Advances in Biochemical Engineering/Biotechnology 187
Series Editor: Roland Ulber

Fred Lisdat
Nicolas Plumeré *Editors*

Trends in Biosensing Research

Advances, Challenges and Applications

Springer

187
Advances in Biochemical Engineering/Biotechnology

Aims and Scope

This book series reviews current trends in modern biotechnology and biochemical engineering. Its aim is to cover all aspects of these interdisciplinary disciplines, where knowledge, methods and expertise are required from chemistry, biochemistry, microbiology, molecular biology, chemical engineering and computer science.

Volumes are organized topically and provide a comprehensive discussion of developments in the field over the past 3–5 years. The series also discusses new discoveries and applications. Special volumes are dedicated to selected topics which focus on new biotechnological products and new processes for their synthesis and purification.

In general, volumes are edited by well-known guest editors. The series editor and publisher will, however, always be pleased to receive suggestions and supplementary information. Manuscripts are accepted in English.

In references, Advances in Biochemical Engineering/Biotechnology is abbreviated as *Adv. Biochem. Engin./Biotechnol.* and cited as a journal.

Fred Lisdat • Nicolas Plumeré
Editors

Trends in Biosensing Research

Advances, Challenges and Applications

With contributions by

K. Aran · M. Bagheri · N. Bagheri · F. F. Bier · E. Campbell · N. G. G. Carducci · A. Chamorro · K. De Wael · S. Dey · I. M. El-Sherbiny · A. B. Ganganboina · B. Goldsmith · S. A. Goodchild · K. Hamad-Schifferli · R. Y. A. Hassan · J. Heikenfeld · J. Hengsteler · T. Hianik · D. P. Hickey · K. Ino · L. J. C. Jeuken · F. Joosten · T. C. Karabulut · D. Kohl · S. Kurbanoglu · P. Lieberzeit · T. Luxton · A. McHenry · M. Moarefian · N. Nakatsuka · E. Y. Park · M. Parrilla · A. Porchetta · M. Rossetti · F. W. Scheller · T. Schlotter · H. Shiku · S. Spagnolo · A. Stuber · M. Thompson · Y. Utagawa · R. Van Echelpoel · A. F. T. Waffo · C. Walti · Z. Watkins · A. Yarman · I. Zebger · X. Zhang

Springer

Editors
Fred Lisdat
Biosystems Technology
Technical University of Applied Sciences
Wildau
Wildau, Germany

Nicolas Plumeré
Electrobiotechnology
Technical University Munich
Munich, Germany

ISSN 0724-6145 ISSN 1616-8542 (electronic)
Advances in Biochemical Engineering/Biotechnology
ISBN 978-3-031-56912-8 ISBN 978-3-031-56913-5 (eBook)
https://doi.org/10.1007/978-3-031-56913-5

This Springer imprint is published by the registered company Springer Nature Switzerland AG
The registered company address is: Gewerbestrasse 11, 6330 Cham, Switzerland

Preface

The continuous pursuit towards detecting extremely small concentrations of analytes with ever-increasing complexity in an expanding diversity of sample matrices has driven innovation in the field of biosensing. Another driving force can be identified in the need to measure biochemical parameters quasi-instantly at the point of need and thus, making analytical devices more accessible. With this book, we highlight how the boundaries in detection limits and sensitivities have been pushed for a variety of analytes and how the design of detection methodologies has been revolutionized to fit the needs of specific applications.

Within the book we follow the classical definition of a biosensor as an analytical tool comprising as heart elements a recognition element and a transduction system – both in close contact. This makes the biosensing field highly interdisciplinary and thus, innovations are driven by different developments. Materials, immobilization strategies, and new methodologies are in the focus. Within this book, the analyte is the molecule which is targeted, and the probe or capture molecule is the recognition site. Although not always in separate chapters, we cover the different kinds of recognition elements – from well-known biomolecules to non-biological approaches. We also illustrate how well-established transduction strategies such as field effect sensing can be revolutionized by new production technologies and immobilization methodologies which widen the applicability. This may underline the dynamic character in the biosensor research field. The book is not intended to introduce into the basic techniques for transduction such as voltammetry, amperometry, surface acoustic waves, surface plasmon resonance, fluorescence, and others. Here, the reader is referred to the various books and reviews covering these topics. Instead, the primary focus lies on highlighting recent developments in the biosensor field. While analytical performance remains important, the emphasis is on the operational principle. As such, the intention is not to be comprehensive, but rather to present illustrative examples to introduce the reader with emerging aspects of biosensor development.

This is highlighted from the first chapter on chimeric protein switch biosensors, where the fusion of recognition and reporter elements paves the way for rapid and efficient analyte detection in complex samples, to the exploration of solid-state

nanopores for biomolecular analysis, which unlocks new possibilities in DNA and protein sequencing.

The applications of graphene-based field effect biosensors and the integration of gold nanoparticles in plasmonic and nanophotonic biosensing showcase the coupling of cutting-edge materials with biological recognition elements leading to innovative transduction principles, marking a significant leap towards portable and cost-effective diagnostic tools.

The advances in DNA-based scaffolds and molecularly imprinted polymers offer unique advantages in the realm of biomolecular recognition. Microbial biosensors emerge as a novel approach, harnessing the metabolic activity of microorganisms to convert chemical signals into electrical outputs, thereby expanding the horizon of environmental monitoring and medical diagnostics.

The convergence of wearable technologies and skin-interfaced systems for continuous biochemical sensing opens avenues for personalized health monitoring, promising a future where real-time data empowers individuals to take control of their well-being.

In the pursuit of precision and sensitivity, aptamer-based biosensors for bacterial detection and signal-amplified nanobiosensors for virus detection using advanced nanomaterials highlight the potential for biosensing complex biological analytes at minute concentrations.

The chapter on microarray-based electrochemical biosensing offers insights into the versatility of array-based detection methodologies, presenting a comprehensive overview of electrochemical techniques applied to high-throughput biosensing.

Finally, the chapter on the electrochemical sensing of illicit drugs underscores the pivotal role of biosensors in addressing societal challenges, offering solutions through rapid, on-site detection methodologies.

Each chapter within this book represents a milestone in the journey towards a future where biosensors go beyond boundaries, transforming the landscape of healthcare, environmental monitoring, and beyond. It is our hope that this book serves as both – a guide and an inspiration to all those embarking on the path of biosensor research, fostering collaboration and innovation

Munich, Germany — Nicolas Plumere
Wildau, Germany — Fred Lisdat

Contents

Adv Biochem Eng Biotechnol (2024) 187: 1–36
https://doi.org/10.1007/10_2023_241

Published online: 26 January 2024

Chimeric Protein Switch Biosensors

Emma Campbell, Timothy Luxton, Declan Kohl, Sarah A. Goodchild, Christoph Walti, and Lars J. C. Jeuken

Contents

Emma Campbell and Timothy Luxton contributed equally to this work.

E. Campbell, T. Luxton, and D. Kohl
School of Biomedical Sciences, University of Leeds, Leeds, UK

S. A. Goodchild
Defence Science and Technology Laboratory, Salisbury, UK

C. Walti
School of Electronic and Electrical Engineering, University of Leeds, Leeds, UK

L. J. C. Jeuken (✉)
School of Biomedical Sciences, University of Leeds, Leeds, UK

Leiden Institute of Chemistry, Leiden University, Leiden, The Netherlands
e-mail: l.j.c.jeuken@lic.leidenuniv.nl

Abstract Rapid detection of protein and small-molecule analytes is a valuable technique across multiple disciplines, but most in vitro testing of biological or environmental samples requires long, laborious processes and trained personnel in laboratory settings, leading to long wait times for results and high expenses. Fusion of recognition with reporter elements has been introduced to detection methods such as enzyme-linked immunoassays (ELISA), with enzyme-conjugated secondary antibodies removing one of the many incubation and wash steps. Chimeric protein switch biosensors go further and provide a platform for homogenous mix-and-read assays where long wash and incubation steps are eradicated from the process. Chimeric protein switch biosensors consist of an enzyme switch (the reporter) coupled to a recognition element, where binding of the analyte results in switching the activity of the reporter enzyme on or off. Several chimeric protein switch biosensors have successfully been developed for analytes ranging from small molecule drugs to large protein biomarkers. There are two main formats of chimeric protein switch biosensor developed, one-component and multi-component, and these formats exhibit unique advantages and disadvantages. Genetically fusing a recognition protein to the enzyme switch has many advantages in the production and performance of the biosensor. A range of immune and synthetic binding proteins have been developed as alternatives to antibodies, including antibody mimetics or antibody fragments. These are mainly small, easily manipulated proteins and can be genetically fused to a reporter for recombinant expression or manipulated to allow chemical fusion. Here, aspects of chimeric protein switch biosensors will be reviewed with a comparison of different classes of recognition elements and switching mechanisms.

Graphical Abstract

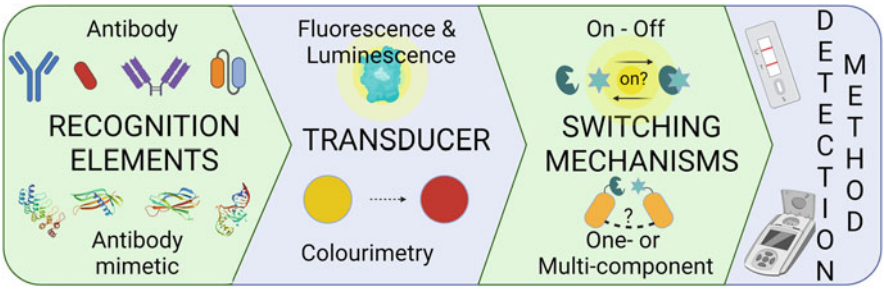

Keywords Enzyme, Point-of-Care Biosensor, Recognition element, Switching mechanism

1 Introduction

Biosensors are typically comprised of three components: a recognition element, a transduction element, and an interface, typically visual or electronic, to communicate the result to the user [1]. Biosensors supersede traditional testing methods enabling the measurement of an analyte of interest quickly, accurately, and at a much lower cost than lengthy lab-based testing; crucially biosensors allow analyte detection at the 'point-of-need' [1]. Biosensors have been implemented in a number of applications including clinical diagnostics [2], environmental pollution monitoring [3], biological warfare [4], and food safety [5].

Biosensors can be categorised into whole-cell sensors, where an analyte can be detected within a living cell [6]; cell-free sensors, genetic systems where the recognition of analyte regulates reporter gene expression [7]; enzymatic sensors, where an enzyme turns over the analyte and the products are measured, such as the glucose sensor [8]; and bio-affinity sensors, where a biorecognition element is used in vitro to capture the analyte from a sample and the transduction element converts the binding event into a signal. Bio-affinity sensors are derived from lab-based immunoassays, such as the very successful enzyme-linked immunosorbent assay (ELISA), where analyte capture and signal transduction are usually separated by wash-steps [9]. These steps can be automated in point-of-care (POC), lab-on-a-chip microfluidic sensors [10], however few have been commercialised [9]. Lateral flow tests (LFTs) are immunodetection devices that produce an optical signal upon protein detection, beneficial for testing that requires a positive or negative result without quantification. They have a long history of use, e.g. in home pregnancy testing and have been widely adopted over the course of the COVID-19 pandemic, due to their low cost, ease of use and utility in low resource settings. Despite their broad uptake, LFTs are semi-quantitative, and often have limited sensitivity that may not be sufficient for some applications [9]. In contrast, protein or enzyme switches, the focus of this chapter, enables highly sensitive quantitative analyte detection at the point-of-need, while retaining the benefits of LFT such as low cost, simplicity for the user and application at the point-of-need. Chimeric protein switch biosensors are defined as sensors in which the reporter and recognition element are fused in a single design (Fig. 1). They can be grouped into (a) domain-inserted allosteric switches, (b) modular allosteric switches, and (c) proximity switches [9, 11]. Here, we first review recognition elements used in chimeric protein switch biosensors, followed by an overview of successful switching mechanisms.

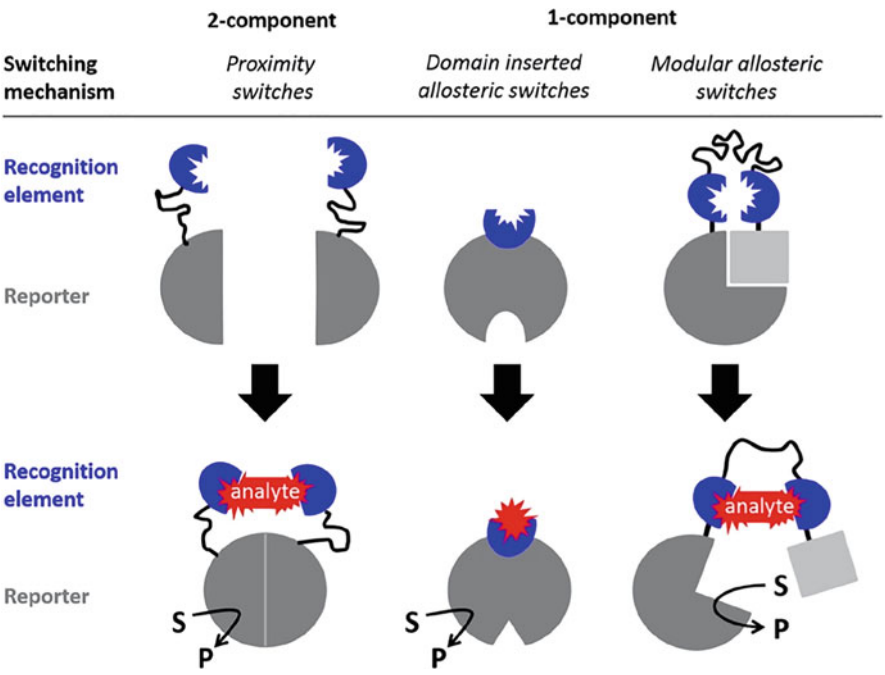

Fig. 1 Switching mechanism classifications of chimeric protein switches. Reprinted from Ref. [9] Copyright 2020 according to CC-BY license

2 Recognition Elements

2.1 Antibodies as Recognition Elements

Antibodies (Immunoglobulin, Ig) were the first and still most utilised recognition elements in immunoassays and bio-affinity sensors. Antibodies are characteristically 'Y' shaped and are approximately 150 kDa in size. Their structure is made up of four chains, two identical heavy chains and two identical light chains, with disulphide bonds linking a light chain to each heavy chain and the two heavy chains together (Fig. 2) [12]. The heavy chains are composed of four regions, three constant regions, and one variable region. The sequences of the heavy chain constant regions determine the class of the immunoglobulin as IgG, IgD, IgM, IgA or IgE [13]. The light chains can be divided into two regions, a constant and a variable region. The antigen-binding sites of an antibody lie in the complementarity-determining regions (CDRs). These regions determine the specificity of the antibody and are located in the heavy and light chain variable regions [13]. The constant regions, on the other hand, determine the immune response to binding the antigen, known as effector functions [14].

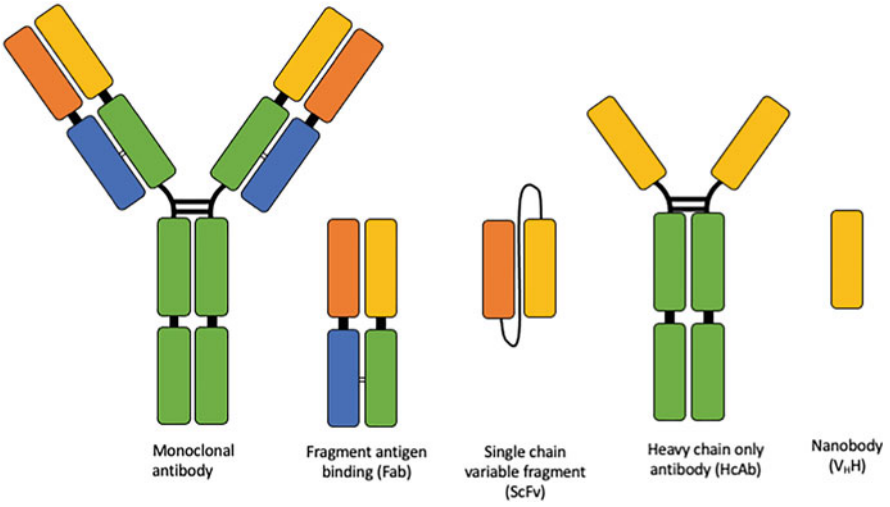

Fig. 2 Antibodies and their fragments used as recognition elements for chimeric protein biosensors. Heavy chain constant domains are depicted in green; light chain constant domains are depicted in blue; heavy chain variable domains are depicted in yellow; light chain variable domains are depicted in orange

The sequences of the constant regions are typically maintained, conversely, the variable regions display a high degree of diversity in its sequences. Sequence diversity in the binding region allows for specific binding to large numbers of analytes and is a result of somatic hypermutation and gene recombination, an immune process that occurs in B cell development in response to exposure of foreign antigens [12]. This ability for sequence diversity is what allows the adaptive immune system to respond to innumerable threats to a host organism [15], and it is this ability that is exploited in biotechnology.

Due to the specificity to their associated antigen, antibodies have been an essential tool in diagnostic tests, and remain a dominating technology for biomolecular analysis [13]. Polyclonal antibodies refer to a non-homogenous pool of antibodies (Igs), where each antibody typically has a different affinity and usually binds to a different part of the analyte (different epitopes) [13]. Polyclonal antibodies are produced through eliciting an immune response in an animal. After a series of injections of the antigen, blood is extracted, and the produced antibodies are purified. Monoclonal antibodies (mAbs), on the other hand, are a single Ig protein (usually an IgG) with a single affinity for their target analyte. Monoclonal antibodies are produced through hybridoma technology [12, 16], in which the effective antibody can be carried forward for monoclonal antibody production [13]. Hybridoma cells are a fusion of B-cells, which are short-lived, and immortal myeloma cells, resulting in an immortalised antibody-producing cell line and, therefore, a maintained source of the selected mAbs [17]. Being able to produce antibodies that are highly specific and highly reproducible has paved the way for tests that are both reliable and

accurate, revolutionising diagnostic technologies [13]. A combination of different antibody types and specificities can be used as capture elements and/or detection elements in assays such as ELISA and fluoroimmunoassays (FIA) to measure the amount of an analyte in a sample [18]. Further, polyclonal and monoclonal antibodies are extensively used in the development of biosensors, which has been previously reviewed [12, 19–21].

Biosensors and immunoassays rely on the antibody's specific affinity to the target of interest. These targets include large macromolecules, such as proteins, larger units such as bacteria, or even small molecules [22]. Whilst antibodies are the most widely used binding proteins, there are limitations to their use and production. Antibodies are typically heat sensitive and for their stability they require disulphide bonds and glycosylation [23]. This complex macromolecular structure makes whole antibodies difficult to express in bacteria, so production is often expensive, requiring the use of animal immunisation or mammalian cell culture [23]. Additionally, there are a number of factors that can result in production of poor antibodies, including mixed hybridoma cultures, poor downstream testing, or antibodies not working well together in an assay. Poor-quality antibodies then raise questions about the reproducibility of antibodies, where researchers have struggled to reproduce the results of published papers [24]. The applications for antibodies are vast, and that is seen in the comprehensive use of antibodies. However, an antibody is only as good as the target it is raised against, as well as the validation carried out subsequent to its selection [25]. Using whole proteins as selection targets is the traditional method for antibody selection [26], but issues may arise if the obtained antibody is cross-selective, with affinities for homologous proteins [25, 27]. To combat inadvertently selecting an antibody against epitopes that are present in multiple analogous proteins, antibodies can be selected against specific epitopes [28–30], provided that the epitopes are stable as isolated peptides. Selecting antibodies against specific epitopes may lead to antibodies that do not have affinity for the whole, folded analyte protein if the epitope is not surface exposed or sterically presented in the same context in the native protein. Thus, care needs to be taken when selecting epitopes for antibody selection.

Small molecules require attachment to a protein carrier to create haptens that illicit an immune response. Typically, it is more challenging to select antibodies against small molecules. Despite this, antibodies with high affinities against small molecules have been produced [22, 31–33]. As with antibodies selected against proteins, stringent validation is needed when being selected against haptens. Since the small molecule needs a larger carrier for antibody production, the resultant antibody may have interactions with a linker or the carrier protein, or a complex of the small molecule and protein carrier [24].

2.2 *Antibody Fragments as Recognition Elements in Chimeric Protein Biosensors*

When looking for highly specific and sensitive recognition elements, antibodies have been the gold-standard. However, antibodies have numerous limitations that impede them as effective recognition elements in biosensors, particularly chimeric protein switch biosensors. Chimeric proteins can be engineered at the genomic level or by chemical conjugation of the antibody with the reporter protein. However, as mentioned, bacteria are unable to produce antibodies, and thus chimeric proteins engineered at the genomic level would need to be expressed in cell cultures. Furthermore, their large size means that when chimeras are formed by chemical conjugation, a heterogenous chimera sample is obtained, affecting the biosensor's performance. The modularity of antibodies allows for the uncoupling of the domains via genetic or biochemical means, enabling the engineering of simplified custom binders. The uncoupling of antibody domains produces antibody fragments with a variety of domain combinations (Fig. 2).

The fragment antigen binding (Fab) region of an antibody is composed of one variable domain and one constant domain from each of the light and heavy chains that make up an antibody [34]. The variable domains contain the antibody paratope, made up of complementary determining regions (CDRs) which are specific to an antigen epitope; the most essential region of an antibody when utilising it for the purpose of detection. Fab regions can be generated from the enzymatic cleavage of a whole antibody with the enzyme papain [35], however, in the context of chimeric protein biosensors it is more practical to recombinantly express chimeras of the Fab region with the reporter protein. Further antibody fragments can be obtained from Fabs. Single chain variable fragments (ScFv) contain the heavy chain (V_H) and light chain (V_L) variable domains linked by a flexible amino acid (AA) linker, most commonly glycine and serine-rich and ~15 residues long [36] (Fig. 2). Singular V_H and V_L domains can also be isolated, although producing these as soluble proteins can be difficult due to the naturally occurring hydrophobic interface between the V_H and V_L domains. The introduction of hydrophilic residues into the V_H/V_L interface has shown improvements in solubility and stability of isolated human V_H or V_L domains [37]. Many of these fragments can be efficiently selected via affinity selection techniques such as with the construction of phage display libraries, using synthetic, naïve, or immune libraries. Synthetic libraries are built on the genetic framework of an antibody fragment with the introduction of randomised sequences into the CDRs and naïve libraries are constructed with the B-cells of unimmunised donors, both of which limit the requirement of animal immunisation. However immune libraries, which require animal immunisation, tend to be more reliable in the generation of high-affinity reagents [38–41]. Molecular display techniques are discussed in more detail in the antibody mimetic section of this book chapter.

Production of Fab, ScFv and V_H fragments is simplified due to the removal of the fragment crystallisation (FC) region of the antibody which eliminates the need for glycosylation and therefore removes the need for mammalian expression systems

[42]. Additionally, the reduced size of the binding protein makes the process of creating a chimeric protein biosensor by genetic fusion easier, as antibody fragments might be easier to express recombinantly with a reporter protein. Despite this simplified structure, Fab fragments, ScFvs and V_H domains still contain disulphide bonds (Fab: 5-6, ScFv: 2, V_H: 1), therefore, an oxidising environment is needed to facilitate native folding of the proteins. Yeasts (*Saccharomyces cerevisiae* and *Pichia pastoris*) are regularly used for the expression of Fab and ScFv fragments. They are the simplest organism that contain an endoplasmic reticulum which aids post-translational modifications, such as the formation of disulphide bonds [43].

Production in bacterial systems (*Escherichia coli*) is advantageous during the research stage as it enables fast production of many different biosensing constructs. However, the reducing environment of the cytoplasm prevents intradomain disulphide bonds from forming, meaning antibody fragments produced in the cytoplasm must frequently be refolded from inclusion bodies under oxidising conditions in vitro [44]. Antibody fragment production can also be directed to occur in the periplasm of *E. coli*, where the environment is oxidising. The volume of the periplasm is much smaller than the cytoplasm and the pathways that secrete proteins from the cytoplasm for folding have a limited capacity, which can become overloaded. This results in lower yields of correctly folded proteins [45]. When expressing chimeric protein biosensors that include multiple ScFvs alongside reporter proteins, *E. coli,* in our experience, is not a reliable host for producing soluble, correctly folded proteins. However, the K-12 type strain RV308 (DE3) expresses insoluble protein as inclusion bodies, and demonstrates less degradation of soluble protein compared to *E. coli* strain BL21(DE3) [46]. The RV308 host strain provides a cheaper alternative for the expression of antibody fragments as inclusion bodies in the cytoplasm with high-yield expression [47]. This does, however, requires the development of a successful refolding procedure when expressing genetically fused chimera proteins.

2.3 Nanobodies as Recognition Elements

Heavy-chain-only antibodies (HcAb) were discovered in 1993 in the sera of camelid species [48]. Compared to the standard mammalian immunoglobulin, HcAbs structurally lack any kind of light chain and only have two of the usual three heavy chain constant domains (Fig. 2). The variable domain of each heavy chain contains three CDRs for antigen recognition. Although they contain only 50% of the binding loops found in IgGs, HcAbs have comparable affinity [49]. Not long after their discovery, the variable domains of HcAbs were isolated and coined V_HH (Fig. 2). HcAbs have also been observed in the sera of elasmobranchs, known as the immunoglobulin new antigen receptor (IgNAR) [50]. These homodimeric HcAbs differ from the camelid HcAbs by three extra constant domains on each chain of the native immunoglobulin. The isolated variable domains (V_{NAR}) also differ slightly, with 2 CDRs (CDR1 and CDR3), and two smaller hypervariable regions (HV2 and HV4) in place of CDR2.

V_{NAR} domains can be further categorised into four isotypes based on the position and number of non-canonical cysteine residues [51]. The collective term for V_HH and V_{NAR} domains is nanobodies or single-domain antibodies (SdAbs). Alongside the high affinity binding and small size (12–15 kDa), the lack of a hydrophobic V_H/V_L domain interface makes them more soluble, another desirable trait for protein engineering. Nanobodies are commonly selected through immune libraries. This involves the immunisation of camelid or shark species, followed by the removal of peripheral blood lymphocytes, extraction of RNA from B-cells, and subsequence synthesis of cDNA. Further selection and affinity maturation of nanobodies can then occur via phage display. Yeast and bacterial display have also been used for this purpose [52]. Nanobodies have been championed for their expression in bacterial systems; however, reports of chimeric proteins involving nanobodies typically use mammalian or yeast expression systems to aid proper folding [53]. In our experience, bacterial hosts do not have the machinery necessary to produce soluble proteins when working with multi-domain chimeric proteins containing V_HH or V_{NAR} domains. Bacterial expression of chimeras with nanobodies is possible, but may need to rely on refolding from inclusion bodies to successfully produce pure proteins [54].

The stability and size of nanobodies has made them versatile tools in developing biosensors. Two V_HHs raised against non-overlapping epitopes of the ectodomain of EGFR (~190 kDa dimer) have been conjugated to semiconductor quantum dot nanocrystals (QD) or terbium (Tb) via bioconjugation techniques. Due to the distance dependence of this detection system, the use of small V_HH domains is advantageous compared to conventional antibodies. V_HH domains can also be used in protein switch biosensors for small molecule recognition. Dimerised V_HH domains form a binding pocket for small molecules, as seen in ScFvs and Fab fragments. Hapten-induced dimerisation of V_HHs provides a 2:1 binding stoichiometry for small molecules, demonstrated in a sensor for caffeine [55, 56].

So far there is little published research utilising V_{NAR} domains as chimeric protein biosensors, with most work focusing on their binding properties in analytical assays such as ELISAs, in vivo diagnostic imaging, and their potential as therapeutic agents. But their potential value in point of care (POC) diagnostic settings has been well documented in reviews [51] (Table 1).

2.4 Antibody Mimetics as Recognition Elements

Antibody mimetics or non-immunoglobin binding proteins are small, single-domain binding proteins that are made up of a conserved scaffold region and a synthetically engineered variable region. Without the natural immune system to rely upon, antibody mimetics with high specificity for analytes need to be selected from protein libraries in the lab with display methods [58, 59]. There are several display methods available for selecting proteins with the desired affinity to analytes of interest. Display methods refer to the presentation of recognition element variants, most

Table 1 Overview of the characteristic of antibody-based binders used in chimeric protein biosensors. Adapted from Ref. [57] Copyright 2021 according to CC-BY license

Antibody-based binder	Size	Production	References
Antibody	~150 kDa	Hybridoma or recombinant DNA technology & mammalian cell expression	[26, 30]
Fragment antibody binding (Fab)	~50 kDa	Proteolysis (e.g. with papain, IdeS, or GingisKHANTM) or recombinant DNA technology and mammalian, yeast, or bacterial cell expression	[35, 42]
Single chain variable fragment (ScFv)	~25 kDa	Recombinant DNA technology and yeast or bacterial cell expression	[36, 44, 47]
Nanobodies	~ 15 kDa	Recombinant DNA technology and plant, mammalian, yeast, or bacterial cell expression	[53, 54]

commonly proteins, to select binders against a target analyte. The most commonly used display method, phage display, uses bacteriophages that contain the recognition element as a fusion with a coat protein, thus presenting the recognition element on the coat of the phage, while retaining the genetic information that encodes that protein within the phage genome. Where in antibody production diversity is produced through somatic hypermutation and gene recombination, diversity in libraries of other protein scaffolds is introduced synthetically. DNA plasmid libraries coding phage containing different recognition element variants are transformed into *E. coli,* which then produce the phage library. The analyte of interest is immobilised onto a surface and the phage library is introduced. Phages presenting recognition elements that bind to the target analyte are identified through panning. Non-binders are washed away, whilst binders are eluted, transformed into *E. coli* and the process is repeated over a number of rounds of affinity selection known as 'panning' rounds (Fig. 3a). Binders are then sequenced, produced and characterised, before introduction into a biosensor detection system. Other display methods utilise cell surface expression of the target analyte in yeast and bacterial cells, and more recently methods that use RNA-templates, such as ribosome display, have been developed that work completely in vitro. They all follow the general concept of converting genetic material into the protein phenotype to select proteins with affinity to a target analyte (Fig. 3b). There are in-depth reviews of the molecular display techniques available for selecting binding proteins [60, 61].

The standard scaffold structure of mimetic binding proteins allows for genetic randomisation of the variable regions, providing a diverse selection of binding proteins with target specificity and high affinity. In addition, desirable protein scaffolds can be selected based on other criteria that ensure downstream utility is optimal. Lower molecular weight, cysteine-free, structures are typically selected to try to ensure that binding reagents are easy to manufacture recombinantly in simple heterologous expression systems [9, 59, 62]. Many antibody mimetic binding

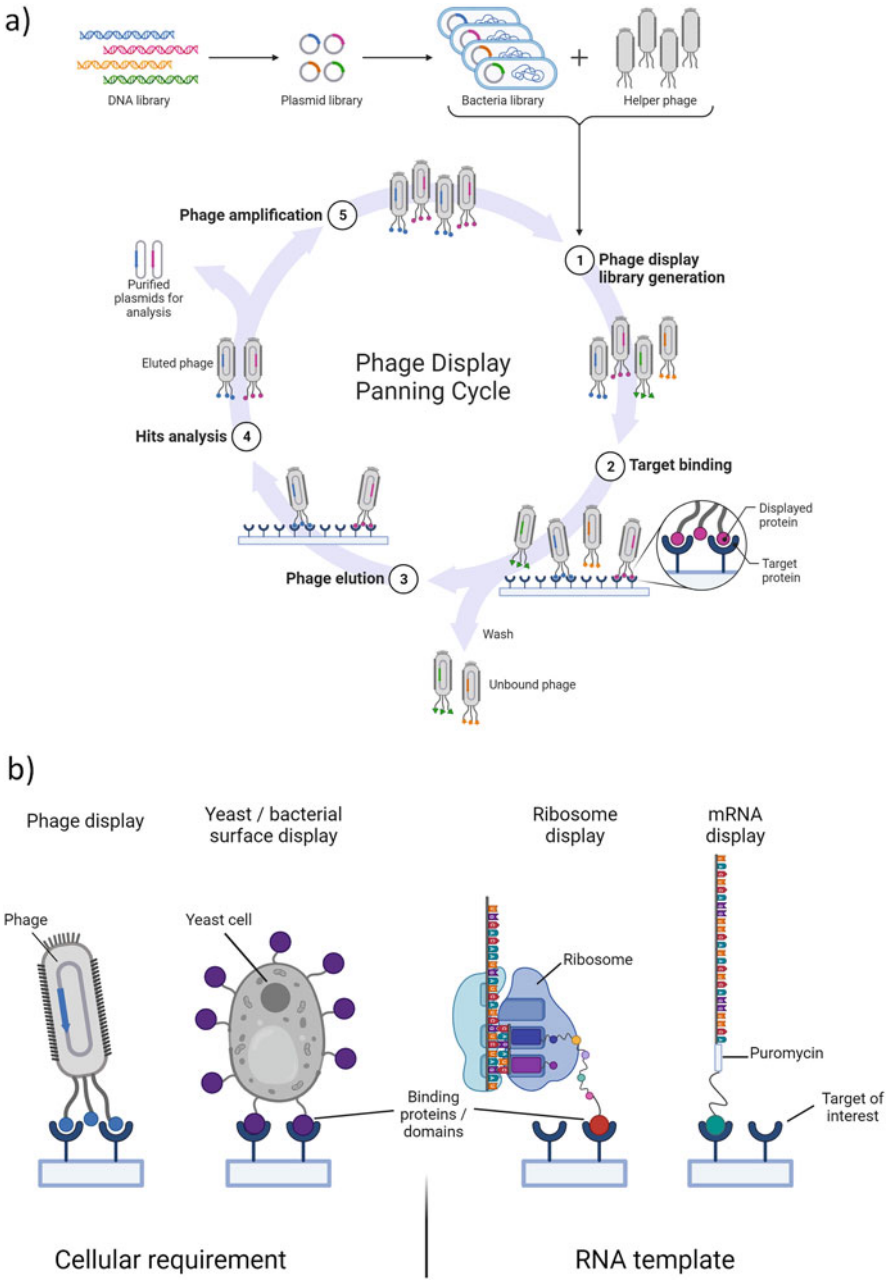

Fig. 3 (**a**) Example phage display panning cycle. Phage libraries presenting recognition element variants are introduced to the immobilised target analyte, high-affinity binders are kept, whilst low-affinity and non-binders are washed away. Binders are eluted and amplified, and the panning cycle is repeated. (**b**) Example molecular display methods used for peptide selection. Phage display is the most well-known and commonly used technique. Other display techniques such as cell surface display and RNA-based display are being developed for the discovery of new binding proteins. Figures (**a**) and (**b**) made with or taken from Biorender.com

proteins have been developed [58], and only a selection will be further explored here as recognition elements in chimeric protein switch biosensors.

Designed ankyrin repeat proteins (DARPins) derived from the naturally occurring binding proteins, ankyrin repeat proteins, are an example of an antibody mimetic protein [63]. Randomisation of the 7 variable amino acids per repeat unit results in large DARPin libraries for selection purposes [64]. The small size of DARPins (14–18 kDa) and the absence of disulphide bonds make them ideal candidates for bacterial expression, enabling production with limited aggregation [65] and incorporation into multi-domain biosensors. This, together with high affinity binding properties, makes DARPins attractive for the design of chimeric protein switch biosensors [66, 67]. However, there have been reports of diminished binding affinity of DARPins when fused to reporter proteins [68].

Another example of antibody mimetic binders with the potential to be implemented as recognition elements are monobodies. Monobodies are built on a scaffold of human fibronectin tenth type III domain, which function as ligand-binding domains in nature [69, 70]. With display-based selection processes, monobodies have been developed against several target analytes such as kinase domains implicated in human health and disease [71, 72], the SARS-CoV2 spike protein [73], tumour biomarkers [74] and monoclonal antibodies [75]. Although monobodies possess the desirable properties to be used as recognition elements within chimeric protein biosensors, their use has so far been focused on therapeutics and as imaging probes for in vivo diagnostics [74].

Affimer binding proteins are another group of antibody mimetic binder based on a cystatin scaffold, with two hypervariable loops for high affinity binding [76]. The ‘consensus concept’ [77] was used to improve the thermostability of the cystatin to produce the synthetic Adhiron scaffold, resulting in a scaffold thermal stability of Tm = 101°C [76]. Affimer proteins are selected against specific targets through phage display [78, 79], with numerous examples published [76, 80–83]. Affimer proteins are small proteins (~12 kDa) without cysteines or disulphide bridges in the scaffold structure. This makes them easy to express in *E. coli* and allows for both site-specific labelling [76], and inclusion in large multi-domain protein switches without misfolding and aggregation complications [84]. Although Affimers can be raised against small molecules [76], Affimers against macromolecules typically have a higher affinity. The use of Affimers as recognition elements in chimeric protein switch biosensors is explored later in this chapter.

2.5 *Peptides as Recognition Elements*

Synthetic peptides can be used as biorecognition elements for chimeric biosensors. As peptides are small and easy for *E. coli* to produce, with no protein folding, disulphide bond formation, or glycosylation required, they may be suitable for fusion with reporter elements in a chimeric sensor. Peptides are short amino acid chains and can be arbitrarily synthesised through solid-phase peptide synthesis

(SPPS) to create a peptide library [85]. Alternatively, peptides can be selected through phage display, with peptide phage libraries commercially available, or mRNA display libraries which covalently combine the genotype coding sequence and the phenotype peptide sequence in one molecule [86]. Peptides, either selected through display methods or synthetically produced, are then characterised through assays and peptides that bind specifically to a target of interest identified. Peptides as recognition elements can give a high affinity to their targets, as with proteins, as well as being easy to synthesise, modify, and produce in bacteria if part of a larger construct [85]. Research has also shown that specificity to the target and stability of the peptide can be improved through the introduction of a hydrocarbon 'staple' between amino acids in the peptide [87]. The use of peptides in chimeric protein switch biosensors is discussed later in this chapter.

2.6 Aptamers as Recognition Elements

Nucleic acid aptamers are short oligonucleotides that form a specific 3D structure with a high affinity to their target molecule which have emerged in the past 20 years as another alternative to antibodies [88]. Their dissociation constants have been reported in the picomolar range against their targets. They bind to their target through salt bridges, van der Waals forces, hydrophobic and other electrostatic interactions [89]. Their small size has also been exploited for use in therapeutics, drug delivery and cell imaging [90]. Aptamers are readily available to bind a variety of biomarkers and pathogens and have been shown to have great biotechnological potential.

In contrast to antibodies, aptamers are produced via chemical synthesis, instead of using in vivo or in vitro mammalian cells, resulting in no batch-to-batch variation. As aptamers are synthesised chemically, reporter molecules or other binding molecules required for biosensor design, need to be chemically attached at precise locations to avoid interference with binding. Aptamers are selected through a process known as Systematic Evolution of Ligands by Exponential Enrichment (SELEX). Compared to antibody selection, SELEX is quicker, more cost-effective, and allows for selection of binders against molecules that would otherwise be toxic to mammals [91]. In SELEX the target of interest is introduced to a single-stranded DNA or RNA library. Non-binding strands are then removed, whilst binders are amplified via polymerase chain reaction (PCR) and used for the next round after converting the double-stranded amplicons into a new single-stranded pool [92]. This process is repeated until the pool is dominated by sequences that bind to the target. DNA sequencing techniques (Sanger sequencing, Illumina, etc,) are used to identify the sequence of aptamers [93]. Several aspects of the isolation process can be customised, including the ionic strength, pH, temperature, and overall chemical environment to optimise binding in an environment that is relevant to the application [94]. The selection of nucleic acid aptamers as binding elements is particularly advantageous when selecting a binder against a small molecule. Antibody selection

requires small molecules to be conjugated to proteins to elicit an immune response [22], and phage display for antibody mimetic protein selection requires immobilisation of the small molecule to a surface, usually conjugated to a protein that can then be immobilised [64, 78, 79]. Both these approaches can alter the chemical structure of the target analyte, resulting in weak binders to the unmodified target, or binders to the protein-molecule complex. Aptamers can be selected against unmodified small molecules in solution through Capture-SELEX. In Capture-SELEX, the library of capture oligonucleotides includes a docking sequence region and are flanked by primer regions. The oligonucleotides are attached to beads using oligonucleotides complementary to the docking region. The small molecule target is then introduced to the bead-bound oligonucleotides. If any of the capture oligonucleotides have a sufficiently high affinity to the target, the nucleotide detaches from the bead, and binds to the target. Non-binders remain on the bead and are removed, whilst binders are amplified by PCR through the flanking primer regions. This process is then repeated for a number of additional cycles [95]. A detailed review on existing SELEX methods has been published [96]. Several aptamers against small molecules have been selected including Aptamers against cocaine, mycotoxins, and pharmaceuticals [97].

The use of aptamers tackles many of the production and development hurdles that face antibodies. Aptamers can be easily amplified, are very stable and not immunogenic [98]. Due to the reliance on living animals for development of antibodies, it makes development of antibodies against some toxic elements and non-immunogenic proteins impractical whereas, in theory, aptamers can be selected against any target [99]. Despite this, aptamers are vulnerable to nucleases and other proteins, present in cells and blood samples, which can break down the oligonucleotides and their 3D structure, preventing them from binding to their desired target [100]. Nanoparticles [98] or chemical modifications can be used to protect them from this breakdown but reduce the number of potential binders in the SELEX process, and may impact affinity to the target of interest. Aptamers also have a tendency to restructure under different ionic or pH conditions limiting their use to the buffer systems used for their selection. The heavily charged nature of aptamers also causes issues with non-specific binding, locked nucleic acids (LNAs) and peptide nucleic acids (PNAs) have been designed as more stable, uncharged alternatives to aptamers [101, 102]. Such chemical modifications can be used to expand the diversity of nucleobase affinity reagents which are otherwise limited by only four nucleic acid building blocks [103].

As with antibodies, care has to be taken with published aptamer sequences. Bottari et al used a number of techniques to measure aptamer binding, including isothermal calorimetry (ITC), and found several published aptamers did not actually bind their respective targets [104]. Also in our experience, several aptamers published to bind antibiotics [105–107] were found to have no or negligible affinity to the target when tested using ITC. Together, this highlights the need for thorough evaluation of selected aptamers.

2.7 De Novo Proteins as Recognition Elements

So far, the discussed recognition elements are all selected through exposure to the target of interest, whether that is via immunisation of animals or through selection from a library. But, analytes can also be targeted through de novo protein design [108, 109]. Here, amino acid monomers are computationally docked to the desired target region and interacting amino acids are stored. Guided by the interacting amino acids, a library of 'miniprotein' scaffolds (50–65 residues) are then computationally docked to the target. The sequences that interface with the target region are further optimised to maximise the number of interactions to the target, this can be done computationally or by creating a synthetic library which is tested and screened to provide more information to the selection process. A second search round is used to improve overall designs, focusing on the designs of the first round that have the best interfaces to the target. Secondary structure motifs that interfaced well with the target region are extracted and clustered, based on their placement and the coordinates of their backbone. Scaffolds are then again docked and superimposed onto the motifs, and the motifs that interact favourably are incorporated into the scaffold. Further interactions to the target are sought through optimising scaffold sequences. The most promising designs are taken forward for experimental validation [108]. This approach may help improve sensor development timelines and improve specificity to the desired target, particularly if analogous proteins to the target exist. For instance, in the development of a biosensor to a virus. This approach will help target regions specific to a more virulent viral strain. Additionally, this can help in the development of biosensors requiring two recognition elements specific to non-overlapping epitopes of the target (Table 2).

3 Sensing Targets

Biosensors need to be specific to the target of interest, so that a signal is not produced in the presence of molecules other than the target of interest. Specificity to the target comes from the recognition elements. As well as specificity, a biosensor needs to be sensitive enough to produce a measurable signal in the presence of the analyte within the desired concentration range. In chimera switch protein biosensors, lack of sensitivity might result from an inability of the target binding event to drive the switching mechanism. Less specific but highly sensitive recognition elements can produce a high background signal when the analyte of interest is not present. Control of sensor component concentrations can typically reduce background binding when using recognition elements with good specificity. Aside from analyte affinity to the recognition elements, sensitivity can be affected by the transduction method (e.g. the enzyme switch) and sensor design. Largely, biosensors can be split into 'switch-off' and 'switch-on' designs (Fig. 4). Switch-off sensors produce a signal in the absence of their target, and when the target is present the signal is inhibited. This sensor

Table 2 Overview of the characteristics of non-immunoglobulin binders used as recognition elements in chimeric protein biosensors. Adapted from Ref. [57] Copyright 2021 according to CC-BY license

Non-immunoglobulin binder	Size	Scaffold	Production	References
Affimer	~12–14 kDa	Cystatin	Phage display and bacterial expression	[76, 78, 79]
DARPins	~14–18 kDa	Ankyrin repeats	Phage or ribosome display and bacterial expression	[63, 65]
Monobodies	~10 kDa	Human fibronectin type III domain	Phage or yeast display and bacterial expression	[69, 70]
Peptides	~5–30 kDa	Amino acid chains	Solid-phase peptide synthesis, phage display and bacterial expression	[85]
Aptamers	~5–30 kDa	Oligonucleotide/protein scaffold	Chemical synthesis (SELEX procedure) or phage display and bacterial expression	[88, 91, 92]
De novo proteins	~5–8 kDa	Amino acid monomers/'Miniprotein'	Computational design, recombinant DNA technology and bacterial expression	[108]

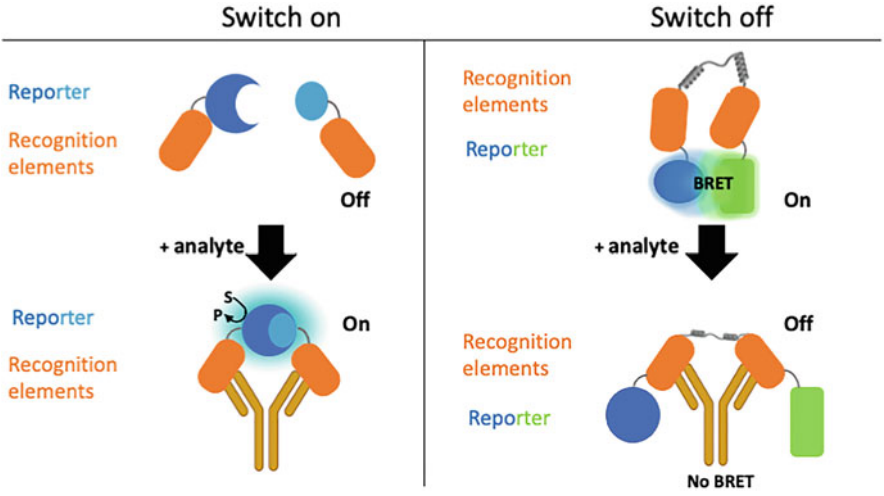

Fig. 4 Schematic examples of 'switch on' and 'switch off' sensor mechanisms. Defined by an increase in signal from baseline (switch on) or a decrease in signal from baseline (switch off)

design, which includes competitive ELISAs, is common for measuring small molecules. Typically, the signal is generated by a tagged target homologue that binds to the recognition element. When the target is present in a sample, it competes for

binding with the tagged homologue and the signal decreases. This sensor design only requires one recognition element and hence is more frequently used for small analytes that have less chemical 'space' for two simultaneous recognition elements to bind. However, at low analyte concentrations, differences in the signal compared to the blank become harder to confidently detect, resulting in lower sensitivity and an increase in error. Switch-off sensors thus typically have a lower sensitivity than switch-on sensors. Switch-on sensors produce a signal in the presence of the target of interest. Generally, two recognition elements specific to non-overlapping target epitopes are needed for a switch-on sensor. This allows for capture and detection of the target, such as in a sandwich ELISA. As a signal is produced in the presence of the target, switch-on sensors tend to be more sensitive as differences in signal compared to the background can be measured even at low analyte concentrations. Switch-on sensors can, however, be difficult to validate when they exhibit high background signal as this must be accounted for in limit of detection and limit of quantification calculations [110].

3.1 Transduction Methods

The methods for producing a signal are known as transduction methods, converting the presence of the target to a measurable signal. These can be categorised into: electrochemical sensors, such as potentiometric, amperometric, and impedimetric; optical sensors, such as colourimetric, spectrophotometric, luminescent, and fluorescent; thermal sensors, such as calorimetric, and thermometric; and mass-based sensors, including magnetoelectric, and piezoelectric sensors [111]. The majority of protein switches are optical sensors and will be the focus of this chapter. Other transduction methods are included in the referenced reviews [1, 111].

A number of optical transduction methods exist, in particular colourimetric, bioluminescent and fluorescent biosensors. Colourimetry is the technique of measuring a colour change that is dependent on the concentration of the target analyte [112]. Colourimetry has been used extensively as a transduction method in protein switches, for instance with β-lactamase:β-lactamase inhibitor protein (BLA-BLIP)-based sensors [11]. The substrate nitrocefin is hydrolysed by β-lactamase from a yellow substrate to a red product, which then can be measured optically. The use of optical transducers limits the requirement for complex instruments with the potential of naked-eye detection, which improves the accessibility and cost-effectiveness of a sensor but restricts its quantitative capabilities. A review on novel approaches for colourimetric measurements, many of which are relevant for point-of-need tests, is referenced [112].

When developing biosensors, chemiluminescence or bioluminescence can be used as transduction methods. Chemiluminescence is the emission of photons as a result of a chemical reaction, which is used by some living organisms to produce light (bioluminescence). Luciferase enzymes are an example of bioluminescent proteins that turn over a substrate to produce light [113]. Although more sensitive

than colourimetric transduction, luminescence is not visible and therefore requires equipment to read the output signal.

Finally, stable fluorescent molecules can be easily attached to recognition elements or linkers to produce sensitive signals in fluorescent biosensors [114]. For instance, the ease of chemical modification of aptamers lends themselves towards fluorescent labelling and numerous diagnostics have been published using fluorophores and quenchers in sensor design. The binding of the aptamer to the target results in a conformational change in the aptamer that is then transduced into a measurable signal due to positions of the fluorophore and quencher [115, 116]. Incorporating fluorescent molecules into sensors also allows for Förster/Bioluminescence resonance energy transfer (F/BRET)-based techniques. FRET occurs through energy transfer between two dipoles, known as dipole-dipole coupling. When the two dipoles are within appropriate proximity and spectral overlap, energy is transferred from an excited state donor fluorophore (D) to an acceptor, a ground state fluorophore or a quencher (A) [117]. BRET is where the energy donor is a bioluminescent molecule, rather than a fluorescent molecule. Both techniques have advantages, FRET produces a stronger signal than BRET and does not require the addition of a substrate. There are several well-documented FRET pairs in literature whereas only a few BRET donors have been identified to date. However, BRET does not require an excitation source which permits the use of simple reading equipment such as smart phones [118] or digital cameras [119]. FRET and BRET as methods are explained in detail in the referenced reviews [117, 120, 121].

3.2 Switching Mechanisms

The mechanism by which a reporter, within a chimeric protein switch biosensor, recovers its activity to transduce a signal in response to analyte binding is known as the switching mechanism. The design of this mechanism aims to maximise the signal-noise ratio (S/N) to obtain a large signal change in response to an analyte.

3.3 One Component Protein Switches

In some instances, all recognition and reporter components of a protein switch are designed and purified as one multimeric polypeptide and can utilise peptide linker regions to connect multiple domains. These are known as one component, or allosteric, protein switches [9, 11]. Generally, allosteric switches are modelled on naturally occurring protein switches that control biomolecular signalling pathways.

Allosteric switches can be categorised as having either a domain inserted or a modular design (Fig. 1). To transduce input to output, domain-inserted switches rely on conformational change within the reporter to switch its activity on (or off). Modular switches limit the conformational change to linker regions which drive

the change in reporter activity. Recombinantly engineering a multidomain protein with the ability to recognise analytes and transduce a signal in a single protein has advantages. It limits the number of steps necessary in the resulting detection assay, typically creating a 'one-pot' assay. It also decreases the number of proteins to be expressed and purified for the assay. Still, as highlighted in the previous sections, there are challenges posed by the expression of multidomain proteins. The multidomain structure these switches possess can end up as large (>80 kDa) proteins, each domain of which must be correctly folded to generate a functional product. The host expression system must also navigate the correct folding of the overall structure, with the possibility of adjacent domains sterically hindering one another. The lack of machinery available in bacterial expression systems to aid in correctly folding such large and complex proteins can result in the formation of unfolded, or aggregated, insoluble protein.

3.3.1 Domain-Inserted Design

Domain-inserted protein switches depend on the direct fusion of a recognition element to a reporter protein. The reporter protein undergoes a conformational change in response to the target analyte binding to the fused recognition element (Fig. 1). The development of these switches requires allosteric coupling of the recognition and reporter elements to allow transduction through residues that are adjacent in the tertiary protein structure [9, 11, 122, 123]. Direct fusion of a recognition element to a reporter can be challenging and ultimately detrimental to reporter activity or binder affinity. Most successful accounts of domain insertion require the inserted domain to be paralogous to the protein in which it is being inserted [124]. β-lactamase (BLA) is a reporter enzyme readily used throughout the field of synthetic biology and bioengineering, and has been successfully inserted into periplasmic binding proteins (PBPs) to create domain-inserted protein switches [122]. The binding of PBPs to their target analyte causes a conformational change which in turn creates a change in conformation and enzymatic activity of BLA. A similar mechanism has been observed with the insertion of calmodulin into the reporter glutamate dehydrogenase (GDH) [123]. Domain-inserted protein switches have been largely limited to specific, naturally occurring binding proteins that are designed with one target analyte in mind and can be restricted in application to other analytes. In this sense, domain-inserted protein switches are often not modular in design.

The use of a modular approach in which a single switch system can measure a range of analytes by replacing the recognition domain is more challenging. There have been accounts of insertion of binding domains from non-paralogous species such as V_HH nanobodies into the solvent-exposed loop of BLA whilst preserving the functionality of both proteins [125]. However, to create the conformational response necessary to make it a protein switch, the reporter protein usually needs to be inserted into the recognition element. Attempts at this with DARPins and monobodies led to diminished binding affinity, limiting the sensitivity and ability

to trigger switching activity [68]. Domain-inserted designs have been complemented by more modular designs to improve adaptability to a range of analytes.

3.3.2 Modular Design

With few protein families exhibiting conformational changes powerful enough to be exploited for signal transduction, engineering of allosteric regulation has taken precedent with more modular designs (Fig. 1). The use of generic reporters that are structurally separated from recognition elements by polypeptide linkers reduces the risk that either the enzyme switch or the recognition domains are affected by the chimera protein design. Such a modular style thus proposes easy adaptability with interchangeable recognition elements (Fig. 1). Interdomain peptide linkers produce a loosely structured conformation to the sensor in its unbound 'off' state. A large conformational change is driven by ligand binding, the bound 'on' state can cause linkers to become rigid, which in turn shifts the conformation of the reporter element (s). In contrast to domain-inserted designs, where the conformational change typically occurs within one protein domain, these modular designs exploit the disruption of an interaction such as an enzyme-inhibitor complex, a fluorophore and quencher or the distance between donor and acceptor fluorophores.

One such successful modular allosteric switch design exploits enzyme autoinhibition, whereby the 'on-off' state of the switch is controlled by the inhibited and non-inhibited state of the enzyme. The wealth of information available on enzymes, their inhibitors and the biophysical properties of their interactions makes these switches easier to design [11]. TEM-1β-lactamase (BLA) can be used for enzyme autoinhibition with its naturally occurring β-lactamase inhibitor protein (BLIP). The BLA-BLIP complex has been engineered into a modular allosteric switch whereby the enzyme and inhibitor are tethered via a long flexible linker containing two recognition elements (Fig. 5). The use of a long, glycine-serine rich linker between the two recognition elements provides the flexibility for the two recognition elements, raised against non-overlapping epitopes, to bind the analyte in a sandwich (capture-detection) format. In contrast, the short rigid linkers that anchor

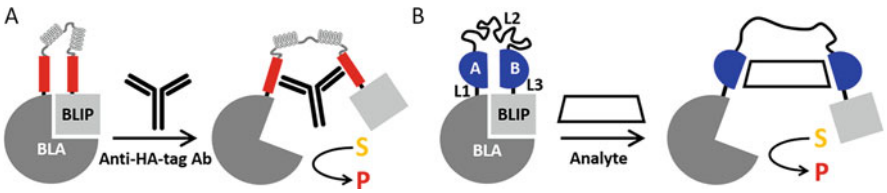

Fig. 5 Chimeric protein switch biosensor design of the BLA-BLIP modular allosteric enzyme switch. (**a**) Original design with peptide epitope sequence recognition elements for the detection of monoclonal antibodies. (**b**) Adapted design with Affimer reagent recognition elements for the detection of multiple protein analytes. Adapted from Ref. [84] Copyright 2019 according to CC-BY license

BLA and BLIP to the recognition elements ensure that binding to the analyte disrupts the enzyme-inhibitor complex (Fig. 5).

This action activates BLA so that its hydrolytic activity can be measured with the addition of a colourimetric substrate. The modular aspect of this switch allows for different recognition elements to be used for a range of targets. This has been demonstrated with peptide epitope sequences (Fig. 5a) [126] and Affimer reagents (Fig. 5b) [84]. The design of this chimeric protein switch biosensor is favourable for the detection of large protein analytes, including antibodies and the multimeric protein biomarker C-reactive protein (CRP).

The BLA-BLIP reporter system has however been adapted for the detection of viral DNA in a single-component modular biosensor [127]. Here, the presence of viral DNA controls BLA inhibition. BLA and BLIP are conjugated to oligonucleotide strands, either side of a region that is complementary to the target viral DNA. In the absence of the target viral DNA, BLIP binds to BLA, inhibiting nitrocefin hydrolysis. When viral DNA is present in the sample, the formation of dsDNA disrupts the BLA-BLIP interaction, resulting in signal generation and viral DNA detection as low as 2 fmol DNA.

Introducing a new reporter, a single component BRET system was created to measure titres of antibodies – LUMABS (LUMinescent AntiBody Sensor) (Fig. 6). Here, the NanoLuc bioluminescent enzyme was used as the donor and the green fluorescent protein mNeonGreen was used as the acceptor, with both proteins fused together by a semi-flexible peptide linker with two peptide recognition elements, specific to the target antibody, included at either end of the peptide linker. In the absence of the antibody target the NanoLuc and mNeonGreen donor and acceptor are held in proximity by a helper domain. The SH3-proline-rich peptide (Sp1) interaction was used as the helper domain, whereby the SH3 protein was fused to the N- terminus of the mNeonGreen protein and the Sp1 peptide was fused to the C-terminus of the NanoLuc. SH3 and Sp1 interact, bringing NanoLuc and mNeonGreen together, allowing BRET from NanoLuc to mNeonGreen. When the target antibody is present in a sample, the antibody binds to the specific peptide epitopes which disrupts the SH3-Sp1 interaction. This separates NanoLuc and mNeonGreen, consequently inhibiting the BRET, giving a measurable signal that

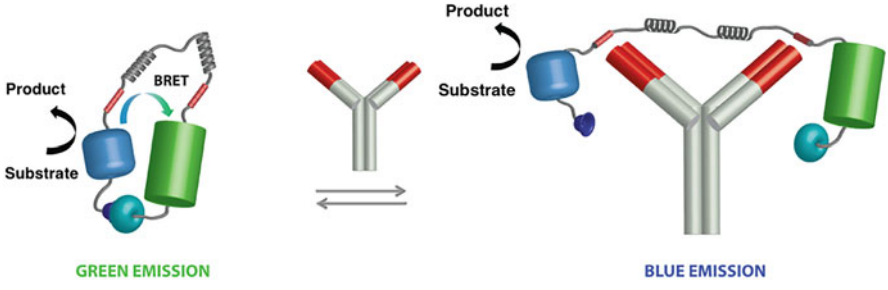

Fig. 6 LUMABs sensor design for antibody detection. Reprinted with permission from Ref [118] Copyright 2016 American Chemical Society

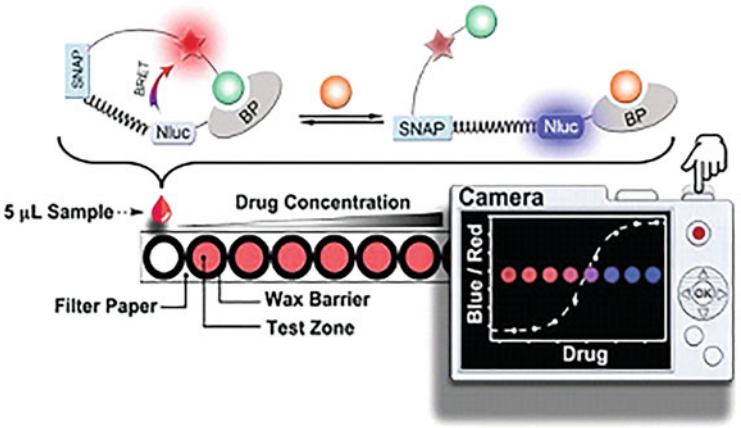

Fig. 7 LUCID sensor design for small molecule drug detection. The LUCID sensor is a fusion protein of NanoLuc luciferase (NLuc), SNAP-tag, and a binding protein (BP). SNAP-tag is labelled with a fluorophore-containing molecule (red star) and a synthetic ligand (green ball) that binds to BP. Wax-printed filter paper is used in the paper-based format and the resulting signal collected using a digital camera. Adapted from Ref. [119] Copyright 2017 according to CC-BY license

is dependent on the concentration of the target antibody. The ratiometric BRET signal produced by the change permits measurements in whole blood, ideal for POC testing [118].

Another one-component modular allosteric switch that uses BRET as a transduction method are the LUCID sensors (luciferase-based indicators of drugs), designed for therapeutic drug monitoring (TDM) in POC settings. LUCID sensors use only one recognition element and do not rely on binding of non-overlapping epitopes to activate the protein-switching mechanism. Instead, displacement of a fluorescent-tagged competitor ligand from the recognition element by the target analyte causes a conformational change within the linker regions of the sensor. Binding of the analyte therefore disrupts BRET between the blue NanoLuc luciferase and red fluorophore, shifting the colour from red to blue in a concentration-dependent manner (Fig. 7). The signal produced permits the quantification of drugs by spotting samples onto paper, followed by analysis with a digital camera. This requirement for non-specific equipment allows these tests to be used in a low-resource environment, often where POC testing is most needed [119].

3.4 Multicomponent Protein Switches

3.4.1 Split Enzymes

Multicomponent switching mechanisms usually rely on the re-complementation of a reporter (Fig. 1). The reporter, most commonly an enzyme, is split into two inactive

fragments that produce no signal when separated [128–131]. It is also possible to exploit the polymerisation process of a multimeric enzyme by modifying the affinity of the associated sub-domains (monomers) [56, 132]. As with most protein switches, the recognition elements selected must bind non-overlapping epitopes of the target analyte to ensure co-localisation of reporter fragments [66, 129, 132–134]. Binding of fused recognition elements to the analyte increases the effective concentration of the reporter fragments, prompting enzyme re-assembly. This results in an increase in signal that is dependent on the concentration of the target analyte; providing that the affinity of the target to the recognition elements is stronger than the consolidation of the reporter enzyme components, so not to drive spontaneous reporter complementation.

Within early examples, two-component proximity switches relied on the split reporter being fused to two proteins that directly interact with one another to drive re-complementation [135, 136]. The system was developed for the analysis of protein–protein interactions (PPI), with an evolution into high-throughput screening (HTS) through the introduction of inhibitors and measurement of the 'off' state of the switch [135]. More recently, improvements in design and development of high affinity binding proteins, such as antibody fragments, antibody mimetics and DNA binders, have opened the possibility of indirect protein detection.

The concept of protein fragment re-complementation to yield active molecules was first observed in β-galactosidase (β-Gal) and ribonuclease [137, 138]. Splitting of a protein for the purpose of measuring its reassembly to monitor PPI was introduced by a split ubiquitin sensor in 1994 [139], however successful reconstitution of ubiquitin was determined by visualisation of ubiquitin-mediated cleavage using blotting methods. Enzymes such as β-Gal have since been split for use in PPI studies. The enzymatic catalysis that produces a fluorescent dye after reconstituting the split parts of the enzyme allows for much easier measurement of PPI and permits such chimeric proteins to work as a tracer of direct PPI within live cells [136]. Chimeric protein biosensors can utilise enzyme complementation for several read-out signals depending on the enzyme and substrate used [56, 66, 67, 131–133, 140].

One development in chimeric protein biosensors exploited the proximity-switching mechanism for the detection of small molecules. Isolated variable (V_H and V_L) domains of a Fab fragment raised against 4-hydroxy-3-nitrophenylacetyl (NP) have been genetically fused to dimerised subunits of the homotetrameric enzyme β-glucuronidase (GUS) to function as a proximity switch [132]. This style of proximity switch relies on high effective concentrations of the chimeric protein driving polymerisation of the dimerised monomers of GUS to produce the fully active homotetrameric enzyme. The sandwich binding pocket created by the V_L and V_H or V_HH domains of an antibody binding to an analyte allows for the detection of small molecules such as NP and caffeine [56].

Improvement of enzyme complementation has largely been focused on luciferases due to their luminescent output and subsequent low background signal, making them highly sensitive in a proximity switch mechanism [66]. A variety of organisms emit light via luciferases which catalyse light-producing reactions, these range from bacteria and fungi to marine life and insects [141]. The splitting of *Renilla* luciferase

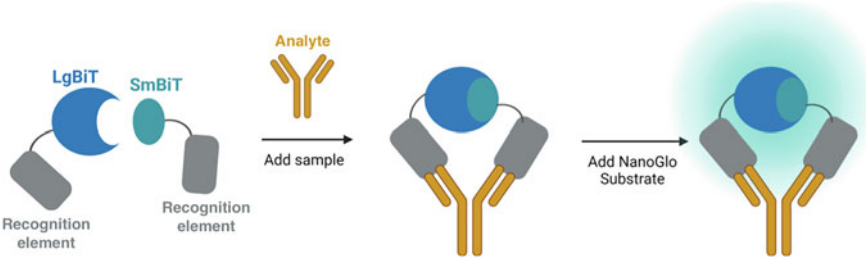

Fig. 8 Schematic diagram of the NanoBiT proximity switch where target-driven co-localisation of the SmBiT and LgBiT fragments results in complementation of the NanoLuc enzyme which emits luminescence with addition of the substrate

[142], *Gaussia* luciferase [143] and firefly luciferase [144] have successfully been used for PPI studies. ScFvs as recognition elements were fused to firefly luciferase fragments and expressed in a cell-free system. This enabled the detection of HER2 in a concentration-dependent manner [145]. However, this was less successful for other targets in the same expression system due to the issues with folding of ScFvs.

To be successfully implemented into a POC setting for in vitro detection of proteins, chimeric biosensor components need to be purified as stable isolated protein. The aforementioned enzyme complementation sensors have been exclusively used in in vivo settings where the sensor components have no need to be extracted from the expression environment. There have been noted issues with the stability of split enzymes in vitro, with the reconstituted activity not reaching that of the wild-type enzyme or high residual activity in the isolated fragments resulting in large background signals and loss of sensitivity [56, 130, 132, 145, 146].

Efforts to optimise a luciferase system resulted in the isolation of an engineered catalytic subunit of the deep-sea shrimp (*Oplophorus gracilirostris*) termed NanoLuc [66, 147]. The high stability and small size of this subunit permitted splitting into two inactive fragments to create a proximity switch system known as the NanoLuc Binary Technology (NanoBiT) (Fig. 8) [148, 149]. The large and small NanoBiT fragments (LgBiT and SmBiT) have been genetically fused to immune and mimetic binding proteins, expressed in *E. coli,* and successfully purified as fully functional chimeric proteins. The NanoBiT system is diverse in its applications with proximity switch assays developed for the detection of large (~270 kDa) and small (~14 kDa) protein biomarkers [148, 149]. An ongoing issue with two-component biosensors is that they are much less sensitive to the orientation of the recognition element binding domains and the analyte. Although this makes their construction easier, the concentration-driven nature means activity is reliant on absolute and relative component concentrations [150]. There is a trade-off between background activity from spontaneous fragment re-complementation and limits to the concentration range that is detectable, as fragment concentrations must be kept below the residual K_d [9]. Component concentrations must also be controlled to limit hook effects at high analyte concentrations: this is where the two sensor components start

Fig. 9 Schematic of Target Engaged Complementation (TEC) split reporter system for the detection of HER2. Reprinted from Ref. [66]. Copyright 2017 according to CC-BY license

binding to two different analyte molecules, omitting the co-localisation of fragments and diminishing the response.

NanoLuc has also been split into three fragments to create a tri-part split luciferase [66, 140, 146]. This involves splitting of NanoLuc into two 11 amino acid β-strand peptides to be fused to recognition elements as chimeric proteins. The use of two smaller peptide reporter fragments improves upon the expression, purification and storage issues commonly seen when creating chimeric proteins with larger more complex reporter proteins. The remainder of the NanoLuc makes up the third component of the switch as a detector protein, or co-operative binder, to limit the hook effect and promote co-localisation (Fig. 9). Dixon et al [66] implemented this system for the detection of HER2 using a Fab fragment and DARPin pair that bind non-overlapping epitopes of the receptor. This alteration of the NanoBiT enables detection of pM concentrations of HER2, with the possibility of adaption for a range of target analytes. Split enzyme systems have the capacity to be used as chimeric protein biosensors with a range of recognition elements facilitating the detection of diverse analytes with diagnostic value.

Fluorescent reporter proteins can also be used in proximity switches: this mechanism is known as biomolecular fluorescence complementation (BiFC) [151]. Two fragments of a fluorescent protein are inactive apart, therefore do not produce a fluorescent signal. Co-localisation of the two inactive fragments permits reassembly of the fluorescent protein resulting in a readable signal. However, as with enzyme re-assembly, spontaneous self-association of the reporter must be considered as background signal. The use of reporters from the green fluorescent protein (GFP) family in BiFC can be slow and result in irreversible complex formation [152, 153], which make them less suitable for rapid analyte detection. However, other fluorescent proteins have been used for BiFC more successfully.

A protein tag derived from apo photoactive yellow protein (PYP) of *Halorhodospira halophila* has been engineered. The protein tag coined FAST (Fluorescence-Activating and absorption-Shifting Tag) forms fluorescent complexes with 4-hydroxybenzylidene rhodanine (HBR) derivatives [154]. FAST was spilt into two inactive loops which maintained some affinity for one another in the presence of HBR derivatives. Fusion of two mammalian binding proteins which interact in the presence of rapamycin resulted in a proximity switch able to image, and measure the presence of rapamycin in vivo [155].

A multi-component biosensor to measure aflatoxin B_1 (AFB_1), a small molecule, using a competitive FRET-based system has been published. Here, two different-sized quantum dots (QD) were used. In proximity, energy transfer occurs from the donor QD (emission: 530 nm) to the acceptor (emission: 650 nm). On the donor QD, multiple AFB_1 molecules were conjugated to the surface. The antibody against AFB_1 was then monovalently conjugated to the acceptor QD. With no AFB_1 present in a sample, the AFB_1 molecule on the donor QD would bind the antibody attached to the acceptor QD, resulting in high FRET and a higher 650 nm emission spectrum. If a sample contained AFB_1, less of the donor QD would be in proximity to the acceptor QD, as the monovalent antibody would be bound by AFB_1 in the sample, resulting in a higher 530 nm emission spectrum and a lower 650 nm emission spectrum [156].

Small molecule toxins, microcystin and nodularin, have been detected in a capture-detection format using ScFv recognition elements. A ScFv labelled with Alexa Fluor 680 and a monoclonal antibody labelled with europium enabled the FRET process to occur in the presence of microcystin or nodularin, within a sandwich binding format [157].

4 Conclusions

Chimeric protein switches permit the direct transduction of analyte binding into a measurable signal using a wash-free, homogenous setup. The general design includes recognition and reporter elements which function together within a switching mechanism, each of these factors impacts the performance of the protein switch. There are a range of binders that have been explored as recognition elements within chimeric protein switches. In some instances, highly specific, naturally occurring binding proteins can be used but these result in limited designs as the naturally occurring binding proteins bind to only one target analyte. These have generally been superseded by antibody-based and non-immunoglobin binding proteins which provide a modular design with the opportunity to be raised against numerous target analytes by swapping of the binding proteins. Each binder has strengths and limitations as a recognition element, depending on their size, affinity, ease of selection and expression conditions. Choosing the best option can depend on their activity once paired with a reporter and switching mechanism.

The reporter element of a chimeric protein switch determines the method of transduction. These are typically colourimetric, fluorescent, or bioluminescent, and can be used alone or in combination with an inhibitor or quencher depending on the switching mechanism. The signal produced must be considered, specifically as the equipment necessary to read the signal would need to be available in the intended setting. The stability of the reporter is also important, as protein engineering to create chimeric proteins by chemical and genetic fusion, or splitting into inactive fragments, can be detrimental to reporter stability and/or activity. The limited number of reporters able to maintain their activity when inserted into the domain of a

recognition element can make domain-inserted protein switches less favourable. Similarly, the splitting of a reporter (split enzyme switch) can be detrimental to recovery of activity. However, intensive research has gone into the design and optimisation of split luciferase systems. Despite that, multi-component switches can suffer from concentration-dependent background activation. One-component modular switches generally do not suffer from concentration dependence and use intact reporters. However, in the case of BLA-BLIP and LUMABS, successful activation of the switch is dependent on exact binding geometries which can be difficult to control when adapting to future targets. Although the general focus of modular protein switches is to create a stable platform with interchangeable recognition elements, the dynamic range of current chimeric protein switches is highly variable. With more focus on creating modular protein switch formats that do not require redesign between target analytes, the prospect of chimeric protein switches being implemented into clinical and real-world settings to compete with the 'gold-standard' analyte measurement assays is improving.

Acknowledgements This work was funded by a CASE studentship to E.C. from the White Rose Mechanistic Biology Doctoral Training Partnership (UK Biotechnology and Biological Sciences Research Council; BB/M011151/1) in conjunction with Dstl, a scholarship from the University of Leeds to T.L., a studentship from the Medical Research Foundation (MRF) to D.K. and the Medical Research Council (MRC; MR/N029976/1).

References

1. Goode JA, Rushworth JVH, Millner PA (2015) Biosensor regeneration: a review of common techniques and outcomes. Langmuir 31(23):6267–6276. https://doi.org/10.1021/la503533g
2. Haleem A, Javaid M, Singh RP, Suman R, Rab S (2021) Biosensors applications in medical field: a brief review. Sens Int 2:100100. https://doi.org/10.1016/j.sintl.2021.100100
3. Gavrilaș S, Ursachi C, Perța-Crișan S, Munteanu FD (2022) Recent trends in biosensors for environmental quality monitoring. Sensors (Basel) 22(4). https://doi.org/10.3390/s22041513
4. Pohanka M (2019) Current trends in the biosensors for biological warfare agents assay. Materials (Basel) 12(14). https://doi.org/10.3390/ma12142303
5. Thakur MS, Ragavan KV (2013) Biosensors in food processing. J Food Sci Technol 50(4): 625–641. https://doi.org/10.1007/s13197-012-0783-z
6. Bousse L (1996) Whole cell biosensors. Sens Actuators B 34(1):270–275. https://doi.org/10.1016/S0925-4005(96)01906-5
7. Zhang L, Guo W, Lu Y (2020) Advances in cell-free biosensors: principle, mechanism, and applications. Biotechnol J 15(9):2000187. https://doi.org/10.1002/biot.202000187
8. Newman JD, Setford SJ (2006) Enzymatic biosensors. Mol Biotechnol 32(3):249–268. https://doi.org/10.1385/MB:32:3:249
9. Adamson H, Jeuken LJC (2020) Engineering protein switches for rapid diagnostic tests. ACS Sens 5(10):3001–3012. https://doi.org/10.1021/acssensors.0c01831
10. Samiei E, Tabrizian M, Hoorfar M (2016) A review of digital microfluidics as portable platforms for lab-on a-chip applications. Lab Chip 16(13):2376–2396. https://doi.org/10.1039/C6LC00387G
11. Stein V, Alexandrov K (2015) Synthetic protein switches: design principles and applications. Trends Biotechnol 33(2):101–110. https://doi.org/10.1016/j.tibtech.2014.11.010

12. Conroy PJ, Hearty S, Leonard P, O'Kennedy RJ (2009) Antibody production, design and use for biosensor-based applications. Semin Cell Dev Biol 20(1):10–26. https://doi.org/10.1016/j.semcdb.2009.01.010
13. Sharma S, Byrne H, O'Kennedy RJ (2016) Antibodies and antibody-derived analytical biosensors. Essays Biochem 60(1):9–18. https://doi.org/10.1042/EBC20150002
14. Schroeder Jr HW, Cavacini L (2010) Structure and function of immunoglobulins. J Allergy Clin Immunol 125(2 Suppl 2):S41–S52. https://doi.org/10.1016/j.jaci.2009.09.046
15. McCullough KC, Summerfield A (2005) Basic concepts of immune response and defense development. ILAR J 46(3):230–240
16. Köhler G, Milstein C (1975) Continuous cultures of fused cells secreting antibody of predefined specificity. Nature 256:495–497
17. Parray HA, Shukla S, Samal S, Shrivastava T, Ahmed S, Sharma C et al (2020) Hybridoma technology a versatile method for isolation of monoclonal antibodies, its applicability across species, limitations, advancement and future perspectives. Int Immunopharmacol 85:106639. https://doi.org/10.1016/j.intimp.2020.106639
18. Darwish IA (2006) Immunoassay methods and their applications in pharmaceutical analysis basic methodology and recent advances. Int J Biomed Sci 2(3):217–235
19. Zeng X, Shen Z, Mernaugh R (2012) Recombinant antibodies and their use in biosensors. Anal Bioanal Chem 402:3027–3038. https://doi.org/10.1007/s00216-011-5569-z
20. Byrne B, Stack E, Gilmartin N, O'Kennedy R (2009) Antibody-based sensors: principles, problems and potential for detection of pathogens and associated toxins. Sensors 9:4407–4445. https://doi.org/10.3390/s90604407
21. Iqbal SS, Mayo MW, Bruno JG, Bronk BV, Batt CA, Chambers JP (2000) A review of molecular recognition technologies for detection of biological threat agents. Biosens Bioelectron 15:549–578
22. Al Qaraghuli MM, Palliyil S, Broadbent G, Cullen DC, Charlton KA, Porter AJ (2015) Defining the complementarities between antibodies and haptens to refine our understanding and aid the prediction of a successful binding interaction. BMC Biotechnol:15. https://doi.org/10.1186/s12896-015-0217-x
23. Tiede C, Tang AA, Deacon SE, Mandal U, Nettleship JE, Owen RL et al (2014) Adhiron: a stable and versatile peptide display scaffold for molecular recognition applications. Protein Eng Des Sel 27(5):145–155. https://doi.org/10.1093/protein/gzu007
24. Weller MG (2016) Quality issues of research antibodies. Anal Chem Insights 11:21–27. https://doi.org/10.4137/ACI.S31614
25. Bordeaux J, Welsh A, Agarwal S, Killiam E, Baquero M, Hanna J et al (2010) Antibody validation. Biotechniques 48(3):197–209. https://doi.org/10.2144/000113382
26. Liew OW, Ling SSM, Lilyanna S, Zhou Y, Wang P, Chong JPC et al (2021) Epitope-directed monoclonal antibody production using a mixed antigen cocktail facilitates antibody characterization and validation. Commun Biol 4(1):441. https://doi.org/10.1038/s42003-021-01965-x
27. Saper CB, Sawchenko PE (2003) Magic peptides, magic antibodies: guidelines for appropriate controls for immunohistochemistry. J Comp Neurol 465:161–163. https://doi.org/10.1002/cne.10858
28. Arnon R, Maron E, Sela M, Anfinsen CB (1971) Antibodies reactive with native lysozyme elicited by a completely synthetic antigen. Proc Natl Acad Sci 68(7):1450–1455. https://doi.org/10.1073/pnas.68.7.1450
29. Sutcliffe JG, Shinnick TM, Green N, Lerner RA (1983) Antibodies that react with predetermined sites on proteins. Science 219(4585):660–666. https://doi.org/10.1126/science.6186024
30. Nilsson P, Paavilainen L, Larsson K, Odling J, Sundberg M, Andersson AC et al (2005) Towards a human proteome atlas: high-throughput generation of mono-specific antibodies for tissue profiling. Proteomics 5(17):4327–4337. https://doi.org/10.1002/pmic.200500072

31. Palliyil S, Downham C, Broadbent I, Charlton K, Porter AJ (2014) High-sensitivity monoclonal antibodies specific for homoserine lactones protect mice from lethal Pseudomonas aeruginosa infections. Appl Environ Microbiol 80(2):462–469. https://doi.org/10.1128/AEM.02912-13
32. Charlton K, Harris WJ, Porter AJ (2001) The isolation of super-sensitive anti-hapten antibodies from combinatorial antibody libraries derived from sheep. Biosens Bioelectron 16(9–12):639–646. https://doi.org/10.1016/s0956-5663(01)00192-0
33. Clementi ME, Marini S, Condò SG, Giardina B (1991) Antibodies against small molecules. Ann Ist Super Sanita 27(1):139–143
34. Crivianu-Gaita V, Thompson M (2016) Aptamers, antibody scFv, and antibody Fab' fragments: an overview and comparison of three of the most versatile biosensor biorecognition elements. Biosens Bioelectron 85:32–45. https://doi.org/10.1016/j.bios.2016.04.091
35. Crivianu-Gaita V, Romaschin A, Thompson M (2015) High efficiency reduction capability for the formation of Fab′ antibody fragments from F(ab)2 units. Biochem Biophys Rep 2:23–28. https://doi.org/10.1016/j.bbrep.2015.04.004
36. Sun H, Wu GM, Chen Y, Tian Y, Yue YH, Zhang GL (2014) Expression, production, and renaturation of a functional single-chain variable antibody fragment (scFv) against human ICAM-1. Braz J Med Biol Res 47(7):540–547. https://doi.org/10.1590/1414-431X20143276
37. Rouet R, Dudgeon K, Christie M, Langley D, Christ D (2015) Fully human VH single domains that rival the stability and cleft recognition of camelid antibodies. J Biol Chem 290(19):11905–11917. https://doi.org/10.1074/jbc.M114.614842
38. Li K, Zettlitz KA, Lipianskaya J, Zhou Y, Marks JD, Mallick P et al (2015) A fully human scFv phage display library for rapid antibody fragment reformatting. Protein Eng Des Sel 28(10):307–316. https://doi.org/10.1093/protein/gzv024
39. Watkins NA, Du LM, Scott JP, Ouwehand WH, Hillery CA (2003) Single-chain antibody fragments derived from a human synthetic phage-display library bind thrombospondin and inhibit sickle cell adhesion. Blood 102(2):718–724. https://doi.org/10.1182/blood-2002-11-3497
40. Huang G, Zhong Z, Miersch S, Sidhu SS, Hou SC, Wu D (2018) Construction of synthetic phage displayed fab library with tailored diversity. J Vis Exp 1(135):1–16. https://doi.org/10.3791/57357
41. Omar N, Lim TS (2018) Construction of naive and immune human fab phage-display library. Methods Mol Biol 1701:25–44. https://doi.org/10.1007/978-1-4939-7447-4_2
42. Kayser V, Chennamsetty N, Voynov V, Forrer K, Helk B, Trout BL (2011) Glycosylation influences on the aggregation propensity of therapeutic monoclonal antibodies. Biotechnol J 6(1):38–44. https://doi.org/10.1002/biot.201000091
43. Woycechowsky KJ, Raines RT (2000) Native disulfide bond formation in proteins. Curr Opin Chem Biol 4(5):533–539. https://doi.org/10.1016/s1367-5931(00)00128-9
44. Rouet R, Lowe D, Dudgeon K, Roome B, Schofield P, Langley D et al (2012) Expression of high-affinity human antibody fragments in bacteria. Nat Protoc 7(2):364–373. https://doi.org/10.1038/nprot.2011.448
45. Gaciarz A, Veijola J, Uchida Y, Saaranen MJ, Wang C, Hörkkö S et al (2016) Systematic screening of soluble expression ofantibody fragments in the cytoplasm of E. coli. Microb Cell Fact 15(1):22. https://doi.org/10.1186/s12934-016-0419-5
46. Marisch K, Bayer K, Cserjan-Puschmann M, Luchner M, Striedner G (2013) Evaluation of three industrial Escherichia coli strains in fed-batch cultivations during high-level SOD protein production. Microb Cell Fact 12(1):58. https://doi.org/10.1186/1475-2859-12-58
47. Yuasa N, Koyama T, Fujita-Yamaguchi Y (2014) Purification and refolding of anti-T-antigen single chain antibodies (scFvs) expressed in Escherichia coli as inclusion bodies. Biosci Trends 8(1):24–31. https://doi.org/10.5582/bst.8.24
48. Hamers-Casterman C, Atarhouch T, Muyldermans S, Robinson G, Hammers C, Songa EB et al (1993) Naturally occurring antibodies devoid of light chains. Nature 363(6428):446–448. https://doi.org/10.1038/363446a0

49. Arbabi-Ghahroudi M (2017) Camelid single-domain antibodies: historical perspective and future outlook. Front Immunol 8(1589). https://doi.org/10.3389/fimmu.2017.01589
50. Greenberg AS, Avila D, Hughes M, Hughes A, McKinney EC, Flajnik MF (1995) A new antigen receptor gene family that undergoes rearrangement and extensive somatic diversification in sharks. Nature 374(6518):168–173. https://doi.org/10.1038/374168a0
51. Cheong WS, Leow Y, Majeed A, Leow H (2020) Diagnostic and therapeutic potential of shark variable new antigen receptor (VNAR) single domain antibody. Int J Biol Macromol 147:369–375. https://doi.org/10.1016/j.ijbiomac.2020.01.039
52. Muyldermans S (2021) A guide to: generation and design of nanobodies. FEBS J 288(7): 2084–2102. https://doi.org/10.1111/febs.15515
53. Yamagata M, Sanes JR (2018) Reporter-nanobody fusions (RANbodies) as versatile, small, sensitive immunohistochemical reagents. Proc Natl Acad Sci 115(9):2126–2131. https://doi.org/10.1073/pnas.1722491115
54. Xu L, Song X, Jia L (2016) A camelid nanobody against EGFR was easily obtained through refolding of inclusion body expressed in E.coli. Biotechnol Appl Biochem:64. https://doi.org/10.1002/bab.1544
55. Sonneson GJ, Horn JR (2009) Hapten-induced dimerization of a single-domain VHH camelid antibody. Biochemistry 48(29):6693–6695. https://doi.org/10.1021/bi900862r
56. Su J, Beh C, Ohmuro-Matsuyama Y, Kitaguchi T, Hoon S, Ueda H (2019) Creation of stable and strictly regulated enzyme switch for signal-on immunodetection of various small antigens. J Biosci Bioeng 128(6):677–682. https://doi.org/10.1016/j.jbiosc.2019.05.015
57. Olaleye O, Govorukhina N, van de Merbel NC, Bischoff R (2021) Non-antibody-based binders for the enrichment of proteins for analysis by mass spectrometry. Biomol Ther 11(12). https://doi.org/10.3390/biom11121791
58. Yu X, Yang Y-P, Dikici E, Deo SK, Daunert S (2017) Beyond antibodies as binding partners: the role of antibody mimetics in bioanalysis. Annu Rev Anal Chem 10(1):293–320. https://doi.org/10.1146/annurev-anchem-061516-045205
59. Peltomaa R, Benito-Peña E, Barderas R, Moreno-Bondi MC (2019) Phage display in the quest for new selective recognition elements for biosensors. ACS Omega 4(7):11569–11580. https://doi.org/10.1021/acsomega.9b01206
60. Galán A, Comor L, Horvatić A, Kuleš J, Guillemin N, Mrljak V et al (2016) Library-based display technologies: where do we stand? Mol Biosyst 12(8):2342–2358. https://doi.org/10.1039/C6MB00219F
61. Ullman CG, Frigotto L, Cooley RN (2011) In vitro methods for peptide display and their applications. Brief Funct Genomics 10(3):125–134. https://doi.org/10.1093/bfgp/elr010
62. Löfblom J, Frejd FY, Ståhl S (2011) Non-immunoglobulin based protein scaffolds. Curr Opin Biotechnol 22(6):843–848. https://doi.org/10.1016/j.copbio.2011.06.002
63. Binz HK, Stumpp MT, Forrer P, Amstutz P, Plückthun A (2003) Designing repeat proteins: well-expressed, soluble and stable proteins from combinatorial libraries of consensus ankyrin repeat proteins. J Mol Biol 332(2):489–503. https://doi.org/10.1016/s0022-2836(03)00896-9
64. Stumpp MT, Binz HK, Amstutz P (2008) DARPins: a new generation of protein therapeutics. Drug Discov Today 13(15):695–701. https://doi.org/10.1016/j.drudis.2008.04.013
65. Münch RC, Mühlebach MD, Schaser T, Kneissl S, Jost C, Plückthun A et al (2011) DARPins: an efficient targeting domain for lentiviral vectors. Mol Ther 19(4):686–693. https://doi.org/10.1038/mt.2010.298
66. Dixon AS, Kim SJ, Baumgartner BK, Krippner S, Owen SC (2017) A tri-part protein complementation system using antibody-small peptide fusions enables homogeneous immunoassays. Sci Rep 7(1):8186. https://doi.org/10.1038/s41598-017-07569-y
67. Kim SJ, Dixon AS, Owen SC (2021) Split-enzyme immunoassay to monitor EGFR-HER2 heterodimerization on cell surfaces. Acta Biomater 135:225–233. https://doi.org/10.1016/j.actbio.2021.08.055

68. Nicholes N, Date A, Beaujean P, Hauk P, Kanwar M, Ostermeier M (2016) Modular protein switches derived from antibody mimetic proteins. Protein Eng Des Sel 29(2):77–85. https://doi.org/10.1093/protein/gzv062
69. Koide A, Bailey CW, Huang X, Koide S (1998) The fibronectin type III domain as a scaffold for novel binding proteins11Edited by. J Wells J Mol Biol 284(4):1141–1151. https://doi.org/10.1006/jmbi.1998.2238
70. Batori V, Koide A, Koide S (2002) Exploring the potential of the monobody scaffold: effects of loop elongation on the stability of a fibronectin type III domain. Protein Eng 15(12):1015–1020. https://doi.org/10.1093/protein/15.12.1015
71. Carrasco-López C, Zhao EM, Gil AA, Alam N, Toettcher JE, Avalos JL (2020) Development of light-responsive protein binding in the monobody non-immunoglobulin scaffold. Nat Commun 11(1):4045. https://doi.org/10.1038/s41467-020-17837-7
72. Hantschel O, Biancalana M, Koide S (2020) Monobodies as enabling tools for structural and mechanistic biology. Curr Opin Struct Biol 60:167–174. https://doi.org/10.1016/j.sbi.2020.01.015
73. Kondo T, Matsuoka K, Umemoto S, Fujino T, Hayashi G, Iwatani Y et al (2022) Monobodies with potent neutralizing activity against SARS-CoV-2 Delta and other variants of concern. Life Sci Alliance 5(6):e202101322. https://doi.org/10.26508/lsa.202101322
74. Park S-H, Park S, Kim D-Y, Pyo A, Kimura RH, Sathirachinda A et al (2015) Isolation and characterization of a monobody with a fibronectin domain III scaffold that specifically binds EphA2. PloS One 10(7):e0132976. https://doi.org/10.1371/journal.pone.0132976
75. Sullivan MA, Wentworth T, Kobie JJ, Sanz I (2012) Anti-idiotypic monobodies for immune response profiling. Methods 58(1):62–68. https://doi.org/10.1016/j.ymeth.2012.07.009
76. Tiede C, Bedford R, Heseltine SJ, Smith G, Wijetunga I, Ross R et al (2017) Affimer proteins are versatile and renewable affinity reagents. Elife 6:e24903. https://doi.org/10.7554/eLife.24903
77. Lehmann M, Loch C, Middendorf A, Studer D, Lassen SF, Pasamontes L et al (2002) The consensus concept for thermostability engineering of proteins: further proof of concept. Protein Eng Des Sel 15(5):403–411. https://doi.org/10.1093/protein/15.5.403
78. Tang AA-S, Tiede C, Hughes DJ, McPherson MJ, Tomlinson DC (2017) Isolation of isoform-specific binding proteins (Affimers) by phage display using negative selection. Sci Signal 10(505):eaan0868. https://doi.org/10.1126/scisignal.aan0868
79. Tang AAS, Tiede C, McPherson MJ, Tomlinson DC (2021) Isolation of artificial binding proteins (Affimer reagents) for use in molecular and cellular biology. In: Poterszman A (ed) Multiprotein complexes: methods and protocols. Springer US, New York, pp 105–121
80. Martin HL, Bedford R, Heseltine SJ, Tang AA, Haza KZ, Rao A et al (2018) Non-immunoglobulin scaffold proteins: precision tools for studying protein-protein interactions in cancer. N Biotechnol 45:28–35. https://doi.org/10.1016/j.nbt.2018.02.008
81. Koutsoumpeli E, Tiede C, Murray J, Tang A, Bon RS, Tomlinson DC et al (2017) Antibody mimetics for the detection of small organic compounds using a quartz crystal microbalance. Anal Chem 89(5):3051–3058. https://doi.org/10.1021/acs.analchem.6b04790
82. Sharma R, Deacon SE, Nowak D, George SE, Szymonik MP, Tang AAS et al (2016) Label-free electrochemical impedance biosensor to detect human interleukin-8 in serum with sub-pg/ml sensitivity. Biosens Bioelectron 80:607–613. https://doi.org/10.1016/j.bios.2016.02.028
83. Xie C, Tiede C, Zhang X, Wang C, Li Z, Xu X et al (2017) Development of an Affimer-antibody combined immunological diagnosis kit for glypican-3. Sci Rep 7(1):9608. https://doi.org/10.1038/s41598-017-10083-w
84. Adamson H, Ajayi MO, Campbell E, Brachi E, Tiede C, Tang AA et al (2019) Affimer–enzyme–inhibitor switch sensor for rapid wash-free assays of multimeric proteins. ACS Sensors 4(11):3014–3022. https://doi.org/10.1021/acssensors.9b01574
85. Liu Q, Wang J, Boyd BJ (2015) Peptide-based biosensors. Talanta 136:114–127. https://doi.org/10.1016/j.talanta.2014.12.020

86. Wang H, Liu R (2011) Advantages of mRNA display selections over other selection techniques for investigation of protein-protein interactions. Expert Rev Proteomics 8(3):335–346. https://doi.org/10.1586/epr.11.15
87. Thean D, Ebo JS, Luxton T, Lee XEC, Yuen TY, Ferrer FJ et al (2017) Enhancing specific disruption of intracellular protein complexes by hydrocarbon stapled peptides using lipid based delivery. Sci Rep 7(1):1763. https://doi.org/10.1038/s41598-017-01712-5
88. Lakhin AV, Tarantul VZ, Gening LV (2013) Aptamers: problems, solutions and prospects. Acta Nat 5(4):34–43
89. Ku T-H, Zhang T, Luo H, Yen TM, Chen P-W, Han Y et al (2015) Nucleic acid aptamers: an emerging tool for biotechnology and biomedical sensing. Sensors 15(7):16281–16313. https://doi.org/10.3390/s150716281
90. Song K-M, Lee S, Ban C (2012) Aptamers and their biological applications. Sensors 12(1): 612–631
91. Siddiqui MZ (2010) Monoclonal antibodies as diagnostics; an appraisal. Indian J Pharm Sci 72(1):12–17. https://doi.org/10.4103/0250-474x.62229
92. Yang K-A, Pei R, Stojanovic MN (2016) In vitro selection and amplification protocols for isolation of aptameric sensors for small molecules. Methods 106:58–65. https://doi.org/10.1016/j.ymeth.2016.04.032
93. Cho M, Xiao Y, Nie J, Stewart R, Csordas AT, Oh SS et al (2010) Quantitative selection of DNA aptamers through microfluidic selection and high-throughput sequencing. Proc Natl Acad Sci U S A 107(35):15373–15378. https://doi.org/10.1073/pnas.1009331107
94. Nutiu R, Li Y (2005) In vitro selection of structure-switching signaling aptamers. Angew Chem Int Ed Engl 44(7):1061–1065. https://doi.org/10.1002/anie.200461848
95. Stoltenburg R, Nikolaus N, Strehlitz B (2012) Capture-SELEX: selection of DNA aptamers for aminoglycoside antibiotics. J Anal Methods Chem 1(14):415697. https://doi.org/10.1155/2012/415697
96. Mascini M, Palchetti I, Tombelli S (2012) Nucleic acid and peptide aptamers: fundamentals and bioanalytical aspects. Angew Chem Int Ed Engl 51(6):1316–1332. https://doi.org/10.1002/anie.201006630
97. Ni S, Yao H, Wang L, Lu J, Jiang F, Lu A et al (2017) Chemical modifications of nucleic acid aptamers for therapeutic purposes. Int J Mol Sci 18(8):1683. https://doi.org/10.3390/ijms18081683
98. Ireson CR, Kelland LR (2006) Discovery and development of anticancer aptamers. Mol Cancer Ther 5(12):2957–2962. https://doi.org/10.1158/1535-7163.Mct-06-0172
99. Yi S, Citartan M, Tang TH (2014) Aptamers as a replacement for antibodies in enzyme-linked immunosorbent assay. Biosens Bioelectron 64C:392–403. https://doi.org/10.1016/j.bios.2014.09.026
100. Jarczewska M, Rębiś J, Górski Ł, Malinowska E (2018) Development of DNA aptamer-based sensor for electrochemical detection of C-reactive protein. Talanta 189:45–54. https://doi.org/10.1016/j.talanta.2018.06.035
101. Pellestor F, Paulasova P (2004) The peptide nucleic acids (PNAs), powerful tools for molecular genetics and cytogenetics. Eur J Hum Genet 12(9):694–700. https://doi.org/10.1038/sj.ejhg.5201226
102. Vester B, Wengel J (2004) LNA (locked nucleic acid): high-affinity targeting of complementary RNA and DNA. Biochemistry 43(42):13233–13241. https://doi.org/10.1021/bi0485732
103. Gawande BN, Rohloff JC, Carter JD, von Carlowitz I, Zhang C, Schneider DJ et al (2017) Selection of DNA aptamers with two modified bases. Proc Natl Acad Sci U S A 114(11): 2898–2903. https://doi.org/10.1073/pnas.1615475114
104. Bottari F, Daems E, de Vries AM, Van Wielendaele P, Trashin S, Blust R et al (2020) Do aptamers always bind? The need for a multifaceted analytical approach when demonstrating binding affinity between aptamer and low molecular weight compounds. J Am Chem Soc 142(46):19622–19630. https://doi.org/10.1021/jacs.0c08691

105. Paniel N, Istamboulie G, Triki A, Lozano C, Barthelmebs L, Noguer T (2017) Selection of DNA aptamers against penicillin G using capture-SELEX for the development of an impedimetric sensor. Talanta 162:232–240. https://doi.org/10.1016/j.talanta.2016.09.058
106. Lee AY, Ha NR, Jung IP, Kim SH, Kim AR, Yoon MY (2017) Development of a ssDNA aptamer for detection of residual benzylpenicillin. Anal Biochem 531:1–7. https://doi.org/10.1016/j.ab.2017.05.013
107. Zhao J, Guo W, Pei M, Ding F (2016) GR–Fe3O4NPs and PEDOT–AuNPs composite based electrochemical aptasensor for the sensitive detection of penicillin. Anal Methods 8(22): 4391–4397. https://doi.org/10.1039/c6ay00555a
108. Cao L, Coventry B, Goreshnik I, Huang B, Sheffler W, Park JS et al (2022) Design of protein-binding proteins from the target structure alone. Nature 605(7910):551–560. https://doi.org/10.1038/s41586-022-04654-9
109. Huang P-S, Boyken SE, Baker D (2016) The coming of age of de novo protein design. Nature 537(7620):320–327. https://doi.org/10.1038/nature19946
110. Armbruster DA, Pry T (2008) Limit of blank, limit of detection and limit of quantitation. Clin Biochem Rev 29(Suppl 1):S49–S52
111. Polat EO, Cetin MM, Tabak AF, Bilget Güven E, Uysal BÖ, Arsan T et al (2022) Transducer Technologies for Biosensors and Their Wearable Applications. Biosensors 12(6):385
112. Fernandes GM, Silva WR, Barreto DN, Lamarca RS, Lima Gomes PCF, Flávio da S Petruci J et al (2020) Novel approaches for colorimetric measurements in analytical chemistry – a review. Anal Chim Acta 1135:187–203. https://doi.org/10.1016/j.aca.2020.07.030
113. Dixon AS, Schwinn MK, Hall MP, Zimmerman K, Otto P, Lubben TH et al (2016) NanoLuc complementation reporter optimized for accurate measurement of protein interactions in cells. ACS Chem Biol 11(2):400–408. https://doi.org/10.1021/acschembio.5b00753
114. Syahir A, Usui K, Tomizaki K-y, Kajikawa K, Mihara H (2015) Label and label-free detection techniques for protein microarrays. Microarrays 4(2):228–244
115. Stojanovic MN, de Prada P, Landry DW (2000) Fluorescent sensors based on aptamer self-assembly. J Am Chem Soc 122(46):11547–11548. https://doi.org/10.1021/ja0022223
116. Arroyo-Currás N, Somerson J, Vieira PA, Ploense KL, Kippin TE, Plaxco KW (2017) Real-time measurement of small molecules directly in awake, ambulatory animals. Proc Natl Acad Sci U S A 114(4):645–650. https://doi.org/10.1073/pnas.1613458114
117. Algar WR, Hildebrandt N, Vogel SS, Medintz IL (2019) FRET as a biomolecular research tool – understanding its potential while avoiding pitfalls. Nat Methods 16(9):815–829. https://doi.org/10.1038/s41592-019-0530-8
118. Arts R, den Hartog I, Zijlema SE, Thijssen V, van der Beelen SHE, Merkx M (2016) Detection of antibodies in blood plasma using bioluminescent sensor proteins and a smartphone. Anal Chem 88(8):4525–4532. https://doi.org/10.1021/acs.analchem.6b00534
119. Xue L, Yu Q, Griss R, Schena A, Johnsson K (2017) Bioluminescent antibodies for point-of-care diagnostics. Angew Chem Int Ed Engl 56(25):7112–7116. https://doi.org/10.1002/anie.201702403
120. Piston DW, Kremers G-J (2007) Fluorescent protein FRET: the good, the bad and the ugly. Trends Biochem Sci 32(9):407–414. https://doi.org/10.1016/j.tibs.2007.08.003
121. Dale NC, Johnstone EKM, White CW, Pfleger KDG (2019) NanoBRET: the bright future of proximity-based assays. Front Bioeng Biotechnol:7. https://doi.org/10.3389/fbioe.2019.00056
122. Tullman J, Nicholes N, Dumont MR, Ribeiro LF, Ostermeier M (2016) Enzymatic protein switches built from paralogous input domains. Biotechnol Bioeng 113(4):852–858. https://doi.org/10.1002/bit.25852
123. Guo Z, Johnston WA, Stein V, Kalimuthu P, Perez-Alcala S, Bernhardt PV et al (2016) Engineering PQQ-glucose dehydrogenase into an allosteric electrochemical Ca(2+) sensor. Chem Commun (Camb) 52(3):485–488. https://doi.org/10.1039/c5cc07824e
124. Guntas G, Mansell TJ, Kim JR, Ostermeier M (2005) Directed evolution of protein switches and their application to the creation of ligand-binding proteins. Proc Natl Acad Sci 102(32): 11224–11229. https://doi.org/10.1073/pnas.0502673102

125. Crasson O, Rhazi N, Jacquin O, Freichels A, Jérôme C, Ruth N et al (2015) Enzymatic functionalization of a nanobody using protein insertion technology. Protein Eng Des Sel 28(10):451–460. https://doi.org/10.1093/protein/gzv020
126. Banala S, Aper SJ, Schalk W, Merkx M (2013) Switchable reporter enzymes based on mutually exclusive domain interactions allow antibody detection directly in solution. ACS Chem Biol 8(10):2127–2132. https://doi.org/10.1021/cb400406x
127. Janssen BMG, Engelen W, Merkx M (2015) DNA-directed control of enzyme–inhibitor complex formation: a modular approach to reversibly switch enzyme activity. ACS Synth Biol 4(5):547–553. https://doi.org/10.1021/sb500278z
128. Drikic M, Olsen S, De Buck J (2019) Detecting total immunoglobulins in diverse animal species with a novel split enzymatic assay. BMC Vet Res 15(1):374. https://doi.org/10.1186/s12917-019-2126-z
129. Ni Y, Rosier BJHM, van Aalen EA, Hanckmann ETL, Biewenga L, Pistikou A-MM et al (2021) A plug-and-play platform of ratiometric bioluminescent sensors for homogeneous immunoassays. Nat Commun 12(1):4586. https://doi.org/10.1038/s41467-021-24874-3
130. Guo Z, Murphy L, Stein V, Johnston WA, Alcala-Perez S, Alexandrov K (2016) Engineered PQQ-glucose dehydrogenase as a universal biosensor platform. J Am Chem Soc 138(32):10108–10111. https://doi.org/10.1021/jacs.6b06342
131. Fleming A (1945) Penicillin Nobel Lectures 83–93
132. Su J, Dong J, Kitaguchi T, Ohmuro-Matsuyama Y, Ueda H (2018) Noncompetitive homogeneous immunodetection of small molecules based on beta-glucuronidase complementation. Analyst 143(9):2096–2101. https://doi.org/10.1039/c8an00074c
133. Dixon AS, Baumgartner BK, Krippner S, Shawn O (2016) Bioluminescence activated by antibody-enzyme fragment complementation following target engagement. Frontiers in bioengineering and biotechnology conference abstract: 10th world biomaterials congress. Montréal, Canada, p 1
134. Ng KK, Reinert ZE, Corver J, Resurreccion D, Hensbergen PJ, Prescher JA (2021) A bioluminescent sensor for rapid detection of PPEP-1, a clostridioides difficile biomarker. Sensors (Basel) 21(22):7485. https://doi.org/10.3390/s21227485
135. Hashimoto J, Watanabe T, Seki T, Karasawa S, Izumikawa M, Seki T et al (2009) Novel in vitro protein fragment complementation assay applicable to high-throughput screening in a 1536-well format. J Biomol Screen 14(8):970–979. https://doi.org/10.1177/1087057109341406
136. Rossi F, Charlton CA, Blau HM (1997) Monitoring protein-protein interactions in intact eukaryotic cells by beta-galactosidase complementation. Proc Natl Acad Sci U S A 94(16):8405–8410. https://doi.org/10.1073/pnas.94.16.8405
137. Richards FM (1958) On the enzymatic activity of subtilisin-modified ribonuclease. Proc Natl Acad Sci U S A 44(2):162–166. https://doi.org/10.1073/pnas.44.2.162
138. Ullmann A, Jacob F, Monod J (1967) Characterization by in vitro complementation of a peptide corresponding to an operator-proximal segment of the beta-galactosidase structural gene of Escherichia coli. J Mol Biol 24(2):339–343. https://doi.org/10.1016/0022-2836(67)90341-5
139. Johnsson N, Varshavsky A (1994) Split ubiquitin as a sensor of protein interactions in vivo. Proc Natl Acad Sci U S A 91(22):10340–10344. https://doi.org/10.1073/pnas.91.22.10340
140. Kim SJ, Dixon AS, Adamovich PC, Robinson PD, Owen SC (2021) Homogeneous immunoassay using a tri-part split-luciferase for rapid quantification of anti-TNF therapeutic antibodies. ACS Sens 6(5):1807–1814. https://doi.org/10.1021/acssensors.0c02642
141. Weissleder R, Ntziachristos V (2003) Shedding light onto live molecular targets. Nat Med 9(1):123–128. https://doi.org/10.1038/nm0103-123
142. Paulmurugan R, Gambhir SS (2003) Monitoring protein−protein interactions using split synthetic renilla luciferase protein-fragment-assisted complementation. Anal Chem 75(7):1584–1589. https://doi.org/10.1021/ac020731c

143. Remy I, Michnick SW (2006) A highly sensitive protein-protein interaction assay based on Gaussia luciferase. Nat Methods 3(12):977–979. https://doi.org/10.1038/nmeth979
144. Paulmurugan R, Umezawa Y, Gambhir S (2002) Noninvasive imaging of protein–protein interactions in living subjects by using reporter protein complementation and reconstitution strategies. Proc Natl Acad Sci 99(24):15608–15613
145. Stains CI, Furman JL, Porter JR, Rajagopal S, Li Y, Wyatt RT et al (2010) A general approach for receptor and antibody-targeted detection of native proteins utilizing split-luciferase reassembly. ACS Chem Biol 5(10):943–952. https://doi.org/10.1021/cb100143m
146. Ohmuro-Matsuyama Y, Ueda H (2018) Homogeneous noncompetitive luminescent Immunodetection of small molecules by ternary protein fragment complementation. Anal Chem 90(5):3001–3004. https://doi.org/10.1021/acs.analchem.7b05140
147. Verhoef LG, Mattioli M, Ricci F, Li YC, Wade M (2016) Multiplex detection of protein-protein interactions using a next generation luciferase reporter. Biochim Biophys Acta 1863(2):284–292. https://doi.org/10.1016/j.bbamcr.2015.11.031
148. Adamson H, Ajayi MO, Gilroy KE, McPherson MJ, Tomlinson DC, Jeuken LJC (2022) Rapid quantification of C. difficile glutamate dehydrogenase and toxin B (TcdB) with a NanoBiT split-luciferase assay. Anal Chem 94(23):8156–8163. https://doi.org/10.1021/acs.analchem.1c05206
149. McArthur N, Cruz-Teran C, Thatavarty A, Reeves GT, Rao BM (2022) Experimental and analytical framework for "Mix-and-Read" assays based on split luciferase. ACS Omega 7(28):24551–24560. https://doi.org/10.1021/acsomega.2c02319
150. Edwardraja S, Guo Z, Whitfield J, Lantadilla IR, Johnston WA, Walden P et al (2020) Caged activators of artificial allosteric protein biosensors. ACS Synth Biol 9(6):1306–1314. https://doi.org/10.1021/acssynbio.9b00500
151. Kerppola TK (2008) Bimolecular fluorescence complementation (BiFC) analysis as a probe of protein interactions in living cells. Annu Rev Biophys 37(1):465–487. https://doi.org/10.1146/annurev.biophys.37.032807.125842
152. Magliery TJ, Wilson CGM, Pan W, Mishler D, Ghosh I, Hamilton AD et al (2005) Detecting protein−protein interactions with a green fluorescent protein fragment reassembly trap: scope and mechanism. J Am Chem Soc 127(1):146–157. https://doi.org/10.1021/ja046699g
153. Ghosh I, Hamilton AD, Regan L (2000) Antiparallel leucine zipper-directed protein reassembly: application to the green fluorescent protein. J Am Chem Soc 122(23):5658–5659
154. Plamont M-A, Billon-Denis E, Maurin S, Gauron C, Pimenta FM, Specht CG et al (2016) Small fluorescence-activating and absorption-shifting tag for tunable protein imaging in vivo. Proc Natl Acad Sci 113(3):497–502. https://doi.org/10.1073/pnas.1513094113
155. Tebo AG, Gautier A (2019) A split fluorescent reporter with rapid and reversible complementation. Nat Commun 10(1):2822. https://doi.org/10.1038/s41467-019-10855-0
156. Xu W, Xiong Y, Lai W, Xu Y, Li C, Xie M (2014) A homogeneous immunosensor for AFB1 detection based on FRET between different-sized quantum dots. Biosens Bioelectron 56:144–150. https://doi.org/10.1016/j.bios.2014.01.007
157. Akter S, Lamminmäki U (2021) A 15-min non-competitive homogeneous assay for microcystin and nodularin based on time-resolved Förster resonance energy transfer (TR-FRET). Anal Bioanal Chem 413(24):6159–6170. https://doi.org/10.1007/s00216-021-03375-8

Adv Biochem Eng Biotechnol (2024) 187: 37–70
https://doi.org/10.1007/10_2024_252

Published online: 29 February 2024

Applications of Graphene Field Effect Biosensors for Biological Sensing

Kiana Aran, Brett Goldsmith, and Maryam Moarefian

Contents

K. Aran (✉)
Shu Chien-Gene Lay Department of Bioengineering, Jacobs School of Engineering, University of California, San Diego, La Jolla, CA, USA

Division of Geriatrics, Gerontology and Palliative Care, Department of Medicine, School of Medicine, University of California, San Diego, La Jolla, CA, USA

Center for Technologies for Healthy Aging, Institute of Engineering and Medicine, University of California, San Diego, La Jolla, CA, USA

Paragraf, Somersham, UK

CRISPR QC, San Diego, CA, USA
e-mail: karan@ucsd.edu

B. Goldsmith
Paragraf, Somersham, UK

M. Moarefian
University of California, Santa Cruz, CA, USA

Abstract This chapter provides a comprehensive overview of the principles, applications, and advancements in graphene field-effect transistor (gFET) biosensors for biological sensing. The unique properties of graphene that make it ideal for biosensing, including its high conductivity, chemical stability, and ability to facilitate label-free detection, will be discussed. The chapter also explores various applications of gFET biosensors, from detecting pH and salinity changes to complex protein-protein interactions and DNA/RNA sensing. It also addresses the challenges and future directions in gFET biosensor technology, emphasizing the need for scalable manufacturing, sophisticated surface chemistry, and the integration of multiomics approaches to enhance biosensing capabilities.

Graphical Abstract

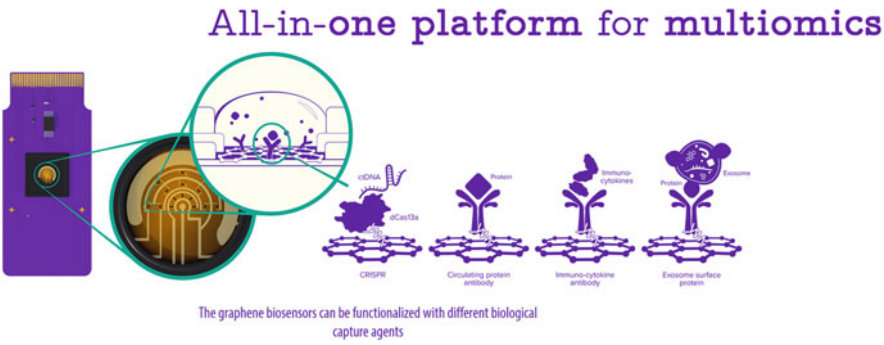

Keywords CRISPR, Field effect Biosesnors, Mutiomics

1 Introduction and Background

Biomedical and environmental testing currently require access to highly specialized facilities or extensive training. Biochemical tests require complex reagents to achieve a simple human readable result such as a color change. Although we have already test systems for providing defined readout with affordable costs (e.g.,

glucose, virus detection, or pregnancy tests), there are still many high-cost tests with insufficient information about human diseases. To maximize information from testing while minimizing costs, biotechnology should leverage complex analysis enabled by advanced portable computing power and use simplified reagents, tools, and processes. This concept can be conceived of as "the internet of biology" in the same way miniaturized electronic sensors have enabled "the internet of things." Nanotechnologists have created proof-of-concept hand-held, easy-to-use personal devices, but none have achieved large-scale manufacturability. We introduce here the concept, principle, and application of the first economical nanoelectronics produced in a commercial foundry. The mass-manufacture of these graphene-based digital biosensors is achieved by successfully integrating graphene into standard electronic high-volume production processes. Access to this type of production opens the door for rapid deployment of nanoelectronic sensors outside the research space. The low power and resource usage of these biosensors enables biotech engineers to gain immediate control over precise biological and environmental data.

The prevailing philosophy in biological testing has been to focus on simple tests with easy to interpret information such as ELISA or lateral flow assays. At the same time, there has been a decades long understanding in device physics and nanotechnology that electrical approaches have the potential to drastically improve the quality, speed, and cost of biological testing provided that computational resources are available to analyze the resulting complex data. It is well established in the nanotechnology literature that techniques such as field effect biosensing are capable of rapid and flexible biological testing. Until now, access to this new technology has been limited to academic researchers focused on bioelectronic devices and their collaborators. Here we show that this capability is retained in an industrially manufactured device, opening access to this technology generally.

The world is entering an inflection point in medical and biological testing with the simultaneous emergence of improved testing technology, advanced software tools, and increased expectations for quality healthcare worldwide. Organizations like the Qualcomm Tricorder XPRIZE and Gates Foundation have pushed for integrations of varied technologies in clinical tests to demonstrate potential application [1]. Traditional healthcare companies market point-of-care tools with limited test libraries [2]. In each case, complex, analyte-specific reagents and intricate protocols are essential for multiple platforms and deep biochemical or clinical expertise to replicate the capability of a central lab [3].

There is a need for information-dense single assays that break the mold of expensive labs running colorimetric and PCR-based assays [4]. Label-free measurement tools based on field-effect sensors should lower the amount for most liquid reagents, decrease power requirements, and shrink the size of handheld testing devices [5]. These tools will be capable of performing a wide variety of chemical and biochemical assays built on top of a single sensor manufacturing chain, leading to lower overall cost for biological measurements.

The unique attributes that are required to build effective field effect biosensors are a combination of semiconductor behavior with chemical stability of the sensor

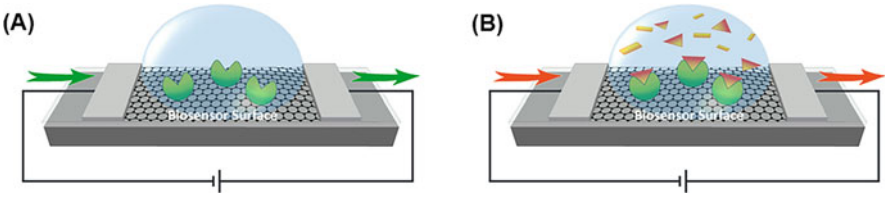

Fig. 1 A schematic view of the surface of an Agile R100 biosensor chip. (**a**) Immobilized probe bound to biosensor chip. (**b**) Capture probe binding on the biosensor surface detected using FEB and the change in current

surface in air and salt water [6]. Materials like silicon require oxide layers between the transistor channel and the environment, limiting the sensitivity of field effect sensors made using those conventional materials [5]. Materials, such as graphene, carbon nanotubes, and molybdenum disulfide have the unique combination of chemical stability and electric field sensitivity desirable to create sensitive electronic interfaces to biological molecules [7]. This has led to a dense literature covering chemical and biological sensors using these materials [8–20]. Several attempts were made to produce carbon nanotube biosensors for biomedical use in the early part of the twenty-first century with limited results due to manufacturing difficulties [14]. Fabrication techniques using molybdenum disulfide have not matured sufficiently for devices to move beyond the proof of concept stage [15].

2 Principle of Operation

2.1 Overview

With graphene-based biosensors, scientists have direct visibility into the binding interactions that natively occur in biological systems without intermediary translations from optical data. In particular, graphene biosensors using field effect biosensing (FEB) offer a label-free technology for measuring biomolecular interactions. FEB, an electrical technique, measures the current across a graphene biosensor surface functionalized with immobilized biomolecular capture probes (Fig. 1a). Any interaction or binding that occurs on the biosensor surface causes a change in conductance of the biosensor that is monitored in real-time (Fig. 1b), enabling accurate kinetic, affinity, and concentration measurements. These measurements are consistent with other biosensor advancements that aim to achieve label-free detection for biochemical analysis. This includes impedimetric techniques, surface plasmon resonance-based optical detection systems, or mass-sensitive devices, such as surface acoustic wave devices (SAW) [21].

Graphene FEB sensors integrate biologically active materials (i.e., the immobilized capture probe) with graphene-based electronics to detect the binding of an analyte in solution. When analyte binds to the probe, the charge distribution at

the surface changes, triggering a change in graphene field effect transistor (gFET) electrical characteristics. This can be obtained by measuring the source and drain current, which effectively converts biological events into electrical signals, such as current. Current (I) changes are directly linked to the analyte concentration, and the concentration of the analyte as well as the kinetic binding data and affinity of the analyte to the target can be detected.

The general concept of biosensing was introduced by Clark in continuous monitoring of chemical composition of blood in cardiovascular surgery as early as 1962 [22]. Additionally, the concept of charge detection, which is the foundational research for graphene FEB, is not new and has been utilized in the insulated-gate field-effect transistor (IGFET) [23] or metal-oxide-semiconductor field-effect transistor (MOSFET) starting from the 1960s [24]. The MOSFET is composed of a silicon substrate that has connections for the source and drain, as well as a layer of silicon dioxide on top. In the typical MOSFET setup, the oxide is coated with a gate metal. When a gate potential is applied, a conducting channel is generated in the silicon, which can be measured as a resistance between the source and drain. Adapting the MOSFET design to operation in liquid for sensing application has been reported by Bergveld in 1970 [25]. The so-called ion-sensitive field effect transistors (ISFETs) are composed of source and drain areas connected by a semiconducting channel of different doping. In ISFETs, the reference electrode (RE) passes no current and utilizes applying the gate voltage while providing a constant potential to the solution. The conductance of the channel is modulated by the potential of the liquid gate. The conducting channel in the semiconductor is separated from the solution by a passivation layer put in place to prevent chemical oxidation of the silicon by water. The concept has been originally developed for ion sensing. Here an ion-selective membrane has been coupled to the gate insulator to allow a defined potential formation in dependence on the respective ion concentration in solution [26].

Later this concept has been extended to biomolecular sensing (BioFET) [25]. Here different principles have been used. In combination with enzymes (ENFET) the detection is based on the production/consumption of an ionic edduct/product (often H+) during the biomolecular conversion which changes the potential at the interface ion-selective membrane/solution and subsequently the source-drain current. This approach is not only valuable for single metabolites but also for measuring cellular activities. [27, 28] One notable commercially successful application of this technology is Ion Torrent, which detects H+ production when nucleotides are incorporated during DNA sequencing [29].

To expand the utilization of BioFETs, approaches were developed where specific biological receptors (or probes) are conjugated on the gate to directly capture the desired analytes based on bioaffinity [30]. The specific binding event is directly transduced, and various BioFETs have been developed for the detection of nucleotides [31–33] and proteins [34–36]. However, it was realized that the charge situation plays an important role and also the ion concentration in solution. The ions in solution can screen part of the charge of the surface attached biomolecule. This can be expressed by the Debye length. This Debye length screening is

proportional to the reciprocal of the square root of the ionic strength and is quite small in physiological solutions, less than 1 nm [37–39]. This has limited the application to mainly highly charged molecules.

On the other hand, organic field-effect transistors (OFETs) represent the next stage of development in transistor technology. OFETs use organic semiconducting materials such as polymers, instead of traditional inorganic materials like silicon. There are several advantages to using organic materials in transistors: (1) Flexibility: Organic materials can be printed on flexible substrates, allowing for the creation of flexible and conformable electronic devices. (2) Low-cost fabrication: Organic materials are less expensive to produce and process than inorganic materials, making them an attractive option for large-scale production. (3) Solution-processability: Organic materials can be dissolved in solvents and processed using solution-based techniques such as inkjet printing, roll-to-roll printing, and spray coating. (4) Tunability: The electronic properties of organic materials can be easily tuned by modifying the chemical structure of the material, enabling the creation of a wide range of devices with varying properties. OFETs have several potential applications, including flexible displays, smart sensors, and wearable electronics. Additionally, the use of organic materials in transistors is environmentally friendly, as organic materials are often biodegradable and can be recycled. Overall, the development of OFETs represents a significant advancement in transistor technology and has the potential to revolutionize the field of electronics with its unique advantages.

2.2 gFET FEB Compact Model

In order to illustrate the advantages of graphene-based field effect transistors first the conditions of operation of a silicon based ISFET or BioFET will be described. The presence of bound charged biomolecules at the sensing surface of the transistor will be detected by changes in channel conductance of the FET due to a change in the effective gate potential. The sensing surface in a BioFET consists of the interface between a passivating layer + ion-selective layer, such as silicon nitride, and the solution.

The amount of bound biomolecules changes the charge at the sensor's surface, thus modifying the gate on the transistor. The charge per biomolecule depends upon the biochemistry, with dependence on the pH of the aqueous solution and the biomolecules' isoelectric points [40, 41]. Historically, in commercial ISFET applications, the signal of interest is the shift in threshold voltage V_T from the addition of ΔV_I [26]. but the source-drain current can also be followed resulting in better sensitivities which is shown in the following equation:

$$I_{SD} = \frac{W}{L}\left((V_{GS} - V_T)V_{DS} - 0.5V_{DS}^2\right)\mu_{eff}C_g \tag{1}$$

where W is the width of the channel, L is the length of the channel, V_{GS} is the gate-source voltage, V_{DS} is the drain-source bias, and μ_{eff} is the effective mobility incorporating the effects of finite contact resistance. It should be emphasized that in this equation, the capacitance of the gate insulator C_g is contained instead of the double layer capacitance C_{DL} which directly influences the source-drain current.

In these silicon devices, the dielectric in between the channel and the liquid introduces not only a small capacitance but may also cause background signal due to the interposing charge traps between the channel and liquid [42, 43]. In gFETs, the channel material is a single atomic layer of carbon in the form of chemical vapor deposition (CVD) grown graphene [44, 45]. This has beneficial electronic and chemical effects for biosensing. The graphene surface is chemically compatible with biological electrolytes, so dielectric passivation layers are not required. This enables direct interaction with the conduction channel via simple functionalization chemistries. In addition, the conductivity of gFETs is extremely sensitive to interactions near the channel because of its two-dimensional structure, as all atoms are surface atoms [46].

Rather than using the source-drain follower measurement scheme commonly used for silicon ISFETS, gFET FEB sensors reported in the literature are usually operated as signal amplifiers, in which the gFET output current response ΔI_D is measured [37, 45, 47–49]. In this case the external operational amplifier (op-amp) which is an integrated circuit for amplifying weak electric signals will be configured as a transimpedance amplifier. Using the typical small signal FET model [45], the change in drain current from a binding event at the surface can be approximated as:

$$\Delta I_D = \frac{W}{L} V_{DS}\, \mu_{eff} \frac{C_{FET}\, \Delta\sigma}{C_{DL} + C_{FET}} \tag{2}$$

where C_{FET} is the field effect transistor capacitance and C_{DL} is the double layer capacitance. In comparing Eqs. 1 and 2, it can be seen that the overall gain is an increase in the current response by a factor equal to the transconductance $g_m = (W/L)V_{DS}\, \mu_{eff}\, C_{FET}$. Graphene has high intrinsic carrier mobility ($\mu > 2{,}000\ cm^2\ V\ s^{-1}$) compared with silicon, leading to an advantage over silicon in this amplification mode. This advantage in transconductance is compounded in biosensing applications because of the increased C_{FET} in graphene compared to silicon/insulator structures. This is because C_{FET} is a series combination of all the capacitances between the interface and the channel, which includes the capacitance of the dielectric passivation layer in silicon, which isn't present in graphene. In gFETs C_{FET} can be comparable to C_{DL}, leading to a higher overall gain [50, 51].

Beyond the increase in signal gain and the lower noise due to no charge traps between the channel and the liquid, a gFET's ability to operate in amplification mode with high transconductance devices allows for multimodal sensing. Multimodal sensing involves the integration of multiple sensors or sensing modalities, such as optical, acoustic, and electrical sensors, to provide a more comprehensive and accurate understanding of the environment or system being monitored. For instance, a multimodal biosensor may include electrodes for measuring neuron spikes

electrical signal, optical sensors for measuring blood oxygen levels, and accelerometers for measuring body movement and activity. Changes in the total gate capacitance C_T and changes in the channel mobility μ_{eff} modulate the transconductance and can be detected by sweeping the liquid gate voltage to measure the I(Vg) transfer curves. This requires using both a gate electrode and a reference electrode in a manner similar to how an electrochemical cell uses a counter electrode and a reference electrode to ensures the potential is properly measured while sweeping [52]. This uses a gate circuit design similar to an electrochemical potentiostat, allowing for very accurate and dynamic control of the liquid potential and continuous measurement of the current vs gate voltage transfer curve. From this, features such as the charge neutrality potential, resistance, surface charge density, mobility, and capacitance can all be extracted simultaneously.

Changes in capacitance result from the displacement of charges in the liquid by the presence of the biomolecules, which can change the double layer capacitance of the channel with the liquid gate [45]. In this case, the biomolecules do not need to be necessarily charged to be sensed but sensitivity might be limited. Mobility changes will be stronger in the opposite limit of strongly charged targets, where charges near the channel can scatter charge carriers, thereby decreasing the mobility [37, 49].

The biomolecules in reality will not assemble as uniform layer of charges right at the interface, but rather will sit some distance away from the FET channel. If the biomolecules sit much farther away than the Debye length, the ions in solution will nearly completely screen the charges of the biomolecule, and they will not materially affect the gate potential of the device. Modern gFET biosensor designs mitigate Debye screening by employing the Donnan effect concept from membrane science. As usual in biosensors based on affinity the capture molecules are immobilized in a layer – here on top of the graphene channel. These layers are composed of various types of molecules with different functions, including biological receptor molecules for the analyte of interest, linker molecules if the biological receptor cannot be directly attached, and blocking molecules such as BSA and PEG to passivate the empty linkers and channel. [13, 47–51, 53] As with the analytes of interest, the organic molecules used in the Donnan layer will usually be charged when in buffer solution, depending on their isoelectric point and the local pH. Larger biomolecules cannot generally penetrate the layer, so the layer is mainly permeable for ions (and small molecules). A concentration gradient is formed between the immobile charged molecules within the layer and the mobile ions in the bulk solution, which in turn creates a potential difference between the bulk solution and the immobilized layer. The potential within the layer, the Donnan potential, is sensitive to pH and ionic concentration [54, 55], and this is the potential directly sensed by the FET. The Donnan potential changes as new biomolecules are bound to or released from the layer of biomolecules immobilized on the surface of the gFET.

Adding a Donnan layer to the interface has led to the modern era of biosensor FETs that can operate even in physiologically relevant, high ionic strength buffers [13, 56–59]. The effect enables sensor to be much more sensitive to bound analyte than under a double layer alone, because, in Donnan equilibrium, the double layer is moved away from the surface of the FET and instead forms at the Donnan layer

interface [55]. If the biological receptors are captured within the Donnan layer and so beneath the double layer, the screening is much reduced because of the decreased concentration of mobile ions [53]. Capacitance mode sensing also benefits from the presence of the Donnan layer, as C_{FET} must be modified to include the series capacitance of the Donnan layer, C_{Don}, which will be smaller than the double layer capacitance and can therefore limit the total capacitance. C_{Don} is proportional to the ionic strength and thereby is more sensitive to changes in ionic concentration than the double layer capacitance which is proportional to the square root of the ionic strength. The presence of large biomolecules, even outside the double layer, can cause large shifts in C_{FET} and the transconductance [57]. This requires that C_{Don} is the limiting term in C_{FET}, true for gFETs, but may not be true in silicon BioFETs with passivating layers that themselves limit C_{FET}.

A current model incorporating these concepts is shown in Eq. 3.

$$I \approx \frac{W}{L}\,\mu\, C_{tot}\, V_{DS}\left(V_{CNP} - V_g + 2.3\,\phi_{th}\alpha\,\Delta pH + (1-\alpha)\Delta\varphi_D\right) \tag{3}$$

where I is the current, μ is the charge carrier mobility, C_{tot} is the total capacitance per unit area, V_{cnp} is the charge neutrality point (CNP) potential, V_g is the gate voltage, alpha is pH sensitivity factor, ΔpH is the pH shift from the neutral surface, $\Delta\varphi_D$ is the Donnan potential which is explained in Eq. 5, and φ_{th} is the thermal voltage at room temperature. In the context of a liquid gate or pH sensor, the thermal voltage should be thought of as a thermodynamic potential driven by a change in ionic concentration at a surface. It is typically constructed as $R*T/F$ with T being temperature, R being the ideal gas constant and F being Faraday's constant.

This model generally relates the current (I) to typical electrical properties such as the charge carrier mobility (μ), total capacitance per unit area (C_{tot}), width (W) and length (L) of the graphene channel, source-drain voltage applied directly to the graphene (V_{DS}), and the gate voltage (V_g) relative to the charge neutrality point (CNP) potential (V_{CNP}). The CNP voltage here is the gate voltage at which there is a minimum in conduction at neutral pH. The capacitance between the graphene and the liquid, C_g, is a series combination of the graphene quantum capacitance, the double layer capacitance, and the Donnan capacitance. It is important to note that Eq. 3 is only valid for hole conduction and does not account for non-linear gate effects near the CNP voltage. It can be combined with a more complete foundational graphene FET model as in Eq. 4:

$$I_{ds} = \frac{\mu\, W\, V_{DS}}{L}\,\sqrt{{C_{tot}}^2\left(V_{CNP} - V_g + 2.3\,\phi_{th}\alpha\,\Delta pH + (1-\alpha)\Delta\varphi_D\right)^2 + 4\frac{{n_0}^2}{q^2}} \tag{4}$$

Here n_o represents the charge density of conduction-band, q is the charge density of valence-band, and $\Delta\varphi_D$ is the Donnan potential (see Eq. 5). With appropriate

construction of the C_{tot} term, this model can be used to represent electron and hole conduction regimes, and close to the CNP. This model encompasses effects from the liquid gate, surface chemistry, and biochemistry. The remaining undescribed terms in Eqs. 3 and 4 are corrections to the gate voltage due to the influence of pH changes and the Donnan potential. This model assumes operation of the sensor near room temperature, for an equivalent gate voltage less than the CNP voltage, for source-drain voltages below 1 V, and for a channel length greater than 10 μm.

Electronic sensitivity to pH is typically attributed to proton binding to a gate dielectric. For graphene transistors, there is no gate dielectric, but this form of pH sensitivity has been shown to apply through direct shifts in the apparent Dirac voltage [60, 61]. The surface pH sensitivity factor (α) is a material dependent value. For clean isolated graphene, α is a very low 0.02, but in practice this value is increased by the presence of oxides and nitrides used in device fabrication; α values for practical graphene transistors are around 0.37 [62–64]. This term is combined with the thermal voltage (ϕ_{th}), about 26 mV, and pH shift from a neutral surface (ΔpH) to produce the equivalent gate voltage due to pH. The thermal voltage of 26 mV multiplied by a factor of 2.3 that comes from the use of $\log_{10}$ instead of natural log by pH measurement results in the familiar Nernst limit for pH measurements of 59 mV per unit change in pH.

A Donnan potential ($\Delta\varphi_D$) is created when an ion-permeable layer separates two collections of ions, as shown in Eq. 5.

$$\Delta\varphi_D = \phi_{th} \ln \frac{\left(\sqrt{4{c_s}^2 + {c_x}^2} + c_x\right)}{2\,c_s} \tag{5}$$

Here c_s stands for the ionic strength of the bulk solution and c_x for captured probe ionic strength. All together, this model provides a relatively simple framework for thinking about how a gFET FEB biosensor works.

2.3 Structure of gFET Sensor

A diagram of a gFET FEB sensor is shown in Fig. 2a, and a top-down microscopy image of the active region of an example gFET FEB biosensor is shown in Fig. 2b. During measurement, a liquid drop is placed onto the circular region defined by the black epoxy shown here. The platinum counter and pseudo-reference electrodes built into the sensor surface control and monitor a voltage in the bulk liquid. A blocking layer and embedded biomolecules such as proteins are immobilized onto 15 graphene channels on the surface. This particular design is intended to lower the possibility that localized mechanical damage, such as from a pipette tip, would completely destroy a sensing channel. There are three sensing channels on the chip, each with five transistors spread around the surface.

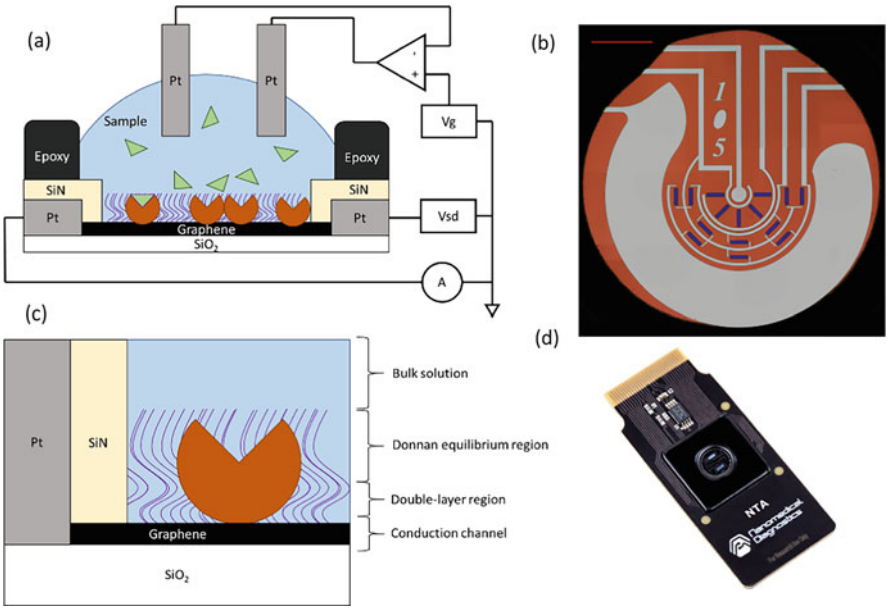

Fig. 2 (**a**) Scheme of the sensor architecture. Circular sections on top of the graphene represent proteins embedded in a blocking layer, represented by curved lines with two Pt electrodes in the liquid as gate and reference and two Pt electrodes on a chip for source and drain. (**b**) A microscopy image showing an entire sensor surface. Red scalebar is 1 mm. There are 15 graphene strips grouped into three groups of five, exposed through the silicon nitride (SiN = Si3N4) protective layer. The center of the circuit is the gate measurement pad (pseudo-reference) and the large pad surrounding the graphene strips is the liquid gate (counter electrode). (**c**) Diagram of the sensor regions near the graphene. The double layer region is $0.3/\sqrt{c_s}$ nm tall, where c_s is the ionic strength of the bulk solution. The Donnan equilibrium region is the thickness of the combined protein and blocking layer on the surface. (**d**) Picture of the complete biosensor

Carbon-based and non-carbon-based nanomaterials are two main categories of electronic and electrochemical biosensors. Graphene field-effect transistors (gFETs) use a three-electrode set up called the source, drain, and gate electrode. gFETs are ion-sensitive and current across graphene channel can be modulated by a liquid gate. While FETs can use any semiconductor material, a higher carrier mobility, and its electrophysical properties make gFETs well suited to biosensing.

gFET sensing is quantified by a transfer curve which is collected as current between sources-drain with respect to the applied gate voltages. The lowest point of the transfer curve is called the Dirac point, or the charge neutrality point (VCNP). While other sensors measure current over time and use electrochemical tags, sensing on gFETs is often in terms of the charge neutrality point, capacitance, transconductivity, and current modulation due to functionalization and biomolecule interaction.

2.4 gFET Sensor Biochemical Interaction Model

gFET FEB sensors are typically used to perform label-free affinity binding assays. It is useful to understand the basics of the biochemical interactions occurring on the graphene surface to understand how to separate measurements of the targeted biochemistry from measurements of background effects or contaminants. While data collected from a real-time, label-free biosensor can be analyzed using several models, the standard approach is to use experiment design so that a first-order chemical interaction can be used to model the data.

The mathematics behind the analysis of label-free biosensor data begins with the 1:1 L model and gets increasingly more detailed as more potential convoluting effects are considered [65]. In its simplest form, the Langmuir model describes the binding of one analyte to one capture molecule to form a complex. Further, all binding sites are assumed to be equal and independent and unaffected by mass transport such as diffusion.

In biochemistry and pharmacology, there are very few reactions that are truly irreversible or truly completely reversible. Analyte molecules are continuously binding and unbinding to the thousands or millions of capture molecules bound to the sensor surface. The often non-equilibrium reaction of capture molecule (M) and analyte (A) can be written as [66]:

$$\mathrm{M} + \mathrm{A} \rightleftharpoons \mathrm{MA} \tag{6}$$

where TA is the complex of the capture molecule with bound analyte.

Therefore, the binding rate of the analyte is:

$$\frac{d[\mathrm{MA}]}{dt} = k_{\mathrm{on}}[\mathrm{M}][\mathrm{A}] - k_{\mathrm{off}}[\mathrm{MA}] \tag{7}$$

where [M] is the unoccupied capture molecule concentration, [A] is the free analyte concentration, [MA] is the concentration of the complex of the capture molecule with bound analyte, k_{on} is the association rate constant, and k_{off} is the dissociation rate constant.

When the system is in equilibrium, the concentrations of capture molecules, analyte, and complex of the capture molecule with bound analyte are no longer time dependent.

$$\frac{d[\mathrm{MA}]}{dt} = k_{\mathrm{on}}[\mathrm{M}][\mathrm{A}] - k_{\mathrm{off}}[\mathrm{MA}] = 0 \tag{8}$$

Then, K_{D} is defined as such and called the dissociation constant.

$$K_D = \frac{k_{off}}{k_{on}} = [M][A]/[MA] \tag{9}$$

In Eq. 7, the number of analyte molecules in each experiment should be several orders of magnitude higher than the number of capture molecules bound to the sensor surface to avoid needing to take into account mass transport effects. Thus, the concentration [A] can be considered constant throughout association since the number of free molecules remains relatively unchanged. Based on this assumption:

$$\frac{d\theta}{dt} = k_{on}(1-\theta)[A] - k_{off} \cdot \theta \tag{10}$$

where θ is the fraction (time-dependent) of occupied probes on the sensor surface.

Solving this differential equation produces the relation:

$$\theta = \left(1 - e^{-k_{obs} \cdot t}\right) \cdot \theta_{eq} \tag{11}$$

where θ_{eq} is the fraction of occupied capture probes once the binding reaction has equilibrated, and k_{obs} is the observed binding rate at a given concentration is defined as:

$$k_{obs} = k_{on}[A] + k_{off} \tag{12}$$

This should be familiar to anyone experienced with conventional label-free sensing systems such as surface plasmon resonance (SPR). Building on the experience from that community, there are some useful guidelines in evaluating biochemical interaction data. One issue is connected to non-specific binding to the sensor surface. Non-specific binding refers to adhesion to the surface or surface chemistry of molecules not targeted by the immobilized capture chemistry. In some cases these are chemical interactions that simply appear as adhesion in the data. The qualitative label of nonspecific binding typically implies a quantitative value for k_{on} of less than 10^5 M^{-1} s^{-1} [67]. To account for this problem calibration is often performed under defined conditions. However, analyzing nonspecific binding is uncertain because, in a genuine sample, accurate kinetic measurement of unknown molecules adsorbing onto the sensor surface is not possible. To address this issue, a different approach is employed by establishing a reference surface without the recognition element and examining the nonspecific binding that occurs there. As a result, in the context of SPR-style sensing, it becomes possible to assess a differential signal to analyze the specific binding and to calculate the rate constant of the specific binding reaction.

For an on-rate of 10^5 M^{-1} s^{-1} you might require many minutes or even hours to achieve half of the equilibrated response to a 1 nM application of [A]. A "specific binder" typically refers to a biochemical system with k_{on} between 10^5 and 10^7 M^{-1} s^{-1}. This is the domain of biochemistry with binding pockets such as antibodies. Here, you will still require several minutes to achieve half of the equilibrated

response to a 1 nM application of [A], and longer time for lower concentrations than 1 nM. Binding rates above this range indicate a steered reaction, where the reaction at the surface is consuming reactants from solution faster than diffusion would normally provide them to the surface. An example of this is a CRISPR complex. Such a reaction is the only case in which a 1 nM application of [A] will achieve at least half the equilibrium response in less than 1 min. These guidelines are presented to help understand how to approach data that shows very fast responses. Very fast label-free sensor responses, including responses on gFETs, are typically due to buffer mismatch, addition of preservatives, or presence of some contamination.

3 Basic Applications

3.1 pH and Salinity

The most basic biochemistry measurements start with detecting changes in pH and salinity. gFET biosensors are sensitive to pH, salinity, and the chemical composition of the buffers applied to them. The exact sensitivity of a gFET sensor depends on its specific design and manufacture, as significant contributions to pH and salinity sensitivity of gFETs come from the substrate on which the graphene is deposited and the processing of the sensor surface prior to use. Examples of some pH and salinity sensing measurements are shown in Fig. 3. The percent change in slope appears to be very high because the slope at "0 salt" or negligible salt is very shallow. Pure DI water is effectively an insulator and the liquid gate will not function well. So in terms of % change, there is a large change because the starting value is quite small. Essentially the "gateablility" of the channel changes in a pronounced way with salt concentration while the (effective) resistance of the channel only changes slightly.

The solutions used in Figs. 2c and 3a are standard 1× phosphate buffered saline (PBS) pH 7.4 1× PBS has a concentration of 0.01 M phosphate buffer concentration, 0.0027 M potassium chloride, and 137 mM sodium chloride or salt concentration. Varying amounts of 100 mM HCl added to 1× PBS to adjust the pH. The sensors were calibrated in pH 7 solutions for these measurements. The solutions used in Fig. 3b, d are NaCl in deionized water.

3.2 Protein-Protein Interactions

Measuring a protein-protein interaction is arguably the most popular and fundamental use of gFET FEB sensors in literature. Here we show an interaction between a monoclonal antibody against human interleukin-6 (anti-IL6) and recombinant human IL6 (IL6). Reagents were sourced from a commercial ELISA kit. IL6 is a well-known cytokine and biomarker related to inflammation, autoimmune diseases,

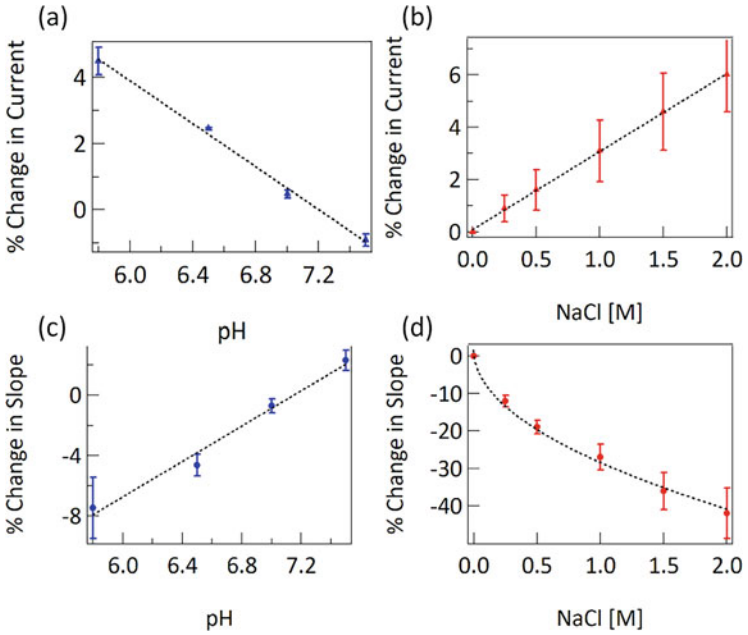

Fig. 3 (**a**) Change in current due to change in pH. Fit is linear with a slope of −3.2% per pH unit. (**b**) Change in current due to change in ionic strength, when pH is held constant. Fit is linear with a slope of 3.0% per molar unit of NaCl. (**c**) Change in slope (dI/dVg) due to change in pH. Fit is linear with a slope of 5.9% per pH unit. (**d**) Change in slope due to change in ionic strength. Response is fit to $-0.3\sqrt{[\mathrm{NaCl}]}$. Each datapoint in this figure is an average of data from four sensor chips

and late-stage cancers. Anti-IL6 was immobilized on graphene chips with a prepared carboxyl surface and activated via standard carbodiimide chemistry in a process shown in Fig. 3 [68]. This approach to surface chemistry is very common in gFET FEB literature. The ethanolamine step here likely presents a dramatic change as it is a charged small molecule that interacts closely with the graphene channel being applied in a low-salt solution.

Figure 4b, c shows the percent change in current and slope responses for 23 different sensor chips all following the same immobilization protocol with the same anti-IL6 reagent. The relatively small variations from chip to chip highlight the stability and reproducibility of the sensors. The immobilization data shows consistent trends. Addition of EDC and sNHS after calibration always leads to a decrease in current, without a change in transconductance slope. This is expected as the carbodiimide chemistry should change the charge at the surface without adding a large amount of material. Addition of the antibody at 30 min leads to a further decrease in current and a large increase in slope. This change is largely due to switching from the pH 6.0 MES buffer used during carboxyl activation to the pH 7.4 PBS pH buffer used during antibody incubation. This highlights the need to limit buffer changes throughout an assay on a gFET, or to make sure the sensor is

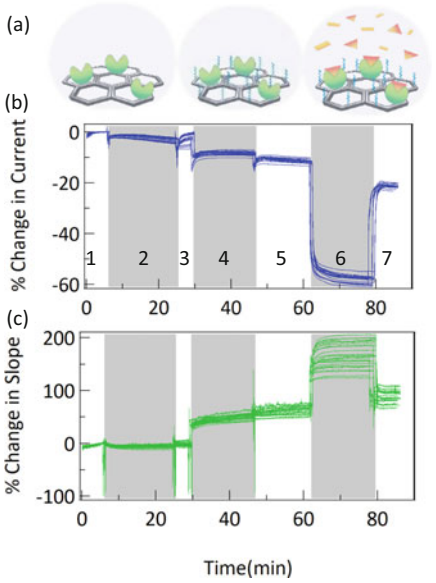

Fig. 4 (**a**) Diagram of the steps of protein immobilization and measurement used here. First, antibodies against IL-6 are immobilized, then PEG is added as a blocker for nonspecific binding, then measurements are performed with IL-6. (**b**) Change in current and (**c**) change in slope (transconductance) for 23 different sensors during immobilization process. Shading is used to delineate steps: 1: calibration in MES buffer, 2: COOH activation by EDC/sNHS incubation in MES buffer, 3: wash in MES, 4: antibody incubation in PBS, 5: PEG incubation in PBS, 6: reaction of remaining COOH groups with ethanolamine, 7: wash in PBS buffer

calibrated and equilibrated in a new buffer when a change in buffer is required. Addition of PEG-amine after anti-IL6 immobilization leads to a small decrease in current and a small increase in slope. This is consistent with association of PEG to the surface to serve as a blocking layer around immobilized protein. After addition of PEG, a complete layer is formed on the graphene surface, enabling a Donnan effect measurement. Addition of ethanolamine (pH 8.0) quenches any remaining activated carboxyl groups, and causes a large decrease in current and a large increase in slope. Rinsing with PBS (pH 7.4) then raises the current and decreases the slope, although never back to the initial starting position. This repeatable set of chemistry and sensor responses indicates both reproducibility of sensor-to-sensor response as well as a detectable and defined change of the surface chemistry due to the immobilization process. These kinds of evaluations of surface chemistry process and repetition across multiple chips are necessary to be confident in subsequent biochemical measurements.

It has to be emphasized here that such approaches are common for several label-free measuring techniques in order to make sure that observed effects can be correlated to a biomolecular event and not to other effects in solution or on the surface. This is often ignored and thus, erroneous conclusions occur.

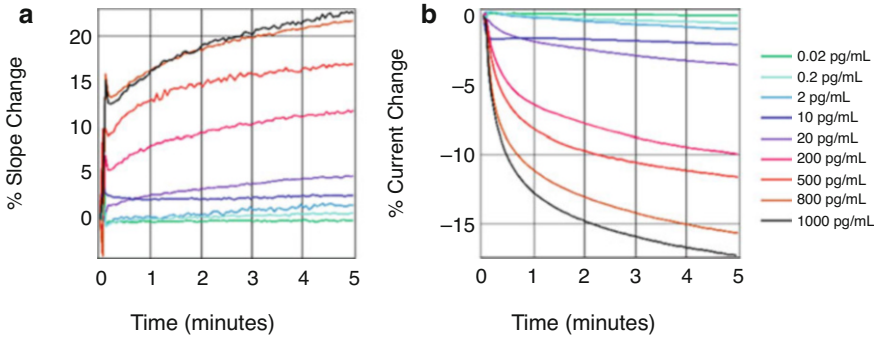

Fig. 5 (**a**) Change in transconductance of sensors functionalized with antibodies against IL-6 to different concentrations of IL6, each measurement from a different sensor chip. (**b**) Simultaneously measured change in current

The effectiveness of this immobilization process is demonstrated in the sensing measurements shown in Fig. 5. Different concentrations of IL6 in PBS were applied to the anti-IL6 immobilized chips. The different concentrations of IL6 lead to different response magnitudes and different speeds of interaction, as expected for any kinetic binding measurement. This data compares well with the metrics provided by the ELISA kit from which the reagents were taken and previous IL6 standard curves gathered on graphene FEB sensors [69]. This is an example of the kind of information available in a real time assay that is not possible in an end-point assay. In addition, it highlights how process, user, and chip variation may be manifested in the data.

When running an ELISA with this kit, the expected lower limit of detection is <2 pg mL^{-1}, and the linear range of response is between 7.8 and 500 pg mL^{-1} (FEB range of response is 2 pg/mL to 1,000 pg/mL). Here, we have reproduced the ELISA quality while adding kinetic information. We have removed the need for labels while providing more information-dense real-time data than an end-point assay technique like ELISA.

3.3 Small Molecule Measurement

Building on sensing protein-protein interaction measurements, the same gFET sensor design can be used for protein-small molecule measurement. This type of measurement is particularly useful for pharmaceutical research. Here, we show an example of a rank-ordering experiment. The purpose of this set of measurements is to compare the relative binding affinities of several small molecules to the same protein. When working with small molecules, it is important to perform appropriate controls. Nonspecific binding of small molecules to graphene is extremely common. If a complete concentration vs response curve can be taken, a comparison of the

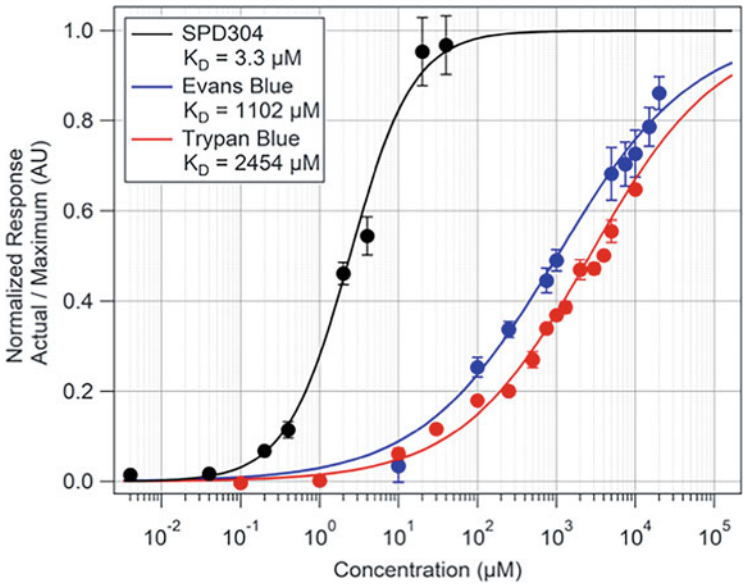

Fig. 6 Dose-response curves generated for TNFα interacting with SPD304 (black; $K_D = 3.3 \pm 0.7$ µM), Evans Blue (blue; $K_D = 1{,}102 \pm 107$ µM), and Trypan Blue (red; $K_D = 2{,}454 \pm 415$ µM). The determined *K*d values are given in the legend. For comparison: The IC_{50} of each inhibitor respectively is 22 µM, 750 µM, and 1,000 µM [1]

calculated kinetics relative to values obtained from other methods can be a helpful check that nonspecific binding is not dominating the observed response.

In this case, the small molecules SPD304, Evans Blue, and Trypan Blue were investigated as drug compounds interacting with the target protein, Tumor Necrosis Factor alpha (TNFα). The assay buffer for all small molecules composed of 1× PBS (0.01 M phosphate buffer concentration, 0.0027 M potassium chloride, 137 mM sodium chloride, pH 7.4), and multiple concentrations were measured for each small molecule.

Fresh assay buffer was added to the chip with the immobilized protein to calibrate a baseline measurement for 5 min, followed by the addition of the compound in assay buffer for 10 min to measure association. After the association measurement was complete, assay buffer was added to measure dissociation of the interaction. Recall that unlike a pure electrochemical sensor, a properly constructed FEB surface is sensitive to changes in the charges within the immobilized layer through measurement of changes in the Donnan potential. When a small molecule displaces the normal salts and hydrogen bonding network on a protein, there is an overall change in this value.

A dose-response curve of the current measurement is plotted in Fig. 6 as the sensor response versus concentration of the compound as the compound interacts with the target protein TNFα. Affinity ranking is determined from the dose-response curves and the associated kinetic binding data. The affinity ranking is comparable to

the rank ordering of the known IC_{50} values: $K_D = 3.3 \pm 0.7$ μM SPD304, $K_D = 1{,}102 \pm 107$ μM Evans Blue, and $K_D = 2{,}454 \pm 415$ μM Trypan Blue compared to $IC_{50} = 22$ μM, 750 μM, and 1,000 μM respectively [70, 71]. The results show that an important drug discovery measurement, affinity ranking for small molecule biochemistry, can be performed on gFET FEB sensors.

4 Bioaffinity-Based Detection

4.1 DNA and RNA Detection

Perhaps the most important area of active research in gFET biosensors is the detection of DNA and RNA. Affinity-based biosensors for nucleic acid detection can be useful after a sample amplification process such as PCR. An affinity-based biosensor provides little advantage when used in conjunction with sample amplification, and does not address the fundamental limitations of sample amplification. Where gFET sensors provide a unique capability is as a solid-state sensor that incorporates new signal amplification techniques, such as the use of CRISPR. These approaches can match the sensitivity of sample amplification, while avoiding the largest problem of sample amplification, which is the potential amplification of contaminating sequences.

As with some small molecules, nonspecific binding of DNA to the surface of the graphene can affect sensor effectiveness. In addition, when DNA associates with the graphene surface, this interaction can disrupt the hydrogen bonds between complementary DNA strands, decreasing the binding affinity of complimentary DNA strands. Since this is valid for all biosensors with immobilized capture probes, care has to be taken during immobilization.

Even with these complications, a gFET FEB sensor can differentiate target DNA from DNA with even a single nucleotide polymorphism (SNP) in a simple affinity sensor mode using a probe DNA attached to the graphene surface. Single stranded probe DNA attached to the graphene gives a negative V_{CNP} shift after immobilization. When a matching single-stranded DNA molecule is detected, a further negative V_{CNP} shift occurs, while non-matching sequences gave significantly smaller shift in V_{CNP}. This negative shift after target addition should match the shift found when double-stranded DNA is bound to the graphene, indicating that hybridization occurs on probe attached to the graphene [72]. There are reports of gFET affinity binding sensors detecting DNA and RNA at extraordinarily low concentrations. Such results need to be considered in context with theoretical limits of detection based on the expected binding kinetics, measurement time, and diffusion. Using Eqs. 11 and 12 above, it is easy to quickly calculate how long a measurement should take for a particular concentration of DNA.

By bending or crumpling, the graphene layer gFET sensing capabilities can be enhanced due to the changes in the Debye length [73]. In order to evaluate this, a DNA probe has been tethered to both crumpled and flat gFETs and a complementary

strand was added to the gFET. Displayed crumpled graphene enhanced the detection of DNA hybridization at LOD of 20 aM, while the flat gFETs displayed a signal change at 2 pM. Additionally, a DNA probe was tethered to the crumbled gFET complementary, to the target miRNA or Let-7b in human serum. While a shift is seen at 20 aM, the standard deviation makes it difficult to differentiate. Another strategy for enhancing sensitivity is using peptide nucleic acid (PNA). PNA is a synthetic oligo, with a peptide backbone in the place of (deoxy)ribose sugar–phosphate chain. PNAs are more stable and have less negative charge, which improves the probe proximity to the graphene surface. The LOD of DNA concentration using PNA was shown to be 600 zM which is more sensitive than using DNA probes. Crumbled gFETs sensor shows unprecedented and incomparable sensitivity without target amplification. While the results are undebatable impressive, it is important to keep in mind what the resolution of any machine is when examining small shifts, even if the fold change is large. The error of the machine nor signal-to-noise ratio are discussed in the paper, making it difficult to fully assess.

Another way to improve the sensitivity of a gFET sensor for detecting nucleic acids is to use a CRISPR complex to improve the binding and search capabilities of the biochemistry. This can be particularly useful when working with real biological samples that contain small copy numbers of long strands of DNA. This way the novel and ultrasensitive gFET biosensor is combined with the selectivity and specificity of CRISPR-Cas system [47, 74]. Such accurate measurement is specifically useful for the detection of single-point mutation and single-gene disorders such as sickle cell anemia [75, 76] or SARS-Cov2 variants without amplification [74]. This section gives first a comprehensive description about CRISPR-Cas detection system and applications. Then, we will explain the mechanism of CRISPR-Cas gFET detection platforms.

4.2 CRISPR-Cas System

CRISPR (Clustered Regularly Interspaced Short Palindromic Repeats) [77] and associated protein (Cas) has been established as a bacterial immune system [78] evolved in Bacteria and Archaea [79] against bacteriophage invasion. The CRISPR locus has two main parts which when transcribed, become the CRISPR-Cas system. The first part of the CRISPR locus is the Cas operon, which codes for a wide variety of Cas proteins [80]. The Cas protein, or CRISPR-associated protein, is an endonuclease responsible for the binding and cleavage in CRISPR-Cas systems. The other component of the CRISPR locus is the CRISPR array, which contains spacer regions. When transcribed and spliced, these spacer regions become the CRISPR RNA or crRNA, which forms a complex with the Cas protein and guides the endonuclease to the target region of DNA (deoxynucleic acids) or RNA. When the Cas protein and crRNA come together, they form the ribonucleoprotein complex or RNP.

Protospacer Adjacent Motif (PAM), a three to six specific nucleotide sequences (e.g., spCas9, NGG, N can be A/TG/C) is required at the target site to be recognized by the RNP complex to complement with crRNA and cleave the sequence [81].

The trans-activating CRISPR RNA or "tracer RNA," pairs with the CRISPR RNA (crRNA) to create a functional guide RNA (gRNA). Within this gRNA complex, the tracrRNA acts as a handle for the Cas9 enzyme, while the crRNA spacer sequence guides the complex to a specific viral sequence that matches it. The potential of CRISPR-Cas system to precisely cleave at specific site and easy to engineer guide RNA (=tracerRNA+crRNA) has opened a new frontier in gene editing. For instance, the first pig-to-human heart transplant has been enabled by CRISPR genome editing [82].

In the CRISPR-Cas system, the concept of classes and types is used to categorize and classify different variants of CRISPR systems based on their molecular components and mechanisms of action. Based on the number of subunits in the molecular structure, CRISPR-Cas systems have been divided into two classes, both of which have multiple types and subtypes.

Class I contains types I, III, and IV, made up of multi-subunit complexes [83] These complexes have a broader variety of enzymatic activity including auxiliary messenger molecules, such as cyclic oligoadenylates (cOAs) which can provide additional cleavage events. The most well-known type of Class I is type III which contains Cas10 and a set of auxiliary subunits called Csm and Cmr [84].

Class II contains types II, V, and VI, which only have a single subunit. While 90% of CRISPR systems fall under Class I, they are significantly less well studied than their Class II counterparts, which contain Cas 9 in type II, Cas 12 in type V, and Cas13 in type VI [83]. Because many clinical applications use Class II CRISPR complexes, this is what we will be focusing on for electrical sensing. Cas 9 and guide-RNA (gRNA) complex specifically target and cut dsDNA. However, Class I complexes offer advantages for some applications where the detection of various byproducts can be further utilized for biosensing. For Class II CRISPR complexes, gRNA is made up of two different sections, which can be synthetically produced as a single unit, called the single guide RNA or sgRNA. The crRNA or CRISPR RNA has one segment that is complementary to the target sequence, while the tracrRNA fits into the scaffold of the Cas protein. If both the PAM and target sequence are present, Cas will bind and cut the DNA or RNA.

There are two distinct types of cleavage that Cas can have cis or trans cleavage. Cis cleavage is when the Cas complex cuts at the target region. Trans cleavage, also known as collateral cleavage or non-specific cleavage, occurs during target recognition when the activated RNP complex non-discriminately cleaves either RNA or DNA at off-target sites that partially match the guide sequence of gRNA or crRNA.

Cas9 targets dsDNA and exhibits only cis-cleavage, making it particularly useful for gene editing applications and is also used for CRISPR diagnostic and dead-Cas9-mediated imaging applications. Cas12 recognizes and exhibits cis cleavage on dsDNA and trans-cleavage after target recognition and cleaves ssDNA and Cas 13 targets RNA and displays both cis and trans cleavage [85]. Most of these technologies use Cas9, Cas12, and Cas13 either in isolation or grouped together.

However, this field is very much still in its nascence – so more research is conducted about other CRISPR Cas systems, specifically in type I.

4.3 CRISPR-Cas Powered gFET Biosensor

Because of CRISPR-Cas gene editing potential and also for many analytical applications several systems have been described in the literature in combining CRISPR-Cas system with gFET biosensors. Recently, CRISPR Cas13a target detection-mediated collateral cleavage was utilized to detect SARS-CoV2 and respiratory syncytial virus samples without the need for PCR analysis. For instance, functionalized RNA reporter sequence is trans-cleaved upon Cas13a activation by Li et al. gFET platform for amplification-free detection of SARS-CoV-2 virus [86]. In their platform, a PolyU reporter RNA oligo was tethered to the surface of the gFET. Then, pre-incubated Cas13a and the target RNA were introduced on the gFET. The presence of the target activates the Cas13a trans-cleavage activity towards the PolyU reporter. The sensor monitors the source-drain current before and after adding the target sequences (SARS-CoV-2 N gene, 1 fM) while keeping a constant source-drain voltage (Vds = 100 mV) and sweeping the gate voltage (Vg) from −1 to 1 V with steps of 10 mV. To optimize the sensor response and to decrease the LOD up to 1aM, incubation time, $MgCl_2$ concentration, Cas13a concentration, polyU probe length, and incubation temperature were tested. To further validate the assay design, respiratory syncytial virus (RSV) was also tested and achieved the LOD of 1 aM. The assay was next tested on heat-inactivated SARS-CoV-2 from clinical samples. The assay successfully decimates the difference between positive and negative samples making it comparable to RT-qPCR. The easy programmability of the assay to detect different pathogens displays the robust design of the assay. Since gFETs do not rely on optical sensing, the assays are easily completed by liquid handling devices.

Another successful gFET platform for detecting genetic mutation without DNA amplification developed by Hajian et al. [47] They immobilized CRISPR-Cas9 on gFET to analyze DNA samples collected from in vitro cell lines and clinical samples of DNA with two distinct mutations in patients with Duchenne muscular dystrophy or DMD. In their platform named CRISPR-chip, standard carbodiimide chemistry is used to link dCas9 (catalytically deactivated Cas9) to lattice of the graphene. A scrambled gRNA sequence has been applied in order to access the specificity of the detection. In the clinical investigation, authors demonstrate by targeting exon 51 in the dystrophin gene, the CRISPR-Chip differentiates between healthy and patient samples, DMD patients with a mutated exon 3, and DMD patients with a mutated exon 51. Their results show CRISPR–Chip generated an enhancement in output signal relative to the samples lacking the DNA target sequence without amplification, within 15 min, and with a sensitivity of 1.7 fM.

As shown in Fig. 7, CRISPR-Cas9 protein was conjugated on a gFET surface to detect Sickle cell and Duchenne muscular dystrophy (DMD)-associated mutations at fM concentrations in extracted human DNA without sample amplification [47,

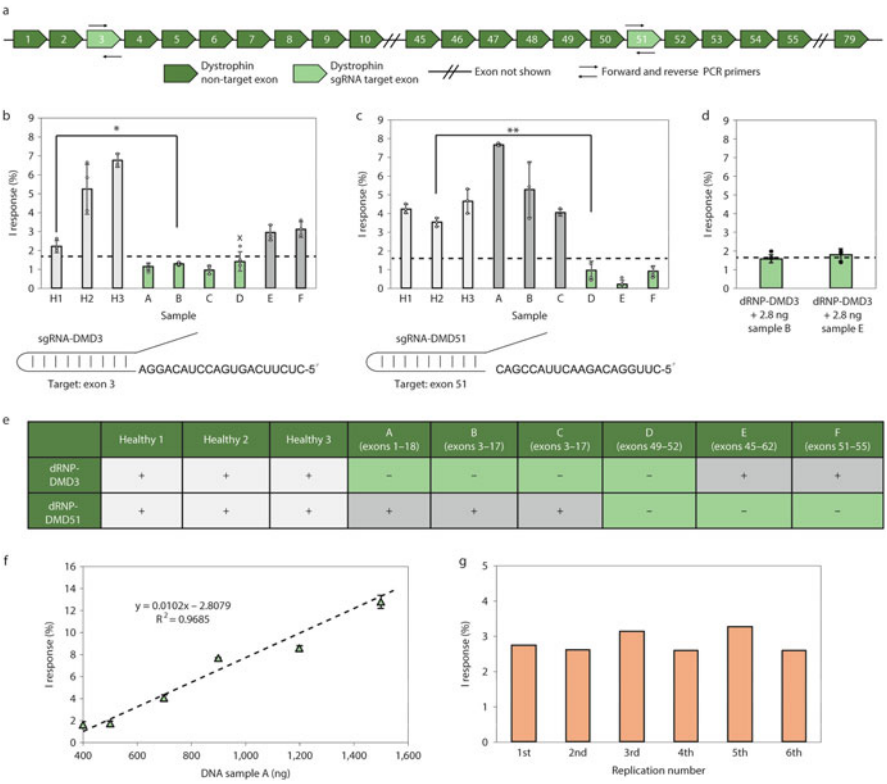

Fig. 7 CRISPR–Chip analysis of healthy and DMD clinical samples for DMD-associated dystrophin exon deletions. (**a**) Schematic of the dystrophin gene with highlighted target exons. (**b**) Top, I response obtained by CRISPR–Chip functionalized with dRNP-DMD3 in the presence of healthy (H1, H2, and H3) and A-F DMD clinical samples (*$P = 0.017$, one-tailed t-test). Bottom, schematic of sgRNA-DMD3, designed to target exon 3. x represents a false negative as confirmed by sequencing. (**c**) Top, I response obtained by CRISPR–Chip functionalized with dRNP-DMD51 in the presence of healthy (H1-H3) and DMD clinical samples, A-F, (**$P = 0.0014$, one-tailed t-test). Bottom, schematic of sgRNA-DMD51, designed to target exon 51. Samples H1-H3 did not lack any Exon in their dystrophin gene. Samples A, B and C were lacking multiple exons including exon 3 as indicated in table e. Sample D, E and F were also lacking multiple exons including exon 51 as indicated in table (**e**, **d**) CRISPR–Chip's negative signal threshold was defined by testing CRISPR–Chips with samples lacking target exons at the highest concentrations of genomic sample obtainable from commercially available buccal swabbing methods to ensure that high sample concentrations would not lead to false positives. (**e**) CRISPR–Chip results for the presence of targeted exons (+) within healthy and DMD clinical samples, as defined by a threshold of 1.73%. (**f**) dRNP-DMD51-functionalized CRISPR–Chip's I response in the presence of varied amounts of clinical sample A (mean; $n = 3$). (**g**) Reproducibility of individual CRISPR–Chips functionalized with dRNP-DMD51 in the presence of clinical sample A. Error bars represent s.d.

75]. In Fig. 7b, c, it can be observed that CRISPR-Chips functionalized with dRNP-DMD3 and dRNP-DMD51 exhibited a significant increase ($P \leq 0.00059$) in signal output when exposed to genomic samples containing the target exons 3 or 51. This

enhancement was observed in comparison to DMD samples that had deletions specifically at exon 3 or 51. Furthermore, additional experiments were conducted to establish a negative signal threshold.

In an additional investigation, Ban et al. have recently developed a single-cell multiomics platform to detect variants of the SARS-Cov2 antigen and viral RNA without amplification [74]. The biosensor platform showcased combines a chimeric probe (RNA-DNA) for detecting RNA using LwaCas13a's collateral cleavage activity. The biosensor has the capability to distinguish unprocessed Saliva samples of SARS-CoV-2, Influenza, and Rhinovirus and a LOD of approximately 65 attomolar (aM) is calculated for viral RNA isolation without the need for amplification.

4.4 Extracellular Vesicles and Cells

In addition to detecting of proteins, small molecules, and nucleic acids as discussed above, gFETs are increasingly being researched for direct detection of cells and extracellular vesicles [87]. For example, exosomes are small extracellular vesicles expelled by both healthy and tumorous cells present in blood serum in high abundance (10^8–10^{11} particles mL^{-1}). The presence of an exosome with cancer-related surface biomarkers and its genetic cargo are important for liquid biopsy diagnostics. By immobilizing anti-CD63 and anti-CD151 antibodies on a graphene channel, a gFET sensor demonstrated specific detection of $CD63^+$ and $CD151^+$exosomes. The change in electrical properties of the graphene in the presence of highly charged captured exosomes resulted in change in electrical parameters of gFET at low concentrations.

Similar device design and surface chemistry for exosome detection can be extended toward monitoring of interactions with cells. An early example of gFET sensing used a device with an array of graphene sensors to track the flow of cells in a microfluidic channel. In addition to this electrical detection, these sensors were built on top of a glass substrate, which allowed simultaneous optical and electrical interrogation of the cells in the channel. The transparent nature of graphene is often emphasized in sensing literature as beneficial to these kinds of combined optical and electrical measurements. While optical graphene materials and electronic graphene tools are both now much more accessible in biology labs, combined systems remain sophisticated nanotechnology tools. Beyond simple detection of cells, the biocompatible nature of graphene enabled gFET sensors for monitoring cardiomyocytes and neuron activity.

5 Requirements for Successful Use

5.1 Scaled Manufacturing

A major hurdle to providing graphene biosensors to biological researchers is the typical manufacture of nanoelectronics in research-oriented clean rooms by teams of research scientists. Increasingly, there are commercial options for obtaining graphene material, graphene chips, and entire gFET FEB sensing systems.

Critically, the cost of graphene and graphene chips has come down significantly. Figure 8 shows the quality assurance results from an example batch of commercially manufactured gFET FEB sensors. For these chips, the cost of graphene was \$0.019 per cm^2. This comes from the average cost of copper foil of \$0.012 per cm^2 and the cost of power to run furnaces to grow the graphene of \$0.007 per cm^2 of grown graphene. This is less than the price of silicon wafer substrates used for these sensors, which was \$0.40 per cm^2 for 150 mm wafers. The cost of processing the wafers through a commercial foundry was 20-fold greater than the cost of the graphene raw

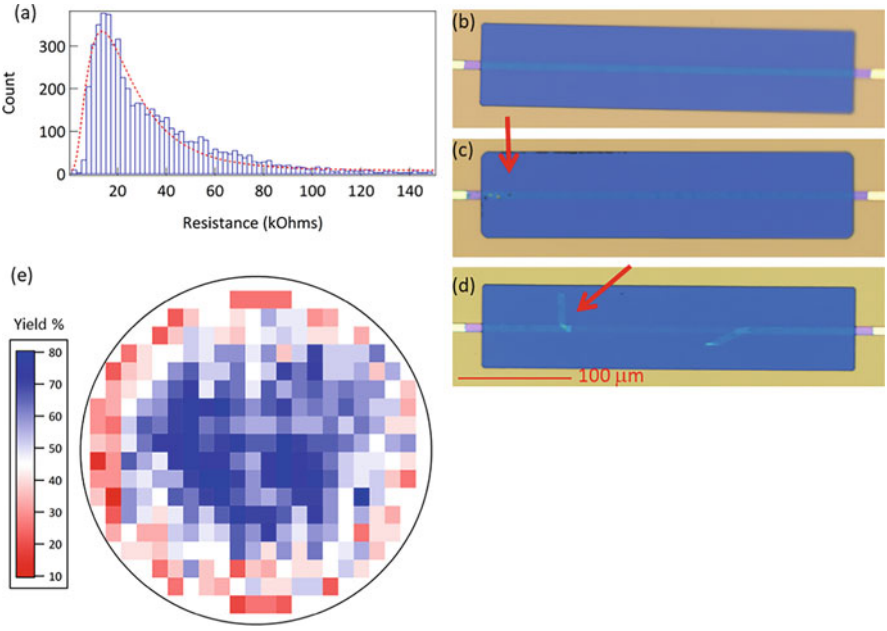

Fig. 8 (**a**) Histogram of test resistances from 5,543 chips. Fit is a log-normal distribution with a peak at 13.6 kΩ and a standard deviation of 9.2 kΩ. This is for a target graphene resistance of 10 kΩ. (**b**) Microscopy image of defect-free graphene sensor (**c**) Microscopy image of a graphene sensor with minor polymer contamination highlighted by the red arrow. (**d**) Microscopy image of a graphene sensor with major graphene tearing highlighted by the red arrow. (**e**) Wafer yield map combining data from 27 wafers, showing cumulative % yield per 0.4 cm^2 area

material, making conventional wafer processing the dominant costs in producing a gFET FEB device.

Figure 8 presents quality assurance data from three production lots comprising 27 150 mm wafers and 7,992 chips produced over the course of 1 year. Quality assurance processes focus on reproducibility and cost rather than searching for occasional outstanding performance. Specifically, this means the usage of automated optical microscopy commonly found associated with commercial silicon fabrication to search for contamination and graphene tearing over entire wafers, rather than using nanotechnology specialized research hardware such as atomic force microscopy or Raman spectroscopy.

Differential interference contrast microscopy is used along with AI-enabled defect identification to perform optical evaluations, such as those shown in Fig. 8b–d. The schematic of the chip side view has been shown in Fig. 2a, b with materials indication. Briefly, yellow material is platinum electrode, blue is the silicon nitride passivation layer, and the line is the graphene electrode.

At the end of the QA process during commercial fabrication, a map of percent yields on different areas of each wafer, shown in Fig. 8e, is produced, and used for chip packaging selection. Although most of the focus for the cost of gFET sensor chips is on wafer scale fabrication issues, the actual driving cost of gFET sensor manufacturing is chip packaging. Costs dominated by packaging are not unique to gFET sensors but are very common across a wide range of electronics. Recently, gFET sensor manufacturers were included in the semiconductor industry working group forming the roadmap for Advanced Packaging. This is the first significant semiconductor roadmap to include graphene chip fabrication which can be found on the Semiconductor Research Corporation Webpage [88].

5.2 Surface Chemistry

When designing your experiment, determining the method of capture molecule immobilization is the first step. Currently, the most common surface chemistries use a pyrene with a butyric acid functional group [89, 90]. This molecule (PBA) can be used as is, or it can be used with an attached N-hydroxysuccinimide ester (PBASE) [91]. Both of these approaches use carbodiimide crosslinker chemistry, but when using PBA, you must apply N-ethyl-N′-(3-dimethylaminopropyl) carbodiimide hydrochloride (EDC) and N-hydroxysulfosuccinimide (sNHS) to activate the carboxylic group immediately prior to use. PBASE does not require this; however, the attached NHS ester will hydrolyze in the presence of water, adding a timing and purity complication to storage and use. Both of these approaches will covalently link to an amine presented by a biomolecule in solution.

Other common surface chemistries include pyrene with a nitrilotriacetic acid (NTA) functional group that will associate with a His tag in the presence of $NiCl_2$, and CLICK chemistry-enabled pyrene linkers. [92]

5.3 Choosing a Capture Molecule for Immobilization

There are many factors to consider when selecting your immobilized capture molecule. First, your target must be able to bind to the graphene biosensor surface. Capture molecule should generally contain a free primary amine to be covalently linked via the common PBA or PBASE chemistries. If this is not the case, more exotic crosslinkers will be necessary. The location of the free primary amine or other binding tag relative to the binding region of the targeted analyte can affect the performance of system as a whole. A binding pocket that is facing down into the graphene will not be effective.

Size also plays an important factor when choosing a recognition element. Smaller immobilized capture probes have reduced interaction surfaces that may be sterically hindered through direct attachment to the surface, and thus obstruct binding to the analyte [93]. For small capture molecules, the use of a spacer arm for attachment to the surface is recommended. The benefit of smaller capture molecules is the proximity of the binding interaction to the graphene surface, which will yield a greater change in electrical properties than when the interaction is further away from the surface (Fig. 9).

Buffer conditions may also affect your choices in recognition elements. Proteins or chemicals in the buffer used during immobilization may interact with your surface chemistry (i.e., bovine serum albumin [BSA] used as a carrier molecule to increase stability of proteins) will also bind along with your specific molecule to the graphene. This can lead to a decrease in signal by reduction in capture probe attachment, or a misleading increase in perceived binding due to your analyte interacting with the nonspecific proteins crosslinked to the surface.

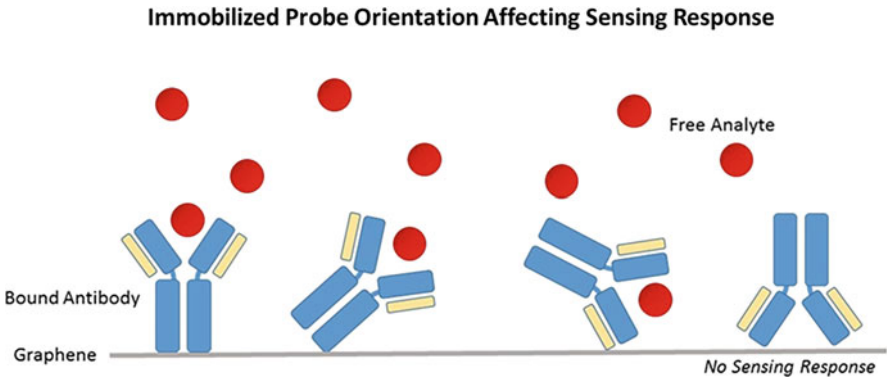

Fig. 9 Orientation of the capture molecule during crosslinking to the surface of a COOH or NHS biosensor chips is a random event. As shown in figure 9, sensing of the analyte by an antibody is only prevented when the variable region of the antibody binds directly to the surface. This is valid for every biosensor construction

If you suspect that specific capture molecule orientation is crucial, alternative binding strategies may be helpful. For specific orientation of a recognition element to a surface, His-tag mediated immobilization to NTA biosensor chips is often used.

5.4 Capture Molecule in Solution

Several factors should also be considered when selecting your capture molecule. Size of the analyte can affect the amount of measurement time needed, as smaller molecules diffuse much faster than larger molecules. Small molecules may also more easily move through a blocking layer made of a polymer such as PEG. However, large molecules tend to show more clear changes in capacitance due to the increased displacement of liquid volume compared to smaller molecules.

5.5 Buffers and Blocking

gFET sensors are versatile and compatible with many commonly used physiological buffers such as phosphate buffered saline (PBS), N-2-hydroxyethylpiperazine-N-2-ethane sulfonic acid (HEPES), and Dulbecco's modified Eagle medium (DMEM). Although graphene literature contains many examples of sensing with extremely dilute buffers, variability in measurement will increase with decreasing salt concentration, and gate voltage control is extremely difficult when using less conductive liquids; consider also the stability and function of the biochemistry in addition to the performance of the gFET when choosing the optimum assay buffers. It is also recommended to avoid buffers with pH $\leq$ 2.0 as extremely low pH can disrupt the pi-pi stacking between commonly used pyrene-based surface chemistries and graphene. The buffers used during EDC/sNHS crosslinking should not include any amine- or carboxylate-containing buffers or components (e.g. Tris–HCl buffer).

As in standard biochemical assays, one goal of blocking is to improve your signal-to-noise ratio by physically blocking nonspecific interactions without interfering with specific binding interactions. An additional goal when using a gFET sensor is to create a Donnan potential at the surface. Polyethylene glycol (PEG) is a common blocker for gFET sensors, as is BSA. In some cases, adding low concentrations of detergents like Tween 20 to the assay buffers may be more effective than a static blocking layer alone.

Ideally, a gFET FEB sensor is equilibrated and calibrated in a buffer that is as similar as that containing the analyte as possible. This prevents changes in composition such as salt concentration, pH, and preservative concentrations from contributing to the sensor response. For example, if your analyte is in human serum, then you may want to use a synthetic serum substitute as your assay buffer during equilibration, in addition to using it as a diluent. Similarly, for animal samples or

cell and tissue lysates, you may want to use a species-specific serum albumin to mimic the nonspecific proteins found in your sample.

5.6 *Looking Forward: Multiomics*

Almost 20 years ago, the Human Genome Project verified something that greatly complicated the way we understand biology: that proteins are not derived from simple expression of the genetic codes in nucleic acid sequences. The human genome contains open reading frames that code for roughly 20,000 canonical proteins. Around 70,000 additional proteins can be created by using alternative splicing of the DNA code. However, to our best understanding, a single human cell contains at least 1,000,000 different forms of proteins.

The elegance of the Central Dogma of biology that information cannot be transferred from protein to protein has been necessarily augmented by an understanding that reality is much more complicated. The definition and construction of a particular protein is due to multiple overlapping parameters such as gene expression and post-translation modifications, which are regulated by interactions with other genetic molecules, methylation, mutation, and transcription factors. In addition, the function of the same protein requires a multitude of interactions between other proteins, small molecules, and metabolic markers. Complexity in biology comes not only from the complexity of the networks of interactions involved, but also in the variations in the parts of those networks. This compounded complexity creates limits to what can be accomplished via reductionist approaches to biology, as well as limits to the usefulness of naive mappings of engineering and computer science concepts into biology.

This understanding led to the creation of the field of systems biology, the study of emergent patterns from the dynamic complexity of biology rather than focusing on a particular type of molecule, such as genomics, proteomics, or metabolomics. An early editorial in Science put it well: "the pluralism of causes and effects in biological networks is better addressed by observing, through quantitative measures, multiple components simultaneously, and by rigorous data integration with mathematical models." This powerful concept offers a way forward to understand how observable traits come about in biological systems and the creation of a new approach to measurement: multiomics.

Multiomics is a challenging idea. Gaining understanding of biology at a system level based on combining a large number of simultaneous measurements including pH, mRNA, DNA, and enzyme activity is going to require far more than "simply" fully realizing gFETs as a multiomics measurement platform. There will remain challenges in sample collection and processing, experiment design, data interpretation, and a host of other issues. Despite all this, "simply" using a single measurement platform to execute a wide range of measurements could open the doors for far more people to try out multiomics studies. To understand and overcome the experimental challenges necessary to standardize and democratize multiomics, we need tools to

enable more experimentation, more data, and more creativity. Many of the most popular biosensing platforms have been widely commercially available for decades, and have developmental histories going back 50 years or more. In comparison, gFETs have only recently gained attention as biosensing platform. Yet in that short time, a tremendous amount of progress has been made, demonstrating capabilities far beyond what has been capable with traditional semiconducting materials. The maturation of graphene device manufacturing in recent years shows broad accessibility through scalable commercialization will be realized in near term [45, 68].

In the last few years, we have seen a change in the character of papers published in gFET sensing literature. It is often the case that different fields and different stages of technology development require different types of studies. Classical gFET literature commonly applied a large number of samples to a small number of test chips in a repeated fashion. This was necessary because of the difficulty in constructing a working sensor. Recently, there have been a few studies that follow the statistical conventions of biology research and apply a smaller number of samples to a larger number of test chips. [47, 94–96] This is a subtle but significant difference. Device designs and analysis are standardizing, while gFET production on a small scale is maturing [45, 68, 97].

In the coming few years, we expect to see a transition in proof-of-concept studies using gFETs from testing a single analyte per sample to testing multiple analytes per sample simultaneously. We have seen studies that used hundreds of gFETs, we should soon see the first biosensing studies that use thousands of gFETs. These are small milestones that do not yet reach the scale of multiplexing and throughput that are common with traditional optical methods. The distinguishing characteristic should be that gFETs can monitor protein, small molecule, and genomic activity together at the same time. This, at last, would indicate a transition from "promise" to reality for gFETs as a multiomics platform.

References

1. Chandler BDL (2014) A doctor in the palm of your hand
2. Chin CD, Sia SK (2012) Commercialization of microfluidic point-of-care diagnostic devices. Lab Chip:2118–2134. https://doi.org/10.1039/c2lc21204h
3. Bingisser R et al (2012) Cardiac troponin: a critical review of the case for point-of-care testing in the ED. Am J Emerg Med 30:1639–1649
4. Giljohann DA, Mirkin CA (2009) Drivers of biodiagnostic development. Nature 462:461–464
5. Lowe BM, Sun K, Zeimpekis I, Skylaris CK, Green NG (2017) Field-effect sensors-from pH sensing to biosensing: sensitivity enhancement using streptavidin-biotin as a model system. Analyst 142:4173–4200
6. Bergveld P (1991) A critical evaluation of direct electrical protein detection methods. Biosens Bioelectron 6:55–72
7. Datta SPA (2016) Future healthcare: bioinformatics, nano-sensors, and emerging innovations. In: Nanosensors: theory and applications in industry, healthcare and defense, p 247
8. Ohno Y, Maehashi K, Yamashiro Y, Matsumoto K (2009) Electrolyte-gated graphene field-effect transistors for detecting pH and protein adsorption. Nano Lett 9:3318–3322

9. Lu Y et al (2012) Graphene-protein bioelectronic devices with wavelength-dependent photoresponse. Appl Phys Lett 100
10. Lerner MB, Dailey J, Goldsmith BR, Brisson D, Charlie Johnson AT (2013) Detecting Lyme disease using antibody-functionalized single-walled carbon nanotube transistors. Biosens Bioelectron 45:163–167
11. Choi Y et al (2012) Single-molecule lysozyme dynamics monitored by an electronic circuit. Science 335:319–324
12. Cohen-Karni T, Qing Q, Li Q, Fang Y, Lieber CM (2010) Graphene and nanowire transistors for cellular interfaces and electrical recording. Nano Lett 10:1098–1102
13. Gao N et al (2016) Specific detection of biomolecules in physiological solutions using graphene transistor biosensors. Proc Natl Acad Sci U S A 113:14633–14638
14. Allen BL, Kichambare PD, Star A (2007) Carbon nanotube field-effect-transistor-based biosensors. Adv Mater 19:1439–1451
15. Sarkar D et al (2014) MoS2field-effect transistor for next-generation label-free biosensors. ACS Nano 8:3992–4003
16. Zuccaro L et al (2015) Real-time label-free direct electronic monitoring of topoisomerase enzyme binding kinetics on graphene. ACS Nano 9:11166–11176
17. Xu S et al (2017) Real-time reliable determination of binding kinetics of DNA hybridization using a multi-channel graphene biosensor. Nat Commun 8:1–10
18. Ang PK et al (2010) A bioelectronic platform using a graphene − lipid bilayer interface. ACS Nano 4:7387–7394
19. Kempaiah R, Chung A, Maheshwari V (2011) Graphene as cellular interface: electromechanical coupling with cells. ACS Nano 5:6025–6031
20. Yang W et al (2010) Carbon nanomaterials in biosensors: should you use nanotubes or graphene. Angew Chem Int Ed 49:2114–2138
21. Mandal D, Banerjee S (2022) Surface acoustic wave (SAW) sensors: physics, materials, and applications. Sensors 22:820
22. Clark Jr LC, Lyons C (1962) Electrode systems for continuous monitoring in cardiovascular surgery. Ann N Y Acad Sci 102:29–45
23. Janata J, Huber RJ (1980) Chemically sensitive field effect transistors. In: Freiser H (ed) Ion-selective electrodes in analytical chemistry. Springer US, pp 107–174. https://doi.org/10.1007/978-1-4684-3776-8_3
24. Sze SM (1981) Semiconductor device development in the 1970s and 1980s – a perspective. Proc IEEE 69:1121–1131
25. Bergveld P (1970) Development of an ion-sensitive solid-state device for neurophysiological measurements. IEEE Trans Biomed Eng BME-17:70–71
26. Bergveld P (2003) Thirty years of ISFETOLOGY: what happened in the past 30 years and what may happen in the next 30 years. Sens Actuators B 88:1–20
27. Milgrew M, Riehle M, DRS, C. (2005) A large transistor-based sensor array chip for direct extracellular imaging. Sens Actuators B 111–112:347–353
28. Fromherz P, Offenhausser A, Vetter T, Weis J (1991) A neuron-silicon junction: a Retzius cell of the leech on an insulated-gate field-effect transistor. Science 252:1290–1293
29. Rothberg JM et al (2011) An integrated semiconductor device enabling non-optical genome sequencing. Nature 475:348–352
30. Forsyth R, Devadoss A (2017) Graphene field effect transistors for biomedical applications: current status and future prospects. Diagnostics. https://doi.org/10.3390/diagnostics7030045
31. Estrela P, Stewart A, Yan F, Migliorato P (2005) Field effect detection of biomolecular interactions. Acta Electrochim 50:4995–5000
32. Gonçalves D, Prazeres DMF, Chu V, Conde JP (2008) Detection of DNA and proteins using amorphous silicon ion-sensitive thin-film field effect transistors. Biosens Bioelectron 24:545–551
33. Sakata T, Kamahori M, Miyahara Y (2004) Immobilization of oligonucleotide probes on Si3N4 surface and its application to genetic field effect transistor. Mater Sci Eng C 24:827–832

34. Caras S, Janata J (1980) Field effect transistor sensitive to penicillin. Anal Chem 52:1935–1937
35. Schasfoort RBM, Kooyman RPH, Bergveldb P, Greve J (1990) A new approach to ImmunoFET operation. Biosens Bioelectron 5:103–124
36. Zayats M, Raitman OA, Chegel VI, Kharitonov AB, Willner I (2002) Probing antigen-antibody binding processes by impedance measurements on ion-sensitive field-effect transistor devices and complementary surface plasmon resonance analyses: development of cholera toxin sensors. Anal Chem 74:4763–4773
37. Andoy NM, Filipiak MS, Vetter D, Gutiérrez-Sanz Ó, Tarasov A (2018) Graphene-based electronic immunosensor with femtomolar detection limit in whole serum. Adv Mater Technol 3:1800186
38. Ping J, Johnson ATC (2016) Quantifying the intrinsic surface charge density and charge-transfer resistance of the graphene-solution interface through bias-free low-level charge measurement. Appl Phys Lett 109:1–15
39. Israelachvili J (2011) Intermolecular and surface forces.3rd edn. Academic Press
40. Schasfoort RBM, Bergveld P, Kooyman RPH, Greve J (1990) Possibilities and limitations of direct detection of protein charges by means of an immunological field-effect transistor. Anal Chim Acta 238:323–329
41. Norde W, Lyklema J (1991) Why proteins prefer interfaces. J Biomater Sci Polym Ed 2:183–202
42. Kutovyi Y et al (2020) Noise suppression beyond the thermal limit with nanotransistor biosensors. Sci Rep 10:12678
43. Liu Y, Georgiou P, Prodromakis T, Constandinou TG, Toumazou C (2011) An extended CMOS ISFET model incorporating the physical design geometry and the effects on performance and offset variation. IEEE Trans Electron Dev 58:4414–4422
44. Lerner MB et al (2017) Large scale commercial fabrication of high quality graphene-based assays for biomolecule detection. Sens Actuators B 239:1261–1267
45. Goldsmith BR et al (2019) Digital biosensing by foundry-fabricated graphene sensors. Sci Rep. https://doi.org/10.1038/s41598-019-38700-w
46. Georgakilas V et al (2016) Noncovalent functionalization of graphene and graphene oxide for energy materials, biosensing, catalytic, and biomedical applications. Chem Rev. https://doi.org/10.1021/acs.chemrev.5b00620
47. Hajian R et al (2019) Detection of unamplified target genes via CRISPR–Cas9 immobilized on a graphene field-effect transistor. Nat Biomed Eng 3:427–437. https://doi.org/10.1038/s41551-019-0371-x
48. Béraud A et al (2021) Graphene field-effect transistors as bioanalytical sensors: design, operation and performance. Analyst 146:403–428
49. Hinnemo M et al (2018) Protein sensing beyond the Debye length using graphene field-effect transistors. IEEE Sens J 18:6497–6503
50. Xia J, Chen F, Li J, Tao N (2009) Measurement of the quantum capacitance of graphene. Nat Nanotechnol 4:505–509
51. Mackin C, McVay E, Palacios T (2018) Frequency response of graphene electrolyte-gated field-effect transistors. Sensors 18:494
52. Mannik J, Goldsmith BR, Kane A, Collins PG (2006) Chemically induced conductance switching in carbon nanotube circuits. Phys Rev Lett. https://doi.org/10.1103/PhysRevLett.97.016601
53. Haustein N, Gutiérrez-Sanz Ó, Tarasov A (2019) Analytical model to describe the effect of polyethylene glycol on ionic screening of analyte charges in transistor-based immunosensing. ACS Sens 4:874–882
54. Das S (2014) Explicit interrelationship between Donnan and surface potentials and explicit quantification of capacitance of charged soft interfaces with pH-dependent charge density. Colloids Surf A Physicochem Eng Asp 462:69–74
55. Ohshima H (2009) Theory of electrostatics and electrokinetics of soft particles. Sci Technol Adv Mater 10

56. Gutiérrez-Sanz Ó, Andoy NM, Filipiak MS, Haustein N, Tarasov A (2017) Direct, label-free, and rapid transistor-based immunodetection in whole serum. ACS Sensors 2:1278–1286
57. Palazzo G et al (2015) Detection beyond Debye's length with an electrolyte-gated organic field-effect transistor. Adv Mater 27:911–916
58. Baldacchini C et al (2020) A reliable BioFET immunosensor for detection of p53 tumour suppressor in physiological-like environment. Sensors 20:6364
59. Park S et al (2020) Interfacial charge regulation of protein blocking layers in transistor biosensor for direct measurement in serum. Biosens Bioelectron 147:111737
60. Mackin C, Palacios T (2016) Large-scale sensor systems based on graphene electrolyte-gated field-effect transistors. Analyst. https://doi.org/10.1039/c5an02328a
61. MacKin C et al (2014) A current-voltage model for graphene electrolyte-gated field-effect transistors. IEEE Trans Electron Dev 61:3971–3977
62. Fu W et al (2011) Graphene transistors are insensitive to pH changes in solution. Nano Lett 11:3597–3600
63. Wang YY, Burke PJ (2013) A large-area and contamination-free graphene transistor for liquid-gated sensing applications. Appl Phys Lett 103
64. Mailly-Giacchetti B et al (2013) PH sensing properties of graphene solution-gated field-effect transistors. J Appl Phys 114
65. Hahnefeld C, Drewianka S, Herberg FW (2004) Determination of kinetic data using surface plasmon resonance biosensors. In: Decler J, Reischl U (eds) Molecular diagnosis of infectious diseases. Humana Press, pp 299–320
66. Malmqvist M (1993) Biospecific interaction analysis using biosensor technology. Nature 361:186–187
67. Myszka DG (2000) Kinetic, equilibrium, and thermodynamic analysis of macromolecular interactions with BIACORE. In: Methods in enzymology, vol 323. Academic Press, pp 325–340
68. Lerner MB et al (2016) Large scale commercial fabrication of high quality graphene-based assays for biomolecule detection. Sens Actuators B. https://doi.org/10.1016/j.snb.2016.09.137
69. Afsahi SJ et al (2017) Towards novel graphene-enabled diagnostic assays with improved signal-to-noise ratio. MRS Adv:1–7. https://doi.org/10.1557/adv.2017.431
70. He MM et al (2005) Small-molecule inhibition of TNF-a. Sci Rep 310:1022–1025
71. Song Y, Buchwald P (2015) TNF superfamily protein–protein interactions: feasibility of small-molecule modulation. Curr Drug Targets 16:393–408
72. Manoharan AK, Chinnathambi S, Jayavel R, Hanagata N (2017) Simplified detection of the hybridized DNA using a graphene field effect transistor. Sci Technol Adv Mater 18:43–50
73. Hwang MT et al (2020) Ultrasensitive detection of nucleic acids using deformed graphene channel field effect biosensors. Nat Commun 11:1543
74. Ban DK et al (2023) A single multiomics transistor for electronic detection of SARS-Cov2 variants antigen and viral RNA without amplification. Adv Mater Technol 8:2201945
75. Balderston S et al (2021) Discrimination of single-point mutations in unamplified genomic DNA via Cas9 immobilized on a graphene field-effect transistor. Nat Biomed Eng 5:713–725
76. Lu H-W et al (2022) The promise of graphene-based transistors for democratizing multiomics studies. Biosens Bioelectron 195:113605
77. Mojica FJ, Ferrer C, Juez G, Rodríguez-Valera F (1995) Long stretches of short tandem repeats are present in the largest replicons of the Archaea Haloferax mediterranei and Haloferax volcanii and could be involved in replicon partitioning. Mol Microbiol 17:85–93
78. Barrangou R et al (2006) Global analysis of carbohydrate utilization by Lactobacillus acidophilus using cDNA microarrays. Proc Natl Acad Sci 103:3816–3821
79. Barrangou R et al (2007) CRISPR provides acquired resistance against viruses in prokaryotes. Science 315:1709–1712
80. van der Oost J, Jore MM, Westra ER, Lundgren M, Brouns SJJ (2009) CRISPR-based adaptive and heritable immunity in prokaryotes. Trends Biochem Sci 34:401–407

81. Mojica FJM, Díez-Villaseñor C, García-Martínez J, Almendros C (2009) Short motif sequences determine the targets of the prokaryotic CRISPR defence system. Microbiology (Reading) 155:733–740
82. Reardon S (2022) First pig-to-human heart transplant: what can scientists learn? Nature 601:305–306
83. Makarova KS et al (2020) Evolutionary classification of CRISPR–Cas systems: a burst of class 2 and derived variants. Nat Rev Microbiol 18:67–83
84. Liu TY, Doudna JA (2020) Chemistry of class 1 CRISPR-Cas effectors: binding, editing, and regulation. J Biol Chem 295:14473–14487
85. Swarts DC, Jinek M (2019) Mechanistic insights into the cis- and trans-acting deoxyribonuclease activities of Cas12a. Mol Cell 73:589–600.e4
86. Li H et al (2022) Amplification-free detection of SARS-CoV-2 and respiratory syncytial virus using CRISPR Cas13a and graphene field-effect transistors. Angew Chem Int Ed Engl 61: e202203826
87. Hajian R et al (2021) Rapid and electronic identification and quantification of age-specific circulating exosomes via biologically activated graphene transistors. Adv Biol 5:2000594
88. Zhirnov V. MAPT roadmap – SRC. Microelectron Adv Packaging Technol Roadmap. https://www.src.org/about/mapt-roadmap/
89. Zhang X et al (2013) Application of graphene–pyrenebutyric acid nanocomposite as probe oligonucleotide immobilization platform in a DNA biosensor. Mater Sci Eng C 33:3851–3857
90. Zhu Y et al (2016) A graphene-based affinity nanosensor for detection of low-charge and low-molecular-weight molecules. Nanoscale 8:5815–5819
91. Wu G, Tang X, Meyyappan M, Lai KWC (2017) Doping effects of surface functionalization on graphene with aromatic molecule and organic solvents. Appl Surf Sci 425:713–721
92. Li H, Papadakis R (2021) Click chemistry enabling covalent and non-covalent modifications of graphene with (poly)saccharides. Polymers 13:142
93. Pollard TD (2010) A guide to simple and informative binding assays. MBoC 21:4061–4067
94. Sandoval JA et al (2020) Novel mTORC1 inhibitors kill glioblastoma stem cells. Pharmaceuticals 13:419
95. Sadlowski C et al (2018) Graphene-based biosensor for on-chip detection of bio-orthogonally labeled proteins to identify the circulating biomarkers of aging during heterochronic parabiosis. Lab Chip 18:3230–3238
96. Qvit N, Disatnik M-H, Sho E, Mochly-Rosen D (2016) Selective phosphorylation inhibitor of delta protein kinase C–pyruvate dehydrogenase kinase protein–protein interactions: application for myocardial injury in vivo. J Am Chem Soc 138:7626–7635
97. Ping J, Vishnubhotla R, Vrudhula A, Johnson ATC (2016) Scalable production of high-sensitivity, label-free DNA biosensors based on back-gated graphene field effect transistors. ACS Nano 10:8700–8704

Adv Biochem Eng Biotechnol (2024) 187: 71–106
https://doi.org/10.1007/10_2023_235

Published online: 26 January 2024

Rationally Designed DNA-Based Scaffolds and Switching Probes for Protein Sensing

Alejandro Chamorro, Marianna Rossetti, Neda Bagheri, and Alessandro Porchetta

Contents

Abstract The detection of a protein analyte and use of this type of information for disease diagnosis and physiological monitoring requires methods with high sensitivity and specificity that have to be also easy to use, rapid and, ideally, single step. In

A. Chamorro, M. Rossetti, N. Bagheri, and A. Porchetta (✉)
Department of Chemistry, University of Rome Tor Vergata, Rome, Italy
e-mail: alessandro.porchetta@uniroma2.it

the last 10 years, a number of DNA-based sensing methods and sensors have been developed in order to achieve quantitative readout of protein biomarkers. Inspired by the speed, specificity, and versatility of naturally occurring chemosensors based on structure-switching biomolecules, significant efforts have been done to reproduce these mechanisms into the fabrication of artificial biosensors for protein detection. As an alternative, in scaffold DNA biosensors, different recognition elements (e.g., peptides, proteins, small molecules, and antibodies) can be conjugated to the DNA scaffold with high accuracy and precision in order to specifically interact with the target protein with high affinity and specificity. They have several advantages and potential, especially because the transduction signal can be drastically enhanced. Our aim here is to provide an overview of the best examples of structure switching-based and scaffold DNA sensors, as well as to introduce the reader to the rational design of innovative sensing mechanisms and strategies based on programmable functional DNA systems for protein detection.

Graphical Abstract

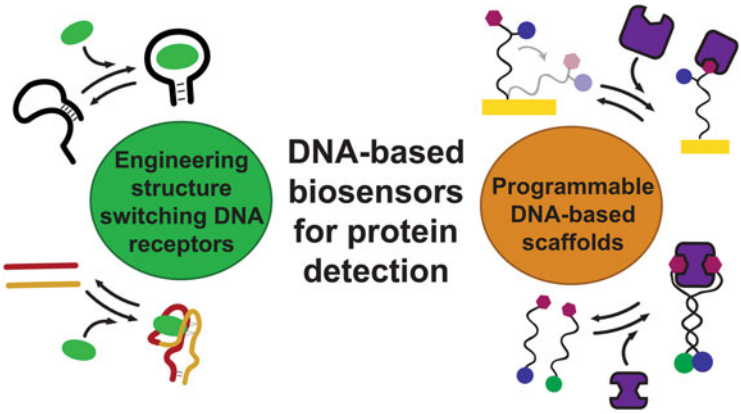

Keyword DNA scaffold, DNA switch, Electrochemical DNA biosensors, Functional DNA nanotechnology

1 Introduction

Detection of protein biomarkers is extremely important for the early diagnostics, treatment, and management of many diseases, as well as in fundamental research and other biomedical applications. Sensitive and accurate detection of proteins in biological fluids, as well as the study of their interactions and their post-translational modifications, is a challenge for research and diagnostic purposes. The high cost and

the complex operating protocols of protein analysis based on the use of laboratory-scale instruments are not able to meet the needs for frequent screening and/or continuous monitoring of patients in primary care, as well as in remote health monitoring systems.

Starting from the 1960s, specific detection of proteins has been achieved mainly through the use of a plethora of immunoassays (immunosorbent colorimetric, Immunoelectrophoresis, Western blot, etc.) capable of detecting and quantifying protein targets in biological fluids. To date, the enzyme-linked immunosorbent assay (ELISA) [1] and Western blot represent the most frequently used techniques. In the last 20 years, apart from these methods, a number of biosensing platforms using appropriate recognition elements (DNA, peptide, synthetic receptors, imprinted polymers, etc.) have been reported for the detection of proteins in solution [2–4]. In particular, many efforts have been directed toward the development of point-of-care (POC) devices for sensitive and specific protein detection, similar to the glucometer in terms of ease-of-operation, response time, operating and equipment costs.

Among them, DNA-based biosensors appear particularly relevant because they harness the design ability of DNA-based systems to easily translate a specific binding event into a measurable signal. Watson-Crick-Franklin base pairing is indeed highly predictable and programmable, and DNA nanotechnologies can be engineered into molecular transduction systems and thus used in conjunction with a variety of material interfaces [5].

In the following chapter, two main approaches developed in the context of protein-responsive nucleic acid-based biosensors are discussed. Specifically, we first introduce the general principles and rules underlying the design of the target-induced structure-switching mechanism (Sects. 2 and 3). Then, we highlight some of the main examples of optical and electrochemical DNA-based biosensors that are based on structure-switching probes (Sect. 4). Finally, we introduce the concept of DNA scaffold showing some applications where simple single and double stranded DNA units can be harnessed as signaling scaffolds that generate a signal output only when in the presence of the specific target protein (Sect. 5).

2 The Many Advantages of Structure-Switching Biosensors

Due to the extraordinary versatility, affinity, and specificity of biomolecular recognition, biosensors [6] have seen significant research advances and commercial exploitation over the last years [7–11]. Besides the amazing recognition properties of biomolecules, however, a significant limitation in the development of biosensing technologies has been represented by the capacity of generating a measurable output in response to the binding of the target molecule [12]. For instance, immunosensors and many other affinity-based biosensors simply rely on bioreceptors that can specifically interact with their targets without emitting electrons or photons upon target binding. To generate a signal in response to target binding most biosensors, as

well as many bioanalytical platforms, require subsequent washings/incubations steps, reagent-intensive procedures, and/or the combination with a secondary recognition element labelled with a tag in order to generate a measurable output. On the contrary, "label-free" biosensors represent an alternative because they are capable of generating an analytical signal in response to the change of an intrinsic property of the receptor upon target recognition, such as subtle changes in molecular mass or charge. To monitor the small changes induced by the unlabelled components, these sensing strategies rely on the use of very sensitive and sophisticated equipment. Among label-free sensing techniques, most famous are the surface plasmon resonance (SPR) [13], field effect transistors [14], quartz microbalances, and microcantilevers [15]. However, they still suffer from a common limitation that is non-specific interaction of contaminants, especially when the sensing platforms are challenged in complex biological matrices.

To overcome this limitation, over millions of years of evolution Nature has optimized a specific class of biomolecules (i.e., switches) operating through the binding-induced structure-switching mechanism that senses chemical/biological inputs and transduce the binding event into a specific biological function [16]. Structure switching generally provides high specificity for the target analyte because the recognition event is not simply mediated by the formation of many weak, non-covalent bonds (e.g., hydrogen bonding and hydrophobic effects) but also requires that the target binding induces a conformational or oligomerization change of the recognition element itself. This dual requirement is essential for initiating the signaling response. Consequently, molecules other than the target, which can nonspecifically interact with the recognition element but lack the capability to induce structural reconfiguration, will not result in signal generation. That prevents interferences and renders the recognition element highly specific. Nature has coupled the structure-switching sensing to an amazing diversity of possible outputs such as enzyme activation/inhibition, gene expression, or opening of an ion channel [17].

Inspired by this naturally occurring mechanism, significant efforts have been vested to take advantage of it for artificial biotechnologies. In particular, since structure switching can be easily combined for the generation of a measurable signal output, biomolecular switches are perfect candidates for biosensing applications. The structural reconfiguration can be either combined with a relative change in FRET efficiency between a fluorophore and quencher pair [18], or with the variation of electron transfer efficiency onto the electrode surface, as well as the activation of a catalytic activity [19]. As a consequence of structure-switching mechanism, these biosensors are generally easy to use, reagentless, and single step, thus, appearing particularly promising for the real-time monitoring of binding events even in complex environments. Among them, engineered protein switches have been widely designed for synthetic biology and sensing applications, and they appear transformative for future point-of-need tests [20, 21]. In this respect, comprehensive reviews of protein switches can better describe their advantages and disadvantages for bioanalytical applications [20].

Design and synthesis of oligonucleotides is still simpler and more affordable than those of protein. As a matter of fact, engineering protein-based recognition elements

becomes a remarkably more challenging endeavor than engineering nucleic acid-based recognition elements. In this line, the superior chemical robustness over time in a wider range of conditions make oligonucleotides superior compared to many proteins. In addition, DNA is a low cost and stable biomolecule easy to synthetize using solid phase synthesis in an automated way [22, 23]. Altogether these features make nucleic acids more accessible and affordable to research labs spread all over the world. Therefore, the literature has experimented a large increase of examples of structure-switching DNA biosensors. Our focus here is on structure-switching DNA biosensors for protein detection. More specifically, we introduce in this Section the basic concept underlying the design of structure-switching DNA receptors and then highlight some applications of structure-switching DNA recognition elements for either point-of-care applications [24] and real-time continuous monitoring [25] of proteins.

3 Engineering Structure Switching DNA Receptors

All the remarkable advantages that structure-switching DNA-based recognition elements offer come at the cost of limited number of DNA sequences that undergo a conformational change upon target binding. Thus, structure switching has to be engineered into those responsive DNA elements that do not change their conformation in response to the binding of the target. Here, we highlight some general rules to help the reader better understand how to design structure-switching DNA receptors.

The physics of structure-switching recognition elements is well described by the population-shift model which provides a route to tune the useful dynamic range of such recognition elements more-or-less at will [26]. According to this model, a DNA-based recognition element can populate two conformational states, i.e., a non-binding and a binding-competent state. The low-energy non-binding state of the DNA recognition element is a more stable conformation and it is always in equilibrium with a less stable, but binding-competent conformation. Target binding stabilizes the latter state thus shifting the equilibrium toward the bound state [26, 27]. Experimental validation of the free energy of the two equilibrium states is crucial to guide the engineering process, and experimental information can be easily obtained from urea [28] or temperature [29] denaturation curves. The equilibrium between the non-binding and binding-competent states is regulated by switching equilibrium constant (K_s, Fig. 1) that can be properly tuned by simply working on the secondary structure of the DNA-based recognition element. As an example, a DNA-based recognition element with a K_s of 0.1 describes a conformational equilibrium where 90% of the recognition element populates the non-binding state. This implies that structure switching is typically connected with a minimal background signal and a substantial signal change upon binding with the target. However, stabilization of the non-binding conformation rises an energetic penalty that target binding must overcome in order to induce the switch. Hence, the concentration of target necessary to trigger the switch (and thus generating a signal)

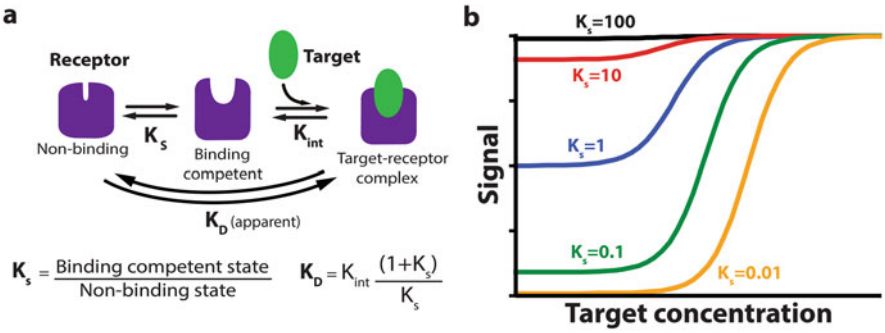

Fig. 1 The population-shift model describes biomolecular receptors operating through structure-switching mechanisms. (**a**) Top, working principle Of the population-shift mechanism. Switching constant (K_S) determines the interconversion between the non-binding and the binding-competent states of the recognition element. The target binding stabilizes the binding-competent state. Bottom, the combination of K_S and intrinsic constant (K_{int}) determines the final observed dissociation constant (K_D) and binding affinity of the recognition element for the target. (**b**) Recognition elements with high K_s have a majority population of receptors in the binding-competent state, which is translated in improved binding affinity (lower K_D) but also lower signal change upon target binding (black and red lines). Enhanced signal changes come at the cost of losing recognition element affinity (K_D). As a general rule, K_S value comprised between 0.1 and 1 offers a good compromise in terms of binding affinity and signal gain of the switch

strongly depends on K_s values, with lower K_s associated to higher observed binding affinity [26]. Thus, it is very important to not over stabilize the non-binding conformation of the recognition element beyond values of K_D required for the specific sensing application. Apparent binding affinities and switching constants can be related through the mathematical expression [26] displayed in Fig. 1a. Generally, achieving a satisfactory compromise between optimal signal-to-noise and strong binding affinity is linked to Ks values falling within the range of 0.1 and 1 with the latter that yields a maximum signal gain of 50% (half population in the binding-competent state in absence of target) while decreasing the observer affinity of the recognition element (K_D) just twofold [27].

Following these basic rules, it is possible to convert a DNA-based recognition element into a switching receptor and also to tune its binding properties and/or signal transduction [30]. In the following subsections, we highlight some of the most relevant strategies for the rational design of structure-switching mechanisms for sensing applications.

3.1 Formation of Duplex Motifs as Regulators of Structure Switching

This category describes the simplest and most straightforward strategy to incorporate a binding-induced structure-switching mechanism into a DNA-based recognition

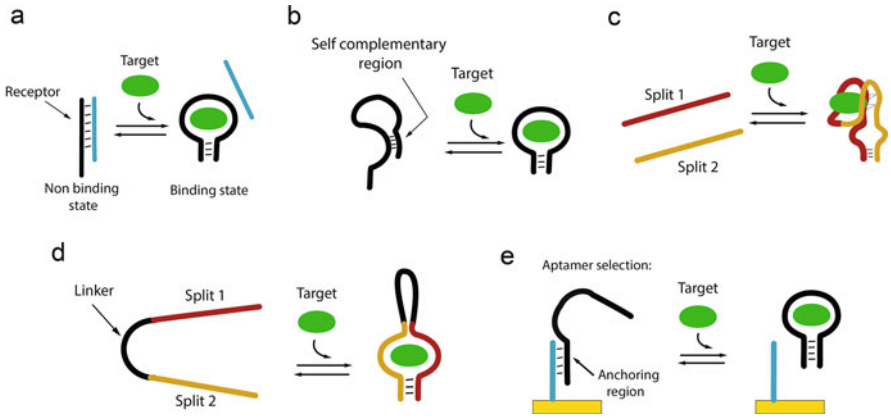

Fig. 2 Different strategies to generate structure-switching aptamers. (**a**) Simplest strategy consists of the addition of a complementary region to the binding site in the recognition element. The target competes for the binding site of the recognition element and disrupts the duplex in order to form the bound complex. (**b**) By introducing self-complementary motifs in the same DNA receptors it is possible to generate a non-binding state. The presence of the target destabilizes the non-binding state and stabilizes the binding conformation [36]. (**c**) Splitting of recognition element into two different subunits that rearrange and fold properly only in presence of the target. (**d**) In some cases, it can be advantageous to integrate the different split subunits in a single molecule connecting them through a linker region. (**e**) Specific selection strategies in aptamer selection make it possible to directly select structure-switching aptamers that intrinsically operate through a conformation change mechanism without needing further modifications

element. The hybridization between a complementary strand (CS) and a DNA-based recognition element generates a duplex structure (i.e., non-binding state) that does not allow the binding of the target molecule. The target has indeed to overcome a free energy penalty to bind to the recognition element, and it will not be able to do so until reaching certain target concentrations. Using a DNA aptamer as a recognition element, this format is known by the name "duplexed aptamer" [31]. For example, the CS can compete with the target for the free DNA recognition element labelled with a reporter molecule. In this approach, the CS binds the recognition element that now populates a non-emitting conformation. When the target is present in a concentration sufficient to displace the CS, structure switching leads to a noteworthy change in the signal (Fig. 2a). In an exhaustive and thorough study using optical characterizations, Lackey and co-workers [32] developed a methodology to study the kinetics of the binding event to recognition events using duplexed aptamer sensors, and demonstrated the switching mechanism behind the L-tyrosinamide binding aptamer. Specifically, they found that the switching mechanism is consistent with a S_N1-like mechanism, in which the complementary strand of the aptamer must dissociate first before aptamer binding to its target. This mechanism, however, is not universal since other aptamers might follow other mechanisms such as induced-fit, in which the target molecule directly interacts with the duplexed recognition elements and facilitates the displacing of the

complementary strand from the aptamer [33]. Another sensing architecture employs labelled CS bound to the DNA recognition element (low background signal) that when displaced by the formation of target-receptor complex generates a response. Dillen A. and colleagues [34] employed this approach in an assay for thrombin detection and extensively examined the associated thermodynamics.

Tuning properly either CS concentration and relative binding affinity between CS and DNA recognition element is fundamental to deploying a working sensor. Essentially, The free energy of the CS interaction with the DNA probe establishes the K_s value linked to the equilibrium between the non-binding and binding states. Therefore, it is important to properly select the length of the complementary motif, i.e., its binding affinity, and also CS concentration to achieve optimal signal gain upon target binding and adequate binding affinity. Besides, since the CS is an independent element added, it can be adapted without affecting intrinsic binding properties and selectivity of the recognition element, as opposed to other mechanisms explained later in the chapter. However, such assay formats are generally limited to end point measurements and are not easily transferrable to continuous monitoring platforms nor reusable biosensors.

An alternative approach consists of the addition of a short self-complementary motif in the sequence of the DNA recognition element itself (Fig. 2b). In this case, the duplex is formed by the self-complementary region and causes the receptor to fold upon itself into a non-binding conformation. The presence of target will push the equilibrium toward the binding competent conformation breaking this self-complementarity interaction and leading the system to the equilibrium bound state. This strategy is also known as the "pseudo knot" approach [35, 36] and has been successfully applied for the thrombin aptamer [37] and later adapted for electrochemical readout [38].

3.2 Splitting DNA-Based Recognition Elements into Two or More Independent Fragments

Here, the DNA recognition element is split into independent sequences not physically linked to each other. The structural change induced by the target binding guides the re-association of the two different subunits in one complex [39]. Not purely a structure switching, since the change in conformation is substituted for the assembly of the subunits, here the main requirement is the formation of secondary structures of the two subunits that still maintain the capacity to interact with the target molecule (Fig. 2c). Even in this case, a remarkable advantage of this approach is the generation of large signal gain upon target binding due to the relative high change in the distance between dissociated subunits that comes into close proximity in the presence of the target. In comparison, typical unimolecular structure-switching bioreceptors can only achieve small structure changes—and so limited signal change—that are basically comprised to the maximum distances within the

recognition element itself. To overcome this limitation, it is also possible to introduce a linker between the subunits involved in the interaction with the target in order to increase signal change upon target binding (Fig. 2d). In principle, this approach could be applied to any aptamer as a generalizable mechanism of signal transduction [40], since it just requires the correct splitting of the aptamer in two different isolated subunits. However, the presence of additional bases can significantly affect the overall secondary structure of the aptamer and its binding affinity for the target molecule.

Reality proves to be more complex and proper assessment of the splitting point in the aptamer is required. A general weakness of the strategy based on split aptamers is the partial re-assemble of the aptamer's subunits often occurring also in the absence of a target. This phenomenon generally results in an increase of the background signal. Furthermore, the approach appears difficult to generalize because splitting the aptamer can also significantly affect intrinsic binding properties and specificity toward the target. As a consequence, the repertoire of split aptamers available still remains limited [39].

3.3 Selection Processes of Structure-Switching DNA Recognition Elements and Their Optimization Through Molecular Engineering

During the selection process of DNA aptamers for non-nucleic acid targets, it is possible to directly select for structure-switching aptamers without the need of further engineering. Initial efforts in this area took advantage of immobilized DNA sequences to a solid surface using libraries containing a complementary docking motif (Fig. 2e). Upon binding with the target, DNA sequences selected and further enriched are those detached from the anchoring sequence. That means that selected aptamers must have undergone a structural change upon target binding inducing strand displacement from the anchoring strand. Different groups have reported successful assays to specifically select small molecules [41] and proteins such as thrombin [42], proving the capacity to successfully select aptamers with structure-switching properties. However, a key limitation of this approach is represented by the fact that the equilibrium state for binding of the sequences to the beads is being constantly re-established with each wash, and thus some non-functional sequences are recovered during the target elution step [43]. An alternative structure-switching SELEX method using a homogenous isolation step can be also performed in order to distinguish between active and inactive library members, without the need to immobilize target or capture strand [41].

Some further engineering strategies, independently of their selection method, can be introduced to induce a conformational change mechanism into non-switchable recognition elements. Either mutations, deletions (truncations), or additions of bases in the recognition element need to be done in a rational way, to

guarantee the binding properties of the aptamer, or to avoid destabilizing the binding conformation (decreasing the K_S) so much that the apparent binding affinity of the recognition element would fall out of the detection range of interest for that target. This approach has been extensively applied in aptamers for detection of small molecules [44–46], and for detection of proteins, for instance, neutrophil gelatinase-associated lipocalin (NGAL) [25]. However, the small changes introduced with respect to the original binding recognition element, require the knowledge of extensive structural information to guide the process in a rational way. Due to the difficulties in obtaining complete structural information for most of the aptamers, guidance in the process of selecting proper single-point mutations is severely limited [46, 47].

4 Protein Detection Using Structure-Switching DNA Receptors

Aptamers are short DNA or RNA single strands (~12–80 nucleotides long) that fold into defined secondary and tertiary structures and can selectively bind to molecular targets, such as small molecules, carbohydrates, proteins, and live cells. In truth, aptamers are selected from libraries [48], typical SELEX library starts with 10^{15} random sequences, of single-stranded oligos. Through sequential steps of binding, eluting, and amplification, DNA sequences capable of binding to the target of interest with high specificity and affinity are enriched within the library. After 5–15 selection cycles and counter-selection steps against potential interferants, the enriched pool is sequenced, and aptamer candidates are identified from the sequencing results using bioinformatics analysis. The selected sequences are chemically synthesized and characterized by their binding ability and specificity to a target. In the last 30 years, more than 30 variants of their process selection (i.e., Systematic Evolution of Ligands by Exponential Enrichment (SELEX)), have been developed [49] and now it is possible to select aptamers that show specificity and affinity comparable to those of antibodies toward their targets. Aptamers, however, are smaller, low-cost bioreceptors that are easier to produce and more straightforward to modify than antibodies.

Consequently, significant progress has been made by both the research community and pharmaceutical companies in the development of aptamer-based technologies, spanning applications from diagnostics to therapeutics [50]. In December 2004, the first aptamer drug was approved by the US Food and Drug Administration (pegaptanib sodium, commercialized under the name of Macugen), and many other aptamers have shown promising results in preclinical research and clinical trials. Among the myriad of aptamer-based biosensor technologies reported in scientific literature, some of them have recently been translated into commercially available diagnostic kit for food safety and biomarker detection [51]. To extend to aptamers all the advantages of the structure-switching binding mechanism

previously described, different molecular designs have been proposed. Since only a few aptamers present structure-switching functionality rationally introduced directly in the selection [52–56] many strategies focused on how to re-create structure-switching behaviors into aptamers that do not undergo a conformational change upon binding to the specific target.

In this section, we only report examples of sensing systems based on structure-switching DNA probes that present a sequence or a motif (i.e., a synthetic aptamer or a consensus sequence) that recognizes the target protein. Nucleic acid-based sensing systems using RNA or other artificial mimics, as well systems where the recognition event is mediated by non-nucleic acid-based elements (i.e., peptides, small molecules and antibodies) will be discussed in the Sect. 5. To help the reader, we have separated subsections for the detection of proteins and transcription factors, also providing a brief overview of DNA-nanoswitches for the activity-based monitoring of repair enzymes.

4.1 Structure-Switching DNA-Based Aptamers for the Optical Detection of Proteins

Pioneer in this field was Ellington's group that designed a new class of recognition elements named aptamer beacons [37]. By appending a complementary DNA motif at the extremity of thrombin-binding aptamer, Ellington and co-workers generated a structure-switching "beacon-like" probe. In the absence of thrombin, the aptamer adopts a stem-loop structure that can be easily visualized by labelling the two termini of the sequence with a fluorophore/quencher pair resulting in a quenched fluorescence emission. Thrombin binding to the G-quadruplex motif triggers the conformation change of the aptamer that ultimately leads to a fluorescence signal increase. This molecular design has been successively developed by many other researchers for bioanalytical and biomedical applications [38, 57–62]. Following these design principles, more recently, a structure-switching aptamer has been selected by Tan and colleagues where a tyrosine kinase-7 (PTK7)-binding aptamer is integrated with a single stranded pH-responsive i-motif allowing for selective binding of PTK-7 recognition elements on the surface of target CCRF-CEM cells [63]. By making use of an i-motif domain, the switching equilibrium is regulated by the pH of cellular microenvironment. At slightly acidic pH (i.e., in tumor microenvironment), the i-motifs enable the binding between the aptamer and the cognate target; at physiological pH (healthy cells) instead, the i-motif structure is switched in a random coil conformation that prevents the recognition event.

Liu's group has also reported on the detection of membrane protein PTK7 on living cells, specifically by employing "beacon-like" aptamers as Surface-Enhanced Raman scattering probe [64]. In the presence of the target protein, the structure switching exposes a DNA portion that triggers an enzyme-mediated signal amplification reaction. This generates Cy5-labelled residual DNA strands, which can

further hybridize with the capture DNA strands immobilized on gold nanoparticles assembled on a functionalized silicon substrate. By integrating SERS, aptamer conformational change, and Exo III enzyme amplification, the sensitivity is superior to that of the commercial ELISA method by several orders of magnitude. However, a common limitation of SERS-based assays showing high sensitivity is that such platforms sometimes exhibit limited accuracy and reliability for quantitative analysis.

Another useful strategy for the design of structure-switching DNA probes was developed by Szostak's group for the detection of ATP [65] and small molecules [66], and later adapted for protein detection. The strategy consists of splitting the aptamer into two or more portions that can associate only in the presence of the specific target. Liu et al. [67] proposed a specific design for the detection of thrombin based on split aptamer-programmed self-assembly of quantum dots (QDs). Specifically, two fragments of the split aptamer are conjugated to different QD populations. The reassembling of the aptamer into a complex through a sandwich-like assay induced by target thrombin leads to self-assembly of fluorescent QDs with a significant fluorescence quenching and band-shift due to exciton energy transfer between QDs. Thanks to the high sensitivity typical of the exciton energy transfer-based fluorescent detection, a limit of detection (LOD) of 15 pM is achieved. Li's group [58] introduced the concept of strand displacement reactions as a means of switching, where a partially complementary strand blocks one aptamer subunit from reassembling into the signaling conformation. Optical aptamer-based assays based on strand displacement reactions employ a binding aptamer modified with a fluorophore that is hybridized with an aptamer-complementary element (i.e., ACE) labelled with a quencher. In the absence of a target, the two tags are in close proximity and the fluorescence signal is quenched. The binding event promotes the folding of the aptamer and the subsequent displacement of the quencher-tagged strand that ultimately results in a fluorescence signal increase. The ACE can be designed of different lengths and complementary to different aptamer's portions, thus allowing straightforward and programmable design features.

One of the limiting steps of the design of duplex aptamers is represented by the velocity of the signal transduction that is mostly governed by the hybridization kinetics of the ACE to the binding aptamer [31]. Recently, precise kinetic control has been reached by Zhang et al. [68] by combining protein-controlled DNA-nanoswitches with a strand displacement reaction to realize a kinetically controlled platform that transduces the presence of ligands (i.e., proteins and small molecules) into the release of an oligonucleotide. Here, the aptamer sequence is designed to be inserted between a toehold and a displacement domain of an invading DNA strand (Fig. 3a). In the absence of the target, the toehold and displacement domains are separated by a long, unstructured aptamer and so the strand displacement reaction on the reporter system is very slow. Upon target binding and consequent aptamer folding, toehold and displacement domains come into closer proximity and therefore are capable of triggering the strand displacement reaction producing fluorescence signal increase. This strategy was successfully demonstrated

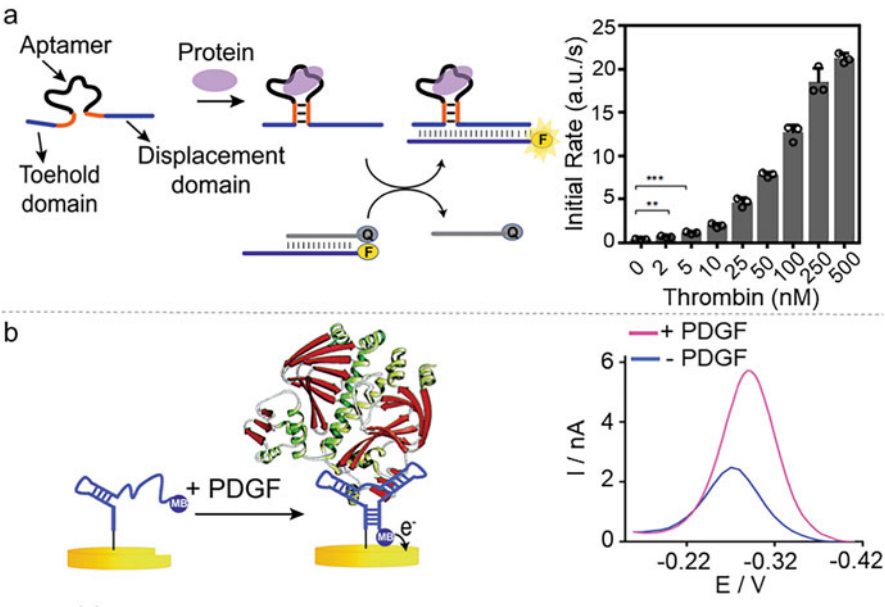

Fig. 3 (**a**) Protein-induced strand displacement reaction. The displacement is triggered by the conformational change induced by the presence of protein. Analysis of initial kinetic rates for the change of fluorescence in the presence of different concentrations of thrombin is shown. Adapted with permission from ref. [68] (Copyright © 2021, Springer Nature). (**b**) Electrochemical aptamer-based (EAB) sensor for the detection of platelet-derived growth factor (PDGF). The PDGF-binding aptamer is attached onto the gold surface and labelled with a redox tag (i.e., methylene blue, MB). Upon target binding, the aptamer folds into a stable three-way junction leading the MB label close to the electrode surface, allowing a more efficient electron transfer. (Right) Voltammograms (square wave voltammetry, SWV) of EAB sensor's response in 50% serum, before (blue line) and after (pink line) incubation with 50 nM PDGF. Adapted with permission from ref. [82] (Copyright © 2007, American Chemical Society)

for the detection of thrombin and PDGF achieving a LOD of 0.96 nM and 0.73 nM, respectively. Furthermore, using this strategy, Zhang et al. reported on the capability to realize orthogonal transduction, logical operations, and DNA-based amplification reactions.

Recently, some in vivo biosensing platforms based on structure-switching aptamers have been also reported [69–71]. For example, imaging of thrombin in living mice has been reported by Zhang et al. [72]. The authors showed that using thrombin-binding aptamer in combination with two DNA strands modified with a near-infrared fluorophore/quencher pair (IRDye 800CW/IRDye QC-1), an efficient contact quenching is obtained. With this simple strategy, the selective visualization and quantification of the target protein is reached with a wide linear dynamic range (0–1,000 nM), and a LOD of 112 nM.

Up to date, most of the assays illustrated are based on fluorometric readout thanks to their high sensitivity and facility of DNA labelling. Nevertheless, electrochemical

readouts represent a more suitable option for POC assays: rapid response time of analysis, feasibility to miniaturize the platforms and to integrate them into low cost, microfluidic devices. However, most electrochemical biosensors for protein detection do not operate in a sample-in-answer-out manner, especially when tested with unprocessed clinical samples. They, instead, generally require multiple washing steps and the addition of reagents to process the sample.

4.2 Structure-Switching Electrochemical Aptamer-Based Biosensors for Protein Detection

Pioneering works carried out by Plaxco's group [38, 73, 74] have demonstrated how to overcome many of the issues mentioned above using Electrochemical Aptamer-based biosensors (EAB sensors). EAB sensors have been reported as one of the most promising tools for both in vitro and in vivo monitoring of small molecules and proteins [25, 75–80]. This is principally due to the enhanced specificity of the structure-switching mechanism of DNA aptamers and the ability of EAB sensors to perform well when placed in whole blood and in living body. EAB sensors are indeed rapid, reversible, reagentless, and can be easily adapted to new targets by simply changing the aptamer sequence. They are prepared in a simple way using redox-reporter- and thiol-modified DNA aptamers immobilized on a gold electrode [81]. In this way, as an example, it is possible to monitor the folding into a triple-stem conformation of the PDGF-responsive aptamer upon binding to PDGF (LOD = 1 nM in blood serum, Fig. 3b) [82]. As a result of the conformational change mechanism, the electrochemical tag comes closer to the electrode surface, generating an increase in the electrochemical signal due to improved electron transfer between the redox tag and the working electrode (Fig. 3b, right). By adopting the same approach, the detection of thrombin was also achieved, reporting a detection LOD of 6.4 nM [38]. In this specific case, the binding event causes a conformational change that inhibits the electron transfer between the redox tag (i.e., methylene blue) and the electrode surface, generating a current decrease. Similarly, Liu and co-workers, showed the detection of interferon-gamma in the presence of overabundant serum protein [83], such as the detection of tumor necrosis factor-alpha (TNF-α) in blood samples (this last one by using an RNA-based aptamer) [84]. The detection of epithelial tumor marker mucin 1 (MUC1) was reported by Ma et al. demonstrated how the MUC1-responsive aptamer in the absence of the target, folds into a thermodynamically stable hairpin conformation, facilitating the direct electron transfer between the redox tag and the gold electrode, whereas in the presence of MUC1, the aptamer no longer holds its hairpin conformation, moving the redox tag further away from the electrode surface [85]. In the same direction, Zhao et al. developed a folding-based EAB for the detection of vascular endothelial growth factor (VEGF) in human whole blood [86]. Here, the cognate aptamer initially unfolded, upon the binding to VEGF, adopts a stem-loop structure that

forces the redox label to be in close proximity to the electrode. An outstanding detection limit of 5 pM was achieved in 50% of blood serum.

One of the main advantages of structure-switching EAB relies on their capacity of performing seconds-resolved, real-time measurements of molecules which makes the technology very attractive for clinical applications. In this respect, recently, Idili et al. demonstrated the single-step, rapid, reagentless, and quantitative measurement of the SARS-CoV-2 spike (S) protein in biological fluids (serum and artificial saliva) [87]. Plaxco's group has also demonstrated the possibility to use this technology to achieve real-time monitoring of different small molecules and drugs in living rats [44, 45, 78]. Inspired by this approach, more recently, Parolo et al. achieved the first high-frequency, real-time detection with subminute time resolution of Neutrophil Gelatinase-Associated Lipocalin without any sample processing in human urine samples using a urinary catheter [25].

Although the unprecedented performance of EAB sensors in vivo, the platform still requires further optimization before it can see a successful clinical application. In particular, the often-poor match between the affinity of binding aptamers for the specific target in the body where it is not possible to easily adjust the experimental conditions to tune the binding properties of the probe (pH, ionic strength, etc.). Additionally, in some cases, the clinically relevant concentration of the analyte itself, as well as the relatively shallow binding curves connected to "Langmuir-type" binding curves of single-site DNA recognition elements, represent main limitations [88]. As an example, the windows of some target analytes (metabolites, drugs, etc.) in vivo are so narrow that the abilities of EAB biosensor technology do not allow their measurement in the clinically relevant ranges. For example, to transition a noncooperative receptor from 10% occupied to 90% occupied requires an 81-fold change in target concentration, being the midpoint of that 81-fold transition the K_D value. This reduces the ability of aptamer-based sensors to measure small differences in target concentration, limiting the precision of the assay and scope of such technologies in practical way [89]. In the case of protein detection, an additional limitation is represented by the fact that EAB sensors require fast kinetics of target release to provide continuous, real-time in vivo monitoring which is often not possible because protein binding is generally associated to stronger interactions with the DNA probe.

Rationally designed molecular approaches to overcoming these problems can be very tricky to optimize and difficult to predict, especially when the DNA aptamer is longer than 35–45 nt. The difficulties encountered to predict the aptamer folding upon binding to the target, as well as the difficulty of understanding the dependence of conformational changes by the analyte also represent minor issues toward the development of a general platform for POC application in vivo.

To increase sensitivity, also nanostructured materials deposited at the electrode interface (i.e., AuPNs, AgNPs, PtNPs, silica nanoparticles (Si NPs), QDs, magnetic nanoparticles (MNPs), carbon nanotubes (CNTs), and graphene (GNs)) can be used. For a more comprehensive explanation of the effects, benefits, and drawbacks linked to the utilization of nanomaterials in conjunction with DNA biosensors, readers are encouraged to consult specific articles and reviews on this subject [90–92].

4.3 DNA-Based Switches for the Detection of Transcription Factors

Transcription factors (TFs) represent a particular class of proteins involved in the transcription of genes. The binding between the TFs and DNA is highly sequence-specific and play a key role on cells differentiation and growth, such as on the interpretation of the genome information. By working as regulators and selector genes, their mutations and dysregulations are involved in many pathological processes [93].

Vallée-Bélisle and colleagues [94] introduced the rational design of DNA nanoswitches for the detection of transcription factors (TFs). In a seminal study, they presented binding-activated fluorescent DNA probes, referred to as "transcription factor beacons," capable of signaling the presence of three transcription factors (TBP, Myc-Max, and NF-κB) directly in crude nuclear extracts. The transcription factor beacons contain a consensus, double stranded DNA binding sequence able to recognize with extreme specificity the TFs target. These probes are designed in a way that they can populate two different conformations in equilibrium with each other: *a stem-loop structure* containing double stranded consensus sequence for the specific binding of the protein, and *a second structure* where the consensus sequence is sequestered in a stem-loop "non-binding" state. By properly introducing a fluorophore/quencher pair, it is possible to monitor the binding of TFs as a means of fluorescence increase (Fig. 4a). The same strategy has been later adapted to an electrochemical format by simply attaching on a gold electrode the TF beacons labelled with a redox tag (i.e., methylene blue). The probe reconfiguration upon TF binding pushes the electrochemical tag away from the electrode surface generating a change of current [95]. By using microfluidic devices, this technology makes it possible to quantify the proteins showing a detection limit of 4 nM for TATA-binding protein in nuclear cell extracts. This feature together with the easiness of detection, attracted many other researchers that extended on this concept [96]. As an example, Bertucci et al. have successfully adapted the in vitro biosensors to intracellular imaging of nuclear factor kB (NF-kB) using living cancer cells and FRET-based readout [97, 98]. By using lipofectamine-based vectors, the nanodevice was successfully delivered to cultured PC3 cells. The transportation via endosomal escape and the successive diffusion into cytoplasm and nucleus were confirmed through stochastic optical reconstruction microscopy (STORM). The specificity of imaging was also confirmed by transferring the cells with siRNA to knockdown the expression of NF-kB. Recently, Bertucci et al. also demonstrated the application of TF beacons as a molecular translator for the actuation of strand displacement reactions by engineering a toehold-binding domain in the switch that can trigger the strand displacement reaction only upon switch reconfiguration induced by TFs [99]. Beside the obvious biosensing applications, this approach paves the way to rationally control biomolecular communication pathways between nucleic acid-based systems and functional proteins. This approach can be of value for a variety of applications, ranging from synthetic biology to artificial

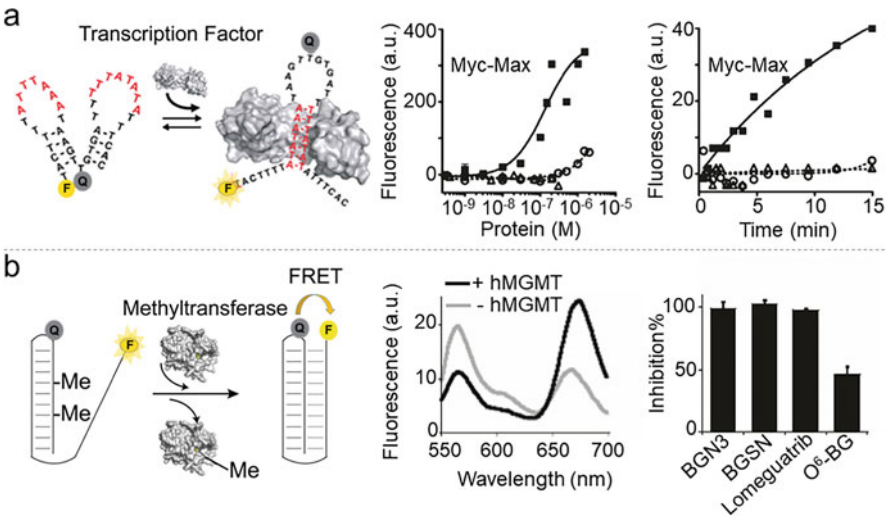

Fig. 4 (**a**) Transcription factor beacon signaling the presence of specific DNA binding proteins. The binding of the TF induces a conformational change that can be detected by properly modifying the beacon with a fluorophore/quencher pair at the extremities of one of the two stems associated to the non-binding state. The equilibrium binding curve (a, center) and kinetic response (a, right) of TF beacons targeting Myc-Max are shown. Adapted with permission from ref. [94] (Copyright © 2011, American Chemical Society). (**b**) Folding upon repair DNA-nanoswitches for the monitoring of the activity of a methyltransferase enzyme (hMGMT). Following the enzymatic reparation, the switch undergoes a conformational change leading to a change in fluorescent signal. Graph in the center of the panel displays the fluorescence spectra in presence and absence of hMGMT. While the graph on the right shows the % Inhibition obtained with the 2-Me Triplex nanoswitch before and after incubation with 5 mM hMGMT at an equimolar concentration of different enzymatic inhibitors. Adapted with permission from ref. [118] (Copyright © 2020, Wiley-VCH GmbH)

transcription-transduction pathways and recreation of cell-like behaviors in biomimetic systems.

We have also designed TF beacons with enzyme-like activity (DNAzymes) by introducing allosteric control over the switching mechanism [100]. The TF-controlled nanozyme shows peroxidase-like catalysis and this provides a means to quantify enzyme activity through a simple colorimetric readout by adding TMB and hydrogen peroxide. The bioassay is cheaper than many other assays based on the use of expensive reagents or labelled molecules. However, the catalytic efficiency of this class of DNAzymes is low and the reaction times limit its applications. Following the TF-induced switching mechanism, recently Zhou's group developed an allosteric DNA-Silver nanocluster (DNA-AgNCs) switch [101]. The fluorescence of DNA-AgNCs is regulated by a guanine-rich enhancer sequence (GRS) that enhances its fluorescence 500-fold when it is close to the DNA-AgNCs. With this strategy, the label-free quantification of NF-κB p50 has been reported showing a LOD of 2 nM.

4.4 Activity-Based Sensors: DNA-Based Switches for the Monitoring of Repair Enzymes

Cells are continuously exposed to endogenous and exogenous mutagens which induce chemical alterations of the DNA structure (i.e., "DNA damage") impacting human health [102]. In response to this, Nature has elaborated a DNA repair machinery reversing the mutagens-induced DNA damage [103] such as base excision repair (BER) [104], mismatch repair [105], nucleotide excision repair [106], and direct damage reversal [107] that collectively represent protective processes blocking the entry of cells into carcinogenesis. An increased risk of developing cancer is generally associated with low DNA repair capacity [108–110], and interindividual variations in DNA repair capacity are thought to determine different susceptibilities to cancer. To date, DNA repair capacity can be assessed indirectly at the level of transcription—for selected genes involved in the different repair pathways—translations (proteomics), and also using single nucleotide polymorphism (SNPs) screening [110]. However, enzyme activity often does not correlate with the rate of transcription/translation, and not even with the amount of protein present, whereas SNPs in repair genes are not always informative when the gene is not expressed [111]. As an alternative, a wide variety of cell-based assays have been reported but they generally require labor-intensive analysis that makes difficult their implementation in a clinical setting (single-cell gel electrophoresis assay, host cell reactivation, etc.). In this regard, chemically modified nucleic acid probes appear promising as they offer many advantages over the traditional methods mentioned above, such as possibility of imaging DNA repair directly in cells and tissues [112], and adaptability for high-throughput assays in biological media. In this respect, we address the reader to the review by Kool's group to learn more about the topic [112].

DNA-nanoswitches can also be used to directly monitor the activity of enzymes involved in DNA repair. Most of these assays employ structure-switching DNA probes that populate a different secondary structure as a result of enzymatic activity, generally a G-quadruplex motif, that is further used to generate a measurable colorimetric, chemiluminescent, or fluorescent output. A significant advancement in the realm of DNA switch sensors for detecting DNA repair enzymatic activity was achieved through the research led by Ren and colleagues. They devised a label-free quadruplex-based functional molecular beacon for the real-time monitoring of Uracil-DNA Glycosylase (UDG) activity, marking a pivotal contribution in this area [113]. The molecular design here makes use of a blocking strand that prevents the proper folding into a G-quadruplex conformation. Specifically, an oligonucleotide presenting several uracil residues binds to a molecular beacon, precluding its folding in a G-quadruplex structure. Upon the removal of uracil residues by UDG, the G-rich portion can fold in a G-quadruplex motif that is finally bound by the N-methyl mesoporphyrin IX (NMM) dye, generating a ∼14-fold enhancement in fluorescence, given the strong interaction between NMM and the folded G-quadruplex. Following this work, several subsequent UDG probes [114, 115] and a T4 PNK probe [116] based on the use of blocking strand have been developed.

Ma and co-workers reported the first luminescent DNA switch-based assay for the detection of nicking endonuclease activity [117]. They synthetized different luminescent Ir(III) complexes presenting a weak affinity toward a DNA duplex and high affinity toward G-quadruplex, that in turn means low and high luminescence signals, respectively. In their assay, the cleavage induced by Nb BbvCI enzyme causes the release of a guanine-rich sequence that folds into a G-quadruplex, enhancing the luminescence of the Ir(III) complexes. The assay was proved in cell extracts showing its potential as a user-friendly and cost-effective switch-on platform. Successively, other complexes were synthesized for the detection of protein tyrosine kinase-7 (PTK7) in aqueous solution [117]. Here, the specific binding between the PTK7 and the sgc8 aptamer triggers the release of the G-quadruplex-forming sequence and consequent luminescent catalytic output.

A new class of DNA nanoswitches for monitoring the activity of methyltransferase activity has been recently reported by our group [118]. We rationally designed folding-upon-repair DNA-nanoswitches that can switch from a duplex conformation (low FRET efficiency) into an FRET-active triplex DNA structure upon human methyltransferase (hMGMT) activity. hMGMT converts O6-methyl-guanine (O6-MeG) nucleobases in the DNA duplex into repaired guanine nucleobases restoring triplex DNA (Fig. 4b). Molecular Dynamics simulations confirm that a methyl group at the guanine O6 position in the duplex portion of the nanoswitch hampers the triplex formation, so that the folding into triplex structure is strictly dependent on the repair activity. The activity of different methyltransferase enzymes has been evaluated also in the presence of several enzyme inhibitors and the assay has been further adapted for drug screening. Another new strategy based on the use of DNAzymes for the monitoring of demethylase activity has been just reported by Jiang's group. They designed fluorogenic DNAzymes, named RADzymes (i.e., repaired and activated DNAzyme), containing single methyl lesion in specific positions that inhibit the catalytic activity of the engineered DNAzymes [119]. The reparation of O6-MeG lesion leads to the restoration of the catalytic activity with generation of fluorescence output with linear correlation with hMGMT concentration in the range between 9 and 540 nM, associated to a limit of detection of 2 nM. The repair activity has been assessed in different cells and under drug treatment, giving promising results. In the same work, the monitoring of ALKBH2 activity was also achieved by engineering a fluorogenic RADzyme containing 3MeC lesions. Successively, epigenetically modified DNAzymes (EMOzymes) were engineered and combined with a CRISPR/Cas12a amplification for the quantification of active GMT [120] showing LOD of 0.05 nM.

5 Programmable DNA Nanostructures as Scaffolds for Biomolecule Detection

In this section, we discuss the use of DNA as a structural material for building scaffolds supporting signaling transduction mechanisms. DNA provides an extraordinarily versatile material for self-assembly and DNA nanostructures have been demonstrated to be useful for biosensing applications. Since DNA thermodynamics is highly predictable, using sequences of limited length (less than 100 nucleotides), it is possible to build simple and more complex nanostructures with precision almost at the level of Armstrongs [121–123]. Moreover, it is possible to control the formation and rearrangement of the DNA structure by tuning experimental conditions (temperature, ionic strength, pH, etc.). Generally, DNA nanostructures take advantage of the canonical Watson-Crick-Franklin base pairing but they can also make use of other types of base pairing, such as non-canonical DNA-RNA base pairing, or Hoogsteen interactions that control the formation of triple helixes [124]. In this context, the capability to build spatially controlled DNA structures at the nanoscale is discussed with regard to biosensing.

5.1 Simple Single and Double Stranded DNA Scaffolds for Sensing Applications

Single or double stranded DNA sequences modified by non-nucleic acid recognition elements represent the simplest DNA scaffold structure that can be employed for biosensing. We highlight here single and double stranded DNA-based scaffolds used in three different classes of bioassays, specifically (i) platforms based on steric hindrance effects, (ii) platforms linked to scaffolds operating through structure-switching mechanisms, and (iii) those that take advantage of proximity-based effects to generate a signal output. In the *first category*, i.e., biosensors based on steric hindrance effects (Fig. 5a), signal generation is directly related to the limited hybridization of the DNA scaffold when it is bound to a large biomolecular target. Specifically, the presence of the target alters the intrinsic mobility and hybridization efficiency with a complementary nucleic acid probe, thus consequently inducing a change in the kinetics and consequently into a measurable output. The *second group* comprises structure-switching DNA scaffolds, where DNA scaffold plays the role of a dynamic reconfigurable unit populating different conformations in the presence and in the absence of the target protein. The interaction of the recognition element covalently conjugated to the DNA scaffold with the target protein induces a structural reconfiguration of the DNA scaffold. In contrast to the sensors based on structure-switching recognition elements, in this case, the target needs to induce a rearrangement into the DNA scaffold. Proximity-based DNA assays (Fig. 5b, c) represent *the third group* of biosensors using single or double stranded DNA structures as target-responsive scaffold elements. In these assays, the DNA scaffolds

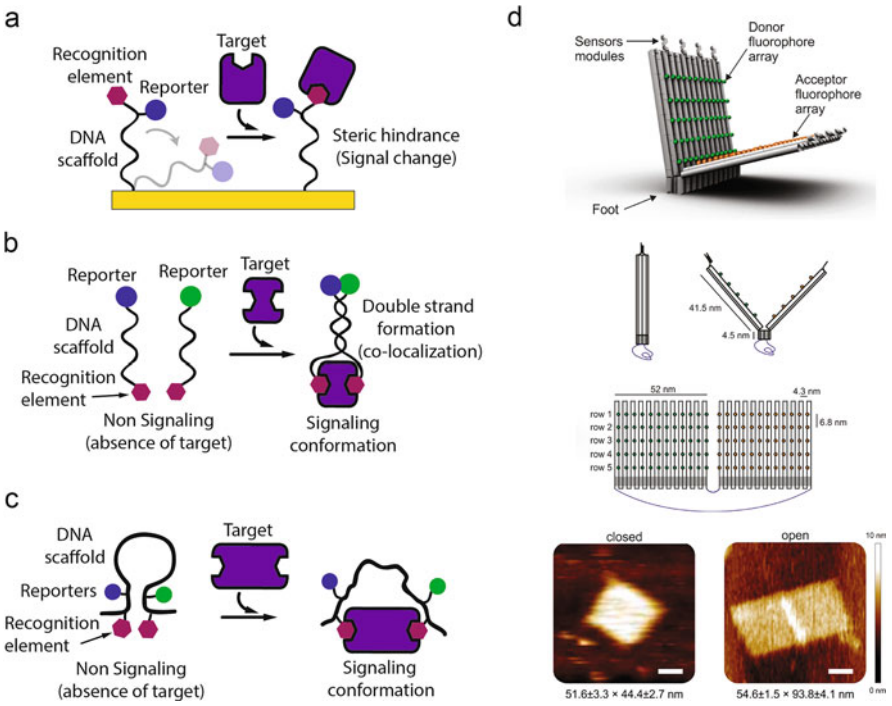

Fig. 5 Sensing approaches supported by DNA-based scaffolds. (**a**) DNA can be used as a scaffold molecule holding both recognition and reporter elements. When the target recognizes the non-nucleic acid recognition element, the efficiency of the scaffold to properly collide with the electrode interface significantly decreases producing current signal change. (**b**) DNA scaffold systems for sensing based on proximity effect. (**c**) The target binding can also induce the structural reconfiguration of a hairpin DNA scaffold resulting in a change of FRET signal. (**d**) Top: target-responsive folding of complex DNA nanostructures of hundreds of nm. Middle: schematic view of the design of an origami "giant" beacon applied for biosensing applications. Bottom: Microscopy images correspond to Atomic Force Microscope (AFM) imaging, scale bars correspond to 20 nm. Adapted with permission from ref. [139] (Copyright© 2018 American Chemical Society)

are also coupled to a reporter system that generates an output signal only when the two DNA elements are co-localized onto the same target acting as a template molecule. Based on the principle of local concentration [125], also referred to as co-localization effect, the simultaneous interaction of the two DNA scaffolds with the same target brings them closer together, thus increasing extraordinarily the effective molar concentration. To be successful, the DNA scaffold strands must be designed in a way that their relative binding affinity is poor when they are free in solution, whereas only upon target binding they can hybridize inducing scaffold interaction and signal generation. Interestingly, thanks to DNA's intrinsic properties, the co-localization-based detection can be connected to a signal amplifying reaction, such as DNA amplification via enzyme-based amplification producing ultrasensitive platforms.

5.2 DNA as Building Block of Complex Nanostructures

Beyond the use of short duplex DNA structures, DNA can be used to build structures in the nano- and microscale when designed and arranged in the proper way. Pioneered by Nandrian C. "Ned" Seeman when introducing the nucleic acid junctions [126], structural DNA nanotechnology rapidly expanded the possibility of properly designing complex DNA-based nanostructures [127] settling the basis for a variety of applications [121]. Most of the mechanisms used to create DNA scaffolds and nanostructures rely on the control and programmability introduced through the use of "sticky ends" to control tile-based self-assembly or the design of more complex origami DNA (such as illustrated in Fig. 5d).

A sticky end is a short single stranded overhang protruding from a double stranded DNA molecules. Examples of tile-based self-assembly are DNA-based nanotubes, [128] where a few strands of DNA assemble into a small structure or "tile," representing the basic building unit of the nanostructure, with a two-dimensional shape similar to a rectangle. Each tile presents short protruding oligos out of the four "corners" of the tile (i.e., sticky ends). The sequence of these sticky ends can be designed in such a way that it hybridizes with other tiles and assembles into bigger DNA-based nanostructure. These initially two-dimensional structures can curve and fold over themselves forming a cylinder/rod-like structure open at both ends. Thanks to DNA's programmability it is possible to build nanotubes with different decorations and homogeneous or heterogeneous composition of its building blocks [129] up to the size of micrometers, so they can be visualized under a fluorescence microscope. By modulating the sticky ends' interaction, it has been also reported the possibility to induce assembling or disassembling of such structures. Ricci and his group have developed many examples where DNA nanotubes are used as supramolecular scaffolds for sensing purposes [130].

W.K. Rothemund instead reported a simple method named DNA origami where a set of properly designed short DNA strands determine the correct folding of a long single strand DNA into desired 2D shapes [131]. Using DNA origami is possible to assemble DNA strands of diverse geometrical shapes. This work settled the basis for later studies where a number of complex and stimuli-responsive 2- and 3-D DNA-based nanostructures have been reported (Fig. 5d) [123, 132]. These DNA-based nanostructures can incorporate a diversity of modifications and components to introduce a wide range of functionalities with applications well beyond biosensing. Therefore, DNA origami design and applications fall out of the scope of this chapter, for further reading of other applications few relevant references have been included: drug delivery applications [133], cargo and release [134, 135], enzymatic activity control [136], and even pore formation on lipidic membranes [137, 138].

5.3 *Electrochemical DNA Scaffold Sensors for Protein and Antibody Detection*

To detect antibody and protein biomarkers, a number of publications reported on the use of redox-tagged DNA signaling scaffolds modified with a non-nucleic acid recognition element, and covalently attached to an interrogating electrode. Specifically, this sensing approach utilizes a rigid but dynamic double stranded DNA scaffold composed of one DNA strand terminally modified with a redox reporter that hybridizes with a second complementary DNA covalently linked to a recognition element [140–144]. The binding of a target protein to the recognition element significantly affects the collisional kinetics of redox-tagged DNA scaffold at the electrode interface (Fig. 6a and b). Key parameters that need special attention here are the size of the recognition element and the target molecule, with particular importance on their relative ratio. In this respect, one of the main limitations is that high molecular weight recognition elements result in a high steric hindrance affecting the intrinsic dynamics of the DNA scaffold, even in the absence of the target molecule. The signal change is instead maximized using a small recognition element having a relatively lower molecular weight in comparison to that of the target protein. Specifically, Kang and co-workers [143] demonstrated that as the recognition element increases in size (more than 70 kDa), the steric bulk reduces the electron transfer also in the absence of the target molecule. By doing so, the current signal is already suppressed to a level that no further signal change upon target binding can be detected. However, this issue was elegantly solved by reducing the size of the recognition elements to the minimal unit interacting with the target. In this particular example, the recognition element was reduced from the whole antigen

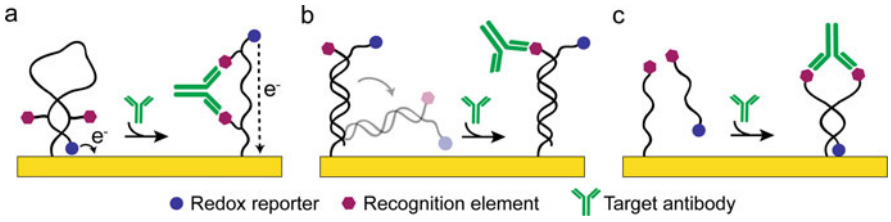

Fig. 6 Example of DNA-based electrochemical sensors for protein detection. (**a**) Structure switching-based electrochemical assays. Conformational change due to the structural reconfiguration of the DNA probe upon antibody binding brings the redox reporter away from the electrode, resulting in reduced electron transfer between the electrode and the redox reporter. Adapted with permission from Ref. [166] (Copyright © 2012, American Chemical Society). (**b**) Steric hindrance-based electrochemical assay. Steric bulk hindrance of the target antibody hinders collisional activity of the DNA probe and hampers electron transfer. Adapted with permission from Ref. [140] (Copyright © 2009, American Chemical Society). (**c**) Proximity-based electrochemical assay. Co-localization of the two antigen-labelled DNA strands on the same target antibody brings the redox reporter closer to the electrode surface and enhances electron transfer. Adapted with permission from Ref. [159] (Copyright © 2020, Wiley)

recognized by the antibodies to the small epitope (region of the antigen) recognized by the antibody [143, 144].

Exploiting the properties of scaffolded DNA sensors that dynamically switch in response to an external electric field [145, 146], Kelley's group reported on reagentless DNA-based scaffold sensors addressing some of the above-mentioned limitations [147]. The method relies on measuring the sensor's electric field-mediated transport using electron transfer kinetics of a reporter molecule attached to DNA. By measuring changes in falling time of the negatively charged DNA probe to the electrode surface upon target binding via chronoamperometry, the presence of a protein bound to the sensor complex can be tracked continuously in real time. This approach provides a generalizable means of monitoring a range of physiologically relevant proteins directly in a variety of body fluids, as well as in living animals. Furthermore, this assay allows direct detection of whole SARS-CoV-2 virions and spike protein in untreated saliva samples of COVID-19 affected patients within minutes [148].

Mimicking the structure of natural Immunoglobulin G antibodies, Idili et al. [149] designed a Y-shaped DNA scaffold containing two redox reporters and two recognition elements at the ends of the DNA arms to detect IgG antibodies in serum and saliva. The bivalent binding of the target antibody to the antigen anchored on the Y-shaped DNA scaffold generates a high steric hindrance effect, reducing the mobility of the DNA scaffold and in turn preventing the redox reporter on the DNA scaffold from reaching the electrode surface. This is reflected in the reduction of the electrochemical signal generated by square wave voltammetry of methylene blue. Thanks to this rationally designed configuration, the authors detected IgG antibody and streptavidin, a multivalent protein, in serum and artificial saliva with detection limits in the low nanomolar range of concentration. Mahshid and co-workers [150] took advantage of steric hindrance effect for the simultaneous one-step detection of large macromolecules (e.g., proteins and antibodies) in whole blood. In this assay, hybridization kinetic of a redox-active signaling strand to a surface-bound capturing strand was inhibited due to the steric hindrance caused by binding of a large macromolecule to the recognition element on the signaling strand. As a result, electrochemical signal was suppressed in proportion to the size and concentration of the target macromolecule. In a follow-up work, a collaboration between Kelley and Vallée-Bélisle groups [151] reported the use of nanostructured microelectrode (NME) as the interface for the steric hindrance-based assay. High curvature structures of NMEs allow immobilization of a longer capturing probe at higher surface density. This improves the detection limit of the platform compared to the previous one (LOD of 10 pM vs LOD of 100 nM for streptavidin as model analyte). They also demonstrated improvements in response time and detection sensitivity as a result of the size-dependent hybridization rates and morphology-induced blocking effects on the electrode surface. These platforms were also used to detect small molecules through a competitive antibody-based assay directly in complex matrices [152, 153].

5.4 *Proximity-Based DNA Scaffold Sensors for Protein and Antibody Detection*

To create a highly selective and more generalizable way to quantify proteins and antibodies, target-induced reconfiguration of signaling DNA scaffolds controlled by proximity effects can be harnessed in order to generate a measurable signal output. In this regard, the typical Y-shaped structure of bivalent IgG antibodies makes them a perfect candidate for the development of proximity-based DNA sensors, as demonstrated by our group [154, 155]. As a matter of fact, the hinge region that links the Fc and Fab portions of an antibody is a flexible tether that allows a quite independent movement of the two Fab arms, thus making the distance between the two binding sites (present at the end of the Fab arms) quite variable. Despite this, the common Y-shaped structural view of an IgG or IgE antibody shows the two binding sites separated by approximately 10–12 nm. This distance can be taken as a reference for the rational design of DNA-based units that can interact only when they are co-localized on the same target antibody at the nanoscale volume.

In this regard, our group reported on the rational design of programmable structure-switching DNA-based scaffolds that combine the advantageous features of DNA-based nanoswitches with those of co-localization-based methods using the principles depicted in Fig. 5b, and exemplified in Fig. 6c for the particular case of antibodies as targets. Although the generation of the signal is associated to a FRET-labelled structure-switching DNA hairpin, all the DNA elements here are used as scaffold molecules where the specific recognition element responsible for antibody binding is chemically conjugated to the DNA. Specifically, the co-localization on the same target antibody of the stem-loop scaffold and its complementary input DNA strand leads the two scaffold units into close proximity, forcing the opening of the stem-loop DNA scaffold with consequent increase of the FRET signal in a concentration-dependent way [154, 155]. This design allows one-step and orthogonal detection of clinically relevant IgG and IgE antibodies in human blood serum and plasma samples in a no-wash format within less than 10 min. The platform has been successfully applied to monitor the immune response of HIV-positive patients treated with a peptide-based (AT20 peptide) phase-I therapeutic vaccine and also proved its capability to differentiate unvaccinated positives from vaccinated patients [155]. One of the major advantages of this design is the capability to recognize any bivalent molecular target for which a recognition element can be conjugated to a nucleic acid strand. This modular and versatile approach has been also used in follow-up work to detect a monoclonal antibody (i.e., trastuzumab) only by changing the Ab-recognizing epitope [154]. Trastuzumab, a growth-inhibitory humanized monoclonal anti-HER2, is currently used for passive immunotherapy in the treatment of breast cancer. Since the therapeutical cut-off value has been set at a relatively high concentration (137 nM), a sensor to monitor the immune response of breast cancer patients under trastuzumab therapy was developed within our group. The reported sensor showed a capability to discriminate positive/negative patients similar to the one obtained by ELISA. By adapting the strategy to a modular design,

we also reported on the detection of small molecules (i.e., antigen) using the same assay through a competitive format [156].

Taking advantage of the proximity effect, Ricci's group also used proteins and bivalent antibodies to control DNA-templated chemical reactions [157, 158]. In their first reported strategy, bivalent binding of a specific IgG antibody to a pair of antigen-conjugated DNA templating strands colocalizes the reactants (the DNA strands) to trigger the copper(I)-catalyzed azide-alkyne cycloaddition (CuAAC) reaction between the reactive elements posed at the 3′- and 5-DNA ends [157]. The confinement of the reactant at the nanoscale due to the DNA hybridization controlled by target antibodies basically increases the effective molarity of reactants, thus allowing the reaction to occur at that concentration (low nanomolar range). The method was characterized by versatility and orthogonality, moreover, by synthesizing the thrombin-binding aptamer, a molecule with potential therapeutic, the authors demonstrated potential utility of their strategy to control the synthesis of functional molecules with specific antibodies. In a follow-up work, the authors also demonstrated the generalizability of their strategy by using protein to control a set of DNA-templated reactions [158]. Following the same concept, our group has recently designed an electrochemical device for the rapid, single-step, and multiplex detection of clinically relevant antibodies in human serum sample [159]. As shown in Fig. 6c, the simultaneous recognition of an antibody target by two antigen-conjugated DNA scaffolds provides a means to induce proximity-dependent DNA hybridization at the electrode interface. By doing so, the redox-labelled DNA scaffold free in solution comes into close proximity to the electrode surface producing an enhanced current signal that is proportional to the antibody concentration. This molecular design clearly demonstrates the impact of the proximity effect on hybridization efficiency, as lower binding affinity (higher *K*d) is reported for the two scaffold DNAs in the absence of the antibody, whereas improved binding affinity is detected in the presence of target antibody in a concentration-dependent fashion.

Similarly, electrochemical proximity assays relying on simultaneous binding of two antibody-modified nucleic acid probes to the same protein can be developed to bring a redox reported into close proximity to the electrode surface. Using this approach, thrombin and insulin were monitored down to the picomolar and femtomolar ranges of concentration, respectively [160, 161]. Furthermore, different proximity assays have been deployed into electro chemiluminescent [162], photoelectrochemical [163], and electrochemical [164] assays to measure alpha-fetoprotein, insulin, prostate-specific antigen proteins, respectively. Although proximity effect offers high selectivity and enhanced sensitivity and allows to monitor a broad range of proteins, the requirement of two distinct binding sites on the same target, the signal might decline at certain regimes of high target-to-probe ratio as analyte excess can drive proximity complexes apart since each target will statistically bind preferentially one of the two strands and not both of them. Besides, the challenging conjugation of certain ligands to the DNA scaffold still represents a potential limitation in some cases [165].

6 Conclusions

The rational design of functional nanostructures and structure-switching probes can be harnessed to develop biosensing platforms for protein detection. Taking advantage of the predictability of DNA interactions and of recent progress in the chemistry of nucleic acids, especially with respect to biomolecule and small molecule conjugation, we are now able to finely control the spatial organization of responsive molecular components into a DNA-based scaffold, as well to predict the dynamic behavior of switchable DNA-based elements upon target binding.

Here, we showed a number of structure-switching DNA probes and programmable DNA scaffold systems with different levels of complexity (2D DNA nanostructures, DNA origami, beacons, etc.) employed to organize molecules (i.e., enzymes, antigens, and peptides) with nanometer precision for biosensing. We believe that in the near future, it will be possible to translate such analytical assays into real and commercially available sensing platforms.

References

1. Lequin RM (2005) Enzyme immunoassay (EIA)/enzyme-linked immunosorbent assay (ELISA). Clin Chem 51:2415–2418. https://doi.org/10.1373/clinchem.2005.051532
2. Vanova V, Mitrevska K, Milosavljevic V, Hynek D, Richtera L, Adam V (2021) Peptide-based electrochemical biosensors utilized for protein detection. Biosens Bioelectron 180: 113087. https://doi.org/10.1016/j.bios.2021.113087
3. Strehlitz B, Nikolaus N, Stoltenburg R (2008) Protein detection with aptamer. Biosens Sens 8: 4296–4307. https://www.mdpi.com/1424-8220/8/7/4296
4. Leca-Bouvier B, Blum LJ (2005) Biosensors for protein detection: a review. Anal Lett 38: 1491–1517. https://doi.org/10.1081/AL-200065780
5. Fortunati S, Pedrini F, Del Grosso E, Baranda Pellejero L, Bertucci A (2022) Design of specific nucleic acid-based biosensors for protein binding activity. Anal Sens 2:e202200037. https://doi.org/10.1002/anse.202200037
6. Thévenot DR, Toth K, Durst RA, Wilson GS (2001) Electrochemical biosensors: recommended definitions and classification 1st International Union of Pure and Applied Chemistry: Physical Chemistry Division, Commission I.7 (Biophysical Chemistry); Analytical Chemistry Division, Commission V.5 (Electroanalytical). Biosens Bioelectron 16:121–131. https://doi.org/10.1016/S0956-5663(01)00115-4
7. Turner APF (2013) Biosensors: sense and sensibility. Chem Soc Rev 42:3184–3196. https://doi.org/10.1039/c3cs35528d
8. Justino CIL, Rocha-Santos TA, Duarte AC, Rocha-Santos TA (2010) Review of analytical figures of merit of sensors and biosensors in clinical applications. Trends Anal Chem 29:1172–1183. https://doi.org/10.1016/j.trac.2010.07.008
9. Arakawa T, Dao DV, Mitsubayashi K (2022) Biosensors and chemical sensors for healthcare monitoring: a review. IEEJ Trans Electr Electron Eng 17:626–636. https://doi.org/10.1002/tee.23580
10. Rosati G, Idili A, Parolo C, Fuentes-Chust C, Calucho E, Hu L, Castro e Silva C d C, Rivas L, Nguyen EP, Bergua JF, Alvárez-Diduk R, Muñoz J, Junot C, Penon O, Monferrer D, Delamarche E, Merkoçi A (2021) Nanodiagnostics to face SARS-CoV-2 and future

pandemics: from an idea to the market and beyond. ACS Nano 15:17137–17149. https://doi.org/10.1021/acsnano.1c06839
11. Sezgintürk MK (2020) Chapter one – introduction to commercial biosensors. In: Sezgintürk MKBT-CB, TA (ed) Commercial biosensors and their applications. Elsevier, pp 1–28. https://doi.org/10.1016/B978-0-12-818592-6.00001-3
12. Vallée-Bélisle A, Plaxco KW (2010) Structure-switching biosensors: inspired by nature. Curr Opin Struct Biol 20:518–526. https://doi.org/10.1016/j.sbi.2010.05.001
13. Masson JF (2017) Surface Plasmon resonance clinical biosensors for medical diagnostics. ACS Sensors 2:16–30. https://pubs.acs.org/doi/10.1021/acssensors.6b00763
14. Manimekala T, Sivasubramanian R, Dharmalingam G (2022) Nanomaterial-based biosensors using field-effect transistors: a review. J Electron Mater 51:1950–1973. https://doi.org/10.1007/s11664-022-09492-z
15. Alvarez M, Lechuga LM (2010) Microcantilever-based platforms as biosensing tools. Analyst 135:827–836. https://doi.org/10.1039/B908503N
16. Plaxco KW, Soh HT (2011) Switch based biosensors: a new approach towards real-time, in vivo molecular detection. Trends Biotechnol 29:1–5. https://doi.org/10.1016/j.tibtech.2010.10.005
17. Gerstein M, Krebs W (1998) A database of macromolecular motions. Nucleic Acids Res 26:4280–4290. https://doi.org/10.1093/nar/26.18.4280
18. Tyagi S, Kramer FR (1996) Molecular beacons: probes that fluoresce upon hybridization. Nat Biotechnol 14:303–308. https://doi.org/10.1038/nbt0396-303
19. Yoshida W, Sode K, Ikebukuro K (2006) Aptameric enzyme subunit for biosensing based on enzymatic activity measurement. Anal Chem 78:3296–3303. https://doi.org/10.1021/ac060254o
20. Stein V, Alexandrov K (2015) Synthetic protein switches: design principles and applications. Trends Biotechnol 33:101–110. https://doi.org/10.1016/j.tibtech.2014.11.010
21. Stein V (2017) Synthetic protein switches: methods and protocols.1st edn. Humana, New York. https://doi.org/10.1007/978-1-4939-6940-1
22. Beaucage SL, Caruthers MH (1981) Deoxynucleoside phosphoramidites – a new class of key intermediates for deoxypolynucleotide synthesis. Tetrahedron Lett 22:1859–1862. https://doi.org/10.1016/S0040-4039(01)90461-7
23. Kosuri S, Church GM (2014) Large-scale de novo DNA synthesis: technologies and applications. Nat Methods 11:499–507. https://doi.org/10.1038/nmeth.2918
24. Zhang Z, Sen P, Adhikari BR, Li Y, Soleymani L (2022) Development of nucleic-acid-based electrochemical biosensors for clinical applications. Angew Chem Int Ed:e202212496. https://doi.org/10.1002/anie.202212496
25. Parolo C, Idili A, Ortega G, Csordas A, Hsu A, Arroyo-Currás N, Yang Q, Ferguson BS, Wang J, Plaxco KW (2020) Real-time monitoring of a protein biomarker. ACS Sensors 5:1877–1881. https://doi.org/10.1021/acssensors.0c01085
26. Vallée-Bélisle A, Ricci F, Plaxco KW (2009) Thermodynamic basis for the optimization of binding-induced biomolecular switches and structure-switching biosensors. Proc Natl Acad Sci 106:13802–13807. https://doi.org/10.1073/pnas.0904005106
27. Harroun SG, Prévost-Tremblay C, Lauzon D, Desrosiers A, Wang X, Pedro L, Vallée-Bélisle A (2018) Programmable DNA switches and their applications. Nanoscale 10:4607–4641
28. Idili A, Ricci F, Vallée-Bélisle A (2017) Determining the folding and binding free energy of DNA-based nanodevices and nanoswitches using urea titration curves. Nucleic Acids Res 45:7571–7580. https://doi.org/10.1093/nar/gkx498
29. You Y, Tataurov AV, Owczarzy R (2011) Measuring thermodynamic details of DNA hybridization using fluorescence. Biopolymers 95:472–486. https://doi.org/10.1002/bip.21615
30. Feagin TA, Maganzini N, Soh HT (2018) Strategies for creating structure-switching aptamers. ACS Sensors 3:1611–1615. https://doi.org/10.1021/acssensors.8b00516

31. Munzar JD, Ng A, Juncker D (2019) Duplexed aptamers: history, design, theory, and application to biosensing. Chem Soc Rev 48:1390–1419. https://doi.org/10.1039/C8CS00880A
32. Lackey HH, Peterson EM, Harris JM, Heemstra JM (2020) Probing the mechanism of structure-switching aptamer assembly by super-resolution localization of individual DNA molecules. Anal Chem 92:6909–6917. https://doi.org/10.1021/acs.analchem.9b05563
33. Munzar JD, Ng A, Corrado M, Juncker D (2017) Complementary oligonucleotides regulate induced fit ligand binding in duplexed aptamers. Chem Sci 8:2251–2256. https://doi.org/10.1039/C6SC03993F
34. Dillen A, Vandezande W, Daems D, Lammertyn J (2021) Unraveling the effect of the aptamer complementary element on the performance of duplexed aptamers: a thermodynamic study. Anal Bioanal Chem 413:4739–4750. https://doi.org/10.1007/s00216-021-03444-y
35. Xiao Y, Lou X, Uzawa T, Plakos KJI, Plaxco KW, Soh HT (2009) An electrochemical sensor for single nucleotide polymorphism detection in serum based on a triple-stem DNA probe. J Am Chem Soc 131:15311–15316. https://doi.org/10.1021/ja905068s
36. Jiang B, Li F, Yang C, Xie J, Xiang Y, Yuan R (2015) Aptamer pseudoknot-functionalized electronic sensor for reagentless and single-step detection of immunoglobulin E in human serum. Anal Chem 87:3094–3098. https://doi.org/10.1021/acs.analchem.5b00041
37. Hamaguchi N, Ellington A, Stanton M (2001) Aptamer beacons for the direct detection of proteins. Anal Biochem 294:126–131. https://doi.org/10.1006/abio.2001.5169
38. Xiao Y, Lubin AA, Heeger AJ, Plaxco KW (2005) Label-free electronic detection of thrombin in blood serum by using an aptamer-based sensor. Angew Chem Int Ed 44:5456–5459. https://doi.org/10.1002/anie.200500989
39. Debiais M, Lelievre A, Smietana M, Müller S (2020) Splitting aptamers and nucleic acid enzymes for the development of advanced biosensors. Nucleic Acids Res 48:3400–3422. https://doi.org/10.1093/nar/gkaa132
40. Stojanovic MN, de Prada P, Landry DW (2000) Fluorescent sensors based on aptamer self-assembly. J Am Chem Soc 122:11547–11548. https://doi.org/10.1021/ja0022223
41. Yang K-A, Barbu M, Halim M, Pallavi P, Kim B, Kolpashchikov DM, Pecic S, Taylor S, Worgall TS, Stojanovic MN (2014) Recognition and sensing of low-epitope targets via ternary complexes with oligonucleotides and synthetic receptors. Nat Chem 6:1003–1008. https://doi.org/10.1038/nchem.2058
42. Oh SS, Plakos K, Lou X, Xiao Y, Soh HT (2010) In vitro selection of structure-switching, self-reporting aptamers. Proc Natl Acad Sci 107:14053–14058. https://doi.org/10.1073/pnas.1009172107
43. Sanford AA, Rangel AE, Feagin TA, Lowery RG, Argueta-Gonzalez HS, Heemstra JM (2021) RE-SELEX: restriction enzyme-based evolution of structure-switching aptamer biosensors. Chem Sci 12:11692–11702. https://doi.org/10.1039/D1SC02715H
44. Idili A, Arroyo-Currás N, Ploense KL, Csordas AT, Kuwahara M, Kippin TE, Plaxco KW (2019) Seconds-resolved pharmacokinetic measurements of the chemotherapeutic irinotecan: in situ in the living body. Chem Sci 10:8164–8170. https://doi.org/10.1039/c9sc01495k
45. Dauphin-Ducharme P, Yang K, Arroyo-Currás N, Ploense KL, Zhang Y, Gerson J, Kurnik M, Kippin TE, Stojanovic MN, Plaxco KW (2019) Electrochemical aptamer-based sensors for improved therapeutic drug monitoring and high-precision, feedback-controlled drug delivery. ACS Sensors 4:2832–2837. https://doi.org/10.1021/acssensors.9b01616
46. Wu Y, Ranallo S, Del Grosso E, Chamoro-Garcia A, Ennis HL, Milosavić N, Yang K, Kippin T, Ricci F, Stojanovic M, Plaxco KW (2022) Using spectroscopy to guide the adaptation of aptamers into electrochemical aptamer-based sensors. Bioconjug Chem. https://doi.org/10.1021/acs.bioconjchem.2c00275
47. Arroyo-Currás N, Dauphin-Ducharme P, Scida K, Chávez JL (2020) From the beaker to the body: translational challenges for electrochemical, aptamer-based sensors. Anal Methods 12:1288–1310. https://doi.org/10.1039/D0AY00026D

48. Bayat P, Nosrati R, Alibolandi M, Rafatpanah H, Abnous K, Khedri M, Ramezani M (2018) SELEX methods on the road to protein targeting with nucleic acid aptamers. Biochimie 154: 132–155. https://doi.org/10.1016/j.biochi.2018.09.001
49. Wu Y, Belmonte I, Sykes KS, Xiao Y, White RJ (2019) Perspective on the future role of aptamers in analytical chemistry. Anal Chem 91:15335–15344. https://doi.org/10.1021/acs.analchem.9b03853
50. Keefe AD, Pai S, Ellington A (2010) Aptamers as therapeutics. Nat Rev Drug Discov 9:537–550. https://doi.org/10.1038/nrd3141
51. Liu S, Xu Y, Jiang X, Tan H, Ying B (2022) Translation of aptamers toward clinical diagnosis and commercialization. Biosens Bioelectron 208:114168. https://doi.org/10.1016/j.bios.2022.114168
52. Yu H, Yang W, Alkhamis O, Canoura J, Yang KA, Xiao Y (2018) In vitro isolation of small-molecule-binding aptamers with intrinsic dye-displacement functionality. Nucleic Acids Res 46:E43. https://doi.org/10.1093/NAR/GKY026
53. Nutiu R, Li Y (2005) In vitro selection of structure-switching signaling aptamers. Angew Chem Int Ed 44:1061–1065. https://doi.org/10.1002/anie.200461848
54. Martini L, Meyer AJ, Ellefson JW, Milligan JN, Forlin M, Ellington AD, Mansy SS (2015) In vitro selection for small-molecule-triggered Strand displacement and riboswitch activity. ACS Synth Biol 4:1144–1150. https://doi.org/10.1021/acssynbio.5b00054
55. Stoltenburg R, Nikolaus N, Strehlitz B (2012) Capture-SELEX: selection of DNA aptamers for aminoglycoside antibiotics. J Anal Methods Chem 1. https://doi.org/10.1155/2012/415697
56. Qu H, Csordas AT, Wang J, Oh SS, Eisenstein MS, Soh HT (2016) Rapid and label-free strategy to isolate aptamers for metal ions. ACS Nano 10:7558–7565. https://doi.org/10.1021/acsnano.6b02558
57. Li JJ, Fang X, Schuster SM, Tan W (2000) Molecular beacons: a novel approach to detect protein – DNA interactions. Angew Chem Int Ed 39:1049–1052. https://doi.org/10.1002/(SICI)1521-3773(20000317)39:6<1049::AID-ANIE1049>3.0.CO;2-2
58. Nutiu R, Li Y (2003) Structure-switching signaling aptamers. J Am Chem Soc 125:4771–4778. https://doi.org/10.1021/ja028962o
59. Li JJ, Fang X, Tan W (2002) Molecular aptamer beacons for real-time protein recognition. Biochem Biophys Res Commun 292:31–40. https://doi.org/10.1006/bbrc.2002.6581
60. Giannetti A, Tombelli S (2021) Aptamer optical switches: from biosensing to intracellular sensing. Sens Actuators Rep 3. https://doi.org/10.1016/j.snr.2021.100030
61. Deng B, Lin Y, Wang C, Li F, Wang Z, Zhang H, Li XF, Le XC (2014) Aptamer binding assays for proteins: the thrombin example – a review. Anal Chim Acta 837:1–15. https://doi.org/10.1016/j.aca.2014.04.055
62. Zheng J, Yang R, Shi M, Wu C, Fang X, Li Y, Li J, Tan W (2015) Rationally designed molecular beacons for bioanalytical and biomedical applications. Chem Soc Rev 44:3036–3055. https://doi.org/10.1039/c5cs00020c
63. Li L, Jiang Y, Cui C, Yang Y, Zhang P, Stewart K, Pan X, Li X, Yang L, Qiu L, Tan W (2018) Modulating aptamer specificity with pH-responsive DNA bonds. J Am Chem Soc 140:13335–13339. https://doi.org/10.1021/jacs.8b08047
64. Li Y, Fang Q, Miao X, Zhang X, Zhao Y, Yan J, Zhang Y, Wu R, Nie B, Hirtz M, Liu J (2019) Aptamer conformation-cooperated enzyme-assisted surface-enhanced Raman scattering enabling ultrasensitive detection of cell surface protein biomarkers in blood samples. ACS Sensors 4:2605–2614. https://doi.org/10.1021/acssensors.9b00604
65. Huizenga DE, Szostak JW (1995) A DNA aptamer that binds adenosine and ATP. Biochemistry 34:656–665. https://doi.org/10.1021/bi00002a033
66. Chen A, Yan M, Yang S (2016) Split aptamers and their applications in sandwich aptasensors. Trends Anal Chem 80:581–593. https://doi.org/10.1016/j.trac.2016.04.006
67. Liu J, Liu Y, Yang X, Wang K, Wang Q, Shi H, Li L (2013) Exciton energy transfer-based fluorescent sensing through aptamer-programmed self-assembly of quantum dots. Anal Chem 85:11121–11128. https://doi.org/10.1021/ac403023p

68. Zhang QL, Wang LL, Liu Y, Lin J, Xu L (2021) A kinetically controlled platform for ligand-oligonucleotide transduction. Nat Commun 12:1–11. https://doi.org/10.1038/s41467-021-24962-4
69. Zheng D, Seferos DS, Giljohann DA, Patel PC, Mirkin CA (2009) Aptamer nano-flares for molecular detection in living cells. Nano Lett 9:3258–3261. https://doi.org/10.1021/nl901517b
70. Shi H, He X, Wang K, Wu X, Ye X, Guo Q, Tan W, Qing Z, Yang X, Zhou B (2011) Activatable aptamer probe for contrast-enhanced in vivo cancer imaging based on cell membrane protein-triggered conformation alteration. Proc Natl Acad Sci U S A 108:3900–3905. https://doi.org/10.1073/pnas.1016197108
71. Wang J, Zhu G, You M, Song E, Shukoor MI, Zhang K, Altman MB, Chen Y, Zhu Z, Huang CZ, Tan W (2012) Assembly of aptamer switch probes and photosensitizer on gold nanorods for targeted photothermal and photodynamic cancer therapy. ACS Nano 6:5070–5077. https://doi.org/10.1021/nn300694v
72. Zhang J, Smaga LP, Satyavolu NSR, Chan J, Lu Y (2017) DNA aptamer-based activatable probes for photoacoustic imaging in living mice. J Am Chem Soc 139:17225–17228. https://doi.org/10.1021/jacs.7b07913
73. Baker BR, Lai RY, Wood MS, Doctor EH, Heeger AJ, Plaxco KW (2006) An electronic, aptamer-based small-molecule sensor for the rapid, label-free detection of cocaine in adulterated samples and biological fluids. J Am Chem Soc 128:3138–3139. https://doi.org/10.1021/ja056957p
74. Xiao Y, Piorek BD, Plaxco KW, Heegert AJ (2005) A reagentless signal-on architecture for electronic, aptamer-based sensors via target-induced strand displacement. J Am Chem Soc 127:17990–17991. https://doi.org/10.1021/ja056555h
75. Plaxco KW, Idili A, Gerson J, Kippin T (2021) Seconds-resolved, in situ measurements of plasma phenylalanine disposition kinetics in living rats. Anal Chem 93:4023–4032. https://doi.org/10.1021/acs.analchem.0c05024
76. Arroyo-Currás N, Dauphin-Ducharme P, Ortega G, Ploense KL, Kippin TE, Plaxco KW (2018) Subsecond-resolved molecular measurements in the living body using chronoamperometrically interrogated aptamer-based sensors. ACS Sensors 3:360–366. https://doi.org/10.1021/acssensors.7b00787
77. Li H, Dauphin-Ducharme P, Arroyo-Currás N, Tran CH, Vieira PA, Li S, Shin C, Somerson J, Kippin TE, Plaxco KW (2017) A biomimetic phosphatidylcholine-terminated monolayer greatly improves the in vivo performance of electrochemical aptamer-based sensors. Angew Chem Int Ed 56:7492–7495. https://doi.org/10.1002/anie.201700748
78. Arroyo-Currás N, Somerson J, Vieira PA, Ploense KL, Kippin TE, Plaxco KW (2017) Real-time measurement of small molecules directly in awake, ambulatory animals. Proc Natl Acad Sci U S A 114:645–650. https://doi.org/10.1073/pnas.1613458114
79. White RJ, Phares N, Lubin AA, Xiao Y, Plaxco KW (2008) Optimization of electrochemical aptamer-based sensors via optimization of probe packing density and surface chemistry. Langmuir. https://doi.org/10.1021/la800801v
80. Chamorro-Garcia A, Gerson J, Flatebo C, Fetter L, Downs AM, Emmons N, Ennis HL, Milosavić N, Yang K, Stojanovic M, Ricci F, Kippin TE, Plaxco KW (2023) Real-time, seconds-resolved measurements of plasma methotrexate in situ in the living body. ACS Sensors 8:150–157. https://doi.org/10.1021/acssensors.2c01894
81. Xiao Y, Lai RY, Plaxco KW (2007) Preparation of electrode-immobilized, redox-modified oligonucleotides for electrochemical DNA and aptamer-based sensing. Nat Protoc 2:2875–2880. https://doi.org/10.1038/nprot.2007.413
82. Lai RY, Plaxco KW, Heeger AJ (2007) Aptamer-based electrochemical detection of picomolar platelet-derived growth factor directly in blood serum. Anal Chem 79:229–233. https://doi.org/10.1021/ac061592s

83. Liu Y, Tuleouva N, Ramanculov E, Revzin A (2010) Aptamer-based electrochemical biosensor for interferon gamma detection. Anal Chem 82:8131–8136. https://doi.org/10.1021/ac101409t
84. Liu Y, Zhou Q, Revzin A (2013) An aptasensor for electrochemical detection of tumor necrosis factor in human blood. Analyst 138:4321–4326. https://doi.org/10.1039/C3AN00818E
85. Ma F, Ho C, Cheng AKH, Yu H-Z (2013) Immobilization of redox-labeled hairpin DNA aptamers on gold: electrochemical quantitation of epithelial tumor marker mucin 1. Electrochim Acta 110:139–145. https://doi.org/10.1016/j.electacta.2013.02.088
86. Zhao S, Yang W, Lai RY (2011) A folding-based electrochemical aptasensor for detection of vascular endothelial growth factor in human whole blood. Biosens Bioelectron 26:2442–2447. https://doi.org/10.1016/j.bios.2010.10.029
87. Idili A, Parolo C, Alvarez-Diduk R, Merkoçi A (2021) Rapid and efficient detection of the SARS-CoV-2 spike protein using an electrochemical aptamer-based sensor. ACS Sensors 6:3093–3101. https://doi.org/10.1021/acssensors.1c01222
88. Ricci F, Vallée-Bélisle A, Simon AJ, Porchetta A, Plaxco KW (2016) Using Nature's "Tricks" to rationally tune the binding properties of biomolecular receptors. Acc Chem Res 49:1884–1892. https://doi.org/10.1021/acs.accounts.6b00276
89. Ortega G, Chamorro-Garcia A, Ricci F, Plaxco KW (2023) On the rational design of cooperative receptors. Annu Rev Biophys. https://doi.org/10.1146/annurev-biophys-091222-082247
90. Luo X, Morrin A, Killard AJ, Smyth MR (2006) Application of nanoparticles in electrochemical sensors and biosensors. Electroanalysis 18:319–326. https://doi.org/10.1002/elan.200503415
91. Zhu C, Yang G, Li H, Du D, Lin Y (2015) Electrochemical sensors and biosensors based on nanomaterials and nanostructures. Anal Chem 87:230–249. https://doi.org/10.1021/ac5039863
92. Bin X, Sargent EH, Kelley SO (2010) Nanostructuring of sensors determines the efficiency of biomolecular capture. Anal Chem 82:5928–5931. https://doi.org/10.1021/ac101164n
93. Farnham PJ (2009) Insights from genomic profiling of transcription factors. Nat Rev Genet 10:605–616. https://doi.org/10.1038/nrg2636
94. Vallée-Bélisle A, Bonham AJ, Reich NO, Ricci F, Plaxco KW (2011) Transcription factor beacons for the quantitative detection of DNA binding activity. J Am Chem Soc 133:13836–13839. https://doi.org/10.1021/ja204775k
95. Bonham AJ, Hsieh K, Ferguson BS, Vallée-Bélisle A, Ricci F, Soh HT, Plaxco KW (2012) Quantification of transcription factor binding in cell extracts using an electrochemical, structure-switching biosensor. J Am Chem Soc 134:3346–3348. https://doi.org/10.1021/ja2115663
96. Li B, Xie S, Xia A, Suo T, Huang H, Zhang X, Chen Y, Zhou X (2020) Recent advance in the sensing of biomarker transcription factors. Trends Anal Chem 132:116039. https://doi.org/10.1038/nrg2636
97. Bertucci A, Guo J, Oppmann N, Glab A, Ricci F, Caruso F, Cavalieri F (2018) Probing transcription factor binding activity and downstream gene silencing in living cells with a DNA nanoswitch. Nanoscale 10:2034–2044. https://doi.org/10.1039/c7nr07814e
98. Glab A, Bertucci A, Martino F, Wojnilowicz M, Amodio A, Venanzi M, Ricci F, Forte G, Caruso F, Cavalieri F (2020) Dissecting the intracellular signalling and fate of a DNA nanosensor by super-resolution and quantitative microscopy. Nanoscale 12:15402–15413. https://doi.org/10.1039/d0nr03087b
99. Bertucci A, Porchetta A, Del Grosso E, Patiño T, Idili A, Ricci F (2020) Protein-controlled actuation of dynamic nucleic acid networks by using synthetic DNA translators. Angew Chem 132:20758–20762. https://doi.org/10.1002/ange.202008553

100. Adornetto G, Porchetta A, Palleschi G, Plaxco KW, Ricci F (2015) A general approach to the design of allosteric, transcription factor-regulated DNAzymes. Chem Sci 6:3692–3696. https://doi.org/10.1039/C5SC00228A
101. Li B, Chen Y, Wang J, Lu Q, Zhu W, Luo J, Hong J, Zhou X (2019) Detecting transcription factors with allosteric DNA-silver nanocluster switches. Anal Chim Acta 1048:168–177. https://doi.org/10.1016/j.aca.2018.10.023
102. Ciccia A, Elledge SJ (2010) The DNA damage response: making it safe to play with knives. Mol Cell 40:179–204. https://doi.org/10.1016/j.molcel.2010.09.019
103. Hoeijmakers JHJ (2001) Genome maintenance mechanisms for preventing cancer. Nature 411: 366–374. https://doi.org/10.1038/35077232
104. Parsons JL, Tait PS, Finch D, Dianova II, Allinson SL, Dianov GL (2008) CHIP-mediated degradation and DNA damage-dependent stabilization regulate base excision repair proteins. Mol Cell 29:477–487. https://doi.org/10.1016/j.molcel.2007.12.027
105. Kunkel TA, Erie DA (2005) DNA mismatch repair. Annu Rev Biochem 74:681–710. https://doi.org/10.1146/annurev.biochem.74.082803.133243
106. de Laat WL, Jaspers NGJ, Hoeijmakers JHJ (1999) Molecular mechanism of nucleotide excision repair. Genes Dev 13:768–785. https://genesdev.cshlp.org/content/13/7/768
107. Gerson SL (2004) MGMT: its role in cancer aetiology and cancer therapeutics. Nat Rev Cancer 4:296–307. https://doi.org/10.1038/nrc1319
108. Mateo J, Carreira S, Sandhu S, Miranda S, Mossop H, Perez-Lopez R, Nava Rodrigues D, Robinson D, Omlin A, Tunariu N, Boysen G, Porta N, Flohr P, Gillman A, Figueiredo I, Paulding C, Seed G, Jain S, Ralph C, Protheroe A, Hussain S, Jones R, Elliott T, McGovern U, Bianchini D, Goodall J, Zafeiriou Z, Williamson CT, Ferraldeschi R, Riisnaes R, Ebbs B, Fowler G, Roda D, Yuan W, Wu Y-M, Cao X, Brough R, Pemberton H, A'Hern R, Swain A, Kunju LP, Eeles R, Attard G, Lord CJ, Ashworth A, Rubin MA, Knudsen KE, Feng FY, Chinnaiyan AM, Hall E, de Bono JS (2015) DNA-repair defects and olaparib in metastatic prostate cancer. N Engl J Med 373:1697–1708. https://doi.org/10.1056/NEJMoa1506859
109. Kiwerska K, Szyfter K (2019) DNA repair in cancer initiation, progression, and therapy – a double-edged sword. J Appl Genet 60:329–334. https://doi.org/10.1007/s13353-019-00516-9
110. Helleday T, Petermann E, Lundin C, Hodgson B, Sharma RA (2008) DNA repair pathways as targets for cancer therapy. Nat Rev Cancer 8:193–204. https://doi.org/10.1038/nrc2342
111. Paz-Elizur T, Elinger D, Leitner-Dagan Y, Blumenstein S, Krupsky M, Berrebi A, Schechtman E, Livneh Z (2007) Development of an enzymatic DNA repair assay for molecular epidemiology studies: distribution of OGG activity in healthy individuals. DNA Repair (Amst) 6:45–60. https://doi.org/10.1016/j.dnarep.2006.08.003
112. Wilson DL, Kool ET (2018) Fluorescent probes of DNA repair. ACS Chem Biol 13:1721–1733. https://doi.org/10.1021/acschembio.7b00919
113. Hu D, Huang Z, Pu F, Ren J, Qu X (2011) A label-free, quadruplex-based functional molecular beacon (LFG4-MB) for fluorescence turn-on detection of DNA and nuclease. Chem A Eur J 17:1635–1641. https://doi.org/10.1002/chem.201001331
114. Lu YJ, Hu DP, Deng Q, Wang ZY, Huang BH, Fang YX, Zhang K, Wong WL (2015) Sensitive and selective detection of uracil-DNA glycosylase activity with a new pyridinium luminescent switch-on molecular probe. Analyst 140:5998–6004. https://doi.org/10.1039/c5an01158b
115. Leung KH, He HZ, Ma VPY, Zhong HJ, Chan DSH, Zhou J, Mergny JL, Leung CH, Ma DL (2013) Detection of base excision repair enzyme activity using a luminescent g-quadruplex selective switch-on probe. Chem Commun 49:5630–5632. https://doi.org/10.1039/c3cc41129j
116. He HZ, Leung KH, Wang W, Chan DSH, Leung CH, Ma DL (2014) Label-free luminescence switch-on detection of T4 polynucleotide kinase activity using a G-quadruplex-selective probe. Chem Commun 50:5313–5315. https://doi.org/10.1039/c3cc47444e
117. Lu L, Shiu-Hin Chan D, Kwong DWJ, He H-Z, Leung C-H, Ma D-L (2014) Detection of nicking endonuclease activity using a G-quadruplex-selective luminescent switch-on probe. Chem Sci 5:4561–4568. https://doi.org/10.1039/C4SC02032D

118. Farag N, Mattossovich R, Merlo R, Nierzwicki Ł, Palermo G, Porchetta A, Perugino G, Ricci F (2021) Folding-upon-repair DNA nanoswitches for monitoring the activity of DNA repair enzymes. Angew Chem Int Ed 60:7283–7289. https://doi.org/10.1002/anie.202016223
119. Wang X, Yi X, Huang Z, He J, Wu Z, Chu X, Jiang JH (2021) "Repaired and Activated" DNAzyme enables the monitoring of DNA alkylation repair in live cells. Angew Chem Int Ed 60:19889–19896. https://doi.org/10.1002/anie.202106557
120. Huang J, Wang J, Wu Z, He J, Jiang JH (2022) Profiling demethylase activity using epigenetically inactivated DNAzyme. Biosens Bioelectron 207. https://doi.org/10.1016/j.bios.2022.114186
121. Seeman NC, Sleiman HF (2017) DNA nanotechnology. Nat Rev Mater 3:17068. https://doi.org/10.1038/natrevmats.2017.68
122. Lu C-H, Cecconello A, Willner I (2016) Recent advances in the synthesis and functions of reconfigurable interlocked DNA nanostructures. J Am Chem Soc 138:5172–5185. https://doi.org/10.1021/jacs.6b00694
123. Hong F, Zhang F, Liu Y, Yan H (2017) DNA origami: scaffolds for creating higher order structures. Chem Rev 117:12584–12640. https://doi.org/10.1021/acs.chemrev.6b00825
124. Takahashi S, Sugimoto N (2021) Watson–Crick versus Hoogsteen base pairs: chemical strategy to encode and express genetic information in life. Acc Chem Res 54:2110–2120. https://doi.org/10.1021/acs.accounts.0c00734
125. Zhang H, Li F, Dever B, Wang C, Li X-F, Le XC (2013) Assembling DNA through affinity binding to achieve ultrasensitive protein detection. Angew Chem Int Ed 52:10698–10705. https://doi.org/10.1002/anie.201210022
126. Seeman NC (1982) Nucleic acid junctions and lattices. J Theor Biol 99:237–247. https://doi.org/10.1016/0022-5193(82)90002-9
127. Seeman NC (2003) DNA in a material world. Nature 421:427–431. https://doi.org/10.1038/nature01406
128. Green LN, Subramanian HKK, Mardanlou V, Kim J, Hariadi RF, Franco E (2019) Autonomous dynamic control of DNA nanostructure self-assembly. Nat Chem 11:510–520. https://doi.org/10.1038/s41557-019-0251-8
129. Gentile S, Del Grosso E, Prins LJ, Ricci F (2021) Reorganization of self-assembled DNA-based polymers using orthogonally addressable building blocks. Angew Chem Int Ed 60:12911–12917. https://doi.org/10.1002/anie.202101378
130. Ranallo S, Sorrentino D, Ricci F (2019) Orthogonal regulation of DNA nanostructure self-assembly and disassembly using antibodies. Nat Commun 10:5509. https://doi.org/10.1038/s41467-019-13104-6
131. Rothemund PWK (2006) Folding DNA to create nanoscale shapes and patterns. Nature 440:297–302. https://doi.org/10.1038/nature04586
132. Dey S, Fan C, Gothelf KV, Li J, Lin C, Liu L, Liu N, Nijenhuis MAD, Saccà B, Simmel FC, Yan H, Zhan P (2021) DNA origami. Nat Rev Methods Prim 1:13. https://doi.org/10.1038/s43586-020-00009-8
133. Douglas SM, Marblestone AH, Teerapittayanon S, Vazquez A, Church GM, Shih WM (2009) Rapid prototyping of 3D DNA-origami shapes with caDNAno. Nucleic Acids Res 37:5001–5006. https://doi.org/10.1093/nar/gkp436
134. Zhao Z, Fu J, Dhakal S, Johnson-Buck A, Liu M, Zhang T, Woodbury NW, Liu Y, Walter NG, Yan H (2016) Nanocaged enzymes with enhanced catalytic activity and increased stability against protease digestion. Nat Commun 7:10619. https://doi.org/10.1038/ncomms10619
135. Ijäs H, Hakaste I, Shen B, Kostiainen MA, Linko V (2019) Reconfigurable DNA origami nanocapsule for pH-controlled encapsulation and display of cargo. ACS Nano 13:5959–5967. https://doi.org/10.1021/acsnano.9b01857
136. Grossi G, Dalgaard Ebbesen Jepsen M, Kjems J, Andersen ES (2017) Control of enzyme reactions by a reconfigurable DNA nanovault. Nat Commun 8:992. https://doi.org/10.1038/s41467-017-01072-8

137. Lanphere C, Offenbartl-Stiegert D, Dorey A, Pugh G, Georgiou E, Xing Y, Burns JR, Howorka S (2021) Design, assembly, and characterization of membrane-spanning DNA nanopores. Nat Protoc 16:86–130. https://doi.org/10.1038/s41596-020-0331-7
138. Xing Y, Dorey A, Jayasinghe L, Howorka S (2022) Highly shape- and size-tunable membrane nanopores made with DNA. Nat Nanotechnol 17:708–713. https://doi.org/10.1038/s41565-022-01116-1
139. Selnihhin D, Sparvath SM, Preus S, Birkedal V, Andersen ES (2018) Multifluorophore DNA origami beacon as a biosensing platform. ACS Nano 12:5699–5708. https://doi.org/10.1021/acsnano.8b01510
140. Cash KJ, Ricci F, Plaxco KW (2009) An electrochemical sensor for the detection of protein–small molecule interactions directly in serum and other complex matrices. J Am Chem Soc 131:6955–6957. https://doi.org/10.1021/ja9011595
141. Bonham AJ, Paden NG, Ricci F, Plaxco KW (2013) Detection of IP-10 protein marker in undiluted blood serum via an electrochemical E-DNA scaffold sensor. Analyst 138:5580–5583. https://doi.org/10.1039/C3AN01079A
142. Ogden NE, Kurnik M, Parolo C, Plaxco KW (2019) An electrochemical scaffold sensor for rapid syphilis diagnosis. Analyst 144:5277–5283. https://doi.org/10.1039/C9AN00455F
143. Kang D, Parolo C, Sun S, Ogden NE, Dahlquist FW, Plaxco KW (2018) Expanding the scope of protein-detecting electrochemical DNA "Scaffold" sensors. ACS Sensors 3:1271–1275. https://doi.org/10.1021/acssensors.8b00311
144. Parolo C, Greenwood AS, Ogden NE, Kang D, Hawes C, Ortega G, Arroyo-Currás N, Plaxco KW (2020) E-DNA scaffold sensors and the reagentless, single-step, measurement of HIV-diagnostic antibodies in human serum. Microsyst Nanoeng 6:13. https://doi.org/10.1038/s41378-019-0119-5
145. Rant U, Arinaga K, Fujita S, Yokoyama N, Abstreiter G, Tornow M (2004) Dynamic electrical switching of DNA layers on a metal surface. Nano Lett 4:2441–2445. https://doi.org/10.1021/nl0484494
146. Langer A, Hampel PA, Kaiser W, Knezevic J, Welte T, Villa V, Maruyama M, Svejda M, Jähner S, Fischer F, Strasser R, Rant U (2013) Protein analysis by time-resolved measurements with an electro-switchable DNA chip. Nat Commun 4:2099. https://doi.org/10.1038/ncomms3099
147. Das J, Gomis S, Chen JB, Yousefi H, Ahmed S, Mahmud A, Zhou W, Sargent EH, Kelley SO (2021) Reagentless biomolecular analysis using a molecular pendulum. Nat Chem 13:428–434. https://doi.org/10.1038/s41557-021-00644-y
148. Yousefi H, Mahmud A, Chang D, Das J, Gomis S, Chen JB, Wang H, Been T, Yip L, Coomes E, Li Z, Mubareka S, McGeer A, Christie N, Gray-Owen S, Cochrane A, Rini JM, Sargent EH, Kelley SO (2021) Detection of SARS-CoV-2 viral particles using direct, reagent-free electrochemical sensing. J Am Chem Soc 143:1722–1727. https://doi.org/10.1021/jacs.0c10810
149. Idili A, Bonini A, Parolo C, Alvarez-Diduk R, Di Francesco F, Merkoçi A (2022) A programmable electrochemical Y-shaped DNA scaffold sensor for the single-step detection of antibodies and proteins in untreated biological fluids. Adv Funct Mater:2201881. https://doi.org/10.1002/adfm.202201881
150. Mahshid SS, Camiré S, Ricci F, Vallée-Bélisle A (2015) A highly selective electrochemical DNA-based sensor that employs steric hindrance effects to detect proteins directly in whole blood. J Am Chem Soc 137:15596–15599. https://doi.org/10.1021/jacs.5b04942
151. Mahshid SS, Vallée-Bélisle A, Kelley SO (2017) Biomolecular steric hindrance effects are enhanced on nanostructured microelectrodes. Anal Chem 89:9751–9757. https://doi.org/10.1021/acs.analchem.7b01595
152. Mahshid SS, Ricci F, Kelley SO, Vallée-Bélisle A (2017) Electrochemical DNA-based immunoassay that employs steric hindrance to detect small molecules directly in whole blood. ACS Sensors 2:718–723. https://doi.org/10.1021/acssensors.7b00176

153. Zhou W, Mahshid SS, Wang W, Vallée-Bélisle A, Zandstra PW, Sargent EH, Kelley SO (2017) Steric hindrance assay for secreted factors in stem cell culture. ACS Sensors 2:495–500. https://doi.org/10.1021/acssensors.7b00136
154. Mocenigo M, Porchetta A, Rossetti M, Brass E, Tonini L, Puzzi L, Tagliabue E, Triulzi T, Marini B, Ricci F, Ippodrino R (2020) Rapid, cost-effective peptide/nucleic acid-based platform for therapeutic antibody monitoring in clinical samples. ACS Sens 5:3109–3115. https://doi.org/10.1021/acssensors.0c01046
155. Porchetta A, Ippodrino R, Marini B, Caruso A, Caccuri F, Ricci F (2018) Programmable nucleic acid nanoswitches for the rapid, single-step detection of antibodies in bodily fluids. J Am Chem Soc 140:947–953. https://doi.org/10.1021/jacs.7b09347
156. Rossetti M, Ippodrino R, Marini B, Palleschi G, Porchetta A (2018) Antibody-mediated small molecule detection using programmable DNA-switches. Anal Chem 90:8196–8201. https://doi.org/10.1021/acs.analchem.8b01584
157. Baranda Pellejero L, Mahdifar M, Ercolani G, Watson J, Brown T, Ricci F (2020) Using antibodies to control DNA-templated chemical reactions. Nat Commun 11:6242. https://doi.org/10.1038/s41467-020-20024-3
158. Baranda Pellejero L, Nijenhuis MAD, Ricci F, Gothelf KV (2022) Protein-templated reactions using DNA-antibody conjugates. Small:2200971. https://doi.org/10.1002/smll.202200971
159. Rossetti M, Brannetti S, Mocenigo M, Marini B, Ippodrino R, Porchetta A (2020) Harnessing effective molarity to design an electrochemical DNA-based platform for clinically relevant antibody detection. Angew Chem Int Ed 59:14973–14978. https://doi.org/10.1002/anie.202005124
160. Hu J, Yu Y, Brooks JC, Godwin LA, Somasundaram S, Torabinejad F, Kim J, Shannon C, Easley CJ (2014) A reusable electrochemical proximity assay for highly selective, real-time protein quantitation in biological matrices. J Am Chem Soc 136:8467–8474. https://doi.org/10.1021/ja503679q
161. Hu J, Wang T, Kim J, Shannon C, Easley CJ (2012) Quantitation of femtomolar protein levels via direct readout with the electrochemical proximity assay. J Am Chem Soc 134:7066–7072. https://doi.org/10.1021/ja3000485
162. Wang X, Gao H, Qi H, Gao Q, Zhang C (2018) Proximity hybridization-regulated immunoassay for cell surface protein and protein-overexpressing cancer cells via electrochemiluminescence. Anal Chem 90:3013–3018. https://doi.org/10.1021/acs.analchem.7b04359
163. Wen G, Ju H (2016) Enhanced photoelectrochemical proximity assay for highly selective protein detection in biological matrixes. Anal Chem 88:8339–8345. https://doi.org/10.1021/acs.analchem.6b02740
164. Ren K, Wu J, Yan F, Ju H (2014) Ratiometric electrochemical proximity assay for sensitive one-step protein detection. Sci Rep 4:4360. https://doi.org/10.1038/srep04360
165. Bezerra AB, Kurian ASNN, Easley CJ (2021) Nucleic-acid driven cooperative bioassays using probe proximity or split-probe techniques. Anal Chem 93:198–214. https://doi.org/10.1021/acs.analchem.0c04364
166. Vallée-Bélisle A, Ricci F, Uzawa T, Xia F, Plaxco KW (2012) Bioelectrochemical switches for the quantitative detection of antibodies directly in whole blood. J Am Chem Soc 134:15197–15200. https://doi.org/10.1021/ja305720w

Adv Biochem Eng Biotechnol (2024) 187: 107–148
https://doi.org/10.1007/10_2023_234

Published online: 27 October 2023

Imprinted Polymers on the Route to Plastibodies for Biomacromolecules (MIPs), Viruses (VIPs), and Cells (CIPs)

Xiaorong Zhang, Aysu Yarman, Mahdien Bagheri, Ibrahim M. El-Sherbiny, Rabeay Y. A. Hassan, Sevinc Kurbanoglu, Armel Franklin Tadjoung Waffo, Ingo Zebger, Tutku Ceren Karabulut, Frank F. Bier, Peter Lieberzeit, and Frieder W. Scheller

Contents

This chapter is devoted to Klaus Mosbach for his groundbreaking contributions in bioanalysis.

X. Zhang, F. F. Bier, and F. W. Scheller (✉)
Institute for Biochemistry and Biology, Universität Potsdam, Potsdam, Germany
e-mail: fschell@uni-potsdam.de

A. Yarman
Molecular Biotechnology, Faculty of Science, Turkish-German University, Istanbul, Turkey

M. Bagheri and P. Lieberzeit (✉)
Department of Physical Chemistry, Faculty for Chemistry, University of Vienna, Vienna, Austria
e-mail: peter.lieberzeit@univie.ac.at

I. M. El-Sherbiny and R. Y. A. Hassan
Nanoscience Program, University of Science and Technology (UST), Zewail City of Science and Technology, Giza, Egypt

Center for Materials Science (CMS), Zewail City of Science and Technology, Giza, Egypt

S. Kurbanoglu
Department of Analytical Chemistry, Faculty of Pharmacy, Ankara University, Ankara, Turkey

A. F. T. Waffo and I. Zebger
Institut für Chemie, PC 14 Technische Universität Berlin, Berlin, Germany

T. C. Karabulut
TOBIO Pharmaceuticals, Istanbul, Turkey

Abstract Around 30% of the scientific papers published on imprinted polymers describe the recognition of proteins, nucleic acids, viruses, and cells. The straightforward synthesis from only one up to six functional monomers and the simple integration into a sensor are significant advantages as compared with enzymes or antibodies. Furthermore, they can be synthesized against toxic substances and structures of low immunogenicity and allow multi-analyte measurements via multi-template synthesis. The affinity is sufficiently high for protein biomarkers, DNA, viruses, and cells. However, the cross-reactivity of highly abundant proteins is still a challenge.

Graphical Abstract

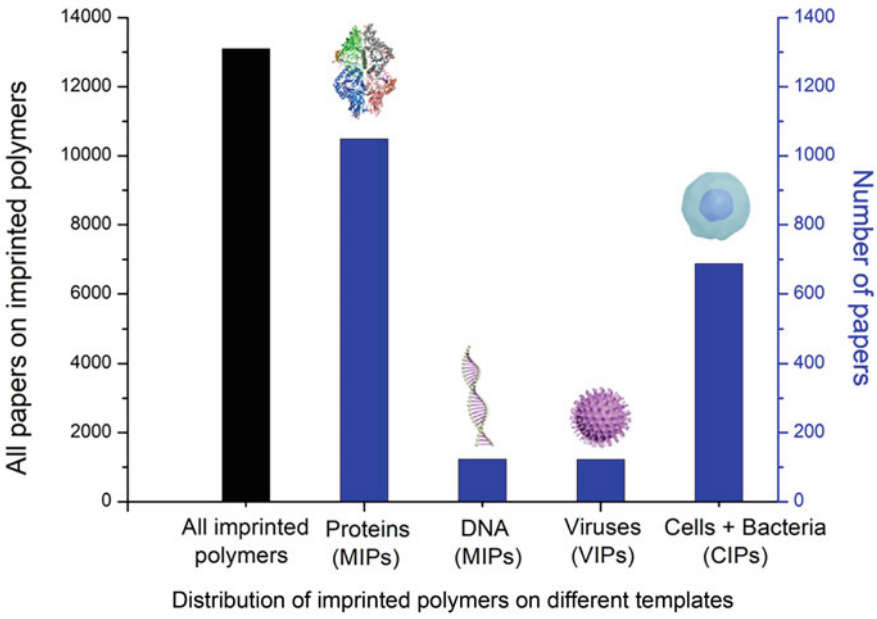

Keywords Biomimetic sensors, Cell-Imprinted Polymers (CIPs), MIPs for proteins and nucleic acids, Plastibodies, Virus-Imprinted Polymers (VIPs)

1 Introduction

The concept of polymers comprising memory for a specific template was proposed as early as 1931 by the Russian scientist Polyakov [1]. However, a real breakthrough has been only achieved almost 50 years after this first report by Wulff and Mosbach [1–3]. In the early phase, imprinted polymers have been developed exclusively for low-molecular substances. Starting from 1984 till present almost 10% of papers describe receptors for biomacromolecules, especially proteins and nucleic acids. These biomimetic recognition elements constitute the "real Molecularly Imprinted Polymers" (MIPs). Derived from this MIP concept imprinted polymers for viruses and cells have been developed. While the term MIP is in general used in the literature for all types of imprinted polymers, we use in this chapter the terms "Virus-Imprinted Polymer (VIP)" and "Cell-Imprinted Polymer (CIP)" as these targets do not comprise molecules.

We found in the *web of sciences* a total of around 13,000 papers describing imprinted polymers (Fig. 1). This number is in agreement with the number of papers

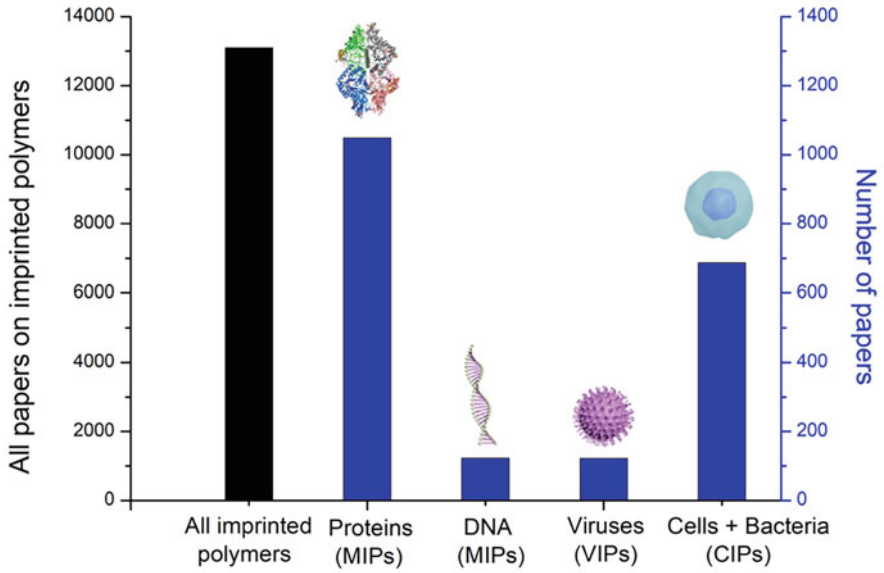

Fig. 1 The number of publications on Imprinted Polymers from 1990 till 2022 (Source: Web of science)

of 7,562 reported by Scopus in September 2020 for a period of 10 years. Last year (2022) around 1,000 papers on imprinted polymers were published. At present the number of papers on cells corresponds to 60% of the research articles of protein-based MIPs (60 papers in 2022). With the outbreak of SARS, the number of papers on virus sensors reached about 17 articles in 2022. The total number of publications on MIPs for nucleic acids is only 122 including 17 papers in 2022. Obviously, it is hard to compete with the high performance of the already established DNA analysis.

2 Polymer Synthesis: From Bulk Polymers to Nano-MIPs and Fully-Electrochemical Sensors

Thermal or photo-initiation is utilized in conventional bulk imprinting. In these processes, the template, functional monomers, and crosslinkers are polymerized together. Before the removal of the template, the bulk polymer is crushed and fractionated resulting in imprinted particles. At the end of these procedures, the prepared polymer has template-specific binding sites. During the preparation, the template can be entrapped into the polymer matrix hampering the template removal and therefore slowing down the binding and analysis of the target analyte [4]. Such challenges can be circumvented by reducing the thickness of the imprinted layer to that of the target analyte (surface imprinting) [5–11]. Herein, the synthesis has been optimized by screening the interaction of monomer libraries with the immobilized

template [12]. Furthermore, docking studies were helpful regarding the selection of functional monomers, crosslinkers, and an optimization of template-monomer ratio [13].

The first MIP for proteins utilized hydrogels with low crosslinking degree and large pores [14–17]. However, these gels are not preferred because they are very fragile. Significant progress has been made by applying innovative methods from polymer chemistry for the synthesis of imprinted polymers for biomacromolecules, cells, and viruses:

- Emulsion or precipitation polymerization techniques were used to prepare micro- or nano-MIPs [18–22].
- Core-shell nanoparticles were utilized as carrier in the synthesis. In such systems, magnetic forces have been used for separation. Furthermore, the readout by intrinsic fluorescence was implemented [23–25].
- Solid-phase synthesis methods were successfully utilized to prepare MIPs on functionalized beads (e.g., from glass) covered with the oriented template (Fig. 2).
- Stamp-like surface patterning (micro-contact printing) was frequently used for CIP synthesis. This method involved the pressing of a template-loaded stamp into the surface of a soft polymer layer [7, 10, 27–29].
- Nanosphere lithograph allows the oriented imprinting of the immobilized template [30].
- In addition, several electrochemical methods were utilized for the formation of surface-imprinted polymers for all types of target analytes. Electropolymerization of electroactive monomers or the self-polymerization of autoxidizable substances like dopamine under ambient oxygen atmosphere is a straightforward method to synthesize ultrathin MIP layers on planar or nanostructured transducers [4, 9, 11, 31–36].

Within the application of electrochemical methods, the polymer layer is formed from one or two monomers without using a crosslinker. Electropolymerization provides control of the polymer thickness by adjusting the charge during

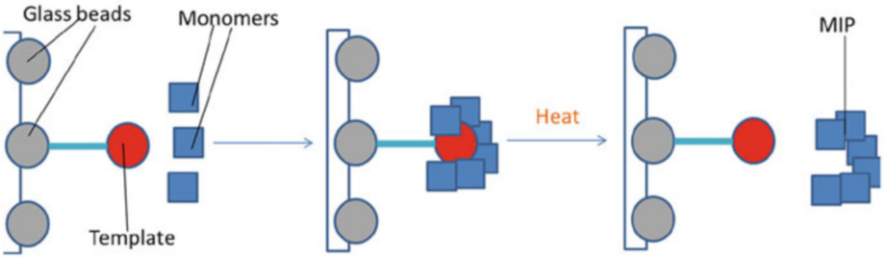

Fig. 2 Solid-phase approach: the polymerization occurs around the template immobilized on glass beads https://www.mdpi.com/2079-4983/13/1/12. Reproduced from Parisi et al. [26]. It is licensed under a Creative Commons Attribution 4.0 International License (CC BY 4.0) https://creativecommons.org/licenses/by/4.0/

electrosynthesis. On the other hand, during self-polymerization, film synthesis requires tedious control of the spontaneous polymerization process. Electropolymerization is only applicable on conductive surfaces, while self-polymerization is suited for all surfaces. Moreover, taking advantage of the nanotechnological integration of metallic and carbon-based nanomaterials such as nanoparticles or graphene into the polymer layer increases the binding capacity and improves the electrochemical signal.

In contrast to the preparation of antibodies, the MIP synthesis provides recognition elements, which harbor the template. In this case, its removal is required before the first and after each measurement. The constraint of a mandatory regeneration between subsequent measurements is comparable with that present in immunosensors. While a regeneration of aptamers is doable by simple thermal treatment, there is no generally applicable procedure reported in the literature to regenerate imprinted polymers [37]. Different chemical and physical treatments have been utilized for the removal of proteins, DNA, viruses, and cell targets including changes in pH or ionic strength, elevated temperature, detergents, electrode potential, or ultrasound (Table 1).

Generally, since several different treatments are combined, a compromise has to be achieved between the efficiency of template removal and maintaining the integrity of the polymer.

For example, proteolytic digestion is appropriate for the removal of proteins under mild conditions; however, the protein fragments may also strongly bind to the MIP [38]. Imprinted polymers based on thermoresponsive polymers have been reported to allow the temperature-controlled soft release of the template [20, 39].

3 Signal Readout and Measuring

The signal generation of MIP sensors has many common aspects with immunosensing, but inherent effects in the polymer matrix can interfere with the readout of the recognition in the binding sites. Electrochemical and optical techniques are generally used in the readout of MIP sensors [4, 58]. Furthermore, piezoelectric [54, 55], thermal [22], and micromechanical [59] transducers have also been used especially in VIP and CIP sensors.

The target protein can be directly monitored during all steps of synthesis, as well as the respective rebinding by evaluating the faradaic current of prosthetic groups [60, 61]; the formation of redox-active products by enzymes [40, 61, 62]; and the fluorescence of aromatic amino acids or a fluorophore of the protein moiety (GFP) [63]. Furthermore, vibrational spectroscopic techniques like Raman and surface-enhanced Raman, as well as infrared (IR) spectroscopy [64–66], or recently also surface-enhanced infrared absorption (SEIRA) spectroscopy [38] allow not only to follow and evaluate all steps of the MIP synthesis and the analyte rebinding with a particular specificity for the target protein via its amide (I and II) absorptions, but also to structurally characterize the polymer and the mechanism of its formation via

Table 1 Methods of template removal for MIP-based protein sensors

Detection method	Template	Monomer type	Removal conditions	Reference
Electrochemical				
	Tyrosinase	Scopoletin or *o*-phenylenediamine	0.1 M NaOH (overnight)	[40]
	Human serum albumin	Scopoletin	5 mM NaOH (10 min), 5% SDS (5 min), 5 mM NaOH (10 min), and finally with ddH_2O	[41]
	Human serum albumin	Bis (2, 2′-bithien-5-yl) methane	30% NaOH for 45 min at 40 °C	[42]
	Cancer antigen 15-3	2-aminophenol	0.5 M oxalic acid (12 h) and 0.1 M phosphate buffer (1 h)	[43]
	Cancer antigen 15-3	*o*-phenylenediamine	Trypsin (90 min, 36°C) and finally with ddH_2O	[44]
	Prostate-specific antigen	Pyrrole	5 mM oxalic acid	[45]
	Acetylcholinesterase	Carboxylate-modified derivative of 3,4-propylenedioxythiophene	50 mM glycine-HCl buffer, pH 2.2 (16 min)	[46]
	Carcinogenic embryonic antigen	Pyrrole	ddH_2O, proteinase K (2 h), PBS, and ddH_2O	[47]
	Interleukin-1β	3,4-ethylenedioxythiophene /4-aminothiophenol	Cyclic voltammetry in 0.1 M PBS, −0.30 V - +0.80 V, 0.10 V/s, 25 cycles	[48]
Optical				
	Ferritin	Scopoletin	5 mM NaOH	[49]
	Hemoglobin	Acrylamide	0.01 M NaCl	[50]
	Lysozyme	Acrylic acid and N, N′-methylenebisacrylamide	1 M NaCl	[51]
	α-Casein	N-isopropylacrylamide, N-tert-butylacrylamide, acrylic acid, N-(3-aminopropyl)methacrylamide HCl, and N,N′-methylenebis(acrylamide)	3 × 30 ml aliquots of ddH_2O at 60°C in ddH_2O (30 ml, 30 min)	[52]
	Avidin	Poly-3,4-ethylenedioxythiophene doped with poly-styrene sulfonate	Chloroform (15 min)	[8]

(continued)

Table 1 (continued)

Detection method	Template	Monomer type	Removal conditions	Reference
	Horseradish peroxidase	Boronic acid-functionalized magnetic nanoparticles	0.1 M HAc containing 5% SDS (w/v)	[53]
Piezoelectric				
	Oxidized-low-density lipoprotein	Methacrylic acid, N-vinylpyrrolidone	10% aqueous acetic acid solution followed by 0.1% SDS solution and ddH_2O	[54]
	Trypsin	Methacrylic acid	Centrifugation and washing with ddH_2O	[55]
	Glycoprotein 41	Dopamine	5% acetic acid for five times and ddH_2O	[56]
	Ribonuclease A	2,2,3,4,4,4-hexafluorobutyl methacrylate, N-methacryloyl-histidine	3 M NaCl (10 h)	[57]

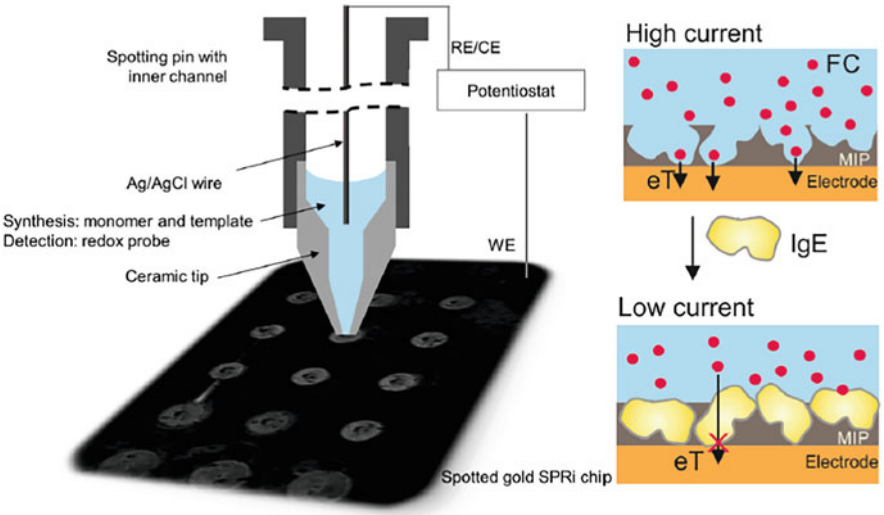

Fig. 3 A schematic diagram of the microelectrospotting/electrochemical readout setup. Reproduced from Supala et al. [68]. It is licensed under a Creative Commons Attribution-NonCommercial-NoDerivatives 4.0 International License (CC BY-NC-ND 4.0) https://creativecommons.org/licenses/by-nc-nd/4.0/

intrinsic bands [67]. The high (spectral) sensitivity of the latter technique will in future also allow us to monitor the conversion of related educts and the formation of products in VIP and CIP systems. Likewise, approaches using techniques such as surface plasmon resonance (SPR)-based sensing, quartz crystal microbalance (QCM), and capacitor or thermistor systems sum up the target binding, nonspecific adsorption to the polymer surface, and different effects of changes in the chemical environment [11].

On the other hand, the frequently applied evaluation of the "gating effect" on the diffusional permeability of a redox marker by the binding of proteins, DNA, viruses, and cells, respectively, reflects "overall effects" [11]. For non-conducting polymers the current signal of the redox marker reflects the occupancy of the pores by the target; i.e., the current decreases with increasing concentration approaching saturation. For conducting polymers both increasing and decreasing currents after target binding have been reported. Electrochemical methods provide a powerful toolbox suitable for simple one-step synthesis of the polymer layer on the transducer surface followed by "electroelution." They are also quite sensitive and selective to the reading of rebinding [11]. This technology has been recently extended to protein microarrays by Gyurcsanyi's group (Fig. 3) [68].

Determination of thermodynamic parameters, e.g., binding, requires the measurement under equilibrium conditions. This prerequisite has been frequently ignored. In this procedure, the sensor is incubated in a solution containing an adequate concentration of the target molecule. Yoshimi et al. introduced this approach for monitoring

theophylline on the basis of the gate effect for a redox marker [69]. On the other hand, for MIPs with a very low rate of dissociation, the measurement can also be performed in a target-free solution. For "dynamic" systems with a medium dissociation rate, the decay of the signal after the removal of the target from the surrounding solution allows the determination of the dissociation constant by SPR and QCM [49, 70].

4 "Whole Analyte": Imprinted Polymers vs. Imprinting of Substructures (Epitope, Engineered Tags, and Labels) of Biomacromolecules and Bioparticles

In analogy to MIPs for small molecules, the first MIPs for the recognition of proteins, cells, viruses, and bionanoobjects applied the whole analyte as the template [71]. However, imprinting of large biological molecules and bioparticles faces challenges due to their complex nature, high cost for pure templates, distribution of heterogeneous binding sites, and difficulties in mass production with high reproducibility [72].

Nevertheless, the analytical performance established in research labs on imprinted polymers for whole proteins or other entire templates in the nanosize range reaches that of immunoassays [73]. Therefore, MIPs have been called plastibodies to address the analogy with antibodies [26]. However, the imprinted polymers interact with the surface of the target molecule which interacts with the walls of the binding pockets. This is also true for surface imprinting of macromolecules where the polymer layer partially entraps the target [5–11]. On the other hand, antibodies bind only to a small area of large antigens—the immunogenic determinant. Mimicking this principle Rachkov and Minoura [74, 75] applied the three N-terminal amino acids of the nonapeptide oxytocin as the template for a MIP which binds the whole peptide. Later on, this approach has been successfully extended to proteins and cells and termed as epitope imprinting to highlight the similarity between epitope MIPs and antibodies [74, 75]. In fact, epitope MIPs are closer to the antigen–antibody reactions because only a very small exposed part of the macromolecule binds to the epitope-shaped cavities.

Such epitope MIPs can recognize the template fragment as well as the respective whole protein [74–81]. Both C- and N-terminal peptides consisting typically of 4 up to 20 amino acids were used as template [75, 77, 80]. Modeling showed that still tripeptides are effective templates to form MIPs with an affinity toward the parent protein in the μM range [82]. Surprisingly, binding of the parent protein to the epitope MIP has also been reported for MIPs which were prepared with non-terminal sequences as templates [83, 84]. Furthermore, functional surface regions of cells and viruses including peptides and especially glycans, e.g., N-acetyl-D-galactosamine, acetylneuraminic acid, and sialic acids [85–87], have been used as templates for MIP synthesis, which are capable of recognizing these bionanoobjects. In nucleic acid

analysis, identification of (short) segments of large molecules is a well-established principle that has also been transferred to MIPs for nucleic acids.

Later on, the epitope approach has been extended to recombinant proteins using peptide tags, e.g., his6-peptide [88], FLAG tag (DYKDDDDK) [89], and StrepTagII (WSHPQFEK), as the template. Furthermore, MIPs based on the imprinting of avidin [90] and "chemical labels," e.g., rhodamine B [91], have been developed for the recognition of the labeled proteins, cells, and nucleic acids.

In addition to small epitopes and tags, subunits of proteins and surface proteins of viruses can be used as the template in the MIP synthesis. A MIP-based biosensor has been developed by imprinting the antigen-binding region Fab fragment for real-time detection of human immunoglobulin G (IgG) [92]. The concept of fragment imprinting was further demonstrated for enzymes by Jeztschmann et al. [93], where the separated oxidase and reductase domains or the whole Cytochrome P450 BM3 have been immobilized on the electrode surface as templates before deposition of the polymer film.

5 MIPs for Recognition of Proteins

At present around 10% of the papers published on imprinted polymers describe the recognition of proteins; for example in 2021, there were 114 dealing with proteins (Source: Web of Science).

5.1 Protein-Imprinted Polymers

The development of MIPs for proteins started with the whole protein imprinting using the glycoprotein ribonuclease A as the template which was entrapped in polysiloxane-coated porous silica by Mosbach's group in 1985 [71].

5.1.1 β-Amyloid

The peptide amyloid β-42 (Aβ-42) is the key biomarker for Alzheimer's disease which is responsible for the formation of senile plaques in the brain. The electrochemical paper-based sensor developed in Sales group [94] comprises a MIP layer that is built up on a carbon ink electrode by electropolymerizing a mixture of the target Aβ-42 and the functional monomer *o*-phenylenediamine (*o*-PD). The template was subsequently removed by enzymatic and acidic treatments. The rebinding was evaluated by square wave voltammetry (SWV) and electrochemical impedance spectroscopy (EIS) using ferricyanide as a redox marker. The response was linear down to 0.1 ng/ml, and repeatability less than 10% was reported.

5.1.2 Choline Esterases

A MIP sensor for the recognition of acetylcholinesterase (AChE) utilized the tetrameric enzyme as template and a 3,4-propylenedioxythiophene derivative for the electrosynthesis of the MIP nanofilm [46]. Prior to MIP synthesis AChE was bound via its peripheral anionic site to a propidium-terminated self-assembled monolayer. Rebinding of AChE to the MIP was demonstrated by measuring the oxidative current of the enzymatically generated thiocholine, which linearly depended on the AChE concentration in a range from 0.04×10^{-6} to 0.4×10^{-6} M. An imprinting factor of 9.9 and a K_d value of 4.2×10^{-7} M were obtained for the MIP. This MIP effectively suppressed the cross-reactivity toward competing proteins and appears promising for assessing AChE activity levels in cerebrospinal fluid.

The first MIP for the recognition of the diagnostically relevant enzyme butyrylcholinesterase (BuChE) was prepared by electropolymerizing a BuChE and *o*-PD containing solution on a glassy carbon electrode [95]. All steps of MIP synthesis and rebinding were characterized by cyclic voltammetry (CV) of the redox maker ferricyanide and the enzymatic activity of BuChE, which was reflected by the anodic oxidation of thiocholine, the reaction product of butyrylthiocholine. The signal depended linearly on the concentrations of BuChE between 50 pM and 2 nM with a detection limit of 14.7 pM. Furthermore, the MIP sensor allowed the indication of pseudo-irreversible inhibitors in the lower mM range.

5.2 Epitope MIPs for Proteins

5.2.1 Immunoglobulins

Immunoglobulins are produced by the B cells of vertebrates in response to invasion by foreign objects, e.g., bacteria and viruses. They are called antibodies, form 4 subclasses, and exhibit a variability of 10^{12} different species. The most common immunoglobulin G (IgG) is a tetrameric Y-shaped glycoprotein with a molecular weight of 150 kDa. It consists of two identical units, each built from two identical heavy and light chains. The arms of the IgG molecule are called antigen-binding fragments (Fab) and form the antigen-binding sites (paratopes). It "neutralizes" foreign molecules and particles by forming immune complexes.

The identification of antibodies that act specifically against different variants of infective germs allows for profiling the humoral immunity of infected and vaccinated subjects, including COVID-19. It is the basis of tracing the immune response during infection and the effect of vaccination [96].

Denizli's group [92] applied the antigen-binding fragment as template for synthesizing a MIP for IgG onto a SPR sensor chip. This Fab-imprinted polymer layer recognizes its template Fab and the whole IgG. The precision of detecting IgG in human plasma using this sensor was 99.1%.

The handle of the Y-shaped IgG molecule—the so-called "fragment crystallizable" (Fc) region—is the binding site of the bacterial protein A. This reaction is used during the chromatographic isolation of IgGs. Therefore, a MIP which binds the Fc domain could substitute protein A in downstream processes. Following this strategy, Sellergren's group developed MIPs with high affinity for the Fc domain [78]. Using solid-phase synthesis, the MIP was deposited around the covalently immobilized template comprising the Fc domain of IgG, the C-terminal 10-mer peptide of IgG, and the whole IgG molecule, respectively. All three MIPs recognized both human and goat IgGs in the nanomolar concentration range.

Using 11-mer peptides as the templates [97], a dual MIP for the depletion of human serum albumin (HSA) and IgG from serum has been developed. The apparent K_d values toward HSA and IgG were 1 and 0.6 μM, respectively.

5.2.2 Cancer Biomarker AFP

Alpha-fetoprotein (AFP) is an important biomarker for the early detection of hepatocellular carcinoma (HCC) [98, 99]. This glycoprotein is produced by the fetal hepatocytes immediately after birth. In healthy adults, the level is below 10 ng/ml (0.15 nM), and a cut-off level of 20 ng/ml (0.3 nM) of AFP in serum is used as an early indication of hepatic carcinoma [98–101]. It has diverse forms of glycosylation, and the one with Lens culinaris agglutinin (LCA)-reactive fraction (AFP-L3) is produced only by cancerous cells [98, 99].

A triple MIP-based plasmonic sandwich assay (triMIP-PISA) was recently developed by Li et al. for cancer diagnosis based on the evaluation of the relative glycosylation expression of the glycoprotein biomarkers (Fig. 4) [102]. This sensor uses two MIPs that recognize either the C-terminal or the N-terminal peptide

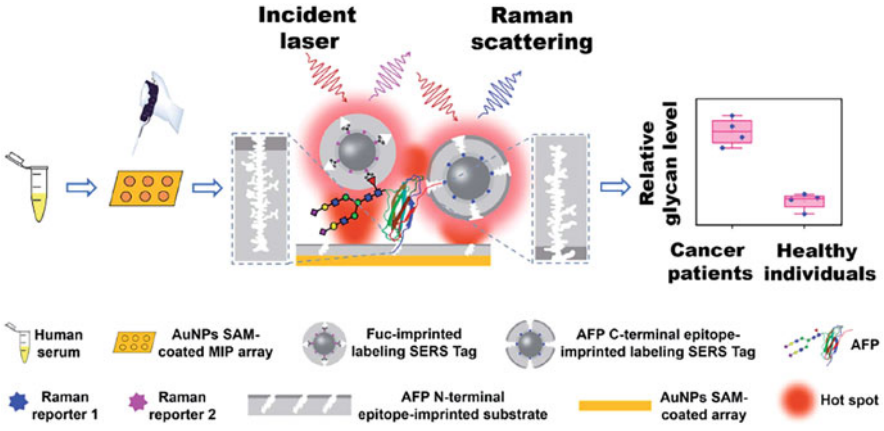

Fig. 4 Schematic illustration of the detection principle of the triMIP-PISA. Reproduced from Pang et al. [102]. It is licensed under a Creative Commons Attribution 3.0 Unported License (CC BY 3.0) https://creativecommons.org/licenses/by/3.0/

sequence of AFP as well as a fucose-imprinted MIP for detection of the fucosylated AFP-L3 fraction. Simultaneous surface-enhanced Raman spectroscopic detection of the total AFP and the AFP-L3 in serum was accomplished, which allows us to distinguish HCC patients from healthy individuals.

5.2.3 Metalloproteinase-1 (MMP-1)

MMP-1 is a biomarker for the diagnosis and progression of idiopathic pulmonary fibrosis. Recently, Kuttner's group [103] developed epitope MIPs utilizing extended-gate field-effect transistors (EG-FET) as the transducer. Surface-exposed epitopes were analyzed by applying BLAST software and the two most suitable sequences were selected according to the location in the MMP-1, length, and aggregation tendency. A mixture of either a 10- or a 12-amino acid peptide and thiazolidine derivatives as functional monomer and bis-EDOT as crosslinker was potentiodynamically polymerized in a solution of organic solvents on the surface of the gate. After template removal, the rebinding of the template peptide resulted in an increase of the differential pulse voltammetry (DPV) current of the redox marker ferricyanide. The authors conclude that the conductivity of the polymer film is increased by filling the binding cavities. Also, the drain current at a constant gate voltage of the EG-FET increased after addition of the template peptide but most important also on interaction with the whole MMP-1. The binding constants determined by the modified Langmuir isotherm were in the order of $10^6\ M^{-1}$ for both the peptide and the MMP-1 protein. The authors claim that the MIP sensor selectively recognizes MMP-1 in buffered serum samples.

5.3 Application of Protein MIPs

A large number of publications report that the required affinity for protein biomarkers has been already achieved for substituting antibodies in clinical diagnostics or environmental analysis [4, 104]. However, many measurements have been carried out in spike pre-treated or semi-synthetic plasma [105–107]. Specificity is frequently claimed on the basis of low cross-reactivity toward irrelevant "interferences" like HRP or BSA in serum or urine [83, 108, 109]. The presence of highly abundant proteins in biological samples, e.g., serum albumin and immunoglobulin in the g/l region, is still a challenge for the detection of protein markers for cancer (prostate-specific antigen), diabetes (insulin), or heart failure (troponin T, myoglobin) in the mg/l to ng/l range [104]. Since MIP sensors represent only one "separation plate," extremely low cross-reactivities are required to prevent saturation of the MIP with serum albumin. Furthermore, electrochemical sensors are especially susceptible to interferences by surface-active constituents of "real sample" which partially block the electrode surface [38].

MIPs for selective protein binding have been successfully exploited mostly in solid-phase extraction and chromatography [107, 110–114], replacement of antibodies in ELISA-derived assays and sensors [4, 9, 115, 116], and the removal of interfering substances [117]. Only a limited number of MIP sensors for biomarkers are already commercially available [118]. Imprinted polymers offer innovative tools not only for clinical and environmental analysis but also for bioimaging, therapy, and protein engineering.

6 Molecularly Imprinted Polymers for Deoxyribonucleic Acid (DNA) Recognition

DNA represents in nature the main vector of genetic information [119]. The length per base of dsDNA is approximately 0.34 nm [120]. Detection of DNA has wide applications in medical diagnostics, food, and environmental monitoring [121–124]. MIPs attract increasing interest due to their low costs, easy preparation, robustness, and comparable affinity to antibodies [118].

Although there are a large number of reports on protein and cell MIPs [118, 125–127], the reported progress for DNA imprinting was impaired due to the structural complexity of the target [128, 129]. Table 2 summarizes several representative MIPs for DNA in chronological order.

6.1 MIPs Based on Nucleosides and Labels as Template

The field of MIPs for nucleic acids was initiated by Piletsky's group [141–143] and Shea [144] with sensors for nucleosides [145–147] and their derivatives [133, 134] and was further developed via oligonucleotides to single-stranded [137, 139] and double-stranded nucleic acids [130, 131, 135, 136, 140].

In order to improve the performance of DNA MIPs, nanoparticles have been integrated into the MIP layer. Novel guanosine-imprinted nanocrystals have been synthesized for DNA recognition based on the ligand exchange approach [133, 134]. According to this approach, the thiol-ligand-modified cadmium sulfide (CdS) quantum dots (QD) nanocrystal was firstly prepared as the substrate and the guanosine-imprinted polymer was formed on the nanocrystal as the surface shell using methacryloylamidohistidine (MAH)-Pt(II)-guanosine as the ligand exchange monomer [133]. The binding of guanosine, guanine, ssDNA (PolyG), and dsDNA was detected based on the fluorescent signal of the QDs. Guanosine ($K_d = 0.21$ μM) and free guanine ($K_d = 1.12$ μM) exhibited an almost 10-fold higher affinity than ssDNA (PolyG) and dsDNA. Moreover, the MIP displayed a higher affinity toward ssDNA (PolyG) than dsDNA. The authors assumed that most imprinted sites recognized two neighboring guanosine nucleotides on the same DNA strand.

Table 2 Representative MIPs for DNA recognition

Target	Template for MIP	Monomer	MIP preparation	Detection	Linear response range, LOD	K_d, IF	Cross-reactivity/ real sample	Reference
DNA used as templates								
Fluorescent-labeled verotoxin dsDNA (34 bp)	Same as target	VDAT, AAm	MIP on a silanized glass surface	Fluorescence intensity, SPR	nd	$K_d = 1.4$ nM	Oligo(dG)-oligo (dC)	[130]
Verotoxin dsDNA (34 bp) dsDNA from λDNA HindIII marker (564 bp)	Same as target	VDAT, AAm	MIP gel	Gel electrophoresis	nd	Nd	DNA mixture	[131]
dsDNA from c-Ha-*ras* gene (73 bp), dsDNA from λDNA HindIII marker (564 bp)	Same as target	VDAT, AAm	MIP gel	Gel electrophoresis	nd	Nd	DNA mixture	[132]
Guanine, guanosine, ssDNA (polyG), dsDNA	Guanosine	MAH-Pt(II)	Guanosine-imprinted nanocrystals based on ligand exchange method	Fluorescence of QDs	nd	$K_d = 206.4$ nM for guanine	Adenosine	[133]

Guanine, guanosine, ssDNA (polyG)	Same as above	Same as above	Same as above	SPR	nd	K_d = 15.2 μM for guanine	dsDNA, adenosine	[134]
Fish sperm dsDNA	Same as target	Pyrrole	Electrosynthesized MIP on PGC	DPV signal of guanine oxidation	nd	nd	nd	[135]
dsDNA from salmon testes	Same as target	Imidazolium ILs	MIP on IL-Fe_3O_4 functionalized silica microspheres	UV-Vis	0.3 - 1.5 mg/ml	IF = 6.6 Adsorption capacity: 162 mg/g	Calf whole blood	[136]
HIV-1 gene ssDNA (21mer)	Same as target	*o*-PD	MIP on ITO	ECL signal of EuS NCs	3 fM – 0.3 nM, LOD = 0.3 fM	nd	Serum samples	[137]
$(AGCT)_3$ ssDNA (12mer)	"Polymerizable nucleoside" complementary to the target	Oligonucleotide, NIPAm, TBAm, AAc	Hybrid oligonucleotide-polymer system	QCM	nd	nd	nd	[138]
Labels and small molecules used as templates								
ssDNA (20mer)	MB	4-VPyr	MIP on CPE	DPV signal of guanine oxidation	0–50 μg/ml (0–7.94 μM), LOD = 8.72 μg/ml (1.38 μM)	nd	One base mismatch DNA, noncomplementary DNA	[139]
BRCA-1 ssDNA	RhB	MAA, Nafion	MIP on GCE modified with AuNPs/rGO	DPV signal of RhB	10 fM – 100 nM, LOD = 2.53 fM	nd	Human serum	[91]
dsDNA from salmon	MG	APTES	MIP on (MPTMS)-capped Mn-doped ZnS QDs	RTP intensity of MIP-QDs,	0.089–1.79 μg/ml (0.068 nM – 1.38 nM)	nd	Urine sample	[140]

(continued)

Table 2 (continued)

Target	Template for MIP	Monomer	MIP preparation	Detection	Linear response range, LOD	K_d, IF	Cross-reactivity/ real sample	Reference
testes (~2000 bp)				fluorescence of MG	LOD = 19.48 ng/ml (14.98 pM)			

Abbreviations: IF: imprinting factor. LOD: limit of detection. nd: not detected. VDAT: 2-vinyl-4,6-diamino-1,3,5-triazine. AAm: acrylamide. NMR: nuclear magnetic resonance. SPR: surface plasmon resonance. DLS: dynamic light scattering. TEM: transmission electron microscopy. MAH-Pt(II): methacryloylamidohistidine-platinum. QDs: quantum dots. PGC: pencil graphite electrode. DPV: differential pulse voltammetry. ILs: ionic liquids. *o*-PD: *o*-phenylenediamine. ITO: indium tin oxide. ECL: electrochemiluminescent. EuS NCs: EuS nanocrystals. NIPAm: *N*-Isopropylacrylamide. TBAm: *N*-*tert*-butylacrylamide. AAc: acrylic acid. MB: methylene blue. 4-VPyr: 4-vinyl pyridine. CPE: carbon paste electrodes. RhB: rhodamine B. MAA: methacrylic acid. GCE: glassy carbon electrode. AuNPs: gold nanoparticles. rGO: reduced graphene oxide. BRCA-1: breast cancer susceptibility gene. MG: malachite green. QDs: quantum dots. MPTMS: mercaptopropyltrimethoxysilane. APTES: (3-aminopropyl)triethoxysilane

Later, Diltemiz et al. applied surface plasmon resonance (SPR) to evaluate the MIP performance [134]. The methacryloyl-(l)-cysteine (MAC) methylester was immobilized on SPR gold chip and the guanosine-imprinted polymer was synthesized on MAC-modified gold surface using the same metal-chelate monomer described before.

Instead of imprinting DNA itself, MIPs for DNA were also prepared by imprinting small molecules which could further react with DNA, so that the challenges related to this macromolecular template could be circumvented and also the affinity could be improved [91, 139, 140].

In 2018, a novel DNA sensor for the breast cancer susceptibility gene BRCA-1 was proposed by imprinting rhodamine B (RhB) on a glassy carbon electrode modified by gold nanoparticles and reduced graphene oxide (AuNPs/GO) [91]. The signal of the target ssDNA was obtained by measuring the DPV signal of RhB (Fig. 5). Based on the recognition of RhB-modified ssDNA, the sensor was able to detect under optimized conditions the target ssDNA in a linear response range from 10 fM to 100 nM with a LOD of 2.53 fM. The recovery in 1:10 diluted human serum was between 97% and 106.4%, suggesting a potential clinical application in real samples.

6.2 DNA-Imprinted Polymers

The first work related to dsDNA-Imprinted Polymer was presented in 2004 [130]. Herein, a verotoxin dsDNA(34 bp)-imprinted polymer was prepared on silanized glass with 2-vinyl-4,6-diamino-1,3,5-triazine (VDAT) as the monomer, which can interact with the adenine-thymine pair (A-T) in the sample DNA. This work opened the possibility to directly imprint the native target dsDNA into the polymer. Later, the authors created a simple and inexpensive detection technique for dsDNA by preparing the MIP as a gel utilizing the same monomer VDAT [131]. The recognition ability of the MIP was evaluated based on the observed capability to hinder the migration of the target dsDNA in the imprinted gel. In this method, no label was required. The MIP gel was able to capture the target dsDNA from mixed dsDNA fragments with different sizes and base pair mismatches. This gel method has been applied for different target dsDNA ranging from 34 bp to 564 bp [131, 132]. However, because of the interaction between the monomer VDAT and the A-T base pair of dsDNA, this MIP gel failed to discriminate between an A-T base pair and T-A base pair.

An electrochemical MIP-based sensor using target dsDNA as the template was reported in 2013 [135]. In this work, the thin polypyrrole layer was formed on a pencil graphite electrode in the presence of the target fish sperm dsDNA using CV or the potential pulse sequences (PPS) method. The DPV signal of guanine oxidation gave information on the binding of target DNA. Pronounced differences in the

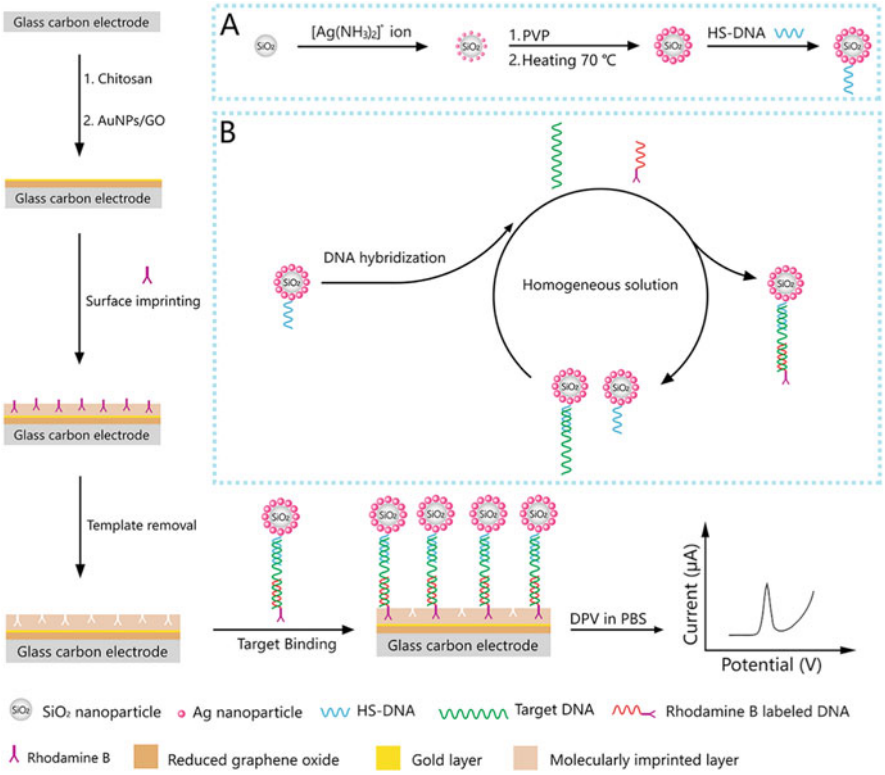

Fig. 5 Schematic representation of a MIP-based sensor fabrication for ssDNA detection [91]. Adapted with permission from Elsevier [91]. Copyright Elsevier, 2018

analytical performance between MIP and NIP were reported. The length of the fish sperm dsDNA can range from 120 to 3,000 nucleotides with the molecular weight from 40 to 1,000 kDa. There was no information about cross-reactivity of this MIP.

A simply and sensitive electrochemiluminescence sensor for HIV gene detection has been presented by Babamiri et al. [137]. The 21mer HIV gene was imprinted on an indium tin oxide (ITO) electrode by electropolymerizing *o*-PD in the presence of the ssDNA. The rebinding was detected by the addition of EuS nanocrystals (EuS NCs) modified with complementary ssDNA. After hybridization, the electrochemiluminescence emission signal of EuS indicated the binding of the target ssDNA to the MIP. This MIP was able to distinguish sequences essentially containing two mismatches from the target DNA and exhibited a detection limit of 0.3 fM. Moreover, this sensor could even detect the target ssDNA from human serum with a recovery of 97–106.4%.

7 Imprinted Polymers for Virus Recognition

Virus infections are a great threat for the entire mankind due to the immense increase of potentially deadly diseases such as acquired immunodeficiency syndrome (AIDS), Ebola, hepatitis, severe acute respiratory syndrome (SARS), corona, avian influenza A H7N9 virus, and dengue virus [148]. Accordingly, high morbidity and mortality rates are attained. Thus, for pandemic control and prevention, a rapid and selective diagnosis of viruses is urgently needed. In this regard, diagnosis of virus infections could be achieved by cell culture (virus propagation), virus-specific IgM antibodies, enzyme-linked immunosorbent assay (ELISA), and polymerase chain reaction (PCR) [149, 150]. However, those methods require expensive enzymes and antibodies for the selective recognition of the analytes. Hence, the development of efficient, cost-effective, and reusable artificial virus receptors was proposed [10, 72, 151, 152].

Development of Imprinted Polymers for virus recognition was pioneered by Dickert [152] and Lieberzeit [10] using micro-contact imprinting on QCM sensors, and then it was extended by Uzun and Denizli [153] to SPR readout.

The use for real-time monitoring of virus and viral infection has been addressed in several research reports [154, 155]. At the beginning of the development, whole-virus particles were used as template in polymer synthesis (VIPs). Derived from the epitope approach of protein MIPs, molecular substructures on the virus surface have been utilized in the synthesis of imprinted polymers for the binding of the whole virus.

7.1 Virus-Imprinted Polymers (VIPs)

Quartz crystal microbalance was combined with micro-contact imprinting to produce the first MIPs for viruses. The MIP for tobacco mosaic virus was fabricated by surface imprinting using a tobacco mosaic virus stamp that was pressed into a copolymer of N-vinylpyrrolidone and methacrylic acid to be spin-coated onto a modified quartz disk. Using the developed chip, it was possible to study dissociation kinetics and viral binding with high reusability and fast responses [152].

VIPs have been evaluated as a synthetic virus neutralizing platform using porcine reproductive and respiratory syndrome virus (PRRSV-1) [156]. During the optimization procedure of this sensor, specificity of virus neutralization alongside the impact of incubation time on the sensor performance was studied. The MIP selectivity was assessed herein by comparing their neutralizing effects on PRRSV-1 to the effects on the unrelated bovine viral diarrhea virus-1. As a result, no significant cross-reactivity was detected. Thus, the VIPs demonstrated effective virus neutralization in a short time (<30 min), while the neutralization effect has been shown to be concentration dependent.

Foot-and-mouth disease (FMDV) diagnosis was carried out using viral Imprinted Polymer (VIP)-based electrochemical sensors [157]. Two different serotypes (FMDV-O and FMDV-SAT2) were identified and determined in real animal samples using two different VIP sensors. In terms of serotype O diagnosis, the selective recognition sites have been designed through the electropolymerization of *o*-aminophenol with the inactivated whole-virus particles on gold screen-printed electrodes (Au-SPEs). Infrared spectroscopy, scanning electron microscopy, atomic force microscopy, and CV have been used for VIP fabrication and characterization. A cross-reactivity study was carried out on several interfering viruses such as lumpy skin disease virus, FMD serotypes A, and SAT2. Detection and quantification limits were estimated to be 2 and 6 ng/ml [158].

Another VIP sensor was developed for the detection of FMDV-SAT2 serotype by the direct electrochemical deposition of FMDV inactivated particles within the poly (*o*-PD) film on gold-copper nanostructured electrodes. This VIP sensor was used for the determination of SAT2 serotype in real clinical field specimens without sample treatment [157].

Recently, a double-mediated impedimetric viral sensor was designed for the rapid detection of the whole SARS-CoV-2 particles. In this study, a mixture of lipophilic electron shuttle (DCIP) and hydrophilic ferricyanide (FCN) was implemented for enhancing the electrochemical signals. Additionally, a nanocomposite (carbon nanotubes/tungsten oxides) was exploited for enlarging the imprinted surface area, as illustrated in Fig. 6. The sensor supported the on-site investigations with a very rapid detection of whole-virus particles in clinical samples [159]. Besides, several respiratory non-targeting viruses were tested including influenza A viruses (H1N1, H5N1, and H3N2), influenza B, human coronaviruses (hCoVs)-OC43, NL63, 229E, and Middle East respiratory syndrome coronavirus (MERS-CoV). In conclusion to this part, virus-designated sensors represent effective diagnostic methods for rapid response, high sensitivity and selectivity, and quantitative determination capability for viruses in real samples without labeling, and without the need for biological molecules such as DNA and RNA.

Using the virus particle as the template, imprinted resonance light-scattering (RLS) sensors have been fabricated and applied for the detection of the Japanese encephalitis virus [160]. With the same RLS technique, the authors further developed a MIP sensor for hepatitis A virus (HAV) detection [161]. Within less than 20 min the sensor was implemented for real sample analysis, for which a linear dynamic range of 0.02–2.0 nM has been achieved with a detection limit of 0.1 pM. The sensor's recovery was evaluated in a range from 88% to 107%, to support the determination of the virus in human serum samples.

A rapid detection and identification of the Zika virus (ZIKV) has been accomplished by utilizing the virus as the template and graphene oxide composites as a platform for the production of a MIP-based electrochemical sensor [162].

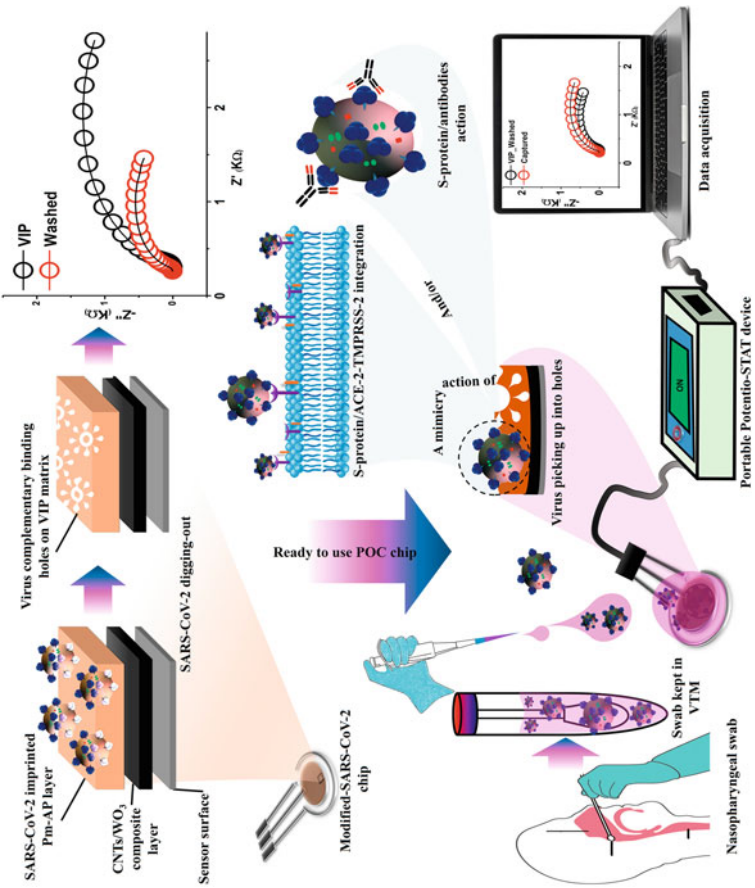

Fig. 6 SARS-CoV-2 VIP nano-disposable sensor chips: fabrication and application in clinical samples [159]

7.2 Sub-Structure Imprinted Polymers for the Recognition of Viruses

A pentadecapeptide (15-mer peptide) has been selected by Tai et al. as a linear epitope of the dengue virus to be exploited as potential template for imprinting on QCM sensors [163]. The imprinted film could recognize both the template and the whole-virus protein. Hence, dengue virus in patients' serum was detected with high accuracy.

Further, using polymeric nanoparticles of methacrylate and acrylate, MIPs have been fabricated by Piletska et al. and implemented for virus screening and identification using different epitopes of adeno-associated viruses (AAV) [164]. On the other hand, a MIP-based sensor was fabricated for the viral hexon protein, the most accessible and abundant surface protein of the human adenovirus type 5 (hAdV5) icosahedral capsid. The corresponding MIP which recognized the entire virus utilized the protein molecule as the template. To validate the sensor's selectivity, two different viruses including hAdV5 and minute virus of mice (MVM) were exposed to the sensor without exhibiting an obvious binding [165].

An electrochemical impedimetric MIP-based sensor has been constructed for dengue virus detection in serum samples during the early stage of the infection. In this context, self-polymerization of dopamine (forming polydopamine (PDA)) was exploited in the presence of target non-structural protein1 (NS1) to create the specific template, in which 0.3 ng/ml was defined as the calculated limit of dengue virus detection [166].

7.3 Functional Proteins of SARS-CoV-2 and Epitopes

For the detection of SARS-CoV-2 in addition to the entire virus or virus-like particles the nucleocapsid protein (N-protein), the spike protein (S-protein), or the receptor binding domain (RBD) was imprinted in the polymer [167–172]. Furthermore, exposed peptide regions of the spike protein were utilized as the template [39, 173–175].

The first MIP sensor for COVID-19 was formed by electropolymerization of m-phenylenediamine around a self-assembled monolayer (SAM) of the N-protein and utilized a redox marker for the electrochemical readout. This sensor revealed a linear response up to 110 fM [167].

Furthermore, a screen-printed carbon electrode loaded with gold/graphene (Au/Gr) nanohybrids used arginine as the functional monomer for an N-protein MIP, exhibiting a wide linear range as well as low detection limit and specific recognition [170].

For the recognition of the S-protein, a polypyrrole layer was electrochemically deposited on platinum black-covered platinum electrodes. Rebinding was analyzed using chronopotentiometry to evaluate the decrease of conductivity by the

displacement of ions by the protein target in the MIP cavities. The S-protein was preferentially bound as compared with HSA, while the imprinting factor was (only) 2.1 [168].

The SARS virus docks via the 26 kDa RBD to the angiotensin-converting enzyme (ACE2) of the host cell [176]. Parisi et al. developed MIPs for the RBD which successfully block the binding of the spike protein to the ACE2 receptor [169, 177]. Besides, Cennamo et al. developed SPR-based MIP sensor using acrylamide as monomer for the specific recognition of the S1 subunit of the spike protein. The sensor was capable of detecting SARS-CoV-2 virions in nasopharyngeal swabs [178].

Cubuk et al. [179] performed molecular docking and molecular dynamics simulation for the interaction of different functional monomers with epitopes of the RBD. 2-acrylamido-2-methylpropanesulfonic acid and itaconic acid were proposed as optimal functional monomers and TEIYQAGST as a template molecule.

The peptide chain starting from L_{455} up to Y_{505} is the binding area of the RBD to the host cell [176]. Gyurcsányi's group applied the nonapeptide G485-Q493 (GFNCYFPLQ) as the template. The peptide was microspotted on gold SPR chips followed by electrodeposition of polyscopoletin and template removal by anodic potential pulses. RBD was bound to the epitope MIP in the lower nanomolar concentration range with K_d values ranging from 2 to 18 nM, while HSA had a negligible effect in 0.5% Tween20 solution [173].

Mizaikoff's group applied the peptide 486-502 of the RBD as template in the synthesis of MIP-covered magnetic nanoparticles (NPs). The NPs were covered with the MIP shell by "self-polymerization" of the peptide containing dopamine solution. The authors concluded that the MIP can differentiate between different viruses; however, no experiments with the RBD or the virus were presented [174].

Recently, MIP Diagnostics presented a thermal resistance sensor based on nano-MIPs for the recognition of the spike protein. The nano-MIPs were prepared by solid-phase synthesis using a decapeptide of an unknown sequence from the spike protein as the template. They were coupled to the electrode surface via electrografted 4-aminobenzoic acid. The company claims that both alpha and delta variants of the spike protein can be determined in clinical samples within 15 min [39].

The hepta-peptide G485 to P491 (GFNCYFP) of the receptor binding domain was used as the template in the electrosynthesis of the respective MIPs (Fig. 7) [180]. It was chemisorbed via its Cys488 in the central position on gold wire electrodes before the deposition of polyscopoletin and template removal by anodic potential pulses. Epitope mapping of six related peptides revealed that the binding affinity was based on the strong interaction between cysteine and Au surface and the number of coinciding amino acids with the template. Both RBD and the spike protein were bound in the lower nM region to the epitope MIP, while HSA exhibited a very low affinity. The high affinity toward the RBD combined with low nonspecific adsorption of HSA allowed the measurement in the 1:20 diluted (spiked) solution of COVID antigen tests.

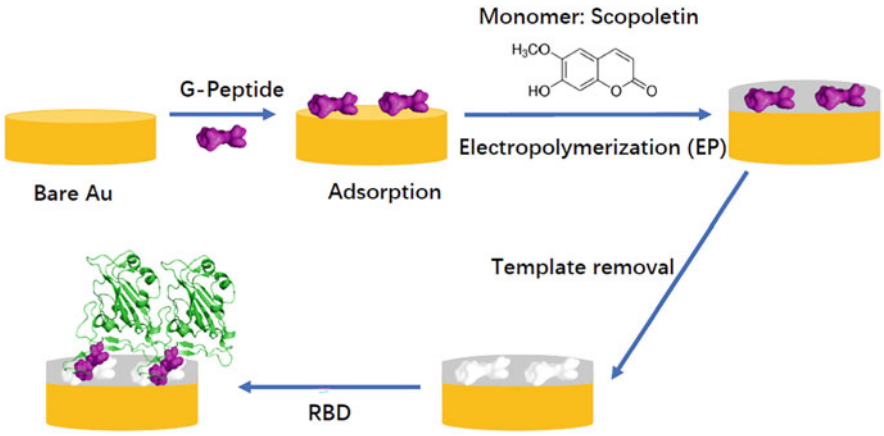

Fig. 7 Schematic of MIP preparation and binding of RBD. The G-peptide (GFNCYFP) was assumed to be adsorbed horizontally on the bare gold via cysteine. Reproduced from Zhang et al. [180]. It is licensed under a Creative Commons Attribution-NonCommercial 3.0 Unported License (CC BY-NC 3.0) https://creativecommons.org/licenses/by-nc/3.0/

8 Imprinted Polymers for the Recognition of Cells

8.1 Cell-Imprinted Polymers (CIPs)

Cell-Imprinted Polymers (CIPs) have been derived from the concept of Molecularly Imprinted Polymers and exclusively use organisms such as yeast, bacteria, mammalian cells, and algae [181] as templates [182].

There is an increasing body of publications stating the use of whole-cell Imprinted Polymers in chemical sensors and bioimaging [183]. CIPs have the advantage of theoretically unlimited shelf life, improved thermal and chemical stability, and straightforward, low-cost manufacturing compared to natural antibodies. Actually, the very first study of microorganism imprinting relied on bacteria as the template: Vulfson and coworkers reported on the synthesis of imprinted polymer microspheres utilizing *Staphylococcus aureus* and *Listeria monocytogenes* as the templates [184]. However, to date the most widely used approach in microorganism imprinting relies on a different technique, namely, stamp imprinting, also called micro-contact stamping. In contrast to emulsion-based strategies [185], this approach provides thin films, which are especially interesting for sensing applications.

The template cells usually bind via adhesion to a flat solid support or are immobilized onto it. Using this setup as a stamp, one can structure a prepolymer film followed by a polymerization step through UV irradiation or heat treatment. This results in a stable layer with the required cavities after removing the template species. As observed for molecular imprinting in general, both the morphology of the imprinted cavity and the exact position of surface functionalities need to be stable

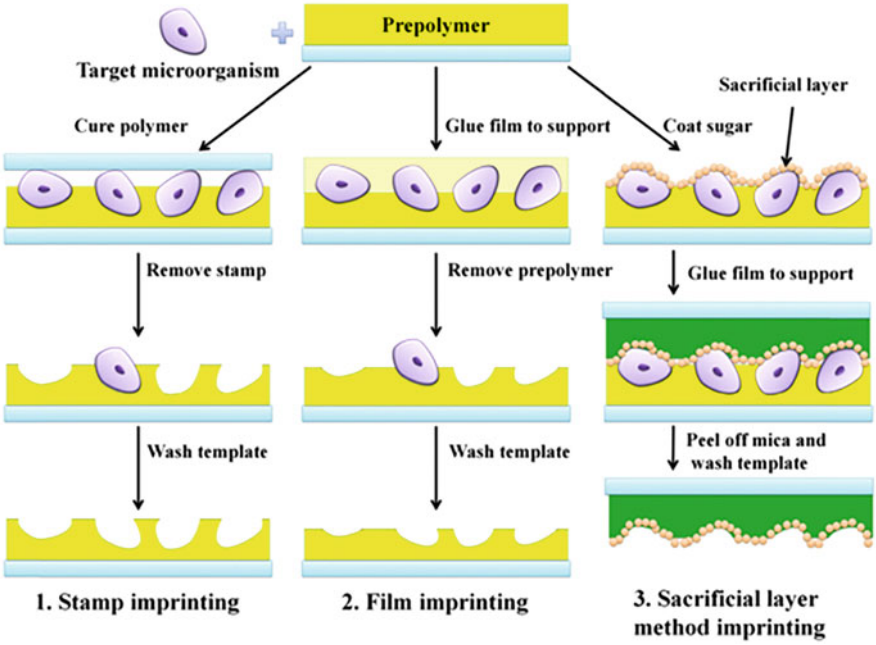

Fig. 8 Schematic procedures for three types of directing cell imprinting. Adapted with permission from [187]. © Elsevier BV, Amsterdam, The Netherlands 2018

and resist harsh conditions, such as thermal stress and solvent exposure. This demands an optimization of the monomer composition for a specific application. For instance, by increasing the degree of crosslinking a well-patterned polymer surface was obtained that facilitates microorganism binding [186].

Direct micro-contact imprinting is the most straightforward technique to obtain high selectivity in microbial imprinting. Figure 8 shows three basic categories of direct imprinting: stamp imprinting, film imprinting, and sacrificial layer imprinting [126]. Stamp imprinting is the most straightforward method: one prepares stamps by coating a solution of target species onto a solid substrate, sometimes containing functional groups for covalent immobilization. After evaporation of the solvent, the resulting stamp is prepared for imprinting. However, the solvent type may considerably influence the imprint process: for example, the use of buffers may lead to the formation of salt crystals on the stamp surfaces. The main drawback of this approach is that the removal of the stamps may be tedious. In the case of fragile cells, it may be better to use film imprinting (also called "sedimentation imprinting"), where the template species is directly deposited on the prepolymer and let to sediment without applying mechanical pressure through a stamp. The sacrificial layer approach is applicable when monomer(s) and template may chemically react with each other. In the case of cell imprinting into polyurethanes, it is beneficial to deposit a thin saccharide film on the stamp to prevent chemical reactions between the isocyanate

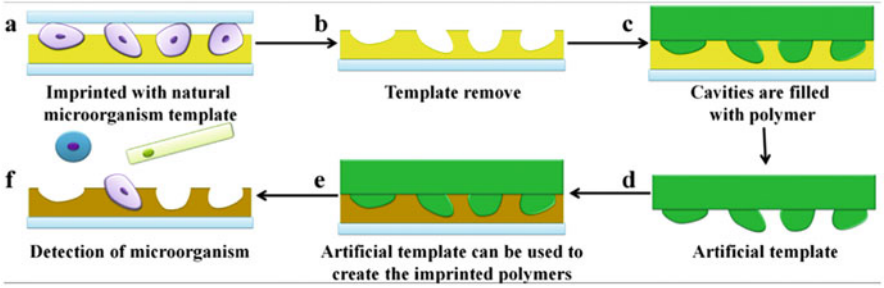

Fig. 9 Schematic procedures for indirect imprinting. Adapted with permission from [187]. © Elsevier BV, Amsterdam, The Netherlands 2018

monomer and primary amino groups on the cell surface. The respective saccharides remain bound in the final CIP and provide it with the necessary non-covalent binding network. Furthermore, this type of approach usually allows a straightforward template removal. However, the need to prepare and wash off the sacrificial layer makes the strategy more tedious.

Direct imprinting implies one major disadvantage, namely the poor stability of natural templates under harsh environments, such as in acids, bases, or organic solvents, which may decrease the selectivity of the finally imprinted layers. One way to overcome this obstacle is to apply indirect micro-contact imprinting as shown in Fig. 9, by creating "artificial cells" from a polymer. To achieve this, one first generates an imprint of the target biospecies in a polymer. In the second step, the cavities are filled with a second prepolymer after the template has been removed. After polymerization, the new material ideally mimics under optimal conditions the shape and functionality of the original cell and thus constitutes an "artificial template" following separation step of the two polymers.

8.2 Imprinting of Cell Substructures

Imprinting with entire cells can be a very tedious process for several reasons: first, they can be rather sensitive to polymerization conditions. Second, the micro-contact printing process requires the immobilization of the cells on a surface as mentioned before. However, together with the stamping process itself this often changes the morphology of cells: they become "flattened" on the surface.

So-called "epitope imprinting" [188] is well known in protein imprinting, where the imprinted cavities behave like natural antibodies in the sense that they bind to their target through a small substructure. In the context of cell imprinting, the respective approach focuses on certain molecular elements on the cell surface, mainly proteins and saccharides. Such kind of cell recognition can be applied for capturing specific cell, such as cancer cells in organs [189].

8.2.1 Imprinting of Membrane Proteins

Membrane proteins are well-known targets in substructure cell imprinting. Choosing this strategy, it is possible to imprint the entire proteins or a corresponding peptide epitope based on affinity binding to cell surface structures. For instance, fibronectin (FN) was imprinted by using silanes as functional monomers and a calcium alginate hydrogel membrane as substrate for the production of fibronectin (FN)-imprinted polysiloxane (FN-MIP) to elevate cell adhesion and favorable cell growth for mouse fibroblasts (L929) [190].

However, the limitations of protein-imprinted polymers are of constant concern. A review from H.R. Culver and N. A. Peppas summarizes challenges and problematic issues including the complexity and large size of protein structures as well as their environmental instability [191].

Indeed, using epitopes rather than the entire target protein as a template offers major advantages for imprinting, including a significant reduction of the cost for MIP production as well as preventing the protein from unfolding during the imprinting process, which ultimately enhances the binding affinity of the created cavities.

8.2.2 Imprinting of Saccharides

More recently, an increasing number of papers report on the usage of saccharides as epitope templates in cell imprinting. Lipopolysaccharide (LPS) imprinting is a perfect example of such an approach: LPS is present on the outer membranes of all Gram-negative bacteria and fulfills an essential role in bacterial resistance with structural modification to avoid the interaction with positively charged antimicrobial peptide receptors. Natural LPS modifications comprise the addition or hydroxylation of fatty acids, and the addition of phosphoethanolamine (PEtN) to the core and lipid A regions, etc. [192].

The LPS consists of two distinct parts: a hydrophilic polysaccharide core and a hydrophobic lipid known as lipid A. Hence, LPS recognition sites on the surface of imprinted hydrogels derived from the utilization of lipid A as a target molecule are suitable to remove LPS from pure water. As a result, the prepared imprinted hydrogels appreciably distinguished the LPS of *E. coli* (toxic LPS) from two other LPS competitors [193]. However, this approach demonstrates only the potential in whole-cell recognition rather than realizing it at the final stage. The latter has been achieved by a different target analyte, namely monosaccharides present on the surfaces of cancer cells. Synthesizing MIP-based fluorescent nanoparticles (NPs) allows us to directly label the target cell. Figure 10 shows both the synthesis approach (Fig. 10a) and the binding assay on the cell surface (Fig. 10b) [194].

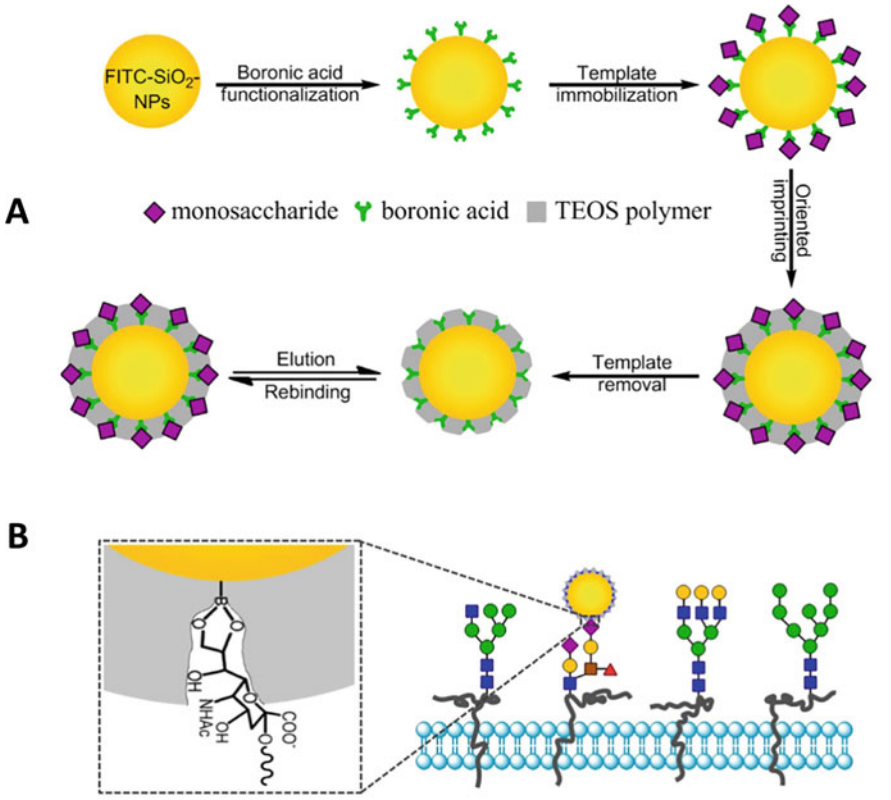

Fig. 10 Monosaccharide-imprinted FITC-doped silica NPs (**a**) and the interaction between MIP NPs and cancer cells (**b**). Reproduced from Wang et al. [194]. It is licensed under a Creative Commons Attribution 4.0 International License (CC BY 4.0) http://creativecommons.org/licenses/by/4.0/

8.3 Applications of Cell Imprinting

Many of the cell concentration and separation techniques are direct binding assays, implying that the number of cells per milliliter (typically expressed as CFU) can be determined by an immediate detection of the trapped cells, mainly bacteria. The main advantage of this assay format is that it offers rapid detection. Overall, the data generated so far clearly indicate that this relatively new approach for quantifying (harmful) microorganisms is highly interesting for real-life analysis problems in environmental samples.

However, applying MIP for cells does not end there: sensors based on MIPs/CIPs have been employed as rapid diagnostic techniques for various diseases: A recent study demonstrated that CIPs synthesized on the surfaces of magnetic particles (magnetic MIPs) are useful to detect *Staphylococcus aureus* in milk and rice

[195]. Zhang et al. developed a pseudo-ELISA to detect *Staphylococcus aureus* in buffer. Unlike the classic sandwich ELISA method, they used synthetic receptors instead of natural antibodies and reported lower limits of detection compared to biologically based assays [196].

Another study used *Escherichia coli* cells imprinted on amino acid-based polymer via micro-contact imprinting on both optical and mass-sensitive devices to quantify this species [197].

Despite these few success stories, creating cavities, which comprise an optimal affinity for selective capture and quantification of microbial cells, still remains a major challenge. Inspired by molecular recognition in nature, CIPs have emerged as a promising strategy for this purpose: they cause relatively low costs, are stable, and are versatile [198].

The development of MIPs to target certain cells like human cancer cells [194] or pathogenic microorganisms has been intensively studied and remarkably assisted the transformation from clinical practice to individualized medicine. However, creating Imprinted Polymers that can transform cell recognition from passive binding to active intervention in cell biology is still an open challenge. Any breakthrough in this area could result in new application paradigms to improve current treatment and diagnostic strategies.

9 Outlook

The clearest advantage of imprinted polymers is the simplicity of preparation and integration in a sensor. They can be easily prepared by using a few monomers and eventually a crosslinker in the form of nanoparticles or deposited on the sensor surface. In the future integration of signal generation in "self-signaling," sensors will allow the decentralized measurement of health parameters, supervision of nutrition, and environmental control. A prerequisite for these applications is a negligible nonspecific interaction of the targets with the polymer surface.

Acknowledgments This book capital is financed under the TKP2021 funding scheme. F. W. S., A. Y. and I.Z. were funded by the Deutsche Forschungsgemeinschaft (DFG, German Research Foundation) under Germany's Excellence Strategy—EXC 2008–390540038 (Unifying Systems in Catalysis—UniSysCat). F. F. B. and X. Z. are indebted for financial support from the German Ministry of Education and Research (BMBF, 01DH20018).

References

1. Polyakov MV (1931) Adsorption properties and structure of silica gel. Zhur Fiz Khim 2:799–895
2. Wulff G, Sarhan A (1972) Use of polymers with enzyme-analogous structures for the resolution of racemates. Angew Chem Int Ed 11:334–342. https://doi.org/10.1002/anie.197203341

3. Arshady R, Mosbach K (1981) Synthesis of substrate-selective polymers by host-guest polymerization. Die Makromol Chemie 182:687–692. https://doi.org/10.1002/MACP.1981.021820240
4. Erdőssy J, Horváth V, Yarman A et al (2016) Electrosynthesized molecularly imprinted polymers for protein recognition. Trends Anal Chem 79:179–190. https://doi.org/10.1016/J.TRAC.2015.12.018
5. Pluhar B, Mizaikoff B (2015) Advanced evaluation strategies for protein-imprinted polymer nanobeads. Macromol Biosci 15:1507–1511. https://doi.org/10.1002/MABI.201500106
6. Van Ho PN, Sussitz HF, Ladenhauf E et al (2018) Combined layer/particle approaches in surface molecular imprinting of proteins: signal enhancement and competition. Sensors 18:180. https://doi.org/10.3390/S18010180
7. Lin H-Y, Hsu C-Y, Thomas JL et al (2006) The microcontact imprinting of proteins: the effect of cross-linking monomers for lysozyme, ribonuclease A and myoglobin. Biosens Bioelectron 22:534–543. https://doi.org/10.1016/j.bios.2006.07.038
8. Menaker A, Syritski V, Reut J et al (2009) Electrosynthesized surface-imprinted conducting polymer microrods for selective protein recognition. Adv Mater 21:2271–2275. https://doi.org/10.1002/adma.200803597
9. Sharma PS, Pietrzyk-Le A, D'Souza F, Kutner W (2012) Electrochemically synthesized polymers in molecular imprinting for chemical sensing. Anal Bioanal Chem 402:3177–3204. https://doi.org/10.1007/s00216-011-5696-6
10. Hayden O, Lieberzeit PA, Blaas D, Dickert FL (2006) Artificial antibodies for bioanalyte detection - sensing viruses and proteins. Adv Funct Mater 16:1269–1278. https://doi.org/10.1002/adfm.200500626
11. Yarman A, Scheller FW (2020) How reliable is the electrochemical readout of MIP sensors? Sensors 20:2677. https://doi.org/10.3390/s20092677
12. Bedwell TS, Anjum N, Ma Y et al (2019) New protocol for optimisation of polymer composition for imprinting of peptides and proteins. RSC Adv 9:27849–27855. https://doi.org/10.1039/c9ra05009d
13. Cowen T, Karim K, Piletsky S (2016) Computational approaches in the design of synthetic receptors – a review. Anal Chim Acta 936:62–74. https://doi.org/10.1016/j.aca.2016.07.027
14. Hjertén S, Liao J-L, Nakazato K et al (1997) Gels mimicking antibodies in their selective recognition of proteins. Chromatographia 44:227–234. https://doi.org/10.1007/BF02466386
15. Takátsy A, Kilár A, Kilár F, Hjertén S (2006) Universal method for synthesis of artificial gel antibodies by the imprinting approach combined with a unique electrophoresis technique for detection of minute structural differences of proteins, viruses, and cells (bacteria): Ia. Gel antibodies against p. J Sep Sci 29:2802–2809. https://doi.org/10.1002/JSSC.200600211
16. Reddy SM, Sette G, Phan Q (2011) Electrochemical probing of selective haemoglobin binding in hydrogel-based molecularly imprinted polymers. Electrochim Acta 56:9203–9208. https://doi.org/10.1016/J.ELECTACTA.2011.07.132
17. Venkataraman AK, Clegg JR, Peppas NA (2020) Polymer composition primarily determines the protein recognition characteristics of molecularly imprinted hydrogels. J Mater Chem B 8:7685–7695. https://doi.org/10.1039/d0tb01627f
18. Tan CJ, Tong YW (2007) Preparation of superparamagnetic ribonuclease A surface-imprinted submicrometer particles for protein recognition in aqueous media. Anal Chem 79:299–306. https://doi.org/10.1021/ac061364y
19. Zhang H (2020) Molecularly imprinted nanoparticles for biomedical applications. Adv Mater 32. https://doi.org/10.1002/adma.201806328
20. Xu J, Ambrosini S, Tamahkar E et al (2016) Toward a universal method for preparing molecularly imprinted polymer nanoparticles with antibody-like affinity for proteins. Biomacromolecules 17:345–353. https://doi.org/10.1021/acs.biomac.5b01454
21. Refaat D, Aggour MG, Farghali AA et al (2019) Strategies for molecular imprinting and the evolution of MIP nanoparticles as plastic antibodies—synthesis and applications. Int J Mol Sci 20:6304. https://doi.org/10.3390/IJMS20246304

22. Crapnell RD, Canfarotta F, Czulak J et al (2019) Thermal detection of cardiac biomarkers heart-fatty acid binding protein and ST2 using a molecularly imprinted nanoparticle-based multiplex sensor platform. ACS Sensors 4:2838–2845. https://doi.org/10.1021/ACSSENSORS.9B01666/SUPPL_FILE/SE9B01666_SI_001.PDF
23. Lin LI, Xiwen HE, Langxing C, Yukui Z (2009) Preparation of novel bovine hemoglobin surface- imprinted polystyrene nanoparticles with magnetic susceptibility. Sci China Ser B Chem 52:1402–1411. https://doi.org/10.1007/s11426-009-0182-0
24. Xu J, Haupt K, Tse Sum Bui B (2017) Core–shell molecularly imprinted polymer nanoparticles as synthetic antibodies in a sandwich fluoroimmunoassay for trypsin determination in human serum. ACS Appl Mater Interfaces 9:24476–24483. https://doi.org/10.1021/acsami.7b05844
25. Dinc M, Esen C, Mizaikoff B (2019) Recent advances on core–shell magnetic molecularly imprinted polymers for biomacromolecules. Trends Anal Chem 114:202–217. https://doi.org/10.1016/j.trac.2019.03.008
26. Parisi OI, Francomano F, Dattilo M et al (2022) The evolution of molecular recognition: from antibodies to molecularly imprinted polymers (MIPs) as artificial counterpart. J Funct Biomater 13:12. https://doi.org/10.3390/JFB13010012
27. Shi H, Tsal WB, Garrison MD et al (1999) Template-imprinted nanostructured surfaces for protein recognition. Nature 398:593–597. https://doi.org/10.1038/19267
28. Chou PC, Rick J, Chou TC (2005) C-reactive protein thin-film molecularly imprinted polymers formed using a micro-contact approach. Anal Chim Acta 542:20–25. https://doi.org/10.1016/j.aca.2004.12.074
29. Ertürk G, Hedström M, Mattiasson B (2016) A sensitive and real-time assay of trypsin by using molecular imprinting-based capacitive biosensor. Biosens Bioelectron 86:557–565. https://doi.org/10.1016/j.bios.2016.07.046
30. Bognár J, Szucs J, Dorkõ Z et al (2013) Nanosphere lithography as a versatile method to generate surface-imprinted polymer films for selective protein recognition. Adv Funct Mater 23:4703–4709. https://doi.org/10.1002/adfm.201300113
31. Scheller FW, Zhang X, Yarman A et al (2019) Molecularly imprinted polymer-based electrochemical sensors for biopolymers. Curr Opin Electrochem 14:53–59. https://doi.org/10.1016/J.COELEC.2018.12.005
32. Malitesta C, Mazzotta E, Picca RA et al (2012) MIP sensors - the electrochemical approach. Anal Bioanal Chem 402:1827–1846. https://doi.org/10.1007/S00216-011-5405-5/FIGURES/8
33. Kalecki J, Cieplak M, Dabrowski M et al (2020) Hexagonally packed macroporous molecularly imprinted polymers for chemosensing of follicle-stimulating hormone protein. ACS Sensors 5:118–126. https://doi.org/10.1021/acssensors.9b01878
34. Cieplak M, Kutner W (2016) Artificial biosensors: how can molecular imprinting mimic biorecognition? Trends Biotechnol 34:922–941. https://doi.org/10.1016/j.tibtech.2016.05.011
35. Palladino P, Minunni M, Scarano S (2018) Cardiac troponin T capture and detection in real-time via epitope-imprinted polymer and optical biosensing. Biosens Bioelectron 106:93–98. https://doi.org/10.1016/J.BIOS.2018.01.068
36. Moreira Gonçalves L (2021) Electropolymerized molecularly imprinted polymers: perceptions based on recent literature for soon-to-be world-class scientists. Curr Opin Electrochem 25:100640
37. Menger M, Yarman A, Erdőssy J et al (2016) MIPs and aptamers for recognition of proteins in biomimetic sensing. Biosensors 6:35. https://doi.org/10.3390/bios6030035
38. Zhang X, Yarman A, Erdossy J et al (2018) Electrosynthesized MIPs for transferrin: plastibodies or nano-filters? Biosens Bioelectron 105:29–35. https://doi.org/10.1016/J.BIOS.2018.01.011
39. McClements J, Bar L, Singla P et al (2022) Molecularly imprinted polymer nanoparticles enable rapid, reliable, and robust point-of-care thermal detection of SARS-CoV-2. ACS Sensors 7:1122–1131. https://doi.org/10.1021/ACSSENSORS.2C00100

40. Yarman A (2018) Development of a molecularly imprinted polymer-based electrochemical sensor for tyrosinase. Turkish J Chem 42:346–354. https://doi.org/10.3906/kim-1708-68
41. Stojanovic Z, Erdőssy J, Keltai K et al (2017) Electrosynthesized molecularly imprinted polyscopoletin nanofilms for human serum albumin detection. Anal Chim Acta 977:1–9. https://doi.org/10.1016/j.aca.2017.04.043
42. Cieplak M, Szwabinska K, Sosnowska M et al (2015) Selective electrochemical sensing of human serum albumin by semi-covalent molecular imprinting. Biosens Bioelectron 74:960–966. https://doi.org/10.1016/j.bios.2015.07.061
43. Pacheco JG, Silva MSV, Freitas M et al (2018) Molecularly imprinted electrochemical sensor for the point-of-care detection of a breast cancer biomarker (CA 15-3). Sens Actuators B 256: 905–912. https://doi.org/10.1016/J.SNB.2017.10.027
44. Gomes RS, Moreira FTC, Fernandes R, Sales MGF (2018) Sensing CA 15-3 in point-of-care by electropolymerizing O-phenylenediamine (oPDA) on Au-screen printed electrodes. PloS One 13:e0196656. https://doi.org/10.1371/journal.pone.0196656
45. Yazdani Z, Yadegari H, Heli H (2019) A molecularly imprinted electrochemical nanobiosensor for prostate specific antigen determination. Anal Biochem 566:116–125. https://doi.org/10.1016/j.ab.2018.11.020
46. Jetzschmann KJ, Jágerszki G, Dechtrirat D et al (2015) Vectorially imprinted hybrid nanofilm for acetylcholinesterase recognition. Adv Funct Mater 25:5178–5183. https://doi.org/10.1002/adfm.201501900
47. Moreira FTC, Ferreira MJMS, Puga JRT, Sales MGF (2016) Screen-printed electrode produced by printed-circuit board technology. Application to cancer biomarker detection by means of plastic antibody as sensing material. Sens Actuators B 223:927–935. https://doi.org/10.1016/j.snb.2015.09.157
48. Cardoso AR, de Sá MH, Sales MGF (2019) An impedimetric molecularly-imprinted biosensor for interleukin-1β determination, prepared by in-situ electropolymerization on carbon screen-printed electrodes. Bioelectrochemistry 130:1–9. https://doi.org/10.1016/j.bioelechem.2019.04.017
49. Bosserdt M, Erdőssy J, Lautner G et al (2015) Microelectrospotting as a new method for electrosynthesis of surface-imprinted polymer microarrays for protein recognition. Biosens Bioelectron 73:123–129. https://doi.org/10.1016/j.bios.2015.05.049
50. Saylan Y, Denizli A (2018) Molecular finger prints of hemoglobin on a nanofilm chip. Sensors 18. https://doi.org/10.3390/s18093016
51. Matsunaga T, Hishiya T, Takeuchi T (2007) Surface plasmon resonance sensor for lysozyme based on molecularly imprinted thin films. Anal Chim Acta 591:63–67. https://doi.org/10.1016/j.aca.2007.02.072
52. Ashley J, Shukor Y, D'Aurelio R et al (2018) Synthesis of molecularly imprinted polymer nanoparticles for α-casein detection using surface plasmon resonance as a milk allergen sensor. ACS Sensors 3:418–424. https://doi.org/10.1021/acssensors.7b00850
53. Lu H, Xu S (2020) Ultrasensitive turn on molecularly imprinted fluorescence sensor for glycoprotein detection based on nanoparticles signal amplification. Sens Actuators B 306: 127566. https://doi.org/10.1016/j.snb.2019.127566
54. Chunta S, Suedee R, Boonsriwong W, Lieberzeit PA (2020) Biomimetic sensors targeting oxidized-low-density lipoprotein with molecularly imprinted polymers. Anal Chim Acta 1116: 27–35. https://doi.org/10.1016/j.aca.2020.04.017
55. Karaseva NA, Pluhar B, Beliaeva EA et al (2019) Synthesis and application of molecularly imprinted polymers for trypsin piezoelectric sensors. Sens Actuators B 280:272–279. https://doi.org/10.1016/J.SNB.2018.10.022
56. Lu C-H, Zhang Y, Tang S-F et al (2012) Sensing HIV related protein using epitope imprinted hydrophilic polymer coated quartz crystal microbalance. Biosens Bioelectron 31:439–444. https://doi.org/10.1016/J.BIOS.2011.11.008

57. Liu S, Zhou D, Guo T (2013) Construction of a novel macroporous imprinted biosensor based on quartz crystal microbalance for ribonuclease A detection. Biosens Bioelectron 42:80–86. https://doi.org/10.1016/j.bios.2012.11.002
58. Ahmad OS, Bedwell TS, Esen C et al (2019) Molecularly imprinted polymers in electrochemical and optical sensors. Trends Biotechnol 37:294–309. https://doi.org/10.1016/J.TIBTECH.2018.08.009
59. El Kirat K, Bartkowski M, Haupt K (2009) Probing the recognition specificity of a protein molecularly imprinted polymer using force spectroscopy. Biosens Bioelectron 24:2618–2624. https://doi.org/10.1016/J.BIOS.2009.01.018
60. Bosserdt M, Gajovic-Eichelman N, Scheller FW (2013) Modulation of direct electron transfer of cytochrome c by use of a molecularly imprinted thin film. Anal Bioanal Chem 405:6437–6444. https://doi.org/10.1007/s00216-013-7009-8
61. Peng L, Yarman A, Jetzschmann KJ et al (2016) Molecularly imprinted electropolymer for a hexameric heme protein with direct electron transfer and peroxide electrocatalysis. Sensors 16:272. https://doi.org/10.3390/s16030272
62. Yarman A (2018) Electrosynthesized molecularly imprinted polymer for laccase using the inactivated enzyme as the target. Bull Korean Chem Soc 39:483–488. https://doi.org/10.1002/bkcs.11413
63. Li S, Yang K, Zhao B et al (2016) Epitope imprinting enhanced IMAC (EI-IMAC) for highly selective purification of His-tagged protein. J Mater Chem B 4:1960–1967. https://doi.org/10.1039/c5tb02505b
64. Moreira FTC, Sharma S, Dutra RAF et al (2014) Protein-responsive polymers for point-of-care detection of cardiac biomarker. Sens Actuators B 196:123–132. https://doi.org/10.1016/J.SNB.2014.01.038
65. Jun-Fei Z, Shi-Li L (2020) Molecularly imprinted polymers-surface-enhanced Raman spectroscopy: state of the art and prospects. Int J Environ Anal Chem 00:1–31. https://doi.org/10.1080/03067319.2020.1738413
66. Guo X, Li J, Arabi M et al (2020) Molecular-imprinting-based surface-enhanced Raman scattering sensors. ACS Sensors 5:601–619. https://doi.org/10.1021/acssensors.9b02039
67. Caserta G, Zhang X, Yarman A et al (2021) Insights in electrosynthesis, target binding, and stability of peptide-imprinted polymer nanofilms. Electrochim Acta 381:138236. https://doi.org/10.1016/j.electacta.2021.138236
68. Supala E, Tamás L, Erdőssy J, Gyurcsányi RE (2020) Multiplexed redox gating measurements with a microelectrospotter. Towards electrochemical readout of molecularly imprinted polymer microarrays. Electrochem Commun 119:106812. https://doi.org/10.1016/J.ELECOM.2020.106812
69. Yoshimi Y, Ohdaira R, Iiyama C, Sakai K (2001) 'Gate effect' of thin layer of molecularly-imprinted poly(methacrylic acid-co-ethyleneglycol dimethacrylate). Sens Actuators B 73:49–53. https://doi.org/10.1016/S0925-4005(00)00671-7
70. Sönmezler M, Özgür E, Yavuz H, Denizli A (2019) Quartz crystal microbalance based histidine sensor. Artif Cells Nanomed Biotechnol 47:221–227. https://doi.org/10.1080/21691401.2018.1548474/SUPPL_FILE/IANB_A_1548474_SM5260.DOCX
71. Glad M, Norrlöw O, Sellergren B et al (1985) Use of silane monomers for molecular imprinting and enzyme entrapment in polysiloxane-coated porous silica. J Chromatogr A 347:11–23. https://doi.org/10.1016/S0021-9673(01)95465-2
72. Amorim MS, Sales MGF, Frasco MF (2022) Recent advances in virus imprinted polymers. Biosens Bioelectron X 10:100131. https://doi.org/10.1016/J.BIOSX.2022.100131
73. Unger C, Lieberzeit PA (2021) Molecularly imprinted thin film surfaces in sensing: chances and challenges. React Funct Polym 161:104855. https://doi.org/10.1016/J.REACTFUNCTPOLYM.2021.104855
74. Rachkov A, Minoura N (2001) Towards molecularly imprinted polymers selective to peptides and proteins. The epitope approach. Biochim Biophys Acta 1544:255–266. https://doi.org/10.1016/S0167-4838(00)00226-0

75. Rachkov A, Minoura N (2000) Recognition of oxytocin and oxytocin-related peptides in aqueous media using a molecularly imprinted polymer synthesized by the epitope approach. J Chromatogr A 889:111–118
76. Yoshimatsu K, Yamazaki T, Hoshino Y et al (2014) Epitope discovery for a synthetic polymer nanoparticle: a new strategy for developing a peptide tag. J Am Chem Soc 136:1194–1197. https://doi.org/10.1021/ja410817p
77. Dechtrirat D, Jetzschmann KJ, Stöcklein WFM et al (2012) Protein rebinding to a surface-confined imprint. Adv Funct Mater 22:5231–5237. https://doi.org/10.1002/adfm.201201328
78. Moczko E, Guerreiro A, Cáceres C et al (2019) Epitope approach in molecular imprinting of antibodies. J Chromatogr B Anal Technol Biomed Life Sci 1124:1–6. https://doi.org/10.1016/j.jchromb.2019.05.024
79. Yang K, Li S, Liu L et al (2019) Epitope imprinting technology: progress, applications, and perspectives toward artificial antibodies. Adv Mater 31:1902048. https://doi.org/10.1002/adma.201902048
80. Nishino H, Huang CS, Shea KJ (2006) Selective protein capture by epitope imprinting. Angew Chem Int Ed 45:2392–2396. https://doi.org/10.1002/anie.200503760
81. Singh M, Gupta N, Raghuwanshi R (2017) Epitope imprinting approach to monitor diseases. J Mol Genet Med 11:1–6. https://doi.org/10.4172/1747-0862.1000270
82. Settipani J, Karim K, Chauvin A et al (2018) Theoretical aspects of peptide imprinting: screening of MIP (virtual) binding sites for their interactions with amino acids, di- and tripeptides. J Chinese Adv Mater Soc 6:301–310. https://doi.org/10.1080/22243682.2018.1467279
83. Tchinda R, Tutsch A, Schmid B et al (2019) Recognition of protein biomarkers using epitope-mediated molecularly imprinted films: histidine or cysteine modified epitopes? Biosens Bioelectron 123:260–268. https://doi.org/10.1016/J.BIOS.2018.09.010
84. Chou CY, Lin CY, Wu CH, Tai DF (2020) Sensing hiv protease and its inhibitor using "helical epitope"-imprinted polymers. Sensors 20:1–10. https://doi.org/10.3390/s20123592
85. Striegler S (2003) Selective carbohydrate recognition by synthetic receptors in aqueous solution. Curr Org Chem 7:81–102. https://doi.org/10.2174/1385272033373201
86. Shinde S, El-Schich Z, Malakpour A et al (2015) Sialic acid-imprinted fluorescent core-shell particles for selective labeling of cell surface glycans. J Am Chem Soc 137:13908–13912. https://doi.org/10.1021/JACS.5B08482
87. Panagiotopoulou M, Salinas Y, Beyazit S et al (2016) Molecularly imprinted polymer coated quantum dots for multiplexed cell targeting and imaging. Angew Chem Int Ed 55:8244–8248. https://doi.org/10.1002/ANIE.201601122
88. Li S, Yang K, Liu J et al (2015) Surface-imprinted nanoparticles prepared with a His-tag-anchored epitope as the template. Anal Chem 87:4617–4620. https://doi.org/10.1021/ac5047246
89. Gómez-Arribas LN, Urraca JL, Benito-Penìa E, Moreno-Bondi MC (2019) Tag-specific affinity purification of recombinant proteins by using molecularly imprinted polymers. Anal Chem 91:4100–4106. https://doi.org/10.1021/acs.analchem.8b05731
90. Brandis A, Partouche E, Yechezkel T et al (2017) A two-step strategy to visually identify molecularly imprinted polymers for tagged proteins. J Sep Sci 40:3358–3367. https://doi.org/10.1002/jssc.201700269
91. You M, Yang S, Tang W et al (2018) Molecularly imprinted polymers-based electrochemical DNA biosensor for the determination of BRCA-1 amplified by SiO2@Ag. Biosens Bioelectron 112:72–78. https://doi.org/10.1016/j.bios.2018.04.038
92. Ertürk G, Uzun L, Tümer MA et al (2011) Fab fragments imprinted SPR biosensor for real-time human immunoglobulin G detection. Biosens Bioelectron 28:97–104. https://doi.org/10.1016/j.bios.2011.07.004
93. Jetzschmann KJ, Yarman A, Rustam L et al (2018) Molecular LEGO by domain-imprinting of cytochrome P450 BM3. Colloids Surf B Biointerfaces 164:240–246. https://doi.org/10.1016/j.colsurfb.2018.01.047

94. Pereira MV, Marques AC, Oliveira D et al (2020) Paper-based platform with an in situ molecularly imprinted polymer for β-amyloid. ACS Omega 5:12057–12066. https://doi.org/10.1021/ACSOMEGA.0C00062/ASSET/IMAGES/LARGE/AO0C00062_0006.JPEG
95. Ozcelikay G, Kurbanoglu S, Zhang X et al (2019) Electrochemical MIP sensor for butyrylcholinesterase. Polymers (Basel) 11:1970. https://doi.org/10.3390/POLYM11121970
96. Ho TS, Du PX, Su WY et al (2022) Development of SARS-CoV-2 variant protein microarray for profiling humoral immunity in vaccinated subjects. Biosens Bioelectron 204:114067. https://doi.org/10.1016/J.BIOS.2022.114067
97. Yang H-H, Lu K-H, Lin Y-F et al (2013) Depletion of albumin and immunoglobulin G from human serum using epitope-imprinted polymers as artificial antibodies. J Biomed Mater Res A 101:1935–1942. https://doi.org/10.1002/jbm.a.34491
98. Wright LM, Kreikemeier JT, Fimmel CJ (2007) A concise review of serum markers for hepatocellular cancer. Cancer Detect Prev 31:35–44. https://doi.org/10.1016/J.CDP.2006.11.003
99. Yuen MF, Lai CL (2005) Serological markers of liver cancer. Best Pract Res Clin Gastroenterol 19:91–99. https://doi.org/10.1016/J.BPG.2004.10.003
100. Karfa P, Roy E, Patra S et al (2016) A fluorescent molecularly-imprinted polymer gate with temperature and pH as inputs for detection of alpha-fetoprotein. Biosens Bioelectron 78:454–463
101. Malati T (2007) Tumour markers: An overview. Indian J Clin Biochem 22:17. https://doi.org/10.1007/BF02913308
102. Pang J, Li P, He H et al (2022) Molecularly imprinted polymers outperform lectin counterparts and enable more precise cancer diagnosis. Chem Sci 13:4589–4597. https://doi.org/10.1039/D2SC01093C
103. Bartold K, Iskierko Z, Borowicz P et al (2022) Molecularly imprinted polymer-based extended-gate field-effect transistor (EG-FET) chemosensor for selective determination of matrix metalloproteinase-1 (MMP-1) protein. Biosens Bioelectron 208:114203. https://doi.org/10.1016/J.BIOS.2022.114203
104. Jetzschmann KJ, Zhang X, Yarman A et al (2017) Label-free MIP sensors for protein biomarkers. In: Label-free biosensing. Springer, Cham, pp 291–321
105. Ozcelikay G, Kurbanoglu S, Yarman A et al (2020) Au-Pt nanoparticles based molecularly imprinted nanosensor for electrochemical detection of the lipopeptide antibiotic drug daptomycin. Sens Actuators B 320:128285. https://doi.org/10.1016/j.snb.2020.128285
106. Truta LAANA, Sales MGF (2019) Carcinoembryonic antigen imprinting by electropolymerization on a common conductive glass support and its determination in serum samples. Sens Actuators B 287:53–63. https://doi.org/10.1016/j.snb.2019.02.033
107. Garcia-Cruz A, Haq I, Di MS et al (2020) Design and fabrication of a smart sensor using in silico epitope mapping and electro- responsive imprinted polymer nanoparticles for determination of insulin levels in human plasma. Biosens Bioelectron 169:112536. https://doi.org/10.1016/j.bios.2020.112536
108. Tu X, Muhammad P, Liu J et al (2016) Molecularly imprinted polymer-based plasmonic immunosandwich assay for fast and ultrasensitive determination of trace glycoproteins in complex samples. Anal Chem 88:12363–12370. https://doi.org/10.1021/acs.analchem.6b03597
109. Xing R, Ma Y, Wang Y et al (2019) Specific recognition of proteins and peptides via controllable oriented surface imprinting of boronate affinity-anchored epitopes. Chem Sci 10:1831–1835. https://doi.org/10.1039/c8sc04169e
110. Wulff G (2013) Forty years of molecular imprinting in synthetic polymers: origin, features and perspectives. Microchim Acta 180:1359–1370. https://doi.org/10.1007/S00604-013-0992-9
111. Sánchez-González J, Odoardi S, Bermejo AM et al (2018) Development of a micro-solid-phase extraction molecularly imprinted polymer technique for synthetic cannabinoids assessment in urine followed by liquid chromatography–tandem mass spectrometry. J Chromatogr A 1550:8–20. https://doi.org/10.1016/j.chroma.2018.03.049

112. Nematollahzadeh A, Shojaei A, Abdekhodaie MJ, Sellergren B (2013) Molecularly imprinted polydopamine nano-layer on the pore surface of porous particles for protein capture in HPLC column. J Colloid Interface Sci 404:117–126. https://doi.org/10.1016/j.jcis.2013.04.004
113. Ambrosini S, Beyazit S, Haupt K, Tse Sum Bui B (2013) Solid-phase synthesis of molecularly imprinted nanoparticles for protein recognition. Chem Commun 49:6746–6748. https://doi.org/10.1039/c3cc41701h
114. Canfarotta F, Poma A, Guerreiro A, Piletsky S (2016) Solid-phase synthesis of molecularly imprinted nanoparticles. Nat Protoc 113(11):443–455. https://doi.org/10.1038/nprot.2016.030
115. Cáceres C, Canfarotta F, Chianella I et al (2016) Does size matter? Study of performance of pseudo-ELISAs based on molecularly imprinted polymer nanoparticles prepared for analytes of different sizes. Analyst 141:1405–1412. https://doi.org/10.1039/C5AN02018B
116. Chianella I, Guerreiro A, Moczko E et al (2013) Direct replacement of antibodies with molecularly imprinted polymer nanoparticles in ELISA—development of a novel assay for vancomycin. Anal Chem 85:8462–8468. https://doi.org/10.1021/ac402102j
117. Rapini R, Canfarotta F, Mazzotta E et al (2019) NanoMIP-based approach for the suppression of interference signals in electrochemical sensors. Analyst 144:7290–7295. https://doi.org/10.1039/c9an01244c
118. Lowdon JW, Diliën H, Singla P et al (2020) MIPs for commercial application in low-cost sensors and assays – an overview of the current status quo. Sens Actuators B Chem 325:128973. https://doi.org/10.1016/J.SNB.2020.128973
119. Minchin S, Lodge J (2019) Understanding biochemistry: structure and function of nucleic acids. Essays Biochem 63:433. https://doi.org/10.1042/EBC20180038
120. Chi Q, Wang G, Jiang J (2013) The persistence length and length per base of single-stranded DNA obtained from fluorescence correlation spectroscopy measurements using mean field theory. Phys A Stat Mech Appl 392:1072–1079. https://doi.org/10.1016/J.PHYSA.2012.09.022
121. Kong D, Wang X, Gu C et al (2021) Direct SARS-CoV-2 nucleic acid detection by Y-shaped DNA dual-probe transistor assay. J Am Chem Soc 143:17004–17014. https://doi.org/10.1021/JACS.1C06325/ASSET/IMAGES/LARGE/JA1C06325_0004.JPEG
122. Jauset-Rubio M, Svobodová M, Mairal T et al (2016) Ultrasensitive, rapid and inexpensive detection of DNA using paper based lateral flow assay. Sci Rep 61(6):1–10. https://doi.org/10.1038/srep37732
123. Dwivedi S, Purohit P, Misra R et al (2017) Diseases and molecular diagnostics: a step closer to precision medicine. Indian J Clin Biochem 32:374–398. https://doi.org/10.1007/S12291-017-0688-8
124. López MM, Bertolini E, Olmos A et al (2003) Innovative tools for detection of plant pathogenic viruses and bacteria. Int Microbiol 6:233–243. https://doi.org/10.1007/S10123-003-0143-Y
125. Gui R, Jin H, Guo H, Wang Z (2018) Recent advances and future prospects in molecularly imprinted polymers-based electrochemical biosensors. Biosens Bioelectron 100:56–70. https://doi.org/10.1016/J.BIOS.2017.08.058
126. Idil N, Mattiasson B (2017) Imprinting of microorganisms for biosensor applications. Sensors (Basel) 17. https://doi.org/10.3390/S17040708
127. Yang Y, Zeng C, Huang J et al (2022) Specific and quantitative detection of bacteria based on surface cell imprinted SERS mapping platform. Biosens Bioelectron 215:114524. https://doi.org/10.1016/J.BIOS.2022.114524
128. Nawaz N, Abu Bakar NK, Muhammad Ekramul Mahmud HN, Jamaludin NS (2021) Molecularly imprinted polymers-based DNA biosensors. Anal Biochem 630. https://doi.org/10.1016/J.AB.2021.114328
129. Cui F, Zhou Z, Zhou HS (2020) Molecularly imprinted polymers and surface imprinted polymers based electrochemical biosensor for infectious diseases. Sensors (Basel) 20. https://doi.org/10.3390/S20040996

130. Slinchenko O, Rachkov A, Miyachi H et al (2004) Imprinted polymer layer for recognizing double-stranded DNA. Biosens Bioelectron 20:1091–1097. https://doi.org/10.1016/j.bios.2004.06.027
131. Ogiso M, Minoura N, Shinbo T, Shimizu T (2006) Detection of a specific DNA sequence by electrophoresis through a molecularly imprinted polymer. Biomaterials 27:4177–4182. https://doi.org/10.1016/J.BIOMATERIALS.2006.03.020
132. Ogiso M, Minoura N, Shinbo T, Shimizu T (2007) DNA detection system using molecularly imprinted polymer as the gel matrix in electrophoresis. Biosens Bioelectron 22:1974–1981. https://doi.org/10.1016/J.BIOS.2006.08.026
133. Diltemiz SE, Say R, Büyüktiryaki S et al (2008) Quantum dot nanocrystals having guanosine imprinted nanoshell for DNA recognition. Talanta 75:890–896. https://doi.org/10.1016/J.TALANTA.2007.12.036
134. Emir Diltemiz S, Denizli A, Ersöz A, Say R (2008) Molecularly imprinted ligand-exchange recognition assay of DNA by SPR system using guanosine and guanine recognition sites of DNA. Sens Actuators B 133:484–488. https://doi.org/10.1016/J.SNB.2008.03.007
135. Ratautaite V, Topkaya SN, Mikoliunaite L et al (2013) Molecularly imprinted polypyrrole for DNA determination. Electroanalysis 25:1169–1177. https://doi.org/10.1002/elan.201300063
136. Dai Q, Wang Y, Xu W et al (2017) Adsorption and specific recognition of DNA by using imprinted polymer layers grafted onto ionic liquid functionalized magnetic microspheres. Microchim Acta 184:4433–4441. https://doi.org/10.1007/S00604-017-2495-6/FIGURES/6
137. Babamiri B, Salimi A, Hallaj R (2018) A molecularly imprinted electrochemiluminescence sensor for ultrasensitive HIV-1 gene detection using EuS nanocrystals as luminophore. Biosens Bioelectron 117:332–339. https://doi.org/10.1016/j.bios.2018.06.003
138. Brahmbhatt H, Poma A, Pendergraff HM et al (2016) Improvement of DNA recognition through molecular imprinting: hybrid oligomer imprinted polymeric nanoparticles (oligoMIP NPs). Biomater Sci 4:281–287. https://doi.org/10.1039/C5BM00341E
139. Muti M, Soysal M, Nacak FM et al (2015) A novel DNA probe based on molecularly imprinted polymer modified electrode for the electrochemical monitoring of DNA. Electroanalysis 27:1368–1377. https://doi.org/10.1002/ELAN.201400672
140. Arslan T, Güney O (2020) Ratiometric sensor based on imprinted quantum dots-cationic dye nanohybrids for selective sensing of dsDNA. Anal Biochem 591:113540. https://doi.org/10.1016/J.AB.2019.113540
141. Piletskii SA, Kukhar VP, Fedoryak DM (1989) Production of polymer sorbents selective to components of nucleic acids. Ukr Khimicheskii Zhurnal 55:872–875
142. Piletskii SA, Dubei IY, Fedoryak DM, Kukhar VP (1990) Substrate-selective polymeric membranes. Selective transfer of nucleic acids components. Biopolim i Kletka 6:55–58
143. Piletsky SA, Fedoryak DM, Atamanenko ID et al (1993) Nucleoside-selective polymers based on methacrylate copolymers. Ukr Khimicheskii Zhurnal 59:1316–1320
144. Shea KJ, Spivak DA, Sellergren B (1993) Polymer complements to nucleotide bases. Selective binding of adenine derivatives to imprinted polymers. J Am Chem Soc 115:3368–3369. https://doi.org/10.1021/JA00061A061/SUPPL_FILE/JA3368.PDF
145. Mathew-Krotz J, Shea KJ (1996) Imprinted polymer membranes for the selective transport of targeted neutral molecules. J Am Chem Soc 118:8154–8155. https://doi.org/10.1021/JA954066J/SUPPL_FILE/JA8154.PDF
146. Spivak DA, Shea KJ (2001) Investigation into the scope and limitations of molecular imprinting with DNA molecules. Anal Chim Acta 435:65–74. https://doi.org/10.1016/S0003-2670(00)01333-7
147. Yoshikawa M, Izumi J-I, Guiver MD, Robertson GP (2001) Recognition and selective transport of nucleic acid components through molecularly imprinted polymeric membranes. Macromol Mater Eng 286:52–59. https://doi.org/10.1002/1439-2054
148. Zaidi SA (2021) An overview of bio-inspired intelligent imprinted polymers for virus determination. Biosensors 11:89. https://doi.org/10.3390/BIOS11030089

149. Nagar PK, Savargaonkar D, Anvikar AR (2020) Detection of dengue virus-specific IgM and IgG antibodies through peptide sequences of envelope and NS1 proteins for serological identification. J Immunol Res 2020:1820325. https://doi.org/10.1155/2020/1820325
150. Chen L, Ruan F, Sun Y et al (2019) Establishment of sandwich ELISA for detecting the H7 subtype influenza A virus. J Med Virol 91:1168–1171. https://doi.org/10.1002/JMV.25408
151. Hayden O, Bindeus R, Haderspöck C et al (2003) Mass-sensitive detection of cells, viruses and enzymes with artificial receptors. Sens Actuators B 91:316–319. https://doi.org/10.1016/S0925-4005(03)00093-5
152. Dickert FL, Hayden O, Bindeus R et al (2004) Bioimprinted QCM sensors for virus detection-screening of plant sap. Anal Bioanal Chem 378:1929–1934. https://doi.org/10.1007/S00216-004-2521-5
153. Uzun L, Say R, Ünal S, Denizli A (2009) Hepatitis B surface antibody purification with hepatitis B surface antibody imprinted poly(hydroxyethyl methacrylate-N-methacryloyl-l-tyrosine methyl ester) particles. J Chromatogr B 877:181–188. https://doi.org/10.1016/J.JCHROMB.2008.12.004
154. Magar HS, Hassan RYA, Mulchandani A (2021) Electrochemical impedance spectroscopy (EIS): principles, construction, and biosensing applications. Sensors 21:6578. https://doi.org/10.3390/S21196578
155. Gast M, Sobek H, Mizaikoff B (2019) Advances in imprinting strategies for selective virus recognition a review. Trends Anal Chem 114:218–232. https://doi.org/10.1016/J.TRAC.2019.03.010
156. Graham SP, El-Sharif HF, Hussain S et al (2019) Evaluation of molecularly imprinted polymers as synthetic virus neutralizing antibody mimics. Front Bioeng Biotechnol 7:115. https://doi.org/10.3389/FBIOE.2019.00115
157. Hussein HA, El Nashar RM, El-Sherbiny IM, Hassan RYA (2021) High selectivity detection of FMDV-SAT-2 using a newly-developed electrochemical nanosensors. Biosens Bioelectron 191:113435. https://doi.org/10.1016/J.BIOS.2021.113435
158. Hussein HA, Hassan RYA, El Nashar RM et al (2019) Designing and fabrication of new VIP biosensor for the rapid and selective detection of foot-and-mouth disease virus (FMDV). Biosens Bioelectron 141:111467. https://doi.org/10.1016/J.BIOS.2019.111467
159. Hussein HA, Kandeil A, Gomaa M et al (2021) SARS-CoV-2-impedimetric biosensor: virus-imprinted chips for early and rapid diagnosis. ACS Sensors 6:4098–4107. https://doi.org/10.1021/ACSSENSORS.1C01614/SUPPL_FILE/SE1C01614_SI_001.PDF
160. Luo L, Yang J, Liang K et al (2019) Fast and sensitive detection of Japanese encephalitis virus based on a magnetic molecular imprinted polymer–resonance light scattering sensor. Talanta 202:21–26. https://doi.org/10.1016/J.TALANTA.2019.04.064
161. Luo L, Zhang F, Chen C, Cai C (2020) Molecular imprinting resonance light scattering nanoprobes based on pH-responsive metal-organic framework for determination of hepatitis A virus. Microchim Acta 187:140. https://doi.org/10.1007/S00604-020-4122-1/TABLES/2
162. Tancharoen C, Sukjee W, Thepparit C et al (2019) Electrochemical biosensor based on surface imprinting for zika virus detection in serum. ACS Sens 4:69–75. https://doi.org/10.1021/ACSSENSORS.8B00885/ASSET/IMAGES/LARGE/SE-2018-00885D_0005.JPEG
163. Tai DF, Lin CY, Wu TZ, Chen LK (2005) Recognition of dengue virus protein using epitope-mediated molecularly imprinted film. Anal Chem 77:5140–5143. https://doi.org/10.1021/AC0504060/ASSET/IMAGES/LARGE/AC0504060F00003.JPEG
164. Piletska EV, Mirkes E, Piletsky SS et al (2020) Combinatorial screening of polymer nanoparticles for their ability to recognize epitopes of AAV-neutralizing antibodies. J Mol Recognit 33:e2824. https://doi.org/10.1002/JMR.2824
165. Gast M, Sobek H, Mizaikoff B (2019) Selective virus capture via hexon imprinting. Mater Sci Eng C 99:1099–1104. https://doi.org/10.1016/J.MSEC.2019.02.037
166. Arshad R, Rhouati A, Hayat A et al (2020) MIP-based impedimetric sensor for detecting dengue fever biomarker. Appl Biochem Biotechnol 191:1384–1394. https://doi.org/10.1007/S12010-020-03285-Y

167. Raziq A, Kidakova A, Boroznjak R et al (2021) Development of a portable MIP-based electrochemical sensor for detection of SARS-CoV-2 antigen. Biosens Bioelectron 178: 113029. https://doi.org/10.1016/j.bios.2021.113029
168. Ratautaite V, Boguzaite R, Brazys E et al (2022) Molecularly imprinted polypyrrole based sensor for the detection of SARS-CoV-2 spike glycoprotein. Electrochim Acta 403:139581. https://doi.org/10.1016/J.ELECTACTA.2021.139581
169. Parisi OI, Dattilo M, Patitucci F et al (2020) "Monoclonal-type" plastic antibodies for SARS-CoV-2 based on molecularly imprinted polymers. bioRxiv:120709. https://doi.org/10.1101/2020.05.28.120709
170. Zhang T, Sun L, Zhang Y (2021) Highly sensitive electrochemical determination of the SARS-COV-2 antigen based on a gold/graphene imprinted poly-arginine sensor. Anal Methods 13: 5772–5776. https://doi.org/10.1039/D1AY01478A
171. Amouzadeh Tabrizi M, Fernández-Blázquez JP, Medina DM, Acedo P (2022) An ultrasensitive molecularly imprinted polymer-based electrochemical sensor for the determination of SARS-CoV-2-RBD by using macroporous gold screen-printed electrode. Biosens Bioelectron 196:113729. https://doi.org/10.1016/J.BIOS.2021.113729
172. Ayankojo AG, Boroznjak R, Reut J et al (2022) Molecularly imprinted polymer based electrochemical sensor for quantitative detection of SARS-CoV-2 spike protein. Sens Actuators B 353:131160. https://doi.org/10.1016/J.SNB.2021.131160
173. Bognár Z, Supala E, Yarman A et al (2022) Peptide epitope-imprinted polymer microarrays for selective protein recognition. Application for SARS-CoV-2 RBD protein. Chem Sci 13:1263–1269. https://doi.org/10.1039/D1SC04502D
174. Fresco-Cala B, Rajpal S, Rudolf T et al (2021) Development and characterization of magnetic SARS-CoV-2 peptide-imprinted polymers. Nanomaterials 11:2985. https://doi.org/10.3390/NANO11112985
175. Yarman A, Kurbanoglu S (2022) Molecularly imprinted polymer-based sensors for SARS-CoV-2: where are we now? Biomimetics 7:58. https://doi.org/10.3390/BIOMIMETICS7020058
176. Liu Z, Xiao X, Wei X et al (2020) Composition and divergence of coronavirus spike proteins and host ACE2 receptors predict potential intermediate hosts of SARS-CoV-2. J Med Virol 92: 595–601. https://doi.org/10.1002/JMV.25726
177. Puoci F (2020) "Monoclonal-Type" plastic antibodies for COVID-19 treatment: what is the idea? J Funct Biomater 11:43. https://doi.org/10.3390/JFB11020043
178. Cennamo N, D'agostino G, Perri C et al (2021) Proof of concept for a quick and highly sensitive on-site detection of SARS-CoV-2 by plasmonic optical fibers and molecularly imprinted polymers. Sensors 21:1681. https://doi.org/10.3390/S21051681
179. Cubuk H, Ozbil M, Cakir Hatir P (2021) Computational analysis of functional monomers used in molecular imprinting for promising COVID-19 detection. Comput Theor Chem 1199: 113215. https://doi.org/10.1016/J.COMPTC.2021.113215
180. Zhang X, Waffo AT, Yarman A et al (2022) How an ACE2 mimicking epitope-MIP nanofilm recognizes template-related peptides and the receptor binding domain of SARS-CoV-2. Nanoscale. https://doi.org/10.1039/D2NR03898F
181. Basak S, Venkatram R, Singhal RS (2022) Recent advances in the application of molecularly imprinted polymers (MIPs) in food analysis. Food Control 139:109074. https://doi.org/10.1016/J.FOODCONT.2022.109074
182. Ostovan A, Arabi M, Wang Y et al (2022) Greenificated molecularly imprinted materials for advanced applications. Adv Mater 34:2203154. https://doi.org/10.1002/ADMA.202203154
183. Arreguin-Campos R, Eersels K, Lowdon JW et al (2021) Biomimetic sensing of Escherichia coli at the solid-liquid interface: from surface-imprinted polymer synthesis toward real sample sensing in food safety. Microchem J 169:106554. https://doi.org/10.1016/J.MICROC.2021.106554

184. Aherne A, Alexander C, Payne MJ et al (1996) Bacteria-mediated lithography of polymer surfaces. J Am Chem Soc 118:8771–8772. https://doi.org/10.1021/JA960123C/ASSET/IMAGES/LARGE/JA960123CF00002.JPEG
185. Gong H, Hajizadeh S, Liu W, Ye L (2021) Imprinted polymer beads loaded with silver nanoparticles for antibacterial applications. ACS Appl Bio Mater 4:2829–2838. https://doi.org/10.1021/ACSABM.1C00045/ASSET/IMAGES/LARGE/MT1C00045_0008.JPEG
186. Chen L, Wang X, Lu W et al (2016) Molecular imprinting: perspectives and applications. Chem Soc Rev 45:2137–2211. https://doi.org/10.1039/C6CS00061D
187. Jia M, Zhang Z, Li J et al (2018) Molecular imprinting technology for microorganism analysis. Trends Anal Chem 106:190–201. https://doi.org/10.1016/J.TRAC.2018.07.011
188. Piletsky S, Canfarotta F, Poma A et al (2020) Molecularly imprinted polymers for cell recognition. Trends Biotechnol 38:368–387. https://doi.org/10.1016/J.TIBTECH.2019.10.002
189. El-Schich Z, Abdullah M, Shinde S et al (2016) Different expression levels of glycans on leukemic cells-a novel screening method with molecularly imprinted polymers (MIP) targeting sialic acid. Tumour Biol 37:13763–13768. https://doi.org/10.1007/S13277-016-5280-Y
190. Liu D, Zhao K, Qi M et al (2018) Preparation of protein molecular-imprinted polysiloxane membrane using calcium alginate film as matrix and its application for cell culture. Polymers (Basel) 10:170. https://doi.org/10.3390/POLYM10020170
191. Culver HR, Peppas NA (2017) Protein-imprinted polymers: the shape of things to come? Chem Mater 29:5753–5761. https://doi.org/10.1021/acs.chemmater.7b01936
192. Tse Sum Bui B, Auroy T, Haupt K (2022) Fighting antibiotic-resistant bacteria: promising strategies orchestrated by molecularly imprinted polymers. Angew Chem Int Ed Engl 61. https://doi.org/10.1002/ANIE.202106493
193. Ogawa KI, Hyuga M, Okada T, Minoura N (2012) Development of lipid A-imprinted polymer hydrogels that selectively recognize lipopolysaccharides. Biosens Bioelectron 38:215–219. https://doi.org/10.1016/J.BIOS.2012.05.028
194. Wang S, Yin D, Wang W et al (2016) Targeting and imaging of cancer cells via monosaccharide-imprinted fluorescent nanoparticles. Sci Rep 6:22757. https://doi.org/10.1038/srep22757
195. Bezdekova J, Zemankova K, Hutarova J et al (2020) Magnetic molecularly imprinted polymers used for selective isolation and detection of Staphylococcus aureus. Food Chem 321:126673. https://doi.org/10.1016/J.FOODCHEM.2020.126673
196. Zhang Z, Guan Y, Li M et al (2015) Highly stable and reusable imprinted artificial antibody used for in situ detection and disinfection of pathogens. Chem Sci 6:2822–2826. https://doi.org/10.1039/C5SC00489F
197. Yilmaz E, Majidi D, Ozgur E, Denizli A (2015) Whole cell imprinting based Escherichia coli sensors: a study for SPR and QCM. Sens Actuators B 209:714–721. https://doi.org/10.1016/J.SNB.2014.12.032
198. Eersels K, Lieberzeit P, Wagner P (2016) A review on synthetic receptors for bioparticle detection created by surface-imprinting techniques—from principles to applications. ACS Sensors 1:1171–1187. https://doi.org/10.1021/ACSSENSORS.6B00572

Adv Biochem Eng Biotechnol (2024) 187: 149–184
https://doi.org/10.1007/10_2023_236

Published online: 26 January 2024

Recent Developments and Applications of Microbial Electrochemical Biosensors

Nunzio Giorgio G. Carducci, Sunanda Dey, and David P. Hickey

Contents

Abstract This chapter provides a comprehensive overview of microbial electrochemical biosensors, which are a unique class of biosensors that utilize the metabolic activity of microorganisms to convert chemical signals into electrical signals. The principles and mechanisms of these biosensors are discussed, including the different types of microorganisms that can be used. The various applications of microbial

N. G. G. Carducci, S. Dey, and D. P. Hickey (✉)
Department of Chemical Engineering and Materials Science, Michigan State University, East Lansing, MI, USA
e-mail: Hickeyd6@msu.edu

electrochemical biosensors in fields such as environmental monitoring, medical diagnostics, and food safety are also explored. The chapter concludes with a discussion of future research directions and potential advancements in the field of microbial electrochemical biosensors.

Graphical Abstract

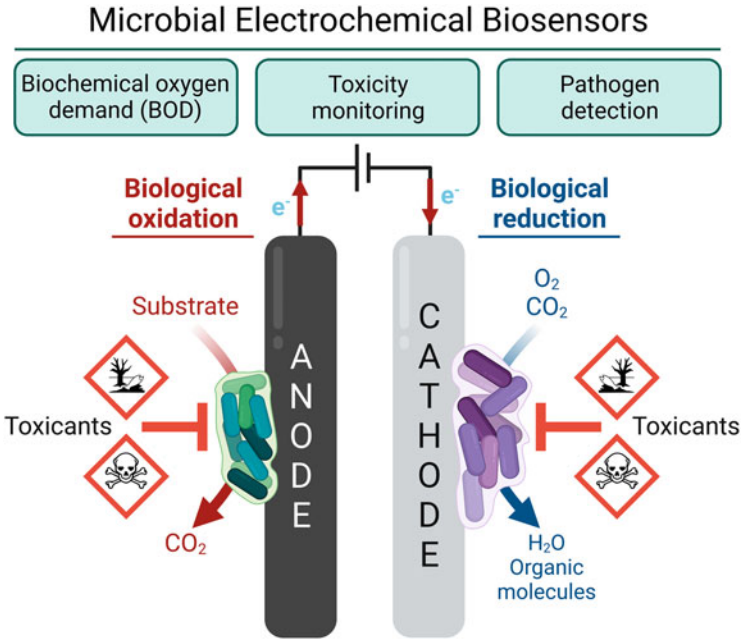

Keywords Bioelectrocatalysis, Extracellular electron transfer, Metabolism, Microbial fuel cell, Wastewater

1 Introduction

Microbial electrochemical biosensors (MEBs) are a unique class of biosensors that utilize the metabolic activity of microorganisms to convert chemical reactions into electrical signals. These biosensors have gained significant attention in recent years due to their potential application in a wide range of fields, such as environmental monitoring, medical diagnostics, and food safety. Unlike traditional biosensors, which typically use enzymes or other biological molecules (e.g., antibodies) to detect specific analytes, MEBs utilize whole cells. This affords them a sensitivity

to any analyte that may alter microbial metabolism and, thus, allows them to be used for detecting a wider range of analytes. The use of whole cells also allows MEBs to be used in environments where traditional biosensors would not be able to function, because the protective cell membrane keeps enzymes from denaturing. Additionally, MEBs can be made more sensitive and specific by genetically engineering the microorganisms to produce specific enzymes or other molecules that can interact with the analytes of interest, making them a versatile tool in the detection and monitoring of various compounds. In this chapter, we will explore the principles and mechanisms of MEBs, the different types of microorganisms that can be used, and the various applications of these biosensors. Specifically, this chapter gives an overview of the mechanisms of electron transfer associated with a microbial electrochemical system and covers recent developments in MEBs. It provides a discussion on the design, applications, working conditions, innovations, and outlook of the MEB-related literature that has been published in the last 5 years.

1.1 Basic MEB Operation

An MEB typically consists of three main components: a microorganism that acts as the biocatalyst, an electrode that serves as the transducer, and an interface that connects the two. The microorganism can be a bacterium, fungus, or algae, and is immobilized on or near the electrode, which is usually made of a conducting material such as gold, carbon, or platinum. When a microorganism reacts with an analyte, it uses the analyte as a substrate to generate electrons as a by-product of metabolism. These electrons are then transported to the electrode resulting in an electrical current, which is proportional to the concentration of the analyte. The electrochemical signal is then sent to a device (e.g., a potentiostat) for measurement and data analysis. The output signal, which can be an electrochemical current or a voltage, is then related to the amount of the analyte present in the sample.

1.2 Brief History of Microbial Electrochemistry and MEBs

Electrochemical phenomena in microorganisms were first detailed by Potter in 1911 [1]. Interest in microbial electrochemical technology (MET) increased sharply in the latter half of the twentieth century after Davis and Yarbrough developed one of the first microbial fuel cells (MFCs) in the early 1960s [2, 3]. While over 100 years have passed since the initial discovery of electroactive microorganisms, the mechanisms underpinning microbial electron transfer have only just started to be understood. Furthermore, some aspects are the subject of considerable debate [4, 5]. Karube and coworkers are often credited with developing the first whole-cell biosensor in 1977, when they reported the use of immobilized microbes in polyacrylamide gel on an oxygen sensing electrode to measure the five-day biochemical oxygen demand of

wastewater [6]. However, it should be noted that Diviés reported the use of a "microbial electrode" for an ethanol assay in a 1975 issue of *Annales de Microbiologie* [7], using *Acetobacter xylinum* (since reclassified as *Gluconobacter xylinus* [8]). Since these initial studies, there has been significant advancement in the capabilities of whole-cell biosensors. Biosensors can use a variety of different biological sensing elements (i.e., cells or enzymes) and physical transducers (i.e., calorimetry, electrochemistry, or spectroscopy), but this chapter will focus on microbial electrochemical biosensors [9]. These are distinct from traditional detection methods, such as gas chromatography, because they do not require sample processing prior to analysis. Additionally, they are intended for repeated or continuous measurement collection, unlike single-use biosensors [10]. It is important to keep in mind that various reports have also referred to such devices as whole-cell biosensors [11, 12], microbial electrochemical sensors [13, 14], microbial electrochemical cell-based sensors [15], electrochemical biosensors [16], and microbial fuel cell-based (MFC-type) sensors [17–20]. Throughout this chapter, these devices will be referred to as microbial electrochemical biosensors (MEBs).

2 Microbial Electrochemical Biosensors

A microbial electrochemical biosensor utilizes a microorganism, most commonly bacteria, to detect the presence of an analyte compound based on the operation principle shown in Fig. 1 [14]. The analyte induces a biological response from the organism, and a transducer then converts the biological response to a measurable signal. Amperometry is the most common operational mode for MEBs; it measures a current signal as a function of time at a constant voltage [9, 21]. Alternatively, current signals can be measured using voltammetric methods, such as cyclic voltammetry and square wave voltammetry, which vary the applied potential as a function of time [22]. The reader is directed to excellent texts on these methods should greater detail be required [21, 23]. The presence of a target analyte can affect microbial metabolism which can change the consumption or production of ionic species [24]. The variation in ion concentration can be monitored by conductometry, which measures changes in the electrical conductivity of the solution over time; however, this detection method is decidedly nonspecific since conductivity can be altered by any ions present in solution. Finally, analytes can be detected by measuring the potential difference between the working and reference electrodes, known as potentiometry. This potential difference can be impacted by changes in concentration or composition of electroactive species, which may vary based on microbial metabolism.

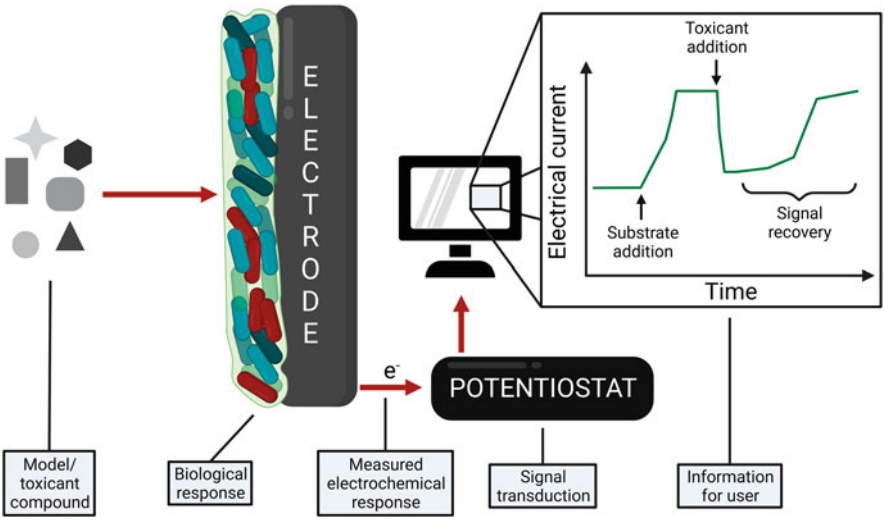

Fig. 1 Operation principle of a biosensor from analyte to microbial response to the transduction to the measured signal readable by end user. (Adapted from Plekhanova and Reshetilov [9] and Noori et al. [12])

2.1 MEB Operation

Unlike enzymatic biosensors, microbial electrochemical biosensors have fewer stability issues because the enzymes are contained within a protective cellular membrane, which allows for a wider range of pH and temperature conditions [25]. The current generated by these microorganisms can be affected by toxicants and other pathogens and, consequently, can also be used to quantify their concentration in a sample. Different sensing applications exist depending on whether the microbes are interfaced to the cathode or anode of the electrochemical device. Anodic applications include measuring biochemical oxygen demand and detecting pathogens. Biochemical oxygen demand (BOD) is the amount of oxygen needed by microorganisms to oxidize a given amount of organic compounds and is, therefore, often used to estimate the total quantity of organic contaminants in a water supply. BOD can be measured with the use of an MEB by monitoring the anodic current produced by oxidation of organic compounds by aerobic electroactive microorganisms during cellular respiration. Unlike direct measurements of dissolved oxygen content for BOD quantification, MEBs are not prone to false background signals caused by reduced inorganic material such as nitrogen compounds, sulfides, and metal salts. At the cathode, microbes can be used for determining the dissolved oxygen concentration or corrosion detection [14]. Microbes can also be used to detect toxicants at the anode or cathode. Furthermore, MEBs can operate either using an external power supply (e.g., as an electrolytic cell) or using the reactions

catalyzed at the anode and cathode to generate its own power (e.g., as a self-powered biosensor). The primary requirement for an MEB to generate its own power, thereby operating as a microbial fuel cell (MFC), is that the difference in formal electrochemical potentials between the cathodic reaction and anodic reaction must be positive (thus corresponding to a spontaneous net reaction),

$$E_{\text{cell}} = E_{\text{cath}} - E_{\text{an}} \tag{1}$$

where E_{cell} is the electrochemical cell potential of the MEB, E_{cath} is the formal redox potential of the cathodic reaction, and E_{an} is the formal redox potential of the anodic reaction [16]. A primary benefit to MEBs that can operate as an MFC is that they do not require an external power source and can be scaled down to the microliter level, improving the portability [15]. One potential limitation of MFC-type MEBs arises because their power output (i.e., signal) depends on the amount of electrical current that can be generated, which, in turn, depends on analyte concentration. Therefore, at low analyte concentrations, there may be insufficient power generated to produce a measurable signal. Garcia and coworkers addressed this potential problem and demonstrated that it is possible to combine an MFC with an MEB to measure lactate concentrations that are too low to generate sufficient power [26]. The MFC provides power using glucose that is present at a relatively high concentration. In a fully self-powered MEB, the MFC provides power for both the applied electrochemical potential in the MEB and the electronics necessary to transmit the signal to an external device. Therefore, the minimum power requirements for a fully self-powered MEB depend on the chosen method of signal recording. For example, miniature data transmission configurations require roughly 10 mW of power, which is too high for miniature MEBs but is plausible for larger MEBs (where a miniature MEB is defined as having a total volume <5 mL and projected electrode area <10 cm^2) [15, 27–29].

The primary crux of electrochemical detection methods is the trade-off between sensitivity and specificity. While electrochemical responses are very sensitive to changes in analyte concentration, they can be affected by electroactive chemical species present in the sample that are not derived from the microbial sensing element. This is useful in determining whether a toxicant or other analyte is present, but it is extremely difficult to determine if the detection signal is caused by one or more analytes [9]. When detecting analytes, values often reported in the literature are the limit of detection, linear range, and IC_{50}. The *limit of detection* (LOD) is the lowest analyte concentration that can be reliably distinguished from analytical noise. This is distinct from the *limit of quantitation* (LOQ), which is the lowest concentration value that meets pre-established requirements for bias and error. The *linear range* is the effective detection range of the sensor where the analyte concentration has a linear relationship with the measured biological signal. The half maximal inhibitory concentration (IC_{50}) is the concentration of a compound required to reduce metabolic function by half.

2.2 Anodic MEBs

As described above, biochemical, or biological, oxygen demand (BOD) is the amount of oxygen required by microorganisms to oxidize a given amount of biodegradable organic compounds [30, 31]. BOD is often used in water quality assessments to describe the biodegradable organic content of a water supply. Similarly, chemical oxygen demand (COD) is a way to estimate the non-biodegradable organic compounds present. Currently, COD and BOD can be measured using either colorimetric (commonly through an oxidative reaction with Cr(VI)) or electrochemical (using an oxygen-permeable electrode to directly measure the dissolved oxygen concentration) assays. However, colorimetric detection kits require toxic reagents and long response times (a few hours for COD and 5 days for BOD) [14, 32]. Aerobic electroactive microorganisms produce current by oxidizing organic substrates and can, therefore, be used to measure the biodegradable fraction of organic material in a water sample. Electrochemical techniques (e.g., MEBs) are capable of much faster response times and can quickly calibrate electrical current output to the concentration of organic compounds in an aqueous sample [14, 33]. As a demonstration of this response time, Wang and coworkers recently designed an MEB that could detect changes in BOD as small as 10 mg/L within 5 min [34]. A summary of recently reported MEBs used for BOD monitoring is provided in Table 1.

Toxicant detection is one of the most heavily researched applications of MEBs, and several types of pollutants have been studied including heavy metals, pesticides, and antibiotics. MEBs used for toxicant detection emphasize portability and quick detection times. These design considerations facilitate use in remote areas that do not have access to expensive and specialized lab equipment normally required for analytical applications, such as water purity tests and mass spectrometers [14]. A schematic of an anodic MEB is shown in Fig. 2. Because electroactive bacteria can produce current as a by-product of metabolism, current through a circuit can be correlated to the concentration of a toxicant that inhibits metabolism. Alternatively, non-electroactive bacteria can be genetically engineered to produce electroactive compounds, giving greater specificity for target analytes. This is done using genetic promoter sequences that are activated in the presence of specific analyte molecules. One application of this strategy involves the activation of an operon promoter sequence, P_{ars}, by arsenic species that results in the production of an electrochemically detectable small molecule [39, 40]. Sánchez and coworkers demonstrated this using an engineered *E. coli* strain containing P_{ars} for the detection of arsenite in one of the first MEBs to receive regulatory approval for field use in Canada [40]. In this MEB, As(III) binds to the *arsR* repressor protein, which releases it from its DNA binding site at the P_{ars} promoter sequence and, thus, increases expression of the *lacZ* gene. *LacZ* expression encodes for the β-galactosidase enzyme, which then cleaves 4-aminophenyl β-D-galactopyranoside (PAPG) to give the electrochemically active redox molecule, 4-aminophenol (PAP). In this way, the amount of PAP produced is proportional to the amount of As(III) present. Similarly, Sciuto and coworkers

Table 1 Recently reported MEBs for BOD quantification

MEB type	Application	Sample type	Linear range and LOD	Reference
Four single-chamber sensors in parallel	Online sensor for rapid BOD measurements	Correlate organic matter concentration in aqueous samples	Linear ranges from 10–50 and 50–500 mg BOD/L	[34]
Double-chamber MFC	Rapid BOD measurements using partial coulombic yield	Correlate organic matter concentration in aqueous samples	Linear range: 37.5–375 mg BOD/L	[35]
Three-electrode cell	Detection of BOD and nitrate w/ pure *Shewanella loihica* culture	Correlate organic matter and nitrate concentrations in aqueous samples	Linear range: 0–130.5 mg BOD/L Linear range: 0–3.6 mg/L NO_3^- LOD: 0.75 NO_3^-	[36]
Three-electrode cell w/redox mediator	Detection of BOD w/-immobilized *Bacillus subtilis*	Correlate organic matter concentration in aqueous samples	Linear range: 4–60 mg BOD/L LOD: 1.8 mg BOD/L	[37]
Single-chamber MFC w/air cathode	Detection of BOD in hypersaline solutions w/ alginate-encapsulated *Salinivibrio* sp. EAGSL	Correlate organic matter concentration in aqueous, high-salinity samples	Linear range: 2,400–10,000 mg BOD/L	[38]

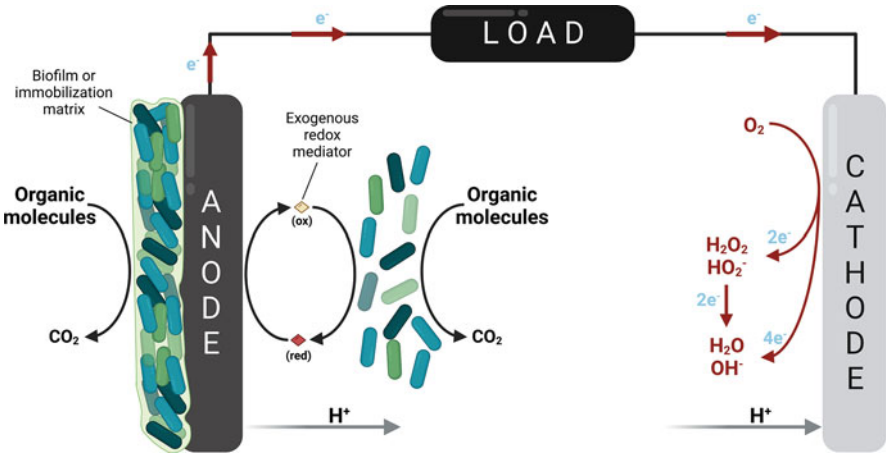

Fig. 2 Schematic of an anodic microbial electrochemical biosensor used to detect organic analytes. Electrons from oxidation are transferred either through direct contact of the immobilized cells or mediated transfer via a redox mediator

constructed a miniaturized MEB with P_{ars}-engineered *E. coli* to produce a redox mediator in response to As(III) [39]. The system exhibited good specificity for As (III) and did not produce a false-positive signal in the presence of Hg(II) and Cd(II). In the same work, they demonstrated the modularity of this approach by preparing an MEB using an *E. coli* strain modified with a different promoter operon to enable the detection of Hg(II) with good specificity against As(III) and Cd(II). The device achieved LODs (10 ppb for As(III) and 1 ppb for Hg(II)) that were an order of magnitude lower than the concentrations deemed dangerous by the World Health Organization (WHO).

Alternatively, the use of specific bacterial strains can also improve detection of a particular analyte. Wu et al. recently developed a novel MEB that used a mixed culture containing nitrifying bacteria to detect trichloroacetic acid [41]. This analyte is important because it is a toxic by-product of chlorine in the treatment of wastewater, and early warning systems are needed since current analytical methods are complex and expensive. Some MEBs can also be used as recovery devices for metal contaminants. Busnelli and coworkers recently used a *Pseudomonas veronii* 2E MEB to detect and remove Cu(II) and Cd(II) in 50 mL bioreactors [22].

MEBs have also been designed to detect the presence of pathogenic bacteria. Yang et al. developed a two-way redox-cycling system (illustrated in Fig. 3) for detecting the pathogenic anaerobe, *Pseudomonas aeruginosa*, indirectly with the use of *Shewanella oneidensis* MR-1. *P. aeruginosa* secretes two electroactive biomarkers, pyocyanin and 1-hydroxyphenazine, that can be electrochemically oxidized (above −0.30 V vs SCE) or reduced (below −0.45 V vs SCE), respectively. While both biomarkers can be detected by direct electrochemistry, *S. oneidensis* is capable of reducing electrochemically oxidized pyocyanin and oxidizing electrochemically reduced 1-hydroxyphenazine, thereby amplifying their corresponding current and dramatically increasing their sensitivity. Detection of the biomarker pyocyanin, indicative of *Pseudomonas aeruginosa* infections, was achieved with an LOD of 304 pM and about 302 times greater sensitivity over the unamplified method. The LOD for 1-hydroxyphenazine was 1.5 nM with a sensitivity 579 times greater than the unamplified method (4.0 μA nM^{-1} vs 6.9 nA nM^{-1}). Importantly, these LOD values are much lower than the concentrations reported in *P. aeruginosa*-infected patients (1–100 μM) [42]. Alternatively, an electrochemical sensor variation of an MEB can utilize an initially abiotic electrode. Electroactive pathogenic bacteria can then interface with the electrode and generate a signal [43, 44]. While they fall outside of the scope of this chapter, other types of electrochemical sensors are more commonly studied to detect pathogens through telltale metabolic compounds or signaling molecules [14]. Abiotic electrodes rather than whole cells are used as sensing elements in this scenario. For example, *P. aeruginosa* secretes phenazines, a class of redox mediators, which can be detected using electrochemical methods [45].

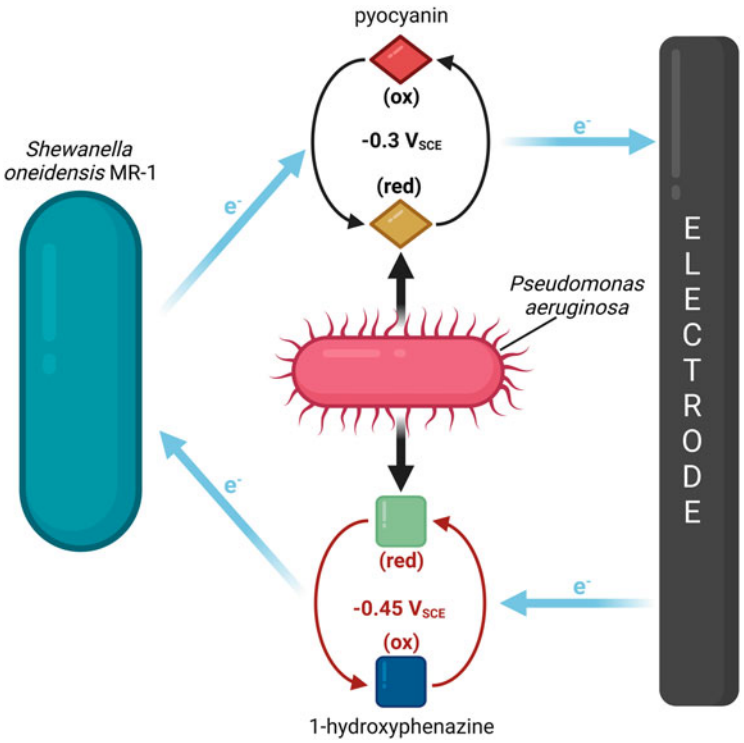

Fig. 3 Schematic representation of a microbial electrochemical biosensor using two-way redox cycling to catalytically amplify an electrochemical signal. Here, *Shewanella oneidensis* MR-1 can biochemically recycle two redox-active biomarkers secreted by the pathogenic anaerobe, *Pseudomonas aeruginosa* (Adapted from Yang et al. [42])

2.3 Cathodic MEBs

Using a biocathode as the MEB's sensing element can facilitate toxicant detection similarly to a bioanode MEB configuration (Fig. 4). A biocathode can also be used to measure dissolved oxygen concentration and detect surface corrosion, but these types of sensors typically do not utilize a whole cell sensing element [14]. A notable difference of using a biocathode sensing element is that electrotrophic bacteria require oxygen instead of biodegradable organic feedstocks, though a reactant for the anode counter-reaction is still necessary [14, 33]. The most common counter-reaction at an abiotic anode is water oxidation but can include the oxidation of organic compounds (such as methanol or formate) to carbon dioxide. Furthermore, cathodic MEBs are capable of detecting aqueous or gaseous analytes. Jiang et al. developed the first MFC-type MEB capable of air quality monitoring in 2018 [47]. The sensor used a gas diffusion biocathode to detect waterborne and airborne contaminants and had an LOD of 20 ppm for formaldehyde. Nitrites have also been

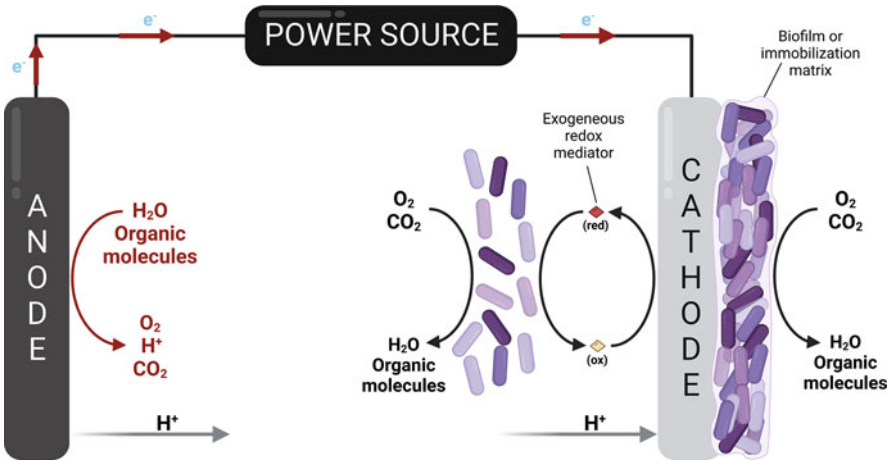

Fig. 4 Schematic of a cathodic microbial electrochemical biosensor to detect dissolved oxygen. Electrode polarization is powered by an external source to provide electrons to electrotrophic bacteria for either oxygen reduction or the reduction of carbon dioxide to organic molecules [9, 12]

quantified using nitrite-oxidizing bacteria on a biocathode with an LOD of 2.39 μM [48].

Interestingly, there is some evidence that biocathode-based MEBs generally exhibit higher sensitivities than their anodic counterparts. One such case was made in a report where oxygen-reducing microbial cathodes were incubated in tap water by Prévoteau et al. [33]. Their device showed higher sensitivity for six heavy metals and organic pollutants compared to anodic MEBs tested with the same analytes. They suggested that the increased sensitivity could be due to either (1) cathodic biofilms being thinner and more sparse than anodic biofilms, leaving the cells more exposed to toxic shocks, or (2) inherent sensitivities of the bacteria comprising anodic and cathodic biofilms to the target analytes. Additional cases for greater sensitivity in biocathodes have been made by multiple publications, including work by Zang et al., who studied a suspended microorganism, *S. oneidensis* MR-1, capable of bidirectional extracellular electron transfer (EET) (e.g., analyte detection using the electrode as an electron donor or an electron acceptor). They found that an MEB constructed with *S. oneidensis* MR-1 had up to 2.7 times higher sensitivity when operating as a reductive biocatalyst (a biocathode) vs an oxidative biocatalyst (a bioanode) [49, 50]. After rigorous testing, they concluded that cathodic EET had a greater contribution to electron transfer in the respiratory chain than anodic EET, and thus, a cathodic sensing configuration showed a larger response to changes in cellular metabolism. Additionally, it was noted that the working potentials varied in each configuration, and the higher currents may be attributed to higher overpotentials of the cathodic EET.

Dissolved oxygen (DO) concentration measurements are useful in monitoring ecosystems of water bodies for eutrophication events [51]. Water bodies undergo eutrophication when essential nutrients like phosphorous and nitrogen are

introduced in abnormal quantities, often as a result of agricultural runoff [52]. The excess nutrients cause algae blooms and microbial degradation of the compounds, which deplete the water's DO level. This has a cascading effect on other organisms, such as fish, which require oxygen to survive. Sensors to measure dissolved oxygen concentrations do not typically utilize a biocathode [51, 53]. Rather, the bioanode is embedded in anaerobic sediment and the abiotic cathode is in the water column above. The dissolved oxygen concentration can then be correlated using the cell voltage because the number of electrons used for the oxygen reduction reaction at the cathode depends on the rate of electron transfer from the exoelectrogens on the bioanode. A primary drawback of these sensors is that they require a constant and continuous supply of organic feedstock for the bioanode, which is not feasible in field operation [51].

Biofilms are also known to affect metal corrosion, a phenomenon that can be used to measure bacterial activity in water and soil samples [54, 55]. MEB corrosion sensors have been applied in industrial cooling systems using natural water sources that can introduce bacteria and damage components [14]. Like the previously discussed pathogen electrochemical biosensors, microorganisms are not inherently present on the electrode surface [56]. Rather, the sensor relies on the colonization of the electrode by bacteria that form a biofilm. The establishment of a biofilm on the metal leads to cathodic depolarization, where the metal donates electrons to the electrotrophic bacteria and dissolved oxygen is the terminal oxidant. As a result, MEBs can also be used to monitor microbial activity in other settings. One such application is monitoring bioremediation of soil, where microorganisms are used to break down soil contaminants such as herbicides and petroleum compounds. Microbial activity can be measured via corrosion potential using MEBs instead of standard microbiological analysis, which requires access to specialized analytical equipment such as DNA sequencing and mass spectrometry [14, 55, 57].

2.4 Analytes

MEBs utilize two routes of analyte detection, inhibition, or direct sensing. Many MEBs detect the presence of an analyte through inhibition of microbial metabolism. Toxicant compounds negatively affect cells through multiple pathways.

2.4.1 Inhibition Sensing

Heavy metals can inhibit enzymes by displacing other molecules such as sulfate or binding to sulfhydryl groups [58]. Other toxicants like organic pollutants can disrupt the cellular membrane in addition to inhibiting enzymes [59, 60]. Studies have tested many heavy metal species and model compounds to emulate real-world contamination. Various organic compounds have been used to test the effectiveness of MEBs, including pesticides [9], aromatic compounds, hydrocarbons [15], and volatile fatty

Table 2 Recently reported inhibition sensing MEBs

Analyte	Limit of detection[a]	Inoculum	Reference
Cyclohexane carboxylic acid	50 mg COD L^{-1}	Mixed	[64]
Pb(II)	1 mg L^{-1}	Mixed	[33]
Cr(VI)	0.5 mg L^{-1}		
Hg(II)	0.5 mg L^{-1}		
Formaldehyde	1 mg L^{-1}		
Benzalkonium chloride	10 mg L^{-1}		
2,4-dichlorophenol	1 mg L^{-1}		
Cu(II)	IC50 10.12	*Saccharomyces cerevisiae*	[65]
Cd(II)	IC50 13.88		
Ni(II)	IC50 17.06		
Pb(II)	IC50 34.56		
3,5-dichlorophenol	IC50 16.48		
4-chlorophenol	IC50 34.40		
Phenol	IC50 44.55		
Acetate	30 mg L^{-1}	Mixed	[66]
Trichloroacetic acid	20 μg L^{-1}	Mixed	[41]
Atrazine	0.05 ppm	Mixed	[67]
Diuron	0.5 μM	*Synechocystis* PCC6803	[68]
Atrazine	10 μM		
Paraquat	0.5 μM		
4-nitrophenol	67.1 mg L^{-1}	Mixed	[69]
Cd(II)	0.2 μM	*Pseudomonas veronii* 2E	[22]
Cu(II)	2.4 μM		
Atrazine	1 nM	*Chlamydomonas reinhardtii*	[70]
As(III)	MIC 15 mM	*Achromobacter xylosoxidans* BHW-15	[71]

IC inhibitory concentration; *MIC* minimum inhibitory concentration

[a] LOD values are listed as reported. However, caution should be used when comparing values as ppm and mg L^{-1} are often equated without accounting for the compound's molecular weight (i.e., 10 ppm = 10 mg L^{-1}). According to the EPA, to convert values in mg L^{-1} to ppm, multiply the mg L^{-1} value by 24,500 and divide by the molecular weight of the compound [63]

acids [61], and have been compiled in previously published reviews. MEBs have also been used to quantify microbial activity in aquatic environments by linking current density to ATP content and enzymatic activity [62]. Table 2 lists the analytes used to test some recently developed MEBs that utilize inhibition sensing.

2.4.2 Direct Sensing

Alternatively, MEBs can detect analytes directly where the presence of the analyte compound increases the current that is generated by the microorganism. The

Table 3 Recently reported direct-sensing MEBs

Analyte	Limit of detection[a]	Inoculum	Reference
As(III)	1.5 ppb	Recombinant *Escherichia coli*	[39]
Hg(II)	0.1 ppb		
As(III)	2.2 ppb	Recombinant *E. coli*	[40]
Glucose	1.4 mM	Recombinant *S. cerevisiae*	[73]
Cholesterol	2 mM		
Catechol	0.1 μM	Recombinant *E. coli*	[74]
Pyocyanin	12.5 nM	Recombinant *E. coli*	[75]
Autoinducer-2	6.25 nM		
Pyocyanin	47 pM	*Shewanella oneidensis* MR-1	[72]
Pyocyanin	304 pM	*S. oneidensis* MR-1	[42]
1-hydroxyphenazine	1.5 nM		
Dicamba	0.9 μM	Recombinant *E. coli*	[76]
Roundup	0.2 μM		
Riboflavin	0.85 nM	*S. oneidensis* MR-1	[77]
Thiosulfate	0.1 mM	Recombinant *E. coli*	[78]

[a] LOD values are listed as reported. However, caution should be used when comparing values as ppm and mg L^{-1} are often equated without accounting for the compound's molecular weight (i.e., 10 ppm = 10 mg L^{-1}). According to the EPA, to convert values in mg L^{-1} to ppm, multiply the mg L^{-1} value by 24,500 and divide by the molecular weight of the compound [63]

previously mentioned BOD sensors from Table 1 operate via this principle where an increase in organic substrate will lead to an increase in the current signal. Direct sensing of analytes can also be achieved through genetic modification where promoter sequences are used to link the presence of a target analyte with the production of a redox-active molecule [39]. The redox-active molecule results in an increase in the current signal. Electroactive bacteria have also been used to detect redox-active analytes by amplifying their electrochemical signal as shown earlier in Fig. 3 [42, 72]. Recent MEBs that utilize direct sensing are listed in Table 3.

3 Bioelectrochemical Interfaces

3.1 Methods of Extracellular Electron Transfer

Electrons can be transferred either through a direct contact interface between the biological cell and electrode, known as *direct extracellular electron transfer* (DEET), or transferred using a redox mediator, known as *mediated extracellular electron transfer* (MEET) [4, 79]. Studies of EET are primarily based around two model bacteria, *Geobacter sulfurreducens* and *Shewanella oneidensis*, which are both dissimilatory metal-reducing bacteria (DRMB) [4]. In dissimilatory metal reduction, the metal remains outside the cellular envelope [80], and electrons are

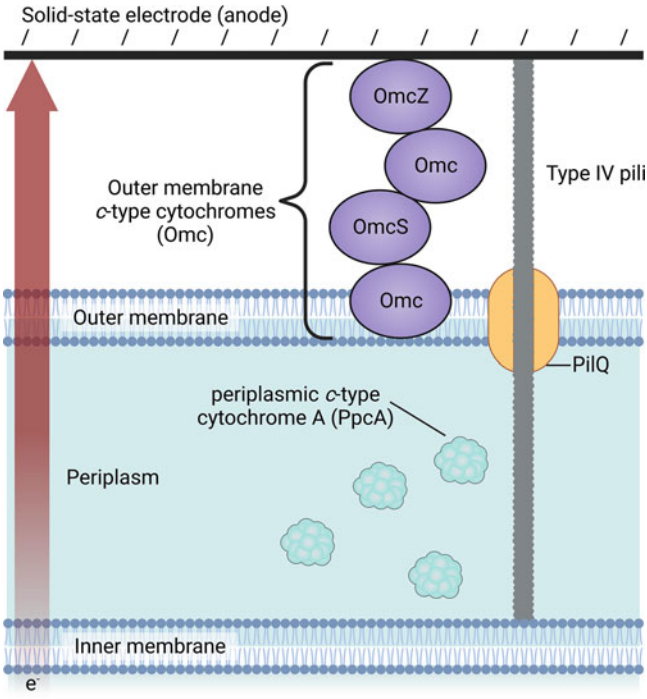

Fig. 5 Illustration of direct extracellular electron transfer pathways in *Geobacter sulfurreducens*. Electron transfer can occur via either c-type cytochromes in outer-membrane proteins or type IV pili (nanowires). (Adapted from Kumar et al. [4])

transferred through direct contact, as is the case with *c*-type cytochromes in *S. oneidensis* or through conductive structures called nanowires [4, 81].

C-*type cytochromes* are hemeproteins that use oxidation and reduction reactions to transfer electrons [82]. They enable DEET by transferring electrons between the intracellular electron transport chain and an extracellular acceptor like an electrode [83]. *S. oneidensis* carries out DEET through metal-reduction (MTR) proteins and *c*-type cytochromes [4]. The *c*-type cytochromes of *S. oneidensis* have been studied both in purified form and in vivo [84]. Despite the well-documented existence of cytochrome complexes, their structures are largely unknown, and attempts to crystalize the Mtr complex of *S. oneidensis* have not been successful [85]. However, the crystal structure of the MtrAB protein complex in *Shewanella baltica* OS185 was recently obtained and characterized by Edwards and coworkers [85]. *Geobacter* species utilize different outer-membrane *c*-type cytochromes (OMCs) that can interact with periplasmic *c*-type cytochromes that are shown in Fig. 5 [4]. Some bacteria also have unique conductive structures that facilitate long-range electron transfer.

One of the earliest works on mediator-less MFCs was done by Kim and coworkers. They demonstrated that cell suspensions of a metal-reducing bacteria

Shewanella putrefaciens when grown anaerobically become electrochemically active with a reduction potential of −0.15 V vs SCE [86]. It was not electrochemically active under aerobic conditions, which suggested that for *S. putrefaciens,* DEET can be only achieved at anaerobic conditions. The authors proposed that the electrochemical activity was due to the presence of electrochemically active cytochromes on the surface of the bacterial cells. The genomic analysis of *S. oneidensis* showed that it has 43 possible cytochrome *c* genes, whereas *Geobacter sulfurreducens* has more than 100 [87]. A few other noteworthy studies have also demonstrated that sulfate-reducing bacteria such as *Desulfovibrio desulfuricans* generate electricity in an MFC by using the sulfate/sulfide as their electron mediator along with the potential cytochrome c proteins that they possess [88]. Mishra and Verma recently published an article evaluating the performance of yeast-based microbial fuel cells that use banana peel waste as a fuel source. It generated a maximum power output of 86.9 mW m^{-2} primarily due to the presence of microbial consortia innate to the banana slurry such as *Pseudomonas, Chryseobacterium, Flavobacterium, Stenotrophomonas, Chryseolinea, Rhodococcus,* and *Rhizobium* [89].

Conductive structures that enable long-range DEET in microbes have collectively been referred to as "*nanowires*," but the structural composition can differ between species. Nanowires were initially discovered in *G. sulfurreducens* by Reguera and coworkers to be type IV pili (Fig. 5) [90]. These pili have subsequently been characterized by multiple methods such as cryo-electron microscopy and conductive-tip atomic force microscopy [5, 91]. *S. oneidensis* also has similar structures that have been referred to as nanowires [92, 93]. However, in vivo labeling fluorescence and electron cryotomography revealed that *S. oneidensis* nanowires are in fact extensions of the outer membrane that enable DEET through embedded MTR proteins and OMCs (Fig. 6) [94].

Electrons can also be transferred through indirect or mediated extracellular electron transfer (MEET) [79]. In MEET, intermediate, electroactive compounds undergo reduction-oxidation reactions to shuttle electrons between the bacteria and the electrode. Humic substances or metals act as redox mediators in natural environments [95]. Various redox mediators have been tested including phenazines (neutral red and pyocyanin), benzoquinones, and other redox-active dyes (methyl viologen and methylene blue) [96]. Recent reviews by Weliwatte et al. [96], Gemünde et al. [97], and Martinez and Alvarez [98] cover the topic extensively. Some bacteria secrete their own redox mediators in the form of flavins as is the case with *S. oneidensis*, shown in Fig. 6 [99]. Further study indicated that the secreted flavins receive electrons from decaheme cytochromes, MtrC and OmcA, on the outer membrane [100]. The reduced flavin can then mediate electron transfer to the solid-state electrode, returning to its oxidized state. In addition to recyclable redox mediator compounds, hydrogen, H_2, acts as a one-way electron shuttle for many bacterial species [101].

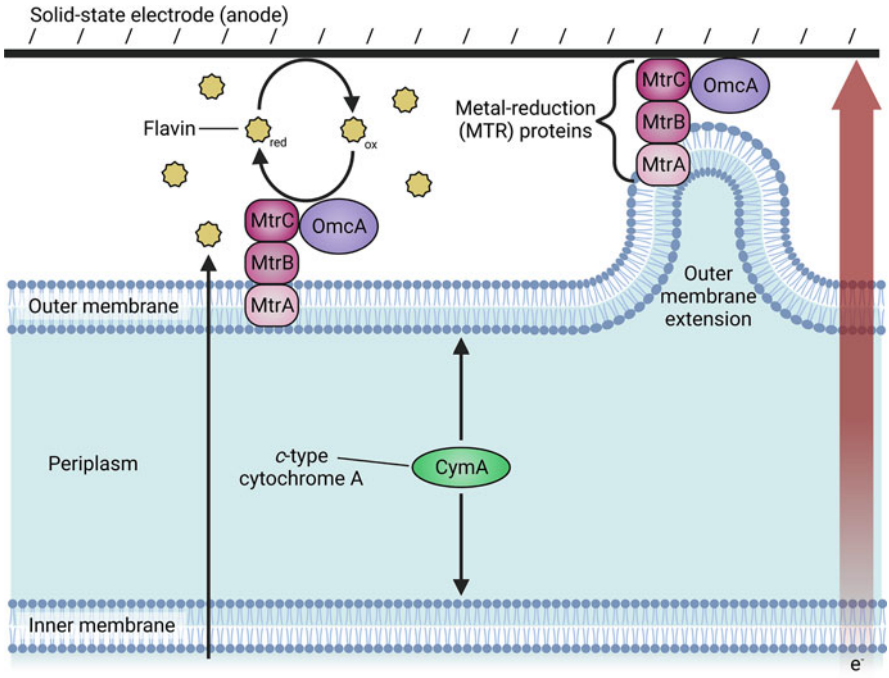

Fig. 6 Illustration of direct and mediated extracellular electron transfer pathways in *Shewanella oneidensis*. Electron transfer to an electrode occurs via either secreted small redox-active molecules or directly through metal-reducing proteins in the outer cell membrane. (Adapted from Kumar et al. [4])

3.2 Electron Transfer in MEBs

From a thermodynamic perspective, the electron transfer between a microbe and an electrode occurs because electrons move from high potential to low potential, analogous to electrochemical reactions [23, 102]. The direction of extracellular electron transfer (EET) defines two subtypes of microorganisms, exoelectrogens and electrotrophs. *Exoelectrogens* donate electrons to an electrode by oxidizing organic compounds, and *electrotrophs* accept electrons from an electrode to reduce organic compounds, metals, or CO_2 [103, 104]. Exoelectrogens have also been referred to as electrochemically active bacteria (EAB) [105], anode-respiring bacteria [106], and electricigens [107]. Exoelectrogenic archaea and eukaryotes have also been discovered [104]. Microbial fuel cells (MFCs) can utilize exoelectrogens instead of a catalyst at the anode to produce current, shown in Fig. 7 [103]. Exoelectrogens generate current by oxidizing organic material and exchanging excess electrons with an electrode instead of being incorporated into reduced metabolic products [79]. The counter-electrode reaction at the cathode is the oxygen reduction reaction that proceeds through a two- or four-electron pathway, depending on the medium. Since current generation can be correlated with the concentration of

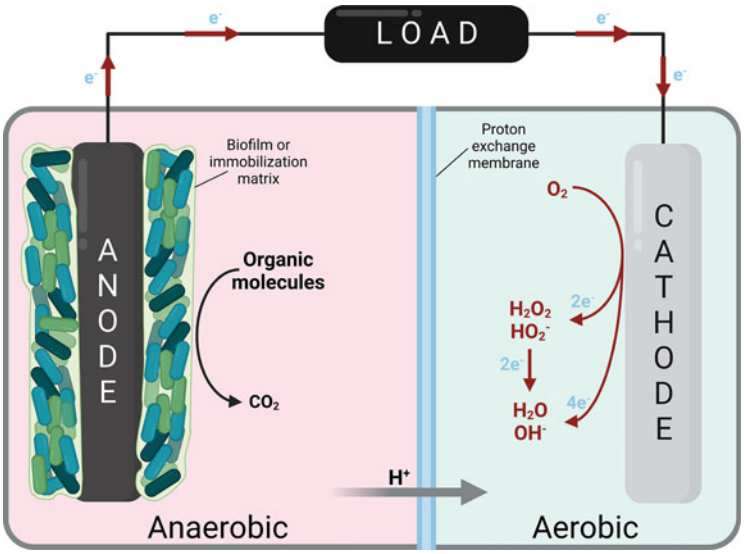

Fig. 7 Illustration of a microbial fuel cell. Electrons can be transferred from the microorganism to the electrode either directly or mediated through a conductive immobilization material

organic material, the microbes can be used to measure the level of organic material present in an aqueous sample as discussed above [14].

Electrotrophic microorganisms take up electrons from an electrode [103]. Before electrodes were used as electron donors to bacteria, it was known that bacterial biofilms could oxidize metals and use the electrons to reduce oxygen [54]. Subsequent research by Park and Zeikus found that the phenazine neutral red could facilitate MEET between a cathode and *Actinobacillus succinogenes* to reduce fumarate [108]. Gregory et al. were the first to document electrotrophic behavior in a pure culture without an exogenous redox mediator [109]. They found that *Geobacter metallireducens* reduced nitrate to nitrite with the cathode as the sole electron donor. These early studies laid the foundation for the development of microbial electrosynthesis. Cathodes can be used to drive biocatalytic reactions such as microbial electrosynthesis, water purification, and microbial electrofermentation (EF) [104, 110, 111]. The electrochemical reactions that form the basis of these processes can be used for biosensing applications as well.

4 MEB Materials and Construction

4.1 Electrode Materials

A wide variety of electrode materials have been used in MEBs, such as metals, ceramics, and polymers [112]. Carbon-based materials (carbon felt, carbon cloth,

carbon paper, etc.) are commonly used as the working electrode, because they are cheap to manufacture, they are easily modified, and biological cells can easily attach and form biofilms [24, 113]. For those unfamiliar with electrochemistry terminology, the working electrode (WE) can be either the anode or cathode, but it is always the electrode at which the reaction of interest is occurring. For MEBs, the working electrode will be the electrode that is interfaced with the microbial cells acting as the sensing element. The reaction at the counter-electrode (CE) is rarely discussed at length in MEB publications, but the primary CE reaction in aqueous systems is the oxygen reduction reaction at the cathode or the oxidation of organic compounds at the anode [14].

Biocompatibility of the electrode material with the biological sensing element is necessary for a successful MEB. Some electrode materials prevent biofilm formation of certain species, as is the case with *Shewanella* spp. on gold electrodes [114]. Depending on the inoculating culture, some electrode materials may be less effective and consequently affect sensing performance [34]. Of course, electrode materials need to be coupled with effective immobilization strategies to ensure a good interface between the microbes and the electrode.

4.2 Immobilization Methods

For an MEB to be effective, immobilization materials must allow for efficient electron transfer between the microorganism and the electrode [14]. To this end, various chemical and physical immobilization methods have been developed. Physical immobilization methods are defined by the nonspecific adsorption onto a permeable electrode surface and rely on the diffusion of microbes into rigid pores. The primary drawback to this approach is the limited ability of analytes to diffuse into the rigid porous structure. Chemical methods can be further categorized as either covalent or non-covalent. Covalent immobilization methods rely on the formation of chemical bonds directly between chemical functionalities on the electrode surface and species on the exterior of a microbe's outer cell wall. While immobilization through direct covalent linkages results in strong adhesion of cells to the electrode surface, the harsh reagents and conditions used for these chemical reactions often have an adverse effect on cell viability [24]. Therefore, covalent immobilization is not commonly employed in modern MEB applications. Non-covalent chemical immobilization methods are preferred in MEBs since they require milder reaction conditions and do not significantly affect cellular function. These methods include the use of polymer hydrogels to entrap microbes on or near an electrode surface and make use of non-covalent interactions such as ionic, polar, or hydrogen bonds or by hydrophobic interactions. A summary of immobilization materials is provided in Table 4 and has been described in recent reviews [9, 24, 115, 116].

Beyond immobilization of microorganisms, electrode surfaces and biofilms can be modified to help promote electron transfer between the microorganism and the electrode [117]. As an example, multi-walled carbon nanotubes (MWCNTs) have

Table 4 Cell immobilization materials used in MEBs

Matrix	Class of compounds	Reference
Natural polymers		
Agarose	Linear polysaccharide derived from red algae	[120]
Alginate	Alginic acid salts: calcium and magnesium alginates	[121, 122]
Chitosan	Amino sugar, linear polysaccharide derivative	[118, 123]
Collagen	Protein that forms the basis of connective tissues of multicellular organisms	[124]
Carrageenan	Polysaccharide similar to agar in composition and properties	[125]
Gelatin	Partially hydrolyzed collagen capable of retaining water	[126]
Cellulose	Polysaccharide, the main component of the cell walls of all higher plants; cheapest substrate available	[127]
Synthetic polymers		
Poly(pyrrole)	Ion-exchange resins or insoluble carriers with porous surfaces; porous surface catches and holds cells	[128]
Poly(ethyleneimine)		[129]
Poly(vinyl alcohol)		[130–133]
Poly(methacrylate)		[134, 135]
Poly(thiophene)		[136, 137]
Inorganic materials		
Zeolites	Silicates	[122]
Silica	Polymorphic modifications of silicon dioxide	[138]
Glass	The main component is silicon dioxide	[122, 139]
Activated carbon	Amorphous carbon without a clear structure almost free of impurities; porous with high adsorption capacity	[140]

been found to improve MEB sensitivity; however, their use introduces significant electrochemical noise. As a result, the incorporation of MWCNTs at an MEB electrode does not improve the sensor's limit of detection [118]. One subset of polymers used for microbial entrapment utilize an electrically conductive backbone (e.g., polyaniline) to help improve the efficiency of electron transfer between microbes and the electrode. While not discussed further here, MEBs using electrically conductive polymers were reviewed recently for the interested reader [11].

As an alternative to incorporating redox species in the immobilization matrix, electron transfer efficiency can be improved through direct functionalization of electrodes with redox mediators. Recently, graphene was functionalized with molybdenum polysulfides (MoS_x) to detect a group of endogenous redox mediators, phenazine derivatives, which are secreted by the pathogen *Pseudomonas aeruginosa* [45]. The incorporation of redox mediators directly onto the electrode surface can help to significantly improve the device shelf life. Uria and coworkers recently developed an MEB with screen-printed graphite electrodes that has a shelf life of up to a year [119]. The device had an activity loss of 50% over the course of the first month of storage but no further losses over the remaining 11 months.

Alternatively, microorganisms can naturally immobilize themselves on the electrode through the formation of biofilms [4, 141]. The drawback of relying solely on a biofilm is that it can take microbes several days to form a fully mature biofilm that can be used for biosensing; however, the biofilm can help protect the biological sensing element during repeated toxicant exposure, reducing the frequency of recalibration. Biofilm development can be affected by shear stress [18, 20]. It is therefore important to consider fluid mechanics, especially in cases of flow-through MEBs that are used for continuous measurement of a flow stream such as wastewater [142]. Once the electrode material and immobilization method have been chosen, the microorganism culture must be incubated to interface with the electrode. Some have incubation times of several hours, but MEBs requiring biofilm formation, such as MFC-type biosensors, can have start-up times of several days or months [14, 34].

5 Organisms Used in MEBs

5.1 Monoculture MEBs

Microorganisms convert biochemical energy into ATP using a cascade of reactions to transfer electrons. As described in detail in Sect. 3, EET plays a pivotal role in fabricating microbial fuel cells and electrolysis cells, collectively known as microbial electrochemical cells (MXCs). A microbial electrolysis cell requires a power input, unlike a microbial fuel cell. An MEB can utilize microbial electrolysis to treat wastewater and produce hydrogen fuel as shown in Fig. 8. A popular way to design MXCs is to exploit the anaerobic respiration capacities of anode-respiring bacteria (ARB). The ARB typically undergoes EET for the respiration of insoluble Fe (III) and Mn oxides. *Geobacteraceae* and *Deltaproteobacteria* families are well studied for their applications in current-generating MXCs. Badalamenti et al. showed that higher current densities can be achieved by pure ARB in MXCs using *Geoalkalibacter. Glk. ferrihydriticus* and *Glk. subterraneus* were tested for generating currents using poised electrodes in alkaline (pH ~9.3) and saline conditions (1.7% NaCl), respectively [143]. The acetate-fed *Glk. subterraneus* biofilms generated current at 0.04 V vs Ag/AgCl under saline conditions at a pH of 7.2 within 3 days of inoculation. The coulombic efficiency ranged from 55 to 119%. On the other hand, Glk. *ferrihydriticus* generated current at pH 9.3, with current densities ranging from 5 to 8.3 A m^{-2}. The high current densities achieved using the *Geoalkalibacter* species make them promising candidates for MXCs to treat alkaline and saline wastewater produced in the textile and brewing industries.

MXCs are also used as platforms for studying photosynthetic cultures which have direct applications in understanding photo-kinetics and energy conversion. The role of green sulfur bacteria to generate current in MXCs was investigated by Badalamenti et al. A comparison was drawn based on the light responsiveness in monocultures and cocultures of *Geobacter* and *Chlorobium.* The *Chlorobium* cultures were maintained under constant illumination at pH 7.2 in $NaHCO_3$ buffer and

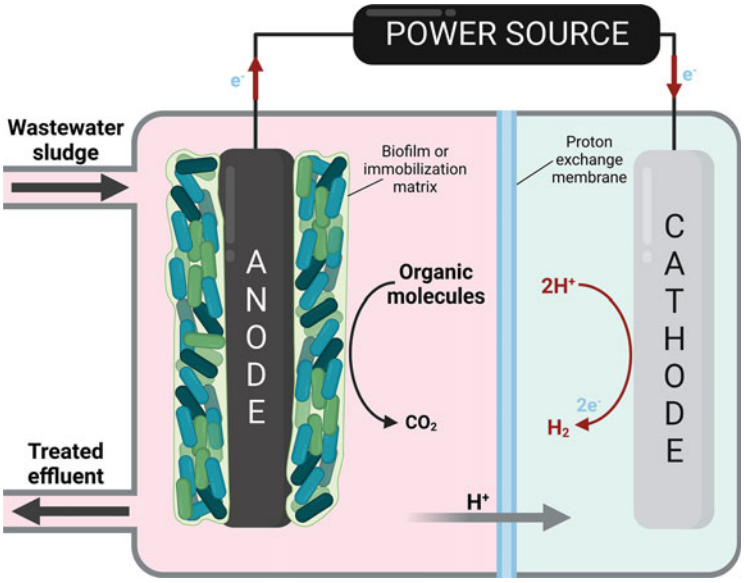

Fig. 8 Illustration of a microbial electrolysis cell. Electrons can be transferred from the microorganism to the electrode either directly or mediated through a conductive immobilization material

the *Geobacter* cultures in acetate and ferric pyrophosphate buffer under N_2:CO_2 atmosphere [144]. The monocultures were studied using an MXC setup and their electrochemical behavior was compared against the coculture. No exogenous electron donors were present in the setup and the anode acted as the only electron receptor. In cocultures, the *Geobacter* cells adhered to the electrode surface and acted as the biosensing interface for the *Chlorobium*-driven carbon metabolism.

Organophosphates (OPs), which are commonly used in pesticides, pose dangerous environmental effects. Organophosphate hydrolases (OPH) can capture and enzymatically degrade OPs by incorporating them into genetically modified microorganisms [145]. Thus, microbes that express OPH innately or extrinsically (such as genetically engineered *E. coli*) have been used extensively for detecting and degrading OPs. Karbelkar et al. developed a dual-species technology that targets and degrades parathion-type OPs using *E. coli* and *S. oneidensis* [145]. The *E. coli* cells were engineered to produce OPH that releases p-nitrophenol (p-NP) when it degrades OP-containing pesticides. The electrochemically active *S. oneidensis* expresses a critical protein CmycA in the presence of p-NP. After validating the monocultures individually, the authors confirmed that in a coculture the *E. coli* degrades the OP which releases p-NP and the *S. oneidensis* detects the degradation product by generating current as a readout signal.

5.2 *Mixed Culture Consortium MEBs*

In fields such as synthetic biology, where a single reaction or product is desired, a single microbial population is often employed in which the genetic circuits of a selected microbe are tuned to amplify a single metabolic pathway [146]. However, with the increase in circuit complexity, the number of engineering challenges increases, and engineered monocultures tend to suffer from poor stability and may require higher maintenance [147]. Because of this, the majority of MEB research relies on the use of a mixed-culture microbial consortium [148]. This enables the division of labor between different strains and improves the circuit's overall efficiency. Mixed cultures are easily obtained from wastewater treatment facilities and other processes that utilize microbial treatment methods; these cultures have the benefit of having already established a symbiotic community to survive in harsh conditions. The most popular applications of these mixed microbial consortium systems include toxicity detection, wastewater treatment, and biomanufacturing processes [149]. Gao developed a benzoquinone-mediated MEB to detect multiple pollutants using a consortium of microorganisms [150]. Mixed cell cultures of *E. coli, Bacillus subtilis*, and *Saccharomyces cerevisiae* were used as the components for developing a biofilm that can detect heavy metal ions (Cu^{2+}, Cd^{2+}), pesticides, and dichlorophenol in wastewater.

6 Limitations to MEBs

Despite significant advances in MEB capabilities, further research is required to overcome remaining shortcomings. MEBs need to be calibrated to correlate electrical current with analyte concentration. One of the main difficulties in using biological cells as a sensing element is that any change in the population or community of interfaced cells will affect the device's accuracy. A previous study found that running an MEB intermittently instead of continuously improved the device sensitivity [17]. A study by Chu et al. found that incubating a biocathode of activated sludge at anodic potentials before reversing the polarity improved the biocathode's response to formaldehyde [151]. However, the strategy was ineffective at recovering the baseline signal after toxicant exposure.

Calibration is critical for accurate reporting of analyte concentrations, but it has been previously noted that the properties of the chosen calibration solution (e.g., composition) greatly affect the accuracy of the MEB [64, 152]. Recalibration is necessitated by several other limitations of MEBs. While previous studies have shown that MEBs can recover well from toxicant shocks, repeated exposure would require recalibration of the device since diminishing the microorganism population would thereby affect the measured current response, leading to inaccurate measurements [33, 46, 153]. In this regard, some progress has been made for BOD MEBs. Spurr and coworkers were able to maintain mixed-culture MFCs operated in batch

and flow modes for 800 days with minimal drift between recalibrations; however, this was made possible by tight control of operating and environmental conditions, something that is rarely possible in field applications [154]. The authors noted that increasing external resistance resulted in a significant decrease in the calibration's upper limit from 240 to 30 mg L^{-1} O_2 BOD_5. Furthermore, dynamic cell populations, both genotypically and phenotypically, will also necessitate recalibration [155].

Contamination by preexisting microbial communities in the sample is also a significant concern for MEB implementation [36]. This effect was evaluated by Xiao and coworkers [156]. They established that the presence of bacteria (electroactive or not) in wastewater samples affected the subsequent measurements of BOD by the mixed bacterial inoculum in a micro-scale MFC-type biosensor. Despite the samples having significantly different BOD levels, the measured current from the bioanode was statistically unchanged due to the variance in microbial populations. The goal for biosensors to be reusable is hampered by the fact that repeated exposure to a different medium can change the microbial population present on the electrode surface, thereby affecting the calibration and sensitivity of the MEB. Another oft-noted limitation of MEBs is that they lack specificity to a particular toxicant. However, this is more aptly described as a double-edged sword. Real-world applications can require a nonspecific but highly sensitive recognition element, as is the case with contamination of water sources, where a quick initial assessment may be required to determine if any of a panel of potential toxicants are present. Subsequent detailed analytical procedures, such as mass spectrometry or high-performance liquid chromatography, can then be used to accurately determine what pollutants are present. Another advantage of MEBs over current analytical methods is that MEBs can determine the amount of an analyte that is biologically available to the microorganisms, which is not necessarily equal to the total concentration present in the sample [9].

7 State of the Art and Outlook

An overview of microbial electrochemical biosensors and the fundamental electron transfer phenomena has been presented, and the applications and limitations of this type of sensor have been summarized. Considerable innovations in MEBs have been made over (esp.) the last 5 years to improve characteristics ranging from device portability to sensitivity. MEBs offer greater stability compared to other biosensors, because whole cells have greater tolerance to varied environmental conditions. MEBs hold significant potential as early warning systems for pollution events in wastewater treatment and portable analytical tools for quick assessment of water quality among other applications.

The physical design and configuration of MEBs have been the subject of recent publications seeking to improve MEB performance. To this end, it is also necessary

to characterize electrical parameters of the electrochemical cell, such as internal resistance and capacitance. These parameters are traditionally found using electrochemical characterization methods such as electrochemical impedance spectroscopy (EIS) and cyclic voltammetry (CV). Electrochemical impedance (which is measured by EIS) accounts for the complexities of an electrical circuit that cannot be described with resistance alone. Unfortunately, the use of EIS and CV adversely affects the microbial sensing element and requires long recovery times when measurements are taken during operation. Adekunle et al. demonstrated use of a software sensor to successfully model their MFC-type MEB with an equivalent circuit model to accurately monitor the electrical parameters without affecting the sensor during operation [142]. Physical design innovations have also been made by combining multiple sensors to improve accuracy. Jia et al. developed a novel MEB design by combining two biocathode MFCs with an upflow anaerobic sludge blanket. By placing the biocathodes in the suspended and sludge layers of the upflow anaerobic sludge blanket, they could effectively quantify COD and total volatile fatty acid concentration, respectively [157]. Despite the intended reusability of MEBs, design improvements are also necessary to avoid the use of unsustainable components. Progress has been made in sustainability by using self-powered MFC-type biosensors as well as environmentally conscious paper-based designs, which were comprehensively reviewed by Chung and Dhar [158]. Cai et al. very recently developed a proof-of-concept rechargeable MEB for water quality monitoring [13]. The device was charged by reducing CO_2 to acetate and formate, which would be consumed by the bioanode during the discharging process. In addition to self-powered MEBs designs that use chemical substrates, MEBs can also be self-powered by storing energy in redox polymers, as demonstrated by Grattieri and coworkers [38]. Their COD monitoring device used a disposable cathode coated with a conductive redox polymer composed of poly(vinylpyridine) and ruthenium, which was charged by oxidizing the redox polymer. The redox polymer also increased the sensitivity of the device by one order of magnitude. Another design innovation is the use of multi-stage MFCs, which can extend the concentration range in which an analyte can be accurately detected [32]. Multi-stage MFCs have been recently applied to improve MEB detection ranges of BOD, from an upper limit of 340 mg L^{-1} BOD_5 to 720 mg L^{-1} BOD_5 [32], and chromium, from an upper limit of 30–90 mg L^{-1} [159]. A multi-stage MFC MEB developed by Godain et al. allowed for better distinction between changes in 4-nitrophenol concentration vs changes in the BOD of the feed [153]. In addition to physical design considerations, steps are also being taken to address biological aspects of MEBs.

Biofilm stability is a primary concern for widespread use of MEBs, because the calibration between measured current and toxicant concentration is dependent on the microbial sensing element maintaining a stable population [160]. To this end, antibiotic composite electrodes using azithromycin were tested by Wang and coworkers to prevent contamination of the bioanode by undesired bacteria [160]. They found that appropriate dosing of azithromycin improved the sensitivity and reduced the start-up period. Unlike previous studies using soluble antibiotics,

azithromycin is insoluble, which facilitates the fabrication of a composite graphite powder electrode that can be used in a continuous-flow MEB without leeching antibiotic into the flow stream. The azithromycin was successfully able to enrich the bioanode by selecting against aerobic gram-positive cocci and gram-negative *Bacillus*.

Another primary issue facing MEBs is selectivity. Few publications test their devices with real samples such as wastewater [14, 37, 48]. They often use controlled tests where a specific analyte is individually added to a sample. In cases where real-world samples are used, the goal is primarily sensitivity, determining when any potential toxicant signal appears as opposed to specific detection of a particular chemical species. While MEBs can have high sensitivity, they fall short in determining the exact compound that results in the detection signal. Nevertheless, MEB specificity can be improved through genetic engineering. One of the goals of genetic modification is to have microbes produce an electroactive compound in response to the presence of a particular analyte. *E. coli* has been modified to produce electroactive 4-aminophenol (PAP), an electroactive redox mediator. PAP can then be detected through cyclic voltammetry at the platinum working electrode [39]. This miniaturized device, developed by Sciuto and coworkers, allows for on-site monitoring of water supplies. Sánchez et al. used the arsenic-responsive *ars* promoter sequence to activate a gene for 4-aminophenol production in recombinant *E. coli* [40]. This enabled selective detection of As(III) because the gene encoding the redox mediator requires that the promoter be activated by the presence of As(III). As covered in a previous section, Yang et al. were able to substantially increase the electrochemical response of pyocyanin and 1-hydroxyphenazine by linking them to a redox-cycling system with *S. oneidensis* MR-1 [42]. Initial research has been conducted on using machine learning algorithms to allow for simultaneous quantification of multiple analytes. Du et al. were able to accurately quantify three toxicants introduced in random concentrations, but the use of machine learning in MEBs remains largely untested and lacks the true selectivity of genetic engineering methods [161].

In addition to sensing capabilities, improvements are also necessary in terms of MEB sensitivity, especially for toxicant monitoring since some sensors are not yet fully capable of detecting some toxicants at or below their maximum allowable concentration based on water standards. Recent developments have shown that cathodic biofilms can exhibit an order of magnitude higher sensitivity to toxicants compared to anodic biofilms [33, 49]. Selectivity is also desired for implementable MEBs for pathogen detection [14]. In terms of future research, the ability to maintain and recover interfaced biofilms should be further explored to improve the reusability of MEBs, especially after toxicant shocks. Electrochemical engineering of immobilization materials and redox mediators could provide pathways to further improve MEB sensitivity and performance.

References

1. Potter MC (1911) Electrical effects accompanying the decomposition of organic compounds. Proc R Soc Lond B 84:260–276. https://doi.org/10.1098/rspb.1911.0073
2. Davis JB, Yarbrough HF (1962) Preliminary experiments on a microbial fuel cell. Science 137:615–616. https://doi.org/10.1126/science.137.3530.615
3. Davis JB (1963) Generation of electricity by microbial action. Adv Appl Microbiol 5:51–64. https://doi.org/10.1016/S0065-2164(08)70006-6
4. Kumar A, Hsu LH-H, Kavanagh P et al (2017) The ins and outs of microorganism–electrode electron transfer reactions. Nat Rev Chem 1:0024. https://doi.org/10.1038/s41570-017-0024
5. Lovley DR, Walker DJF (2019) Geobacter protein nanowires. Front Microbiol 10. https://doi.org/10.3389/fmicb.2019.02078
6. Karube I, Mitsuda S, Matsunaga T, Suzuki S (1977) A rapid method for estimation of BOD by using immobilized microbial cells. J Ferment Technol 55:243–248
7. Diviés C (1975) Remarks on ethanol oxidation by an "Acetobacter xylinum" microbial electrode (author's transl). Ann Microbiol (Paris) 126:175–186
8. Shankaran DR (2018) Cellulose nanocrystals for health care applications. In: Applications of nanomaterials. Elsevier, pp 415–459
9. Plekhanova YV, Reshetilov AN (2019) Microbial biosensors for the determination of pesticides. J Anal Chem 74:1159–1173. https://doi.org/10.1134/S1061934819120098
10. Thévenot DR, Toth K, Durst RA, Wilson GS (2001) Electrochemical biosensors: recommended definitions and classification. Biosens Bioelectron 16:121–131. https://doi.org/10.1016/S0956-5663(01)00115-4
11. Lakard B (2020) Electrochemical biosensors based on conducting polymers: a review. Appl Sci 10:6614. https://doi.org/10.3390/app10186614
12. Noori MT, Thatikayala D, Pant D, Min B (2022) A critical review on microbe-electrode interactions towards heavy metal ion detection using microbial fuel cell technology. Bioresour Technol 347:126589. https://doi.org/10.1016/j.biortech.2021.126589
13. Cai J, Huang H, Li Z et al (2022) A rechargeable microbial electrochemical sensor for water biotoxicity monitoring. Biosens Bioelectron X 10:100132. https://doi.org/10.1016/j.biosx.2022.100132
14. Simoska O, Gaffney EM, Minteer SD et al (2021) Recent trends and advances in microbial electrochemical sensing technologies: an overview. Curr Opin Electrochem 30:100762. https://doi.org/10.1016/j.coelec.2021.100762
15. Hyun Chung T, Meshref MNA, Ranjan Dhar B (2021) A review and roadmap for developing microbial electrochemical cell-based biosensors for recalcitrant environmental contaminants, emphasis on aromatic compounds. Chem Eng J 424:130245. https://doi.org/10.1016/j.cej.2021.130245
16. Grattieri M, Minteer SD (2018) Self-powered biosensors. ACS Sens 3:44–53. https://doi.org/10.1021/acssensors.7b00818
17. Jiang Y, Liang P, Liu P et al (2017) Enhancement of the sensitivity of a microbial fuel cell sensor by transient-state operation. Environ Sci Water Res Technol 3:472–479. https://doi.org/10.1039/C6EW00346J
18. Shen Y, Wang M, Chang IS, Ng HY (2013) Effect of shear rate on the response of microbial fuel cell toxicity sensor to Cu(II). Bioresour Technol 136:707–710. https://doi.org/10.1016/j.biortech.2013.02.069
19. Xu M, Li J, Liu B et al (2021) The evaluation of long term performance of microbial fuel cell based Pb toxicity shock sensor. Chemosphere 270:129455. https://doi.org/10.1016/j.chemosphere.2020.129455
20. Zhai J, Dong S (2022) Recent advances in microbial fuel cell-based toxicity biosensors: strategies for enhanced toxicity response. Curr Opin Electrochem 34:100975. https://doi.org/10.1016/j.coelec.2022.100975

21. Bard AJ, Faulkner LR (2001) Electrochemical methods: fundamentals and applications.2nd edn. Wiley, New York
22. Busnelli MP, Lazzarini Behrmann IC, Ferreira ML et al (2021) Metal-Pseudomonas veronii 2E interactions as strategies for innovative process developments in environmental biotechnology. Front Microbiol 12. https://doi.org/10.3389/fmicb.2021.622600
23. Fuller TF, Harb JN (2018) Electrochemical engineering.1st edn. Wiley, Hoboken
24. Lei Y, Chen W, Mulchandani A (2006) Microbial biosensors. Anal Chim Acta 568:200–210. https://doi.org/10.1016/j.aca.2005.11.065
25. Lim JW, Ha D, Lee J et al (2015) Review of micro/nanotechnologies for microbial biosensors. Front Bioeng Biotechnol 3. https://doi.org/10.3389/fbioe.2015.00061
26. Garcia SO, Ulyanova YV, Figueroa-Teran R et al (2016) Wearable sensor system powered by a biofuel cell for detection of lactate levels in sweat. ECS J Solid State Sci Technol 5:M3075–M3081. https://doi.org/10.1149/2.0131608jss
27. Dai Z, Xu Z, Wang T et al (2019) In-situ oil presence sensor using simple-structured upward open-channel microbial fuel cell (UOC-MFC). Biosens Bioelectron X 1:100014. https://doi.org/10.1016/j.biosx.2019.100014
28. Fan Y, Qian F, Huang Y et al (2021) Miniature microbial fuel cells integrated with triggered power management systems to power wastewater sensors in an uninterrupted mode. Appl Energy 302:117556. https://doi.org/10.1016/j.apenergy.2021.117556
29. Qian F, Morse DE (2011) Miniaturizing microbial fuel cells. Trends Biotechnol 29:62–69. https://doi.org/10.1016/j.tibtech.2010.10.003
30. Woodard & Curran, Inc. (2006) Waste characterization. In: Industrial waste treatment handbook. Elsevier, pp 83–126
31. Jouanneau S, Recoules L, Durand MJ et al (2014) Methods for assessing biochemical oxygen demand (BOD): a review. Water Res 49:62–82. https://doi.org/10.1016/j.watres.2013.10.066
32. Spurr MWA, Yu EH, Scott K, Head IM (2018) Extending the dynamic range of biochemical oxygen demand sensing with multi-stage microbial fuel cells. Environ Sci (Camb) 4:2029–2040. https://doi.org/10.1039/C8EW00497H
33. Prévoteau A, Clauwaert P, Kerckhof F-M, Rabaey K (2019) Oxygen-reducing microbial cathodes monitoring toxic shocks in tap water. Biosens Bioelectron 132:115–121. https://doi.org/10.1016/j.bios.2019.02.037
34. Wang Z, Liao C, Zhong Z et al (2023) Design, optimization and application of a highly sensitive microbial electrolytic cell-based BOD biosensor. Environ Res 216:114533. https://doi.org/10.1016/j.envres.2022.114533
35. Gao Y, Yin F, Ma W et al (2020) Rapid detection of biodegradable organic matter in polluted water with microbial fuel cell sensor: method of partial coulombic yield. Bioelectrochemistry 133:107488. https://doi.org/10.1016/j.bioelechem.2020.107488
36. Yi Y, Zhao T, Xie B et al (2020) Dual detection of biochemical oxygen demand and nitrate in water based on bidirectional Shewanella loihica electron transfer. Bioresour Technol 309:123402. https://doi.org/10.1016/j.biortech.2020.123402
37. Hu J, Li Y, Gao G, Xia S (2017) A mediated BOD biosensor based on immobilized B. Subtilis on three-dimensional porous graphene-polypyrrole composite. Sensors 17:2594. https://doi.org/10.3390/s17112594
38. Grattieri M, Hickey DP, Alkotaini B et al (2018) Hypersaline microbial self-powered biosensor with increased sensitivity. J Electrochem Soc 165:H251–H254. https://doi.org/10.1149/2.1051805jes
39. Sciuto EL, Petralia S, Meer JR, Conoci S (2021) Miniaturized electrochemical biosensor based on whole-cell for heavy metal ions detection in water. Biotechnol Bioeng 118:1456–1465. https://doi.org/10.1002/bit.27646
40. Sánchez S, McDonald M, Silver DM et al (2021) The integration of whole-cell biosensors for the field-ready electrochemical detection of arsenic. J Electrochem Soc 168:067508. https://doi.org/10.1149/1945-7111/ac049e

41. Wu H, Li A, Wang J et al (2022) A novel electrochemical sensor based on autotropic and heterotrophic nitrifying biofilm for trichloroacetic acid toxicity monitoring. Environ Res 210: 112985. https://doi.org/10.1016/j.envres.2022.112985
42. Yang Y, Yu Y-Y, Shi Y-T et al (2019) In vivo two-way redox cycling system for independent duplexed electrochemical signal amplification. Anal Chem 91:4939–4942. https://doi.org/10.1021/acs.analchem.9b00053
43. Karbelkar AA, Furst AL (2020) Electrochemical diagnostics for bacterial infectious diseases. ACS Infect Dis 6:1567–1571. https://doi.org/10.1021/acsinfecdis.0c00342
44. Simoska O, Stevenson KJ (2019) Electrochemical sensors for rapid diagnosis of pathogens in real time. Analyst 144:6461–6478. https://doi.org/10.1039/C9AN01747J
45. Zhou K, Kammarchedu V, Butler D et al (2022) Electrochemical sensors based on MoS_x-functionalized laser-induced graphene for real-time monitoring of phenazines produced by *Pseudomonas aeruginosa*. Adv Healthc Mater 11:2200773. https://doi.org/10.1002/adhm.202200773
46. Chu N, Liang Q, Hao W et al (2021) Microbial electrochemical sensor for water biotoxicity monitoring. Chem Eng J 404:127053. https://doi.org/10.1016/j.cej.2020.127053
47. Jiang Y, Liang P, Huang X, Ren ZJ (2018) A novel microbial fuel cell sensor with a gas diffusion biocathode sensing element for water and air quality monitoring. Chemosphere 203: 21–25. https://doi.org/10.1016/j.chemosphere.2018.03.169
48. Li X, Yang X, Cui M et al (2022) A novel electrochemical sensor based on nitrite-oxidizing bacteria for highly specific and sensitive detection of nitrites. Sci Total Environ 826:154178. https://doi.org/10.1016/j.scitotenv.2022.154178
49. Zang Y, Zhao H, Cao B et al (2022) Enhancing the sensitivity of water toxicity detection based on suspended Shewanella oneidensis MR-1 by reversing extracellular electron transfer direction. Anal Bioanal Chem 414:3057–3066. https://doi.org/10.1007/s00216-022-03919-6
50. Jiang Y, Liang P, Liu P et al (2017) A novel microbial fuel cell sensor with biocathode sensing element. Biosens Bioelectron 94:344–350. https://doi.org/10.1016/j.bios.2017.02.052
51. Song N, Yan Z, Xu H et al (2019) Development of a sediment microbial fuel cell-based biosensor for simultaneous online monitoring of dissolved oxygen concentrations along various depths in lake water. Sci Total Environ 673:272–280. https://doi.org/10.1016/j.scitotenv.2019.04.032
52. Lemley DA, Adams JB (2019) Eutrophication. In: Encyclopedia of ecology. Elsevier, pp 86–90
53. Olias LG, Otero AR, Cameron PJ, di Lorenzo M (2020) A soil microbial fuel cell-based biosensor for dissolved oxygen monitoring in water. Electrochim Acta 362:137108. https://doi.org/10.1016/j.electacta.2020.137108
54. Dexter SC, Gao GY (1988) Effect of seawater biofilms on corrosion potential and oxygen reduction of stainless steel. Corros Sci 44:717–723. https://doi.org/10.5006/1.3584936
55. Cristiani P, Franzetti A, Bestetti G (2008) Monitoring of electro-active biofilm in soil. Electrochim Acta 54:41–46. https://doi.org/10.1016/j.electacta.2008.01.107
56. Mollica A, Cristiani P (2003) On-line biofilm monitoring by "BIOX" electrochemical probe. Water Sci Technol 47:45–49. https://doi.org/10.2166/wst.2003.0277
57. Domínguez-Garay A, Boltes K, Esteve-Núñez A (2016) Cleaning-up atrazine-polluted soil by using microbial electroremediating cells. Chemosphere 161:365–371. https://doi.org/10.1016/j.chemosphere.2016.07.023
58. Olaniran A, Balgobind A, Pillay B (2013) Bioavailability of heavy metals in soil: impact on microbial biodegradation of organic compounds and possible improvement strategies. Int J Mol Sci 14:10197–10228. https://doi.org/10.3390/ijms140510197
59. Murínová S, Dercová K (2014) Response mechanisms of bacterial degraders to environmental contaminants on the level of cell walls and cytoplasmic membrane. Int J Microbiol 2014:1–16. https://doi.org/10.1155/2014/873081

60. Bouarab-Chibane L, Forquet V, Lantéri P et al (2019) Antibacterial properties of polyphenols: characterization and QSAR (quantitative structure–activity relationship) models. Front Microbiol 10. https://doi.org/10.3389/fmicb.2019.00829
61. Sun H, Xiao K, Zeng Z et al (2022) Electroactive biofilm-based sensor for volatile fatty acids monitoring: a review. Chem Eng J 449:137833. https://doi.org/10.1016/j.cej.2022.137833
62. Fernandez-Gatell M, Sanchez-Vila X, Puigagut J (2022) Power assisted MFC-based biosensor for continuous assessment of microbial activity and biomass in freshwater ecosystems. Sci Total Environ 833:155165. https://doi.org/10.1016/j.scitotenv.2022.155165
63. United States Environmental Protection Agency (1999) Appendix B: RMP guidance for offsite consequence analysis
64. Chung TH, Meshref MNA, Dhar BR (2020) Microbial electrochemical biosensor for rapid detection of naphthenic acid in aqueous solution. J Electroanal Chem 873:114405. https://doi.org/10.1016/j.jelechem.2020.114405
65. Gao G, Fang D, Yu Y et al (2017) A double-mediator based whole cell electrochemical biosensor for acute biotoxicity assessment of wastewater. Talanta 167:208–216. https://doi.org/10.1016/j.talanta.2017.01.081
66. Kretzschmar J, Koch C, Liebetrau J et al (2017) Electroactive biofilms as sensor for volatile fatty acids: cross sensitivity, response dynamics, latency and stability. Sens Actuators B Chem 241:466–472. https://doi.org/10.1016/j.snb.2016.10.097
67. Chouler J, di Lorenzo M (2019) Pesticide detection by a miniature microbial fuel cell under controlled operational disturbances. Water Sci Technol 79:2231–2241. https://doi.org/10.2166/wst.2019.207
68. Tucci M, Bombelli P, Howe CJ et al (2019) A storable mediatorless electrochemical biosensor for herbicide detection. Microorganisms 7:630. https://doi.org/10.3390/microorganisms7120630
69. Spurr MWA, Yu EH, Scott K, Head IM (2020) A microbial fuel cell sensor for unambiguous measurement of organic loading and definitive identification of toxic influents. Environ Sci (Camb) 6:612–621. https://doi.org/10.1039/C9EW00849G
70. Attaallah R, Antonacci A, Mazzaracchio V et al (2020) Carbon black nanoparticles to sense algae oxygen evolution for herbicides detection: atrazine as a case study. Biosens Bioelectron 159:112203. https://doi.org/10.1016/j.bios.2020.112203
71. Diba F, Khan MZH, Uddin SZ et al (2021) Bioaccumulation and detoxification of trivalent arsenic by Achromobacter xylosoxidans BHW-15 and electrochemical detection of its transformation efficiency. Sci Rep 11:21312. https://doi.org/10.1038/s41598-021-00745-1
72. Yang Y, Yu Y-Y, Wang Y-Z et al (2017) Amplification of electrochemical signal by a whole-cell redox reactivation module for ultrasensitive detection of pyocyanin. Biosens Bioelectron 98:338–344. https://doi.org/10.1016/j.bios.2017.07.008
73. Zhao S, Guo D, Zhu Q et al (2020) Display of microbial glucose dehydrogenase and cholesterol oxidase on the yeast cell surface for the detection of blood biochemical parameters. Biosensors (Basel) 11:13. https://doi.org/10.3390/bios11010013
74. Zhang Z, Liu J, Fan J et al (2018) Detection of catechol using an electrochemical biosensor based on engineered Escherichia coli cells that surface-display laccase. Anal Chim Acta 1009:65–72. https://doi.org/10.1016/j.aca.2018.01.008
75. VanArsdale E, Pitzer J, Wang S et al (2022) Enhanced electrochemical measurement of β-galactosidase activity in whole cells by coexpression of lactose permease, LacY. Biotechniques 73:233–237. https://doi.org/10.2144/btn-2022-0090
76. VanArsdale E, Tsao C, Liu Y et al (2019) Redox-based synthetic biology enables electrochemical detection of the herbicides Dicamba and roundup via rewired *Escherichia coli*. ACS Sens 4:1180–1184. https://doi.org/10.1021/acssensors.9b00085
77. Yu Y-Y, Wang J-X, Si R-W et al (2017) Sensitive amperometric detection of riboflavin with a whole-cell electrochemical sensor. Anal Chim Acta 985:148–154. https://doi.org/10.1016/j.aca.2017.06.053

78. Atkinson JT, Su L, Zhang X et al (2022) Real-time bioelectronic sensing of environmental contaminants. Nature 611:548–553. https://doi.org/10.1038/s41586-022-05356-y
79. Schröder U, Harnisch F, Angenent LT (2015) Microbial electrochemistry and technology: terminology and classification. Energ Environ Sci 8:513–519. https://doi.org/10.1039/C4EE03359K
80. Liermann LJ, Hausrath EM, Anbar AD, Brantley SL (2007) Assimilatory and dissimilatory processes of microorganisms affecting metals in the environment. J Anal At Spectrom 22:867. https://doi.org/10.1039/b705383e
81. Myers JM, Myers CR (2001) Role for outer membrane cytochromes OmcA and OmcB of *Shewanella putrefaciens* MR-1 in reduction of manganese dioxide. Appl Environ Microbiol 67:260–269. https://doi.org/10.1128/AEM.67.1.260-269.2001
82. Nomenclature Committee of the International Union of Biochemistry (NC-IUB) (1992) Nomenclature of electron-transfer proteins. Recommendations 1989. J Biol Chem 267:665–677. https://doi.org/10.1016/S0021-9258(18)48544-4
83. Rowe AR, Salimijazi F, Trutschel L et al (2021) Identification of a pathway for electron uptake in Shewanella oneidensis. Commun Biol 4. https://doi.org/10.1038/s42003-021-02454-x
84. Han R, Li X, Wu Y et al (2017) In situ spectral kinetics of quinone reduction by c-type cytochromes in intact Shewanella oneidensis MR-1 cells. Colloids Surf A Physicochem Eng Asp 520:505–513. https://doi.org/10.1016/j.colsurfa.2017.02.023
85. Edwards MJ, White GF, Butt JN et al (2020) The crystal structure of a biological insulated transmembrane molecular wire. Cell 181:665–673.e10. https://doi.org/10.1016/j.cell.2020.03.032
86. Kim BH, Ikeda T, Park HS et al (1999) Electrochemical activity of an Fe(III)-reducing bacterium, Shewanella putrefaciens IR-1, in the presence of alternative electron acceptors. Biotechnol Tech 13:475–478. https://doi.org/10.1023/A:1008993029309
87. Methé BA, Nelson KE, Eisen JA et al (2003) Genome of *Geobacter sulfurreducens:* metal reduction in subsurface environments. Science 302:1967–1969. https://doi.org/10.1126/science.1088727
88. Yu L, Zhang E, Yang L et al (2023) Combining biological denitrification and electricity generation in methane-powered microbial fuel cells. J Environ Sci 130:212–222. https://doi.org/10.1016/j.jes.2022.10.013
89. Verma M, Mishra V (2023) Bioelectricity generation by microbial degradation of banana peel waste biomass in a dual-chamber S. cerevisiae-based microbial fuel cell. Biomass Bioenergy 168:106677. https://doi.org/10.1016/j.biombioe.2022.106677
90. Reguera G, McCarthy KD, Mehta T et al (2005) Extracellular electron transfer via microbial nanowires. Nature 435:1098–1101. https://doi.org/10.1038/nature03661
91. Filman DJ, Marino SF, Ward JE et al (2019) Cryo-EM reveals the structural basis of long-range electron transport in a cytochrome-based bacterial nanowire. Commun Biol 2:219. https://doi.org/10.1038/s42003-019-0448-9
92. Gorby YA, Yanina S, McLean JS et al (2006) Electrically conductive bacterial nanowires produced by Shewanella oneidensis strain MR-1 and other microorganisms. Proc Natl Acad Sci 103:11358–11363. https://doi.org/10.1073/pnas.0604517103
93. Pirbadian S, Barchinger SE, Leung KM et al (2014) *Shewanella oneidensis* MR-1 nanowires are outer membrane and periplasmic extensions of the extracellular electron transport components. Proc Natl Acad Sci 111:12883–12888. https://doi.org/10.1073/pnas.1410551111
94. Subramanian P, Pirbadian S, El-Naggar MY, Jensen GJ (2018) Ultrastructure of *Shewanella oneidensis* MR-1 nanowires revealed by electron cryotomography. Proc Natl Acad Sci 115:247–255. https://doi.org/10.1073/pnas.1718810115
95. Roden EE, Kappler A, Bauer I et al (2010) Extracellular electron transfer through microbial reduction of solid-phase humic substances. Nat Geosci 3:417–421. https://doi.org/10.1038/ngeo870

96. Weliwatte NS, Grattieri M, Minteer SD (2021) Rational design of artificial redox-mediating systems toward upgrading photobioelectrocatalysis. Photochem Photobiol Sci 20:1333–1356. https://doi.org/10.1007/s43630-021-00099-7
97. Gemünde A, Lai B, Pause L et al (2022) Redox mediators in microbial electrochemical systems. ChemElectroChem 9. https://doi.org/10.1002/celc.202200216
98. Martinez CM, Alvarez LH (2018) Application of redox mediators in bioelectrochemical systems. Biotechnol Adv 36:1412–1423. https://doi.org/10.1016/j.biotechadv.2018.05.005
99. von Canstein H, Ogawa J, Shimizu S, Lloyd JR (2008) Secretion of flavins by Shewanella species and their role in extracellular electron transfer. Appl Environ Microbiol 74:615–623. https://doi.org/10.1128/AEM.01387-07
100. Coursolle D, Baron DB, Bond DR, Gralnick JA (2010) The Mtr respiratory pathway is essential for reducing flavins and electrodes in *Shewanella oneidensis*. J Bacteriol 192:467–474. https://doi.org/10.1128/JB.00925-09
101. Claassens NJ, Cotton CAR, Kopljar D, Bar-Even A (2019) Making quantitative sense of electromicrobial production. Nat Catal 2:437–447. https://doi.org/10.1038/s41929-019-0272-0
102. Morgado L, Bruix M, Pessanha M et al (2010) Thermodynamic characterization of a triheme cytochrome family from Geobacter sulfurreducens reveals mechanistic and functional diversity. Biophys J 99:293–301. https://doi.org/10.1016/j.bpj.2010.04.017
103. Logan BE (2009) Exoelectrogenic bacteria that power microbial fuel cells. Nat Rev Microbiol 7:375–381. https://doi.org/10.1038/nrmicro2113
104. Logan BE, Rossi R, Ragab A, Saikaly PE (2019) Electroactive microorganisms in bioelectrochemical systems. Nat Rev Microbiol 17:307–319. https://doi.org/10.1038/s41579-019-0173-x
105. Chang I-S, Moon H-S, Bretschger O et al (2006) Electrochemically active bacteria (EAB) and mediator-less microbial fuel cells. J Microbiol Biotechnol 16:163–177
106. Rittmann BE, Krajmalnik-Brown R, Halden RU (2008) Pre-genomic, genomic and post-genomic study of microbial communities involved in bioenergy. Nat Rev Microbiol 6:604–612. https://doi.org/10.1038/nrmicro1939
107. Lovley DR (2006) Bug juice: harvesting electricity with microorganisms. Nat Rev Microbiol 4:497–508
108. Park DH, Zeikus JG (1999) Utilization of electrically reduced neutral red by *Actinobacillus succinogenes*: physiological function of neutral red in membrane-driven fumarate reduction and energy conservation. J Bacteriol 181:2403–2410. https://doi.org/10.1128/JB.181.8.2403-2410.1999
109. Gregory KB, Bond DR, Lovley DR (2004) Graphite electrodes as electron donors for anaerobic respiration. Environ Microbiol 6:596–604. https://doi.org/10.1111/j.1462-2920.2004.00593.x
110. Jourdin L, Burdyny T (2021) Microbial electrosynthesis: where do we go from here? Trends Biotechnol 39:359–369
111. Moscoviz R, Toledo-Alarcón J, Trably E, Bernet N (2016) Electro-fermentation: how to drive fermentation using electrochemical systems. Trends Biotechnol 34:856–865. https://doi.org/10.1016/j.tibtech.2016.04.009
112. Banakar M, Hamidi M, Khurshid Z et al (2022) Electrochemical biosensors for pathogen detection: an updated review. Biosensors (Basel) 12:927. https://doi.org/10.3390/bios12110927
113. Su L, Jia W, Hou C, Lei Y (2011) Microbial biosensors: a review. Biosens Bioelectron 26:1788–1799. https://doi.org/10.1016/j.bios.2010.09.005
114. Kane AL, Bond DR, Gralnick JA (2013) Electrochemical analysis of *Shewanella oneidensis* engineered to bind gold electrodes. ACS Synth Biol 2:93–101. https://doi.org/10.1021/sb300042w

115. Hui Y, Huang Z, Alahi MEE et al (2022) Recent advancements in electrochemical biosensors for monitoring the water quality. Biosensors (Basel) 12:551. https://doi.org/10.3390/bios12070551
116. Lagarde F, Jaffrezic-Renault N (2011) Cell-based electrochemical biosensors for water quality assessment. Anal Bioanal Chem 400:947–964. https://doi.org/10.1007/s00216-011-4816-7
117. Jiang Z, Zhang D, Zhou L et al (2018) Enhanced catalytic capability of electroactive biofilm modified with different kinds of carbon nanotubes. Anal Chim Acta 1035:51–59. https://doi.org/10.1016/j.aca.2018.06.077
118. Plekhanova T, Bykov et al (2019) Multiwalled carbon nanotubes and the electrocatalytic activity of Gluconobacter oxydans as the basis of a biosensor. Biosensors (Basel) 9:137. https://doi.org/10.3390/bios9040137
119. Uria N, Fiset E, Pellitero MA et al (2020) Immobilisation of electrochemically active bacteria on screen-printed electrodes for rapid in situ toxicity biosensing. Environ Sci Ecotechnol 3:100053. https://doi.org/10.1016/j.ese.2020.100053
120. Bettaieb F, Ponsonnet L, Lejeune P et al (2007) Immobilization of E. coli bacteria in three-dimensional matrices for ISFET biosensor design. Bioelectrochemistry 71:118–125. https://doi.org/10.1016/j.bioelechem.2007.02.004
121. Wasito H, Fatoni A, Hermawan D, Susilowati SS (2019) Immobilized bacterial biosensor for rapid and effective monitoring of acute toxicity in water. Ecotoxicol Environ Saf 170:205–209. https://doi.org/10.1016/j.ecoenv.2018.11.141
122. Lee JI, Karube I (1996) Reactor type sensor for cyanide using an immobilized microorganism. Electroanalysis 8:1117–1120. https://doi.org/10.1002/elan.1140081208
123. Odaci D, Timur S, Telefoncu A (2009) A microbial biosensor based on bacterial cells immobilized on chitosan matrix. Bioelectrochemistry 75:77–82. https://doi.org/10.1016/j.bioelechem.2009.01.002
124. Zhao L, He L, Chen S et al (2017) Microbial BOD sensors based on Zr (IV)-loaded collagen fiber. Enzyme Microb Technol 98:52–57. https://doi.org/10.1016/j.enzmictec.2016.11.010
125. Held M, Schuhmann W, Jahreis K, Schmidt H-L (2002) Microbial biosensor array with transport mutants of Escherichia coli K12 for the simultaneous determination of mono-and disaccharides. Biosens Bioelectron 17:1089–1094. https://doi.org/10.1016/S0956-5663(02)00103-3
126. Akyilmaz E, Dinçkaya E (2005) An amperometric microbial biosensor development based on Candida tropicalis yeast cells for sensitive determination of ethanol. Biosens Bioelectron 20:1263–1269. https://doi.org/10.1016/j.bios.2004.04.010
127. Chen J, Jin Y (2011) Sensitive lactate determination based on acclimated mixed bacteria and palygorskite co-modified oxygen electrode. Bioelectrochemistry 80:151–154. https://doi.org/10.1016/j.bioelechem.2010.07.004
128. Kaur A, Ibrahim S, Pickett CJ et al (2014) Anode modification to improve the performance of a microbial fuel cell volatile fatty acid biosensor. Sens Actuators B Chem 201:266–273. https://doi.org/10.1016/j.snb.2014.04.062
129. Lazzarini Behrmann IC, Grattieri M, Minteer SD et al (2020) Online self-powered Cr (VI) monitoring with autochthonous pseudomonas and a bio-inspired redox polymer. Anal Bioanal Chem 412:6449–6457. https://doi.org/10.1007/s00216-020-02620-w
130. Liu L, Liu C, Shang L et al (2010) Viable but nonculturable cells used in biosensor fabrication for long-term storage stability. Talanta 83:31–35. https://doi.org/10.1016/j.talanta.2010.08.034
131. Han X, Chen L, He D et al (2019) Bacteria-immobilized preparation as the microbial probe for electrochemical susceptibility test. Int J Electrochem Sci 14:2833–2845. https://doi.org/10.20964/2019.03.45
132. Tag K, Riedel K, Bauer H-J et al (2007) Amperometric detection of Cu2+ by yeast biosensors using flow injection analysis (FIA). Sens Actuators B Chem 122:403–409. https://doi.org/10.1016/j.snb.2006.06.007

133. Lehmann M, Riedel K, Adler K, Kunze G (2000) Amperometric measurement of copper ions with a deputy substrate using a novel Saccharomyces cerevisiae sensor. Biosens Bioelectron 15:211–219. https://doi.org/10.1016/S0956-5663(00)00060-9
134. Wong LS, Lee YH, Surif S (2013) Performance of a cyanobacteria whole cell-based fluorescence biosensor for heavy metal and pesticide detection. Sensors 13:6394–6404. https://doi.org/10.3390/s130506394
135. Ergön-Can T, Erhan E, Algur ÖF (2015) Poly(glycidyl methacrylate-co-3-thienylmethylmethacrylate) as an immobilization matrix for microbial glycerol biosensing based on Gluconobacter oxydans. Mater Sci Eng C 56:432–437. https://doi.org/10.1016/j.msec.2015.07.006
136. Odaci D, Kiralp Kayahan S, Timur S, Toppare L (2008) Use of a thiophene-based conducting polymer in microbial biosensing. Electrochim Acta 53:4104–4108. https://doi.org/10.1016/j.electacta.2007.12.065
137. Tuncagil S, Odaci D, Yildiz E et al (2009) Design of a microbial sensor using conducting polymer of 4-(2,5-di(thiophen-2-yl)-1H-pyrrole-1-l) benzenamine. Sens Actuators B Chem 137:42–47. https://doi.org/10.1016/j.snb.2008.10.067
138. Yu D, Volponi J, Chhabra S et al (2005) Aqueous sol–gel encapsulation of genetically engineered Moraxella spp. cells for the detection of organophosphates. Biosens Bioelectron 20:1433–1437. https://doi.org/10.1016/j.bios.2004.04.022
139. Mulchandani A, Mulchandani P, Chauhan S et al (1998) A potentiometric microbial biosensor for direct determination of organophosphate nerve agents. Electroanalysis 10:733–737. https://doi.org/10.1002/(SICI)1521-4109(199809)10:11<733::AID-ELAN733>3.0.CO;2-X
140. Tucci M, Grattieri M, Schievano A et al (2019) Microbial amperometric biosensor for online herbicide detection: photocurrent inhibition of Anabaena variabilis. Electrochim Acta 302:102–108. https://doi.org/10.1016/j.electacta.2019.02.007
141. Conners EM, Rengasamy K, Bose A (2022) Electroactive biofilms: how microbial electron transfer enables bioelectrochemical applications. J Ind Microbiol Biotechnol 49. https://doi.org/10.1093/jimb/kuac012
142. Adekunle A, Gomez Vidales A, Woodward L, Tartakovsky B (2021) Microbial fuel cell soft sensor for real-time toxicity detection and monitoring. Environ Sci Pollut Res 28:12792–12802. https://doi.org/10.1007/s11356-020-11245-6
143. Badalamenti JP, Krajmalnik-Brown R, Torres CI (2013) Generation of high current densities by pure cultures of anode-respiring *Geoalkalibacter* spp under alkaline and saline conditions in microbial electrochemical cells. MBio:4. https://doi.org/10.1128/mBio.00144-13
144. Badalamenti JP, Torres CI, Krajmalnik-Brown R (2014) Coupling dark metabolism to electricity generation using photosynthetic cocultures. Biotechnol Bioeng 111:223–231. https://doi.org/10.1002/bit.25011
145. Karbelkar AA, Reynolds EE, Ahlmark R, Furst AL (2021) A microbial electrochemical technology to detect and degrade organophosphate pesticides. ACS Cent Sci 7:1718–1727. https://doi.org/10.1021/acscentsci.1c00931
146. Roell GW, Zha J, Carr RR et al (2019) Engineering microbial consortia by division of labor. Microb Cell Fact 18:35. https://doi.org/10.1186/s12934-019-1083-3
147. Ghosh S, Chowdhury R, Bhattacharya P (2016) Mixed consortia in bioprocesses: role of microbial interactions. Appl Microbiol Biotechnol 100:4283–4295. https://doi.org/10.1007/s00253-016-7448-1
148. Wang B, Barahona M, Buck M (2013) A modular cell-based biosensor using engineered genetic logic circuits to detect and integrate multiple environmental signals. Biosens Bioelectron 40:368–376. https://doi.org/10.1016/j.bios.2012.08.011
149. Duncker KE, Holmes ZA, You L (2021) Engineered microbial consortia: strategies and applications. Microb Cell Fact 20:211. https://doi.org/10.1186/s12934-021-01699-9
150. Gao G, Qian J, Fang D et al (2016) Development of a mediated whole cell-based electrochemical biosensor for joint toxicity assessment of multi-pollutants using a mixed microbial consortium. Anal Chim Acta 924:21–28. https://doi.org/10.1016/j.aca.2016.04.011

151. Chu N, Jiang Y, Zhang L et al (2022) Biocathode prepared at low anodic potentials achieved a higher response for water biotoxicity monitoring after polarity reversal. Sci Total Environ 847: 157553. https://doi.org/10.1016/j.scitotenv.2022.157553
152. Kale MM, Mehrotra I (2009) Rapid determination of biochemical oxygen demand. Int J Chem Mol Eng 3:133–140
153. Godain A, Spurr MWA, Boghani HC et al (2020) Detection of 4-nitrophenol, a model toxic compound, using multi-stage microbial fuel cells. Front Environ Sci 8. https://doi.org/10.3389/fenvs.2020.00005
154. Spurr MWA, Yu EH, Scott K, Head IM (2021) No re-calibration required? Stability of a bioelectrochemical sensor for biodegradable organic matter over 800 days. Biosens Bioelectron 190:113392. https://doi.org/10.1016/j.bios.2021.113392
155. Brehm-Stecher BF, Johnson EA (2004) Single-cell microbiology: tools, technologies, and applications. Microbiol Mol Biol Rev 68:538–559. https://doi.org/10.1128/MMBR.68.3.538-559.2004
156. Xiao N, Selvaganapathy PR, Wu R, Huang JJ (2020) Influence of wastewater microbial community on the performance of miniaturized microbial fuel cell biosensor. Bioresour Technol 302:122777. https://doi.org/10.1016/j.biortech.2020.122777
157. Jia H, Liu W, Wang J et al (2018) Optimization of sensing performance in an integrated dual sensors system combining microbial fuel cells and upflow anaerobic sludge bed reactor. Chemosphere 210:931–940. https://doi.org/10.1016/j.chemosphere.2018.07.119
158. Chung TH, Dhar BR (2021) Paper-based platforms for microbial electrochemical cell-based biosensors: a review. Biosens Bioelectron 192:113485. https://doi.org/10.1016/j.bios.2021.113485
159. Wu L-C, Wang G-H, Tsai T-H et al (2019) Three-stage single-chambered microbial fuel cell biosensor inoculated with Exiguobacterium aestuarii YC211 for continuous chromium (VI) measurement. Sensors 19:1418. https://doi.org/10.3390/s19061418
160. Wang S, Qi X, Jiang Y et al (2022) An antibiotic composite electrode for improving the sensitivity of electrochemically active biofilm biosensor. Front Environ Sci Eng 16:97. https://doi.org/10.1007/s11783-022-1518-7
161. Du L, Yan Y, Li T et al (2022) Machine learning enables quantification of multiple toxicants with microbial electrochemical sensors. ACS ES&T Eng 2:92–100. https://doi.org/10.1021/acsestengg.1c00287

Adv Biochem Eng Biotechnol (2024) 187: 185–222
https://doi.org/10.1007/10_2023_237

Published online: 26 January 2024

Applications of Gold Nanoparticles in Plasmonic and Nanophotonic Biosensing

Kimberly Hamad-Schifferli

Contents

Abstract The unique properties of plasmonic nanoparticles and nanostructures have enabled a broad range of applications in a diverse set of fields, ranging from biological sensing, cancer therapy, to catalysis. They have been some of the most studied nanomaterials due in part to their chemical stability and biocompatibility as well as supporting theoretical efforts. The synthesis and fabrication of plasmonic nanoparticles and nanostructures have now reached high precision and sophistication. We review here their fundamental optical properties, discuss their tailoring for biological environments, and then detail examples on how they have been used to innovate in the biological and biomedical fields.

K. Hamad-Schifferli (✉)
Department of Engineering, School for the Environment, University of Massachusetts Boston, Boston, MA, USA
e-mail: kim.hamad@umb.edu

Graphical Abstract

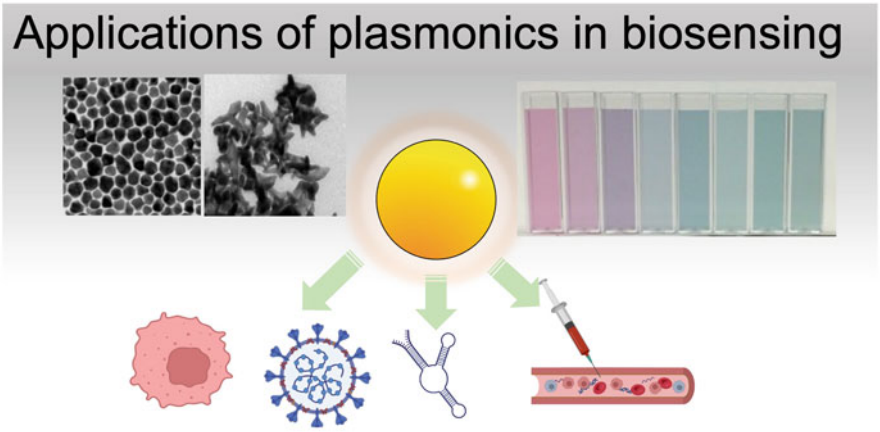

Keywords Gold nanoparticles, Photothermal, Plasmon-enhanced fluorescence, Plasmonics, Surface-enhanced Raman spectroscopy, Surface plasmon resonance

1 Introduction

Plasmonic nanoparticles and nanostructures have enabled a wealth of applications, ranging from sensing to catalytic uses. Their successful use in such a broad application space can be attributed to many factors. This includes the robustness of their synthesis and fabrication techniques, unique chemical stability, and advancements in chemistries and materials science to make them compatible in many environments, especially biological ones. In addition, the success of simulations and theory to describe their optical behavior has facilitated the design and tailoring of plasmonic structures with desired properties [1]. These are the pillars that have supported this discipline as it innovates new applications in sensing for biomedical and biological applications (Fig. 1).

There are many reports and works covering single aspects of their applications in depth, such as their photonic properties, abilities to enhance Raman scattering, and numerous others. Because plasmonic materials have had a unique impact on medical applications, we focus here on innovations in the biological fields. We first discuss the fundamental properties of plasmonic nanoparticles, how they are synthesized and fabricated, and routes for their modification for sensing and then describe the state of the art of their applications for biosensing in various fields.

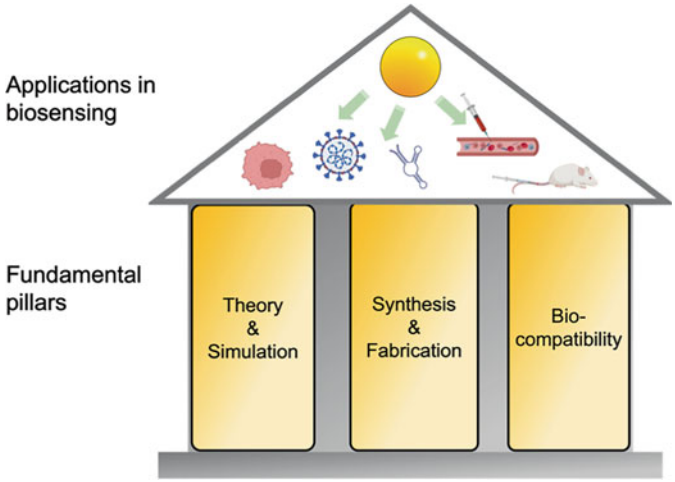

Fig. 1 The field of biosensing with plasmonics has been supported by the pillars of robust theory and simulation, synthesis and fabrication, and bioconjugation and biocompatibility strategies

2 Plasmonic Properties of Gold Nanoparticles

Investigation of the surface plasmon resonance (SPR) of gold nanoparticles has been going on for centuries, where the unique properties of gold formulations of glass give rise to the unique colors of the Lycurgus Cup (fourth century AD), and later to impart a brilliant red to stained glass windows in medieval Europe. The SPR is the coherent motion of electrons in the metal that arises from interaction with an electromagnetic field. Irradiation of the nanoparticle with light induces a polarization of the electrons, which can move more rapidly with respect to the gold lattice core. At the surface of the nanoparticle, the charge oscillation results in a net charge difference, and thus a restoring force results in a charge oscillation. If the frequency of light is resonant with this electron motion, it results in a strong optical absorption, which is the SPR. The frequency at which the SPR occurs depends on the size and shape of the nanoparticle, in addition to other parameters such as the index of refraction of the nanoparticle surroundings. For gold nanoparticles, the SPR occurs in the visible, giving rise to their strong red color. Noble metals (Au, Cu, Ag, etc.) have conduction band electrons that can be treated to an approximation as freely moving with respect to the ions of the lattice, and thus have a higher polarizability compared to other metals. This results in a narrow resonance and a strong absorption peak.

In particular, the success of using Mie theory (1908) to describe the properties of colloidal gold nanoparticles has been central for the practical use of plasmonics. Mie solved Maxwell's equation for the interaction of an electromagnetic field with a small spherical metal and described the interaction of light with the metal by scattering, absorption, and extinction (Fig. 2a) [3]. Mie theory works well for

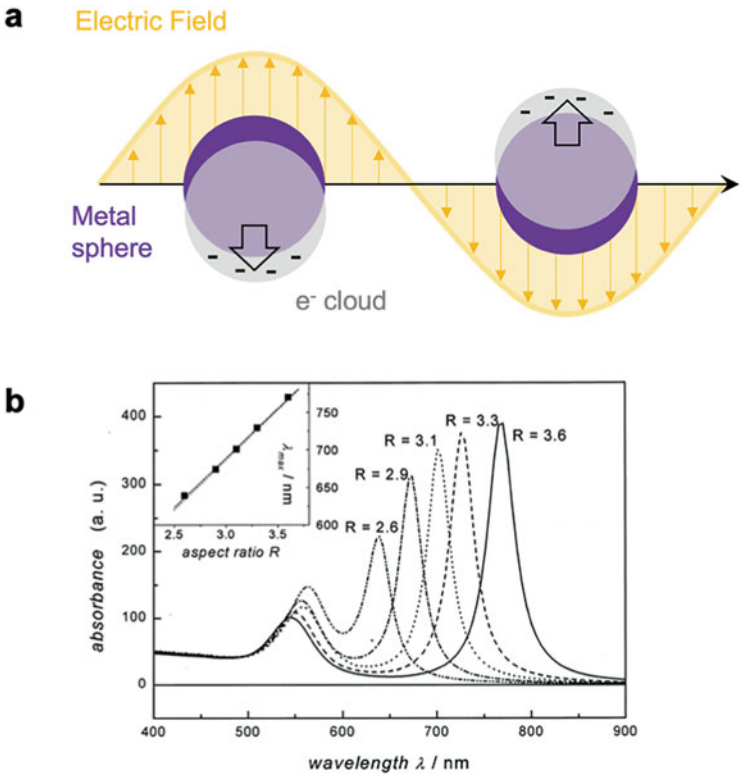

Fig. 2 (**a**) Oscillations in a spherical particle induced by an electromagnetic wave. (**b**) Simulations of nanorod absorption spectra, exhibiting an LSPR maxima shift with the aspect ratio R of the particle. From [2] Reprinted with permission from S. Link, M. B. Mohamed, and M. A. El-Sayed *Journal of Physical Chemistry B* 1999. Copyright 1999 American Chemical Society

describing nanoparticles 10 nm and larger, where it can completely describe the optical cross sections of a spherical nanoparticle of Au.

In addition, Mie's theory has been used successfully to describe the size dependence of the optical spectra, i.e., the blue shift of the SPR with decreasing nanoparticle size. While Mie's theory described only spherical nanoparticles, the extension of the theory to describe other shapes was achieved by Gans [4]. Gans broke the symmetry of spherical properties to introduce an aspect ratio. This extended the description of their shape dependence to include a longitudinal and transverse SPR, or the LSPR and TSPR (Fig. 2b). This has fueled numerous theoretical studies of plasmonics, where we now have a deep understanding of their optical properties. Furthermore, this deep understanding of their optical properties has laid the groundwork for their applications, where theory and simulations have been used to guide their design and use in applications.

3 Synthesis/Fabrication of Gold Nanostructures

The fabrication of noble metal and metal oxide nanostructures with a high degree of control has been key to the growth of the field of plasmonics. Nanostructures can be synthesized and fabricated in a broad variety of ways, ranging from wet chemical synthesis to patterning on substrates. Fabrication techniques are now highly sophisticated with an exquisite degree of control. One can precisely control the spacing and arrangements of structures, including complex geometries. Both solution synthesis (bottom-up) and fabrication (top-down) approaches have met with success through continual innovation.

3.1 Solution Synthesis of Gold Nanoparticles

Gold nanoparticles are the most studied plasmonic nanomaterial, which can be partially attributed to the fact that their synthesis is centuries old. They are responsible for the vibrant colors (Fig. 3a) in stained glass windows, where glass formulations with gold were known to yield red. The sols from Michael Faraday were made in 1856 as washes from gold films, and the colloids are still stable today.

Because gold nanoparticles are synthesized in solution, it has greatly facilitated the processing of and chemical conjugation to nanostructures, opening up the ability to use nanoparticles attached to different chemical moieties, incorporate them into polymers, cast as films, and many other formats. In particular, the aqueous synthesis of gold nanoparticles enabled their interfacing to biological molecules, as biological environments are aqueous.

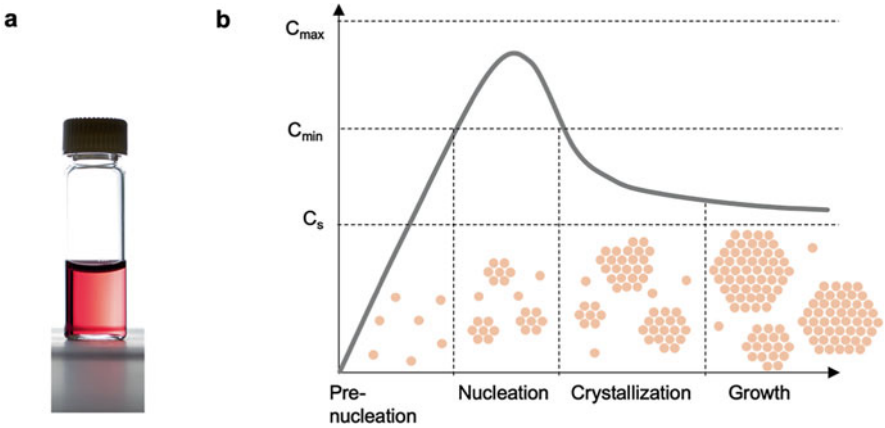

Fig. 3 (**a**) Solution of colloidal gold nanoparticles, exhibiting a strong red color due to their SPR. (**b**) LaMer theory of the nucleation and growth

The synthesis of nanoparticles has been described by LaMer theory (Fig. 3b), which describes the growth of sols in solution by conceptually separating the nucleation and growth steps. There are three stages to the particle growth. The ions, or monomer, first must reach a critical concentration for nucleation. In the second stage, nucleation occurs, which decreases the concentration of the monomer in the solution as they are incorporated into the nuclei. In the third stage, the concentration of the monomer in the solution decreases, which adsorbs to the crystal to increase its size, where the growth regime occurs. $C_{\min}$ is the minimum supersaturation for nucleation and $C_{\max}$ is the limiting supersaturation. C_s is the saturation concentration, or the solubility of the monomer.

For gold nanoparticles, synthesis is achieved by the reduction of a gold salt, typically $HAuCl_4\ 3H_2O$ [5]. Often $NaBH_4$ has been used as a reductant for organic phase synthesis. In the aqueous phase, the classic Turkevich synthesis utilizes trisodium citrate to reduce the Au salt. This results in water-soluble nanoparticles ~10 nm in diameter [6]. This is much more attractive for biological applications, especially compared to the alternative of synthesizing the nanoparticles initially in nonaqueous solutions, and then transferring them to the aqueous phase. This phase transfer must occur by ligand exchange, which is not always straightforward, nor 100% efficient.

3.1.1 Varying Nanoparticle Size and Shape

One aspect of synthesis that is desirable is the ability to control nanoparticle size and shape, which has been explored extensively for gold nanoparticles. Numerous shapes and broad size ranges are possible by varying reaction conditions, with tight control over the size distribution, which can routinely be down to a few percent. Complex structures are now routinely achievable, such as rods, cubes, stars, flowers, and hollow cages, which allows one to tailor the optical properties by tailoring its structure.

The size dependence of spherical gold nanoparticles was first explored by modifying the Turkevich method [7], where the citrate to gold molar ratio was varied. The nanoparticle size decreases with increasing molar ratio of [citrate]/[Au^{III}].

Nanorods

For spherical particles, the shift in SPR with size relatively small. However, changing the shape of the nanoparticles allows for testing Gans theory as a function of particle aspect ratio and shape. The simplest shape that breaks the spherical symmetry is the nanorod, where particle aspect ratio (AR) is greater than 1. Nanorods are ideal for studying the optical properties of SPRs because they possess both a longitudinal SPR (LSPR) and transverse (TSPR). The LSPR is strongly dependent on particle AR and can shift dramatically throughout the visible and NIR, over 100s

of nanometers. This systematic variation of the optical properties has facilitated the study of shape-dependent optical properties (Fig. 4c) [9, 10].

Furthermore, the LSPR peak is narrow relative to its shift, so it is possible to synthesize particles that can be excited in a nearly mutually exclusive fashion at two different wavelengths.

To yield particles that are rod shaped, it requires more growth along one axis compared the other. The most commonly used approach for nanorod synthesis is a two-step method in the presence of the amphiphilic ligand cetyltrimethylammonium bromide (CTAB) [11, 12]. First, gold seeds are grown in CTAB by the reduction of $HAuCl_4$ by $NaBH_4$. Then, the seeds are introduced into a growth solution with $AgNO_3$, $HAuCl_4$, and ascorbic acid which results in directional growth along one axis, resulting in rod-shaped particles. The synthesis can be modified to include other surfactants to increase the AR. Addition of benzyldimethylhexadecylammonium chloride (BDAC) to CTAB can grow additional lobes on the ends of the nanorods, resulting in "nanobones" that have a peak LSPR further out to the infrared (1,100 nm) [13].

Nanoshells

Gold nanoshells are another nanoparticle shape that has been of interest for their shape-dependent plasmonic properties. Shells can be in a core/shell format, which consists of a plasmonic material in a thin shell on top of a dielectric such as SiO_2 or a hollow structure. Nanoshells have a tunable plasmon resonance that shifts with shell thickness over a wide spectral range, similar to nanorods (Fig. 4b). The SPR peak blue shifts with increasing shell thickness, where a 5 nm Au shell has an absorption peak in the NIR (>1,000 nm), and a 20 nm shell is at ~700 nm. Core/shells have the advantage of finer control over the core size, where different nanoparticles or colloids can simply be changed out before shell growth [14].

Nanoshells are made by a two-step process where small (1.4 nm) gold nanoparticles are attached to a larger silica particle or polystyrene particle, which acts as a template. Following this, the nanoparticles are annealed to make a shell. The shell thickness can be controlled by controlling the growth parameters. Nanoshells can also be achieved by synthesizing hollow nanostructures [15]. These can be made by using sacrificial galvanic replacement, where Ag nanoparticles are synthesized, and then introduction of Au^{3+} etches the nanoparticles. Due to the difference in reduction potentials between Ag^+ and Au^{3+} (0.7966 V for Ag^+ vs. 1.498 V for Au^{3+}), Au^{3+} becomes reduced while Ag is oxidized, resulting in a gold shell enclosing an inner cavity. The SPR systematically shifts with increasing Ag:Au molar ratio.

Nanostars

Gold nanostars are another nanoparticle shape that has been attractive due to the fact that their synthesis is a one-step process at room temperature (Fig. 4) [16]. Nanostar

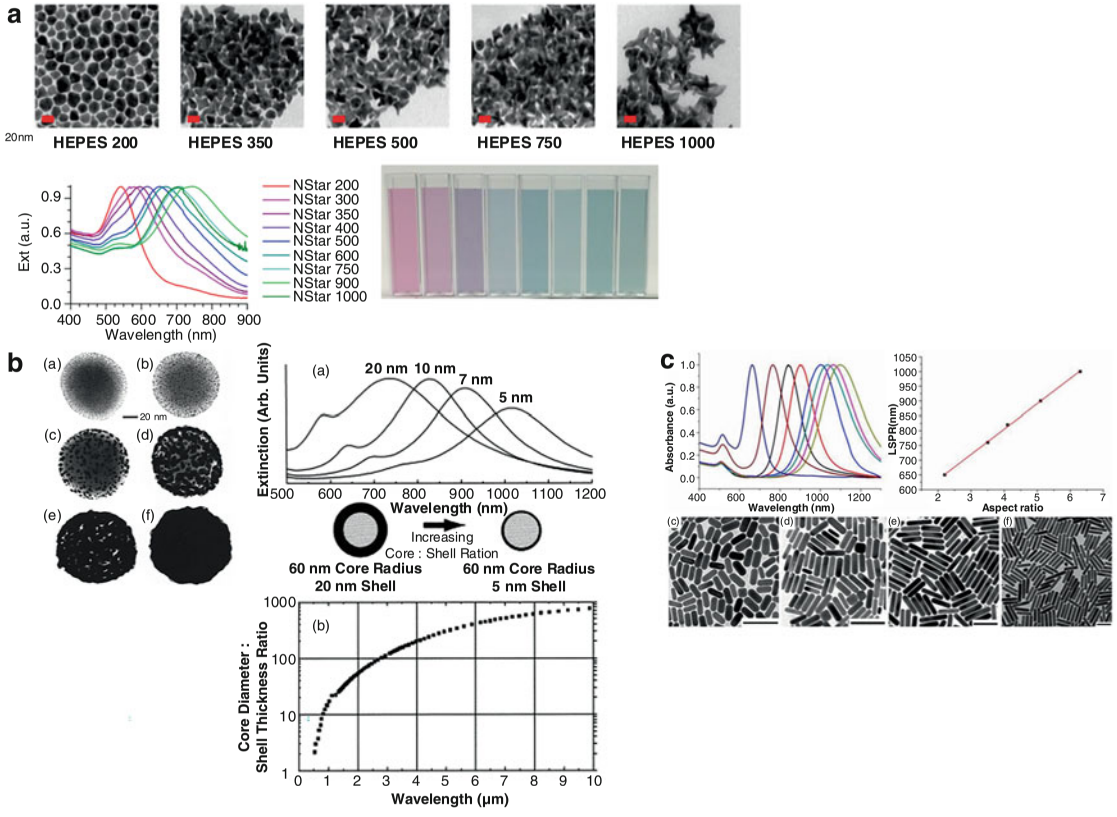

Fig. 4 Different structures of nanoparticles that can be synthesized by solution synthesis. (**a**) Gold nanostars of different arm lengths, which can shift the SPR throughout the visible and result in different colors. (**b**) Gold nanoshells synthesized by Au coating of dielectric templates, where the absorption spectra shift with increasing core:shell thickness [8]. Reproduced with permission from Oldenburg et al., *Chemical Physics Letters*, 1998. (**c**) Gold nanorods of different aspect ratios shift the LSPR to the red with increasing aspect ratio. Reproduced with permission from Wang et al., *Theranostics* 2015 [9]

SPRs can also be tuned across the visible spectrum and into the NIR like nanorods and are much easier to synthesize in comparison [17, 18–21]. Gold nanostar synthesis is performed by reducing a gold salt ($HAuCl_4$ $3H_2O$) with a Goods buffer such as HEPES, which nucleates and grows the nanostars. Tuning the SPR peak wavelength is achieved by varying the HEPES:Au ratio, where higher HEPES ratios grow larger nanostars and redshift the SPR. This also results in particles of different colors, which can be exploited for visual readouts. One benefit is that the resulting gold nanostars are stable in biological fluids because they are synthesized directly in HEPES buffer, which facilitates bioconjugation and incorporation into biological media.

Other Shapes and Compositions

A multitude of other shapes have been achieved, which are too numerous to describe in detail. Some hollow shapes leverage etching techniques such as cubes, triangular plates, and hexagonal plates [22]. Changing the composition of the plasmonic nanomaterial can tune the optical properties. Au and Ag have been alloyed with other materials including other plasmonic metals, transition metals, semiconductors, and dielectrics [23]. Au Alloys with Ag, Pd Pt, etc., to yield AuCu [24] and AuPt nanoparticles [25, 26] have also shown the ability to modify the optical properties with composition.

3.2 Fabrication Techniques

In contrast to wet synthesis approaches, plasmonic nanostructures can be fabricated by deposition techniques such as electron beam (e-beam) lithography, focused ion beam (FIB) lithography, and others [27]. A summary of the resolution and throughput that lithographic techniques can achieve is shown in Fig. 5a. These approaches are top-down, in contrast to the bottom-up approach of solution syntheses, which build nanostructures from atoms. Fabrication techniques are generally much more reproducible than solution-phase techniques, with higher fidelity. Furthermore, they can be used to optimize placement on the substrate, which is difficult to do with solution made nanostructures. This is essential for systems that require periodic structures or holes that are on the nanometer lengthscale. These techniques are much more costly, as they require sophisticated instrumentation with controlled atmospheres such as high vacuum and high voltage sources. In addition, the characterization techniques are also instrument intensive.

3.2.1 Electron-Beam (e-Beam) Lithography

Electron-beam lithography uses scanning of focused electron beams to write patterns on substrates. E-beam lithography is ideal for making nanostructures because of its high resolution, which can be down to a few nanometers for the spot size, and a writing resolution of ~10 nm. It is routinely used to make two-dimensional arrays of nanostructures on a flat substrate, where feature sizes down to the nm range (Fig. 5b). The e-beam is used to write a pattern on a polymer photoresist (typically polymethylmethacrylate, PMMA), which can then be used as a mask for patterning the plasmonic.

First, a thin layer of PMMA is spin coated onto a substrate, which is typically silicon. The e-beam is used to write a pattern on it, which de-cross-links the polymer. The polymer is developed by UV exposure. Following this, Au is evaporated onto the photoresist, and then the PMMA is removed by liftoff, achieved by its dissolution with a solvent. This leaves the Au in the written pattern on the substrate (Fig. 5c). Often there is an initial layer under the photoresist to help with adhesion of the pattern Au structures on the substrate. Alternatively, the pattern photoresist can be etched with a plasma, which is a dry etching form that is highly directional. The plasma etches the Au, and then removal of the photoresist results in a negative of the written pattern (Fig. 5d).

3.2.2 Colloidal Lithography

Another route to pattern substrates is colloidal lithography, or nanosphere lithography (NSL, Fig. 5e). Monolayers of colloidal crystals are used as a mask for the deposition of metal, which is usually deposited by thermal evaporation, atomic layer deposition, or pulsed laser deposition [29, 30]. NSL is a highly efficient way to pattern large areas with high precision, so it is considered a high-throughput approach. Moreover, the method is simple, easy to execute, and inexpensive, especially in comparison with techniques such as e-beam lithography which have intensive instrumentation needs.

NSL uses the self-assembly of monodisperse colloids, often of silica or polystyrene, which pack into hexagonal close packed monolayers on planar substrates, or at the air–water interface. The size of the colloids can range from <100 nm to >1.5 μm. Deposition can be achieved by spin coating, drop coating, or coating at an angle. The monolayers formed are well ordered over long ranges ($>1{,}000$ μm^2). After the monolayers are formed, Au is evaporated over the monolayer and patterns the surfaces in the voids between the spheres. Finally, the colloidal mask is removed by sonication, leaving behind the Au pattern on the surface. Haynes et al. demonstrated the self-assembly of polystyrene latex nanospheres with a diameter of 542 nm, and then evaporating gold, resulting in a regularly patterned substrate that could be used for surface-enhanced Raman spectroscopy (SERS) detection [29].

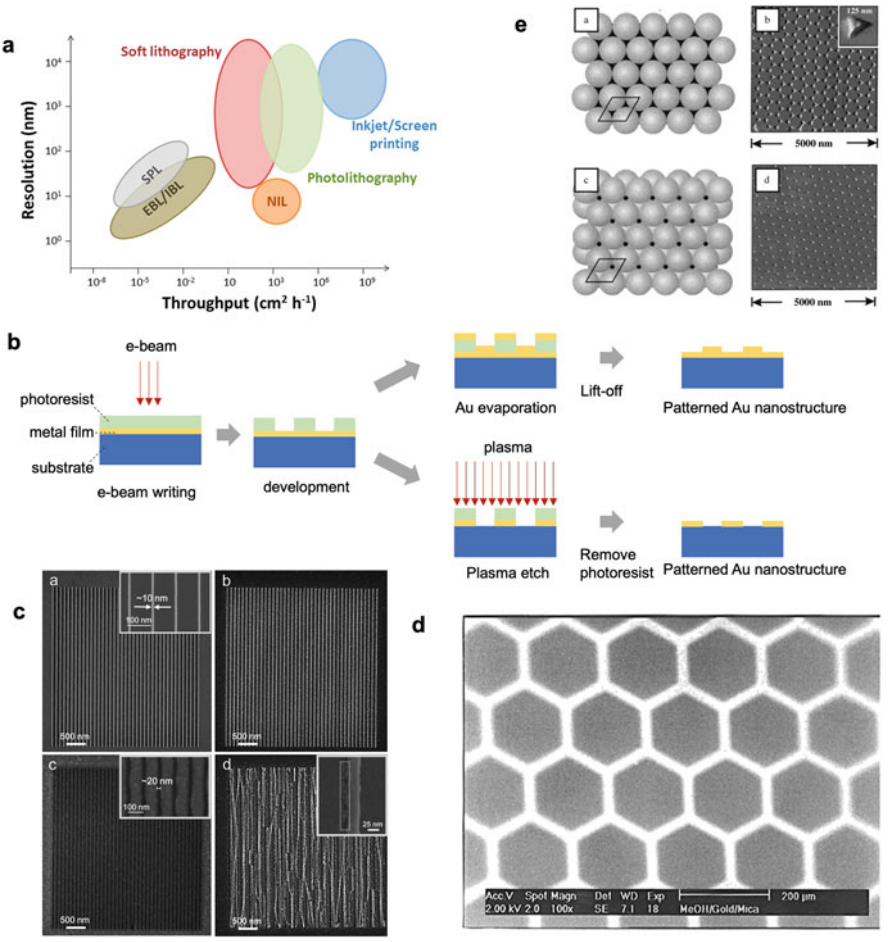

Fig. 5 (**a**) Lithography techniques and the resolution and throughput they can achieve SPL: scanning probe lithography, EBL/IBL: electron/ion beam lithography, NIL: nanoimprint lithography. From [27]. Reproduced from Fruncillo et al., *ACS Sensors*, 2021, 6, 2002–2024. Permissions from Creative Commons license. (**b**) Approach for electron beam lithography that uses the beam to write directly, or to remove the photoresist. (**c**) SEM of structures of gold made by liftoff and (**d**) plasma etching. [28] Reprinted with permission from Dai, Griesser, and Mau, Journal of Physical Chemistry B, 1997, Copyright 1997 American Chemical Society. (**e**) NSL lithography using colloids to create ordered masks through which the gold can be evaporated. Reprinted with permission from Haynes and Van Duyne, Nanosphere Lithography: A Versatile Nanofabrication Tool for Studies of Size-Dependent Nanoparticle Optics, *Journal of Physical Chemistry B*, Copyright 2001 American Chemical Society." From [29]

There are many approaches to change the fabrication techniques to tailor the properties of the surface in colloidal lithography. One can change the size of the colloids to change the periodicity of the deposited Au, evaporated at different angles

to result in different deposited patterns. Alternatively, the colloids can be functionalized with different ligand chemistries to change their interactions and thus geometries, and then multiple layers can be used for more complex structures. Furthermore, the colloidal monolayer can be used as a mask not just for deposition but also for etching by an O_2 plasma or reactive ion etching (RIE).

3.2.3 Soft Lithography

Soft lithography uses elastomeric stamps made of a soft polymer; most commonly used one is polydimethylsiloxane (PDMS) to print structures. Patterned PDMS stamps are formed by casting, usually by creating a mold by photolithography onto a substrate. The PDMS is poured over the mold and then can be used to stamp the pattern. The "ink" for stamps can be molecules but also gold nanoparticles, resulting in the formation of plasmonic arrays. The instrumentation requirement outside of the mold formation is simple, and the technique is relatively simple to carry out.

3.3 Surface Functionalization Techniques

Often the plasmonic nanomaterial needs to be interfaced to a molecular species to enable sensing, such as a protein or antibody that can bind to a specific target or permit in vivo targeting and/or cell uptake. Surface passivation plays a critical role in preventing nanoparticles from aggregating. Thus, the plasmonic material needs to be chemically conjugated or interfaced to some molecular species, as well as have customized surface properties for stability in the biological media (Fig. 6).

For gold and silver, there are many functionalization techniques available, and chemistries for these two materials are now well established. Many of these functionalization chemistries are robust, are repeatable, and can be done at scale, especially for gold surfaces. Gold can be functionalized by small molecules, polymers, biomolecules, and shells of other inorganic materials to result in core/shell particles [31].

For gold nanoparticles made by the Turkevich synthesis, they possess citrate on the surface, which can be easily exchanged with higher affinity ligands such as thiols. The chemical functionalization of gold nanoparticles has often relied on thiol chemistry to bind to the gold, adapted from the self-assembled monolayer (SAMs) field. These monolayers were alkanethiols that are closely packed, resulting in high van der Waals stabilization and the strong enthalpic benefit of Au-S binding to overcome the penalty in entropy. Many molecules are available, where the terminal species can be different functional end groups (where $R = COO^-$ for negatively charged particles, and $R = NH^{3+}$ for positive), and this interchanging of molecular groups has enabled a wide variety of functions.

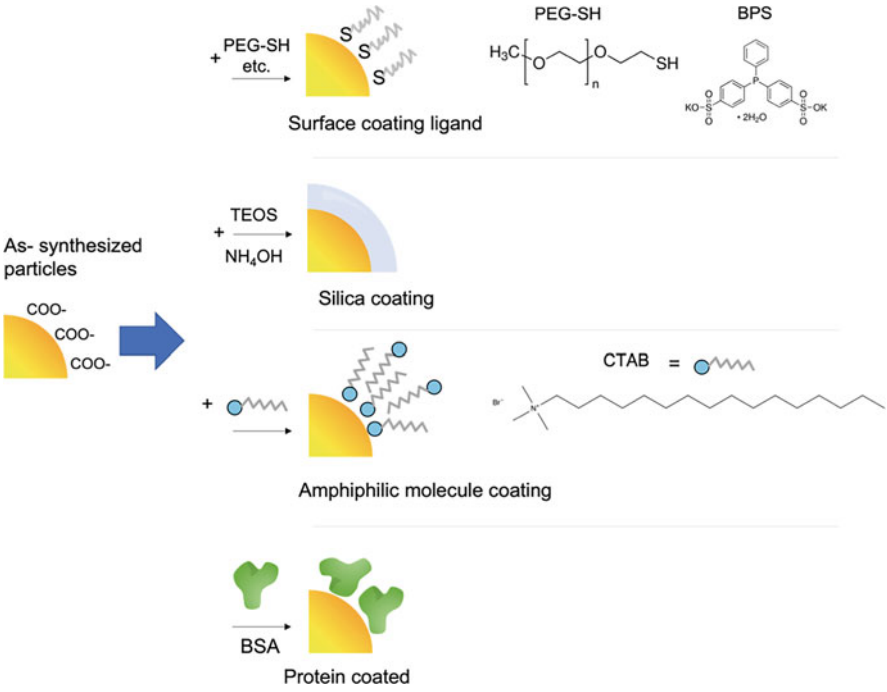

Fig. 6 Strategies to modify the particle surfaces, by addition of surface capping ligands such as PEG-SH or BPS, silica coating by the Stöber process, coating with amphiphilic molecules such as CTAB, which form a bilayer on the surface, or surface blocking with proteins such as BSA to prevent non-specific adsorption

Some nanoparticle syntheses are conducted in solution with surface passivation molecules that are more challenging to replace. Gold nanorods are synthesized in cetyltrimethyl ammonium bromide (CTAB), an amphiphilic molecule that forms a bilayer around the nanorod. CTAB must be present at concentrations greater than the critical micelle concentration stabilization, which is ~1 mM. Thus, it is difficult to remove all residual CTAB from nanorods. Exchange routes to remove CTAB can be achieved by multiple phase transfers between aqueous and organic phases [32].

Coating Au nanoparticles with silica has been desirable for improving biocompatibility ($Au@SiO_2$) to facilitate linking to biomolecules, which is achieved by the modified Stöber process using tetraorthosilicate (TEOS), which is a sol-gel process.

Protein adsorption is another surface treatment, where proteins are used to coat the surface and potentially reduce non-specific adsorption. The most common protein for this purpose is bovine serum albumin (BSA), as it is inexpensive and a highly stable soluble protein. Often, the nanoparticles are simply mixed in solution with BSA, and free BSA is removed by spin centrifugation washes.

3.4 Bioconjugation Techniques and Bioassembly

For biological sensing applications, the nanostructures need to be attached to biological molecules to impart biological function or recognition. The bioconjugation can enable targeting a specific cell or tumor site via ligand–receptor interactions, or the biological species is the payload to be delivered. Plasmonic nanomaterials have been attached to proteins, nucleic acids, and small molecules. Covalent attachment strategies have been well studied in the literature and have been successful for a broad number of biological species [33]. Bioconjugation has been predominantly studied for gold nanoparticles because of the many available facile surface modification chemistries, in addition to the superior biocompatibility and stability of gold.

Typically, the purpose of the biological species is to act as an affinity reagent that binds to a target with high specificity [34]. Biofunctionalization has enabled in vivo targeting where the nanoparticles are introduced by injection, and then transported through the bloodstream to target specific sites such as tumors. Antibodies are the most commonly used targeting species, as they possess high specificity for a target and bind with high affinity, which are typically in the nanomolar range.

The use of other protein-ligand binding (streptavidin-biotin) is among the strongest, with an affinity in the 10^{-14} M range. DNA and RNA can also be used for recognition, as decoration with an oligonucleotide of a certain sequence enables binding to a specific complementary strand. Alternatively, they can function as aptamers that bind specifically to different species, ranging from ions and small molecules to proteins. The exquisite specificity of nucleic acids in combination with their broad availability due to commercial synthesis has resulted in their use as a construction material, where structures can be designed by DNA sequence.

The nanostructure can also be functionalized with peptides that bind to a target, though often they possess lower affinity compared to antibodies.

3.4.1 Gold-Thiol Chemistry

The predominant route for conjugation is gold-thiol chemistry, which was originally adapted from the self-assembled monolayer studies (Fig. 7a). Thiols readily form Au-S bonds and can be conveniently appended to DNA at the termini during DNA synthesis. The naturally occurring amino acid cysteine possesses a thiol group [35] and can also be appended to the protein in expression via mutations. Naturally occurring cysteines can be used, but this has the potential to interfere with protein structure and result in denaturation, especially since cysteines often form structural dithiol linkages in proteins.

Gold-thiol conjugation can be achieved by incubation of the thiolated biomolecule with the nanoparticle or gold surface in solution, as the interaction is spontaneous. This is often followed by separation of the free biomolecule by spin centrifugation or washes.

3.4.2 Click Chemistry

A highly popular route for nanostructure functionalization is click chemistry (Fig. 7c) [36], which has linkages that are easy to make [37–39]. Click chemistry reactions are rapid, regiospecific, and modular. Generally reactions are achieved under simple and feasible reaction conditions. Consequently, due to its robustness and versatility, click chemistry has made chemical modification much more accessible to those in different fields, including materials science. Many commercially available nanoparticles and bioreagents are sold with reactive groups that can be used in click reactions. Click chemistry comes in hundreds of different options, so a summary of the field will not be described here. One of the most used is the copper-catalyzed azide reaction where a 1,3-dipolar cycloaddition of an alkyne and azide yields a triazole. Other chemical reactions for conjugation [33] include zero-length crosslinking using NH_2 to react with COO groups. Nanostructures are coated with a thiolated molecule that has a COO^- group on the other end, often by an alkanethiol. The COO- can be reacted with an amine using 1-ethyl-3-(3-dimethylaminopropyl) carbodiimide hydrochloride, or EDC.

N-hydroxysuccinimide (NHS) esters are another popular reactive group, as they react with primary amines to form an amide bond (Fig. 7c). The amine can be easily

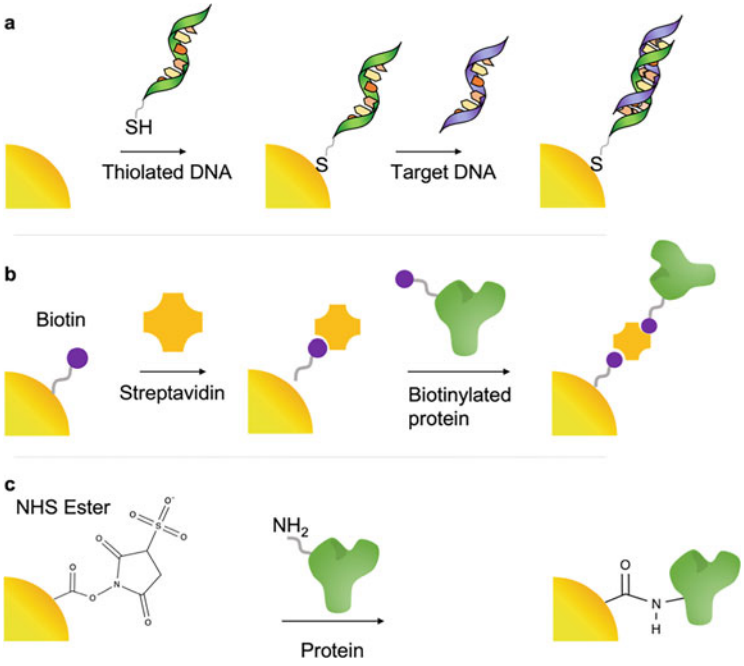

Fig. 7 Bioconjugation strategies to link nanoparticles to proteins and DNA. (**a**) Thiols on DNA can form a covalent bond, and then be used to capture the complementary strand, (**b**) biotin-streptavidin can be used to append biotin-functionalized proteins or DNA, (**c**) click chemistry such as NHS esters can link to primary amines on proteins or DNA

appended to DNA during synthesis, or one can leverage naturally occurring primary amines in proteins, where the amino acid lysine has an amine group.

If the nanostructure is coated with silica, then functionalization of the silica shell can be achieved by a condensation reaction between the silica surface and a given trialkoxysilane $(RO)_3SiR'$ [40, 41], and then can be conjugated to amine-terminated DNA oligonucleotides.

3.4.3 Protein-Ligand Binding

Streptavidin/biotin (Fig. 7b) has been used as a binding system as it has a high binding affinity. Streptavidin has four binding sites that can bind to biotin, with affinities on the order of femtomolar. Biotin modifications are commercially available for oligonucleotides and proteins, facilitating this approach.

Other strategies to develop expressible tags include Spy Catcher/SpyTag, which uses a peptide that binds with high affinity to protein. The tag can be genetically engineered as an appendage to the protein sequence, so the attachment can be achieved by expression.

3.4.4 Adsorption Techniques

Finally, the biological species can be conjugated to the plasmonic material by physisorption, where the biological species interacts with the gold or other material by non-covalent interactions [42]. This is typically achieved by incubation of the nanoparticle in solution with the biomolecule, which adsorbs to the nanoparticle surface, and then by spin centrifugation to isolate the unbound biomolecules away from the nanoparticle. The downsides of this approach are that yields can be low, where the amount of affinity agent does not adsorb to the nanoparticle. In addition, the biomolecule is free to adapt a range of orientations on the nanoparticle surface, where some orientations may sterically hinder its ability to bind to its target, so even if it is on the nanoparticle surface, it cannot function. However, changing the pH or surface charge of the nanoparticle can favor certain protein orientations over others [43, 44].

3.4.5 Bioassembly

For some applications, more complex structures are desirable, for which the recognition properties of biological molecules can be leveraged. DNA can be used as an exquisite recognition system, where a DNA sequence can discriminate target sequences that differ by a single nucleotide. Consequently, DNA has been utilized as a programmable construction material to aggregate and link together nanostructures in solution. This has been greatly facilitated by the fact that DNA oligonucleotides can be custom synthesized inexpensively, up to kilobases long. In

addition, RNA and DNA can also be used as binding affinity agents where they bind as aptamers, which are short oligonucleotides that bind to proteins and small molecules.

4 Plasmonic Sensing Applications

We now discuss the different ways in which plasmonic materials have been used for biosensing. Because of the multitude of novel properties of plasmonics, they have been versatile in enhancing biosensing for medical, biological, and many other purposes.

4.1 Colorimetric Sensing

4.1.1 Presence of Color

The most straightforward application of plasmonic particles is to use them colorimetrically. Gold nanoparticles absorb light strongly due to their SPR. A 10 nm Au nanoparticle has a molar extinction coefficient of ~10^8 M^{-1} cm^{-1}, which is several orders of magnitude higher compared to small molecule chromophores and dyes. Thus, simply the presence of a nanoparticle can enable colorimetric sensing. This property of gold nanoparticles has been utilized for many sensing applications.

One of the most widely used applications in recent years has been for the visual readout in lateral flow immunoassays, which is the format of paper diagnostics used for pregnancy testing, diagnosis of COVID-19 infections in patients, detection of pathogenic species present in food, and numerous other applications (Fig. 8a) [45–47]. The assays recognize a biomarker by the use of antibodies specific for the target of interest [34]. The antibodies are immobilized at the test area and also conjugated to the nanoparticle. If the biomarker is present, it binds to both the nanoparticle-Ab conjugates and the antibodies immobilized at the test line, and this double-binding event is referred to as sandwich formation. The two antibodies that form the sandwich are referred to as a pair. The sandwich formation event accumulates nanoparticles at the test line, and due to the strong optical absorption of the nanoparticles, this gives rise to a red color that can be detected by eye. Thus, the spatial location in combination with the optical absorption can be used to determine a binding event. Tests can read out simply by visual confirmation, or be obtained quantitatively by mobile phone images or scanning on a simple desktop scanner. Commercial lateral flow readers can be used for more sensitive readout.

While immunoassays are often used as diagnostics to provide only a yes/no answer, the intensity of the test line varies with the antigen concentration, [48] so the test line intensity can be used quantitatively. This can be achieved by image analysis from mobile phone images or instrumentation that reads RGB intensity of

the strip, which can often be low cost. To adapt an immunoassay for different targets, the antibodies used in the test are changed to be specific for the target of interest [34].

4.1.2 Multicolor Sensing

The optical properties of plasmonic nanoparticles can be leveraged to yield multicolor assays [49, 50], which takes advantage of the fact that the SPR of silver and gold nanoparticles shifts over a broad wavelength range through the visible spectrum with particle size [51]. Thus, it is easy to have visually distinct colors. This was used to create multiplexed immunoassays that could distinguish between Ebola glycoprotein, dengue virus nonstructural protein 1 (NS1), and yellow fever NS1 (Fig. 8b) [52], and in another case for food safety applications, with the detection of aflatoxin B1 and type-B fumonisins [50]. Ultimately, the color of the test line can be used to determine which biomarker was present. This relies on good separation of the colors in RGB space. However, if discrimination by eye is not feasible, RGB image analysis can be used.

Furthermore, multicolored immunoassays can give new capabilities to diagnostics. For example, by introducing additional even just one additional color to an assay, the test can be used to detect a range of species and thus be used as an array for pattern recognition, where a different antigen results in a "fingerprint" that is the product of color and spatial location. This can in turn enable the repurposing of cross-reactive antibodies for the detection of new antigens. This was deployed by Rodriguez-Quijada et al. [49] where antibodies for dengue and zika were used to detect NS1 of yellow fever virus, without the need for yellow fever antibodies. First, the dengue and antibodies are screened for which pairs can bind to each of the antigens, in this case dengue, zika, and yellow fever (Fig. 8d), and the intensity of the test line is quantified. Then, a strategic arrangement of immobilized antibodies and antibodies conjugated to nanoparticles of different colors is determined. In this case, dengue antibodies were conjugated to the red nanoparticles and zika antibodies to blue nanostars. Also, the assay required two separate locations, where dengue antibodies were spotted at one location and zika at the other. When this test was run with dengue NS1, two red spots appeared. If zika NS1 was run, the spots were purple. If yellow fever NS1 was run, it resulted in one red spot. This shows that this assay, using only zika and dengue antibodies, could detect yellow fever while still being able to distinguish it from zika and dengue.

While the test results were distinguishable by eye, image analysis can be used to quantitatively discriminate the test patterns. In addition, machine learning of the test images was used train the computer to recognize which spatial arrangements of colors are due to which biomarkers, thus allowing identification of diseases. This approach has been demonstrated for other virus types such as filoviruses [53].

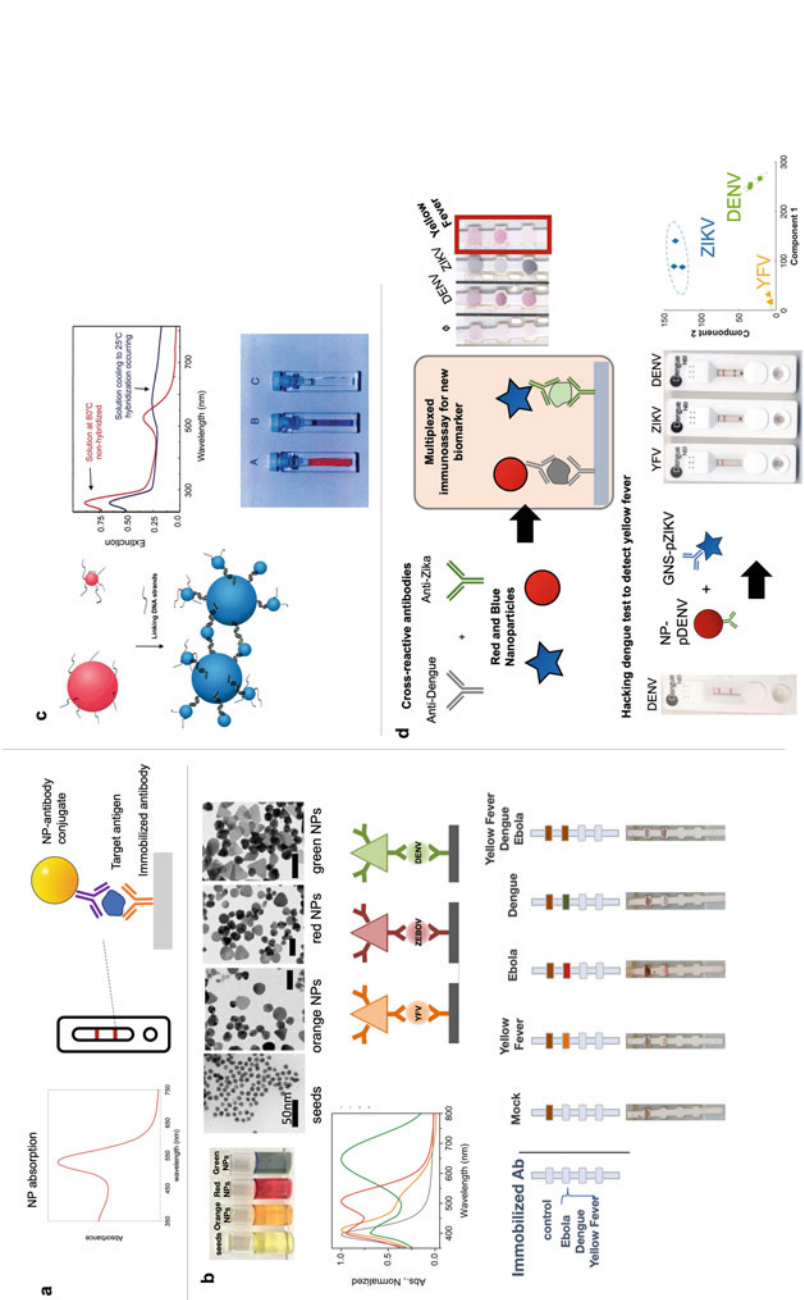

Fig. 8 Colorimetric readouts of nanoparticles. (**a**) The SPR of spherical red nanoparticles has been exploited as the visible color in rapid tests. The target antigen, if present, binds to antibodies conjugated to nanoparticles and also antibodies immobilized on the paper strip. (**b**) Multicolor immunoassays for yellow fever virus (YFV), Ebola virus (ZEBOV), and dengue virus (DENV) using silver nanoplates, which exhibit different colors due to their different sizes. (**c**)

Fig. 8 (continued) Aggregation-based colorimetric changes result from DNA linked to DNA that binds to a complementary strand, bringing the nanoparticles in proximity, and shifting the absorption spectra. This results in a color change from red to blue. Reprinted with permission from Mirkin., Programming the Assembly of Two- and Three-Dimensional Architectures with DNA and Nanoscale Inorganic Building Blocks, *Inorganic Chemistry*, 2001. Copyright 2001 American Chemical Society. (**d**) Multicolor nanoparticles in immunoassays can enable repurposing of antibodies to detect antigens that the antibodies were not raised against. This can be achieved by hacking existing tests for dengue so that they can detect yellow fever, with machine learning analysis

4.1.3 Aggregation-Based Colorimetric Changes

Another colorimetric approach utilizes the fact that the color of nanoparticles changes due to their aggregation state. When nanoparticles are in proximity of one another (i.e., within a few nanoparticle lengths), then the SPR of one particle is affected by the presence of another, shifting its resonance frequency to longer wavelengths. The shift in the collective SPR results in a visually striking color change from red (disaggregated particles) to blue (aggregated particles). This dramatic color change can be used to detect the presence of different analytes that induce a change in the aggregation state, such as the presence of target DNA strands (Fig. 8c), and this phenomenon has been well described theoretically [54].

This phenomenon has been used for sensing of DNA, where the nanoparticles are functionalized with probe strands that can bind to both ends of a target strand. Thus, if the DNA target is present, it assembles a cluster of nanoparticles, bringing them in proximity to one another, and shifting the collective SPR. This results in a color change from red to blue. Numerous variations on this aggregation-based sensing have been investigated since its discovery. Often, it relies on salt-induced aggregation of the nanoparticles, where the DNA on the nanoparticle is an aptamer that can bind to a specific target. If the target is not present, the aptamers stabilize the nanoparticles, which then do not aggregate at high salt concentrations. This results in a red color. If the target is present, then the aptamers bind to the target and no longer stabilize the nanoparticles, resulting in particle aggregation, and a shift to a blue color. This was utilized for the detection of ochratoxin A, a toxin found in food [55].

The DNA strands on the nanoparticles can also be in the form of an aptamer that binds to small molecules or ions, which has been utilized to sense Pb^{2+}. If the Pb^{2+} is not present, the nanoparticles aggregate, yielding a blue solution, but if the Pb^{2+} is present, the aptamers on the nanoparticle bind to it, dispersing the particles and resulting in a red solution [56, 57].

4.2 Plasmonic Biosensors

One application of the plasmonic properties of nanoparticles is the use of an SPR to sense the presence of analytes. This relies on the fact that the SPR of a plasmonic material is sensitive to the refractive index, n, of the medium in its surroundings, which can be leveraged for sensing. Incident light on a gold surface creates a plasmon oscillation, generating an electric field in the vicinity of the surface. This reduces the intensity of the reflected light at a particular angle θ. To detect a species, the surface is functionalized with a binding affinity agent and the analyte solution is flowed over it. If the surface species binds to the target, then the local n is changed, and this shifts the angle at which the dip in intensity occurs. The angle of reflection is measured on the backside using a prism. The intensity at the detector measured as a

function of time is the sensorgram, and has a typical response where it increases with time and then saturates. This signal is compared to a background sensorgram, where the signal is measured for a solution with no analyte is flowed over the surface [58].

SPR is a label-free, robust, and sensitive technique for characterizing protein–ligand interactions, where it can be used to measure binding in real time, yielding values for k_{on}, k_{off}, and K_D. Because it relies on a sensor surface, the protein must be immobilized by some chemical strategy. This confines the sensing area to the surface, so the amount of protein that the technique probes can be limited. To address this limitation, it has been determined that functionalization of the sensor surface with a hydrogel matrix such as dextran can increase binding capacity by increasing the adsorbed analyte per unit area. Because the dextran is a porous gel, transport of the analyte is not hindered. Overall, this can greatly improve the sensitivity [59].

Innovations in SPR sensing have included interfacing to microfluidic devices, and which can integrate sample preparation steps so that raw sample can be added directly. Recent forms include dengue diagnostics that can read DNA biomarkers directly in blood [60] or detection of live viruses of vesicular stomatitis virus and pseudotyped Ebola [61].

4.3 Surface-Enhanced Raman Spectroscopy, SERS

The Raman spectrum of a molecule is its vibrational fingerprint and thus unique to its molecular structure. Thus, it has the potential to be used to identify a chemical species in a sample. However, the Raman scattering effect is weak with a very low cross section, where only 1 in 10^7 photons undergoes inelastic scattering. However, it was discovered that the scattering intensity is greatly enhanced when the molecule is in the presence of a strong electric field (Fig. 9a). One can generate extremely high electric fields using metals with nanoscale features [62]. For spherical gold nanoparticles, the field enhancement can enable the detection of trace amounts of analyte, down to attomolar (aM) concentrations.

Since the discovery of the field enhancement effect in the 1970s, SERS has emerged as an important analytical tool for detection, especially in biosensing [63]. In particular, the ability to use noble metal nanoparticles to enhance spectra has been leveraged in a variety of ways. Even though SERS is still not completely understood, [64] extensive modeling of the enhancement phenomenon has aided in its widespread use [65].

SERS poses many advantages as an analytical tool. It is a label-free technique, where the Raman spectrum is a fingerprint of a unique analyte, and can be performed on solids, liquids, gases, and complex mixtures.

The ability of noble metal nanoparticles and nanomaterials to increase the Raman intensity is quantified as an enhancement factor (EF), defined as

$$\mathrm{EF} = \frac{I_{\mathrm{SERS}}}{I_{\mathrm{Raman}}} \cdot \frac{N_{\mathrm{Raman}}}{N_{\mathrm{SERS}}} \cdot \frac{P_{\mathrm{Raman}}}{P_{\mathrm{SERS}}} \cdot \frac{t_{\mathrm{Raman}}}{t_{\mathrm{SERS}}} \quad (1)$$

where I is the peak intensity, N is the number of the contributing reporter molecules, P is the laser power, and t the integration time. The subscripts Raman indicate measurements on the reporter molecule alone, and SERS indicates the measurement when the reporter molecule is enhanced by a plasmonic structure. Typical EFs for spherical nanoparticles are on the order of 10^5, and the highest values have been on the order of 10^9 and higher.

Because enhancement can be optimized by varying the nanostructure parameters, there have been many studies in the SERS field to increase EFs or use SERS for different detection modalities.

4.3.1 Hotspot Engineering

In order to increase the localized electric fields, novel plasmonic structures have been engineered to optimize Raman hotspots that can increase enhancement several fold. The SERS intensity is proportional to E^4, where E is the local electric field, so engineering hotspots have the potential to greatly enhance SERS sensitivity. Creating complex structures with controlled shapes and arrangements can improve enhancement far beyond that of a roughened metal surface. Hotspots can take on many forms, where they can be the gaps between noble metal particles, cavities designed to have particular shapes, core-shell particles, or periodic arrays of metal structures. While both fabricated and solution-phase approaches forms have yielded different ways to achieve this, top-down fabrication techniques are much better in controlling the dimensions of nanostructures and also the distances between them [66].

Fabricated arrays allow for precise arrangements of nanostructures [67, 68] such as arrays of nanopillars over large areas. This has enabled the detection of hepatitis A virus at low levels (Fig. 9b) [69]. In addition, structures that have designed gaps such as nanocrescent particles (Fig. 9c) can also increase the electric field [70].

Solution-phase approaches are much less precise in comparison, as control over interparticle spacing. In this case, solution approaches have instead sought to make particles with engineered cavities, or to use controlled nanoparticle aggregation to create hotspots between particles. Changing the colloidal particle shape can also create hotspots, where star-shaped nanostars or nanorods have pointed structures that can create strong local electric fields [19, 71, 72].

4.3.2 SERS Nanotags

For biological sensing the target species are proteins, DNA, or small molecules. These have complex Raman spectra, especially proteins. Moreover, different

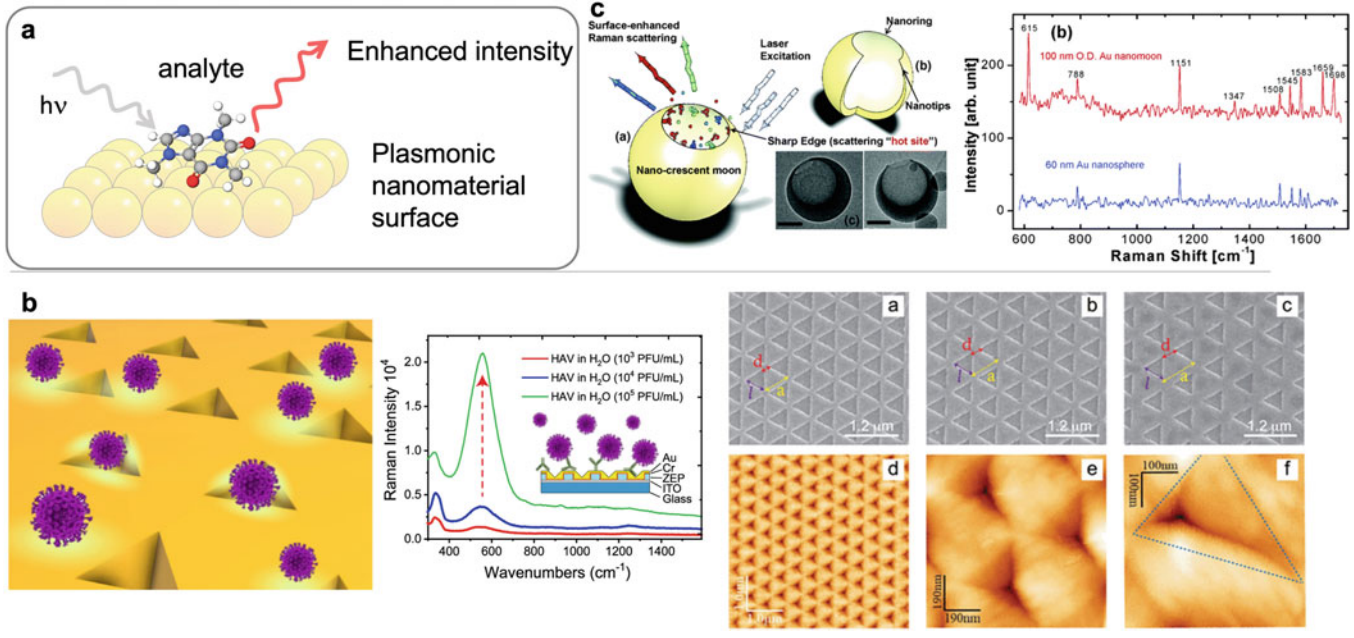

Fig. 9 (**a**) SERS occurs on metal nanostructures, which enhances the Raman spectra by several orders of magnitude. (**b**) Periodic nanoholes in substrates have been used for the detection of hepatitis A virus. From [69] (**c**) Crescent structures engineered for SERS hotspots which exhibit enhancements higher than spherical nanoparticles [70]. Reprinted with permission from Yu Lu, Gang L. Liu, Jaeyoun Kim, et al., *Nano Letters*, 2005. Copyright 2005 American Chemical Society

proteins and DNA have shared chemical groups (i.e., amides, primary amines, carboxylic acids), making it difficult to distinguish the target from other species present.

A format that gets around this problem is the SERS nanotag, where an affinity agent specific to the target, typically an antibody, is conjugated to a plasmonic nanoparticle, and the nanoparticle is functionalized with a Raman reporter (Fig. 10a). Thus, the antibody provides specificity, while the reporter molecule provides a SERS signal. The reporter is chosen so that it has well-defined and intense peaks, and thus is distinguishable from other species that may be present. Thus, the presence of the biological species is read out by the signal of the Raman reporter [73]. Nanotags were first developed for SERS imaging of species cells [74] and can be used in a multiplexed format, where each nanoparticle is decorated with its own Raman reporter. Thus, the different targets can be distinguished by the different SERS spectral signals. Because of the requirement for conjugation to the nanoparticle, often thiol-based molecules are used, such as 4-MBA or 4-nitrobenzenethiol, which are small and thus have distinct spectra.

The nanotag format has also been utilized for multiplexed immunoassays that can distinguish between zika and dengue NS1 in a paper strip [75–77]. Traditional paper strip assays have limited sensitivity due to their visual readout. However, SERS readouts can decrease the limit of detection by two orders of magnitude or more (Fig. 10c).

Much of the promise of SERS nanotags is its potential for multiplexed readout, where different SERS nanotags can detect the presence of different targets. Increasing the multiplexing requires multiple Raman reporters. While it is easy to select two reporters that are well separated spectrally, it becomes more challenging for higher numbers of reporters. Strategies for reporter selection include quantifying reporter overlap in a correlation matrix (Fig. 10d). In addition, linear discriminant analysis was used to evaluate spectral separation for five reporter molecules [78]. It is also possible to use combinations of reporters in different ratios, in a barcode method, similar to what is used for fluorescent dyes in beads in high-throughput screening assays. This strategy has been used to reach over 50 unique Raman codes [79] and demonstrated on peptide libraries (Fig. 10b) [80, 81].

Another way to increase SERS nanotag sensitivity is to use AuAg alloys as a material for the nanoparticle [82–84]. The alloy combines the strong SERS enhancement from Ag with biocompatibility of Au, resulting in enhancement factors higher than Au nanostars by a factor of 10.

4.3.3 Plasmonic Imaging

Plasmonic materials also create the opportunity for plasmonic imaging [85]. Another approach is plasmonic resonance energy transfer (PRET), where energy transfer occurs from a target molecule to the plasmonic structure. Park et al. demonstrate this on mesoporous-silica nanospheres with an optical nanocrescent antenna (MONA) for both imaging and control for light-driven delivery [85]. Nanocrescents have an

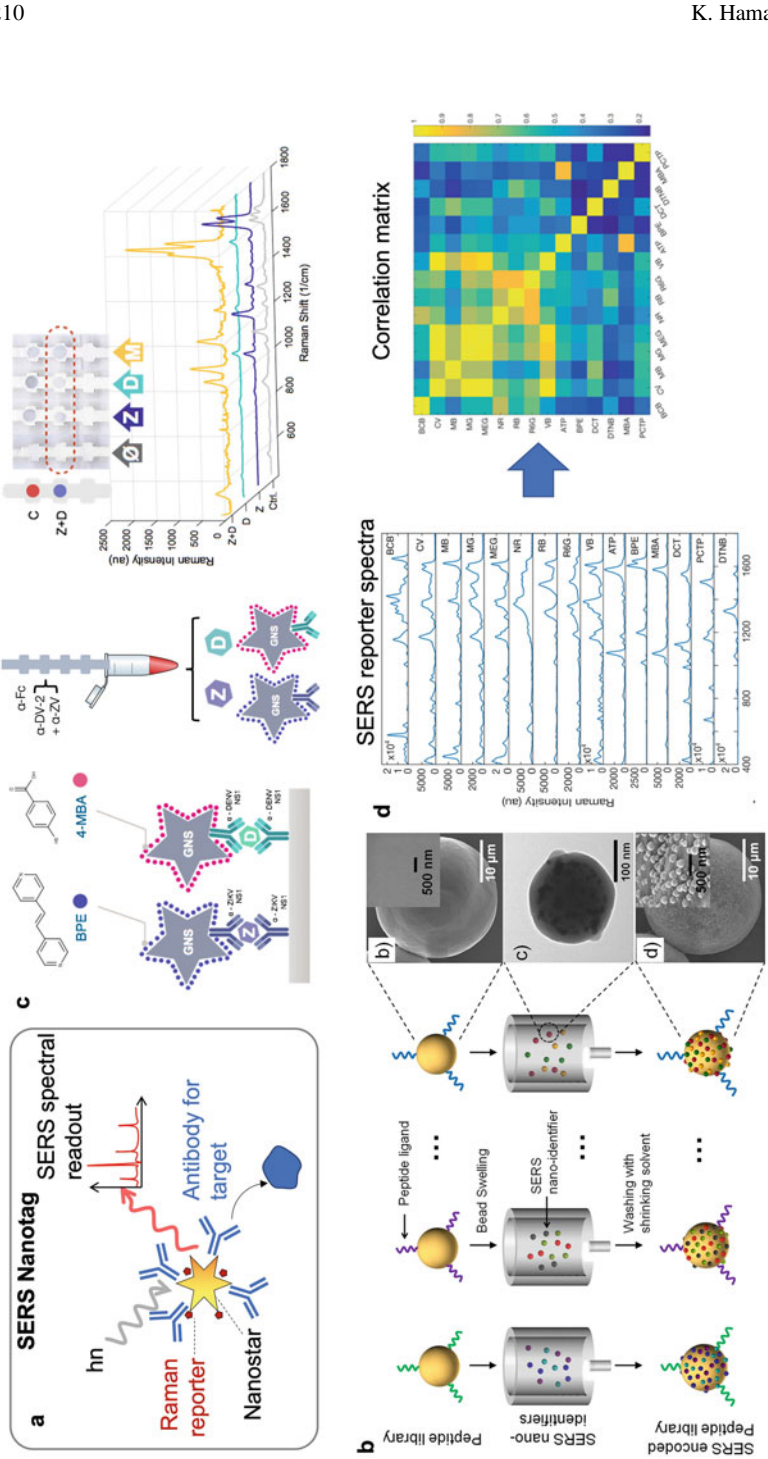

Fig. 10 (**a**) Structure of a SERS nanotag (**b**) SERS barcoding to identify peptides. From [81] Creative Commons Attribution 4.0 International License, (**c**) SERS nanotags for multiplexed detection of zika and dengue in an immunoassay. From [78], (**d**) correlation matrix for choosing multiple reporters based on their spectra. Yellow indicates high overlap, blue low overlap. From [76]

asymmetry to their shape which focuses the thermal gradient in the particle when excited by a laser. They used MONA for release in doxorubicin in cancer cells (MCF-7) and then imaging the impacts of the release.

SERS can also be used for imaging can also be via the enhanced Raman signal. Jiminez de Aberasturi et al. used SERS nanotags consisting of Au nanorods and nanostars as the plasmonic materials, which were decorated with two distinct reporters, 2-naphthalenethiol (2NAT) and biphenyl-4-thiol (4BPT). They demonstrate 3D imaging in layers of fibroblast cells [86], a structurally complex biological sample.

4.4 Plasmon-Enhanced Fluorescent Sensing

Plasmonics can also be used to enhance fluorescence, known as surface plasmon-enhanced fluorescence spectroscopy (PEF or SPFS) or metal-enhanced fluorescence (MEF). This occurs by electric field effects like SERS for the Raman events. Like SERS, it is dependent on the shape of the plasmonic material and the distance between the fluorophore and the plasmonic material. Also similar to SERS, many different nanoparticle shapes have been investigated for optimization of PEF (gold nanorods, shells, pyramids, core-shell particles, etc.) [87]. PEF can increase fluorescence dramatically and lower limit of detection. However, nanoparticles possess a strong absorption, so quenching effects can occur, where the dye fluorescence is absorbed by the nanoparticle. Thus, depending on the separation and orientation, either phenomenon can dominate.

PEF was used to create a COVID-19 antibody test for detection of IgG and IgM [88] where the structure was a grating-coupled fluorescent plasmonic (GC-FP) to enhance fluorescence of a secondary antibody appended with a dye molecule (e.g., Alexa 647). The GC-FP could attain an LOD of <2 ng and can be read out in 30 min.

PEF has also been used for detection of bacterial pathogens, including *E. coli* O157:H7 which is a major threat to food safety. O157:H7 is challenging to detect because the number of cells that can induce illness is extremely low, <10–100. Thus, this places stringent benchmarks on any detection technique. Typically for bacterial detection, samples are brought back to a lab to culture the cells and thus grow them to a high concentration. However, Huang et al. [89] were able to use PEF induced by a planar film to increase fluorescence and thus detect the species directly, with an LOD of <10 cfu/mL and short detection times (40 min). This greatly reduces the time for detection, as culturing can take days.

4.5 Photothermal Excitation of Nanoparticles

Because plasmonic nanoparticles have extremely high absorption cross section, they can convert the energy of absorbed light into heat, resulting in heat localized to the

nanoparticle. This property of nanoparticles has been exploited for externally controlled localized heating, where laser irradiation at the SPR can be used to generate heat to burn tumors or induce a thermally triggered change such as the release of a drug. For gold nanorods and nanostars, their NIR absorption coincides with the window where tissue absorbs minimally, which is ~800 to 1,100 nm, making them attractive for through-tissue applications, facilitating nanomedicine applications in vivo (Fig. 11c).

4.5.1 Ultrafast Excitation

Ultrafast excitation at the SPR with pulses on the order of femtoseconds (fs) has been used to induce a rapid temperature rise in nanoparticles, which induces melting or thermally triggered release. The fs pulse excites the electrons in the particle, perturbing the electron distribution (Fig. 11a). Initially the relaxation occurs via electron thermalization, by e-e scattering, and establishes a new Fermi electron distribution that corresponds to a new higher temperature. This occurs extremely fast, on the timescales of 500 fs for gold. This is followed by exchange of energy between the electrons and the lattice by electron–phonon coupling and occurs over the timescale of ps. These electron–phonon coupling rates are shape/size dependent. Following this, there is energy exchange between the particle and the surrounding medium by phonon–phonon coupling. This exchange is also size dependent and occurs over several hundred picoseconds. The laser irradiation generates heat, and because it is on the ultrafast timescale, it is faster than the dissipation rate to the surrounding and thus melts the nanoparticles (Fig. 11b). For nanoparticles that are different shapes than sphere, this results in a nanoparticle shape change. The shape change was observed by TEM imaging and results in a change in the optical absorption where the LSPR and the TSPR are not impacted [13, 90]. This confirms the transformation of the particle from a rod into a sphere.

The ligand on the nanoparticle surface matters as it can affect the thermal dissipation rates [93, 94]. For ligands that are not covalently attached, they can still impact thermal dissipation and release rates, as they impact by influencing the rate of exchange that can sometimes be by exchange [95]. Furthermore, the shape change can also depend on the particle ligand [96].

4.5.2 Continuous Wave Excitation

Continuous wave (cw) excitation at the SPR can also be used to excite nanoparticles, and is more convenient as the lasers are more portable compared to ultrafast excitation. The laser excitation still excites the plasmon and generates heat, but does not melt the nanoparticles. Continuous wave light is much easier from an instrumentation perspective, as ultrafast pulsed lasers are expensive, not portable, and not as compatible with fiber optics. In contrast, cw laser light can easily be sent

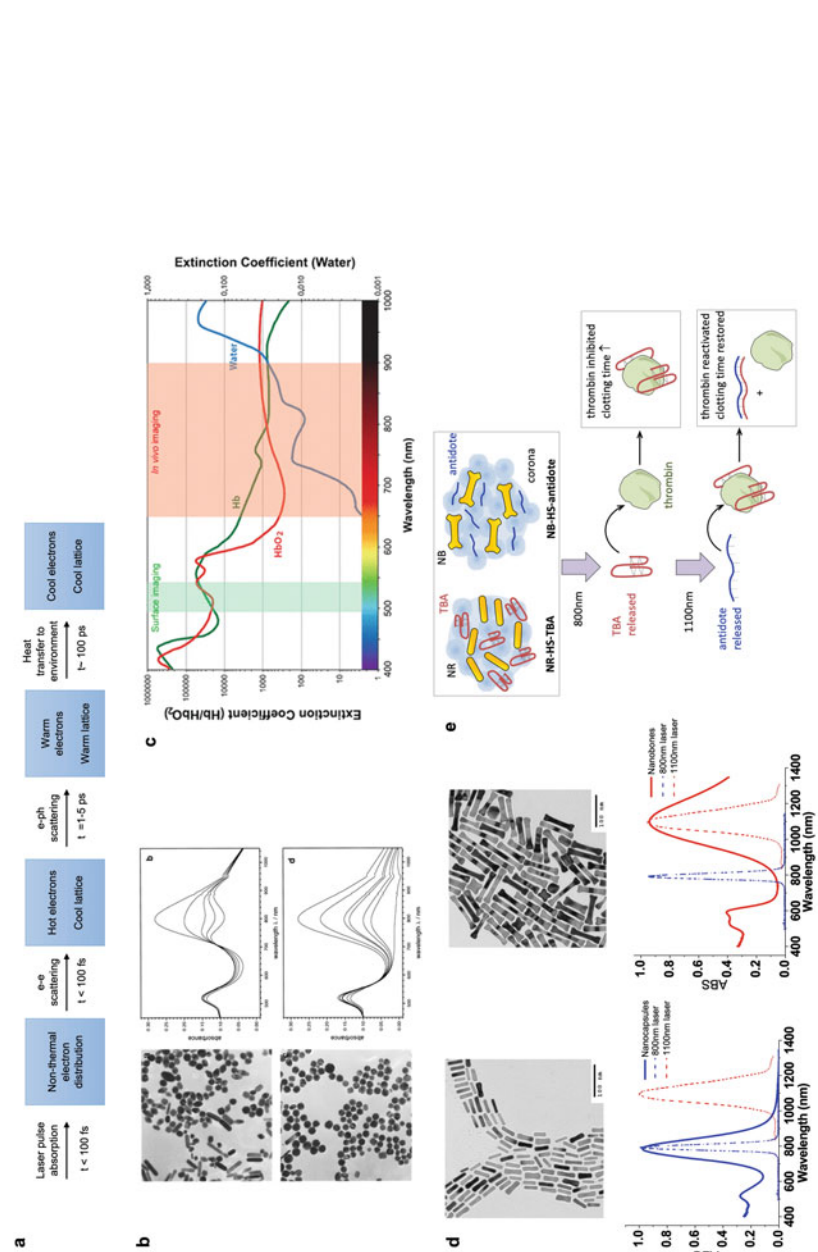

Fig. 11 (**a**) Photothermal mechanism upon irradiation of a nanoparticle with an ultrafast laser pulse. (**b**) Ultrafast irradiation at the LSPR of nanorods induces a shape change, and a decrease in the LSPR peak. From [90] Reprinted with permission from S. Link, C. Burda, B. Nikoobakht, et al., *Journal of Physical Chemistry B*, 2000. Copyright 2000 American Chemical Society; (**c**) tissue window relative to the visible and NIR spectrum, [91] Reprinted with permission from Hisataka Kobayashi, Mikako Ogawa, Raphael Alford, et al., *Chemical Reviews*, 2010,. Copyright 2010 American Chemical Society. (**d**) Nanorods of two different aspect ratios have LSPR that can be selectively excited at two different wavelengths, 800 nm (blue) and 1,100 nm (red). From [13]. (**e**) Selective release of thrombin binding aptamer (TBA) and its complement can be used to switch blood clotting on and off. From [92]

down a fiber optic, so the working format can be more amenable to excitation in hard to reach locations such as inside the body.

4.5.3 Applications of Photothermal Excitation

Phototriggered Release

The ability to heat nanoparticles by an external laser excitation has been exploited in numerous formats, and has been particularly attractive for drug delivery [97]. The main goal of drug delivery is that one wants to control the dosage and timing of a drug. Because laser excitation can control heating, one has the ability to externally control when drug release occurs from a nanoparticle carrier instead of having to rely on passive release. The nanoparticle can be taken up into a cell or be transported in vivo, and the absorption peak of the nanoparticle can be tuned to coincide with the tissue window. It requires conjugation of the nanoparticle to the payload or targeting species, so one has to control particle surface chemistry. If the nanoparticle is irradiated by an ultrafast pulse, the mechanism of release occurs via breakage of the Au-S bond. For cw excitation, release is by thermolysis, where DNA is released from its complement by heat.

This approach has been used to trigger the release of chemotherapeutic agents in cancer cells and in vivo, such as the release of doxorubicin from liposomes [98] or the photosensitizer chlorine e6 (Ce6) for use in photodynamic cancer therapy (PDT) [99].

Multiplexed Triggered Release

The controlled release of multiple species enables the technique to be more powerful, as biological reactions often do not have single inputs but multiple ones. Multiplexed control opens the door to controlling more exciting biological processes. By strategically tuning the size and shape of the nanoparticles used, they can be tailored to absorb at different wavelengths, enabling excitation at multiple wavelengths to selectively control release (Fig. 11d). For example, gold nanorods of different aspect ratios possess LSPR peaks at 800 nm and 1,100 nm, so laser excitation at either wavelength can selectively heat each nanorod, triggering the release of different DNA strands [13]. This was extended to control blood clotting, by loading on the nanorods aptamers that bind and inhibit thrombin, a protein in the blood clotting cascade (Fig. 11e) [92]. The second nanorod possessed the complement to the aptamer, which would inhibit the aptamer when released. Thus, the nanorods could be used to switch on and off blood clotting by external excitation. Selective release has been used for gene circuits in cells [100], where the payload released was siRNA.

Photothermal Signal

The photothermal effect has also been used to enhance the signal in immunoassays, to improve their sensitivity over visual readout [101, 102]. Laser excitation heats the nanoparticles in the test area and the temperature change can be measured with a thermal camera. Wang et al. demonstrated this approach could yield an eightfold enhancement in lateral flow assays for influenza, malaria, and *Clostridium difficile* [103].

5 Conclusions and Future Directions

In summary, there have been a wealth of applications for biosensing with nanoplasmonics and nanophotonics, which has been strengthened by the robust successes of the pillars supporting this discipline, which are theory, synthesis and fabrication, and biocompatibility.

The understanding of their fundamental properties has been bolstered by a long history of theory and simulations. This has been synergistically supported by the numerous and versatile ways to fabricate, pattern, functionalize, and conjugate plasmonic materials. Plasmonics have the rare advantage of possessing both effective chemical synthesis and top-down fabrication techniques. These have enabled routine tailoring of the optical properties by changing their size, shape, and spatial arrangement, with control over wide spatial and wavelength ranges.

One additional aspect that needs to be considered are the environmental effects of plasmonic materials. The globe does not have an unlimited supply of gold, where gold production is already declining and deemed to be unsustainable by 2050 by the World Gold Council [104]. There are efforts in gold recycling, where material can be recovered from electronics waste. In addition, some of the phenomena studied traditionally for plasmonics are now being discovered for other materials. For example, it was discovered that Raman enhancement can also be achieved in dielectric materials such as TiO_2 and that SERS does not require a plasmon. This opens the opportunity to use non-noble metals for some of these biosensing applications [105, 106].

Looking forward, innovation in biosensing seeks to move toward more complex and real biological environments, such as sensing and control in cells and in vivo. Clinical needs are often urgent and help drive innovation. With new biological sensing challenges such as viral outbreaks and novel cancer therapies, the need for novel sensing approaches has only grown.

Acknowledgments The author acknowledges funding from NIH (AI151547) and UMass Boston.

References

1. Dreaden EC, Alkilany AM, Huang X, Murphy CJ, El-Sayed MA (2012) The golden age: gold nanoparticles for biomedicine. Chem Soc Rev 41(7):2740–2779
2. Link S, Mohamed MB, El-Sayed MA (1999) Simulation of the optical absorption spectra of gold nanorods as a function of their aspect ratio and the effect of the medium dielectric constant. J Phys Chem B 103(16):3073–3077
3. Mie G (1908) Articles on the optical characteristics of turbid tubes, especially colloidal metal solutions. Ann Phys 25(3):377–445
4. Link S, El-Sayed MA (2003) Optical properties and ultrafast dynamics of metallic nanocrystals. Annu Rev Phys Chem 54(1):331–366
5. Brust M, Walker M, Bethell D, Schiffrin DJ, Whyman R (1994) Synthesis of thiol-derivatised gold nanoparticles in a two-phase liquid–liquid system. J Chem Soc Chem Commun 7:801–802
6. Turkevich J, Stevenson PC, Hillier J (1951) A study of the nucleation and growth processes in the synthesis of colloidal gold. Discuss Faraday Soc 11:55–75
7. Shi L, Buhler E, Boué F, Carn F (2017) How does the size of gold nanoparticles depend on citrate to gold ratio in Turkevich synthesis? Final answer to a debated question. J Colloid Interface Sci 492:191–198
8. Oldenburg SJ, Averitt RD, Westcott SL, Halas NJ (1998) Nanoengineering of optical resonances. Chem Phys Lett 288(2):243–247
9. Wang S, Xi W, Cai F, Zhao X, Xu Z, Qian J, He S (2015) Three-photon luminescence of gold nanorods and its applications for high contrast tissue and deep in vivo brain imaging. Theranostics 5(3):251–266
10. Huang X, Neretina S, El-Sayed MA (2009) Gold Nanorods: from synthesis and properties to biological and biomedical applications. Adv Mater 21(48):4880–4910
11. Jana NR, Gearheart L, Murphy CJ (2001) Wet chemical synthesis of high aspect ratio cylindrical gold nanorods. J Phys Chem B 105(19):4065–4067
12. Nikoobakht B, El-Sayed MA (2003) Preparation and growth mechanism of gold nanorods (NRs) using seed-mediated growth method. Chem Mater 15(10):1957–1962
13. Wijaya A, Schaffer SB, Pallares IG, Hamad-Schifferli K (2009) Selective release of multiple DNA oligonucleotides from gold nanorods. ACS Nano 3(1):80–86
14. Hirsch LR, Gobin AM, Lowery AR, Tam F, Drezek RA, Halas NJ, West JL (2006) Metal nanoshells. Ann Biomed Eng 34(1):15–22
15. Schwartzberg AM, Olson TY, Talley CE, Zhang JZ (2006) Synthesis, characterization, and tunable optical properties of hollow gold nanospheres. J Phys Chem B 110(40):19935–19944
16. Fabris L (2020) Gold nanostars in biology and medicine: understanding physicochemical properties to broaden applicability. J Phys Chem C 124(49):26540–26553
17. Chandra K, Culver KSB, Werner SE, Lee RC, Odom TW (2016) Manipulating the anisotropic structure of gold nanostars using good's buffers. Chem Mater 28(18):6763–6769
18. de Puig H, Tam JO, Yen C-W, Gehrke L, Hamad-Schifferli K (2015) The extinction coefficient of gold nanostars. J Phys Chem C 119:17408–17415
19. Khoury CG, Vo-Dinh T (2008) Gold nanostars for surface-enhanced Raman scattering: synthesis, characterization and optimization. J Phys Chem C 112(48):18849–18859
20. Dam DHM, Culver KSB, Odom TW (2014) Grafting aptamers onto gold nanostars increases in vitro efficacy in a wide range of cancer cell types. Mol Pharm 11(2):580–587
21. Xie J, Lee JY, Wang DIC (2007) Seedless, surfactantless, high-yield synthesis of branched gold nanocrystals in HEPES buffer solution. Chem Mater 19(11):2823–2830
22. Orendorff CJ, Sau TK, Murphy CJ (2006) Shape-dependent plasmon-resonant gold nanoparticles. Small 2(5):636–639
23. Ha M, Kim J-H, You M, Li Q, Fan C, Nam J-M (2019) Multicomponent plasmonic nanoparticles: from heterostructured nanoparticles to colloidal composite nanostructures. Chem Rev 119(24):12208–12278

24. Xu Z, Lai E, Shao-Horn Y, Hamad-Schifferli K (2012) Compositional dependence of the stability of AuCu alloy nanoparticles. Chem Commun 48(45):5626–5628
25. Xu Z, Xu Z, Carlton CE, Allard LF, Shao-Horn Y, Hamad-Schifferli K (2010) Direct colloidal route for Pt-covered AuPt bimetallic nanoparticles. J Phys Chem Lett 1(17):2514–2518
26. Lu Y-C, Xu Z, Gasteiger HA, Chen S, Hamad-Schifferli K, Shao-Horn Y (2010) Platinum-gold nanoparticles: a highly active bifunctional electrocatalyst for rechargeable lithium-air batteries. J Am Chem Soc 32(135):12170–12171
27. Fruncillo S, Su X, Liu H, Wong LS (2021) Lithographic processes for the scalable fabrication of micro- and nanostructures for biochips and biosensors. ACS Sens 6(6):2002–2024
28. Dai L, Griesser HJ, Mau AWH (1997) Surface modification by plasma etching and plasma patterning. J Phys Chem B 101(46):9548–9554
29. Haynes CL, Van Duyne RP (2001) Nanosphere lithography: a versatile nanofabrication tool for studies of size-dependent nanoparticle optics. J Phys Chem B 105(24):5599–5611
30. Lotito V, Zambelli T (2015) Self-assembly and nanosphere lithography for large-area plasmonic patterns on graphene. J Colloid Interface Sci 447:202–210
31. Weare WW, Reed SM, Warner MG, Hutchison JE (2000) Improved synthesis of small (dCORE ≈ 1.5 nm) phosphine-stabilized gold nanoparticles. J Am Chem Soc 122(51): 12890–12891
32. Wijaya A, Hamad-Schifferli K (2008) Ligand customization and DNA functionalization of gold nanorods via round-trip phase transfer ligand exchange. Langmuir 24(18):9966–9969
33. Hermanson GT (2013) Chapter 6 – heterobifunctional Crosslinkers. In: Hermanson GT (ed) Bioconjugate techniques3rd edn. Academic Press, Boston, pp 299–339
34. Mata Calidonio J, Hamad-Schifferli K (2023) Biophysical and biochemical insights in the design of immunoassays. Biochim Biophys Acta 1867(1):130266
35. Aubin-Tam M-E, Hamad-Schifferli K (2005) Gold nanoparticle-cytochrome *c* complexes: the effect of nanoparticle ligand charge on protein structure. Langmuir 21(26):12080–12084
36. Kolb HC, Finn MG, Sharpless KB (2001) Click chemistry: diverse chemical function from a few good reactions. Angew Chem Int Ed 40(11):2004–2021
37. van der Meer SB, Loza K, Wey K, Heggen M, Beuck C, Bayer P, Epple M (2019) Click chemistry on the surface of ultrasmall gold nanoparticles (2 nm) for covalent ligand attachment followed by NMR spectroscopy. Langmuir 35(22):7191–7204
38. Boisselier E, Salmon L, Ruiz J, Astruc D (2008) How to very efficiently functionalize gold nanoparticles by "click" chemistry. Chem Commun 44:5788–5790
39. Moses JE, Moorhouse AD (2007) The growing applications of click chemistry. Chem Soc Rev 36(8):1249–1262
40. Li H, Chen X, Shen D, Wu F, Pleixats R, Pan J (2021) Functionalized silica nanoparticles: classification, synthetic approaches and recent advances in adsorption applications. Nanoscale 13(38):15998–16016
41. Liu S, Zhang Z, Wang Y, Wang F, Han M-Y (2005) Surface-functionalized silica-coated gold nanoparticles and their bioapplications. Talanta 67(3):456–461
42. Vertegel AA, Siegel RW, Dordick JS (2004) Silica nanoparticle size influences the structure and enzymatic activity of adsorbed lysozyme. Langmuir 20(16):6800–6807
43. Bayraktar H, You C-C, Rotello VM, Knapp MJ (2007) Facial control of nanoparticle binding to cytochrome c. J Am Chem Soc 129(10):2732–2733
44. Ruiz G, Tripathi K, Okyem S, Driskell JD (2019) pH impacts the orientation of antibody adsorbed onto gold nanoparticles. Bioconjug Chem 30(4):1182–1191
45. Rodríguez-Quijada C, Lyons C, Santamaria C, Quinn S, Tlusty M, Shiaris M, Hamad-Schifferli K (2020) Optimization of paper-based nanoparticle immunoassays for direct detection of the bacterial pathogen V. Parahaemolyticus in oyster hemolymph. Anal Methods 12(23):3056–3063
46. Hristov DR, Gomez-Marquez J, Wade D, Hamad-Schifferli K (2021) SARS-CoV-2 and approaches for a testing and diagnostic strategy. J Mater Chem B 9(39):8157–8173

47. Hristov DR, Rodríguez-Quijada C, Gomez-Marquez J, Hamad-Schifferli K (2019) Designing paper-based immunoassays for biomedical applications. Sensors 19(3):554
48. de Puig Guixé H, Bosch I, Gehrke L, Hamad-Schifferli K (2017) Challenges of the nano-bio interface in lateral flow and dipstick immunoassays. Trends Biotechnol 35(12):1169–1180
49. Rodríguez-Quijada C, Gomez-Marquez J, Hamad-Schifferli K (2020) Repurposing old antibodies for new diseases by exploiting cross reactivity and multicolored nanoparticles. ACS Nano 14(6):6626–6635
50. Anfossi L, Di Nardo F, Russo A, Cavalera S, Giovannoli C, Spano G, Baumgartner S, Lauter K, Baggiani C (2019) Silver and gold nanoparticles as multi-chromatic lateral flow assay probes for the detection of food allergens. Anal Bioanal Chem 411(9):1905–1913
51. Homan KA, Souza M, Truby R, Luke GP, Green C, Vreeland E, Emelianov S (2012) Silver nanoplate contrast agents for in vivo molecular photoacoustic imaging. ACS Nano 6(1): 641–650
52. Yen C-W, de Puig H, Tam J, Gómez-Márquez J, Bosch I, Hamad-Schifferli K, Gehrke L (2015) Multicolored silver nanoparticles for multiplexed disease diagnostics: distinguishing dengue, yellow fever, and Ebola viruses. Lab Chip 15:1638–1641
53. de Puig H, Bosch I, Salcedo N, Clavet C, Hamad-Schifferli K, Collins JJ, Gehrke L (2022) Specific viral antigen detection using cross-reactive antibody pairs: implications for outbreak preparedness. Nano Today
54. Storhoff JJ, Lazarides AA, Mucic RC, Mirkin CA, Letsinger RL, Schatz GC (2000) What controls the optical properties of DNA-linked gold nanoparticle assemblies? J Am Chem Soc 122(19):4640–4650
55. Yang C, Wang Y, Marty J-L, Yang X (2011) Aptamer-based colorimetric biosensing of ochratoxin a using unmodified gold nanoparticles indicator. Biosens Bioelectron 26(5): 2724–2727
56. Zahra QU, Luo Z, Ali R, Khan MI, Li F, Qiu B (2021) Advances in gold nanoparticles-based colorimetric aptasensors for the detection of antibiotics: an overview of the past decade. Nanomaterials 11(4)
57. Liu J, Lu Y (2004) Optimization of a Pb2+-directed gold nanoparticle/DNAzyme assembly and its application as a colorimetric biosensor for Pb2+. Chem Mater 16(17):3231–3238
58. Nguyen HH, Park J, Kang S, Kim M (2015) Surface plasmon resonance: a versatile technique for biosensor applications. Sensors:10481–10510
59. Löfås S, Malmqvist M, Rönnberg I, Stenberg E, Liedberg B, Lundström I (1991) Bioanalysis with surface plasmon resonance. Sens Actuators B 5(1):79–84
60. Vázquez-Guardado A, Mehta F, Jimenez B, Biswas A, Ray K, Baksh A, Lee S, Saraf N, Seal S, Chanda D (2021) DNA-modified plasmonic sensor for the direct detection of virus biomarkers from the blood. Nano Lett 21(18):7505–7511
61. Yanik AA, Huang M, Kamohara O, Artar A, Geisbert TW, Connor JH, Altug H (2010) An Optofluidic nanoplasmonic biosensor for direct detection of live viruses from biological media. Nano Lett 10(12):4962–4969
62. Sharma B, Frontiera RR, Henry A-I, Ringe E, Van Duyne RP (2012) SERS: materials, applications, and the future. Mater Today 15(1):16–25
63. Bantz KC, Meyer AF, Wittenberg NJ, Im H, Kurtuluş Ö, Lee SH, Lindquist NC, Oh S-H, Haynes CL (2011) Recent progress in SERS biosensing. Phys Chem Chem Phys 13(24): 11551–11567
64. Moskovits M (2013) Persistent misconceptions regarding SERS. Phys Chem Chem Phys 15(15):5301–5311
65. Schatz GC (1984) Theoretical studies of surface enhanced Raman scattering. Acc Chem Res 17(10):370–376
66. Wang H, Levin CS, Halas NJ (2005) Nanosphere arrays with controlled Sub-10-nm gaps as surface-enhanced Raman spectroscopy substrates. J Am Chem Soc 127(43):14992–14993

67. Ikegami S, Benirschke RC, Fakhrai-Rad H, Motamedi MH, Hockett R, David S, Lee HK, Kang J, Gniadek TJ (2021) Target specific serologic analysis of COVID-19 convalescent plasma. PloS One 16(4):e0249938
68. Shumaker-Parry JS, Rochholz H, Kreiter M (2005) Fabrication of crescent-shaped optical antennas. Adv Mater 17(17):2131–2134
69. Palermo G, Rippa M, Conti Y, Vestri A, Castagna R, Fusco G, Suffredini E, Zhou J, Zyss J, De Luca A, Petti L (2021) Plasmonic metasurfaces based on pyramidal nanoholes for high-efficiency SERS biosensing. ACS Appl Mater Interfaces 13(36):43715–43725
70. Lu Y, Liu GL, Kim J, Mejia YX, Lee LP (2005) Nanophotonic crescent moon structures with sharp edge for ultrasensitive biomolecular detection by local electromagnetic field enhancement effect. Nano Lett 5(1):119–124
71. Folks C, Phuyal US, Rajesh M, Arja N, Gladden M, Hamm L, De Silva Indrasekara AS (2021) Fabrication and comparative quantitative analysis of plasmonic-polymer nanocomposites as optical platforms. Langmuir 37(44):12853–12866
72. Indrasekara ASDS, Meyers S, Shubeita S, Feldman LC, Gustafsson T, Fabris L (2014) Gold nanostar substrates for SERS-based chemical sensing in the femtomolar regime. Nanoscale 6(15):8891–8899
73. Gao J, Sánchez-Purrà M, Huang H, Wang S, Chen Y, Yu X, Luo Q, Hamad-Schifferli K, Liu S (2017) Synthesis of different-sized gold nanostars for Raman bioimaging and photothermal therapy in cancer nanotheranostics. Sci China Chem 60(9):1219–1229
74. Lenzi E, Jimenez de Aberasturi D, Liz-Marzán LM (2019) Surface-enhanced Raman scattering tags for three-dimensional bioimaging and biomarker detection. ACS Sensors 4(5): 1126–1137
75. Sánchez-Purrà M, Roig-Solvas B, Versiani A, Rodriguez-Quijada C, de Puig H, Bosch I, Gehrke L, Hamad-Schifferli K (2017) Design of SERS nanotags for multiplexed lateral flow immunoassays. Mol Syst Design Eng 2:401–409
76. Sanchez-Purra M, Roig-Solvas B, Rodríguez-Quijada C, Leonardo B, Hamad-Schifferli K (2018) Reporter selection for nanotags in multiplexed surface enhanced Raman spectroscopy assays. ACS Omega 3(9):10733–10742
77. Wang G, Park H-Y, Lipert RJ, Porter MD (2009) Mixed monolayers on gold nanoparticle labels for multiplexed surface-enhanced Raman scattering based immunoassays. Anal Chem 81(23):9643–9650
78. Sánchez-Purrà M, Carré Camps M, de Puig Guixé H, Bosch I, Gehrke L, Hamad-Schifferli K (2017) SERS-based sandwich immunoassays for multiplexed detection of Zika and dengue viral biomarkers, ACS. Infect Dis 3(10):767–776
79. Rodal-Cedeira S, Vázquez-Arias A, Bodelón G, Skorikov A, Núñez-Sánchez S, Laporta A, Polavarapu L, Bals S, Liz-Marzán LM, Pérez-Juste J, Pastoriza-Santos I (2020) An expanded surface-enhanced Raman scattering tags library by combinatorial encapsulation of reporter molecules in metal nanoshells. ACS Nano 14(11):14655–14664
80. Kang H, Jeong S, Koh Y, Geun Cha M, Yang J-K, Kyeong S, Kim J, Kwak S-Y, Chang H-J, Lee H, Jeong C, Kim J-H, Jun B-H, Kim Y-K, Hong Jeong D, Lee Y-S (2015) Direct identification of on-bead peptides using surface-enhanced Raman spectroscopic barcoding system for high-throughput bioanalysis. Sci Rep 5(1):10144
81. Kim J-H, Kang H, Kim S, Jun B-H, Kang T, Chae J, Jeong S, Kim J, Jeong DH, Lee Y-S (2011) Encoding peptide sequences with surface-enhanced Raman spectroscopic nanoparticles. Chem Commun 47(8):2306–2308
82. Jackson JB, Halas NJ (2004) Surface-enhanced Raman scattering on tunable plasmonic nanoparticle substrates. Proc Natl Acad Sci 101(52):17930–17935
83. Russo L, Merkoçi F, Patarroyo J, Piella J, Merkoçi A, Bastús NG, Puntes V (2018) Time- and size-resolved plasmonic evolution with nm resolution of galvanic replacement reaction in AuAg nanoshells synthesis. Chem Mater 30(15):5098–5107

84. Russo L, Sanchez-Purra M, Rodríguez-Quijada C, Leonardo BM, Puntes V, Hamad-Schifferli K (2019) Detection of resistance protein A (MxA) in paper-based immunoassays with surface enhanced Raman spectroscopy with AuAg nanoshells. Nanoscale 11(22):10819–10827
85. Park Y, Yoon HJ, Lee SE, Lee LP (2022) Multifunctional cellular targeting, molecular delivery, and imaging by integrated mesoporous-silica with optical nanocrescent antenna: MONA. ACS Nano 16(2):2013–2023
86. Jimenez de Aberasturi D, Henriksen-Lacey M, Litti L, Langer J, Liz-Marzán LM (2020) Using SERS tags to image the three-dimensional structure of complex cell models. Adv Funct Mater 30(14):1909655
87. Badshah MA, Koh NY, Zia AW, Abbas N, Zahra Z, Saleem MW (2020) Recent developments in plasmonic nanostructures for metal enhanced fluorescence-based biosensing. Nanomaterials
88. Cady NC, Tokranova N, Minor A, Nikvand N, Strle K, Lee WT, Page W, Guignon E, Pilar A, Gibson GN (2021) Multiplexed detection and quantification of human antibody response to COVID-19 infection using a plasmon enhanced biosensor platform. Biosens Bioelectron 171: 112679
89. Huang C-J, Dostalek J, Sessitsch A, Knoll W (2011) Long-range surface plasmon-enhanced fluorescence spectroscopy biosensor for ultrasensitive detection of E. coli O157:H7. Anal Chem 83(3):674–677
90. Link S, Burda C, Nikoobakht B, El-Sayed MA (2000) Laser-induced shape changes of colloidal gold nanorods using femtosecond and nanosecond laser pulses. J Phys Chem B 104(26):6152–6163
91. Kobayashi H, Ogawa M, Alford R, Choyke PL, Urano Y (2010) New strategies for fluorescent probe design in medical diagnostic imaging. Chem Rev 110(5):2620–2640
92. de Puig Guixé H, Cifuentes Rius A, Flemister D, Baxamusa SH, Hamad-Schifferli K (2013) Selective light-triggered release of DNA from gold nanorods switches blood clotting on and off. PloS One 8(7):e68511
93. Alper JD, Hamad-Schifferli K (2010) Effect of ligands on thermal dissipation from gold nanorods. Langmuir 26(6):3786–3789
94. Schmidt AJ, Alper JD, Chiesa M, Chen G, Das SK, Hamad-Schifferli K (2008) Probing the gold nanorod-ligand-solvent interface by plasmonic absorption and thermal decay. J Phys Chem C 112(35):13320–13323
95. Alper JD, Crespo M, Hamad-Schifferli K (2009) Release mechanism of octadecyl rhodamine B chloride from Au nanorods by ultrafast laser pulses. J Phys Chem C 113(15):5967–5973
96. Horiguchi Y, Honda K, Kato Y, Nakashima N, Niidome Y (2008) Photothermal reshaping of gold nanorods depends on the passivating layers of the nanorod surfaces. Langmuir 24(20): 12026–12031
97. Haine AT, Niidome T (2017) Gold nanorods as nanodevices for bioimaging, photothermal therapeutics, and drug delivery. Chem Pharm Bull 65(7):625–628
98. Agarwal A, Mackey MA, El-Sayed MA, Bellamkonda RV (2011) Remote triggered release of doxorubicin in tumors by synergistic application of thermosensitive liposomes and gold nanorods. ACS Nano 5(6):4919–4926
99. Xu Y, He R, Lin D, Ji M, Chen J (2015) Laser beam controlled drug release from Ce6–gold nanorod composites in living cells: a FLIM study. Nanoscale 7(6):2433–2441
100. Lee SE, Liu GL, Kim F, Lee LP (2009) Remote optical switch for localized and selective control of gene interference. Nano Lett 9(2):562–570
101. Liu Y, Zhan L, Shen JW, Baro B, Alemany A, Sackrison J, Mitjà O, Bischof JC (2021) fM–aM detection of the SARS-CoV-2 antigen by advanced lateral flow immunoassay based on gold nanospheres. ACS Appl Nano Mater 4(12):13826–13837
102. Qin Z, Chan WCW, Boulware DR, Akkin T, Butler EK, Bischof JC (2012) Significantly improved analytical sensitivity of lateral flow immunoassays by using thermal contrast. Angew Chem Int Ed 51(18):4358–4361
103. Wang Y, Qin Z, Boulware DR, Pritt BS, Sloan LM, González IJ, Bell D, Rees-Channer RR, Chiodini P, Chan WCW, Bischof JC (2016) Thermal contrast amplification reader yielding

8-fold analytical improvement for disease detection with lateral flow assays. Anal Chem 88(23):11774–11782
104. The World Gold Council. www.gold.org
105. Alessandri I (2013) Enhancing Raman scattering without plasmons: unprecedented sensitivity achieved by TiO2 shell-based resonators. J Am Chem Soc 135(15):5541–5544
106. Alessandri I, Lombardi JR (2016) Enhanced Raman scattering with dielectrics. Chem Rev 116(24):14921–14981

Adv Biochem Eng Biotechnol (2024) 187: 223–282
https://doi.org/10.1007/10_2023_238

Published online: 26 January 2024

Wearing the Lab: Advances and Challenges in Skin-Interfaced Systems for Continuous Biochemical Sensing

Zach Watkins, Adam McHenry, and Jason Heikenfeld

Contents

Abstract Continuous, on-demand, and, most importantly, contextual data regarding individual biomarker concentrations exemplify the holy grail for personalized health and performance monitoring. This is well-illustrated for continuous glucose monitoring, which has drastically improved outcomes and quality of life for diabetic patients over the past 2 decades. Recent advances in wearable biosensing technologies (biorecognition elements, transduction mechanisms, materials, and integration schemes) have begun to make monitoring of other clinically relevant analytes a reality via minimally invasive skin-interfaced devices. However, several challenges

Z. Watkins (✉), A. McHenry, and J. Heikenfeld
Department of Biomedical Engineering, University of Cincinnati, Cincinnati, OH, USA
e-mail: watkinzl@mail.uc.edu

concerning sensitivity, specificity, calibration, sensor longevity, and overall device lifetime must be addressed before these systems can be made commercially viable. In this chapter, a logical framework for developing a wearable skin-interfaced device for a desired application is proposed with careful consideration of the feasibility of monitoring certain analytes in sweat and interstitial fluid and the current development of the tools available to do so. Specifically, we focus on recent advancements in the engineering of biorecognition elements, the development of more robust signal transduction mechanisms, and novel integration schemes that allow for continuous quantitative analysis. Furthermore, we highlight the most compelling and promising prospects in the field of wearable biosensing and the challenges that remain in translating these technologies into useful products for disease management and for optimizing human performance.

Graphical Abstract

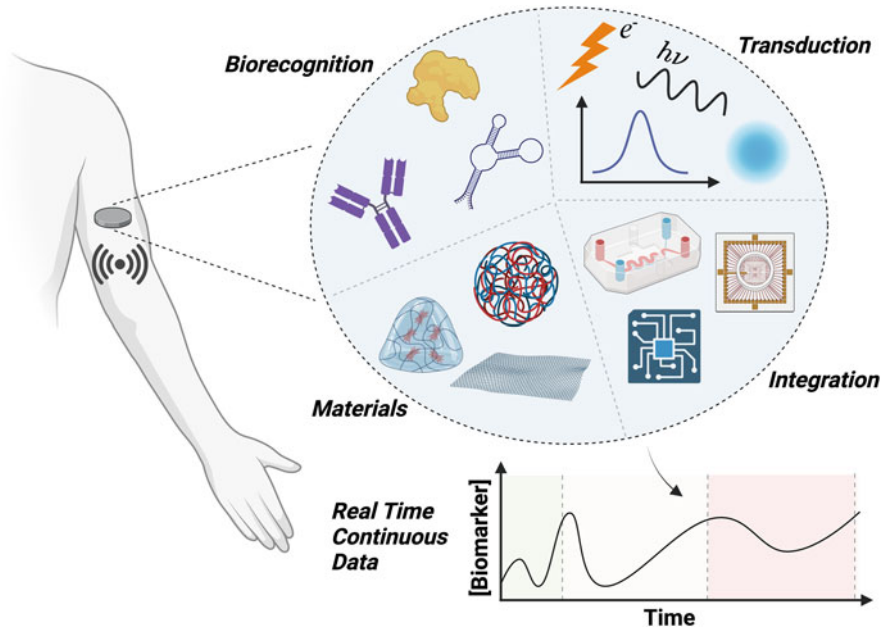

Keywords Biosensing, Electrochemical, Interstitial fluid, Optical, Sweat, Wearables

1 Introduction

On-demand access to data regarding levels of circulating analytes indicative of human health and performance has long been promised as the next breakthrough for personalized medicine [1]. While advancements in analytical techniques in the clinical laboratory and extensive developments in point-of-care assays for the measurement of specific analytes have undoubtedly improved patient care, an emerging wave of continuous wearable platforms promises the ability to harness this information as patients go about their daily lives. These devices not only offer access to more time-resolved data via high-frequency monitoring, but more importantly can provide *contextual* information corresponding to specific life events that may help establish individual trends and patterns. The power of such data is well-illustrated for glucose, where continuous glucose monitors (CGMs) have been demonstrated to improve both glycemic control and overall disease burden for diabetic patients compared to self-monitoring with fingerstick blood glucose test strips [2].

With the global market value for continuous glucose monitoring projected to exceed $10 billion within the next 5 years [3], commercial and clinical success unfortunately remains out of reach for wearable devices that can measure other analytes. Despite extensive development over the past 50 years, electrochemical enzymatic sensors like those used in continuous glucose monitors are limited in their generalization due to a finite number of suitable oxidoreductase enzymes found in nature for the detection of a diverse set of relevant analytes. Thus, there is a large unmet need for modalities and devices that could measure other target molecules for a broad range of applications. Some pertinent examples include measuring analytes that could (1) help alleviate disease burden for those with chronic conditions, (2) improve outcomes for patients requiring postoperative monitoring, (3) revolutionize hormone monitoring for patients suffering from infertility and other endocrine disorders, and (4) improve performance for athletes, military personnel, and those with labor-intensive jobs. Recent advances in biorecognition elements, transduction mechanisms, materials, and integration schemes have begun to make continuous wearable biosensing for other analytes a conceivable reality; however, several challenges remain that are current topics of investigation for those in the field.

In this chapter, we focus specifically on biomolecular sensing modalities that can provide continuous measurements of relevant analytes via minimally invasive interfaces with the skin. This primarily includes chemical sensors that are deployable via wearable devices that attach directly to the skin, but we will also briefly look toward the next frontier of devices that can be implanted into the dermis and interfaced with across the skin for long-term biosensing. We will not spend time discussing wearable sensors that interface with mucosal surfaces, such as those for saliva or tears, as these devices are extensively reviewed elsewhere [1, 4–9], and currently the most compelling wearable demonstrations focus on devices that interface with the skin. While saliva and tears may offer non-invasive biofluid sources for some applications,

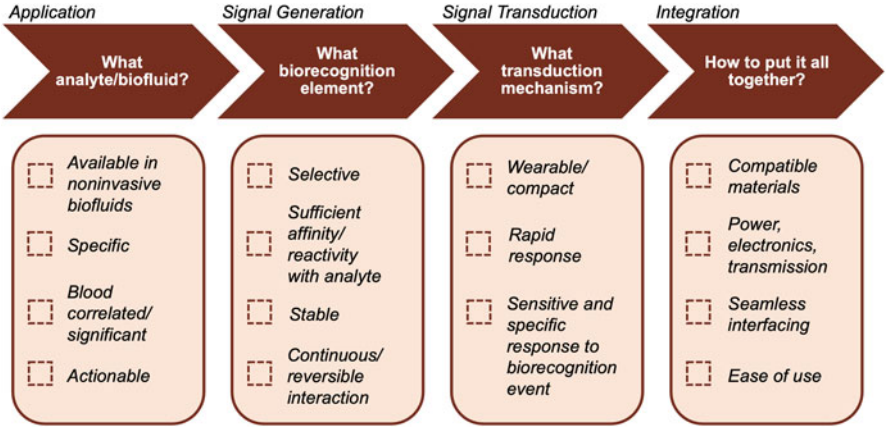

Fig. 1 Application-oriented framework for developing a wearable biosensing platform for the continuous biochemical monitoring of relevant analytes

issues with continuity of biofluid access, excessive contamination, and impracticality of continual device deployment have largely precluded most applications to date [1, 6].

This discussion follows a generalizable framework that can be readily adopted in the process of developing a wearable biosensing device for a given application (Fig. 1), as expanded on in the subsequent sections of this chapter. In general, analytes worth pursuing should be specific and actionable with temporal fluctuations that justify continuous monitoring or longer-term changes that could benefit from more frequent longitudinal monitoring. For example, glucose levels can vary drastically over short timeframes (i.e., minutes-hours) based on the body's metabolic state and in response to the consumption of food [10]. On-demand access to glucose levels provides the insight to make lifestyle changes in the forms of dietary and medication habits and is thus highly actionable. On the other hand, while longitudinally measuring C-reactive protein (CRP) may provide general insights into the inflammatory state of the body, it does not provide specific information that can lead to targeted resolution without additional diagnostic information. However, in conjunction with continuous measures of other markers, such as IL-1β, CRP may be a useful indicator that can help evaluate effectiveness of therapy against the specific cause of inflammation or infection over a given course of treatment [11].

Once a target analyte or multiple relevant analytes have been identified, one must first assess the availability of those analytes in biofluids suitable for wearable biosensing and whether or not the concentration of analyte in that particular biofluid has the potential to provide meaningful data. Secondly, a specific biorecognition element that is capable of interacting with the analyte of interest must be chosen such that the biomolecular event between the two can generate an appreciable signal for detection in the physiological or therapeutic range of the analyte being measured. This event must then be transduced appropriately via a modality that is suitable for

wearable biosensing and must do so in a manner that maintains sufficient sensitivity and selectivity of the interaction to a degree that a discernable signal can be produced with adequate resolution for the application. All of these elements must be compatible with robust integration schemes into ergonomic wearable devices, complete with appropriate materials, electronics, and proper biofluid access such that continuous measurements can be made as one goes about their daily life. This chapter therefore highlights the recent advancements in these various aspects and emphasizes the fundamental challenges the field still faces in achieving these ends.

A final consideration is that these devices should ideally be cost-effective and capable of lasting for long enough to justify monitoring in a continuous and longitudinal fashion. For example, if a device costing $100 only lasted for 6 h at a time, the estimated price for 2 weeks' worth of data, mirroring that of commercial CGMs, would exceed $5,000. Furthermore, the burden of repeated device application would hardly provide any additional benefits beyond those provided by point-of-care assays. As miniaturized electronics and device power capabilities continue to advance at a rapid pace, it appears as if the largest bottleneck for emerging wearable biosensors moving forward will be the longevity of their sensing and transducing elements. As such, we will conclude our discussion by highlighting the most promising modalities and prospects for advancing the commercial and clinical success of biosensors beyond that of current continuous glucose monitors.

2 Beyond Glucose: Relevant Analytes and How to Access Them for Continuous Wearable Monitoring

The first step in crafting a wearable device for on-demand monitoring requires identification of analytes worth pursuing for human health, disease, and performance assessment through an application-oriented lens. One-to-two-week wearable continuous glucose monitoring is a historical achievement in the management of diabetes, as it has enabled precision dosing of insulin and allowed for insight into potential lifestyle modifications that can improve glycemic control [12]. As a result, long-term outcomes for these patients have significantly improved [2, 13]. While glucose monitoring serves as the current benchmark for continuous wearable biosensing, few demonstrations for continuous sensing of other analytes have even come close to such success. There are numerous other analytes that could benefit from more frequent, longitudinal monitoring in a wearable device, including hormones, therapeutic drugs, and cardiac biomarkers to name a few.

Target analytes worth pursuing are ideally specific to a certain disease state and are resultingly actionable or reflect a physiological disturbance that is largely correctable. For disturbances that are not specific to a certain pathophysiology, the measured analyte should be one that must be maintained at certain levels for proper bodily functioning. For example, there are numerous conditions that can lead to hypo- or hypernatremia (i.e., low or high blood Na^+ levels, respectively); however,

these levels must be tightly regulated in order to maintain transmembrane potentials required for necessary cellular operations. Therefore, while not specific to any one disease state, information regarding Na^+ and other electrolyte levels is highly actionable, as treatment can be initiated to correct the imbalance, while the primary cause of the disturbance is further investigated. Cardiac troponin I on the other hand is a highly specific biomarker that is indicative of cardiac cell death, and therefore monitoring of this biomarker can identify the onset of a myocardial infarction and thus inform treatment decisions for preventing further myocardial damage.

Furthering this notion of application-oriented development, one must determine how the analyte of interest can be feasibly accessed and measured in a wearable device. While blood serves as the gold standard biofluid for routine clinical analysis, it is invasive and currently impractical to have an indwelling intravenous sensor for continuous monitoring in ambulatory individuals given the risk of infection. As a result, peripheral biofluids such as sweat and interstitial fluid have gained considerable attention for continuous wearable biosensing applications due to their availability via minimally invasive interfaces with the skin. Methods of biofluid access at the skin interface are expanded upon in the subsequent sections but can be broadly categorized into 3 main approaches including (1) transdermal extraction, (2) surface collection of natural perspiration, and (3) minimally invasive disruption of the epidermal barrier to transdermally access underlying ISF. In light of these options, the presence and significance of specific analytes in either sweat or interstitial fluid must first be carefully assessed to determine the feasibility of peripheral monitoring for a given application.

Table 1 provides concentrations and characteristics of some common clinically relevant analytes spanning from ions, metabolites, and small lipophilic molecules to larger peptide and protein biomarkers. Several of these analytes have concentrations in ISF and sweat that are drastically different from those seen in routine blood analysis, while many have not been assessed in these fluids due to the difficulties of sample collection and analysis using gold standard assays. Based on the dynamic partitioning of analytes from blood into sweat and ISF, as elaborated on in Sects. 2.1 and 2.2, certain biomarkers may be highly dilute or completely absent in these fluids and thus raises an important consideration for application-oriented device development. Furthermore, one must consider the significance of analyte levels measured in these peripheral biofluids, as they may not necessarily be reflective of systemic phenomena. If analyte levels in these fluids are not correlative to blood levels, it may suggest local analyte production/accumulation and therefore one must evaluate if such information has utility for a given analyte [6, 14, 15].

Another consideration for real-time, on-demand biosensors is the temporal resolution needed for a given application and the relationship between changes in analyte concentrations in the blood and those in the biofluid being analyzed. For example, it is known that glucose levels exhibit an average delay of 5–10 min in order for changes in blood to be reflected in ISF concentrations [18, 36, 37]. Devices measuring analytes in sweat and ISF must account for such "physiological lag times" if real-time monitoring with high temporal resolution is desired. With regard to frequency of monitoring, few analytes have temporal fluctuations that vary as

Table 1 Comparison of multiple analytes spanning several classes in sweat and interstitial fluid. Adapted from Heikenfeld et al. [6]; copyright 2019 Springer Nature

	Molecular weight (Da)	Hydrophilicity/ lipophilicity	Blood plasma	Interstitial fluid	Sweat	References
Na^+	23	Hydrophilic (charged)	135–145 mM	Similar to blood plasma	10 s of mM	[16]
K^+	39	Hydrophilic (charged)	3.5–5 mM	Similar to blood plasma	~5–15 mM	[17]
Glucose	180	Hydrophilic (polar)	4.1–6.9 mM	Similar to blood plasma	<5% of blood plasma (0.01–0.20 mM)	[18, 19]
Lactate	90	Hydrophilic (charged)	0.5–10 mM	Similar to blood plasma	~5–10 s mM	[20]
Steroid hormones (e.g., cortisol)	200–400	Highly lipophilic	*Total:* 100 s of nM *Unbound:* 10 s of nM	[Unbound] similar to blood plasma	[Unbound] similar to blood plasma	[21, 22]
Classic small molecules pharmaceuticals (e.g., warfarin)	200–600	>90% are moderately to highly lipophilic	Therapeutic ranges vary based on drug potency, many >90% bound; pM to mM	[Unbound] similar to blood plasma for many highly lipophilic drugs	[Unbound] similar to blood plasma for many highly lipophilic drugs	[6, 14, 23, 24]
Insulin	5,808	Hydrophilic (pI = 5.4)	Fasting: <174 pM Post-prandial: 0.2–2 nM	~21–55% of blood plasma	15–100 pM[a]	[25–27]
Brain natriuretic peptide (BNP)	3,464	Hydrophilic (pI = 10.95)	Healthy: 5–14 pM Heart failure: >23 pM	Lack of report	1.4–2 pM[a]	[28, 29]
Cardiac troponin I (cTnI)	24 kDa	Hydrophilic (pI = 9.9)	Healthy: < 1.7 pM Myocardial infarction: > 17 pM	Lack of report	3–45 fM[a]	[30, 31]
C-reactive protein (CRP)	120 kDa	Hydrophilic (pI = 6.3)	Healthy: 3–33 nM Inflammation/infection: 100–1,000 nM	Lack of report	8 pM-250 pM	[11, 32, 33]

(continued)

Table 1 (continued)

	Molecular weight (Da)	Hydrophilicity/ lipophilicity	Blood plasma	Interstitial fluid	Sweat	References
Cytokines (e.g., IL-1, TNF-α)	~6–70 kDa	Hydrophilic (pI varies)	pM to nM	80% of blood plasma	<0.1% of blood plasma	[6, 34]
Antibodies (e.g., IgG, IgM, IgE)	~150–990 kDa	Hydrophilic (pI varies)	Varies; total ~0.4–16 mg/mL	15–25% of blood plasma	Local or very highly diluted	[6, 34]

Key: IL-1 = interleukin-1, TNF-a = tissue necrosis factor alpha

pI = isoelectric point, which indicates how charged a protein is at physiological pH based on its deviation from 7.4 [35]

[a] Reflects lack of report in sweat. However, due to physiologically similar partitioning pathways [6], data are provided from concentrations measured in salivary fluid as an estimate of concentrations that may be present in sweat

rapidly and drastically as glucose and consequently require prompt resolving actions, such as insulin or oral glucose administration. Therefore, it is likely that most analytes worth pursuing for continuous sensing will benefit from more long-term longitudinal monitoring to analyze trends over several hours, days, or weeks. In these cases, concerns with lag time may not be a pertinent issue. Furthermore, predictive algorithms have been developed to account for these lag times for glucose [38] and are likely adaptable to the real-time measurement of other analytes.

The following sections review the specific approaches, opportunities, and challenges for minimally invasive continuous biosensing in sweat and interstitial fluid. The physiology of analyte partitioning for each is briefly overviewed to provide insights into which analytes may be available for direct chemical detection and to highlight important biological considerations for continuous monitoring. The common methods of biofluid access for peripheral monitoring are also reviewed with their corresponding advantages and limitations for wearable devices.

2.1 Sweat Biosensing

Sweat presents an appealing biofluid option for non-invasive continuous biomonitoring given that it is readily accessible on the surface of the skin for in situ analysis without the need for compromising skin barrier function. Eccrine sweat glands are distributed throughout the skin with a density of 50–500 glands/cm^2 depending on location [39] with typical sweat production rates that vary from 0.01 to 2 μL min^{-1} cm^{-2} depending on the body's hydration and thermoregulatory status [40]. Sweat secretion occurs in a pulsatile manner and is controlled via acetylcholine agonism of muscarinic receptors on secretory cells and periglandular myoepithelial cells under sympathetic nervous system control [41]. Sweat glands are highly vascularized in the dermis and are bathed in dermal interstitial fluid, both of which are key factors that determine sweat composition as the glands carry out their exocrine function within their local environment [42].

Eccrine sweat is primarily composed of water and electrolytes under the tight regulation of aquaporins and specific ion transporters. Notably, sweat also contains a plethora of other analytes originating from blood, ISF, and the eccrine gland itself which can include local waste products, metabolites, proteins, and other compounds that may be of interest for biomonitoring [43]. However, given that secretory cells are connected by tight intercellular junctions that limit paracellular partitioning into sweat glands, some larger analytes found in circulation may be highly diluted or completely excluded from sweat. We refer to prior review articles for an in-depth analysis of sweat analyte partitioning with regard to peripheral biomonitoring [6, 40, 44]. In brief, most analytes readily available for monitoring in sweat are those that can either paracellularly traverse secretory cell tight junctions or passively diffuse through their cell membranes. This predominately includes electrolytes, metabolites, and small lipophilic molecules such as steroid hormones and classic drugs, though

certain proteins may also be present with considerable dilution compared to blood concentrations (see Table 1).

While establishing biofluid access to measure these analytes is not a concern for sweat due to its availability at the skin surface, issues with small sample volumes (i.e., ~nLs), biofluid continuity, and reliable sweat–sensor coupling have presented considerable challenges for the field. In 2013, Jia et al. were able to demonstrate the first integrated on-body sweat biosensor by directly coupling an enzyme-based tattoo onto the skin for electrochemical lactate detection [45]. While these early approaches of direct sensor-to-skin contact opened the door to wearable sweat biosensing [45–48], concerns of variable sweat composition (e.g., mixing of old and new sweat) and unreliable transport of sweat to sensing interfaces have led to a push toward advances in reliable sweat sampling via microfluidic coupling [6, 7, 49]. Relying on sweat secretory driving pressures that range from 2.4 to 2.9 kPa [50], microfluidic devices have recently been engineered to achieve consistent and predictable manipulations of the small sample volumes that can be reasonably collected from a patch on an individual's skin [50–55].

Given that most early demonstrations of wearable sweat biosensing were geared toward applications for active individuals that naturally sweat (e.g., athletes, military personnel, etc.), researchers relied on exercise- or heat-induced sweating to produce sufficient sample volumes for adequate analyte detection. These initial successes harnessed considerable attention for extending continuous sweat sensing to sedentary individuals not actively sweating for health monitoring applications. To achieve this, Kim et al. demonstrated the first wearable sweat sensing device with integrated sweat stimulation in 2016 using local iontophoretic delivery of the cholinergic agent pilocarpine [56], similar to clinical tests for measuring sweat chlorides in cystic fibrosis diagnosis [57]. Iontophoresis is a common transdermal drug delivery method that involves applying voltage across the skin in order to drive charged species into the dermis based on their migration in the resulting electric field (not to be confused with reverse iontophoresis; see *Interstitial Fluid Biosensing*). Most iontophoretic delivery is performed under a constant current density (e.g., typical values of ~0.1–0.5 mA/cm^2) via feedback control of the applied voltage in response to the variable resistance of the skin in order to achieve a constant flux (i.e., mol s^{-1} cm^{-2}) of the species being delivered [58]. As a result, iontophoresis can be leveraged to precisely deliver positively charged cholinergic agents, such as acetylcholine and pilocarpine, to sweat glands in the dermis via electrorepulsion from a positively charged anode at the skin surface in order to stimulate sweat production for continuous biosensing in sedentary individuals.

Initial demonstrations of sweat biosensing with integrated sweat stimulation [56, 59, 60] revealed a viable approach for overcoming challenges associated with inadequate sweat generation, increasing natural baseline sweat rates of <1 nL/min/gland to >5–10 nL/min/gland via iontophoretic delivery of pilocarpine, for example [61]. These studies demonstrated that continuous wearable sweat sensing could be an achievable reality and that iontophoretic sweat stimulation with a suitable agent would be a prerequisite for long-duration measurements to ensure biofluid continuity for most applications involving individuals at rest [6]. However, due to the rapid

metabolism and short-lived effects of agents such as acetylcholine and pilocarpine (i.e., several minutes to ~1.5 h), prolonged measurement over several hours requires repeated and sustained delivery which can cause excessive skin irritation and potential tissue damage [58, 61]. The Heikenfeld group later expanded on iontophoretic sweat sensing schemes by utilizing carbochol, a slowly metabolized cholinergic agent with both muscarinic and nicotinic agonism, which was shown to produce longer duration and more controllable local sweating due to the sudomotor stimulation of sweat glands adjacent to the site of iontophoretic delivery [62, 63, 61]. Precise iontophoretic delivery of carbochol was shown to produce stable sweat generation rates over several hours at lower doses and less overall current exposure/charge injection compared to other agents [61], thus enabling safe, multi-day sensing of stimulated sweat. This breakthrough led to the first validation of a continuous and blood-correlated sweat-sensing device with integrated sweat stimulation by Hauke et al. in 2018 [53].

Despite these recent advances, there are still considerable challenges that warrant further investigation in order to translate continuous sweat biosensing into clinical and commercial viability. One issue that is specific to monitoring in sweat is the variable salinity and pH of the biofluid (pH ~4.5–7), which can drastically alter the performance of biosensing elements. Recent efforts have attempted to isolate sensors from these changes [64] and from potential contaminates at the skin surface (e.g., bacteria and sebum) [65] via oil-impregnated membranes. Other approaches have focused on measuring pH, temperature, and electrolyte concentrations in efforts to provide dynamic sensor correction as skin temperature and sweat composition fluctuate over time [66–71]. Additional challenges include the dependence of sweat composition and resulting analyte concentrations on sweat rate. It is well known that Na^+ and Cl^- levels are heavily dependent on sweat rate due to reabsorption along the secretory duct [40, 72, 73], while glucose levels also show considerable dependence [19, 74]. As a result, compensation for sweat rate has also been explored by employing integrated sweat rate sensors and corrective algorithms [75].

Overall, the largest uncertainty for sweat biosensing is the presence of certain analytes in sweat and the clinical significance of their concentrations as they relate to systemic phenomena. The goal of monitoring in sweat for most analytes is for the concentrations measured to serve as a non-invasive proxy for blood measurements. As discussed previously, it is possible that some analytes worth pursuing may not be present in sweat and, even if they are present, may not correlate significantly to blood concentrations. Recently, there have been demonstrations of increasing paracellular permeability to enhance analyte flux into sweat via local delivery of agents that can modulate intercellular tight junctions [74]. However, such efforts must be critically evaluated on an individual analyte basis and assessed in conjunction with iontophoretic stimulation for continuous monitoring as biology may ultimately be restrictive in what analytes can be measured in sweat with any appreciable diagnostic utility.

2.2 Interstitial Fluid Biosensing

Compared to sweat, the interstitial fluid (ISF) surrounding the cells of the dermis and subcutaneous fat provides a much richer source of relevant analytes given that it is directly connected to the bloodstream via extensive networks of continuous capillaries [76]. Considering that these semipermeable capillaries are designed to deliver nutrients and remove waste from the skin, they also effectively serve as the route by which analytes from blood partition into dermal and subcutaneous interstitial fluids. Two predominant types of continuous capillaries exist in the skin, those fenestrated with diaphragms and those without fenestrations [77]. Fluidic connection between the blood and interstitial fluid is established both through these diaphragmed fenestrations and through the loose adherens junctions between adjacent capillary endothelial cells. The sum of the hydrostatic and osmotic pressures between blood and interstitial fluid (~2–20 mmHg net gradient) leads to a net advective flow of filtered blood plasma into the interstitial space as described by the Starling principle [78–80]. As fluid moves from the microvasculature into the interstitium, analytes from the blood can potentially enter ISF via one or more distinct mechanisms: (1) *paracellular transport* through capillary fenestrations and/or loose adherens junctions between adjacent endothelial cells, (2) *transcellular diffusion* across the plasma membranes of capillary endothelial cells, or (3) *active transcytosis* across endothelial cells via caveolae or clathrin-coated vesicles.

Many low molecular weight species (<1 kDa), particularly ions and small polar molecules (e.g., glucose and urea), can freely traverse intercellular junctions and thus predominately partition via the paracellular route. This results in concentrations in ISF that are often nearly identical to those in blood plasma for these analytes. It is well known that ions, such as Na^+, K^+, and H^+ (i.e., pH), are consistent across blood and interstitial fluid since precise concentrations are necessary for proper cellular function [81]. Additionally, it has been repeatedly shown that ISF glucose mirrors that of blood, attributable to its small size and polar nature enabling unrestricted movement across adherens junctions [18, 36]. For small hydrophobic compounds, such as steroid hormones and classic lipophilic drugs, the situation is complicated by the fact that these compounds exist in blood primarily bound to large plasma proteins (e.g., albumin) which cannot freely pass from blood to ISF [23, 24]. For example, cortisol (362 Da) exists in circulation ~90–95% bound to both corticosteroid-binding globulin and albumin at total physiological concentrations ranging from 50 to 700 nM. Since cortisol is highly lipophilic, the unbound molecules are free to diffuse across endothelial plasma membranes to equilibrate between blood and ISF [6]. As a result, unbound concentrations of cortisol in blood plasma (i.e., ~5–50 nM) are fairly consistent with those in ISF. Similarly, ISF concentrations for other highly bound analytes, such as small molecule drugs, are largely expected to mirror their unbound blood plasma concentrations [23, 82] (see Table 1).

Regarding paracellular partitioning of larger analytes, such as proteins, the capillaries act as both a size-exclusive and charged barrier to passive transport, resulting in selective filtration from blood to ISF. It has been shown that size-

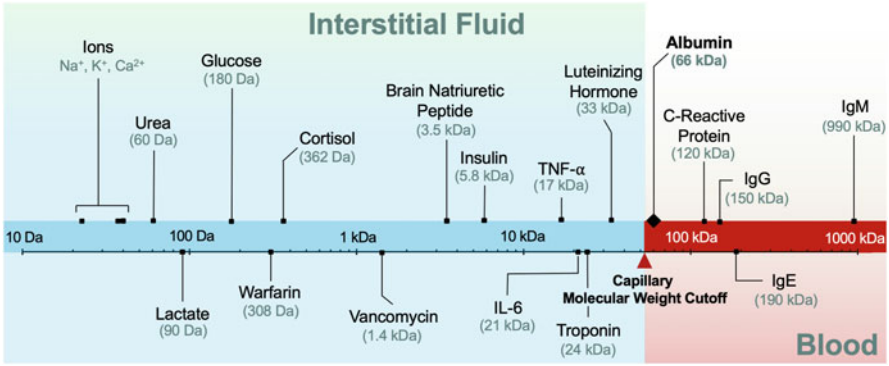

Fig. 2 Size of clinically relevant analytes that may be capable of partitioning into interstitial fluid based on an estimated capillary molecular weight cutoff ~60–70 kDa (~6–7 nm diameter) for paracellular partitioning. Adapted from Ono et al. [76] under a Creative Commons license CC BY 4.0

restricted transport into ISF through the adherens junctions becomes dominant near 65 kDa based on average interendothelial pore sizes of around 6–7 nm [76]. While capillary fenestrations provide larger physical pore sizes of up to 60–80 nm, the estimated upper limit for paracellular transport is reportedly <6–12 nm due to the charge barrier imposed by the anionic layer of proteoglycans and glycosaminoglycans along the capillary lumen known as the glycocalyx [77]. As a result, some larger and highly charged protein-based macromolecules, such as peptide hormones, antibodies, cytokines, and lipoproteins, are largely filtered from the blood plasma that enters ISF.

Figure 2 shows a collection of exemplary analytes that may be capable of paracellular partitioning or alternatively may be excluded from ISF based on these physiological upper limits. However, this does not take into account the active transport of large macromolecules across endothelial cells or the dynamic remodeling of interendothelial junctions based on extracellular stimuli. Insulin, for example, has been shown to bind endothelial receptors on the capillary lumen that initiate clathrin-dependent endocytosis with subsequent exocytosis into the interstitial space [83]. However, due to its small size (5.8 kDa), paracellular partitioning still plays a significant role in insulin delivery to tissues [84]. Albumin, on the other hand, is too large for unimpeded paracellular partitioning but has been shown to enter ISF in small quantities predominately via caveolae-mediated vesicular transport [85, 86]. Regardless of size, local inflammation can drastically increase extravasation of large analytes due to inflammatory mediators initiating cellular signaling that can disrupt interendothelial junctions and upregulate luminal analyte receptors [87]. Therefore, in relating blood concentrations of large macromolecules to those in ISF, active transport and the effects of stimuli like inflammation must be carefully considered. We refer to prior reviews for a more in-depth analysis of dynamic analyte partitioning and the resulting physiological considerations for ISF monitoring [6, 14].

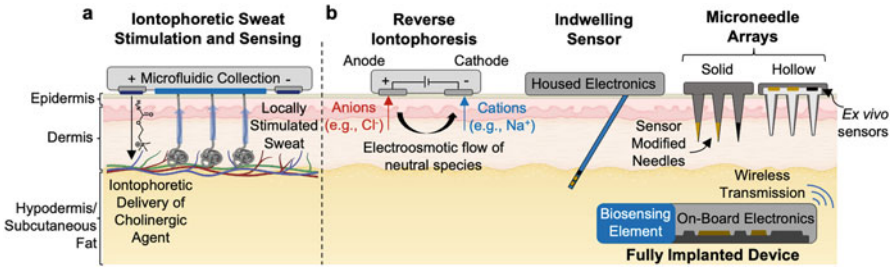

Fig. 3 Overview of leading strategies for skin-interfaced biosensing for both (**a**) sweat and (**b**) interstitial fluid. Adapted from Friedel et al. [14]; copyright 2023 Springer Nature

While interstitial fluid may provide access to a more diverse set of analytes that have a higher potential for correlation with blood concentrations, minimally invasive access to interstitial fluid compared to sweat is considerably more challenging. Traditional analysis of ISF has relied on sample extraction via vacuum/suction blisters, pressure-based needle withdrawal, or microdialysis, all of which are susceptible to artifacts and infeasible for long-term continuous monitoring [14]. The first attempt at a wearable device for interstitial fluid monitoring was the GlucoWatch Biographer, which was based on the principle of reverse iontophoresis to continually extract interstitial glucose for external sensing [88]. Reverse iontophoresis is similar to iontophoretic drug delivery in that it involves the application of a potential across two electrodes placed on the skin; however, instead of delivering a charged species into the dermis, the resulting flow of ions is used to extract diluted ISF and bring neutral species, such as glucose, to the surface via electroosmosis (Fig. 3). While the GlucoWatch was later discontinued due to issues of accuracy and skin irritation from the applied potential [89], recent efforts have attempted to address these concerns by employing lower current densities (~0.25 mA/cm^2 vs. ~0.5 mA/cm^2 for the GlucoWatch) for shorter periods of time [59, 90–92] and increasing flux through the local delivery of charged species such as hyaluronic acid [93].

Other strategies for minimally invasive access to analytes in interstitial fluid for continuous monitoring have involved compromising the epidermal barrier to achieve direct coupling to underlying dermal and hypodermal interstitial fluids. The most prevalent examples are those employed by leading diagnostic companies (e.g., Abbott, Dexcom, and Medtronic) where wire-based or thin-film electrode arrays are transdermally placed 5–9 mm beneath the skin surface via a custom inserter that leaves the necessary on-body electronics adhesively attached to the skin. These devices represent the current benchmark for on-body biosensing with accurate continuous measurements for up to 2 weeks and have been extensively studied and reviewed owing to their unrivaled commercial and clinical success [94, 95]. Other approaches have focused on utilizing microneedle arrays, which may obviate the need for complex inserters and are overall less invasive given that they typically penetrate less than 1 mm into the dermis and are $<$200 μm in diameter.

Recent demonstrations have utilized both solid microneedle arrays with functionalized needles placed directly into the dermis [96–99] and hollow microneedle arrays, where the lumen of the microneedle creates a fluidic path to ex vivo housed sensors allowing for more versatile device design [100–104]. A new frontier of implantable devices has also gained traction, exemplified by the Senseonics Eversense, where the device is fully implanted in the dermis and interfaced with the skin via an external reader [105, 106]. These approaches are summarized in Fig. 3 alongside the leading approach for continuous sweat biosensing, which was recently shown to be compatible with integration into a dual sweat/ISF biosensing device [59].

Given these approaches, several physiological considerations must be taken into account to ensure reliable and accurate biosensing. One consideration is that the dermis is typically under negative pressures of −1 to −4 mmHg relative to atmospheric pressure due to constant lymphatic clearance [107], which may complicate hollow microneedle-based approaches that rely on fluidic coupling and analyte transport to ex vivo sensing elements. Additionally, any device that disrupts the epidermal barrier to access ISF will inevitably induce a local inflammatory response, which may transiently increase vascular permeability in the short term and initiate a foreign body response in the long term, both of which may diminish sensor accuracy and confound correlation to blood concentrations [108]. Lastly, the local production of certain analytes (e.g., cytokines, inflammatory markers) and the local utilization of analytes (e.g., glucose uptake into adipose cells) at the sensing location must be accounted for if the data are to be used as a proxy for systemic phenomena [14]. Similar to sweat biosensing, further investigation is needed to evaluate what analytes can be measured in ISF with appreciable diagnostic utility, which ultimately may be accelerated by the development of robust biosensors utilizing the technological advances detailed below [109].

3 Choosing the Most Appropriate Biorecognition Element

Once a suitable biomarker has been identified and its presence in either interstitial fluid or sweat has been established, careful consideration must be given to the biomolecules capable of selective recognition of the analyte to be measured. Biorecognition elements can be divided into two broad categories depending on whether they catalyze a chemical reaction involving the analyte (i.e., catalytic/reactivity based) or if they simply interact with the analyte via non-covalent intermolecular forces with a certain affinity (i.e., affinity-based). Such elements can be found in nature, chemically modified, or synthetically derived to mimic naturally occurring biomacromolecules. When assessing key criteria for selecting suitable biorecognition elements, they should ideally be (1) selective for the target analyte against chemically similar species, (2) stable in complex biofluids,

(3) capable of generating a measurable interaction with analyte in the concentration range relevant to the application, and (4) kinetically tuned to respond appropriately and reversibly to changes in concentrations. Below we will discuss the benefits and limitations associated with the major classes of these elements for continuous wearable biosensing and highlight the recent progress in advancing molecular biorecognition, as summarized in Fig. 4.

3.1 Reactivity Based

In 1962, Clark and Lyons published the first conceptualization of a biosensor that could capitalize on the specific reactivity of glucose and oxygen with the enzyme glucose oxidase (GOx) such that glucose could be detected indirectly by the proportional decrease in oxygen concentration measured at an amperometric sensor [110]. Shortly thereafter, Clark demonstrated that retaining GOx near a platinum anode with cellophane allowed him to measure glucose in whole blood via detection of the hydrogen peroxide produced in the catalyzed reaction [111, 112]. This success opened the door to the field of biosensing, as this concept was quickly adapted to the use of other enzymes, such as urease [113] and lactate dehydrogenase [114], with varying immobilization strategies and transduction schemes.

Enzymes comprise the entirety of the reactivity-based biorecognition elements and also represent the class of biosensor that has achieved the greatest commercial success due to the widespread adoption of fingerstick and continuous glucose monitors for diabetes management. Enzymatic sensors rely on the catalysis and specific chemical reactivity of a target analyte with a particular enzyme to produce a new species. A generalized reaction scheme for enzymatic catalysis can be expressed as:

$$E + S \underset{k_r}{\overset{k_f}{\rightleftharpoons}} ES \xrightarrow{k_{cat}} E + P \tag{1}$$

where E is the enzyme that catalyzes the reaction of substrate S to product P through the formation of an enzyme substrate complex ES. Assuming reversible formation of this complex with respective forward and reverse rate constants, k_f and k_r, and an irreversible conversion to P with rate constant k_{cat}, rearrangement of the rate equations associated with Reaction 1 gives rise to the Michaelis-Menten equation:

$$V \equiv \frac{d[P]}{dt} = \frac{V_{max}[S]}{K_M + [S]} \propto \text{signal} \tag{2}$$

where V is the rate of the product formation, V_{max} is the maximum rate obtainable under saturating conditions, and K_M is the Michaelis constant, which is defined as:

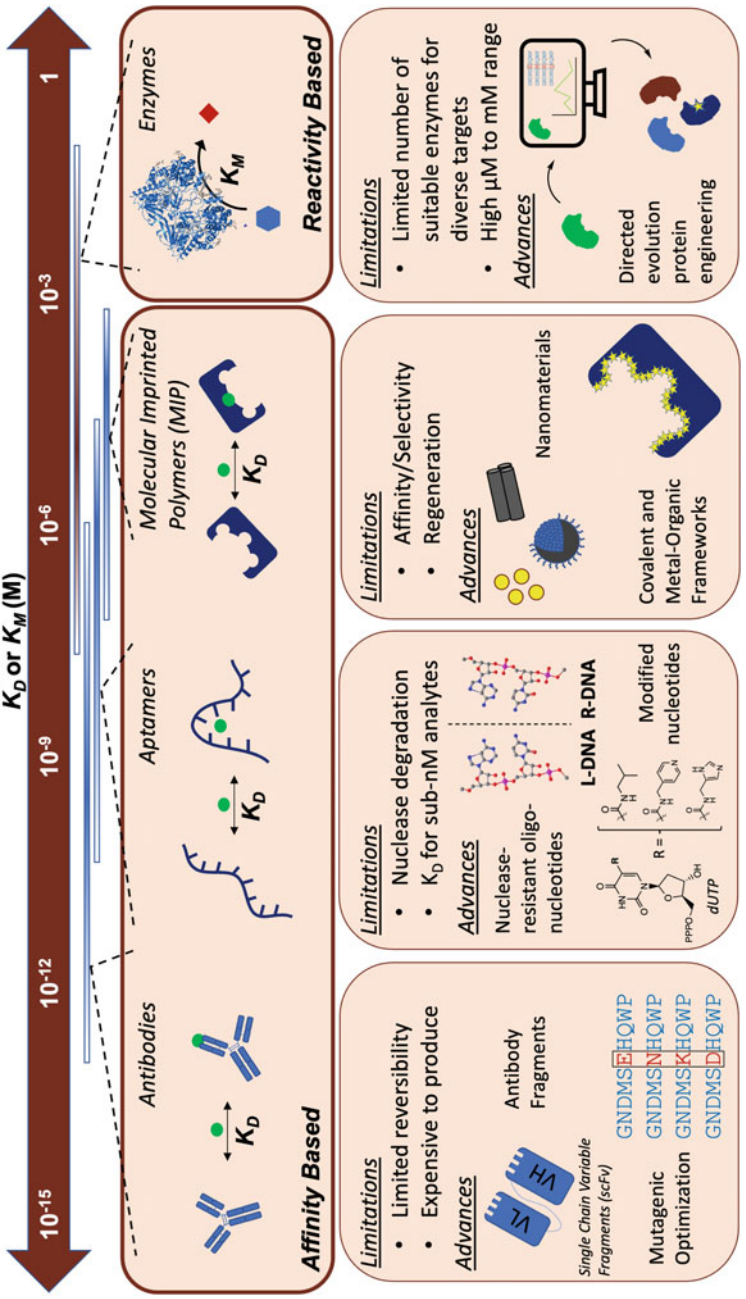

Fig. 4 Overview of the leading biorecognition elements most promising for wearable biosensing, including limitations and recent advances for each class

$$K_M \equiv \frac{k_r + k_{\text{cat}}}{k_f} \tag{3}$$

and represents the concentration of substrate that results in a rate that is ½$V_{\max}$ at equilibrium. K_M and $V_{\max}$ are intrinsic properties of an enzyme/substrate pair in a given system as $V_{\max}$ is related to k_{cat} and the overall enzyme concentration, $[E_0]$, via $V_{\max} = k_{\text{cat}}\ [E_0]$. These parameters relate to the *activity* of an enzyme, which is defined as the amount of substrate an enzyme can catalyze into product in a given amount of time (i.e., μmol/min) under specified conditions, and thus are key factors in an enzyme's performance as a recognition element in a biosensing system.

As denoted in Eq. 2, the rate of product formation is directly related to the concentration of the analyte being measured. Therefore, enzymatic biosensors in the general sense rely on the generation of a product that can be specifically detected either optically or electrochemically, which can then be related back to the concentration of analyte being measured. This may include the production of an electroactive species or the production of a species that results in a color change or change in fluorescence of the sample. Beyond the direct detection of enzymatic products, other transduction schemes for enzymatic sensors may involve the use of shuttle species known as mediators that can facilitate rapid downstream analyte detection, or involve the direct coupling and proper orientation of enzymes to a transducer, as is the case for enzymes undergoing direct electron transfer with an electrode upon analyte conversion. Since reaction rate is the determining factor for signal generation, flux of analyte to the sensing interface is a critical aspect of performance for systems utilizing enzymatic biorecognition [115]. As a result, enzyme immobilization and encapsulation strategies are important design considerations for integrated continuous sensing devices, as demonstrated by the use of flux-limiting membranes to tune the dynamic range of commercially available continuous glucose monitors [116, 117].

A major benefit of using enzymes for biorecognition lies in the versatility of the immobilization strategies that can be used to contain enzymes at the sensing interface for continuous monitoring. There have been several approaches demonstrated in the literature for enzyme immobilization, including physical adsorption, covalent coupling, polymeric encapsulation, and cross-linking entrapment [118]. Since most enzymes undergo minimal conformational change in catalyzing a reaction [119], signal generation is not heavily dependent on the physical mobility of the enzyme at the site of containment. However, if the native structure of the enzyme is drastically altered during the immobilization process, the activity of the enzyme may be significantly reduced [115]. Therefore, methods that minimize loss of activity and minimize the amount of enzyme needed to generate appreciable signal once immobilized are desirable [118]. Recent approaches have focused on layer-by-layer assembly techniques to create multilayer architectures that minimize loss of enzyme activity for more sensitive analyte detection [120, 121]. Other key considerations for enzyme immobilization include the long-term stability of the biorecognition layer in complex media and the ease of incorporation into robust

device designs such that signals can be transduced appropriately. We refer to prior reviews for a more in-depth analysis of the benefits and drawbacks of specific enzyme immobilization strategies for biosensing applications [118, 122, 123], along with the incorporation of specific mediators that can lead to more sensitive and specific analyte detection [115].

Since enzymes are highly complex biological catalysts, they are predominately found in nature and isolated from biological sources, such as bacteria and yeast. As a result, enzymatic biorecognition is limited to analytes that are substrates for naturally occurring enzymes where there is conversion to a product that can be specifically detected. Furthermore, most enzymatic sensors have insufficient limits of detection to measure low concentration analytes (i.e., pM to nM) and are typically limited to analytes that are present in the high μM to mM concentration range (e.g., glucose, lactate, and ethanol). Recent efforts have been aimed toward the reengineering of enzymes to improve sensitivity for biosensing applications, aided by computational modeling to drive directed evolution mutagenesis and the incorporation of site-specific chemical modifications [124, 125]. Other emerging innovations include the development of artificial enzymes and nanozymes, which obviate the need for natural enzymes by achieving catalysis with sophisticatedly designed nanomaterials [126, 127]. While these analogues may achieve superior stability in complex biological media, they currently lack the specificity offered by their naturally derived counterparts [126]. Ultimately, enzyme-based biosensing is currently confined to a limited subset of small molecule targets as catalytic biorecognition is not suitable for measurement of some analytes, such as large protein-based biomarkers. Thus, many applications of continuous wearable biosensing will be reliant on affinity-based biorecognition and its accommodation of a more diverse catalog of target analytes.

3.2 *Affinity Based*

Affinity-based biosensors rely on the equilibrium between the bound and unbound states of a bioreceptor molecule with a target analyte given by:

$$T + R \underset{k_{\text{off}}}{\overset{k_{\text{on}}}{\rightleftharpoons}} TR_{\text{complex}} \tag{4}$$

where T is the target that specifically binds at a singular binding site to receptor R, forming an intermolecular complex TR with an association rate constant of k_{on}. The ratio of the dissociation rate constant, k_{off}, and k_{on} gives rise to the dissociation constant, K_D, which is a measure of binding affinity between the target and biorecognition element at equilibrium.

$$K_D \equiv \frac{k_{\text{off}}}{k_{\text{on}}} = \frac{[T][R]}{[TR]} \tag{5}$$

The dissociation constant represents the equilibrium concentration of target at which the fraction of available receptors bound to target (f_{bound}) is 50%. By solving the following rate law equation associated with Reaction 4:

$$\frac{d[TR]}{dt} = k_{\text{on}}[T][R] - k_{\text{off}}[TR] \tag{6}$$

with the assumption that $[T] >> [R]$ (i.e., $[T]$ is relatively constant), the relationship between the concentration of target and the fraction of receptors bound *at equilibrium* can be derived to give rise to the Langmuir equation:

$$f_{\text{bound}} \equiv \frac{[TR]}{[R] + [TR]} = \frac{[T]}{[T] + K_D} \propto \text{signal} \tag{7}$$

where the signal provided by the interaction between the target and receptor is either proportional or inversely proportional to the fraction of bound biorecognition elements. For multivalent receptors with more than one target binding site, Eq. 7 can be generalized to the Langmuir–Hill equation, which takes into account the effects of cooperative binding [128]. While there have been demonstrations of multivalent biorecognition elements in efforts toward signal amplification and dynamic range modulation [129], analyte binding at equilibrium for most biosensors at a given temperature follows a simple Langmuir isotherm, which mirrors the mathematical relationships seen in Michaelis-Menten kinetics of enzymatic systems.

An important consideration for wearable affinity-based biosensors is the trade-off between the binding affinity at equilibrium (i.e., thermodynamics) and the response time of the sensor (i.e., kinetics), determining its practical "reversibility" over a given operational timeframe. It is known that k_{on} is largely dictated by the physical and structural properties of receptor–analyte binding and is typically limited to values of 10^5–10^7 s^{-1} M^{-1} for large biomacromolecules [130, 131]. Therefore, for most biosensors, the K_D is predominately determined by k_{off}, with higher affinity receptors requiring slower off-rates [132]. The rate of equilibration for a sensor in the presence of a given target concentration can be realized via the *transient* solution to Eq. 6:

$$f_{\text{bound}}(t) = \frac{[T]}{[T] + K_D} \left(1 - e^{-(k_{\text{on}}[T] + k_{\text{off}})t}\right) \tag{8}$$

This relationship presents an extraordinary challenge in terms of sensor equilibration times for low concentration analytes that require high-affinity bioreceptors in order to make meaningful measurements. For example, an insulin sensor with an adequate K_D of 500 pM attempting to measure a postprandial concentration of 1 nM

with a typical k_{on} of 10^6 s^{-1} M^{-1} [131] would take ~45 min to reach 98% of its equilibrium value, a time by which insulin concentrations may have fallen drastically back toward basal levels. Lubken et al. recently provided an insightful analysis on this issue by modeling the dynamic response of affinity-based sensors for low-abundance analytes [133] and proposed solutions that may achieve more rapid quantification by controlling sample volumes and flow at the sensing interface [134]. However, these approaches still rely on full equilibration and may overly complicate device design. Recently, Maganzini et al. demonstrated a signal processing approach that analyzes the sensor's kinetic response in the frequency domain in order to track fluctuating concentrations of analytes in real time without the need for reaching equilibrium [135]. It is likely that a combination of these approaches and others will be necessary for accurate on-demand quantification of analytes in the pM to sub-pM concentration ranges, especially for analytes that fluctuate more rapidly.

Other considerations for affinity-based biosensors include their means of signal generation upon analyte binding and how the bound fraction can produce some specific change in the sensing environment that can be appropriately transduced and quantified. Some examples of binding-induced changes seen in affinity-based biorecognition include changes in receptor conformation, changes in supramolecular chemistry, changes in local charge distribution/permittivity, changes in optical properties, changes in mass/diffusivity, and the induction of subsequent chemical or physical events that may be specifically transduced. Additionally, it is also important to consider the effects different sample media will have on analyte binding. For example, the variable salinity and pH of sweat may drastically change the affinity of a biorecognition element for its target and therefore must be accounted for in such environments. Furthermore, the long-term stability of a given biorecognition element in complex biofluids such as sweat and ISF must also be considered as denaturation may occur over time due to hydrolysis, enzymatic degradation, or non-specific interactions with other molecules.

Below, we explore these considerations for the major classes of affinity-based biorecognition elements and review their suitability for use in continuous wearable platforms. Furthermore, we highlight the specific challenges each face and the emerging innovations that seek to overcome these obstacles.

3.2.1 Antibodies

Antibody-based biorecognition platforms are a mainstay in clinical diagnostics owing to their high sensitivity and selectivity, commonly seen in the form of enzyme-linked immunosorbent assays (ELISA) and lateral flow assays (LFA). Given their widespread use, there has been much interest in leveraging antibodies into reagent-free and continuous immunosensing platforms for wearable applications. While antibodies can bind a wide range of molecules and demonstrate high-affinity binding to their target ($K_D \sim 10^{-7}$–10^{-12} M) with unmatched specificity, issues with sensor reversibility have largely precluded continuous operation,

effectively limiting immunosensors to single-use point-of-care applications. Although the binding of an antibody to its antigen is technically reversible in the thermodynamic sense, the slow off-rates that accompany the low K_D values of antibodies make them practically irreversible on the operational timescales needed for continuous, on-demand biosensing. If immunosensors are used for repeated measures in practice, they often have to rely on denaturants, such as detergents or chaotropic agents (i.e., urea, guanidinium hydrochloride), to disrupt antibody–analyte binding and regenerate the sensor for further quantification [136]. Some recent demonstrations have achieved semi-continuous quantification with antibodies in various biofluids; however, they required exogenous reagents [137], utilized complex processing not suitable for wearable biosensing [138], or lacked evidence of regeneration in situ [11, 139]. Ultimately, there have been no demonstrations to date detailing a continuous reversible immunosensor that can track fluctuations of an analyte in real time via a reagent-free wearable platform.

Other key considerations for immunosensors include the process of generating quality antibodies with the high affinity and selectivity expected of antibody–antigen binding pairs. Antibodies, like enzymes, are derived from natural sources but typically involve more complex protocols using animals and/or cell cultures making antibody production expensive and labor-intensive. These methods rely on the ability of an antigen to initiate an immune response in a mouse, rabbit, or cell line, which poses challenges for generating antibodies against target molecules with limited immunogenicity; however, there are known strategies for inducing humoral immunity against small molecules (i.e., haptens) by utilizing proper protein carriers [140]. Due to the complexities of production, animal-derived antibodies may also suffer from batch-to-batch variations [141], which can drastically affect sensor reproducibility. The end product of antibody production is a large (>100 kDa) and intricate protein with a distinct quaternary structure that is susceptible to denaturation and degradation, which can limit the operational lifetimes of immunosensors [142]. While the structure of native antibodies makes them versatile in their conjugation to sensing interfaces, such as electrode surfaces and nanoparticles, their large size makes them unfit for some sensing transduction mechanisms [143] (*see* Sect. 4.2.4).

Despite these shortcomings, recent advancements in immunoengineering and protein engineering have led to considerable progress toward antibodies and antibody fragments that are capable of high affinity and reversible binding to targets with superior long-term stability in biosensing environments. Approaches such as directed evolution mutagenesis and phage display biopanning have been shown to produce antibody mutants that have fast dissociation rates while maintaining sufficient affinity to target [144]. These methods offer the ability to tune binding affinities and kinetic responses of antibodies such that they can be tailored for a particular application. Additionally, there has been a recent emergence of the use of antibody fragments such as single-domain antibodies (sdAb), antigen-binding fragments (Fab), single chain variable fragments (scFv), and camelid nanobodies (VHH) [145], which can be readily produced via recombinant technologies to make antibodies cheaper and more reproducible [141]. The reduced size and complexity of

these fragments also make them more stable for long-term use in sensing systems [142, 143] and allow them to be compatible with transduction schemes such as those utilized in field-effect transistors [146]. While these innovations have yet to be demonstrated in devices for wearable biosensing, they provide a promising area of future development for continuous immunosensing of analytes in sweat and ISF.

3.2.2 Oligonucleotides (Aptamers)

Aptamers are short oligonucleotide sequences of single-stranded DNA or RNA that can be selected and synthetically produced to specifically bind a broad range of target analytes ranging from small molecules [147], to peptide hormones [148], and even whole cells via the binding of specific cell surface proteins [149]. Aptamers, along with complementary oligonucleotides for detecting specific genetic sequences, are attractive options for biosensor applications given their relatively simple synthesis and cost-effective production on large scales compared to antibodies [142, 143]. Sequences that can sensitively and selectively bind a given target analyte are identified through an in vitro method known as systematic evolution of ligands by exponential enrichment (SELEX) [150, 151]. Through this process, a random library of 10^{12}–10^{15} different sequences is exposed to the intended target and taken through several rounds of selection and counter-selection to identify sequences that exhibit the highest affinity for the target while ensuring minimal cross-reactivity with close analogues [152]. Once an appropriate sequence has been identified, it can be produced in large-scale quantities via solid-phase synthesis at a low cost with minimal batch-to-batch variability.

Most selected aptamers are ~30–70 nucleotides long and take on unique secondary structures based on intramolecular complementary base pairing, a process that is highly predictable and enables precise molecular modeling [153]. Most aptamer biosensing takes advantage of the fact that aptamers are flexible and can undergo large conformational changes upon target binding. This allows the interaction to be detected and transduced in a reagent-free manner by various optical and electrochemical techniques, typically facilitated by the covalent attachment of optical tags or redox reporters. Aptamers can also be modified with a variety of linkage chemistries such that they can be readily conjugated to sensing interfaces for analyte binding and detection [154]. The small size of aptamers compared to other biorecognition elements allows them to be compatible with most transduction schemes and can be readily re-engineered to meet the requirements of most applications [143].

While aptamers offer benefits in terms of ease of production and simplicity in device integration, there have been concerns regarding the susceptibility of aptamers to enzymatic degradation. Attempts have been made to utilize peptide nucleic acids (PNA) to increase stability by replacing the sugar-phosphate backbone with peptide linkages [155]; however, this still leaves aptamers susceptible to peptidase cleavage and degradation. Other approaches have focused on using left-handed DNA or RNA aptamers, which can still demonstrate affinity for target but are capable of evading

enzymatic degradation due to the stereospecificity of nucleases for naturally occurring right-handed DNA. L-DNA aptamers have shown superior stability in complex biological media when incorporated into electrochemical platforms [156] and thus will likely be a prerequisite for long-term use of aptamer-based sensors.

Another current limitation of aptamer-based sensors is the limited range of affinities that aptamers typically display for their target ($K_D \sim 10^{-5}$–10^{-9} M), precluding many applications measuring low-abundance analytes in the pM to nM range. Additionally, the selectivity of aptamer biorecognition elements for their targets can be a concern in some cases given that aptamers are typically less selective than their antibody counterparts [142, 143]. These issues are especially pressing in the selection of aptamers for small hydrophobic molecules that share many close analogues, such as those for steroid hormones (e.g., cortisol) [157]. Recent progress in advanced SELEX protocols, including selection under specialized conditions (e.g., solutes, solvents, pH, and temperature), has enabled the identification of more sensitive and selective sequences for analyte binding [147, 158]. Other approaches to increasing aptamer binding affinity have focused on incorporating chemical modifications [153] and introducing non-native bases during the SELEX process [159, 160], which have successfully led to the generation of aptamers with K_D's in the 10^{-10}–10^{-12} range. While there is still a trade-off that must be established between increased affinity and prolonged dissociation rates, these innovations offer promising tools for tailoring aptamer sequences to specific applications for robust biorecognition.

3.2.3 Others

While often not seen as traditional biorecognition elements, the following affinity-based entities have utility in continuous wearable biosensing and offer potential alternatives to antibodies and aptamers for certain applications. We briefly detail the specific benefits and drawbacks of *ionophores, peptide-based biorecognition elements,* and *molecularly imprinted polymers* and the advances recently demonstrated for each.

Ionophores are molecules typically found in the cell membranes of certain microbes that are capable of reversible binding with a specific ion and thus are often used to develop ion-selective membranes [161]. A pertinent example includes the use of valinomycin as a selective recognition element for K^+ in membrane cocktails for ion-selective electrodes (ISEs), which have been repeatedly shown to be capable of continuously measuring levels in sweat via potentiometric analysis [47, 49]. Despite being validated in several wearable sweat-sensing demonstrations, devices incorporating ionophores into miniaturized ISE formats still face challenges of signal drift, calibration, and stability over long durations due to lack of robust integration schemes and current demonstrations utilize materials that may not be biocompatible for intradermal ISF monitoring applications [162]. Additionally, the availability of specific ionophores that exhibit minimal affinity for other ions may be limited among naturally occurring ionophores. However, recent advances in

synthetic ionophore development [161] and in materials optimization for ionophore integration into ion-selective membranes have led to significant improvements in these areas. Progress has also been made in preparing stable solid contacts of ion-selective membranes with electrode materials which may result in more accurate and versatile use of ionophores in future wearable biosensing applications [163].

Peptide-based biorecognition elements (PBREs) are small sequences of amino acids (i.e., typically <50 AAs) that can be selected to selectively bind a broad range of target analytes, similar to aptamers. Sequences that have high affinity for a given target are typically screened and identified via biopanning using combinatorial phage display libraries [164]. Unlike their antibody counterparts, PBREs do not rely on animal immunogenicity for generation and can be easily synthesized for reproducible production [165]. Recent developments have focused on in silico methods of evolving higher affinity PBREs using computational modeling of peptide–analyte interactions [166]. However, these methods are currently complex and highly involved; thus, future efforts will need to focus on more streamlined identification of high-performing PBREs suitable for biosensing applications. Of note, naturally occurring proteins have also been demonstrated as affinity-based recognition elements in biosensing applications [167], illustrating the compatibility of non-antibody PBREs with transduction schemes suitable for wearable biosensing.

Molecularly imprinted polymers (MIPs) are an emerging class of synthetic biorecognition elements that use the target molecule of interest as a template during polymerization to form a selective affinity-based layer that can be used for optical or electrochemical analyte detection [168]. MIPs are an attractive option for wearable biosensing given that they are cheap, are easy to produce, and can typically be generated in situ during sensor fabrication for seamless integration. This is commonly achieved via electropolymerization of monomers such as o-phenylenediamine (OPD) [169] and 3-aminophenylboronic acid (APBA) [71, 170, 171], or by UV irradiation of compounds such as methacrylic acid (MAA) [172], among many others. Once polymerization is complete, the template molecule can be removed via a washing protocol to condition the MIP for subsequent analyte detection in the desired biofluid. Apparent affinities for MIP typically are in the millimolar to micromolar range ($K_D \sim 10^{-3}$–10^{-6}) [173], making it difficult to detect low-abundance analytes. Furthermore, MIPs are highly heterogeneous and deformable recognition elements, which may result in lack of specificity and loss of analyte-binding capacity over time. Recent work has focused on the incorporation of metal- and covalent-organic frameworks in order to improve the mechanical and chemical stability of MIPs such that they can achieve higher affinity and selectivity for their target [174]. Other advances have included the addition of nanomaterials such as gold nanoparticles [169], silver nanowires [171], and redox nanoreporters [71] for more sensitive analyte detection. There has also been significant progress in MIPs for protein recognition applications, a topic that will be treated in a separate chapter of this book. Despite these innovations, the regeneration of MIPs still remains an issue for many systems, typically requiring extensive wash steps [171, 172], and more research is needed regarding in situ regeneration methods in order for MIPs to see widespread adoption in continuous wearable devices [71].

4 Transduction Mechanisms Suitable for Wearable Devices

With a suitable biorecognition element selected for a given target analyte, careful consideration must be given to the transduction mechanism used to detect, amplify, and convert the biorecognition event into a quantifiable signal for determination of analyte concentration. In order for a biosensor to have utility in continuous wearable monitoring, it must be reagent-free, self-contained, and capable of repeated quantification with minimal user involvement for real-time in situ analysis. As a result, methods requiring washing/regeneration steps, prolonged incubations, or the external addition of exogenous reactants (e.g., secondary antibody and chromogenic substrate) are not well suited for wearable devices.

Furthermore, the sensing modality must be compatible with the challenging conditions that may be experienced with a skin-interfaced system, which include excessive motion, moisture, and mechanical deformations, and must meet the criteria of being small, compact, and not overly complex such that it can be crafted into a feasibly wearable device. Thermal/calorimetric transduction mechanisms are largely unsuitable for wearable applications given exposure to highly variable ambient conditions and fluctuating skin temperatures. Gravimetric and piezoelectric methods, exemplified by quartz crystal microbalances (QCM), are likely too sensitive and are susceptible to fouling and motion artifacts from limb movement, though they may have utility in self-powered biosensing applications [175]. Some more specialized transduction techniques, like surface plasmon resonance (SPR), are currently too cumbersome to incorporate into a device that could be applied to the skin for continuous use. It appears that basic optical and electrochemical transduction mechanisms are the most suitable options for continuous skin-interfaced biosensing, which is supported by the overwhelming body of literature focused on these approaches for wearable demonstrations [1, 7–9, 109].

When choosing an appropriate transduction mechanism from the various optical and electrochemical methods available, another consideration is the compatibility of the technique with the biorecognition element that will be used. Some biorecognition elements can be easily conjugated with optical or redox-active tags to help facilitate specific signal transduction, while other sensing schemes may be capable of "label-free" operation without tags. Even though a biorecognition element may bind or interact with an analyte with sufficient affinity, it may not generate a signal that is readily transducible for certain systems. An example of this would be an enzymatic reaction that does not involve electron transfer (i.e., not an oxidoreductase) or does not create a product that can be specifically detected via optical or electrochemical means. Another example would be an aptamer that has sufficient affinity for its target but does not undergo a large enough conformational change to elicit a sensor response for common transduction techniques [176]. Finally, one must consider whether the transduction mechanism affects the integrity of the biorecognition element, as seen in the effects of certain electrochemical techniques on charged aptamers and proteins due to the applied electric fields [177–179].

All of the aforementioned considerations contribute to the overall sensitivity and specificity of a sensing scheme complete with compatible biorecognition and transducing elements. Sensitivity is defined as the ratio of change in sensor response, S, to the change in concentration of target, T, expressed as $\Delta S/\Delta[T]$, and is a function of the signal generated due to biorecognition, the amplification of that signal in a given sensing scheme, and how well a certain transduction mechanism can quantify that particular signal. The specificity of a biosensor is largely determined by the selectivity of the biorecognition element; however, based on the transduction mechanism used, interferences and non-specific binding to sensing interfaces may lead to false positives that can reduce specific analyte detection. All of these factors contribute to a sensor's limit of detection (LOD), which is commonly taken to be the concentration at which the signal generated is greater than 3 standard deviations above the average signal of a suitable blank [180].

Below we detail these considerations for the major transduction mechanisms used in optical and electrochemical biosensing. In doing so, we highlight the benefits and limitations of each and the recent demonstrations that present innovative solutions for robust signal transduction in continuous wearable biosensing systems.

4.1 Optical Biosensing at the Skin Interface

Optical transduction relies on the transmission and detection of light to indicate changes in analyte concentration. The two most common optical techniques are colorimetry, which measures changes in the absorbance of visible light, and fluorescent or phosphorescent detection, which relies on changes in emission upon excitation of a sample with a specific light source. These techniques are illustrated in Fig. 5, with exemplary biorecognition elements and transduction schemes shown for each.

Many optical biosensing methods can be readily integrated into skin-interfaced systems as there are no complicated electrode designs or elaborate electronics involved and data can easily be collected via a cell phone camera or handheld reader. However, this makes it difficult for high-frequency monitoring and may necessitate on-chip/wearable readers for continuous operation, which, along with excitation light sources required for fluorescent/phosphorescent detection, can complicate miniaturized device design. Most demonstrations of wearable optical biosensors are skin surface-based and are subject to variable ambient lighting conditions, which can confound measurement accuracy and precision. Advances in optical fibers [100, 101, 181, 182] and implantable hydrogels [105, 106] may pose options for intradermal ISF sensing; however, these approaches will necessarily be subject to background interferences present in dermal and subcutaneous tissues. Overall, optical transduction may be a feasible option for some applications but requires consideration of the specific benefits and challenges detailed in the following sections.

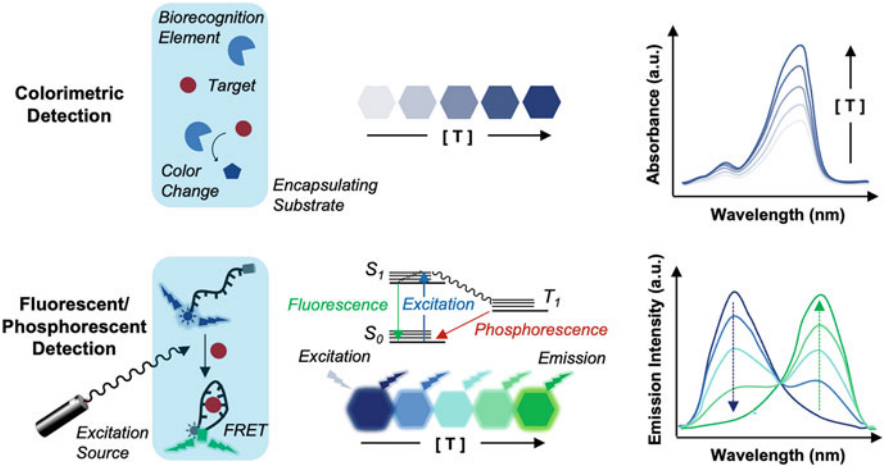

Fig. 5 Optical biosensing transduction schemes including colorimetric detection via changes in color intensity upon interaction of biorecognition elements with target analyte and fluorescent detection relying on a change in fluorescence emission with varying target analyte concentrations in response to an excitation light source. Here, a ratiometric FRET-based fluorescent detection scheme is illustrated, where the emission becomes increasingly intense at one wavelength while becoming less intense at the original fluorescent wavelength in response to increasing analyte

4.1.1 Colorimetric

Colorimetric analysis relies on visible changes in color to detect the presence of a particular analyte and quantify its concentration in a given sample. This method is commonly seen in simple qualitative point-of-care devices, such as lateral flow assays (LFAs) for influenza and at-home pregnancy tests, where a positive result is evident to the naked eye based on the observed color [183]. In quantitative laboratory analysis, colorimetry typically involves measuring the absorbance of light at different wavelengths via spectrophotometry and discerning analyte concentrations according to the Beer–Lambert law [184]. Since spectrophotometers are largely infeasible for wearable devices, mobile readers and cell phone cameras are often utilized instead for cheap and simple analysis. As a result, RGB [51], HSV [185], or CIE 1931 [186] color space values from the images captured by digital camera arrays are commonly used as proxies for absorption spectra in the quantification of target analyte concentrations [187].

Color change of a sample can be elicited via a variety of transduction schemes that may lead to sensitive and specific detection of a target analyte given an appropriate biorecognition element. One example is the direct participation of an enzymatic product in a chemiluminescent reaction, as seen with specific oxidases that produce H_2O_2 upon reaction with target analyte, which can oxidize luminol in the presence of a metal catalyst [188]. Alternatively, an enzyme may produce a chemical species that can participate in a secondary enzymatic reaction to contribute

to a color change. This is most commonly achieved by coupling the aforementioned oxidase reactions to those of horseradish peroxidase (HRP), which, in the presence of the oxidase-produced H_2O_2, can oxidize and change the color of common chromogenic substrates such as 3,3′,5,5′-tetramethylbenzidine (TMB) [189], o-dianisidine [190], and potassium iodine [51]. Finally, an enzymatic reaction can catalyze a product that results in a local pH change, which can be quantified by the color of a pH-sensitive dye or material [185, 186], although for sweat sensing this method requires correction for natural pH fluctuations, compromising accuracy.

Nonenzymatic methods for wearable colorimetric biosensing are less common but may include transduction schemes such as those utilizing gold nanoparticles (AuNPs) conjugated with biorecognition elements, such as antibodies and aptamers. AuNPs exhibit unique optical properties based on local surface plasmon resonance (LSPR) effects, appearing red when dispersed in solution. When these particles aggregate, the LSPR changes and the solution resultingly becomes dark purple [191]. Reversible binding of analytes to affinity-based biorecognition elements decorated on the surface of these particles can modulate interparticle distance and thus can create a concentration-dependent colorimetric response [192–194], which may have utility in some wearable applications.

Colorimetric transduction is most feasibly executed at the skin surface and is thus a well-suited option for on-demand sweat sensing. The Rogers Research Group has published extensively on the wearable colorimetric sensing of sweat using aforementioned transduction schemes, pre-incorporating the necessary reagents for enzymatic detection into reaction chambers of eloquently designed microfluidic devices [51, 55, 195, 196]. Colorimetric analysis of ISF is also possible; however, it typically requires microneedle-based extraction for ex vivo measurements at the surface of the skin [185, 189, 197]. For both sweat and extracted ISF, in situ analysis using cell phones may be subject to error based on differences in camera sensor arrays and variable ambient lighting; however, recent advances have shown reliable measurement of analytes in various conditions by incorporating reference color patches to overcome these challenges [55, 196]. Currently, most demonstrations leveraging wearable colorimetric biosensing require on-board incorporation of regents, such as chromogenic substrates for HRP [51, 185, 190, 196, 197]. While this approach has been shown to achieve short-term semi-continuous quantification, it is ultimately limited by the amount of reagent that can be feasibly incorporated into the device. Thus, while these devices may be useful for short-term sensing over several hours, more long-term longitudinal monitoring is likely unfeasible with most colorimetric modalities.

4.1.2 Fluorescence/Phosphorescence

Fluorescent and phosphorescent detection primarily differ from colorimetry in the fact that they require a specific excitation light source in order to observe a response, a design criterion that makes these modalities far less common for wearable biosensing. Fluorescence is the process by which certain molecules can absorb

light to result in an excited singlet state and reemit light at a different wavelength as the molecule undergoes vibrational relaxation and photon emission upon return to its ground state. Phosphorescence also relies on the promotion of electrons into orbitals of higher energy; however, a change in electron spin forbids immediate relaxation and thus the molecule must proceed through a triplet state, resulting in much longer emission lifetimes (ms to mins) compared to those for fluorescence (ns to μs). In both fluorescence and phosphorescence, the light emitted is typically of lower energy due to non-radiative losses and is thus of a longer wavelength resulting in a deviation between excitation and emission spectra known as Stokes shift. Based on these fundamental aspects, transduction using these two phenomena may rely on changes in emission intensity, changes in emission lifetime, or changes in emission spectra [198].

The additional complexities of fluorescent and phosphorescent transduction, such as the requirement of an excitation source, currently complicate device development for wearable monitoring and, as a result, there are far fewer demonstrations in the literature detailing devices that are capable of continuous skin-interfaced biosensing using these approaches. Kim et al. recently demonstrated a fluorescent-based microfluidic sweat-sensing device for glucose and ascorbic acid using an HRP-coupled enzymatic detection scheme similar to those for colorimetric analysis but instead using a substrate that can undergo fluorescence once reduced by HRP [199], which faces the same limitations as those seen for colorimetric devices. The only other approach that has shown proven results in vivo is that of the Senseonics Eversense implantable continuous glucose monitor [106], which achieves excitation and fluorescent detection in an integrated hydrogel capsule that can be implanted in the dermis for long-term sensing up to 90 days. This device leverages hydrogel-conjugated boronic acid derivatives that can selectively bind glucose to disrupt photoinduced electron transfer within the matrix, thus resulting in a concentration-dependent increase in fluorescence from incorporated polyaromatic cyclic hydrocarbons [105, 200]. This approach has also been shown to be compatible with molecular imprinting techniques and other fluorescent species, such as carbon quantum dots, which can be used to tune optical properties and improve sensitivity/specificity [201]. As for phosphorescent detection, an emerging oxygen-responsive phosphorescent hydrogel [202] has been recently leveraged to detect local O_2 depletion from GOx to modulate emission lifetime for continuous glucose quantification [203].

Other fluorescent sensing schemes show promise for continuous wearable biosensing; however, they are less proven in practice and will need to overcome considerable technical challenges before adoption into feasibly deployable devices. Many biorecognition elements can be easily conjugated with fluorescent tags and quenchers such that fluorescence is modulated upon analyte binding [204]. This has been demonstrated with aptamer-functionalized microneedles for in vivo glucose measurements; however, the specific transduction scheme lacked the ability for continuous in situ monitoring [98]. Recent attempts have been made to incorporate a similar aptamer-based molecular beacon assay onto an optical fiber device [182]; however, this approach will require rigorous material optimization before it is a

feasible option for insertion into ISF continuous operation. Such schemes may also be compatible with Förster resonance energy transfer (FRET) detection, which may offer a ratiometric and calibration-free solution for more sensitive and accurate measurements as emission is shifted from a donor fluorophore at one wavelength to an acceptor fluorophore at another wavelength based on analyte binding in a concentration-dependent manner (See Fig. 5) [205].

Overall, fluorescent and phosphorescent detection offer sensitive and versatile transduction schemes with the potential to be leveraged in wearable biosensing platforms if careful consideration is given to the limitations of such systems. Other than concerns of increased device complexity due to the need for an excitation source, issues with light scattering in the body, autofluorescence of tissues/biofluids, and photobleaching/photodegradation of fluorescent tags all may reduce the signal-to-noise ratio and reduce sensing performance [198]. However, with appropriate fluorophore selection, optimized excitation/emission waveguiding, proper light filtering, and robust integration schemes, these transduction mechanisms show promise for achieving long-term, skin-interfaced continuous biosensing for analytes beyond glucose.

4.2 Electrochemical Transduction

Compared to optical transduction techniques, electrochemical analysis is currently better suited for high-frequency continuous monitoring in wearable devices as biorecognition events are directly converted into electrical signals that can be easily processed via integrated circuits and on-board electronics. These systems can be easily miniaturized and interfaced with the skin such that electrodes are seamlessly coupled to biofluids at the skin surface or intradermally for on-demand in situ quantification. Complete with adequate powering and wireless communication, fully integrated wearable devices can be crafted without the need for external readers or user manipulation.

Electrochemical biosensing inevitably involves the immobilization or localization of biorecognition elements near a sensing electrode. This may be achieved via encapsulation near the surface, often seen in enzymatic systems, or through the formation of mixed self-assembled monolayers containing both biorecognition and passivating elements at the electrode surface. A major consideration for electrochemical transduction is the effect of the technique on the integrity of the sensing interface and the biorecognition element used. For example, the applied electric fields used in voltammetric techniques can potentially disrupt self-assembled monolayers on electrode surfaces, especially for negatively charged biorecognition elements such as aptamers [177, 179, 206]. Other considerations include the presence of competing redox processes at the electrode surface, such as the reduction of oxygen, and the effects of electric double layer charging upon the application of a voltage, both of which can obscure and overwhelm the faradaic signals that are being measured [207]. Electrochemical biosensing may also involve the use of redox

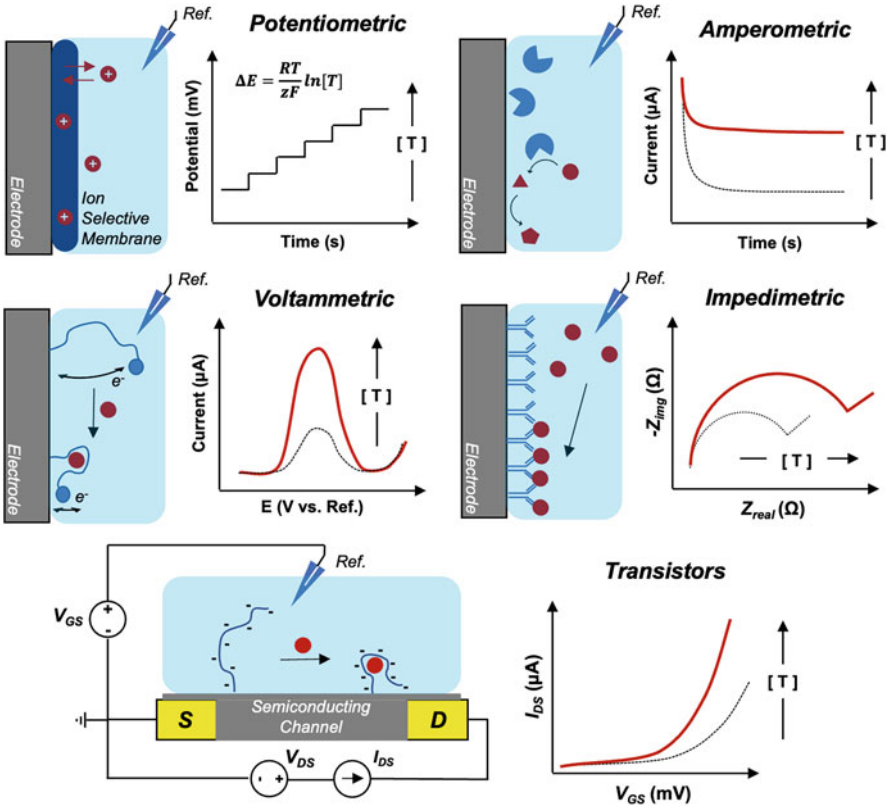

Fig. 6 Leading electrochemical transduction mechanisms for wearable biosensing with examples of suitable biorecognition elements for analyte detection

reporters, such as methylene blue, which can be conjugated to a biosensing element for sensitive and specific detection of analyte and thus care must be taken in choosing an appropriate tag in these instances [208, 209].

Figure 6 provides a summary of the leading electrochemical techniques for wearable biosensing and provides examples of transduction schemes that may be used with each based on different biorecognition elements. Below we detail these methods and highlight their utilization in various schemes for continuous wearable biosensing, emphasizing the benefits and challenges associated with each.

4.2.1 Potentiometry

The most rudimentary electrochemical technique available is potentiometry, which involves passive measurement of the open circuit electrochemical potential at a given interface compared to a known, chemically stable reference potential (e.g.,

Ag/AgCl in a solution of constant Cl^- concentration). This technique is most commonly seen in ion-selective electrodes (ISEs), where an ion-sensitive membrane at the electrode surface results in a concentration-dependent change in electrode potential due to the specific binding of target ions to ionophores embedded in the membrane. The change in the open circuit electrode potential, E, measured against a stable reference electrode in response to target ion, X, is ideally governed by the Nernst equation:

$$E = E_0 + \frac{RT}{z_i F} \ln\left[\frac{X}{X_0}\right]$$

where E_0 is the open circuit potential (vs. ref.) measured at a detection limit of $[X_0]$, R is the universal gas constant, T is the temperature in Kelvin, z_i is the charge of the ion for which the membrane is selective, and F is Faraday's constant. Beyond ISEs, this technique has also been applied to enzymatic biorecognition schemes. Recently, the detection of urea in sweat was achieved based on the fact that its decomposition via urease results in a local change in pH which can be detected potentiometrically using electrodes coated with pH-sensitive polymers such as polyaniline [70].

A significant benefit of potentiometric sensing is that it is passive, which effectively reduces sensor power requirements and may lead to longer sensor lifetimes due to the lack of voltage-induced degradation. The maximum sensitivity obtainable for these sensors, however, is limited by the ideal Nernstian response, which is ~59 mV/z_i for a sensor at room temperature. Typically, polymeric coatings such as Nafion™ and polyvinyl chloride (PVC) are used to exclude inferences and ensure specificity [70]; however, the nonidealities of these materials can lead to deviations from a Nernstian response and lower sensor performance. Another key consideration for potentiometric sensors is that they must be used in conjugation with a stable reference electrode in order to make precise measurements. Numerous wearable devices have implemented ISEs for potentiometric analysis of electrolytes, and it is likely they will be a mainstay of multiplexed sweat-sensing platforms. Other applications of potentiometry are likely limited, and more advanced electrochemical techniques will be needed for the measurement of most analytes.

4.2.2 Voltammetric Techniques

In contrast to potentiometry, voltammetric methods involve the application of a potential or a range of potentials to an electrode in order to measure the current response. The simplest voltammetric technique is chronoamperometry, a process by which a sufficient potential necessary to oxidize or reduce the species of interest is held for a given duration and the current is measured as a function of time. Chronoamperometry is the most commonly employed technique for enzymatic biosensing and is well suited for this application given that the current measured at a specific time is proportional to the reaction rate which, as mentioned

previously, is proportional to analyte concentration [115]. The current measured in chronoamperometry, however, is also susceptible to contributions from electroactive interferences in biofluids, such as ascorbic acid, which can confound sensor calibrations. Common approaches to this problem include the use of redox mediators, such as Prussian blue, to lower the overpotential necessary to oxidize/reduce enzymatic products [118] or the use of additional layers such as layer-by-layer [120, 121] or polymeric encapsulation [115] approaches to exclude interferences from the electrode surface. Beyond enzymatic sensors, chronoamperometry has also been demonstrated for use with methylene blue-labeled aptamers for sub-second resolved measurements in vivo [210] and may be useful for high-frequency monitoring applications.

More advanced voltammetric techniques involve measuring current as a function of the applied potential in response to a particular potential waveform. Common techniques include linear sweep methods, such as cyclic voltammetry (CV) [211], and pulse-based methods, such as square wave voltammetry (SWV), differential pulse voltammetry (DPV), and AC voltammetry (ACV) [207]. SWV is the most sensitive of voltammetric techniques as it effectively reduces the capacitive contributions to the measured current. These techniques not only serve as a means of quantifying target analytes but also serve as powerful tools in characterizing a particular biosensing system for optimization prior to use. While voltammetric techniques may offer sensitive quantification in various electrochemical transduction schemes, one must carefully consider the presence of competitive faradaic processes in a given sensing environment, such as those involved in the oxygen reduction reaction (ORR), and their contributions must be managed accordingly for accurate voltammetric sensing [212].

Some of the most promising examples of biosensing that have tremendous potential to be leveraged into platforms for continuous wearable monitoring include those utilizing voltammetry for electrochemical aptamer-based (EAB) sensing [213]. This modality relies on the formation of a mixed monolayer of redox-tagged aptamers and passivating moieties, such as 6-mercapto-1-hexanol (MCH), to create a sensing interface that can mitigate non-specific binding and interferences while specifically reporting target concentrations via binding-induced conformational changes in the aptamer. These changes can resultingly modulate electron transfer between the redox tag (e.g., methylene blue) and the electrode surface (e.g., gold), which can be readily measured as a change in current using SWV [176]. The Plaxco group and others have published over a dozen demonstrations of these sensors successfully detecting a broad range of target analytes in vivo when placed in the jugular veins of live rats [214–217]. These sensors are able to sensitively and specifically quantify target analytes in these challenging in vivo environments and do so continuously with high temporal resolution all the while achievable with ultrasimple fabrication and integration schemes. Recently, there have been demonstrations of EAB sensing in the ISF of rats [99, 218] with parallel efforts toward the first demonstrations in human subjects [219]. While there are certainly translational challenges that must be overcome, such as multi-day sensor longevity in complex media [177, 206], this specific biorecognition and transduction pairing shows great

promise for a versatile platform that can be adapted to many applications for continuous wearable monitoring of sweat or ISF [217].

4.2.3 Impedimetric Techniques

Electrochemical impedance spectroscopy (EIS) techniques are attractive for biosensing applications due to their non-destructive character and high degree of measurement sensitivity [220]. The basic principle of EIS relies on the application of a small sinusoidal perturbation voltage in the linear range of response (typically around 5–10 mV in amplitude) in order to measure the resulting current response over a range of frequencies [221]. Measurements can be done at the open circuit potential of the system but also under forced oxidation or reduction conditions. Assuming a time-invariant system, impedance is derived from the measured current and applied perturbation voltage via Ohm's law and can be expressed as a complex function via Euler's relationship such that:

$$Z(j\omega) \equiv \frac{E(j\omega)}{I(j\omega)} = \frac{E_0 \sin(\omega t)}{I_0 \sin(\omega t + \phi)} = \mid Z \mid e^{j\phi}$$

where E is the applied sinusoidal perturbation voltage with amplitude E_0, I is the resulting measured current with amplitude I_0 and phase shift ϕ, j is the imaginary unit, and Z is the complex impedance of the system with magnitude $|Z|$ and phase ϕ, both of which are functions of angular frequency, ω, where $\omega = 2\pi f$ and f is the frequency in Hz. Based on the analysis of the impedance in the frequency domain, equivalent circuit models can be created to isolate certain aspects contributing to a system's impedance, such as the charge transfer resistance (R_{ct}) and interfacial capacitance of the electric double layer (C_{EDL}).

Impedimetric techniques can be categorized into two broad classes of analysis: faradic and non-faradaic impedance spectroscopy. Faradaic analysis typically utilizes solution-phase redox couples such as $[Fe(CN)_6]^{3-}/[Fe(CN)_6]^{4-}$ to measure changes in charge transfer resistance, which largely precludes wearable applications due to the need for reagent addition. As a result, most wearable demonstrations have focused on non-faradaic measurements based on changes in interfacial capacitance [11, 139, 164, 222, 223]. However, these methods are highly sensitive and are subject to poor specificity for target as non-specific binding events can lead to changes in capacitance not associated with change in target analyte concentrations. Recent advances in this approach have focused on incorporating nanoporous materials [222] and room temperature ionic liquids [139] at the sensing interface; however, more work is needed to improve specificity in these systems for robust wearable biosensing. Downs et al. recently showed the ability of methylene blue-tagged aptamers to undergo sensitive faradaic impedimetric analysis without the need for solution-phase redox reporters by monitoring changes in the phase of the impedance [224], an approach that is more specific and better equipped for wearable biosensing.

EIS ultimately is a powerful tool for system characterization; however, significant work is needed in order for this transduction scheme to see broad adoption for continuous monitoring in biofluids with either label-free or redox-tagged approaches. For example, EIS is inherently very sensitive to fouling of the sensor surface, which can cause measurement inaccuracy due to non-specific changes in measured impedance not resulting from analyte biorecognition. For a more in-depth analysis of these techniques and their potential use, we refer to prior reviews on EIS fundamentals and applications [220, 221, 225].

4.2.4 Transistors

Field-effect transistors (FET) have long been seen as an attractive transduction option for wearable biosensors due to the label and reagent-free nature of the modality and the ease of robust, miniaturized sensor fabrication. Bergveld introduced the concept of the first ion-sensitive FET (ISFET) in 1970 [226], which was shortly adapted to the realm of biosensing in 1980 by Caras and Janata through the addition of an enzyme biorecognition layer to enable detection of penicillin [227]. Since then, the concept has been further extended to include conjugation of antibodies, DNA receptors, and other enzymes to this architecture, often referred to as bioFETs, for specific detection and quantification of various analytes in biologically relevant media.

Transduction of specific biomolecular events is typically achieved by conjugating biorecognition elements to the semiconducting channel spanning the drain and source of a device possessing an architecture similar to a metal-oxide semiconductor field-effect transistor (MOSFET). However, instead of a metal gate, the bioFET is electrochemically gated by the solution to be tested via a reference electrode [228]. As the biorecognition event occurs, the surface charge at the gate changes, thus altering the gate voltage and causing a change in the current between source and drain electrodes [229].The sensor response is gathered by measuring this change in drain-to-source current (I_{DS}) upon changes in analyte concentration under optimized biasing drain-to-source (V_{DS}) and gate-to-source voltages (V_{GS}). Calibration curves are typically constructed by determining the most sensitive change in I_{DS} based on different biasing voltages derived from the transfer curves obtained from sweeping V_{GS} over a certain range. Recent efforts have achieved more reproducible sensor responses by dividing the absolute change in I_{DS} by the slope of the transfer curve (i.e., dI_{DS}/dV_{GS}), also known as the transconductance, at the most sensitive V_{GS} biasing point in order to mitigate batch-to-batch variations [230].

Common materials used for the semiconducting channels of FETs include silicon dioxide (SiO_2), indium tin oxide (ITO), and other metal oxides. More recent advances try to avoid thick insulating layers with high capacitance by utilizing nanomaterials such as silicon nanoribbons, silver nanowires, and 2D structures, such as graphene and molybdenum sulfide (MoS_2), in order to achieve more sensitive detection [231, 232]. Particularly for graphene-based transistors, recent progress will be described in a separate chapter of this book. Similar detection

schemes have also been achieved with organic electrochemical transistors (OECTs) by utilizing electroconductive polymers, such as PEDOT:PSS, as the semiconducting channel, relying on charge injection into the material to modulate the gate voltage as opposed to charge accumulation at the surface for FETs [172, 233]. All of these materials are compatible with microscale fabrication techniques on flexible substrates, such as polyimide, parylene, and PET, making these devices suitable for integration into feasible wearable platforms [234].

Since field-effect transistors rely on variations in surface charge at the semiconducting channel, one challenge that is largely unique to this modality is that, in order for biorecognition events to be transduced, they occur within the Debye length of the channel surface such that surface charge is perturbed in the presence of analyte [234]. This renders this modality virtually incompatible for operation with larger biorecognition elements, such as antibodies, as antigen-binding sites often extend out from the surface far beyond the Debye length. Recent demonstrations with antibody fragments and nanobodies have aimed to overcome this issue with considerable success due to their drastically reduced size [146]. Some aptamer constructs may also extend beyond the Debye length and therefore rational design and reengineering of these sequences can be applied to ensure robust signaling using this transduction mechanism [235]. Other approaches will be discussed in the chapter on graphene-based transistors as biosensors.

While this modality is promising, there are some concerns with specificity, continuous operation, and long-term stability in complex biofluid media that currently limit widespread adoption. Though these sensors can be quite sensitive, changes in the local environment due to non-specific adsorption of proteins and other molecules to the semiconducting material can drastically change transfer curve characteristics and lead to inaccurate results. Recently, Wang et al. developed an integrated wearable FET sensing device for measurement of cortisol in sweat [236]. While these sensors showed low limits of detection, only single point on-body measurements were achieved due to issues with sensor regeneration and rapid degradation in biofluid. Considerable efforts to develop robust antifouling and regeneration strategies for this modality will be required to enable multi-day wearable biosensing, along with careful consideration of biorecognition element design with regard to the Debye length limitations.

5 Advances in Materials, Methods, and Interfaces for Integrated Wearable Devices

The following section briefly overviews several of the many integrative aspects that should be considered when bridging the components that constitute a complete device for a given application. Particular emphasis is placed on the recent advances in materials and methods that can contribute to the creation of robust sensing platforms for durable and reliable long-term wearable monitoring.

5.1 Materials

Materials science acts as the bridge between the different facets of biosensing, and it is thus critical that appropriately optimized materials are implemented both at the sensing interface and the skin interface to obtain sensitive, stable, conformable, and biocompatible devices that can continuously measure analytes over long durations via minimally invasive sweat or ISF access.

5.1.1 Sensing Interface

Choice of electrode material is a key consideration for electrochemical biosensors as it is important that an electrode can demonstrate sufficient conductivity and high electrochemical stability under the operation modes needed for transduction. Carbon electrodes are common in biosensing applications given that they are cheap to fabricate and have wide electrochemical potential windows [237]. Gold is also routinely used due to its inert nature and the ability to form self-assembled monolayers on the surface using thiolated moieties [238]. Recent advances in nanomaterials have expanded the options for highly sensitive transducing surfaces, as seen with carbon nanotubes, graphene, and organic-inorganic nanohybrid composite materials [239]. Additionally, the creation of porous and nanostructured surfaces, such as in nanoporous gold [191, 240] and metal oxides [222, 241], has been extensively shown to enhance the loading of biorecognition elements onto transducing surfaces to increase signal and response to analyte [242, 243].

Beyond the properties of the electrode material itself, the incorporation of surface modifications to the electrode surface is also important to ensure sensitive and specific detection. Electrochemical aptamer sensors, for example, typically rely on self-assembled monolayers on gold in order to both immobilize the biorecognition element and block the surface with passivating moieties, such as 6-mercapto-1-hexanol (MCH). As a result, the longevity of these sensors is highly dependent on overall monolayer stability. Recent advancements have focused on incorporating biomimetic zwitterionic monolayer moieties to reduce non-specific adsorption [244] and increasing lateral van der Waals interactions between adjacent monolayer molecules in efforts to increase monolayer stability and prolong operational lifetimes [177, 245]. It is likely that a combination of these two approaches will be necessary to mitigate fouling and monolayer desorption over multi-day timescales for continuous electrochemical aptamer sensing [177]. Other examples of surface modifications to enhance sensing interfaces are seen in the use of room temperature ionic liquids (RTILs), which have been shown to stabilize biorecognition elements for longer-term sensing [11, 139]; however, concerns over their reliable incorporation in many systems for continuous in situ analysis may limit their broad applicability.

5.1.2 Sensor Coatings/Membranes

Methods of membrane and polymeric encapsulation are well established for enzymatic sensors and are used to reduce interferences, incorporate redox mediators and nanomaterials, mitigate electrode biofouling, and improve overall performance in complex biological fluids [115, 123]. While this process will inevitably reduce enzyme activity, robust encapsulation is often readily achievable since enzymes only have to undergo minimal conformational changes to catalyze reactions and the reduced activity can be accounted for via the use of excess enzyme. Typically, polymers can be applied to these sensors as part of enzyme immobilization [122], through layer-by-layer approaches [120, 121], or by post hoc addition of a protective hydrogel matrix [246].

The process of applying polymeric coatings to other sensing modalities, such as electrochemical aptamer sensors, is more nuanced as the capacity for a biorecognition element to undergo analyte-dependent conformational change after in situ polymerization may be limited. Electrochemical aptamer sensors have been shown in the past to have superior operational stability when protected with prefabricated commercially available membranes, such as polysulfone [215]; however, incorporation of membranes in this manner is technically challenging for many deployable devices. Watkins et al. recently demonstrated that this modality could be made compatible with the application of a zwitterionic polysulfobetaine hydrogel to aptamer sensors fabricated on nanostructured gold, thereby preventing degradation in complex media on multi-day timescales [177]. It is clear that optimizing these protective strategies by incorporating robust anti-biofouling and biocompatible hydrogel and polymeric networks will ultimately be necessary for long-term monitoring using sensing modalities beyond enzymatic sensors.

5.1.3 Skin Interface

Devices interfacing with the skin surface must have a high degree of skin conformability and the materials utilized should ideally be selected to match the viscoelastic properties of the tissue for maximal wearability. Thus, optimal materials should demonstrate both flexibility and stretchability while maintaining the durability to stay intact during everyday movements and impacts to the device. Elastomers, such as polydimethylsiloxane (PDMS), polyurethane (PU), and polyimide (PI), are soft and stretchable polymers that can be tuned to be highly conformal for wearable applications [247]. Choi et al. recently demonstrated the compatible incorporation of both elastomeric and rigid materials into a wearable microfluidic device in order to mitigate damage from deformation all the while maintaining appropriate conformability for a sweat-based colorimetric platform [55]. Wearable electrochemical devices, on the other hand, often face the fundamental challenge that most conductive materials have poor stretchability; however, the design of serpentine and mesh-like structures, along with the use of compatible nanocomposite materials, has

allowed for electronics to be seamlessly incorporated into flexible substrates [8, 247].

Other considerations for materials selection at the skin–sensor interface include the choice of adhesive that can resist moisture and delamination from the skin during everyday movement. Traditional medical grade adhesives have relied largely on silicone and acrylate-based polymers, and recent advancements have focused on improving and expanding upon these approaches for more durable adhesion [248]. 3 M has traditionally been a leader in medical adhesive offerings and recently developed a material that can be worn for over 21 days [249], improving upon the 14-day rating of their current adhesives used in CGM devices. Regarding adhesive lifetime, there may be an upper limit to how long something can feasibly adhere to the skin given the 21–40 day turnover of the epidermis [14]. Ultimately, all materials used at the skin interface must be durable, biocompatible, and not cause skin irritation in order to be suitable for multi-day to multi-week wearable monitoring.

5.2 Methods

In addition to material selection, there are certain methodological aspects that also significantly contribute to biosensing performance. Below we detail some of the key considerations in device operation that are critical to achieving accurate and reliable concentrations measurement from wearable devices.

5.2.1 Power and Wireless Communication

Beyond colorimetric biosensing, all other biosensing modalities have power requirements in order to operate, which include powering the necessary light source and photodetector circuits for on-chip fluorometric/phosphorescent analysis or supplying power to an integrated circuit potentiostat [250] for electrochemical transduction. Additionally, on-board data processing and transmission to a cell phone or other portable reader also contribute to power consumption, and therefore, there is a trade-off between the amount of data acquired and how long a device can be powered for continuous monitoring. Power requirements are typically met using high-capacity lithium or silver oxide batteries directly integrated into the device; however, novel research is currently aimed at self-powered platforms [251] that can harvest energy from solar cells [252], biofuel cells [253], or motion-based piezoelectric devices [175]. For implantable devices, common approaches include charging via wireless inductive coupling through the skin, as seen with the Senseonics Eversense [106]. Ultimately, with power requirements of integrated circuits being minimized at a rapid pace, along with batteries achieving ever higher energy densities, device power is a critical design consideration though likely not a major bottleneck for achieving multi-day to multi-week monitoring.

In terms of data communication with external devices, such as cell phones, the 3 most common approaches for wearable platforms are based on radio-frequency transmission and include Bluetooth low energy (BLE) [236], radio-frequency identification (RFID) [254], and near-field communication (NFC) [106]. The benefit of NFC and RFID is that they do not require a power source; however, they are limited in their transmission range (i.e., ~0.2 and 5 m, respectively). BLE has the fastest and most long-range transmission (i.e., up to 100 m) at the cost of power consumption; however, today's technology requires very little energy. These technologies can be easily incorporated into on-board electronics for seamless transfer of sensor readouts directly to a mobile device for on-demand monitoring.

5.2.2 Calibration, Algorithms, and Operational Strategies

In order for a biosensing modality to accurately report measurements of a target analyte, the sensor response over the desired concentration range must be established in a manner that is highly predictable. Calibration can be done on an individual basis, either during fabrication or by the end user, or through batch calibration methods, where a representative sample is taken for each set of sensors. The most optimal circumstance is to have a system that is capable of "calibration-free" operation, where the response is related to some intrinsic aspect of the modality such that routine calibration is not needed. This is often seen in ratiometric sensor responses, as exemplified by many FRET-based detection schemes (see Fig. 5). Recently, electrochemical aptamer sensors were shown to be capable of calibration-free operation by exploiting the dependence of the modality on the SWV frequency used for voltammetric interrogation [255]. Other approaches, such as those seen for FET biosensing [230], aim to normalize the sensor response to variables that are largely dependent on inter-device differences in efforts to mitigate batch-to-batch variations.

Beyond calibration, device-specific algorithms and operational strategies can be utilized to maximize device performance by improving measurement accuracy and extending device lifetime. Pertinent examples include the compensation for ISF lag times in CGM devices [38] and the dynamic correction for temperature, salinity, and pH for sweat-based devices [66–71]. Recent efforts have also been geared toward modulating device operation to minimize the degradation of sensing elements while still maintaining adequate data collection, as recently demonstrated for electrochemical aptamer sensors through the optimization of voltammetric interrogation techniques [177, 211, 256]. Other algorithmic considerations include in situ regeneration methods, such as analyte-binding modulation via applied electric fields, a promising yet underdeveloped practice [257]. Ultimately, with machine learning and artificial intelligence becoming more advanced, corrective and adaptive algorithms will likely be critical components in realizing the full potential of wearable biosensing.

5.2.3 Integrative Aspects and Considerations

Putting it all together, wearable biosensing devices have been shown to take on many forms, such as in smart wristbands [47], epidermal tattoos [45, 56, 90], smart textiles [258, 259], wearable microfluidics [195], indwelling probes [94, 95], and implantable hydrogel capsules [105, 106, 200]. As mentioned previously, long-term wearable biosensing for sweat analysis will inevitably require integrated sweat stimulation and proper coupling to surface-mounted microfluidics [53], and thus, integrative schemes must be appropriately engineered to accommodate these features. As for ISF monitoring, intradermal approaches are likely to be the most fruitful, and therefore compensation for biofouling and the foreign body response is a necessity. Beyond the incorporation of biocompatible and protective antifouling materials, some devices have also incorporated the slow secretion of drugs, such as dexamethasone, to suppress the local immune response around the device [106].

Other integrative aspects include developing devices that can measure multiple analytes at once through multiplexed [47, 197] or multimodal [195, 199] operation. Multiplexed operation refers to the simultaneous measure of multiple analytes in one integrated device (i.e., glucose and K+) and may be carried out by one or more biosensing modalities while multimodal operation integrates two or more detection schemes into a single device (i.e., utilizing different biorecognition elements and/or transduction mechanisms). Recent demonstrations have also achieved the simultaneous measurement of an analyte and delivery of related substances in a single device [67, 196], an approach that may be leveraged for achieving operation toward closed-loop feedback systems [103]. Ultimately, more data and more features require more complex device design, and thus, careful consideration must be given to fabrication and sensor functionalization strategies to maximize overall device performance.

Finally, a vital consideration that is often overlooked in the development of wearable devices for clinical adoption is their ability to be sterilized prior to use. This may be less of a concern for surface-based sweat-sensing devices; however, for those disrupting the epidermal barrier to gain transdermal access to ISF, it is potentially one of the most critical aspects in determining whether a given sensing modality can be made viable or not. Commercial CGMs benefit from the ability of enzymes to be embedded in a matrix that can protect the recognition element from damage when utilizing common sterilization techniques such as ethylene oxide exposure and gamma irradiation [260–262]. Other biorecognition elements may not be capable of functioning with protective encapsulation and therefore may not withstand these necessarily harsh conditions. The disinfection of electrochemical aptamer sensors has recently been demonstrated with moderate success [263]; however, clinical grade sterilization has yet to be achieved for this modality or any other modality beyond amperometric enzymatic sensors. Those in the field will need to dedicate extensive research efforts toward this issue in order to ensure quality sterilization of devices without compromising analytical performance.

6 Major Hurdles and Promising Prospects: Can We Move Beyond Glucose?

Continuous glucose monitors have undoubtedly transformed diabetes management by providing patients with on-demand access to their glucose levels and enabling them to adjust their lifestyle and medication habits accordingly. After over 50 years of research and development efforts, combined with billions of dollars in investment, CGM technology is now widely trusted by doctors and patients alike as devices continue to evolve at a rapid pace. With over five million users worldwide and a growing interest for adoption in type 2 diabetes management [2, 264], these devices are poised to make an even larger impact in the years to come. Despite this growing success, the question remains: can we expect similar success for the continuous monitoring of other analytes in the near future?

As discussed throughout this chapter, the innovations attained for enzymatic biosensing are limited in their applicability to a broader range of clinically relevant analytes for which suitable enzymes are not available. While a handful of other target molecules (e.g., lactate, ethanol, urea) have been measured with repeated success in wearable platforms through the use of their respective oxidoreductases, more versatile biorecognition elements with compatible transduction schemes are needed to enable continuous measurement of other species. Electrochemical aptamer sensors hold tremendous promise as a biosensing platform, with over a dozen demonstrations thus far tracking a diverse set of molecular targets in the veins of live rats [217]. Recently, this success was extended to the measurement of analytes in rat interstitial fluid [99, 218], with parallel efforts geared toward the first demonstrations in human subjects [104]. Despite this progress, there are still significant challenges that must be addressed before these sensors can be successfully translated to long-term use in humans, especially those regarding sensitivity and sensor longevity.

While aptamers are relatively easy to produce and offer the highest versatility in terms of the target analytes they can be selected for, inadequate affinity may result in a lack of sufficiently sensitive measurements of low-abundance analytes. However, recent developments in the incorporation of non-native bases have led to the selection of aptamers that have affinities rivaling those of antibodies [143], as seen with many SOMAmers recently developed by SomaLogic [159]. While this approach inevitably increases equilibration times [135], the trade-off with affinity can be managed accordingly for a given application. Furthermore, significant research has gone into rationally engineering aptamers to maximize sensor response upon analyte binding for a given transduction mechanism [128, 265], thus contributing to the overall sensitivity of aptamer-based sensing platforms. FET-based aptamer sensing may also be a means of achieving ultra-sensitive analyte detection; however, issues with specificity, reversibility, and long-term operation of the modality need to be broadly addressed before widespread adoption is likely feasible [229, 234, 236].

One of the largest remaining bottlenecks for any biosensing modality is the longevity of its sensing elements in complex biofluids such as sweat and ISF.

Most continuous glucose monitors on the market are currently validated for 7–14 days of use before the device needs to be replaced [94, 95], an achievement that sets a high standard for the operational lifetimes of future sensors. Few demonstrations of other modalities have even come close to such long-term continuous operation in vitro, let alone in vivo. Recently, Watkins et al. demonstrated that electrochemical aptamer sensors could withstand >1 week of continuous operation in complex biofluids such as serum; however, several challenges must be addressed before achieving accurate, long-term, continuous use in vivo [177]. With additional research into enhancing monolayer stability and incorporating more robust anti-biofouling protection, this modality may be well poised for deployment in wearable devices for multi-day continuous sensing in the near future.

In this chapter, we have established a comprehensive framework for the development of integrated wearable biosensing platforms for compelling applications beyond glucose monitoring. Such a process requires critical evaluation of all necessary components including analyte access in minimally invasive biofluids, selection of appropriate biorecognition elements with compatible transduction schemes, and integration into fully formed devices with optimal materials and essential methodological considerations. While there are many promising demonstrations currently in the literature, it will take considerable multidisciplinary efforts to translate these technologies from the laboratory into the clinic and eventually onto patients as they go about their daily lives. Extensive validation through ample clinical trial data will be necessary for devices to be eventually leveraged in treatment decisions. The field of wearable biosensing is rapidly evolving, and wearable sensors beyond those for glucose are expected to play an increasingly important role in healthcare in the coming years. Ultimately, these devices have the potential to open the door to a new era of personalized medicine by enabling highly data-driven treatment decisions that can revolutionize patient care and improve overall outcomes.

References

1. Heikenfeld J, Jajack A, Rogers J, Gutruf P, Tian L, Pan T, Li R, Khine M, Kim J, Wang J, Kim J (2018) Wearable sensors: modalities, challenges, and prospects. Lab Chip 18:217–248. https://doi.org/10.1039/C7LC00914C
2. Janapala RN, Jayaraj JS, Fathima N, Kashif T, Usman N, Dasari A, Jahan N, Sachmechi I (2019) Continuous glucose monitoring versus self-monitoring of blood glucose in type 2 diabetes mellitus: a systematic review with meta-analysis. Cureus 11:e5634. https://doi.org/10.7759/cureus.5634
3. Linu D, Dhanashri B, Onkar S (2023) Continuous glucose monitoring systems market by component (sensors, transmitters and receivers), by demography (child population, adult population), by end user (Hospital and Clinics, Home Healthcare, Others): global opportunity analysis and industry forecast, 2021–2031. Allied Market Res
4. Malon RSP, Sadir S, Balakrishnan M, Córcoles EP (2014) Saliva-based biosensors: noninvasive monitoring tool for clinical diagnostics. Biomed Res Int 2014:962903. https://doi.org/10.1155/2014/962903

5. Yu L, Yang Z, An M (2019) Lab on the eye: a review of tear-based wearable devices for medical use and health management. Biosci Trends 13:308–313. https://doi.org/10.5582/bst.2019.01178
6. Heikenfeld J, Jajack A, Feldman B, Granger SW, Gaitonde S, Begtrup G, Katchman BA (2019) Accessing analytes in biofluids for peripheral biochemical monitoring. Nat Biotechnol 37:407–419. https://doi.org/10.1038/s41587-019-0040-3
7. Kim J, Campbell AS, de Ávila BE-F, Wang J (2019) Wearable biosensors for healthcare monitoring. Nat Biotechnol 37:389–406. https://doi.org/10.1038/s41587-019-0045-y
8. Yang Y, Gao W (2019) Wearable and flexible electronics for continuous molecular monitoring. Chem Soc Rev 48:1465–1491. https://doi.org/10.1039/C7CS00730B
9. Zhao J, Guo H, Li J, Bandodkar AJ, Rogers JA (2019) Body-interfaced chemical sensors for noninvasive monitoring and analysis of biofluids. TRECHEM 1:559–571. https://doi.org/10.1016/j.trechm.2019.07.001
10. Kovatchev B, Cobelli C (2016) Glucose variability: timing, risk analysis, and relationship to Hypoglycemia in diabetes. Diabetes Care 39:502–510. https://doi.org/10.2337/dc15-2035
11. Jagannath B, Lin K-C, Pali M, Sankhala D, Muthukumar S, Prasad S (2020) A sweat-based wearable enabling technology for real-time monitoring of IL-1β and CRP as potential markers for inflammatory bowel disease. Inflamm Bowel Dis 26:1533–1542. https://doi.org/10.1093/ibd/izaa191
12. Hirsch IB (2018) Introduction: history of glucose monitoring. American Diabetes Association
13. Danne T, Nimri R, Battelino T, Bergenstal RM, Close KL, DeVries JH, Garg S, Heinemann L, Hirsch I, Amiel SA, Beck R, Bosi E, Buckingham B, Cobelli C, Dassau E, Doyle FJ, Heller S, Hovorka R, Jia W, Jones T, Kordonouri O, Kovatchev B, Kowalski A, Laffel L, Maahs D, Murphy HR, Nørgaard K, Parkin CG, Renard E, Saboo B, Scharf M, Tamborlane WV, Weinzimer SA, Phillip M (2017) International consensus on use of continuous glucose monitoring. Diabetes Care 40:1631–1640. https://doi.org/10.2337/dc17-1600
14. Friedel M, Thompson IAP, Kasting G, Polsky R, Cunningham D, Soh HT, Heikenfeld J (2023) Opportunities and challenges in the diagnostic utility of dermal interstitial fluid. Nat Biomed Eng:1–15. https://doi.org/10.1038/s41551-022-00998-9
15. Young T, Clark V, Arroyo Curras N, Heikenfeld J (2023) Perspective – the feasibility of continuous protein monitoring in interstitial fluid. ECS Sens Plus. https://doi.org/10.1149/2754-2726/accd7e
16. Baker LB, Barnes KA, Anderson ML, Passe DH, Stofan JR (2016) Normative data for regional sweat sodium concentration and whole-body sweating rate in athletes. J Sports Sci 34:358–368. https://doi.org/10.1080/02640414.2015.1055291
17. Baker LB, Stofan JR, Hamilton AA, Horswill CA (2009) Comparison of regional patch collection vs. whole body washdown for measuring sweat sodium and potassium loss during exercise. J Appl Physiol 107:887–895. https://doi.org/10.1152/japplphysiol.00197.2009
18. Schiavon M, Dalla Man C, Dube S, Slama M, Kudva YC, Peyser T, Basu A, Basu R, Cobelli C (2015) Modeling plasma-to-interstitium glucose kinetics from multitracer plasma and microdialysis data. Diabetes Technol Ther 17:825–831. https://doi.org/10.1089/dia.2015.0119
19. Moyer J, Wilson D, Finkelshtein I, Wong B, Potts R (2012) Correlation between sweat glucose and blood glucose in subjects with diabetes. Diabetes Technol Ther 14:398–402. https://doi.org/10.1089/dia.2011.0262
20. Green JM, Bishop PA, Muir IH, McLester Jr JR, Heath HE (2000) Effects of high and low blood lactate concentrations on sweat lactate response. Int J Sports Med 21:556–560. https://doi.org/10.1055/s-2000-8483
21. Steckl AJ, Ray P (2018) Stress biomarkers in biological fluids and their point-of-use detection. ACS Sens 3:2025–2044. https://doi.org/10.1021/acssensors.8b00726
22. Jia M, Chew WM, Feinstein Y, Skeath P, Sternberg EM (2016) Quantification of cortisol in human eccrine sweat by liquid chromatography – tandem mass spectrometry. Analyst 141:2053–2060. https://doi.org/10.1039/C5AN02387D

23. Zhang F, Xue J, Shao J, Jia L (2012) Compilation of 222 drugs' plasma protein binding data and guidance for study designs. Drug Discov Today 17:475–485. https://doi.org/10.1016/j.drudis.2011.12.018
24. Zeitlinger MA, Derendorf H, Mouton JW, Cars O, Craig WA, Andes D, Theuretzbacher U (2011) Protein binding: do we ever learn? Antimicrob Agents Chemother 55:3067–3074. https://doi.org/10.1128/AAC.01433-10
25. Jansson P-AE, Fowelin JP, Von Schenck HP, Smith UP, Lönnroth PN (1993) Measurement by microdialysis of the insulin concentration in subcutaneous interstitial fluid: importance of the endothelial barrier for insulin. Diabetes 42:1469–1473. https://doi.org/10.2337/diab.42.10.1469
26. Bodenlenz M, Schaupp LA, Druml T, Sommer R, Wutte A, Schaller HC, Sinner F, Wach P, Pieber TR (2005) Measurement of interstitial insulin in human adipose and muscle tissue under moderate hyperinsulinemia by means of direct interstitial access. Am J Physiol Endocrinol Metab 289:E296–E300. https://doi.org/10.1152/ajpendo.00431.2004
27. Myette-Côté É, Baba K, Brar R, Little JP (2017) Detection of salivary insulin following low versus high carbohydrate meals in humans. Nutrients 9:1204. https://doi.org/10.3390/nu9111204
28. Packer M (2003) Should B-type natriuretic peptide be measured routinely to guide the diagnosis and Management of chronic heart failure? Circulation 108:2950–2953. https://doi.org/10.1161/01.CIR.0000109205.35813.8E
29. Joharimoghadam A, Tajdini M, Bozorgi A (2017) Salivary B-type natriuretic peptide: a new method for heart failure diagnosis and follow-up. Kardiol Pol 75:71–77. https://doi.org/10.5603/KP.a2016.0097
30. Mahajan VS, Jarolim P (2011) How to interpret elevated cardiac troponin levels. Circulation 124:2350–2354. https://doi.org/10.1161/CIRCULATIONAHA.111.023697
31. Mirzaii-Dizgah I, Riahi E (2013) Salivary troponin I as an indicator of myocardial infarction. Indian J Med Res 138:861–865
32. Sproston NR, Ashworth JJ (2018) Role of C-reactive protein at sites of inflammation and infection. Front Immunol 9:754. https://doi.org/10.3389/fimmu.2018.00754
33. Iyengar A, Paulus JK, Gerlanc DJ, Maron JL (2014) Detection and potential utility of C-reactive protein in saliva of neonates. Front Pediatr 2:131. https://doi.org/10.3389/fped.2014.00131
34. Katchman BA, Zhu M, Blain Christen J, Anderson KS (2018) Eccrine sweat as a biofluid for profiling immune biomarkers. Proteomics Clin Appl 12:1800010. https://doi.org/10.1002/prca.201800010
35. Tokmakov AA, Kurotani A, Sato K-I (2021) Protein pI and intracellular localization. Front Mol Biosci 8
36. Cengiz E, Tamborlane WV (2009) A tale of two compartments: interstitial versus blood glucose monitoring. https://home.liebertpub.com/dia. https://doi.org/10.1089/dia.2009.0002. Accessed 8 Apr 2023
37. Bailey T, Bode BW, Christiansen MP, Klaff LJ, Alva S (2015) The performance and usability of a factory-calibrated flash glucose monitoring system. Diabetes Technol Ther 17:787–794. https://doi.org/10.1089/dia.2014.0378
38. Bequette BW (2010) Continuous glucose monitoring: real-time algorithms for calibration, filtering, and alarms. J Diabetes Sci Technol 4:404–418
39. Taylor NA, Machado-Moreira CA (2013) Regional variations in transepidermal water loss, eccrine sweat gland density, sweat secretion rates and electrolyte composition in resting and exercising humans. Extrem Physiol Med 2:4. https://doi.org/10.1186/2046-7648-2-4
40. Sonner Z, Wilder E, Heikenfeld J, Kasting G, Beyette F, Swaile D, Sherman F, Joyce J, Hagen J, Kelley-Loughnane N, Naik R (2015) The microfluidics of the eccrine sweat gland, including biomarker partitioning, transport, and biosensing implications. Biomicrofluidics 9:031301. https://doi.org/10.1063/1.4921039

41. Hu Y, Converse C, Lyons MC, Hsu WH (2018) Neural control of sweat secretion: a review. Br J Dermatol 178:1246–1256. https://doi.org/10.1111/bjd.15808
42. Cui C-Y, Schlessinger D (2015) Eccrine sweat gland development and sweat secretion. Exp Dermatol 24:644–650. https://doi.org/10.1111/exd.12773
43. Baker LB (2019) Physiology of sweat gland function: the roles of sweating and sweat composition in human health. Temperature (Austin) 6:211–259. https://doi.org/10.1080/23328940.2019.1632145
44. Brothers MC, DeBrosse M, Grigsby CC, Naik RR, Hussain SM, Heikenfeld J, Kim SS (2019) Achievements and challenges for real-time sensing of analytes in sweat within wearable platforms. Acc Chem Res 52:297–306. https://doi.org/10.1021/acs.accounts.8b00555
45. Jia W, Bandodkar AJ, Valdés-Ramírez G, Windmiller JR, Yang Z, Ramírez J, Chan G, Wang J (2013) Electrochemical tattoo biosensors for real-time noninvasive lactate monitoring in human perspiration. Anal Chem 85:6553–6560. https://doi.org/10.1021/ac401573r
46. Bandodkar AJ, Molinnus D, Mirza O, Guinovart T, Windmiller JR, Valdés-Ramírez G, Andrade FJ, Schöning MJ, Wang J (2014) Epidermal tattoo potentiometric sodium sensors with wireless signal transduction for continuous non-invasive sweat monitoring. Biosens Bioelectron 54:603–609. https://doi.org/10.1016/j.bios.2013.11.039
47. Gao W, Emaminejad S, Nyein HYY, Challa S, Chen K, Peck A, Fahad HM, Ota H, Shiraki H, Kiriya D, Lien D-H, Brooks GA, Davis RW, Javey A (2016) Fully integrated wearable sensor arrays for multiplexed in situ perspiration analysis. Nature 529:509–514. https://doi.org/10.1038/nature16521
48. Imani S, Bandodkar AJ, Mohan AMV, Kumar R, Yu S, Wang J, Mercier PP (2016) A wearable chemical–electrophysiological hybrid biosensing system for real-time health and fitness monitoring. Nat Commun 7:11650. https://doi.org/10.1038/ncomms11650
49. Gao F, Liu C, Zhang L, Liu T, Wang Z, Song Z, Cai H, Fang Z, Chen J, Wang J, Han M, Wang J, Lin K, Wang R, Li M, Mei Q, Ma X, Liang S, Gou G, Xue N (2023) Wearable and flexible electrochemical sensors for sweat analysis: a review. Microsyst Nanoeng 9:1–21. https://doi.org/10.1038/s41378-022-00443-6
50. Choi J, Xue Y, Xia W, Ray TR, Reeder JT, Bandodkar AJ, Kang D, Xu S, Huang Y, Rogers JA (2017) Soft, skin-mounted microfluidic systems for measuring secretory fluidic pressures generated at the surface of the skin by eccrine sweat glands. Lab Chip 17:2572–2580. https://doi.org/10.1039/C7LC00525C
51. Koh A, Kang D, Xue Y, Lee S, Pielak RM, Kim J, Hwang T, Min S, Banks A, Bastien P, Manco MC, Wang L, Ammann KR, Jang K-I, Won P, Han S, Ghaffari R, Paik U, Slepian MJ, Balooch G, Huang Y, Rogers JA (2016) A soft, wearable microfluidic device for the capture, storage, and colorimetric sensing of sweat. Sci Transl Med 8:366ra165. https://doi.org/10.1126/scitranslmed.aaf2593
52. Martín A, Kim J, Kurniawan JF, Sempionatto JR, Moreto JR, Tang G, Campbell AS, Shin A, Lee MY, Liu X, Wang J (2017) Epidermal microfluidic electrochemical detection system: enhanced sweat sampling and metabolite detection. ACS Sens 2:1860–1868. https://doi.org/10.1021/acssensors.7b00729
53. Hauke A, Simmers P, Ojha YR, Cameron BD, Ballweg R, Zhang T, Twine N, Brothers M, Gomez E, Heikenfeld J (2018) Complete validation of a continuous and blood-correlated sweat biosensing device with integrated sweat stimulation. Lab Chip 18:3750–3759. https://doi.org/10.1039/C8LC01082J
54. Twine NB, Norton RM, Brothers MC, Hauke A, Gomez EF, Heikenfeld J (2018) Open nanofluidic films with rapid transport and no analyte exchange for ultra-low sample volumes. Lab Chip 18:2816–2825. https://doi.org/10.1039/C8LC00186C
55. Choi J, Chen S, Deng Y, Xue Y, Reeder JT, Franklin D, Oh YS, Model JB, Aranyosi AJ, Lee SP, Ghaffari R, Huang Y, Rogers JA (2021) Skin-interfaced microfluidic systems that combine hard and soft materials for demanding applications in sweat capture and analysis. Adv Healthc Mater 10:2000722. https://doi.org/10.1002/adhm.202000722

56. Kim J, Jeerapan I, Imani S, Cho TN, Bandodkar A, Cinti S, Mercier PP, Wang J (2016) Noninvasive alcohol monitoring using a wearable tattoo-based iontophoretic-biosensing system. ACS Sens 1:1011–1019. https://doi.org/10.1021/acssensors.6b00356
57. Gibson LE, Cooke RE (1959) A test for concentration of electrolytes in sweat in cystic fibrosis of the pancreas utilizing pilocarpine by iontophoresis. Pediatrics 23:545–549
58. Pandey PC, Shukla S, Skoog SA, Boehm RD, Narayan RJ (2019) Current advancements in transdermal biosensing and targeted drug delivery. Sensors 19:1028. https://doi.org/10.3390/s19051028
59. Kim J, Sempionatto JR, Imani S, Hartel MC, Barfidokht A, Tang G, Campbell AS, Mercier PP, Wang J (2018) Simultaneous monitoring of sweat and interstitial fluid using a single wearable biosensor platform. Adv Sci (Weinh) 5:1800880. https://doi.org/10.1002/advs.201800880
60. Emaminejad S, Gao W, Wu E, Davies ZA, Yin Yin Nyein H, Challa S, Ryan SP, Fahad HM, Chen K, Shahpar Z, Talebi S, Milla C, Javey A, Davis RW (2017) Autonomous sweat extraction and analysis applied to cystic fibrosis and glucose monitoring using a fully integrated wearable platform. Proc Natl Acad Sci 114:4625–4630. https://doi.org/10.1073/pnas.1701740114
61. Simmers P, Li SK, Kasting G, Heikenfeld J (2018) Prolonged and localized sweat stimulation by iontophoretic delivery of the slowly-metabolized cholinergic agent carbachol. J Dermatol Sci 89:40–51. https://doi.org/10.1016/j.jdermsci.2017.10.013
62. Sonner Z, Wilder E, Gaillard T, Kasting G, Heikenfeld J (2017) Integrated sudomotor axon reflex sweat stimulation for continuous sweat analyte analysis with individuals at rest. Lab Chip 17:2550–2560. https://doi.org/10.1039/C7LC00364A
63. Simmers P, Yuan Y, Sonner Z, Heikenfeld J (2018) Membrane isolation of repeated-use sweat stimulants for mitigating both direct dermal contact and sweat dilution. Biomicrofluidics 12:034101. https://doi.org/10.1063/1.5023396
64. Yuan Y, DeBrosse M, Brothers M, Kim S, Sereda A, Ivanov NV, Hussain S, Heikenfeld J (2021) Oil-membrane protection of electrochemical sensors for fouling- and pH-insensitive detection of lipophilic analytes. ACS Appl Mater Interfaces 13:53553–53563. https://doi.org/10.1021/acsami.1c14175
65. Peng R, Sonner Z, Hauke A, Wilder E, Kasting J, Gaillard T, Swaille D, Sherman F, Mao X, Hagen J, Murdock R, Heikenfeld J (2016) A new oil/membrane approach for integrated sweat sampling and sensing: sample volumes reduced from μL's to nL's and reduction of analyte contamination from skin. Lab Chip 16:4415–4423. https://doi.org/10.1039/C6LC01013J
66. Lee H, Choi TK, Lee YB, Cho HR, Ghaffari R, Wang L, Choi HJ, Chung TD, Lu N, Hyeon T, Choi SH, Kim D-H (2016) A graphene-based electrochemical device with thermoresponsive microneedles for diabetes monitoring and therapy. Nat Nanotechnol 11:566–572. https://doi.org/10.1038/nnano.2016.38
67. Lee H, Song C, Hong YS, Kim MS, Cho HR, Kang T, Shin K, Choi SH, Hyeon T, Kim D-H (2017) Wearable/disposable sweat-based glucose monitoring device with multistage transdermal drug delivery module. Sci Adv 3:e1601314. https://doi.org/10.1126/sciadv.1601314
68. Wiorek A, Parrilla M, Cuartero M, Crespo GA (2020) Epidermal patch with glucose biosensor: pH and temperature correction toward more accurate sweat analysis during sport practice. Anal Chem 92:10153–10161. https://doi.org/10.1021/acs.analchem.0c02211
69. Xuan X, Pérez-Ràfols C, Chen C, Cuartero M, Crespo GA (2021) Lactate biosensing for reliable on-body sweat analysis. ACS Sens 6:2763–2771. https://doi.org/10.1021/acssensors.1c01009
70. Ibáñez-Redín G, Rosso Cagnani G, Gomes NO, Raymundo-Pereira PA, Machado SAS, Gutierrez MA, Krieger JE, Oliveira ON (2023) Wearable potentiometric biosensor for analysis of urea in sweat. Biosens Bioelectron 223:114994. https://doi.org/10.1016/j.bios.2022.114994
71. Wang M, Yang Y, Min J, Song Y, Tu J, Mukasa D, Ye C, Xu C, Heflin N, McCune JS, Hsiai TK, Li Z, Gao W (2022) A wearable electrochemical biosensor for the monitoring of

metabolites and nutrients. Nat Biomed Eng 6:1225–1235. https://doi.org/10.1038/s41551-022-00916-z
72. Sato K, Kang WH, Saga K, Sato KT (1989) Biology of sweat glands and their disorders. I. Normal sweat gland function. J Am Acad Dermatol 20:537–563. https://doi.org/10.1016/S0190-9622(89)70063-3
73. Baker LB (2017) Sweating rate and sweat sodium concentration in athletes: a review of methodology and intra/interindividual variability. Sports Med 47:111–128. https://doi.org/10.1007/s40279-017-0691-5
74. Jajack A, Brothers M, Kasting G, Heikenfeld J (2018) Enhancing glucose flux into sweat by increasing paracellular permeability of the sweat gland. PloS One 13:e0200009. https://doi.org/10.1371/journal.pone.0200009
75. Nyein HYY, Tai L-C, Ngo QP, Chao M, Zhang GB, Gao W, Bariya M, Bullock J, Kim H, Fahad HM, Javey A (2018) A wearable microfluidic sensing patch for dynamic sweat secretion analysis. ACS Sens 3:944–952. https://doi.org/10.1021/acssensors.7b00961
76. Ono S, Egawa G, Kabashima K (2017) Regulation of blood vascular permeability in the skin. Inflamm Regen 37:11. https://doi.org/10.1186/s41232-017-0042-9
77. Sarin H (2010) Physiologic upper limits of pore size of different blood capillary types and another perspective on the dual pore theory of microvascular permeability. Vasc Cell 2:14. https://doi.org/10.1186/2040-2384-2-14
78. Starling EH (1896) On the absorption of fluids from the connective tissue spaces. J Physiol 19:312–326. https://doi.org/10.1113/jphysiol.1896.sp000596
79. Levick JR, Michel CC (2010) Microvascular fluid exchange and the revised Starling principle. Cardiovasc Res 87:198–210. https://doi.org/10.1093/cvr/cvq062
80. Michel CC, Woodcock TE, Curry F-RE (2020) Understanding and extending the Starling principle. Acta Anaesthesiol Scand 64:1032–1037. https://doi.org/10.1111/aas.13603
81. Friedman A (2010) Fluid and electrolyte therapy: a primer. Pediatr Nephrol 25:843–846. https://doi.org/10.1007/s00467-009-1189-7
82. Gonzalez D, Schmidt S, Derendorf H (2013) Importance of relating efficacy measures to unbound drug concentrations for anti-infective agents. Clin Microbiol Rev 26:274–288. https://doi.org/10.1128/CMR.00092-12
83. Azizi PM, Zyla RE, Guan S, Wang C, Liu J, Bolz S-S, Heit B, Klip A, Lee WL (2015) Clathrin-dependent entry and vesicle-mediated exocytosis define insulin transcytosis across microvascular endothelial cells. Mol Biol Cell 26:740–750. https://doi.org/10.1091/mbc.E14-08-1307
84. Bendayan M, Rasio EA (1996) Transport of insulin and albumin by the microvascular endothelium of the rete mirabile. J Cell Sci 109:1857–1864. https://doi.org/10.1242/jcs.109.7.1857
85. Milici AJ, Watrous NE, Stukenbrok H, Palade GE (1987) Transcytosis of albumin in capillary endothelium. J Cell Biol 105:2603–2612. https://doi.org/10.1083/jcb.105.6.2603
86. Bendayan M (2002) Morphological and cytochemical aspects of capillary permeability. Microsc Res Tech 57:327–349. https://doi.org/10.1002/jemt.10088
87. Komarova YA, Kruse K, Mehta D, Malik AB (2017) Protein interactions at endothelial junctions and Signaling mechanisms regulating endothelial permeability. Circ Res 120:179–206. https://doi.org/10.1161/CIRCRESAHA.116.306534
88. Tierney MJ, Tamada JA, Potts RO, Jovanovic L, Garg S, Cygnus Research Team (2001) Clinical evaluation of the GlucoWatch biographer: a continual, non-invasive glucose monitor for patients with diabetes. Biosens Bioelectron 16:621–629. https://doi.org/10.1016/s0956-5663(01)00189-0
89. Vashist SK (2012) Non-invasive glucose monitoring technology in diabetes management: a review. Anal Chim Acta 750:16–27. https://doi.org/10.1016/j.aca.2012.03.043
90. Bandodkar AJ, Jia W, Yardımcı C, Wang X, Ramirez J, Wang J (2015) Tattoo-based noninvasive glucose monitoring: a proof-of-concept study. Anal Chem 87:394–398. https://doi.org/10.1021/ac504300n

91. De la Paz E, Barfidokht A, Rios S, Brown C, Chao E, Wang J (2021) Extended noninvasive glucose monitoring in the interstitial fluid using an epidermal biosensing patch. Anal Chem 93: 12767–12775. https://doi.org/10.1021/acs.analchem.1c02887
92. De la Paz E, Saha T, Del Caño R, Seker S, Kshirsagar N, Wang J (2023) Non-invasive monitoring of interstitial fluid lactate through an epidermal iontophoretic device. Talanta 254: 124122. https://doi.org/10.1016/j.talanta.2022.124122
93. Chen Y, Lu S, Zhang S, Li Y, Qu Z, Chen Y, Lu B, Wang X, Feng X (2017) Skin-like biosensor system via electrochemical channels for noninvasive blood glucose monitoring. Sci Adv 3:e1701629. https://doi.org/10.1126/sciadv.1701629
94. Klonoff DC, Ahn D, Drincic A (2017) Continuous glucose monitoring: a review of the technology and clinical use. Diabetes Res Clin Pract 133:178–192. https://doi.org/10.1016/j.diabres.2017.08.005
95. Cappon G, Vettoretti M, Sparacino G, Facchinetti A (2019) Continuous glucose monitoring sensors for diabetes management: a review of technologies and applications. Diabetes Metab J 43:383–397. https://doi.org/10.4093/dmj.2019.0121
96. Sharma S, Saeed A, Johnson C, Gadegaard N, Cass AE (2017) Rapid, low cost prototyping of transdermal devices for personal healthcare monitoring. Sens Bio-Sens Res 13:104–108. https://doi.org/10.1016/j.sbsr.2016.10.004
97. Ming DK, Jangam S, Gowers SAN, Wilson R, Freeman DME, Boutelle MG, Cass AEG, O'Hare D, Holmes AH (2022) Real-time continuous measurement of lactate through a minimally invasive microneedle patch: a phase I clinical study. BMJ Innov 8. https://doi.org/10.1136/bmjinnov-2021-000864
98. Zheng H, GhavamiNejad A, GhavamiNejad P, Samarikhalaj M, Giacca A, Poudineh M (2022) Hydrogel microneedle-assisted assay integrating aptamer probes and fluorescence detection for reagentless biomarker quantification. ACS Sens 7:2387–2399. https://doi.org/10.1021/acssensors.2c01033
99. Lin S, Cheng X, Zhu J, Wang B, Jelinek D, Zhao Y, Wu T-Y, Horrillo A, Tan J, Yeung J, Yan W, Forman S, Coller HA, Milla C, Emaminejad S (2022) Wearable microneedle-based electrochemical aptamer biosensing for precision dosing of drugs with narrow therapeutic windows. Sci Adv 8:eabq4539. https://doi.org/10.1126/sciadv.abq4539
100. Ranamukhaarachchi SA, Padeste C, Dübner M, Häfeli UO, Stoeber B, Cadarso VJ (2016) Integrated hollow microneedle-optofluidic biosensor for therapeutic drug monitoring in sub-nanoliter volumes. Sci Rep 6:29075. https://doi.org/10.1038/srep29075
101. Ranamukhaarachchi SA, Padeste C, Häfeli UO, Stoeber B, Cadarso VJ (2017) Design considerations of a hollow microneedle-optofluidic biosensing platform incorporating enzyme-linked assays. J Micromech Microeng 28:024002. https://doi.org/10.1088/1361-6439/aa9c9c
102. Parrilla M, Detamornrat U, Domínguez-Robles J, Donnelly RF, De Wael K (2022) Wearable hollow microneedle sensing patches for the transdermal electrochemical monitoring of glucose. Talanta 249:123695. https://doi.org/10.1016/j.talanta.2022.123695
103. Luo X, Yu Q, Liu Y, Gai W, Ye L, Yang L, Cui Y (2022) Closed-loop diabetes Minipatch based on a biosensor and an electroosmotic pump on hollow biodegradable microneedles. ACS Sens 7:1347–1360. https://doi.org/10.1021/acssensors.1c02337
104. Friedel M, Werbovetz B, Drexelius A, Plaxco K, Heikenfeld J (2023) Continuous molecular monitoring of human dermal interstitial fluid with microneedle-enabled electrochemical aptamer sensors
105. Heo YJ, Shibata H, Okitsu T, Kawanishi T, Takeuchi S (2011) Long-term in vivo glucose monitoring using fluorescent hydrogel fibers. Proc Natl Acad Sci 108:13399–13403. https://doi.org/10.1073/pnas.1104954108
106. Joseph JI (2021) Review of the Long-term implantable Senseonics continuous glucose monitoring system and other continuous glucose monitoring systems. J Diabetes Sci Technol 15:167–173. https://doi.org/10.1177/1932296820911919

107. Stewart RH (2020) A modern view of the interstitial space in health and disease. Front Vet Sci 7
108. McClatchey PM, McClain ES, Williams IM, Malabanan CM, James FD, Lord PC, Gregory JM, Cliffel DE, Wasserman DH (2019) Fibrotic encapsulation is the dominant source of continuous glucose monitor delays. Diabetes 68:1892–1901. https://doi.org/10.2337/db19-0229
109. Sempionatto JR, Lasalde-Ramírez JA, Mahato K, Wang J, Gao W (2022) Wearable chemical sensors for biomarker discovery in the omics era. Nat Rev Chem 6:899–915. https://doi.org/10.1038/s41570-022-00439-w
110. Clark Jr LC, Lyons C (1962) Electrode Systems for Continuous Monitoring in cardiovascular surgery. Ann N Y Acad Sci 102:29–45. https://doi.org/10.1111/j.1749-6632.1962.tb13623.x
111. Clark LC Jr (1970) Membrane polarographic electrode system and method with electrochemical compensation
112. Clark LC (1993) Guest editorial. Biosens Bioelectron 8:iii–vii. https://doi.org/10.1016/0956-5663(93)80035-N
113. Guilbault GG, Montalvo JG (1969) Urea-specific enzyme electrode. J Am Chem Soc 91:2164–2165. https://doi.org/10.1021/ja01036a083
114. Suzuki S, Takahashi F, Satoh I, Sonobe N (1975) Ethanol and lactic acid sensors using electrodes coated with dehydrogenase – collagen membranes. BCSJ 48:3246–3249. https://doi.org/10.1246/bcsj.48.3246
115. Rocchitta G, Spanu A, Babudieri S, Latte G, Madeddu G, Galleri G, Nuvoli S, Bagella P, Demartis MI, Fiore V, Manetti R, Serra PA (2016) Enzyme biosensors for biomedical applications: strategies for safeguarding analytical performances in biological fluids. Sensors (Basel) 16:780. https://doi.org/10.3390/s16060780
116. Heller A (1999) Implanted electrochemical glucose sensors for the management of diabetes. Annu Rev Biomed Eng 1:153–175. https://doi.org/10.1146/annurev.bioeng.1.1.153
117. Heller A, Feldman B (2008) Electrochemical glucose sensors and their applications in diabetes management. Chem Rev 108:2482–2505. https://doi.org/10.1021/cr068069y
118. Sassolas A, Blum LJ, Leca-Bouvier BD (2012) Immobilization strategies to develop enzymatic biosensors. Biotechnol Adv 30:489–511. https://doi.org/10.1016/j.biotechadv.2011.09.003
119. Gutteridge A, Thornton J (2004) Conformational change in substrate binding, catalysis and product release: an open and shut case? FEBS Lett 567:67–73. https://doi.org/10.1016/j.febslet.2004.03.067
120. Feifel SC, Kapp A, Lisdat F (2014) Protein multilayer architectures on electrodes for analyte detection. In: Gu MB, Kim H-S (eds) Biosensors based on aptamers and enzymes. Springer, Berlin, pp 253–298
121. Lisdat F (2017) Trends in the layer-by-layer assembly of redox proteins and enzymes in bioelectrochemistry. Curr Opin Electrochem 5:165–172. https://doi.org/10.1016/j.coelec.2017.09.002
122. Nguyen HH, Lee SH, Lee UJ, Fermin CD, Kim M (2019) Immobilized enzymes in biosensor applications. Materials (Basel) 12:121. https://doi.org/10.3390/ma12010121
123. Rodriguez-Abetxuko A, Sánchez-deAlcázar D, Muñumer P, Beloqui A (2020) Tunable polymeric scaffolds for enzyme immobilization. Front Bioeng Biotechnol 8
124. Zhang Y, Ge J, Liu Z (2015) Enhanced activity of immobilized or chemically modified enzymes. ACS Catal 5:4503–4513. https://doi.org/10.1021/acscatal.5b00996
125. Li C, Zhang R, Wang J, Wilson LM, Yan Y (2020) Protein engineering for improving and diversifying natural products biosynthesis. Trends Biotechnol 38:729–744. https://doi.org/10.1016/j.tibtech.2019.12.008
126. Stasyuk N, Smutok O, Demkiv O, Prokopiv T, Gayda G, Nisnevitch M, Gonchar M (2020) Synthesis, catalytic properties and application in biosensorics of nanozymes and electronanocatalysts: a review. Sensors (Basel) 20:4509. https://doi.org/10.3390/s20164509

127. Wang X, Dong S, Wei H (2023) Recent advances on nanozyme-based electrochemical biosensors. Electroanalysis 35:e202100684. https://doi.org/10.1002/elan.202100684
128. Ricci F, Vallée-Bélisle A, Simon AJ, Porchetta A, Plaxco KW (2016) Using nature's "Tricks" to rationally tune the binding properties of biomolecular receptors. Acc Chem Res 49:1884–1892. https://doi.org/10.1021/acs.accounts.6b00276
129. Vorobyeva M, Vorobjev P, Venyaminova A (2016) Multivalent aptamers: versatile tools for diagnostic and therapeutic applications. Molecules 21:1613. https://doi.org/10.3390/molecules21121613
130. Pollard TD (2010) A guide to simple and informative binding assays. MBoC 21:4061–4067. https://doi.org/10.1091/mbc.e10-08-0683
131. Wang X, Hao Z, Olsen TR, Zhang W, Lin Q (2019) Measurements of aptamer–protein binding kinetics using graphene field-effect transistors. Nanoscale 11:12573–12581. https://doi.org/10.1039/C9NR02797A
132. Frutiger A, Tanno A, Hwu S, Tiefenauer RF, Vörös J, Nakatsuka N (2021) Nonspecific binding – fundamental concepts and consequences for biosensing applications. Chem Rev 121:8095–8160. https://doi.org/10.1021/acs.chemrev.1c00044
133. Lubken RM, de Jong AM, Prins MWJ (2022) Real-time monitoring of biomolecules: dynamic response limits of affinity-based sensors. ACS Sens 7:286–295. https://doi.org/10.1021/acssensors.1c02307
134. Lubken RM, Bergkamp MH, de Jong AM, Prins MWJ (2021) Sensing methodology for the rapid monitoring of biomolecules at low concentrations over long time spans. ACS Sens 6:4471–4481. https://doi.org/10.1021/acssensors.1c01991
135. Maganzini N, Thompson I, Wilson B, Soh HT (2022) Pre-equilibrium biosensors as an approach towards rapid and continuous molecular measurements. Nat Commun 13:7072. https://doi.org/10.1038/s41467-022-34778-5
136. Cristea C, Florea A, Tertiș M, Săndulescu R, Cristea C, Florea A, Tertiș M, Săndulescu R (2015) Immunosensors. IntechOpen
137. Poudineh M, Maikawa CL, Ma EY, Pan J, Mamerow D, Hang Y, Baker SW, Beirami A, Yoshikawa A, Eisenstein M, Kim S, Vučković J, Appel EA, Soh HT (2021) A fluorescence sandwich immunoassay for the real-time continuous detection of glucose and insulin in live animals. Nat Biomed Eng 5:53–63. https://doi.org/10.1038/s41551-020-00661-1
138. van Smeden L, Saris A, Sergelen K, de Jong AM, Yan J, Prins MWJ (2022) Reversible immunosensor for the continuous monitoring of cortisol in blood plasma sampled with microdialysis. ACS Sens 7:3041–3048. https://doi.org/10.1021/acssensors.2c01358
139. Munje RD, Muthukumar S, Jagannath B, Prasad S (2017) A new paradigm in sweat based wearable diagnostics biosensors using room temperature ionic liquids (RTILs). Sci Rep 7:1950. https://doi.org/10.1038/s41598-017-02133-0
140. Song J, Wang R-M, Wang Y-Q, Tang Y-R, Deng A-P (2010) Hapten design, modification and preparation of artificial antigens. Chin J Anal Chem 38:1211–1218. https://doi.org/10.1016/S1872-2040(09)60063-3
141. Gray A, Bradbury ARM, Knappik A, Plückthun A, Borrebaeck CAK, Dübel S (2020) Animal-free alternatives and the antibody iceberg. Nat Biotechnol 38:1234–1239. https://doi.org/10.1038/s41587-020-0687-9
142. Crivianu-Gaita V, Thompson M (2016) Aptamers, antibody scFv, and antibody fab' fragments: An overview and comparison of three of the most versatile biosensor biorecognition elements. Biosens Bioelectron 85:32–45. https://doi.org/10.1016/j.bios.2016.04.091
143. Arshavsky-Graham S, Heuer C, Jiang X, Segal E (2022) Aptasensors versus immunosensors – which will prevail? Eng Life Sci 22:319–333. https://doi.org/10.1002/elsc.202100148
144. Fercher C, Jones ML, Mahler SM, Corrie SR (2021) Recombinant antibody engineering enables reversible binding for continuous protein biosensing. ACS Sens 6:764–776. https://doi.org/10.1021/acssensors.0c01510

145. Asaadi Y, Jouneghani FF, Janani S, Rahbarizadeh F (2021) A comprehensive comparison between camelid nanobodies and single chain variable fragments. Biomarker Res 9:87. https://doi.org/10.1186/s40364-021-00332-6
146. Filipiak MS, Rother M, Andoy NM, Knudsen AC, Grimm S, Bachran C, Swee LK, Zaumseil J, Tarasov A (2018) Highly sensitive, selective and label-free protein detection in physiological solutions using carbon nanotube transistors with nanobody receptors. Sens Actuators B 255:1507–1516. https://doi.org/10.1016/j.snb.2017.08.164
147. Ruscito A, DeRosa MC (2016) Small-molecule binding aptamers: selection strategies, characterization, and applications. Front Chem 4
148. Liang S, Kinghorn AB, Voliotis M, Prague JK, Veldhuis JD, Tsaneva-Atanasova K, McArdle CA, Li RHW, Cass AEG, Dhillo WS, Tanner JA (2019) Measuring luteinising hormone pulsatility with a robotic aptamer-enabled electrochemical reader. Nat Commun 10:852. https://doi.org/10.1038/s41467-019-08799-6
149. Takahashi M (2018) Aptamers targeting cell surface proteins. Biochimie 145:63–72. https://doi.org/10.1016/j.biochi.2017.11.019
150. Tuerk C, Gold L (1990) Systematic evolution of ligands by exponential enrichment: RNA ligands to bacteriophage T4 DNA polymerase. Science 249:505–510. https://doi.org/10.1126/science.2200121
151. Ellington AD, Szostak JW (1990) In vitro selection of RNA molecules that bind specific ligands. Nature 346:818–822. https://doi.org/10.1038/346818a0
152. Song K-M, Lee S, Ban C (2012) Aptamers and their biological applications. Sensors 12:612–631. https://doi.org/10.3390/s120100612
153. Duffy K, Arangundy-Franklin S, Holliger P (2020) Modified nucleic acids: replication, evolution, and next-generation therapeutics. BMC Biol 18:112. https://doi.org/10.1186/s12915-020-00803-6
154. Odeh F, Nsairat H, Alshaer W, Ismail MA, Esawi E, Qaqish B, Bawab AA, Ismail SI (2019) Aptamers chemistry: chemical modifications and conjugation strategies. Molecules 25:3. https://doi.org/10.3390/molecules25010003
155. Lai Q, Chen W, Zhang Y, Liu Z (2021) Application strategies of peptide nucleic acids toward electrochemical nucleic acid sensors. Analyst 146:5822–5835. https://doi.org/10.1039/D1AN00765C
156. Shaver A, Kundu N, Young BE, Vieira PA, Sczepanski JT, Arroyo-Currás N (2021) Nuclease hydrolysis does not drive the rapid signaling decay of DNA aptamer-based electrochemical sensors in biological fluids. Langmuir 37:5213–5221. https://doi.org/10.1021/acs.langmuir.1c00166
157. Yang K-A, Chun H, Zhang Y, Pecic S, Nakatsuka N, Andrews AM, Worgall TS, Stojanovic MN (2017) High-affinity nucleic-acid-based receptors for steroids. ACS Chem Biol 12:3103–3112. https://doi.org/10.1021/acschembio.7b00634
158. Zhuo Z, Yu Y, Wang M, Li J, Zhang Z, Liu J, Wu X, Lu A, Zhang G, Zhang B (2017) Recent advances in SELEX technology and aptamer applications in biomedicine. Int J Mol Sci 18:2142. https://doi.org/10.3390/ijms18102142
159. Gold L, Ayers D, Bertino J, Bock C, Bock A, Brody EN, Carter J, Dalby AB, Eaton BE, Fitzwater T, Flather D, Forbes A, Foreman T, Fowler C, Gawande B, Goss M, Gunn M, Gupta S, Halladay D, Heil J, Heilig J, Hicke B, Husar G, Janjic N, Jarvis T, Jennings S, Katilius E, Keeney TR, Kim N, Koch TH, Kraemer S, Kroiss L, Le N, Levine D, Lindsey W, Lollo B, Mayfield W, Mehan M, Mehler R, Nelson SK, Nelson M, Nieuwlandt D, Nikrad M, Ochsner U, Ostroff RM, Otis M, Parker T, Pietrasiewicz S, Resnicow DI, Rohloff J, Sanders G, Sattin S, Schneider D, Singer B, Stanton M, Sterkel A, Stewart A, Stratford S, Vaught JD, Vrkljan M, Walker JJ, Watrobka M, Waugh S, Weiss A, Wilcox SK, Wolfson A, Wolk SK, Zhang C, Zichi D (2010) Aptamer-based multiplexed proteomic technology for biomarker discovery. PloS One 5:e15004. https://doi.org/10.1371/journal.pone.0015004

160. Vaught JD, Bock C, Carter J, Fitzwater T, Otis M, Schneider D, Rolando J, Waugh S, Wilcox SK, Eaton BE (2010) Expanding the chemistry of DNA for in vitro selection. J Am Chem Soc 132:4141–4151. https://doi.org/10.1021/ja908035g
161. Roy A, Talukdar P (2021) Recent advances in bioactive artificial ionophores. Chembiochem 22:2925–2940. https://doi.org/10.1002/cbic.202100112
162. Bühlmann P, Chen LD (2012) Ion-selective electrodes with ionophore-doped sensing membranes. In: Supramolecular chemistry. Wiley
163. Parrilla M, Cuartero M, Crespo GA (2019) Wearable potentiometric ion sensors. Trends Anal Chem 110:303–320. https://doi.org/10.1016/j.trac.2018.11.024
164. Sharma R, Deacon SE, Nowak D, George SE, Szymonik MP, Tang AAS, Tomlinson DC, Davies AG, McPherson MJ, Wälti C (2016) Label-free electrochemical impedance biosensor to detect human interleukin-8 in serum with sub-pg/ml sensitivity. Biosens Bioelectron 80: 607–613. https://doi.org/10.1016/j.bios.2016.02.028
165. Vanova V, Mitrevska K, Milosavljevic V, Hynek D, Richtera L, Adam V (2021) Peptide-based electrochemical biosensors utilized for protein detection. Biosens Bioelectron 180: 113087. https://doi.org/10.1016/j.bios.2021.113087
166. Xiao X, Kuang Z, Slocik JM, Tadepalli S, Brothers M, Kim S, Mirau PA, Butkus C, Farmer BL, Singamaneni S, Hall CK, Naik RR (2018) Advancing peptide-based biorecognition elements for biosensors using *in-silico* evolution. ACS Sens 3:1024–1031. https://doi.org/10.1021/acssensors.8b00159
167. Kang D, Sun S, Kurnik M, Morales D, Dahlquist FW, Plaxco KW (2017) New architecture for reagentless, protein-based electrochemical biosensors. J Am Chem Soc 139:12113–12116. https://doi.org/10.1021/jacs.7b05953
168. Ahmad OS, Bedwell TS, Esen C, Garcia-Cruz A, Piletsky SA (2019) Molecularly imprinted polymers in electrochemical and optical sensors. Trends Biotechnol 37:294–309. https://doi.org/10.1016/j.tibtech.2018.08.009
169. Pereira TC, Stradiotto NR (2019) Electrochemical sensing of lactate by using an electrode modified with molecularly imprinted polymers, reduced graphene oxide and gold nanoparticles. Microchim Acta 186:764. https://doi.org/10.1007/s00604-019-3898-3
170. Zaryanov NV, Nikitina VN, Karpova EV, Karyakina EE, Karyakin AA (2017) Nonenzymatic sensor for lactate detection in human sweat. Anal Chem 89:11198–11202. https://doi.org/10.1021/acs.analchem.7b03662
171. Zhang Q, Jiang D, Xu C, Ge Y, Liu X, Wei Q, Huang L, Ren X, Wang C, Wang Y (2020) Wearable electrochemical biosensor based on molecularly imprinted ag nanowires for noninvasive monitoring lactate in human sweat. Sens Actuators B 320:128325. https://doi.org/10.1016/j.snb.2020.128325
172. Parlak O, Keene ST, Marais A, Curto VF, Salleo A (2018) Molecularly selective nanoporous membrane-based wearable organic electrochemical device for noninvasive cortisol sensing. Sci Adv 4:eaar2904. https://doi.org/10.1126/sciadv.aar2904
173. Ansell RJ (2015) Characterization of the binding properties of molecularly imprinted polymers. In: Mattiasson B, Ye L (eds) Molecularly imprinted polymers in biotechnology. Springer, Cham, pp 51–93
174. Lahcen AA, Surya SG, Beduk T, Vijjapu MT, Lamaoui A, Durmus C, Timur S, Shekhah O, Mani V, Amine A, Eddaoudi M, Salama KN (2022) Metal–organic frameworks meet molecularly imprinted polymers: insights and prospects for sensor applications. ACS Appl Mater Interfaces 14:49399–49424. https://doi.org/10.1021/acsami.2c12842
175. Han W, He H, Zhang L, Dong C, Zeng H, Dai Y, Xing L, Zhang Y, Xue X (2017) A self-powered wearable noninvasive electronic-skin for perspiration analysis based on piezo-biosensing unit matrix of enzyme/ZnO nanoarrays. ACS Appl Mater Interfaces 9:29526–29537. https://doi.org/10.1021/acsami.7b07990
176. Arroyo-Currás N, Dauphin-Ducharme P, Scida K, Chávez JL (2020) From the beaker to the body: translational challenges for electrochemical, aptamer-based sensors. Anal Methods 12:1288–1310. https://doi.org/10.1039/D0AY00026D

177. Watkins Z, Karajic A, Young T, White R, Heikenfeld J (2023) Week-long operation of electrochemical aptamer sensors: new insights into self-assembled monolayer degradation mechanisms and solutions for stability in serum at body temperature. ACS Sens 8:1119–1131. https://doi.org/10.1021/acssensors.2c02403
178. Clark V, Pellitero MA, Arroyo-Currás N (2023) Explaining the decay of nucleic acid-based sensors under continuous voltammetric interrogation. Anal Chem 95:4974–4983. https://doi.org/10.1021/acs.analchem.2c05158
179. Leung KK, Downs AM, Ortega G, Kurnik M, Plaxco KW (2021) Elucidating the mechanisms underlying the signal drift of electrochemical aptamer-based sensors in whole blood. ACS Sens. https://doi.org/10.1021/acssensors.1c01183
180. Long GL, Winefordner JD (1983) Limit of detection a closer look at the IUPAC definition. Anal Chem 55:712A–724A. https://doi.org/10.1021/ac00258a724
181. Chiang C-Y, Huang T-T, Wang C-H, Huang C-J, Tsung-Heng Tsai YS-N, Chen Y-T, Hong S-W, Hsu C-W, Chang T-C, Chau L-K (2020) Fiber optic nanogold-linked immunosorbent assay for rapid detection of procalcitonin at femtomolar concentration level. Biosens Bioelectron 151:111871. https://doi.org/10.1016/j.bios.2019.111871
182. Hariri AA, Cartwright AP, Dory C, Gidi Y, Yee S, Fu K, Yang K, Wu D, Thompson IAP, Maganzini N, Feagin T, Young BE, Afshar BH, Eisenstein M, Digonnet M, Vuckovic J, Soh HT (2023) Continuous optical detection of small-molecule analytes in complex. Biomatrices. 2023.03.03.531030
183. Liu Y, Zhan L, Qin Z, Sackrison J, Bischof JC (2021) Ultrasensitive and highly specific lateral flow assays for point-of-care diagnosis. ACS Nano 15:3593–3611. https://doi.org/10.1021/acsnano.0c10035
184. Mayerhöfer TG, Pahlow S, Popp J (2020) The Bouguer-Beer-Lambert law: shining light on the obscure. ChemPhysChem 21:2029–2046. https://doi.org/10.1002/cphc.202000464
185. He R, Liu H, Fang T, Niu Y, Zhang H, Han F, Gao B, Li F, Xu F (2021) A colorimetric dermal tattoo biosensor fabricated by microneedle patch for multiplexed detection of health-related biomarkers. Adv Sci 8:2103030. https://doi.org/10.1002/advs.202103030
186. Hussain S, Park S (2020) Sweat-based noninvasive skin-patchable urea biosensors with photonic interpenetrating polymer network films integrated into PDMS chips. ACS Sens 5:3988–3998. https://doi.org/10.1021/acssensors.0c01757
187. Huang X, Xu D, Chen J, Liu J, Li Y, Song J, Ma X, Guo J (2018) Smartphone-based analytical biosensors. Analyst 143:5339–5351. https://doi.org/10.1039/C8AN01269E
188. Xu S, Wang Y, Zhou D, Kuang M, Fang D, Yang W, Wei S, Ma L (2016) A novel chemiluminescence sensor for sensitive detection of cholesterol based on the peroxidase-like activity of copper nanoclusters. Sci Rep 6:39157. https://doi.org/10.1038/srep39157
189. Nicholas D, Logan KA, Sheng Y, Gao J, Farrell S, Dixon D, Callan B, McHale AP, Callan JF (2018) Rapid paper based colorimetric detection of glucose using a hollow microneedle device. Int J Pharm 547:244–249. https://doi.org/10.1016/j.ijpharm.2018.06.002
190. Xiao J, Liu Y, Su L, Zhao D, Zhao L, Zhang X (2019) Microfluidic chip-based wearable colorimetric sensor for simple and facile detection of sweat glucose. Anal Chem 91:14803–14807. https://doi.org/10.1021/acs.analchem.9b03110
191. Yi J, Xianyu Y (2022) Gold nanomaterials-implemented wearable sensors for healthcare applications. Adv Funct Mater 32:2113012. https://doi.org/10.1002/adfm.202113012
192. Song K-M, Cho M, Jo H, Min K, Jeon SH, Kim T, Han MS, Ku JK, Ban C (2011) Gold nanoparticle-based colorimetric detection of kanamycin using a DNA aptamer. Anal Biochem 415:175–181. https://doi.org/10.1016/j.ab.2011.04.007
193. Saraf N, Bosak A, Willenberg A, Das S, Willenberg BJ, Seal S (2017) Colorimetric detection of epinephrine using an optimized paper-based aptasensor. RSC Adv 7:49133–49143. https://doi.org/10.1039/C7RA10272K
194. António M, Ferreira R, Vitorino R, Daniel-da-Silva AL (2020) A simple aptamer-based colorimetric assay for rapid detection of C-reactive protein using gold nanoparticles. Talanta 214:120868. https://doi.org/10.1016/j.talanta.2020.120868

195. Bandodkar AJ, Gutruf P, Choi J, Lee K, Sekine Y, Reeder JT, Jeang WJ, Aranyosi AJ, Lee SP, Model JB, Ghaffari R, Su C-J, Leshock JP, Ray T, Verrillo A, Thomas K, Krishnamurthi V, Han S, Kim J, Krishnan S, Hang T, Rogers JA (2019) Battery-free, skin-interfaced microfluidic/electronic systems for simultaneous electrochemical, colorimetric, and volumetric analysis of sweat. Sci Adv 5:eaav3294. https://doi.org/10.1126/sciadv.aav3294
196. Kim J, Wu Y, Luan H, Yang DS, Cho D, Kwak SS, Liu S, Ryu H, Ghaffari R, Rogers JA (2022) A skin-interfaced, miniaturized microfluidic analysis and delivery system for colorimetric measurements of nutrients in sweat and supply of vitamins through the skin. Adv Sci 9: 2103331. https://doi.org/10.1002/advs.202103331
197. Zhu DD, Zheng LW, Duong PK, Cheah RH, Liu XY, Wong JR, Wang WJ, Tien Guan ST, Zheng XT, Chen P (2022) Colorimetric microneedle patches for multiplexed transdermal detection of metabolites. Biosens Bioelectron 212:114412. https://doi.org/10.1016/j.bios.2022.114412
198. Nawrot W, Drzozga K, Baluta S, Cabaj J, Malecha K (2018) A fluorescent biosensors for detection vital body fluids' agents. Sensors (Basel) 18:2357. https://doi.org/10.3390/s18082357
199. Kim S, Lee B, Reeder JT, Seo SH, Lee S-U, Hourlier-Fargette A, Shin J, Sekine Y, Jeong H, Oh YS, Aranyosi AJ, Lee SP, Model JB, Lee G, Seo M-H, Kwak SS, Jo S, Park G, Han S, Park I, Jung H-I, Ghaffari R, Koo J, Braun PV, Rogers JA (2020) Soft, skin-interfaced microfluidic systems with integrated immunoassays, fluorometric sensors, and impedance measurement capabilities. Proc Natl Acad Sci 117:27906–27915. https://doi.org/10.1073/pnas.2012700117
200. Shibata H, Heo YJ, Okitsu T, Matsunaga Y, Kawanishi T, Takeuchi S (2010) Injectable hydrogel microbeads for fluorescence-based in vivo continuous glucose monitoring. Proc Natl Acad Sci 107:17894–17898. https://doi.org/10.1073/pnas.1006911107
201. Wang H, Yi J, Velado D, Yu Y, Zhou S (2015) Immobilization of carbon dots in molecularly imprinted microgels for optical sensing of glucose at physiological pH. ACS Appl Mater Interfaces 7:15735–15745. https://doi.org/10.1021/acsami.5b04744
202. Kanick SC, Schneider PA, Klitzman B, Wisniewski NA, Rebrin K (2019) Continuous monitoring of interstitial tissue oxygen using subcutaneous oxygen microsensors: in vivo characterization in healthy volunteers. Microvasc Res 124:6–18. https://doi.org/10.1016/j.mvr.2019.02.002
203. Dong P, Ko BS, Lomeli KA, Clark EC, McShane MJ, Grunlan MA (2022) A glucose biosensor based on phosphorescence lifetime sensing and a thermoresponsive membrane. Macromol Rapid Commun 43:2100902. https://doi.org/10.1002/marc.202100902
204. Li N, Ho C-M (2008) Aptamer-based optical probes with separated molecular recognition and signal transduction modules. J Am Chem Soc 130:2380–2381. https://doi.org/10.1021/ja076787b
205. Verma AK, Noumani A, Yadav AK, Solanki PR (2023) FRET based biosensor: principle applications recent advances and challenges. Diagnostics 13:1375. https://doi.org/10.3390/diagnostics13081375
206. Shaver A, Arroyo-Currás N (2022) The challenge of long-term stability for nucleic acid-based electrochemical sensors. Curr Opin Electrochem 32:100902. https://doi.org/10.1016/j.coelec.2021.100902
207. Pellitero MA, Shaver A, Arroyo-Currás N (2019) Critical review – approaches for the electrochemical interrogation of DNA-based sensors: a critical review. J Electrochem Soc 167:037529. https://doi.org/10.1149/2.0292003JES
208. Kang D, Zuo X, Yang R, Xia F, Plaxco KW, White RJ (2009) Comparing the properties of electrochemical-based DNA sensors employing different redox tags. Anal Chem 81:9109–9113. https://doi.org/10.1021/ac901811n
209. Pellitero MA, Kundu N, Sczepanski J, Arroyo-Currás N (2023) Os(II/III) complex supports pH-insensitive electrochemical DNA-based sensing with superior operational stability than the

benchmark methylene blue reporter. Analyst 148:806–813. https://doi.org/10.1039/D2AN01901A
210. Arroyo-Currás N, Dauphin-Ducharme P, Ortega G, Ploense KL, Kippin TE, Plaxco KW (2018) Subsecond-resolved molecular measurements in the living body using chronoamperometrically interrogated aptamer-based sensors. ACS Sens 3:360–366. https://doi.org/10.1021/acssensors.7b00787
211. Pellitero MA, Curtis SD, Arroyo-Currás N (2021) Interrogation of electrochemical aptamer-based sensors via peak-to-peak separation in cyclic voltammetry improves the temporal stability and batch-to-batch variability in biological fluids. ACS Sens 6:1199–1207. https://doi.org/10.1021/acssensors.0c02455
212. Chen A, Shah B (2013) Electrochemical sensing and biosensing based on square wave voltammetry. Anal Methods 5:2158–2173. https://doi.org/10.1039/C3AY40155C
213. Xiao Y, Lubin AA, Heeger AJ, Plaxco KW (2005) Label-free electronic detection of thrombin in blood serum by using an aptamer-based sensor. Angew Chem Int Ed 44:5456–5459. https://doi.org/10.1002/anie.200500989
214. Ferguson BS, Hoggarth DA, Maliniak D, Ploense K, White RJ, Woodward N, Hsieh K, Bonham AJ, Eisenstein M, Kippin T, Plaxco KW, Soh HT (2013) Real-time, aptamer-based tracking of circulating therapeutic agents in living animals. Sci Transl Med 5:213ra165. https://doi.org/10.1126/scitranslmed.3007095
215. Arroyo-Currás N, Somerson J, Vieira PA, Ploense KL, Kippin TE, Plaxco KW (2017) Real-time measurement of small molecules directly in awake, ambulatory animals. Proc Natl Acad Sci U S A 114:645–650. https://doi.org/10.1073/pnas.1613458114
216. Dauphin-Ducharme P, Yang K, Arroyo-Currás N, Ploense KL, Zhang Y, Gerson J, Kurnik M, Kippin TE, Stojanovic MN, Plaxco KW (2019) Electrochemical aptamer-based sensors for improved therapeutic drug monitoring and high-precision, feedback-controlled drug delivery. ACS Sens 4:2832–2837. https://doi.org/10.1021/acssensors.9b01616
217. Downs AM, Plaxco KW (2022) Real-time, in vivo molecular monitoring using electrochemical aptamer based sensors: opportunities and challenges. ACS Sens 7:2823–2832. https://doi.org/10.1021/acssensors.2c01428
218. Wu Y, Tehrani F, Teymourian H, Mack J, Shaver A, Reynoso M, Kavner J, Huang N, Furmidge A, Duvvuri A, Nie Y, Laffel LM, Doyle FJI, Patti M-E, Dassau E, Wang J, Arroyo-Currás N (2022) Microneedle aptamer-based sensors for continuous, real-time therapeutic drug monitoring. Anal Chem 94:8335–8345. https://doi.org/10.1021/acs.analchem.2c00829
219. Friedel M, Werbovetz B, Drexelius A, Watkins Z, Bali A, Plaxco KW, Heikenfeld J (2023) Continuous molecular monitoring of human dermal interstitial fluid with microneedle-enabled electrochemical aptamer sensors. Lab Chip 23:3289–3299. https://doi.org/10.1039/D3LC00210A
220. Riedel M, Lisdat F (2018) Biosensorial application of impedance spectroscopy with focus on DNA detection. In: Schöning MJ, Poghossian A (eds) Label-free biosensing: advanced materials, devices and applications. Springer, Cham, pp 133–178
221. Lisdat F, Schäfer D (2008) The use of electrochemical impedance spectroscopy for biosensing. Anal Bioanal Chem 391:1555–1567. https://doi.org/10.1007/s00216-008-1970-7
222. Munje RD, Muthukumar S, Panneer Selvam A, Prasad S (2015) Flexible nanoporous tunable electrical double layer biosensors for sweat diagnostics. Sci Rep 5:14586. https://doi.org/10.1038/srep14586
223. Lin K-C, Jagannath B, Muthukumar S, Prasad S (2017) Sub-picomolar label-free detection of thrombin using electrochemical impedance spectroscopy of aptamer-functionalized MoS 2. Analyst 142:2770–2780. https://doi.org/10.1039/C7AN00548B
224. Downs AM, Gerson J, Ploense KL, Plaxco KW, Dauphin-Ducharme P (2020) Subsecond-resolved molecular measurements using electrochemical phase interrogation of aptamer-based sensors. Anal Chem 92:14063–14068. https://doi.org/10.1021/acs.analchem.0c03109

225. Magar HS, Hassan RYA, Mulchandani A (2021) Electrochemical impedance spectroscopy (EIS): principles, construction, and biosensing applications. Sensors (Basel) 21:6578. https://doi.org/10.3390/s21196578
226. Bergveld P (1970) Development of an ion-sensitive solid-state device for neurophysiological measurements. IEEE Trans Biomed Eng BME-17:70–71. https://doi.org/10.1109/TBME.1970.4502688
227. Steve C, Jiri J (1980) Field effect transistor sensitive to penicillin. Anal Chem 52:1935–1937. https://doi.org/10.1021/ac50062a035
228. Janata J, Huber RJ (1980) Chemically sensitive field effect transistors. In: Freiser H (ed) Ion-selective electrodes in analytical chemistry. Springer US, Boston, pp 107–174
229. Kaisti M (2017) Detection principles of biological and chemical FET sensors. Biosens Bioelectron 98:437–448. https://doi.org/10.1016/j.bios.2017.07.010
230. Ishikawa FN, Curreli M, Chang H-K, Chen P-C, Zhang R, Cote RJ, Thompson ME, Zhou C (2009) A calibration method for nanowire biosensors to suppress device-to-device variation. ACS Nano 3:3969–3976. https://doi.org/10.1021/nn9011384
231. Nehra A, Pal Singh K (2015) Current trends in nanomaterial embedded field effect transistor-based biosensor. Biosens Bioelectron 74:731–743. https://doi.org/10.1016/j.bios.2015.07.030
232. Meng Z, Stolz RM, Mendecki L, Mirica KA (2019) Electrically-transduced chemical sensors based on two-dimensional nanomaterials. Chem Rev 119:478–598. https://doi.org/10.1021/acs.chemrev.8b00311
233. Bidinger SL, Keene ST, Han S, Plaxco KW, Malliaras GG, Hasan T (2022) Pulsed transistor operation enables miniaturization of electrochemical aptamer-based sensors. Sci Adv 8:eadd4111. https://doi.org/10.1126/sciadv.add4111
234. Sung D, Koo J (2021) A review of BioFET's basic principles and materials for biomedical applications. Biomed Eng Lett 11:85–96. https://doi.org/10.1007/s13534-021-00187-8
235. Nakatsuka N, Yang K-A, Abendroth JM, Cheung K, Xu X, Yang H, Zhao C, Zhu B, Rim YS, Yang Y, Weiss PS, Stojanović MN, Andrews AM (2018) Aptamer-field-effect transistors overcome Debye length limitations for small-molecule sensing. Science 362:319–324. https://doi.org/10.1126/science.aao6750
236. Wang B, Zhao C, Wang Z, Yang K-A, Cheng X, Liu W, Yu W, Lin S, Zhao Y, Cheung KM, Lin H, Hojaiji H, Weiss PS, Stojanović MN, Tomiyama AJ, Andrews AM, Emaminejad S (2022) Wearable aptamer-field-effect transistor sensing system for noninvasive cortisol monitoring. Sci Adv 8:eabk0967. https://doi.org/10.1126/sciadv.abk0967
237. Joshi P, Mishra R, Narayan RJ (2021) Biosensing applications of carbon-based materials. Curr Opin Biomed Eng 18:100274. https://doi.org/10.1016/j.cobme.2021.100274
238. Gooding JJ, Darwish N (2012) The rise of self-assembled monolayers for fabricating electrochemical biosensors – an interfacial perspective. Chem Rec 12:92–105. https://doi.org/10.1002/tcr.201100013
239. Kour R, Arya S, Young S-J, Gupta V, Bandhoria P, Khosla A (2020) Review – recent advances in carbon nanomaterials as electrochemical biosensors. J Electrochem Soc 167:037555. https://doi.org/10.1149/1945-7111/ab6bc4
240. Downs AM, Gerson J, Hossain MN, Ploense K, Pham M, Kraatz H-B, Kippin T, Plaxco KW (2021) Nanoporous gold for the miniaturization of in vivo electrochemical aptamer-based sensors. ACS Sens 6:2299–2306. https://doi.org/10.1021/acssensors.1c00354
241. Bukkitgar SD, Kumar S, Pratibha SS, Singh V, Raghava Reddy K, Sadhu V, Bagihalli GB, Shetti NP, Venkata Reddy C, Ravindranadh K, Naveen S (2020) Functional nanostructured metal oxides and its hybrid electrodes – recent advancements in electrochemical biosensing applications. Microchem J 159:105522. https://doi.org/10.1016/j.microc.2020.105522
242. Soleymani L, Fang Z, Sargent EH, Kelley SO (2009) Programming the detection limits of biosensors through controlled nanostructuring. Nat Nanotechnol 4:844–848. https://doi.org/10.1038/nnano.2009.276
243. Holzinger M, Le Goff A, Cosnier S (2014) Nanomaterials for biosensing applications: a review. Front Chem 2

244. Li H, Dauphin-Ducharme P, Arroyo-Currás N, Tran CH, Vieira PA, Li S, Shin C, Somerson J, Kippin TE, Plaxco KW (2017) A biomimetic phosphatidylcholine-terminated monolayer greatly improves the in vivo performance of electrochemical aptamer-based sensors. Angew Chem Int Ed 56:7492–7495. https://doi.org/10.1002/anie.201700748
245. Shaver A, Curtis SD, Arroyo-Currás N (2020) Alkanethiol monolayer end groups affect the Long-term operational stability and Signaling of electrochemical, aptamer-based sensors in biological fluids. ACS Appl Mater Interfaces 12:11214–11223. https://doi.org/10.1021/acsami.9b22385
246. Herrmann A, Haag R, Schedler U (2021) Hydrogels and their role in biosensing applications. Adv Healthc Mater 10:2100062. https://doi.org/10.1002/adhm.202100062
247. Xu K, Lu Y, Takei K (2019) Multifunctional skin-inspired flexible sensor systems for wearable electronics. Adv Mater Technol 4:1800628. https://doi.org/10.1002/admt.201800628
248. Wong SHD, Deen GR, Bates JS, Maiti C, Lam CYK, Pachauri A, AlAnsari R, Bělský P, Yoon J, Dodda JM (2023) Smart skin-adhesive patches: from design to biomedical applications. Adv Funct Mater 33:2213560. https://doi.org/10.1002/adfm.202213560
249. Myhre P, Smith G (2023) Evaluation of wear time for various extended Wear adhesive tapes on human volunteers: 21-day study. 3M Med Mater Technol
250. Brown EW, Glasscott MW, Conley K, Barr J, Ray JD, Moores LC, Netchaev A (2022) ACEstat: a DIY guide to unlocking the potential of integrated circuit Potentiostats for open-source electrochemical analysis. Anal Chem 94:4906–4912. https://doi.org/10.1021/acs.analchem.1c04226
251. Grattieri M, Minteer SD (2018) Self-powered biosensors. ACS Sens 3:44–53. https://doi.org/10.1021/acssensors.7b00818
252. O'Connor TF, Zaretski AV, Savagatrup S, Printz AD, Wilkes CD, Diaz MI, Sawyer EJ, Lipomi DJ (2016) Wearable organic solar cells with high cyclic bending stability: materials selection criteria. Sol Energy Mater Sol Cells 144:438–444. https://doi.org/10.1016/j.solmat.2015.09.049
253. Pinyou P, Conzuelo F, Sliozberg K, Vivekananthan J, Contin A, Pöller S, Plumeré N, Schuhmann W (2015) Coupling of an enzymatic biofuel cell to an electrochemical cell for self-powered glucose sensing with optical readout. Bioelectrochemistry 106:22–27. https://doi.org/10.1016/j.bioelechem.2015.04.003
254. Rose DP, Ratterman ME, Griffin DK, Hou L, Kelley-Loughnane N, Naik RR, Hagen JA, Papautsky I, Heikenfeld JC (2015) Adhesive RFID sensor patch for monitoring of sweat electrolytes. IEEE Trans Biomed Eng 62:1457–1465. https://doi.org/10.1109/TBME.2014.2369991
255. Idili A, Parolo C, Ortega G, Plaxco KW (2019) Calibration-free measurement of phenylalanine levels in the blood using an electrochemical aptamer-based sensor suitable for point-of-care applications. ACS Sens 4:3227–3233. https://doi.org/10.1021/acssensors.9b01703
256. McHenry A, Friedel M, Heikenfeld J (2022) Voltammetry peak tracking for longer-lasting and reference-electrode-free electrochemical biosensors. Biosensors 12:782. https://doi.org/10.3390/bios12100782
257. Goode JA, Rushworth JVH, Millner PA (2015) Biosensor regeneration: a review of common techniques and outcomes. Langmuir 31:6267–6276. https://doi.org/10.1021/la503533g
258. He W, Wang C, Wang H, Jian M, Lu W, Liang X, Zhang X, Yang F, Zhang Y (2019) Integrated textile sensor patch for real-time and multiplex sweat analysis. Sci Adv 5:eaax0649. https://doi.org/10.1126/sciadv.aax0649
259. Hatamie A, Angizi S, Kumar S, Pandey CM, Simchi A, Willander M, Malhotra BD (2020) Review – textile based chemical and physical sensors for healthcare monitoring. J Electrochem Soc 167:037546. https://doi.org/10.1149/1945-7111/ab6827
260. von Woedtke T, Jülich W-D, Hartmann V, Stieber M, Abel PU (2002) Sterilization of enzyme glucose sensors: problems and concepts. Biosens Bioelectron 17:373–382. https://doi.org/10.1016/s0956-5663(01)00310-4

261. Shah R, Yang Q, Mucic RC, Wang J-HL (2019) Enzyme matrices for use with ethylene oxide sterilization
262. Grucela MM, Gao J (2022) Method of packaging analyte sensors
263. Chung J, Sepunaru L, Plaxco KW (2022) On the disinfection of electrochemical aptamer-based sensors. ECS Sens Plus 1:011604. https://doi.org/10.1149/2754-2726/ac60b2
264. Jackson MA, Ahmann A, Shah VN (2021) Type 2 diabetes and the use of real-time continuous glucose monitoring. Diabetes Technol Ther 23:S-27. https://doi.org/10.1089/dia.2021.0007
265. Porchetta A, Vallée-Bélisle A, Plaxco KW, Ricci F (2012) Using distal-site mutations and allosteric inhibition to tune, extend, and narrow the useful dynamic range of aptamer-based sensors. J Am Chem Soc 134:20601–20604. https://doi.org/10.1021/ja310585e

Adv Biochem Eng Biotechnol (2024) 187: 283–316
https://doi.org/10.1007/10_2023_240

Published online: 26 January 2024

Solid-State Nanopores for Biomolecular Analysis and Detection

Annina Stuber, Tilman Schlotter, Julian Hengsteler, and Nako Nakatsuka

Contents

Abstract Advances in nanopore technology and data processing have rendered DNA sequencing highly accessible, unlocking a new realm of biotechnological opportunities. Commercially available nanopores for DNA sequencing are of biological origin and have certain disadvantages such as having specific environmental requirements to retain functionality. Solid-state nanopores have received increased

Annina Stuber, Tilman Schlotter, and Julian Hengsteler contributed equally to this work.

A. Stuber, T. Schlotter, J. Hengsteler, and N. Nakatsuka (✉)
Laboratory of Biosensors and Bioelectronics, Institute for Biomedical Engineering, ETH Zürich, Zürich, Switzerland
e-mail: nakatsuka@biomed.ee.ethz.ch

attention as modular systems with controllable characteristics that enable deployment in non-physiological milieu. Thus, we focus our review on summarizing recent innovations in the field of solid-state nanopores to envision the future of this technology for biomolecular analysis and detection. We begin by introducing the physical aspects of nanopore measurements ranging from interfacial interactions at pore and electrode surfaces to mass transport of analytes and data analysis of recorded signals. Then, developments in nanopore fabrication and post-processing techniques with the pros and cons of different methodologies are examined. Subsequently, progress to facilitate DNA sequencing using solid-state nanopores is described to assess how this platform is evolving to tackle the more complex challenge of protein sequencing. Beyond sequencing, we highlight the recent developments in biosensing of nucleic acids, proteins, and sugars and conclude with an outlook on the frontiers of nanopore technologies.

Graphical Abstract

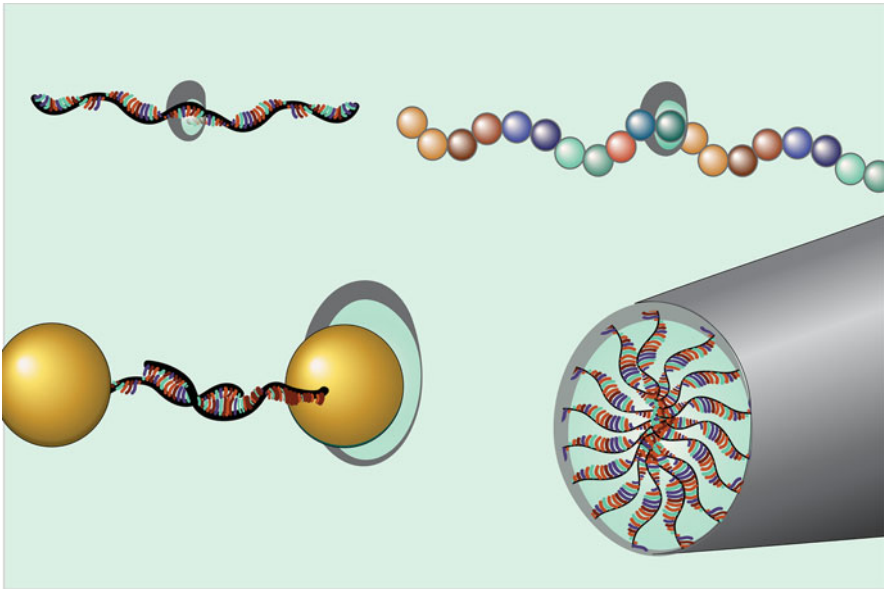

Keywords Aptamers, Biosensing, DNA origami, Genomics, Ionic current, Multiomics, Proteomics, RNA, Sequencing, Single molecule

1 Introduction to Solid-State Nanopores

Nanopore technologies have advanced in recent decades as powerful analytical tools for single-molecule biosensing. The concept of detecting biomolecules through confined nanopores originated over three decades ago for nucleic acid sequencing [1]. In the original configuration inspired by biological processes of membrane transport, the nanopore was a biological protein, alpha-hemolysin, inserted into a lipid bilayer separated by two *cis* and *trans* compartments [2]. Based on the nanoscale dimensions of the alpha-hemolysin nanopore, only single-stranded oligonucleotides and not double-stranded sequences were expected to translocate through the pore. Modulation of the ionic current flowing through the pore from *cis* to *trans* observed in a time-dependent recording enabled differentiation of nucleic acid bases based on the amplitude of current blockades. Today, this technology has been commercialized by Oxford Nanopore.

However, the prospects of nanopore-based biosensing extend far beyond nucleic acid sequencing as summarized in various recent reviews that highlight diverse applications [3, 4] including strategies toward single-molecule protein sequencing [5–7]. While biological nanopores have high reproducibility due to defined channel sizes, certain challenges arise such as the lipid bilayer instability in certain environments, which limits the applied voltage range, use of chemical additives, pH, temperature, and pressure. Further, the lateral diffusion of biological nanopores in the lipid bilayer impedes spatial localization [8]. Several reviews have covered the challenges and opportunities associated with biological nanopores [9, 10]. Alternatively, solid-state nanopores are localized and size tunable to specific applications, albeit with issues such as experimental variability and nonspecific interactions that cause nanopore clogging. Nonetheless, advances in surface chemistries, materials science, and fabrication technologies have improved the robustness of solid-state nanopore biosensors [11].

Herein, we review recent solid-state nanopore innovations to highlight the advances in this field while navigating readers to existing comprehensive review articles that cover specific areas in depth. We first provide a brief background on the working principles of solid-state nanopore-based biosensors and discuss advances in nanopore materials and architectures. Then, we highlight innovative ways in which remaining challenges of solid-state nanopores are being tackled with evolving technologies that are pushing the limits of bioanalytical analysis and detection.

2 Working Principle and Tuning Properties of Nanopores

Ionic current-based solid-state nanopore measurements are conducted by applying a voltage bias between two electrodes each located in two chambers – *cis* and *trans* – separated by a nanoscale orifice. Ionic flux through the nanopore is converted into an electrical current via charge transfer across the solid-liquid interface at the respective

electrode immersed in solution. Several processes influence this charge transfer: (1) the formation of an electric double layer (EDL) at the electrode interface that shields the surface from the ionic bulk, (2) redox reactions at the electrode surface, and (3) mass transport mechanisms. In this section, we briefly cover each of these effects and demonstrate the importance of the choice of nanopore and electrode materials due to different interfacial mechanisms that influence nanopore measurements [12].

2.1 The Electric Double Layer at the Electrode Interface

The electrostatic field from the EDL extends into solution from the electrode surface establishing an electrode potential (i.e., surface potential, E_0), characteristic of the electrode material. Different models have been established to describe the regions of the EDL depending on their constitution and distance from the surface. Most often, the EDL is described as three layers (Fig. 1a). The inner layer is composed of solvent molecules and ions that are specifically adsorbed to the surface forming the inner Helmholtz plane (IHP) at the center of the adsorbed ions. The subsequent layer, constituted by the outer Helmholtz plane (OHP), is formed by solvated ions. These first two layers together are called the Stern layer. The third diffuse, or Gouy-Chapman layer, involves nonspecifically adsorbed ions due to thermal motion in the solution. Formation of the different layers and their implication for electrochemical measurements have been summarized in this prior review [13].

The characteristic EDL equivalent circuit is modeled with three capacitors in series (Fig. 1b). While the potential drop across the Stern layer follows a linear trend (C_{IHP} and C_{OHP}), in the diffuse layer, the potential decays exponentially, modeled by the variable capacitance, C_D in the equivalent circuit. In steady state, the capacitive behavior of the electrode inhibits charges from being transferred across the interface independent of the potential applied by an external voltage source. In such a case, the hypothetical electrode characterized by an absence of faradaic current between the electrode surface and the solution is called an ideal polarizable electrode.

2.2 Redox Reactions at Electrode Surfaces

However, such an ideal polarizable electrode does not exist. At sufficiently large, applied potentials, a redox reaction at the electrode surface occurs. A charge transfer during the redox reaction leads to the conversion of the ionic current into a faradaic current, which can then be measured with electronic instrumentation. The magnitude of the potential that needs to be applied depends on the electrode material. In contrast to the ideal polarizable electrode, an ideal non-polarizable electrode can be modeled by an electric short; there is no potential change upon charge transfer. Typically, a realistic electrode model equivalent circuit consists of a capacitive part due to the

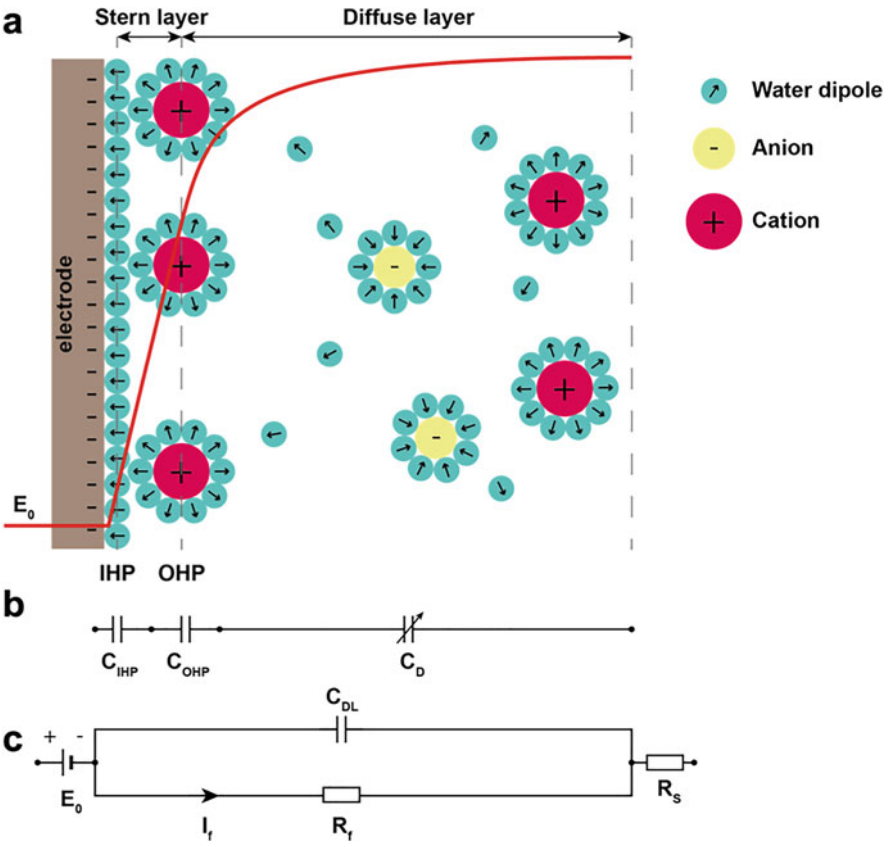

Fig. 1 Formation of an electrical double layer at the electrode liquid interface. (**a**) Schematic of the constitution of the electrical double layer (EDL) with the Stern layer comprising of the inner- and outer-Helmholtz plane (IHP and OHP, respectively) and the diffuse layer extending from the OHP to the bulk of the solution. The potential drop across the EDL is linear in the Stern layer while it decreases exponentially in the diffuse layer. (**b**) The EDL is modeled as a series of capacitors, C_{IHP}, C_{OHP}, and C_D (variable capacitance) respectively. (**c**) The total liquid-electrode interface comprises of capacitive (C_{DL}) as well as resistive (R_f) elements depending on the electrode material. The bulk solution is modeled by a series resistance, R_S. The surface potential is represented as E_0 and faradaic currents as I_f. Adapted with permission from [13]

EDL (C_{DL}) and a resistive part (R_f) in parallel to model the faradaic currents (I_f) of the charge transfer (Fig. 1c). The induced noise by capacitive elements in the system lowers the signal to noise ratio and should be avoided (see Sect. 2.4) [11, 14].

The extent of both components, resistive and capacitive, largely depends on the electrode material. The choice of electrode material not only influences the surface redox reaction, but also the formation of the EDL. Electrode materials with close to non-polarizable characteristics are optimal to reduce capacitive effects; a prominent example of such an electrode material is Ag/AgCl. Due to a reversible redox

reaction, the charge accumulation at the interface and thus EDL formation, can be kept to a minimum. The corresponding half-cell reactions are:

$$\mathrm{Ag^{+} + e^{-} \rightleftharpoons Ag}$$
$$\mathrm{AgCl(s) + e^{-} \rightleftharpoons Ag(s) + Cl^{-}}$$

Biosensing is typically conducted in solutions containing chloride ions (Cl^-) such as phosphate-buffered saline. Hence, the Cl^- dissolved from the electrode due to surface redox reaction does not affect the measurements if the overall chloride concentration remains stable. In addition to stability, Ag/AgCl electrodes are ideal due to ease of fabrication and low impedance.

2.3 *Debye Length and Double Layer Formation in the Nanopore*

In addition to the formation of the EDL at the liquid-electrode interface, the surface charge of the nanopore walls influences conductivity changes that drive sensing measurements. This surface charge is influenced by the membrane or pore material as well as eventual surface modifications. Electrostatic attraction of counterions with opposite charges than the pore wall surface will form an EDL. The layer thickness is determined by the Debye length:

$$\text{Debye length} = \sqrt{\frac{\varepsilon_0 \varepsilon_r k_\mathrm{B} T}{2e^2 I}}$$

This double layer length is a function of the permittivity of free space (ε_0), the dielectric constant (ε_r), the Boltzmann constant (k_B), the absolute temperature (T), the elementary charge (e), and the ionic strength of the electrolyte (I). Thus, the Debye length inside the nanopore depends on the composition of the electrolyte and varies on the order of nanometers from the channel wall. Different characteristics are observed depending on the salt concentration. High salt content leads to a thin EDL (e.g., at physiological salt content, the Debye length is <1 nm), where the transport behavior through the nanopore is minimally influenced by surface charge; the bulk salt concentration dominates over the charge distribution at the nanopore walls. Alternatively, when the ionic content is so low that the EDL overlaps within the center of the nanopore, surface charge effects dominate transport inside the nanopore and ion selectivity to cations or anions is observed. This ion selectivity leads to unique transport properties such as diode-like behavior [15, 16].

In nanopores with asymmetric pore shapes (e.g., nanopipettes or truncated nanopores), ion current rectification (ICR), a non-Ohmic behavior of the nanopore resistance, is observed [15, 17–21]. The origins of this effect lie in both the broken symmetry of the pore geometry as well as the surface charge at the solid/liquid

interface [22]. The current vs. voltage characteristics of such asymmetric nanopores switch from a linear (Ohmic) to a non-linear behavior. Depending on the surface charge inside the nanopore, the current in either the cathodic (negatively charged surface) or anodic (positively charged surface) direction is larger than in the opposite direction, leading to a rectified current response. Thus, the ICR effect enables the detection of charged biomolecules that influence the measured current rectification through translocations or interactions with the nanopore surface.

2.4 Mass Transport Mechanisms

Beyond the charge accumulation behavior at the electrode interface and within nanopores, it is important to understand the basic principles of ion, charge, and mass transport through the solid-state nanopore to interpret measured signals. Ionic transduction through the nanopore is influenced by various factors such as the pore size, geometry, and surface charge. Thus, the choice of nanopore material and dimensions must be carefully considered for specific applications. The analyte of interest must reach the pore by some means of mass transport to enable measurements of translocations or interactions. Besides the random movement of molecules through Brownian motion, three different modes of mass transport are considered: (1) migration of charged species driven by an electric field, (2) analyte diffusion from a region of higher to lower concentration eventually leading to an equilibrium state, and (3) convection through mechanically driven motion (e.g., stirring) or hydrodynamic forces. Application of a voltage across the pore is sufficient to drive migration of charged species such as DNA [2, 23]. Applications such as sequencing [24] necessitate precise control over the translocation dynamics, which requires comprehension of the different mass transport mechanisms [25, 26].

Several works have studied and controlled translocation dynamics using various external influences. For example, the influence of a convective flow parallel to the pore membrane on biomolecule capture rate and translocation time was interrogated [27]. Up to a certain threshold value, larger flow rates led to higher DNA capture rates. A tangential convective flow was also used to slow the speed of translocation events through the nanopore for enhanced temporal resolution for signal acquisition. The effects were rationalized by the size and shape dependence of the nanopore capture volume on the tangential flow. In another study, the hydrodynamic behavior of DNA was investigated in a nanofluidic system with integrated nanostructures [28]. Long DNA strands were guided into nanochannels without clogging using nanopillars that changed the fluidic resistance in the vicinity of the channel entrance, which slowed down DNA locomotion. Upon entering the channel, the flow rate of DNA increased due to the decreased cross-sectional area. The abrupt change from slow to fast rates led to stretching of the DNA strands and an overall stabilized speed within the channel. A similar microfluidic chip design was used to stretch and sort DNA molecules prior to translocation through the nanopore [29].

Due to pore dimensions in the range between several tens (<10 nm) and hundreds (>10 nm) of ions, both classical continuous methods and molecular theories as well as hybrid models must be considered when explaining mass transport through a nanopore, which has been summarized in recent publications [30, 31]. In pores <50 nm, the EDL must be considered for the ion transport [32]. When the EDL of two walls is overlapping (usually pores <5 nm), electroneutrality breaks down and the concentration of current carriers is regulated by the pore surface rather than by bulk concentration [33, 34]. Consequently, this effect allows regulation of ion concentration to modulate the transport within nanopores. Reaching a pore size of a single ion leads to a surface charge-dependent state where the passage of ions is allowed or blocked called ionic coulomb blockade [35, 36].

2.5 Noise and Data Analysis for Nanopore Measurements

When measuring low ionic currents down to the single pA range, noise must be reduced as much as possible. The noise is described as the root mean square of the baseline current I_{RMS}, which is defined as the integral of the power spectral density $S(f)$ with respect to the bandwidth at which the ionic current is measured [14, 37–40]:

$$I_{\mathrm{RMS}}^2 = \int_0^{\mathrm{BW}} S(f)\, df$$

Depending on the bandwidth (BW), different contributions to the power spectral density are predominant. At low frequencies, flicker noise also called 1/*f*-noise is dominating. At higher frequencies, white noise or thermal noise is the highest component to the power spectral density. At intermediate bandwidths, the dielectric noise, $S_{\mathrm{dielectric}}$ becomes dominant and at frequencies above 100 kHz, the capacitive noise, $S_{\mathrm{capacitive}}$ takes over:

$$\begin{aligned} S(f) &= S_{\mathrm{flicker}} + S_{\mathrm{white}} + S_{\mathrm{dielectric}} + S_{\mathrm{capacitive}} \\ &= \frac{\alpha_H I^2}{N_c f} + \frac{4k_B T}{R} + 8\pi k_B T C_M D_M f + 4\pi^2((C_M + C_W + C_i + C_v)v_n)^2 f^2 \\ &= A \cdot \frac{1}{f} + B + C \cdot f + D \cdot f^2 \end{aligned}$$

In the equation, α is a constant, I, the ionic current, N_c is the number of charge carriers in the pore volume, f, the bandwidth, k_B, the Boltzmann constant, T, the temperature (in Kelvin), R is the equivalent resistance of the nanopore, C_M and D_M, the membrane capacitance and dielectric constant respectively, and C_W, C_i, C_v, the capacitance of the wiring, amplifier input, and amplifier feedback capacitance

respectively, and ν_n, the voltage noise density (V/√Hz) of the input amplifier [14, 41]. The power spectral density of a measured signal can be calculated from the auto-correlation function of the measured signal itself. Hence, all capacitance effects in the system should be reduced for optimization.

Another challenge in nanopore sensing is the vast amount of data that is produced in massively parallel and high bandwidth measurements, which requires the development of new data structures [42]. Real-time data analysis necessitates signal filtering alongside identification and characterization of translocation events. Further discussions on nanopore data analysis can be found in this prior publication [43]. The process of assigning electrical current levels to individual nucleobases as the DNA passes through the nanopore is called base calling [44]. In the advent of nanopore sequencing, Hidden Markov models, which calculate the highest probability of a next state based on prior states, were commonly used for time series segmentation [45]. Current approaches focus on improving neural networks for data analysis [46–48]. Further, application of a time-varying (non-constant) potential across the pore was also reported to increase the accuracy of DNA sequencing with nanopores [49].

2.6 Nanopore Fabrication, Size Tuning, and Functionalization

In addition to the electrode material, the geometry and orifice size of the nanopore influences the overall measurement sensitivity, as the diameter and shape not only define the size range of translocatable molecules, but also what kind of molecules induce a measurable change in current. Various nanopore materials such as silicon-nitride (SiN) [50], glass nanopipettes [51, 52], oxides [53, 54], and 2-D materials such as graphene [55, 56], hexagonal boron nitride (h-BN) [57], molybdenum disulfide (MoS_2) [57], and tungsten disulfide (WS_2) [58] have been reported. Details on nanopore materials as well as methods for nanopore fabrication are summarized in numerous reviews [11, 59–63]. Herein, we highlight a few state-of-the-art and recently developed techniques for nanopore fabrication, pore size tuning, and routes for functionalization to tackle nanopore stability and nonspecific binding.

Focused ion beam milling and transmission electron microscopy have the potential to make precise pores below 10 nm and enable real-time monitoring of the fabrication process with control over both location and number of pores created [64, 65]. However, both methods are costly in time and instrumentation and are prone to chemical contaminations within the pore. A higher throughput and lower cost method is laser pulling of quartz or borosilicate capillaries to form two pipettes with openings ranging from microns to nanometers at the tip; sizes are tuned based on a variety of pulling parameters including the temperature, force, and velocity [66]. However, it is not possible to monitor the pore formation in real time and characterization of the exact pore dimensions is challenging.

Nevertheless, due to the broad application of nanopipettes in a variety of different disciplines in addition to single molecule sensing and sequencing (e.g., scanning probe microscopy [67], electrochemical measurements [68] or 3-D printing [69]), new laser pulling programs of small nanoscale pipettes are continuously developed. The smallest reported pipette orifice diameters now reach scales down to 1–2 nm [70]. Pushing the dimension limits toward angstrom levels, 2-D slit-like structures have been reported [71]. The angstrom size of the channel that is tuneable through stacking of 2-D material layers comes at the cost of requiring multi-step assembly processes [71]. While the orifice dimensions of these 2-D channels as well as the pore diameters of the nanopipettes can be fine-tuned, both methods are not designed for large-scale production and alternative methods such as controlled electric breakdown (CEB) [72] have been established as reliable and automated techniques for large-scale production [61] (Fig. 2a). Since nanopores formed by traditional CEB are randomly positioned in the membrane, latest research aims to improve the efficiency and robustness of pore formation as well as the pore size control [73] by the additional use of an atomic force microscope [76], local electric field enhancement [77], laser enhancement [78], and on chip electrodes [79].

Alternatively, once a pore is fabricated, there are post-processing techniques to optimize the size of the pore. Pulsing high electric fields have been shown to increase the diameter of existing nanopores with sub-nanometer resolution [80]. This method is advantageous as size tuning can be performed in situ under desired experimental conditions. Visual feedback is not possible during the growth, but the pore dimensions can be extrapolated from the measured conductance between voltage pulses [81]. However, the pore growth rate accelerates with increased pore dimensions in a non-linear manner, rendering reproducible pore formation challenging. Transmission electron microscopy has also been used to expand silicon oxide pores with diameters $>$80 nm [64]. On the contrary, if the pore diameter is $<$50 nm, applying the same technique will result in diameter reduction. Similarly, shrinking SiN nanopores using scanning electron microscopy has been reported [82]. The image magnification and accelerating voltages can be tuned to shrink the pore linearly, implying that this method shrinks the pore at the same rate regardless of the initial diameter.

Chemical routes also enable size tuning of nanopores [83]. Atomic layer deposition coats layers of materials with near-Angstrom precision to shrink nanopore orifices [84]. The advantages of this method include the precise control of membrane thickness based on the number of deposition cycles as well as the possibility to coat different materials. Alternatively, cyclic atomic layer deposition has also been reported to allow 3-D pore tuning, forming conical pores [85]. Tuning both the length of the funnel as well as shrinking the pore diameter to desired dimensions enabled generation of “stalactite-shaped” nanopores. Another method to shrink the opening involves tannic acid modifications, which has the advantage of tuning the thickness reversibly via controlling the amounts of crosslinker present (Fig. 2b) [74]. However, the precision of this method is not at the atomic scale. For both these chemical methods, the deposition occurs over the entirety of the pore as well as the membrane and will not only decrease the pore diameter, but will also increase the

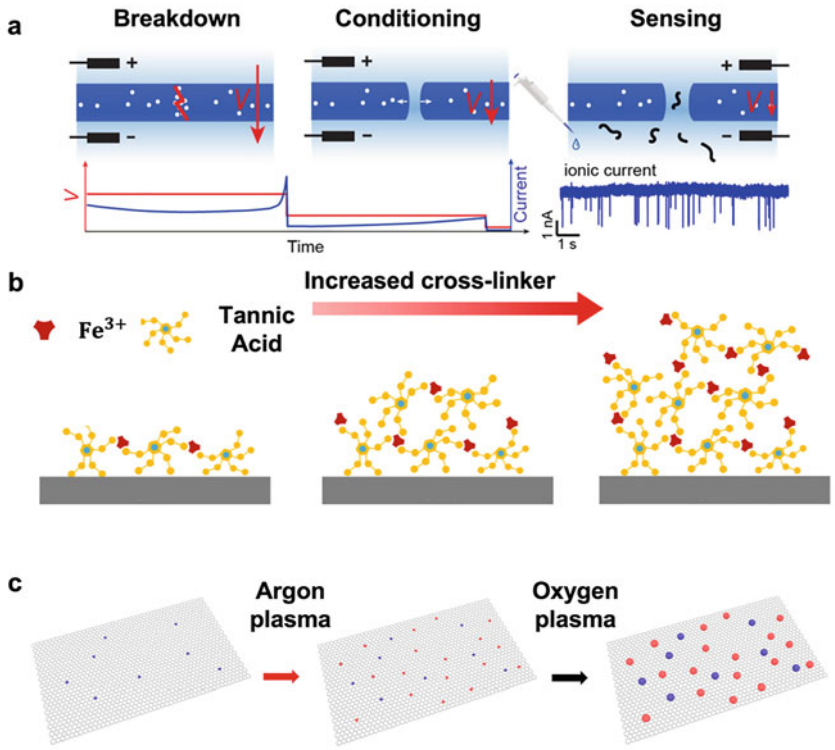

Fig. 2 Physical and chemical processes to fine-tune nanopore size. (**a**) Schematic of the process of controlled electrical breakdown (CEB). Application of a high voltage (V) across a thin isolating membrane induces local stress that causes the material to breakdown and form a pore. An electric field can then be used in a conditioning step to tune the size of the pore [73]. (**b**) Tannic acid crosslinks on a surface in the presence of iron (Fe^{3+}) and can be reversibly tuned by modifying the Fe^{3+} concentration [74]. (**c**) Impurities are generated in graphene sheets using argon plasma, and the impurities are transformed into nanopores by tuning oxygen plasma exposure [75]

membrane thickness, which may not be desirable for certain applications. Alternatively, routes for enlarging nanopores with nanoscale precision have been reported within graphene sheets [75]. Upon exposure to oxygen plasma, the imperfections (initially induced through low-energy argon plasma) can be expanded, however, with limited control over the location of the nanopores in the graphene sheet (Fig. 2c).

Another unique approach to modulate pore sizes involves the integration of DNA origami programmed to adopt various shapes and dimensions. Nanopores were blocked with a 2-D DNA origami cover via an induced electric field [86]. The DNA cover is transparent to ions while blocking larger molecules from entering the pore and can be removed by applying an inverse potential [86]. Recently, this DNA-gate method was endowed with selectivity by incorporating binding

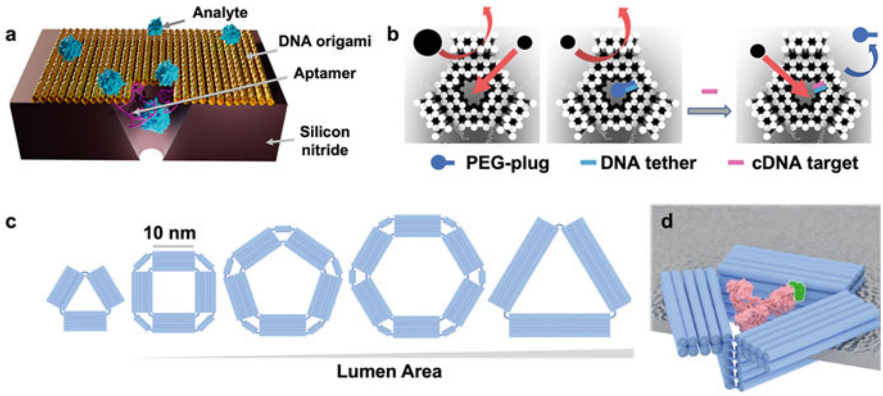

Fig. 3 Engineering DNA origami to generate versatile nanopores. (**a**) A 2-D DNA origami decorated with aptamers immobilized at the entrance of a solid-state nanopore to slow down specific translocation events [87]. (**b**) A DNA origami pore engineered to discriminate molecules based on orifice size. A poly(ethylene glycol) (PEG) plug is tethered to the wall of the nanopore via a short DNA tether strand and partially occludes the opening, limiting molecular passage. Complementary DNA (cDNA) binds competitively with the DNA strand tethering the PEG-plug, releasing the plug, and increasing the pore size [88]. (**c**) A multitude of shapes and sizes of nanopores have been designed using DNA origami. (**d**) The nanopore shape can be tuned to the analyte of interest: a triangular pore allowed increased analyte-shape specificity for the translocation of antibodies with shape complementarity [89]

molecules such as aptamers into the origami structure (Fig. 3a) [87]. Aptamers are versatile, artificial single-stranded oligonucleotide sequences isolated to bind to a specific analyte of interest, and have been incorporated into many biosensing platforms, including nanopores [87, 88].

To enlarge the DNA origami pore in-situ during measurements, a trigger was introduced to enable gating of the pore (Fig. 3b) [88]. The nanopores (~10 nm) were partially occluded due to a poly(ethylene glycol) (PEG) polymer plug (~5 nm) tethered to the pore wall with a short DNA segment, termed a staple. The tether of the PEG-oligo served as a toehold to which a specific single-stranded DNA could competitively bind, and thus detach the plug from inside the nanopore. The size of the nanopore was therefore doubled upon the addition of the specific strand of DNA, enabling larger molecules to pass through. However, once the plug is released, the nanopore orifice size is unalterable; further development is required to enable real-time tuning of the nanopore size.

Harnessing the flexibility of DNA origami assemblies, diverse nanopore shapes ranging from triangles, squares, pentagons, and hexagons between 10 and 20 nm in diameter have been explored (Fig. 3c) [89]. Nanopores with geometries tailored to the analyte of interest (e.g., triangular pores for antibodies) led to increased measurable blockade events (Fig. 3d). The tunability of DNA origami extends beyond modulating pore sizes but also channels and the membranes into which they are incorporated. For example, T-shaped DNA have been immobilized in lipidic membranes due to their specific geometry and hydrophobic motifs [90]. Most engineered

DNA membrane channels have relatively small dimensions (<5 nm in diameter) as larger structures have a tendency of collapsing and have difficulties incorporating into membranes. Recently, DNA origami nanopores with dimensions up to 30 nm have been achieved by coating the negatively charged DNA nanopore surface with positively charged lysine-coupled PEG [91]. This polymer coating prevents the DNA nanopore from disassembling in low ionic environments and minimizes potential nuclease degradation [92]. The ability to tune the nanopore dimensions with nanoscale resolution up to 30 nm combined with the possibility to functionalize specific areas of the pore with recognition elements selectively opens a vast range of possibilities for biosensing.

While advanced nanopore fabrication methods as well as post-modification techniques allow precise tailoring of nanopore dimensions, these proportions are not necessarily maintained over prolonged measurements. Long-term stability is a critical characteristic for a reliable nanopore sensor, especially when pre- and post-calibration steps are necessary when deploying sensors in clinically relevant environments. Conditions necessary for nanopore sensing such as prolonged exposure to ions or static voltages have been shown to enlarge pores after reaching a material-dependent threshold [93–95]. The issue of applied static voltages can be circumvented with the use of controlled, short, pulsed potentials that improve nanopore stability while simultaneously reducing clogging by removing debris within the pore [80, 81]. Accumulation of contaminants at the orifice of the nanopore can also be avoided via washing procedures and optimized storage conditions post-washing have a substantial influence on the nanopore longevity [94]. Treating the nanopore surfaces chemically has also been reported to protect the orifice and help maintain stability, thus promoting a reusable and more reliable sensor [95].

In addition to accumulation of contaminants, a major limitation of solid-state nanopores is the inevitable nonspecific binding to the inner walls, which leads to clogging or convoluted signals of translocating molecules [96]. While being common analytes to study, proteins are especially prone to interact with the walls of synthetic nanopores via intermolecular interactions such as electrostatics, hydrophobic, and van der Waals forces [97]. Nonspecific adhesion to the nanopore walls can lead to signal artifacts, pore clogging, and unresolved translocation events. Nanopore surface coatings can be employed to reduce the influence of these intermolecular interactions, which has been summarized in a recent review (Fig. 4) [98]. Such surface modifications can also increase the stability of synthetic nanopores by reducing the amount of etching that occurs over time in electrolyte solutions leading to changes in pore size [98]. Further, such chemistries can be harnessed to manipulate surface charges to drive certain targets through the pore [99–101].

Chemical modifications of solid-state nanopores are not limited to antifouling applications, but also for applications that necessitate specific interactions achieved through functionalization of biological receptors on the nanopore surface. For biosensing specific analytes of interest, molecular selectivity to differentiate targets from structurally similar or interfering biomolecules is critical. Various modification strategies have been established to endow nanopores with chemical selectivity

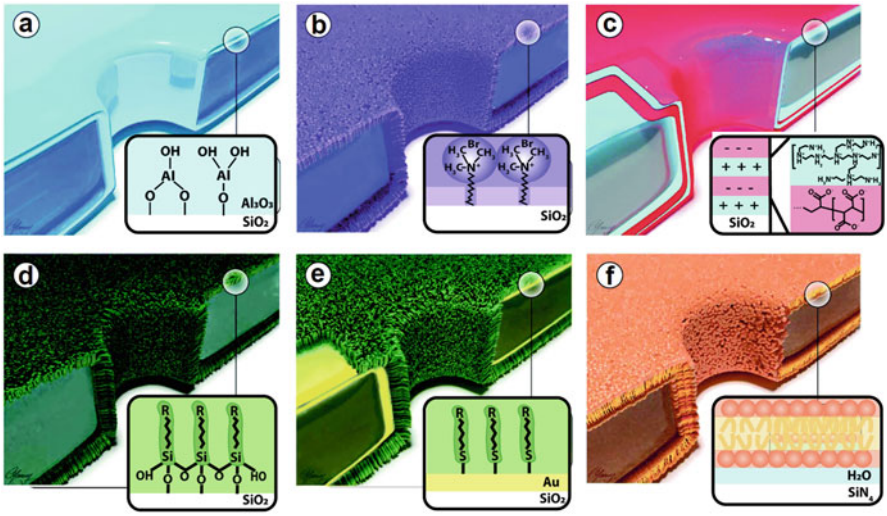

Fig. 4 Schematic cross sections of commonly used nanopore coatings. (**a**) Coating of Al_2O_3 deposited on an SiO_2 membrane. (**b**) Surfactants physisorbed on the nanopore walls. (**c**) Alternating layer-by-layer assembly of positively and negatively charged polymers. (**d**) Silanization of SiO_2 surfaces. (**e**) Self-assembled monolayers of alkanethiols on gold-deposited SiO_2 nanopores. (**f**) Fluid lipid bilayers assembled on SiN nanopore walls. Figure adapted from [98]

[102]. A recent review has summarized the use of polymer-functionalized nanopores that gate molecular transport based on external stimuli [103]. Further, biological protein- [104, 105] and oligonucleotide-based [106–108] receptors have been integrated into nanopores to detect a range of analytes including metal ions [109, 110], small molecules [111–113], nucleic acids [114, 115], or proteins [106, 116]. However, controlling the quality and spatial arrangement/density of the assembled biomolecules inside of nanopores is challenging as there are limited analytical methodologies that can characterize physico-chemical properties at the nanoscale [117, 118]. Thus, quantitative characterization of the surface chemistry on planar surfaces using methods such as quartz crystal microbalance with dissipation monitoring (QCM-D) may give insight into the morphology, surface density, and stability of the assembled biological receptors [112, 119].

3 Advances in Sequencing Using Solid-State Nanopores

Biological nanopores have already been widely deployed for biomolecular diagnostics [120], realized third-generation DNA/RNA sequencing [121], and paved the way for commercially available low-cost DNA sequencing devices [122, 123]. Instead, solid-state systems are now emerging as the next-generation nanopore technology for DNA/RNA sequencing due to the advantages of

processability, robustness, and flexibility in nanopore dimensions compared with biological nanopores [11, 62]. Despite these advantages, solid-state nanopores are not yet commercially used for nucleic acid sequencing, due to challenges such as insufficient spatial and temporal resolution [124]. In this section, we cover recent advances in solid-state nanopore DNA sequencing that are tackling remaining issues and present technological developments toward achieving protein sequencing.

3.1 Tackling Remaining Challenges of Solid-State Nanopore DNA Sequencing

The spatial resolution issue of solid-state nanopores can be addressed by fabricating nanopores out of 2-D materials where the membrane thickness matches the length to each nucleobase [55, 56]. The spacing between two bases in a DNA chain is ~0.34 nm, comparable to the thickness of a single layer of graphene, rendering this material a promising candidate for high-resolution DNA sequencing [125]. Providing adequate spatial resolution also reduces the complexity of the recorded signal. Future applications may include composites of different stacked 2-D materials, which have the potential to improve the temporal resolution [126].

Regarding temporal resolution, slowing down of translocation speeds has posed a major challenge for solid-state nanopores, especially for sequencing [26]. Control of experimental conditions such as electrolyte temperature, salt concentration and content, solution viscosity, and electrical bias has been shown to reduce DNA translocation speeds by an order of magnitude through solid-state nanopores [127, 128]. However, for physiologically relevant recordings, such parameters may not be tunable. Alternatively, DNA molecules tethered to beads have been mechanically manipulated via optical tweezers or magnetic traps [129, 130]. While effective for sequencing methodologies, labeled methods are limiting for biosensing. Existing label-free methods influence the DNA translocation through intermolecular interactions between the nanopore surface and DNA [131] or by modulating the electric field [132, 133].

Alternatively, the porosity at either the entry or exit (*cis* or *trans* respectively) has been tuned to slow DNA translocation. A copolymer nanofiber mesh with tunable chemical and physical properties was electrospun onto the *cis* side, slowing DNA passage due to hydrophobic interactions [134]. In another report, nanopipettes filled with hydrogels enabled slowing of translocating DNA through tuning of the hydrogel mesh size and chemical composition [135]. Despite large nanopipette pore diameters (>20 nm), using engineered hydrogels with tuned mesh sizes and surface charge, short DNA strands (down to 100 base pairs) could be selectively detected.

While slowing down the translocation speeds is one way of achieving the goal of measuring events that are otherwise too fast to be detected, an alternative strategy is to improve the temporal resolution of the instrumentation. Measuring fast events on the order of micro- or nanoseconds, necessitates bandwidths exceeding 1 MHz, in a

frequency range where thermal and capacitive noise are dominating. While temperature is not easily adaptable especially in biological systems, the capacitive effects can be optimized. The choice of pore material and geometry as well as amplifier and interconnect design play an important role in improving the capacitive characteristics of the setup [41]. New developments in complementary metal-oxide-semiconductor (CMOS) design allow reductions in parasitic capacitances of the amplifier circuitry and enable fast signal acquisition at low noise [39, 136]. Highspeed sampling of 40 million samples per second recorded single-stranded DNA translocations at bandwidths of 100 MHz or 100 ns long events [137]. Such strategies to tackle the current shortcomings of DNA sequencing with solid-state nanopores hold great promise for the future of this technology.

3.2 Toward Solid-State Nanopore Protein Sequencing

To unlock the holy grail of single-molecule proteomics, nanopore technologies are evolving beyond oligonucleotide sequencing. Recent reports highlight how biological nanopores are making advances toward achieving the ambitious vision of sequencing peptides or even full-length, unfolded proteins with single-amino acid resolution and discrimination of post-translational modifications [138, 139]. An ideal nanopore sensor for single-cell proteomics must have the following characteristics: high mechanical, thermal, electrical, and chemical stability to withstand non-physiological and protein-denaturing conditions as well as high electrical bias potentials [140–144]. Stability in non-physiological conditions, which is a challenge for biological nanopores, can be addressed by using solid-state materials. For example, heat denaturation and anionic surfactants have been used to facilitate solid-state nanopore sensing of unfolded proteins [145]. Precise size tunability of nanopores for analyte-specific detection is advantageous compared to current membrane-embedded systems [146]. Various studies have correlated molecular dwell times in solid-state nanopores to the pore diameter and slowing translocation times is advantageous for sequencing [145, 147].

To manufacture a spatially resolved nanopore, a pore was integrated into a hollow SiN atomic force microscope (AFM) cantilever using combined Ga-ion beam drilling and afterward He^+-ion sculpturing to shrink down the pore to the desired dimensions [148] (Fig. 5a). A pore pre-confinement was achieved by bringing the integrated nanopore in contact with a rigid glass substrate from solution, which resulted in a change from resistive pulses to conductive peaks upon translocation of the protein, fibronectin (Fig. 5b). Reversible, real-time pore size tuning has been achieved using fluid force microscopy [150] that combines an AFM with integrated microfluidics through a pore. A hollow SiN cantilever with a 300 nm diameter is mounted on the AFM and brought into contact with a soft polymeric substrate [149] (Fig. 5c). The confined nanogap between the cantilever and the soft substrate becomes an interface nanopore (iNP). Using AFM force feedback, iNPs in the range of 2–20 nm can be achieved based on the cantilever indentation force into

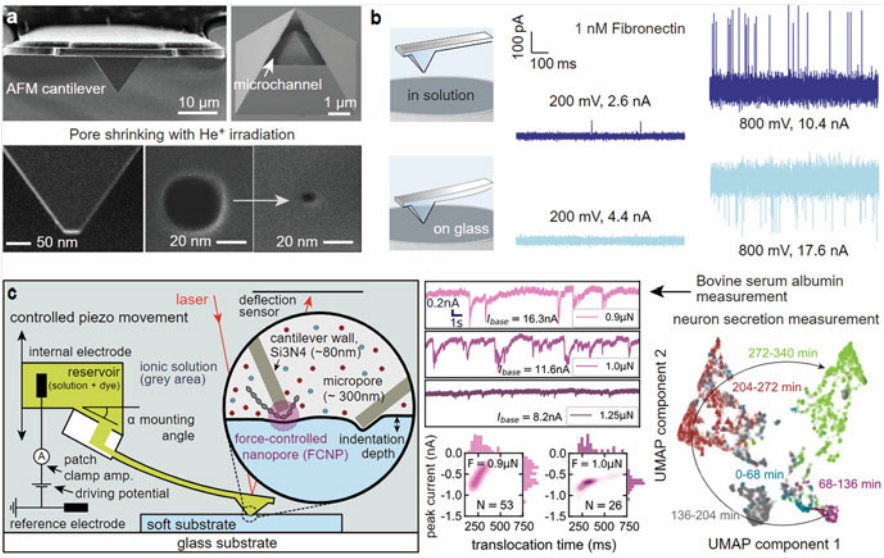

Fig. 5 On-demand pore adjustability with force-controlled interface nanopores (iNPs). (**a**) Scanning electron microscopy image of the hollow atomic force microscopy (AFM) cantilever and cutaway view of a pyramidal apex and embedded microchannel. The pore is drilled and sculpted with a focused He^+ ion beam [148]. (**b**) Translocation of the protein fibronectin through a nanopore in pure solution (top) and on glass (bottom). Inversion from resistive pulse to conductive pulse is observed when approaching a substrate. (**c**) Schematic of the force-controlled iNP with pore-dimension control for bovine serum albumin translocation measurements and long-term recordings (up to ~6 h) next to neural cells [149]

the substrate. Pore size adjustments were demonstrated in situ by controlling bovine serum albumin protein translocation events in a single measurement. At low applied forces (large pore openings), protein translocations were observed, which were hindered by increasing the force exerted by the cantilever, which decreased the pore size mid-recording. Further, the system enabled neuron secretion measurements over several hours.

Several key challenges of conventional nanopore systems can be tackled using iNPs: on-demand pore size adjustability is enabled by positioning two substrates with nanoscale resolution. Moreover, as the iNP is formed at the interface of two surfaces, each side of the nanopore can be individually functionalized with different surface chemistries. To realize single-molecule protein sequencing, current research is focused on distinguishing different amino acids in the backbone of peptides. To detect specific amino acids, aptamers have been integrated into iNPs with tunable pore sizes. Using aptamer-functionalized iNPs, peptides with phenylalanine motifs [151] were discriminated based on specific aptamer-amino-acid interactions [152]. Molecular recognition increased peptide retention times inside the iNP, enabling differentiation between specific vs. nonspecific sequences where

phenylalanine was replaced by structurally similar amino acids (i.e., tyrosine and tryptophan). Discrimination of single amino acids in a peptide backbone is a promising step toward sequencing – an array of different amino acid-specific aptamers functionalized in succession would expand the capabilities of this system.

One of the significant challenges of protein sequencing is distinguishing the current levels of 20 different amino acids and deconvoluting the complex signals for each amino acid. One route to error minimization when reading peptide sequences is to re-read a single molecule [138]. The iNP fabrication based on standard lithographic processes renders this system optimal for serial nanopores enabling multiple re-reads. Further, integration of neural networks has potential in classifying ionic current signals based on specific amino acids [153]. In the future, combining such machine learning algorithms may enable distinguishing similar proteins with single-point mutations or post-translational modifications.

4 Applications Beyond Sequencing Using Solid-State Nanopores

To date, the use of solid-state nanopores extends well beyond sequencing and has been adapted to analyze biomolecular interactions and stochastic processes in diverse systems. Nanopores are advantageous biosensing platforms due to their capacity to convert chemical and structural signatures of diverse analytes into measurable electronic signals. Further, the mechanism of detection enables exploration of large populations of molecules at the single-molecule level. Thus, solid-state nanopores are valuable tools for sensing biomarkers for molecular diagnostic applications [154–157]. While we focus on progress in the biosensing realm, alternative applications that harness the confined nanopore chemical environment have been reported, such as protein nanoreactors [158, 159]. Other reviews have extensively covered many recent advances [4]. Herein, we focus on advances in nucleic acid, protein, sugar, and intracellular sensing using solid-state nanopores reported in the last few years.

4.1 Nucleic Acid Biosensing

Besides single-molecule DNA/RNA sequencing, various applications for nucleic acid sensing with solid-state nanopores have been reported [9]. When the COVID-19 pandemic hit in late 2019, solid-state nanopores were deployed to classify corona virus RNA [160]. An amplification-free approach using solid-state nanopores enabled quantification of multiple RNA types with the possibility to distinguish between viral RNA and a human reference gene. The SARS-CoV-2 RNA was detected directly in clinical patient samples collected by nasal swabs (Fig. 6a).

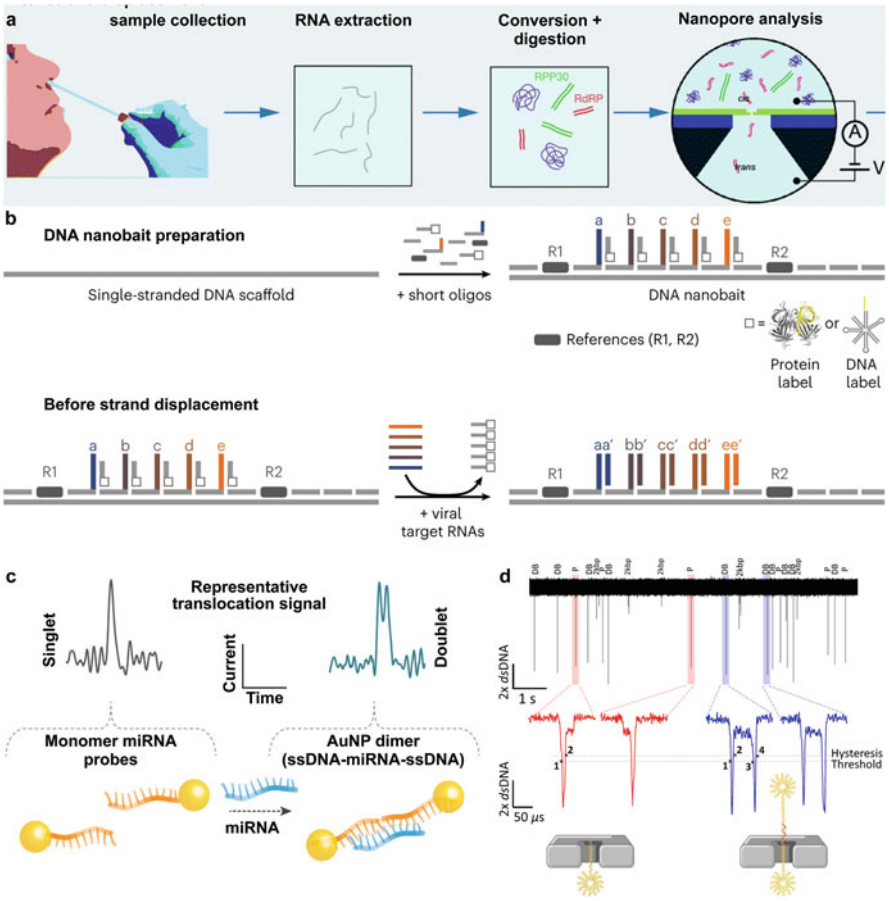

Fig. 6 Strategies for nucleic acid biosensing using solid-state nanopores. (**a**) Detection of Sars-Cov-2 RNA strands using silicon nitride nanopores in clinical samples [160]. (**b**) Multiplexed viral RNA detection via self-assembled DNA nanobaits. Short oligos labeled with either protein or DNA are hybridized to the nanobait. Presence of multiple viral target RNAs competitively displaces tethered labeled strands, which are subsequently analyzed by a nanopore [161]. (**c**) Short miRNA targets are detected via two populations of gold nanoparticles (AuNPs) with half the complementary sequence (monomers) to the target. In the presence of the target miRNA, the nanoparticles dimerize resulting in a doublet signal upon translocation vs. singlet signals for single nanoparticles [160]. (**d**) Digital nanopore sensing that differentiates the fraction of single peak probes vs. doublets from "dumbbells" when two probes are hybridized. Concentration quantification of protein biomarkers is possible due to a digital immunoassay workflow that translates protein amounts to a complementary DNA that hybridizes two nanospheres together [162]

This report demonstrates the potential of single-molecule sensing approaches to overcome remaining challenges of state-of-the-art techniques such as reverse transcription quantitative polymerase chain reaction (RT-qPCR), the most widespread nucleic acid amplification test.

While RT-qPCR is a highly sensitive approach to sense viral nucleic acids in complex biological samples, it has limited multiplexing capabilities. To address the need for simultaneous detection of multiple viruses and variants, programmable DNA was harnessed and coupled to solid-state nanopores [161]. A self-assembled DNA nanobait, consisting of a single-stranded DNA scaffold with attached complementary short oligos were displaced upon exposure to viral target RNAs. This mechanism facilitated the multiplexed identification of different viruses (Fig. 6b). The displaced oligo was tagged with either protein or DNA-based labels to amplify the signals in nanopore recordings. This system enabled simultaneous detection of five different respiratory viruses or SARS-CoV-2 variants in parallel.

An alternative prevalent application is early-stage screening of biomarkers found in low abundance in complex media. Solid-state nanopores coupled to nanoparticle probes that generate characteristic translocation current levels enabled detection of short miRNA sequences upregulated in patients with prostate cancer (Fig. 6c) [163]. Two populations of nanoparticles with half the complementary miRNA sequence are introduced, which dimerize in the presence of the miRNA and form a doublet signal upon translocation, which is distinguishable from the singlet signals from single nanoparticles. This method has also been deployed for the detection of proteins such as procalcitonin, a biomarker for sepsis. Using a similar strategy, DNA hybridization was harnessed for a DNA-protein digital immunoassay for biomarker quantification [163] (Fig. 6d). Nanospheres immobilized with DNA strands detected target proteins such as thyroid-stimulating hormone tagged with complementary sequences, resulting in a distinguishable nanostructure with a double-peak ionic current signature upon translocation. Extracting the ratio of the different signatures in the signal allows for concentration quantification of the target molecule of interest.

The implementation of multiplexed sensing presents a way to increase the information that can be obtained from just one sample. A mobile nanopore at the tip of a nanopipette enabled spatial and temporal control for multiplexed nucleic acid sensing. By gradually approaching a glass slide immobilized with hybrid DNA using an XYZ positioner with nanometer resolution, DNA translocations were re-read with controlled speeds which reduced the error rate [164]. Additionally, by leveraging the XY scanning capability of the positioner, a region of interest can be selected on the glass slide; analysis of different surface-tethered DNA is possible using one nanopore.

In addition to detecting specific nucleic acid sequences and harnessing hybridization events, different nucleic acid conformations can be probed. For example, conformational analysis of RNA (~300–2,000 nucleotides in length) under native conditions was performed using a polymer-electrolyte solid-state nanopore [165]. The polymer in the bath solution enabled control over translocation dynamics of the analyte [166], while allowing the sample containing DNA to be in physiological conditions promoting native DNA folded states.

Rather than differentiating translocating nucleic acid structures, the conformational dynamics of DNA aptamers covalently modified in ~10 nm nanopores has modulated the detection of small molecules such as serotonin [167]. Upon target recognition, aptamer structure-switching modulates the ionic current in a target-

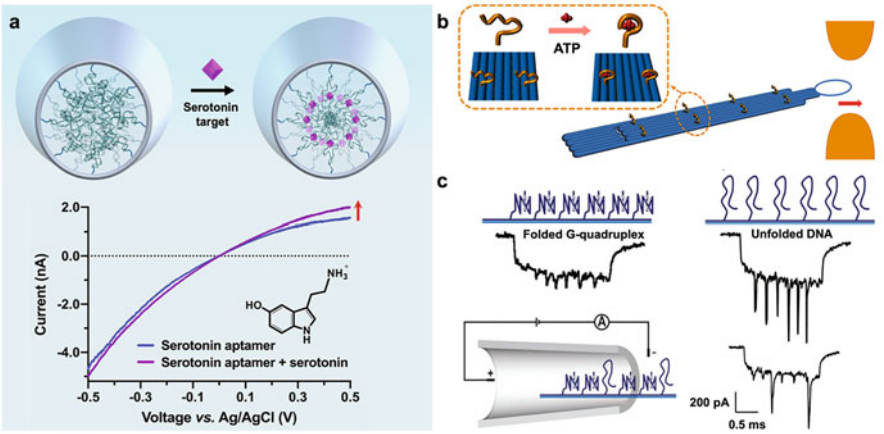

Fig. 7 Harnessing DNA conformational changes for detection in nanopores. (**a**) Aptamers covalently functionalized inside of nanopipettes (10 nm pores) allow detection of serotonin upon target-driven conformational changes that modulate the current flux through the nanopore [167]. The rearrangement of negatively charged aptamers upon serotonin capture inside the nanopore leads to an increase in the ionic current upon application of a positive potential. The non-linear behavior of the ionic current arises from the asymmetric diffusion of ions through the nanopore due to the nanopipette geometry (pore size and conical angle) and the surface charge density of the nanopore walls. (**b**) Aptamers immobilized on a DNA origami raft enabled adenosine triphosphate (ATP) detection based on a characteristic translocation signal generated through different conformations of the ATP aptamers [168]. (**c**) The state and conformation of G-quadruplexes folded on a DNA carrier resulted in specific peaks upon nanopore translocation [169]

specific manner (Fig. 7a). The advantage of this mechanism vs. stochastic detection of analytes is the ability to sense in complex biofluids with high concentrations of interferents. Nonspecific binding to the nanopore surface and entry of proteins $>$10 nm is hindered by completely functionalizing the inside of the ~10 nm nanopore with aptamers ~5 nm in size. Serotonin released from human serotonergic neurons has been quantified at physiologically relevant concentrations using such aptamer-modified nanopipettes [170].

Following a similar mechanistic principle, adenosine-5 triphosphate (ATP) aptamers have been immobilized inside of nanopipettes to allow ATP detection [171]. An increase in current is measured upon ATP binding to aptamers confined within nanopipettes, hypothesized due to pore enlarging upon aptamer structure switching, as well as a local charge increase. Instead of being functionalized inside of nanopore surfaces, ATP aptamers have also been immobilized onto DNA origami ribbons, allowing the detection of small-molecule translocation events (Fig. 7b) [168]. While detection of small molecules such as ATP alone is challenging, target-specific structure switching of ATP-specific aptamers on the DNA origami ribbon led to differentiable conformational states.

Further, to analyze noncanonical DNA motifs such as G-quadruplexes that regulate gene expression and are promising drug targets for cancer, these structures were attached to digitally encoded DNA carriers (similar in design to DNA origami)

that translocate through nanopores (Fig. 7c) [52, 169]. For analysis of G-quadruplexes, it is important to know their conformation and stability. Based on designed positions along the multiplexed DNA carrier, folded vs. unfolded G-quadruplexes (tuned via potassium ions, which specifically stabilizes G-quadruplexes) as well as various structural forms of G-quadruplexes could be discriminated. Instead of using DNA as carriers, aptamer-decorated nanoparticles have also been employed to detect small molecules such as metal ions that alone, cannot generate measurable signals upon nanopore translocation [109]. Upon binding of the small molecule, the rearrangement of the negative charges on the carrier particle modifies translocation speeds, enabling detection. Compared to small molecules, larger species such as proteins are likely to induce measurable signals upon translocation; these signals can be amplified using aptamers as labels. The accumulation of negative charge due to specific aptamer binding allows proteins such as C-reactive protein to be detected in complex environments such as serum [172].

4.2 Protein Biosensing

Solid-state nanopores have advantageous properties for protein sensing [173] as they can operate under a wider range of environmental conditions, including high electrical bias potentials [144], high temperatures [141], and function in the presence of denaturants like sodium dodecyl sulfate [140]. Recent reviews have been published regarding the application of solid-state nanopores for single-molecule protein detection [174, 175]. Thus, we do not delve deep into this literature but instead highlight some works published in the last few years as examples of progress in this field.

Proteins lack routes for amplification, in contrast to nucleic acids that have techniques such as the polymerase chain reaction. However, if used in a cascade with DNA signal amplification, scarce proteins that interact with specific DNA sequences can be detected. For example, a conical nanopore sensor combined with cascade signal amplification was used to detect methyltransferase activity [176], as impaired DNA methyltransferase levels were previously linked to genetic diseases or cancer [177, 178]. Specific recognition of enzymes to a hairpin DNA triggered a hybridization chain reaction to assemble a double-stranded DNA on the surface of the nanopore, which altered the surface charge and in turn, the measured current rectification. Proteins dwelling in nanopipettes induce detectable changes in the surface charge and thus alter the measured current rectification in conical solid-state nanopores. Various strategies have facilitated trapping the protein of interest specifically within the tip of the nanopipette. Some examples include the use of DNA aptamers [106, 179, 180] or alternatively, functionalization with specially designed peptides or proteins for specific target recognition [105, 181].

Using nanopores that have a similar diameter as the analyte of interest, it is possible to approximate the shape, volume, charge, rotational diffusion coefficient, and dipole moment of individual proteins [182]. Due to the rotation of a single non-spherical object during translocation through a cylindrical nanopore, the ionic

current is altered, leading to a characteristic footprint of the protein. Unmodified proteins have also been distinguished based on their size and conformation using electro-osmotic traps formed by docking a DNA origami sphere that seals off the nanopore [183]. Different fibril sizes of amyloid-beta plaques that play a critical role in the progression of Alzheimer's disease were discriminated using conical nanopores of various geometries functionalized with PEG to increase the dwell time of fibers inside the nanopore through molecular crowding [184]. Comparing experimental results of transport selectivity based on either size exclusion or molecular recognition with computational models that realistically simulate protein trajectories and probabilities of target binding vs. translocation [185] will help to guide future engineering of solid-state nanopores for proteomics.

4.3 Polysaccharides (Sugars) Biosensing

The third field of single-molecule sensing beyond genomics and proteomics, in which nanopore sensors have gained further interest is glycomics, the study of sugars or polysaccharides. Compared to DNA/RNA, which have 4 different nucleotides and proteins/peptides with 20 amino acids, polysaccharides have more than 100 monosaccharides with additional variety in linkage and branching structures (Fig. 8a). While the field of single-molecule glycomics is still in its infancy due to the complexity of polysaccharides, both biological [187] as well as solid-state nanopores have shown potential for the analysis of sugars.

Silicon nitride-based nanopores were used to discriminate heparin, an anticoagulant drug used in the treatment of various blood vessel, heart, and lung conditions, from a structurally similar contaminant that led to adverse clinical consequences including death [188] (Fig. 8b). The contaminant interacted stronger vs. heparin with the unmodified SiN nanopore, leading to higher current blockages in resistive pulse measurements. While heparin is one of the most highly negatively charged biomolecules, many carbohydrate oligomers and polymers are neutral, which renders molecular manipulation via electrophoresis challenging. Thus, chemical tailoring of solid-state nanopores via surface chemistry is a vital consideration for modulating mass transport of sugars in addition to tackling other aspects such as tuning conductance and surface fouling [186]. Other publications have shown the potential of nanopore sensing for glycomics by conducting label-free characterization of plant polysaccharides [189] and single-molecule identification and quantification of glycosaminoglycans [190]. To this end, advances in solid-state nanopore technologies are expanding the repertoire and complexity of biomolecules that can be detected and such platforms will be an integral tool for future multi-omics applications.

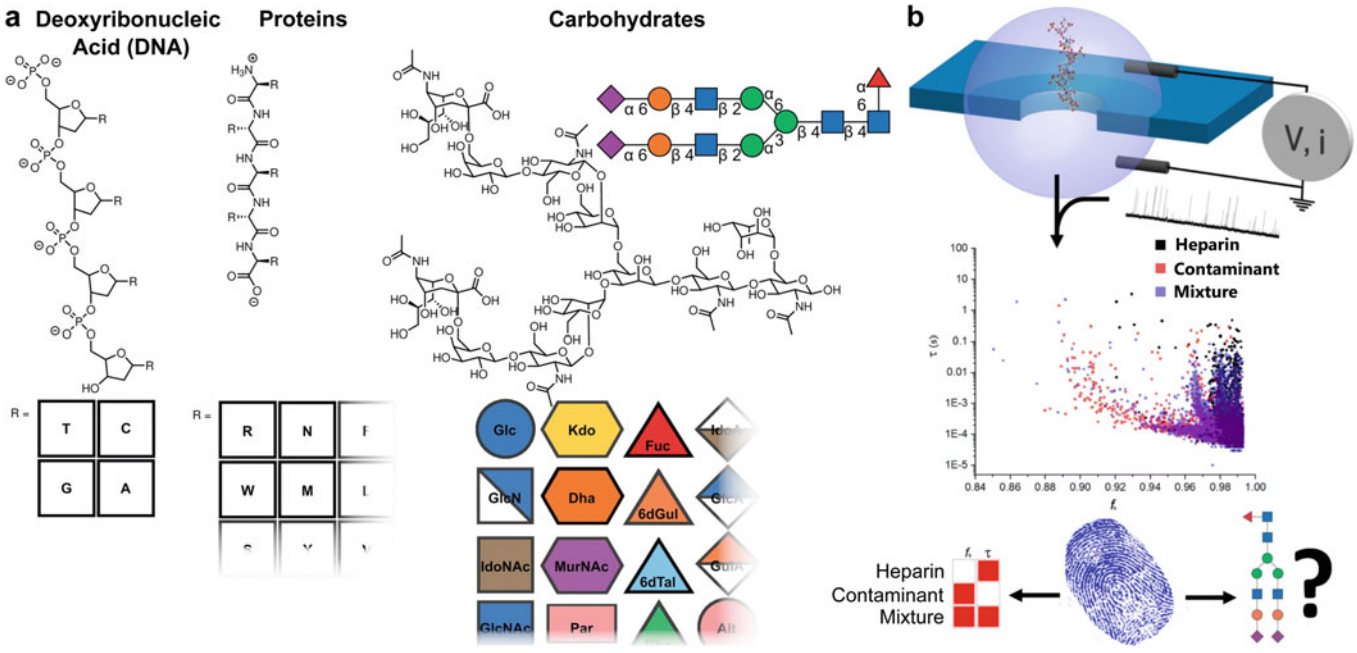

Fig. 8 Nanopore sensing of sugars. (**a**) DNA and protein biopolymer structures are determined by the sequence of 4 or 20 unique monomers (a subset is shown) respectively connected linearly. In contrast, carbohydrate oligo- and polymers consist of sequences of 120 possible monomers (a subset is shown) connected by different linkage types with the possibility of branching. This chemical complexity is reflected in the adoption of drawing conventions to simply and quickly summarize the diversity of information needed for carbohydrate analysis (**b**) Overview of nanopore sensing for glycomics. Passage of a carbohydrate through a nanopore generates a series of measurable current perturbations namely from current blockages. Differences in key characteristics of these current blockages such as the blockage magnitude (f_b) and blockage duration (τ) enabled differentiation of heparin vs. a toxic contaminant vs. a mixture of both. The goal of nanopore glycomics is to determine whether such fingerprints combined with statistical analysis can yield adequate information regarding the sequence [186]

4.4 Biosensing in Live Cells

Measuring analytes inside live cells is possible by exploiting the nanopipette geometry: tips within the range of 50–100 nm in diameter allow repeated intracellular probe insertion without damaging the membrane [191, 192]. Monitoring analyte concentration flux while minimally stressing the cells under physiological environments sheds new light on cell behavior and characteristics. For example, tracking ATP within a cell gives insight into intracellular signaling as well as metabolic states. Following such dynamic processes has been made possible through ATP aptamer-modified nanopipettes [192]. The ATP aptamers undergo conformational changes upon analyte binding and unfold when exposed to UV-light, an external trigger that allows the sensors to be reset for re-use (Fig. 9a). However, we note that exposure to UV-light may result in single-stranded DNA damage for long-term measurements [193] and dynamic target release is necessary for continuous measurements.

Another small molecule, dopamine, has been rendered detectable intracellularly using DNA aptamers to capture and accumulate the charged neurotransmitter within the orifice of the nanopipette [194]. Changes in intracellular signals are detectable in this nanopipette due to its double-barrel geometry, which confines ionic migration

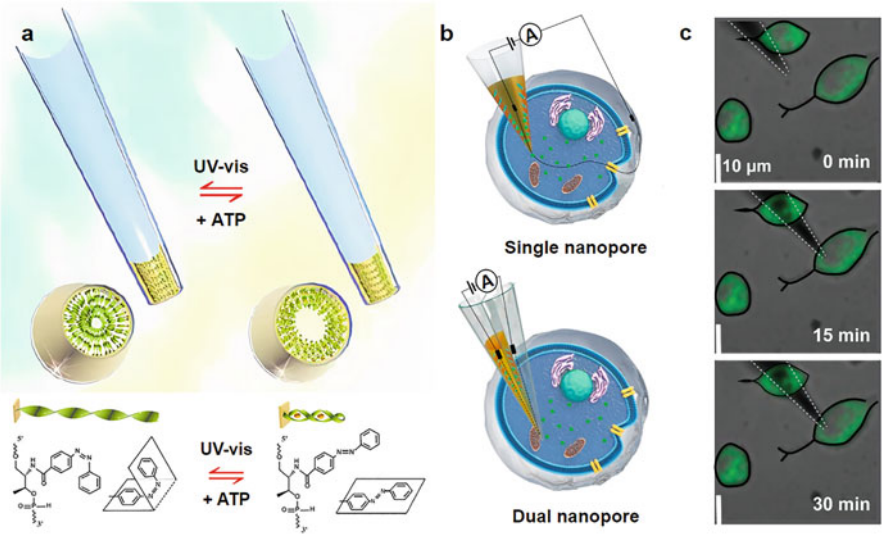

Fig. 9 Intracellular measurements with nanopipette sensors. (**a**) Adenosine triphosphate (ATP) aptamers functionalized inside nanopipettes undergo a reversible conformational change upon ATP recognition and can be unfolded with an external ultraviolet (UV) trigger [192]. (**b**) While single nanopore sensors can measure intracellular, transmembrane current measurements, dual nanopores enable monitoring of more local influences as the distance and thus resistance due to biological material between the two electrodes becomes negligible [191]. (**c**) Cell survival up to 30 min was demonstrated upon insertion of the dual nanopore sensor [191]

within a ~100 nm radius, allowing the trans-membrane resistance to be neglected (Fig. 9b). While the cells survived up to 30 min, it is necessary to assess cell survival for longer-term measurements (Fig. 9c). However, the DNA dopamine aptamer used in this work is deemed not to be an aptamer due to cross-reactivity with any molecule possessing a catechol group, thus likely having issues with selectivity [195–197]. Thus, while aptamers can serve as effective molecular recognition elements for intracellular measurements of small molecules [170], it is important to characterize their selectivity vs. structurally similar molecules [198]. A specific and selective dopamine aptamer [199] has been recently incorporated into nanopipettes with smaller orifices of 10 nm. Rather than detection of charge accumulation, which can also induce signals from nonspecific interactions especially in the complex intracellular environment, aptamer conformational change upon dopamine recognition is the mechanism of signal transduction [200].

The double-barrel nanopipette approach has also been used to monitor the metabolic regulator, protein kinase A, intracellularly [191]. This sensor was not functionalized using aptamers, but instead relied on peptide-affinity probes covalently modified on gold film deposited on the inner surface of one of the dual pores to capture the protein within the orifice. The affinity of the peptide probes to the target was tuned by varying the peptide sequence, to facilitate reversible binding and thus enabling real-time monitoring of the protein. Decreases in current were observed upon protein detection, which was reasoned by pore occlusion due to the capture of protein targets on the nanopore inner surface. Surface charge changes affecting the ICR of the sensor appeared negligible compared to the change in effective pore size.

A strategy allowing both intracellular measurement as well as monitoring events occurring at the membrane consists in combining an AFM cantilever with a nanopore [148], as mentioned prior in Sect. 3.2. Upon application of controlled pressure, the probe can be inserted intracellularly to map the nuclear membrane or to record ionic channels and proteins such as fibronectin. The combination of force with ion-current feedback generates combined information maps, incorporating topography with local ionic current.

5 Prospects: Frontiers of Nanopore Technologies

When observing the rapid advances of the past few years, opportunities of solid-state nanopore systems for biomolecular analysis and detection seem limitless. Since the original study that fabricated nanopores in a SiN membrane to observe the translocation of DNA over two decades ago, there has been significant progress in diverse areas of research. In this review, we covered developments of novel routes of fabrication and pore tuning with increased precision, surface modifications to modulate the chemical properties inside the nanopores, and the emergence of atomically thin 2-D nanopores that have tackled the challenge of spatial resolution. The field has also gained an improved understanding of the physical models that govern ionic flux and molecular interactions inside nanopores through theoretical modeling, which

has led to enhanced control over translocation dynamics. Further, improvements in data analysis for the interpretation of complex signals combined with machine learning algorithms have enabled differentiation of similarly structured biomolecules. We now look to the future of solid-state nanopores where we anticipate technological breakthroughs in single-molecule analysis and biosensing.

An advantage of solid-state systems is that they can be engineered such that several nanopores can be put in series. In such a configuration, single molecules can be re-read several times, which reduces the error rate of the sensors. Moreover, by placing engineered nanopores with various surface modifications in series (e.g., different receptors that bind specifically to different chemical motifs), new information can be extracted from biomolecules (e.g., amino acid sequence), which is impossible using a single nanopore. Careful manipulation of the chemical and physical interactions of biomolecules with the inner surface of each nanopore will be essential to ensure specificity, selectivity, sensitivity, and capture efficiency with adequate temporal resolution. We believe aptamers are promising recognition elements due to the tunability of affinities, inherent selectivity, and ability to increase retention times of analytes through molecular recognition. Coupling aptamers to DNA origami may add another dimension of nanopore control. To date, a dual-constriction biological nanopore [201] and solid-state systems with several pores in series have been presented. Eight non-circular pores in series have been implemented to analyze hepatitis B virus capsid assemblies [202] where the pore is created by closing a nanostructured channel. Recently, a fabrication method to create two to three serial nanopores with cylindrical and conical geometries in plane with the substrate was reported [203]. A two-fold improvement in the precision of resistive-pulse measurements of hepatitis B virus capsids was observed by having multiple pores in series.

For solid-state nanopores that interface with biology (e.g., intracellular measurements in live cells), it will be critical that the insertion of the probe does not perturb the system. To this point, miniaturization of nanopipette orifices is important to minimize cellular damage upon membrane penetration. Further, in complex biological environments, it is necessary to have a reference sensor in parallel for differential measurements to ensure signals arise from specific binding rather than changes in ionic flux. Dopamine nanopipette sensors implanted alongside control sensors modified with scrambled DNA sequences that do not recognize dopamine have enabled the detection of endogenous dopamine released ex vivo in brain slices with the necessary selectivity [204]. In addition to reducing the tip size of nanopipettes, the whole nanopore system has been miniaturized and integrated into microfluidic arrays using microvalves as a cost-effective and portable device [205].

Opportunities for scalable parallelized detection lie in the possibility of integrating solid-state nanopores into other detection modalities such as optics, plasmonics, and electronic transistors [206, 207]. Different sensing methods offer complementary enhancements in overall single-molecule sensitivity, dwell time, detection rate, and scalability – all features that must be tackled to realize single-molecule sequencing or detection of complex biomolecules [208, 209]. We previously described the

possibility of fluidic systems to control the translocation rate either hydrodynamically or through nanostructured elements (Sect. 2.3). In addition, we envision that fluidics can be coupled to nanopore sensors to improve the analysis of complex biological samples. Microfluidics that enable separation via single-molecule resolution gel electrophoresis of thousands of proteins directly extracted from a human cancer cell line have been reported [210]. The combination of the gel slowing down protein flow with a fluidics design that confines proteins near the surface enabled high-resolution imaging of individual proteins in situ. Coupling such a platform that can separate and image proteins prior to detection via solid-state nanopores integrated downstream may permit superior protein classification and analysis. We envision the use of fluorescent labels specifically attached to certain parts of the molecule, e.g., individual amino-acids or post-translational protein modifications [211], facilitating the identification or sorting of biomolecules in complex samples.

Beyond biomedical applications, several works have demonstrated the potential to exploit the intrinsic property of DNA/RNA for information storage. With a theoretical data density of $\sim 4.5 \times 10^7$ GB/g for DNA, 17 exabytes per gram (EB g^{-1}) of storage has been achieved to date [212]. A recent review shows that either sequence (single nucleic-acids) or structure-based (modified DNA stands for better error correction) information storage can be achieved where a nanopore sensor is one possible low-cost read-out device to extract the data [213]. New possibilities also arise with the availability of high-speed electronics for capturing events in timescales faster than 100 ns as well as new algorithms that can deal with the large amounts of data captured, which at these fast sample rates, can easily go up to several tens of MB/s. Thus, technological advances in diverse areas utilizing solid-state nanopores are continually amplifying the opportunities beyond single-molecule analysis and biosensing.

Acknowledgments

The authors acknowledge ETH Zurich for funding and Prof. Janos Vörös for helpful discussions.
Notes The authors declare no competing financial interest.

References

1. Deamer D, Akeson M, Branton D (2016) Nat Biotechnol 34:518
2. Kasianowicz JJ, Brandin E, Branton D, Deamer DW (1996) Proc Natl Acad Sci U S A 93: 13770
3. Wang Y, Zhao Y, Bollas A, Wang Y, Au KF (2021) Nat Biotechnol 39:1348
4. Ying Y-L, Hu Z-L, Zhang S, Qing Y, Fragasso A, Maglia G, Meller A, Bayley H, Dekker C, Long Y-T (2022) Nat Nanotechnol 17:1136
5. Hu ZL, Huo MZ, Ying YL, Long YT (2021) Angew Chem Int Ed 60:14738
6. Alfaro JA, Bohländer P, Dai M, Filius M, Howard CJ, van Kooten XF, Ohayon S, Pomorski A, Schmid S, Aksimentiev A, Anslyn EV, Bedran G, Cao C, Chinappi M, Coyaud E, Dekker C, Dittmar G, Drachman N, Eelkema R, Goodlett D, Hentz S, Kalathiya U, Kelleher NL, Kelly RT, Kelman Z, Kim SH, Kuster B, Rodriguez-Larrea D, Lindsay S, Maglia G, Marcotte EM,

Marino JP, Masselon C, Mayer M, Samaras P, Sarthak K, Sepiashvili L, Stein D, Wanunu M, Wilhelm M, Yin P, Meller A, Joo C (2021) Nat Methods 18:604
7. Restrepo-Pérez L, Joo C, Dekker C (2018) Nat Nanotechnol 13:786
8. Mayer SF, Cao C, Dal Peraro M (2022) iScience 25:104145
9. Venkatesan BM, Bashir R (2011) Nat Nanotechnol 6:615
10. Varongchayakul N, Song J, Meller A, Grinstaff MW (2018) Chem Soc Rev 47:8512
11. Xue L, Yamazaki H, Ren R, Wanunu M, Ivanov AP, Edel JB (2020) Nat Rev Mater 5:931
12. Haywood DG, Saha-Shah A, Baker LA, Jacobson SC (2015) Anal Chem 87:172
13. Guo L (2020) J Neural Eng 17:013001
14. Rosenstein JK, Wanunu M, Merchant CA, Drndic M, Shepard KL (2012) Nat Methods 9:487
15. Siwy ZS (2006) Adv Funct Mater 16:735
16. Huang X, Kong X-Y, Wen L, Jiang L, Huang X, Kong X, Wen L, Jiang L (2018) Adv Funct Mater 28:1801079
17. Sa N, Baker LA (2011) J Am Chem Soc 133:10398
18. Apel PY, Blonskaya IV, Orelovitch OL, Ramirez P, Sartowska BA (2011) Nanotechnology 22:175302
19. Hu K, Wang Y, Cai H, Mirkin MV, Gao Y, Friedman G, Gogotsi Y (2014) Anal Chem 86: 8897
20. Zeng S, Wen C, Solomon P, Zhang S-L, Zhang Z (2019) Nat Nanotechnol 14:1056
21. Poggioli AR, Siria A, Bocquet L (2019) J Phys Chem B 123:1171
22. Wei C, Bard AJ, Feldberg SW (1997) Anal Chem 69:4627
23. Meller A, Nivon L, Branton D (2001) Phys Rev Lett 86:3435
24. Aksimentiev A (2010) Nanoscale 2:468
25. Keyser UF (2011) J R Soc Interface 8:1369
26. Yuan Z, Liu Y, Dai M, Yi X, Wang C (2020) Nanoscale Res Lett 15:1
27. Sohi AN, Beamish E, Tabard-Cossa V, Godin M (2020) Anal Chem 92:8108
28. Wang C, Bruce RL, Duch EA, Patel JV, Smith JT, Astier Y, Wunsch BH, Meshram S, Galan A, Scerbo C, Pereira MA, Wang D, Colgan EG, Lin Q, Stolovitzky G (2015) ACS Nano 9:1206
29. Zrehen A, Huttner D, Meller A (2019) ACS Nano 13:14388
30. Pérez-Mitta G, Toimil-Molares ME, Trautmann C, Marmisollé WA, Azzaroni O (2019) Adv Mater 31:1901483
31. Faucher S, Aluru N, Bazant MZ, Blankschtein D, Brozena AH, Cumings J, Pedro de Souza J, Elimelech M, Epsztein R, Fourkas JT (2019) J Phys Chem C 123:21309
32. Lee C, Joly L, Siria A, Biance A-L, Fulcrand R, Bocquet L (2012) Nano Lett 12:4037
33. Levy A, de Souza JP, Bazant MZ (2020) J Colloid Interface Sci 579:162
34. Luo Z-X, Xing Y-Z, Ling Y-C, Kleinhammes A, Wu Y (2015) Nat Commun 6:1
35. Feng J, Liu K, Graf M, Dumcenco D, Kis A, di Ventra M, Radenovic A (2016) Nat Mater 15: 850
36. Kavokine N, Marbach S, Siria A, Bocquet L (2019) Nat Nanotechnol 14:573
37. Smeets RMM, Keyser UF, Dekker NH, Dekker C (2008) PNAS 105:417
38. Uram JD, Ke K, Mayer M (2008) ACS Nano 2:857
39. Shekar S, Niedzwiecki DJ, Chien CC, Ong P, Fleischer DA, Lin J, Rosenstein JK, Drndić M, Shepard KL (2016) Nano Lett 16:4483
40. Knowles SF, Weckman NE, Lim VJY, Bonthuis DJ, Keyser UF, Thorneywork AL (2021) Phys Rev Lett 127:137801
41. Fragasso A, Schmid S, Dekker C (2020) ACS Nano 14:1338
42. Gamaarachchi H, Samarakoon H, Jenner SP, Ferguson JM, Amos TG, Hammond JM, Saadat H, Smith MA, Parameswaran S, Deveson IW (2022) Nat Biotechnol 8:5386
43. Plesa C, Dekker C (2015) Nanotechnology 26:084003
44. Zhang Y, Akdemir A, Tremmel G, Imoto S, Miyano S, Shibuya T, Yamaguchi R (2020) BMC Bioinformatics 21:1
45. Zhang J, Liu X, Ying YL, Gu Z, Meng FN, Long YT (2017) Nanoscale 9:3458

46. Boža V, Brejová B, Vinař T (2017) PloS One 12:1
47. David M, Dursi LJ, Yao D, Boutros PC, Simpson JT (2017) Bioinformatics 33:49
48. Konishi H, Yamaguchi R, Yamaguchi K, Furukawa Y, Imoto S (2021) Bioinformatics 37: 1211
49. Noakes MT, Brinkerhoff H, Laszlo AH, Derrington IM, Langford KW, Mount JW, Bowman JL, Baker KS, Doering KM, Tickman BI (2019) Nat Biotechnol 37:651
50. Rodríguez-Manzo JA, Puster M, Nicolaï A, Meunier V, Drndić M (2015) ACS Nano 9:6555
51. Freedman KJ, Otto LM, Ivanov AP, Barik A, Oh S-H, Edel JB (2016) Nat Commun 7:1
52. Bell NAW, Keyser UF (2016) Nat Nanotechnol 11:645
53. Larkin J, Henley RY, Jadhav V, Korlach J, Wanunu M (2017) Nat Nanotechnol 12:1169
54. Wang R, Gilboa T, Song J, Huttner D, Grinstaff MW, Meller A (2018) ACS Nano 12:11648
55. Merchant CA, Healy K, Wanunu M, Ray V, Peterman N, Bartel J, Fischbein MD, Venta K, Luo Z, Johnson ATC, Drndić M (2010) Nano Lett 10:2915
56. Schneider GF, Kowalczyk SW, Calado VE, Pandraud G, Zandbergen HW, Vandersypen LMK, Dekker C (2010) Nano Lett 10:3163
57. Gilbert SM, Dunn G, Azizi A, Pham T, Shevitski B, Dimitrov E, Liu S, Aloni S, Zettl A (2017) Sci Rep 7:1
58. Danda G, Masih Das P, Chou YC, Mlack JT, Parkin WM, Naylor CH, Fujisawa K, Zhang T, Fulton LB, Terrones M, Johnson ATC, Drndić M (2017) ACS Nano 11:1937
59. He Y, Tsutsui M, Zhou Y, Miao X-S (2021) NPG Asia Mater 13:48
60. Chen Q, Liu Z (2019) Sensors 19:1886
61. Waugh M, Briggs K, Gunn D, Gibeault M, King S, Ingram Q, Jimenez AM, Berryman S, Lomovtsev D, Andrzejewski L, Tabard-Cossa V (2020) Nat Protoc 15:122
62. Lee K, Park K-B, Kim H-J, Yu J-S, Chae H, Kim H-M, Kim K-B (2018) Adv Mater 30: 1704680
63. Lei X, Zhang J, Hong H, Yuan Z, Liu Z (2022) Micromachines (Basel) 13:923
64. Storm AJ, Chen JH, Ling XS, Zandbergen HW, Dekker C (2003) Nat Mater 2:537
65. Li J, Stein D, McMullan C, Branton D, Aziz MJ, Golovchenko JA (2001) Nature 412:166
66. Zhou Y, Sun L, Watanabe S, Ando T (2022) Anal Chem 94:324
67. Zhu C, Huang K, Siepser NP, Baker LA (2020) Chem Rev 121:11726
68. Ebejer N, Güell AG, Lai SCS, McKelvey K, Snowden ME, Unwin PR (2013) Annu Rev Anal Chem 6:329
69. Hu J, Yu MF (2010) Science 329:313
70. Hengsteler J, Mandal B, Van Nisselroy C, Lau GPS, Schlotter T, Zambelli T, Momotenko D (2021) Nano Lett 21:9093
71. Goutham S, Keerthi A, Ismail A, Bhardwaj A, Jalali H, You Y, Li Y, Hassani N, Peng H, Martins MVS, Wang F, Neek-Amal M, Radha B (2023) Nat Nanotechnol 18:596
72. Kwok H, Briggs K, Tabard-Cossa V (2014) PloS One 9:92880
73. Ying C, Ma T, Xu L, Rahmani M (2022) Nanomaterials 12:2384
74. Wei G, Hu R, Li Q, Lu W, Liang H, Nan H, Lu J, Li J, Zhao Q (2022) Langmuir ACS J Surf Colloids 38:6443
75. Chen X, Zhang S, Hou D, Duan H, Deng B, Zeng Z, Liu B, Sun L, Song R, Du J, Gao P, Peng H, Liu Z, Wang L (2021) ACS Appl Mater Interfaces 13:29926
76. Zhang Y, Miyahara Y, Derriche N, Yang W, Yazda K, Capaldi X, Liu Z, Grutter P, Reisner W (2019) Small Methods 3:1900147
77. Fang S, Yin B, Xie W, Zhou D, Tang P, He S, Yuan J, Wang D (2020) Rev Sci Instrum 91: 093203
78. Ying C, Houghtaling J, Eggenberger OM, Guha A, Nirmalraj P, Awasthi S, Tian J, Mayer M (2018) ACS Nano 12:11458
79. Fried JP, Swett JL, Nadappuram BP, Fedosyuk A, Gee A, Dyck OE, Yates JR, Ivanov AP, Edel JB, Mol JA (2022) Nano Res 15:9881
80. Beamish E, Kwok H, Tabard-Cossa V, Godin M (2012) Nanotechnology 23:405301
81. Beamish E, Kwok H, Tabard-Cossa V, Godin M (2013) J Vis Exp 80:51081

82. Prabhu AS, Freedman KJ, Robertson JWF, Nikolov Z, Kasianowicz JJ, Kim MJ (2011) Nanotechnology 22:425302
83. Mussi V, Fanzio P, Firpo G, Repetto L, Valbusa U (2012) Nanotechnology 23:435301
84. Chen P, Mitsui T, Farmer DB, Golovchenko J, Gordon RG, Branton D (2004) Nano Lett 4: 1333
85. Chernev A, Teng Y, Thakur M, Boureau V, Navratilova L, Cai N, Chen T, Wen L, Artemov V, Radenovic A (2023) Adv Mater 35:2302827
86. Wei R, Martin TG, Rant U, Dietz H (2012) Angew Chem Int Ed 51:4864
87. Pal S, Naik A, Rao A, Chakraborty B, Varma MM (2022) ACS Appl Nano Mater 5:8804
88. Thomsen RP, Malle MG, Okholm AH, Krishnan S, Bohr SSR, Sørensen RS, Ries O, Vogel S, Simmel FC, Hatzakis NS, Kjems J (2019) Nat Commun 10:5655
89. Xing Y, Dorey A, Jayasinghe L, Howorka S (2022) Nat Nanotechnol 17:708
90. Krishnan S, Ziegler D, Arnaut V, Martin TG, Kapsner K, Henneberg K, Bausch AR, Dietz H, Simmel FC (2016) Nat Commun 7
91. Fragasso A, de Franceschi N, Stömmer P, van der Sluis EO, Dietz H, Dekker C (2021) ACS Nano 15:12768
92. Ponnuswamy N, Bastings MMC, Nathwani B, Ryu JH, Chou LYT, Vinther M, Li WA, Anastassacos FM, Mooney DJ, Shih WM (2017) Nat Commun 8:15654
93. Niedzwiecki DJ, DiPaolo B, Lin C-Y, Castan A, Keneipp R, Drndić M (2021) ACS Sens 6: 2534
94. Alawami MF, Bošković F, Zhu J, Chen K, Sandler SE, Keyser UF (2022) iScience 25:104191
95. Chou Y-C, Masih Das P, Monos DS, Drndić M (2020) ACS Nano 14:6715
96. Frutiger A, Tanno A, Hwu S, Tiefenauer RF, Vörös J, Nakatsuka N (2021) Chem Rev 121: 8095
97. Hlady V, Buijs J (1996) Curr Opin Biotechnol 8:72
98. Eggenberger OM, Ying C, Mayer M (2019) Nanoscale 11:19636
99. Yusko EC, Johnson JM, Majd S, Prangkio P, Rollings RC, Li J, Yang J, Mayer M (2011) Nat Nanotechnol 6:253
100. Vaitheeswaran S, Thirumalai D (2008) Proc Natl Acad Sci U S A 105:17636
101. Karmi A, Sakala GP, Rotem D, Reches M, Porath D (2020) ACS Appl Mater Interfaces 12: 14563
102. Lepoitevin M, Ma T, Bechelany M, Janot JM, Balme S (2017) Adv Colloid Interface Sci 250: 195
103. Brilmayer R, Förster C, Zhao L, Andrieu-Brunsen A (2020) Curr Opin Biotechnol 63:200
104. Duznovic I, Gräwe A, Weber W, Müller LK, Ali M, Ensinger W, Tietze A, Stein V (2021) Small 17:2101066
105. Bulbul G, Liu G, Vithalapur NR, Atilgan C, Sayers Z, Pourmand N (2019) ACS Chem Neurosci 10:1970
106. Ren R, Wang X, Cai S, Zhang Y, Korchev Y, Ivanov AP, Edel JB, Ren XR, Wang S, Cai AP, Ivanov BE, Zhang Y, Korchev Y (2020) Small Methods 4:2000356
107. Actis P, Rogers A, Nivala J, Vilozny B, Seger RA, Jejelowo O, Pourmand N (2011) Biosens Bioelectron 26:4503
108. Ding S, Gao C, Gu LQ (2009) Anal Chem 81:6649
109. Mayne L, Lin CY, Christie SDR, Siwy ZS, Platt M (2018) ACS Nano 12:4844
110. Acar ET, Buchsbaum SF, Combs C, Fornasiero F, Siwy ZS (2019) Sci Adv 5:2568
111. Abelow AE, Schepelina O, White RJ, Vallée-Bélisle A, Plaxco KW, Zharov I (2010) Chem Commun (Camb) 46:7984
112. Nakatsuka N, Failletaz A, Eggemann D, Forro C, Voros J, Momotenko D (2021) Anal Chem 93:4033
113. Nakatsuka N, Heard KJ, Failletaz A, Momotenko D, Voros J, Gage FH, Vadodaria KC (2021) Mol Psychiatry 26:2753
114. Mubarak A, Neumann R, Ensinger W (2010) ACS Nano 4:7267

115. Mussi V, Fanzio P, Repetto L, Firpo G, Stigliani S, Tonini GP, Valbusa U (2011) Biosens Bioelectron 29:125
116. Wei R, Gatterdam V, Wieneke R, Tampé R, Rant U (2012) Nat Nanotechnol 7:257
117. Lazzara TD, Kliesch TT, Janshoff A, Steinem C (2011) ACS Appl Mater Interfaces 3:1068
118. Pla-Roca M, Isa L, Kumar K, Reimhult E (2015) ACS Appl Mater Interfaces 7:6030
119. Ananth A, GenuaM AN, Díaz L, Eisele NB, Frey S, Dekker C, Richter RP, Görlich D (2018) Small 14:1703357
120. Taniguchi M, Ohshiro T (2019) Tokeshi M (ed) Applications of microfluidic systems in biology and medicine. Springer, Singapore, pp 301–324
121. Clarke J, Wu HC, Jayasinghe L, Patel A, Reid S, Bayley H (2009) Nat Nanotechnol 4:265
122. Jain M, Fiddes IT, Miga KH, Olsen HE, Paten B, Akeson M (2015) Nat Methods 12:351
123. Lu H, Giordano F, Ning Z (2016) Genomics Proteomics Bioinf 14:265
124. Goto Y, Akahori R, Yanagi I, Takeda K (2020) J Hum Genet 65:69
125. Qiu H, Zhou W, Guo W (2021) ACS Nano 15:18848
126. Balasubramanian R, Pal S, Rao A, Naik A, Chakraborty B, Maiti PK, Varma MM (2020) ACS Appl Bio Mater 4:451
127. Kowalczyk SW, Wells DB, Aksimentiev A, Dekker C (2012) Nano Lett 12:1038
128. Fologea D, Uplinger J, Thomas B, McNabb DS, Li J (2005) Nano Lett 5:1734
129. Hyun C, Kaur H, Rollings R, Xiao M, Li J (2013) ACS Nano 7:5892
130. Keyser UF, Koeleman BN, Van Dorp S, Krapf D, Smeets RMM, Lemay SG, Dekker NH, Dekker C (2006) Nat Phys 2:473
131. Banerjee S, Wilson J, Shim J, Shankla M, Corbin EA, Aksimentiev A, Bashir R (2015) Adv Funct Mater 25:936
132. Wang C, Sensale S, Pan Z, Senapati S, Chang HC (2021) Nat Commun 12:1
133. Di Fiori N, Squires A, Bar D, Gilboa T, Moustakas TD, Meller A (2013) Nat Nanotechnol 8:12
134. Squires AH, Hersey JS, Grinstaff MW, Meller A (2013) J Am Chem Soc 135:16304
135. Al Sulaiman D, Cadinu P, Ivanov AP, Edel JB, Ladame S (2018) Nano Lett 18:6084
136. Venta K, Shemer G, Puster M, Rodríguez-Manzo JA, Balan A, Rosenstein JK, Shepard K, Drndić M (2013) ACS Nano 7:4629
137. Chien CC, Shekar S, Niedzwiecki DJ, Shepard KL, Drndić M (2019) ACS Nano 13:10545
138. Brinkerhoff H, Kang ASW, Liu J, Aksimentiev A, Dekker C (2021) Science 374:1509
139. Nova IC, Ritmejeris J, Brinkerhoff H, Koenig TJR, Gundlach JH, Dekker C (2022) BioRxiv. 2022.11.11.516163
140. Restrepo-Pérez L, John S, Aksimentiev A, Joo C, Dekker C (2017) Nanoscale 9:11685
141. Payet L, Martinho M, Pastoriza-Gallego M, Betton JM, Auvray L, Pelta J, Mathé J (2012) Anal Chem 84:4071
142. Li J, Fologea D, Rollings R, Ledden B (2014) Protein Pept Lett 21:256
143. Freedman KJ, Jürgens M, Prabhu A, Ahn CW, Jemth P, Edel JB, Kim MJ (2011) Anal Chem 83:5137
144. Freedman KJ, Haq SR, Edel JB, Jemth P, Kim MJ (2013) Sci Rep 3:1638
145. Soni N, Freundlich N, Ohayon S, Huttner D, Meller A (2022) ACS Nano 16:11405
146. Hagan JT, Gonzalez A, Shi Y, Han GGD, Dwyer JR (2022) ACS Nano 16:5537
147. Wanunu M, Sutin J, McNally B, Chow A, Meller A (2008) Biophys J 95:4716
148. Aramesh M, Forró C, Dorwling-Carter L, Lüchtefeld I, Schlotter T, Ihle SJ, Shorubalko I, Hosseini V, Momotenko D, Zambelli T, Klotzsch E, Vörös J (2019) Nat Nanotechnol 14:791
149. Schlotter T, Weaver S, Forró C, Momotenko D, Vörös JJ, Zambelli T, Aramesh M (2020) ACS Nano 14:12993
150. Meister AA, Gabi M, Behr P, Studer P, Vörös J, Niedermann P, Bitterli J, Polesel-Maris JJ, Liley M, Heinzelmann H, Zambelli T (2009) Nano Lett 9:2501
151. Cheung KM, Yang KA, Nakatsuka N, Zhao C, Ye M, Jung ME, Yang H, Weiss PS, Stojanović MN, Andrews AM (2019) ACS Sens 4:3308

152. Schlotter T, Kloter T, Hengsteler J, Ragavan S, Hu H, Zhang X, Duru J, Voros J, Zambelli T, Nakatsuka N (2022) Preprint (Version 1) available at Research Square. https://doi.org/10.21203/rs.3.rs-3015491/v1
153. Rodriguez-Larrea D (2021) Biosens Bioelectron 180:113108
154. Wanunu M, Dadosh T, Ray V, Jin J, McReynolds L, Drndić M (2010) Nat Nanotechnol 5:807
155. Wang Y, Zheng D, Tan Q, Wang MX, Gu L-Q (2011) Nat Nanotechnol 6:668
156. Burck N, Gilboa T, Gadi A, Patkin Nehrer M, Schneider RJ, Meller A (2021) Clin Chem 67:753
157. Galenkamp NS, Soskine M, Hermans J, Wloka C, Maglia G (2018) Nat Commun 9:4085
158. Liu W, Yang Z-L, Yang C-N, Ying Y-L, Long Y-T (2022) Chem Sci 13:4109
159. Bayley H, Luchian T, Shin S-H, Steffensen MB (2008) Biophysics 12:251
160. van Kooten XF, Rozevsky Y, Marom Y, Ben Sadeh E, Meller A (2022) Nanoscale 14:4977
161. Bošković F, Zhu J, Tivony R, Ohmann A, Chen K, Alawami MF, Đorđević M, Ermann N, Dias JP, Fairhead M (2021) MedRxiv
162. He L, Tessier DR, Briggs K, Tsangaris M, Charron M, McConnell EM, Lomovtsev D, Tabard-Cossa V (2021) Nat Commun 12:4576
163. Ren R, Sun M, Goel P, Cai S, Kotov NA, Kuang H, Xu C, Ivanov AP, Edel JB (2021) Adv Mater 33:2103067
164. Leitao SM, Navikas V, Miljkovic H, Drake B, Marion S, Pistoletti Blanchet G, Chen K, Mayer SF, Keyser UF, Kuhn A, Fantner GE, Radenovic A (2023) Nat Nanotechnol 18:1078
165. Chau C, Marcuccio F, Soulias D, Edwards MA, Tuplin A, Radford SE, Hewitt E, Actis P (2022) ACS Nano 16:20075
166. Chau CC, Radford SE, Hewitt EW, Actis P (2020) Nano Lett 20:5553
167. Nakatsuka N, Faillétaz A, Eggemann D, Forró C, Vörös J, Momotenko D (2021) Anal Chem 93:4033
168. Ding T, Yang J, Wang J, Pan V, Lu Z, Ke Y, Zhang C (2022) Biosens Bioelectron 195:113658
169. Bošković F, Zhu J, Chen K, Keyser UF (2019) Nano Lett 19:7996
170. Moraldo C, Vuille-dit-Bille E, Shkodra B, Kloter T, Nakatsuka N (2022) J Neurosci Methods 365:109386
171. Cai S-L, Zheng Y-B, Cao S-H, Cai X-H, Li Y-Q (2016) Chem Commun 52:12450
172. Wu J, Liang L, Zhang M, Zhu R, Wang Z, Yin Y, Yin B, Weng T, Fang S, Xie W, Wang L, Wang D (2022) ACS Appl Mater Interfaces 14:12077
173. Robertson JWFF, Reiner JE (2018) Proteomics 18:1800026
174. Hu R, Tong X, Zhao Q (2020) Adv Healthc Mater 9:2000933
175. Meyer N, Abrao-Nemeir I, Janot J-M, Torrent J, Lepoitevin M, Balme S (2021) Adv Colloid Interface Sci 298:102561
176. Zhang S, Shi W, Bin Li K, Han DM, Xu JJ (2022) Anal Chem 94:4407
177. Esteller M (2007) Nat Rev Genet 8:4
178. Choy JS, Wei S, Lee JY, Tan S, Chu S, Lee TH (2010) J Am Chem Soc 132:1782
179. Tang H, Wang H, Yang C, Zhao D, Qian Y, Li Y (2020) Anal Chem 92:3042
180. Hanif S, Liu H-L, Ahmed SA, Yang J-M, Zhou Y, Pang J, Ji L-N, Xia X-H, Wang K (2017) Anal Chem 89:9911
181. Zhang S, Liu G, Chai H, Zhao Y-D, Yu L, Chen W (2019) Electrochem Commun 99:71
182. Yusko EC, Bruhn BR, Eggenberger OM, Houghtaling J, Rollings RC, Walsh NC, Nandivada S, Pindrus M, Hall AR, Sept D, Li J, Kalonia DS, Mayer M (2017) Nat Nanotechnol 12:360
183. Schmid S, Stömmer P, Dietz H, Dekker C (2021) Nat Nanotechnol 16:1244
184. Meyer N, Arroyo N, Janot JM, Lepoitevin M, Stevenson A, Nemeir IA, Perrier V, Bougard D, Belondrade M, Cot D, Bentin J, Picaud F, Torrent J, Balme S (2021) ACS Sens 6:3733
185. Mitscha-Baude G, Stadlbauer B, Howorka S, Heitzinger C (2021) ACS Nano 15:9900
186. Hagan JT, Sheetz BS, Bandara YM, Karawdeniya BI, Morris MA, Chevalier RB, Dwyer JR (2020) Anal Bioanal Chem 412:6639

187. Bayat P, Rambaud C, Priem B, Bourderioux M, Bilong M, Poyer S, Pastoriza-Gallego M, Oukhaled A, Mathé J, Daniel R (2022) Nat Commun 13:1
188. Karawdeniya BI, Bandara YMNDY, Nichols JW, Chevalier RB, Dwyer JR (2018) Nat Commun 9:3278
189. Cai Y, Zhang B, Liang L, Wang S, Zhang L, Wang L, Cui HL, Zhou Y, Wang D (2021) Plant Commun 2:100106
190. Im J, Lindsay S, Wang X, Zhang P (2019) ACS Nano 13:6308
191. Zhang H, Zhao T, Huang P, Wang Q, Tang H, Chu X, Jiang J (2022) ACS Nano 16:5752
192. Yu S-Y, Ruan Y-F, Liu Y-L, Han D-M, Zhou H, Zhao W-W, Jiang D, Xu J-J, Chen H-Y (2021) ACS Sens 6:1529
193. Rastogi RP, Richa A, Kumar MB, Tyagi, Sinha RP (2010) J Nucleic Acids 2010:592980
194. Zhao T, Wang J-W, Zhang H-S, Zheng X, Chen Y-P, Tang H, Jiang J-H (2022) Anal Chem 94:15541
195. Nakatsuka N, Cao HH, Deshayes S, Melkonian AL, Kasko AM, Weiss PS, Andrews AM (2018) ACS Appl Mater Interfaces 10:23490
196. Hou Y, Hou J, Liu X (2021) ChemBioChem 22:1948
197. Álvarez-Martos I, Ferapontova EE (2017) Biochem Biophys Res Commun 489:381
198. Nakatsuka N, Andrews AM (2017) ACS Chem Neurosci 8:218
199. Nakatsuka N, Yang K-A, Abendroth JM, Cheung KM, Xu X, Yang H, Zhao C, Zhu B, Rim YS, Yang Y, Weiss PS, Stojanović MN, Andrews AM (2018) Science 362:319
200. Stuber A, Douaki A, Hengsteler J, Buckingham D, Momotenko D, Garoli D, Nakatsuka N (2023) ACS Nano 17:19168
201. van der Verren SE, van Gerven N, Jonckheere W, Hambley R, Singh P, Kilgour J, Jordan M, Wallace EJ, Jayasinghe L, Remaut H (2020) Nat Biotechnol 38:1415
202. Kondylis P, Zhou J, Harms ZD, Kneller AR, Lee LS, Zlotnick A, Jacobson SC (2017) Anal Chem 89:4855
203. Zhang M, Harms ZD, Greibe T, Starr CA, Zlotnick A, Jacobson SC (2022) ACS Nano 16:7352
204. Stuber A, Cavaccini A, Manole A, Hengsteler J, Burdina A, Patriarchi T, Karayannis T, Nakatsuka N (2023) ACS Meas Sci Au. https://doi.org/10.1021/acsmeasuresciau.3c00047
205. Tahvildari R, Beamish E, Briggs K, Chagnon-Lessard S, Sohi AN, Han S, Watts B, Tabard-Cossa V, Godin M (2017) Small 13:1602601
206. Zhu X, Li X, Gu C, Ye Z, Cao Z, Zhang X, Jin C, Liu Y (2021) ACS Nano 15:9882
207. Li W, Zhou J, Maccaferri N, Krahne R, Wang K, Garoli D (2022) Anal Chem 94:503
208. Rahman M, Sampad MJN, Hawkins A, Schmidt H (2021) Lab Chip 21:3030
209. Spitzberg JD, Zrehen A, van Kooten XF, Meller A (2019) Adv Mater 31:1900422
210. Zrehen A, Ohayon S, Huttner D, Meller A (2020) Sci Rep 10:1
211. Emenike B, Nwajiobi O, Raj M (2022) Front Chem 10:714
212. Organick L, Chen Y-J, Dumas Ang S, Lopez R, Liu X, Strauss K, Ceze L (2020) Nat Commun 11:1
213. Doricchi A, Platnich CM, Gimpel A, Horn F, Earle M, Lanzavecchia G, Cortajarena AL, Liz-Marzán LM, Liu N, Heckel R (2022) ACS Nano 16:17552

Adv Biochem Eng Biotechnol (2024) 187: 317–338
https://doi.org/10.1007/10_2023_229

Published online: 13 June 2023

Microarray-Based Electrochemical Biosensing

Kosuke Ino, Yoshinobu Utagawa, and Hitoshi Shiku

Contents

Abstract Microarrays are widely utilized in bioanalysis. Electrochemical biosensing techniques are often applied in microarray-based assays because of their simplicity, low cost, and high sensitivity. In such systems, the electrodes and sensing elements are arranged in arrays, and the target analytes are detected electrochemically. These sensors can be utilized for high-throughput bioanalysis and the electrochemical imaging of biosamples, including proteins, oligonucleotides, and cells. In this chapter, we summarize recent progress on these topics. We categorize electrochemical biosensing techniques for array detection into four groups: scanning electrochemical microscopy, electrode arrays, electrochemiluminescence, and bipolar electrodes. For each technique, we summarize the key principles and discuss the

K. Ino (✉)
Graduate School of Engineering, Tohoku University, Sendai, Miyagi, Japan
e-mail: kosuke.ino@tohoku.ac.jp

Y. Utagawa
Graduate School of Environmental Studies, Tohoku University, Sendai, Miyagi, Japan

H. Shiku (✉)
Graduate School of Engineering, Tohoku University, Sendai, Miyagi, Japan

Graduate School of Environmental Studies, Tohoku University, Sendai, Miyagi, Japan
e-mail: hitoshi.shiku.c3@tohoku.ac.jp

advantages, disadvantages, and bioanalysis applications. Finally, we present conclusions and perspectives about future directions in this field.

Graphical Abstract

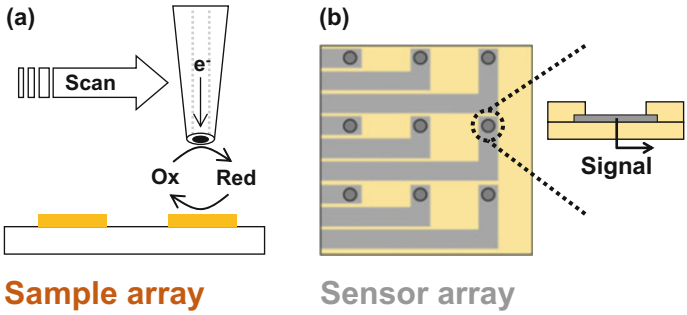

Keywords Bioanalysis, Bipolar electrode array, Electrochemiluminescence, Electrode array, Microarray, Scanning electrochemical microscopy

1 Introduction

Electrochemical biosensing has been widely used in clinical diagnostics, environmental assessment, food analysis, chemical analysis, and basic research [1]. As these applications often require the analysis of many samples, high-throughput and simple assays are desirable. For this purpose, it is advantageous to arrange samples or sensors in dense arrays on a single small chip. Although optical approaches involving fluorescence analysis have been widely used for array sensing, electrochemical systems have also been proposed because of their simplicity, low cost, and high sensitivity. In many electrochemical approaches, the target analytes are captured in arrays and then are electrochemically measured. In other electrochemical approaches, electrochemical sensors or sensing elements are arranged in arrays for target imaging and analyte detection. For array-based electrochemical detection systems and devices, scanning electrochemical microscopy (SECM) and electrochemical chip devices, such as electrode arrays, have been developed (Fig. 1). As a subset of electrode array, bipolar electrode (BPE) arrays are also attractive for bioanalysis because no complex wiring needs to be introduced during the fabrication process. Advantageously, other components, such as microfluidic systems, microwells, and cell culture platforms, can be incorporated into chip devices. In addition to potentiometry, amperometry, and impedance spectroscopy, electrochemiluminescence (ECL) and dielectrophoresis (DEP) have been utilized for detection (Fig. 2). In ECL measurements, electrochemical signals are converted

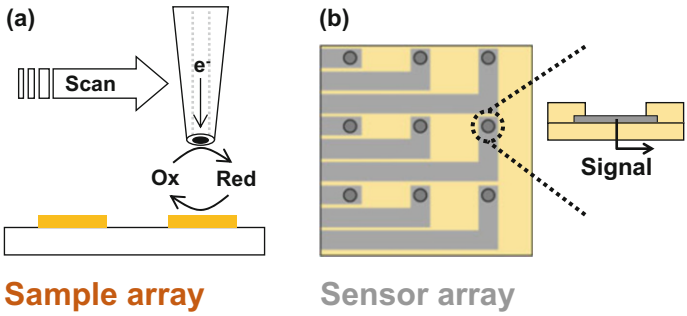

Fig. 1 Electrochemical biosensing in arrays using (**a**) SECM and (**b**) chip devices (e.g., electrode arrays)

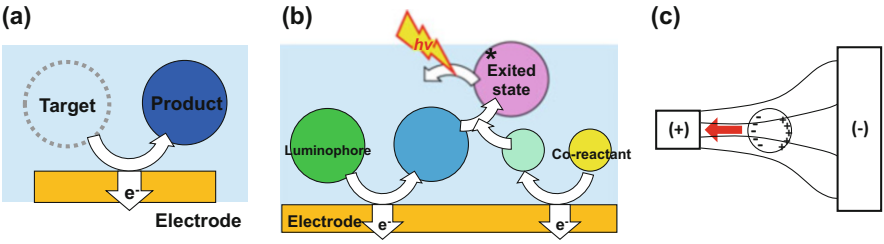

Fig. 2 Electrochemical detection based on (**a**) amperometry, (**b**) ECL, and (**c**) DEP

into optical signals, and the ECL imaging allows the rapid detection of analytes in large areas without electrode arrays or scanning probe electrodes. DEP techniques have been applied to trap biosamples in arrays and then release them, demonstrating the applicability of these approaches for array-based bioanalysis.

In array-based assays, several biocomponents, – mostly proteins and oligonucleotides – have been analyzed for medical checks in samples of blood, sweat, and urine. Biosamples are widely analyzed using immunoassays, including the enzyme-linked immunosorbent assay (ELISA), in which enzymes and redox compounds as labels are electrochemically detected. In addition to conventional ELISA, digital ELISA using beads or droplets has been reported for the detection of single beads or molecules [2]. In a digital ELISA approach, microbeads with antibodies are used to capture one or zero target protein molecules per bead. The microbeads are further modified with antibodies conjugated with enzymes and then are trapped within microwells filled with enzymatic substrates, and the fluorescence products accumulated within the confined microwells are monitored. As the number of target molecules can be measured by counting the positive beads, a high sensitivity is realized. Instead of antibodies in immunoassays, aptamers modified with redox compounds have been used in electrochemical assays. In addition to proteins and oligonucleotides, cells have been analyzed using arrays. Conventional cell-

based assays measure the average response of a cell population. Therefore, these assays are unsuitable for use in monitoring cellular heterogeneity and identifying special cells such as circulating tumor cells. To this end, single-cell analysis is of critical importance [3, 4]. In addition, three-dimensional (3D) cultured cells have attracted considerable attention because they can show in vivo functions, unlike two-dimensional (2D) cultured cells. In particular, spheroids and organoids have been widely analyzed in regenerative medicine and drug screening.

In this chapter, we categorize electrochemical approaches for array-based biosensing into four groups: SECM, electrode arrays, ECL, and BPEs since we see here the most innovative aspects in the last decade. For each technique, we summarize the features of the devices/systems, describe the advantages and disadvantages, and discuss bioanalysis applications. Finally, we present our perspectives on future developments. We previously reviewed microelectrode arrays in cell analysis and engineering [5], and some of those topics are updated herein. As the present chapter focuses on the use of arrays for electrochemical biosensing, to obtain a deeper understanding of other specific themes, we recommend that the reader refer to excellent reviews on the electrochemical analysis of cells [6], electrochemical biosensors for nucleic acids [7–9], and electrochemical biosensors based on nanomaterials [10].

2 SECM

SECM is a type of scanning probe electrochemical microscopy [11] in which an electrode scans the sample and local electrochemical reactions are monitored. In general, only the tip of a disk microelectrode is exposed, and the other areas are covered with an insulating material, such as glass. The probe electrode approaches the sample in a solution wherein a reference/counter electrode is immersed and scans the sample surface. During the scan, a bias is applied between the electrodes to monitor local electrochemical reactions at the tip of the probe electrode. There are different modes of SECM operation [12]. For example, in the "feedback mode," a redox mediator shuttles between the tip and sample (e.g., conductive materials and catalysts), and the tip current is controlled by reactions at the tip and sample [13]. In the so-called generation-collection mode, redox species generated from a sample are detected at the tip. Detailed descriptions of the SECM operation modes can be found in earlier reviews. The SECM technique can be used to evaluate the topographies of samples and activity of biocomponents, e.g. when glucose oxidase is immobilized on a target surface and the solution contains redox mediators, redox currents from the probe electrodes increase because of the redox cycling of the redox mediators between the electrode and enzyme. After XY scanning, redox current values are pseudo-colorized, and a 2D electrochemical image of these values is obtained. The technique can clearly visualize the position but also the activity of glucose oxidase. The fabrication of nanoelectrodes has facilitated the acquisition of electrochemical images on the nanometer scale [14], which is a strong advantage over electrode

arrays. Although SECM is a very useful tool for electrochemical imaging, it suffers from long measurement because of the movement of the probe electrode. To address these issues, the use of microelectrode arrays as probes has been proposed. For example, soft linear Au microelectrode arrays were fabricated using printing technology [15], and a linear array of microelectrodes was used as a probe [16]. The probe mechanically contacts a target and slides along its surface during the scan. Because of its softness and the presence of multiple electrodes, the probe enables rapid SECM imaging on curved substrates.

Application of SECM for bioanalysis can be mainly seen in enzyme activity measurements. These aspects will be illustrated in applications of ELISA, oligonucleotide assays, and cellular analyses. For example, for enzyme imaging SECM was combined with a continuous nanoflow system to achieve high-resolution analysis of enzyme-labeled protein microarrays [17]. In this work, a ring electrode/injector probe equipped with a pump was used. This pump system can introduce a solution containing H_2O_2 and $FcCH_2OH$ to the area under the probe, resulting in a high imaging resolution. Human immunoglobulin G (IgG) spots labeled with anti-human IgG and horseradish peroxidase (HRP) were electrochemically detected by monitoring the reduction currents of $FcCH_2OH^+$ generated by the HRP reaction. In another study, inkjet printing technology was utilized to prepare glucose oxidase, invertase, and HRP spots in 2D arrays, and the printed enzymes were monitored using SECM to reveal the utility of inkjet printing in fabricating 2D enzyme arrays [18].

In addition to enzyme arrays, DNA microarrays have been detected using SECM (Fig. 3a) [19]. Thiolated capture DNA probes are immobilized on a gold substrate, and the target DNA, when present, hybridizes with the capture DNA. Furthermore, biotinylated DNA signal and DNA auxiliary probes hybridize as shown in Fig. 3a, resulting in the formation of DNA concatemers. Finally, streptavidin HRP is linked with the concatemers. The HRP-catalyzed reaction was monitored by reducing enzyme-oxidized benzoquinone. In another study, SiO_2 nanoparticles immobilized on HRP were used for signal amplification [20].

SECM has also been applied for cell analysis in microwell arrays. For example, visualization of the concentrations of dissolved oxygen using SECM allowed the detection of respiratory activity in cellular spheroids (Fig. 3b) [21, 22]. For these experiments, the spheroids were fabricated in microwell arrays. In addition, alkaline phosphatase (ALP), a pluripotent marker in cellular spheroids, was successfully evaluated by detecting the enzymatic product *p*-aminophenol (PAP) after addition of the enzymatic substrate *p*-aminophenol phosphate (PAPP) (Fig. 3c) [23]. Single-cell analysis in arrays has also been performed using SECM. In an electrochemical reporter gene assay, HeLa cells were genetically transfected with a reporter gene to evaluate tumor necrosis factor α [24]. Secreted alkaline phosphatase (SEAP) was selected as the reporter protein. The cells were trapped in microwells filled with PAPP, and the enzymatic products were monitored using SECM. SECM has also been used as an engraving method for cell analysis [25]. In this study, cells were captured in a microwell array, and the microwells were covered with a detection slide to trap cells in confined spaces. During culturing, the cellular secretions of

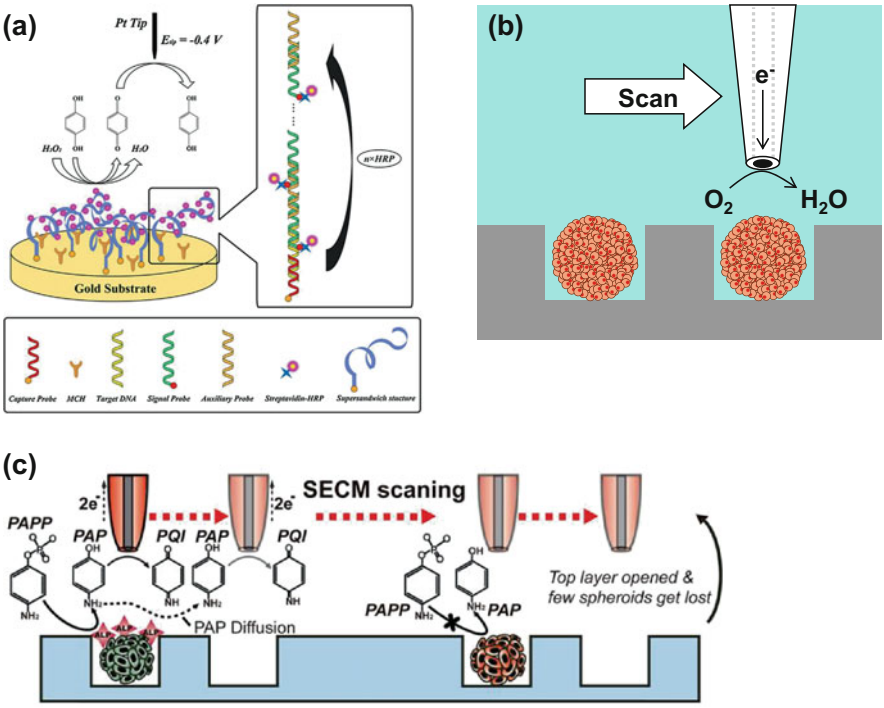

Fig. 3 Array-based bioanalysis using SECM. (**a**) Detection of DNAs. Reproduced with permission from [19]. Copyright 2016, Elsevier. (**b**) Detection of the respiratory activity of cellular spheroids. (**c**) Detection of ALP in cellular spheroids. Reproduced with permission from [23]. Copyright 2019, American Chemical Society

SEAP were trapped and immobilized on the detection slide modified with antibodies for SEAP, which is a similar process to engraving. The immobilized SEAP was then detected using PAPP and SECM. In addition to cell analysis, SECM can be used to evaluate biomaterials in cell cultures. For example, the topography and oxygen permeability around hydrogel microwell arrays were visualized [26].

This chapter focuses on array-based bioanalyses using SECM. However, SECM has also been utilized to analyze inorganic catalysts. This is related to the characterization of the homogeneity of a single catalyst layer or many catalyst materials in an array. For example, SECM was applied to screen CO_2 electroreduction activities [27] and photocatalysts in arrays [28]. A review regarding the use of SECM in analyzing catalytic activity was recently published [29].

3 Electrode Arrays

Electrode array devices have been proposed for high-throughput and rapid array analyses. These devices consist of an array containing multiple electrodes, which can each work individually. Because no scanning process is involved, the analysis time for multiple samples is shorter than in SECM. Moreover, the rapid progress of micro/nanofabrication processes has facilitated the incorporation of multiple microelectrodes into small chip devices. Electrode array devices have been applied not only for high-throughput analysis but also for the electrochemical imaging of biosamples. However, because the number of electrodes in the array is limited, electrochemical images obtained using simple electrode arrays have much lower spatial resolution than SECM images. Simple electrode arrays consist of sensor electrodes, leading electrodes, and connectors. The leading electrodes and connector pads have large areas, and the number of sensors is limited. Also, electrode array devices require numerous bonding pads at their edges, and leading electrodes are needed to connect the sensor electrodes to the pads. Thus, complex wiring is necessary. To reduce the process for the wiring and improve sensor density, switching systems based on field effect transistor and chemical reactions have been proposed, and we present them later. In this section, we discuss simple electrode arrays, wherein the electrodes exhibit 2D or 3D arrangements. We describe electrode arrays with switching systems such as complementary metal oxide semiconductor (CMOS) devices, and finally, we analyze DEP and electrorotation (ROT) devices.

Electrode arrays have been widely utilized for immunosensing. In one study, the coronavirus was identified by employing spike protein S1 as a biomarker [30]. Although the eight electrodes in the device could detect eight different coronaviruses, two electrodes were modified with bovine serum albumin instead of target antigens for use as controls in the study. Further, four electrodes were used for the Middle East respiratory syndrome corona virus (MERS-CoV) antigen and two electrodes were used for human corona virus antigen to enable duplicate measurements. For detection, the electrodes were modified with antigens, and indirect competitive assays were conducted by measuring the redox current of the ferro/ferricyanide redox couple.

Platforms of 96 well plates were utilized for electrochemical bioassays in arrays, although they were not microarrays. Screen-printed electrodes were prepared on the bottoms [31, 32], and wire electrodes were inserted into the top wells [33]. These well plates were used for the electrochemical detection of aflatoxin B_1, magnet-based immunoassays, and the bioelectrochemical analysis of cytochrome P450.

In another system, many sensors were incorporated into a single working electrode without a switching system to achieve digital electrochemical detection [34]. Sensor electrodes of different sizes (1, 2, and 4 mm^2) were connected to a single working electrode. Then, droplets with or without a redox compound at a constant concentration (e.g., 0 or 1 mM) were placed on each sensor. The current signals obtained from the single working electrode were converted into a 3-digit binary number by considering the sensor area and current value. The obtained binary

numbers had one-to-one correspondence with the positions of all three droplets. Although this strategy allows many sensors to be incorporated into a single working electrode, only digital analysis can be performed to judge whether the analytes at the constant concentration are present.

In addition to devices consisting of individual working electrodes, connected electrode arrays have been utilized for bioanalysis, including the sensing of biomarkers in dermal interstitial fluid [35, 36]. For example, microneedle arrays placed on the skin were used to collect and evaluate the components in skin.

DNA detection has also been realized using electrode arrays. For example, 4 × 4 interdigitated electrode arrays (IDAs) with fingers (width and spacing: 600 nm) were fabricated [37]. The IDAs were modified with single-stranded DNAs as capture probes, and the impedance between the fingers in each IDA was monitored after target DNA hybridization, resulting in label-free DNA detection. Apart from impedimetric detection, IDAs were used for oligonucleotide detection based on redox cycling [38]. In this study, a capture oligonucleotide was immobilized on gold IDAs with the aid of a thiol molecule. Then, the target 16S rRNA was captured by hybridization. A detector oligonucleotide labeled with biotin was hybridized to the target RNA, and avidin with ALP was bound to biotin. Finally, PAPP was introduced, and the generated PAP was detected by redox cycling using the IDAs (which means that the substance is oxidized at one finger of the interdigitated electrode and the reaction product subsequently is reduced at the other finger resulting in several detection cycles for one molecule which amplifies the signal). There were 16 electrode pairs, and each IDA consisted of 204 fingers with 800 nm width and 40 nm gap.

Several other strategies that incorporate multiple sensors have also been proposed, including, electrochemical switching systems based on local redox cycling [39–41]. In one device, 32 row and 32 column electrodes were prepared on a single glass substrate. The application of appropriate potentials to these electrodes induced the local redox cycling of analytes, such as PAP, at the crossing points. By monitoring the electrochemical signals, the crossing points could be utilized as individual sensors. Thus, 1,024 sensors were created using only 64 electrodes. In another device, a sensor density of over 1,000 sensors/mm^2 was achieved (Fig. 4a) [39]. Such a device was successfully applied to evaluate the differentiation of embryonic stem (ES) cells (Fig. 4b). Similar systems were also applied to the electrochemical detection of droplet arrays [42, 43].

Microelectrode arrays have also been used in brain studies [44–46]. For example, microelectrode arrays recorded and stimulated electrical signals in neuronal networks in brain tissue. Additionally, 3D electrodes and constructs such as microneedles [47] were developed to monitor 3D brain tissue. Recently, a flexible electrode array was designed to cover cortical spheroids (Fig. 5a) [48]. In this study, a 3D neural interfacial network was successfully monitored using 25 electrodes arranged in a 3D array. CMOS techniques have been used to solve the problem of sensor density. A CMOS-based electrode array device was used for in vitro assays to characterize the neuronal dynamics of single-cell networks (Fig. 5b) [49]. This device consisted of 19,584 recording sites with a density of 3,050 sensors/mm^2. This device allowed induced pluripotent stem cell-derived neuronal cells to be

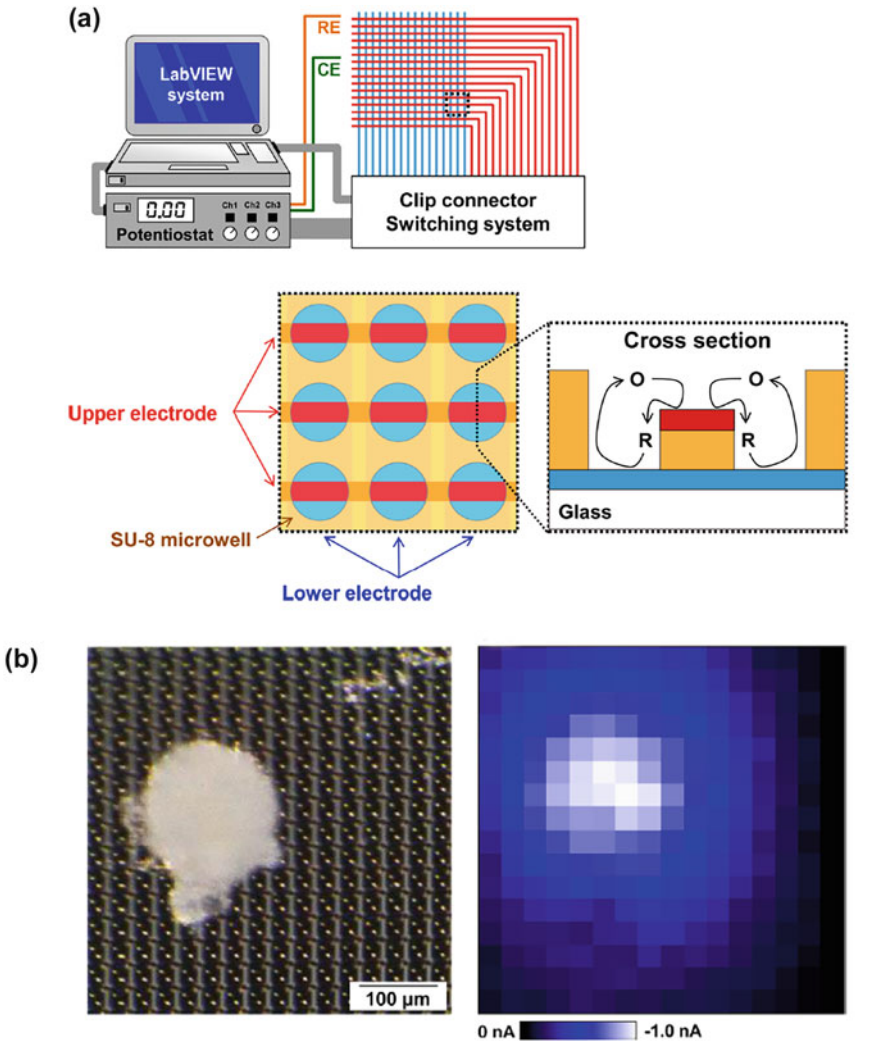

Fig. 4 Local-redox-cycling-based electrochemical imaging device. (**a**) Schematic of device and system. Row and column electrodes are orthogonally crossed, and redox cycling is locally induced only at the crossing points. In this case, 256 crossing points as individual sensors are obtained using only 32 electrodes. (**b**) Optical and electrochemical images of the embryoid body of ES cells. The ALP activity as a differentiation marker was converted into a redox current. The electrochemical image consists of 256 pixels that indicate the current values. Reproduced with permission from [39]. Copyright 2014, American Chemical Society

monitored for several weeks. Another CMOS microelectrode array device was applied for the multiparametric functional imaging of cells and tissues [50]. This device used impedance and electrochemical analyses to visualize cellular attachment, adhesion, and metabolism.

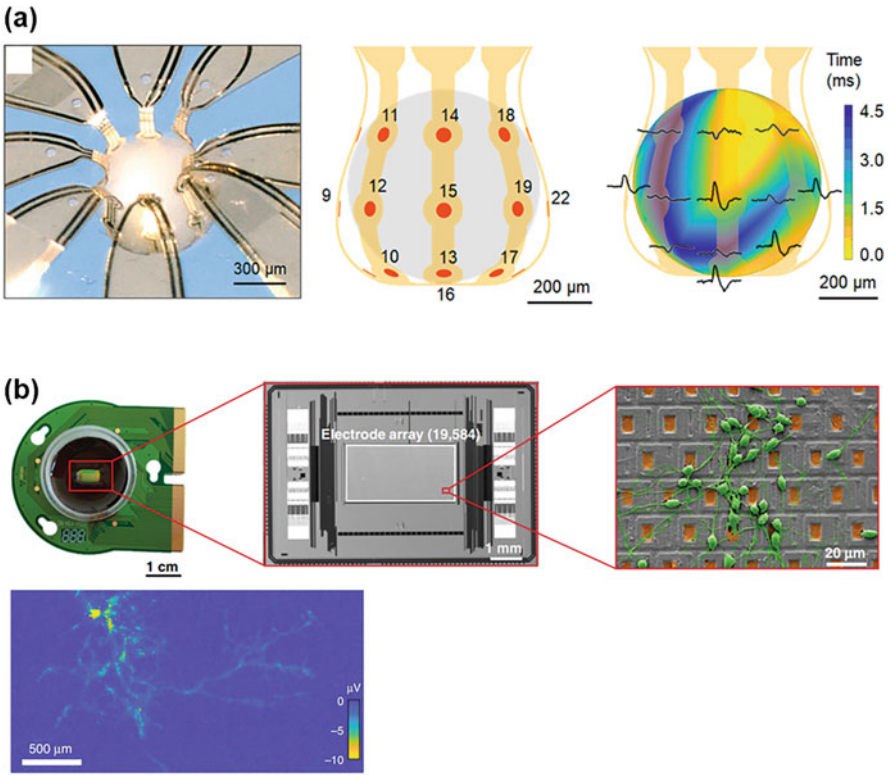

Fig. 5 Electrode arrays for monitoring the neural activity of cells. (**a**) 3D electrode array. Left: optical image of a cortical spheroid enclosed in the device. Middle: position of sensor electrodes. Right: local field potentials from the electrodes. Reproduced from [48]. Licensed under CC BY-NC. Copyright 2021, the authors. (**b**) CMOS device. Top: device structure. Bottom: activity map of neurons. The color represents the potential values. Reproduced from [49]. Licensed under CC BY 4.0. Copyright 2020, the authors

DEP devices have been applied to trap biosamples, such as immunobeads and cells, in arrays. DEP-based analyses can be classified as positive or negative DEP (pDEP and nDEP, respectively) [51]. In pDEP, bioparticles move to areas with strong electric fields. In contrast, in nDEP, bioparticles move away from the areas with strong electric fields. In one study, microbeads for a digital immunoassay were loaded and then efficiently captured in a microwell array consisting of SU-8 as the photoresist, and Au electrodes using pDEP (Fig. 6a) [52]. After the immunoassay, the system was washed by pushing the microbeads out of the microwells using nDEP. This system was used to detect four types of cytokines. Another DEP device was applied to the detection of surface antigens on cells [53]. This microfluidic device consisted of a single-plane indium tin oxide (ITO) electrode and an antibody-modified band array on the top and bottom, respectively. Using nDEP induced by the

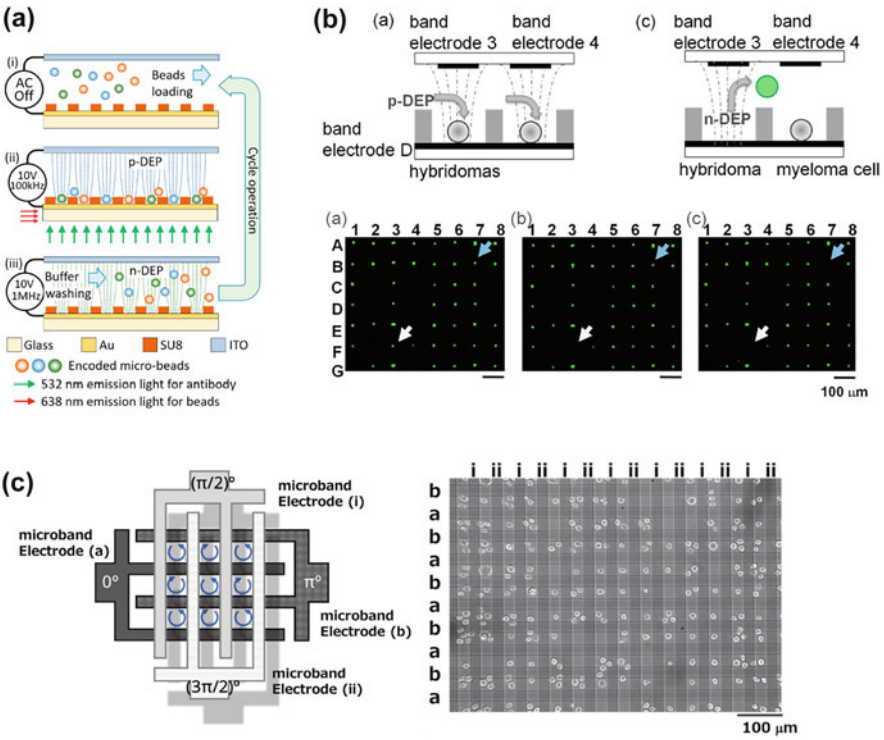

Fig. 6 Manipulation of biobeads in arrays using (**a**, **b**) DEP and (**c**) ROT. (**a**) Schematic illustration of immunoassay combined with DEP. DEP is used to trap immunobeads in the array for multiple rapid detection. Reproduced from [52]. Licensed under CC BY-NC-ND. Copyright 2021, the authors. (**b**) Trapping and releasing cells using DEP. Reproduced with permission from [55]. Copyright 2022, Elsevier. (**c**) Schematic illustration and photo of a cell array. Two pairs of IDAs are set orthogonally to induce ROT in the array. Cells are trapped and rotated at the center of the grids. Reproduced from [57]. Licensed under CC BY 3.0. Copyright 2020, Royal Society of Chemistry

electrode array, target cells with CD33 were pushed onto the area modified with antibodies and captured via immunoreactions. The potential was then switched to remove nontarget cells. The surface antigen was successfully monitored by measuring the efficiency of cell trapping. A DEP device was also used to harvest target single cells from arrays after analysis (Fig. 6b) [54, 55]. This device consisted of microband electrode arrays orthogonally arranged at the top and bottom. First, the cells were trapped in microwell arrays using pDEP. Suitable potentials were then applied to specific electrodes to induce local nDEP only at the target crossing point, resulting in the release of cells from the microwell [55].

In addition to DEP, electrorotation (ROT) has been used to evaluate bioparticles. By employing ROT, torque can be induced in bioparticles. Typically, four electrodes are prepared on a planar substrate to induce a rotating electric field. In contrast, for high-throughput analyses, two sets of IDAs were prepared in a 3D arrangement to

induce ROT in many areas in an array (Fig. 6c) [56, 57]. This device was applied to trap and rotate cells in the array, which facilitated evaluation of their dielectric properties [57].

4 ECL

In ECL detection, electrochemical reactions are converted into luminescent signals. In a typical ECL scheme, luminophores and co-reactants react electrochemically on an electrode to produce excited luminophores, resulting in ECL emission (Fig. 2b). $Ru(bpy)_3^{2+}$/tri-*n*-propylamine (TPA) and luminol/H_2O_2 have been widely used for ECL emission. A single working electrode can visualize electrochemical reactions over large areas without complex wiring, which is an advantage over electrode arrays. Compared to that of fluorescence detection, the ECL method exhibits an almost zero background because it does not require excitation light, resulting in highly sensitive assays. However, there are fewer reactions that are suitable for ECL-based bioanalysis, especially for cell analysis. Therefore, new reactions and strategies that use ECL are desirable. As the ECL signals depended strongly on the surface conditions, the use of clean electrodes in every analysis is necessary, which may be a disadvantage compared to fluorescence techniques. In contrast, surface fouling due to bioreactions, such as cellular activity may be monitored using the ECL approach.

ECL can be observed in bioanalyses including immunoassays, and oligonucleotide assays. Recently, novel strategies for use in cell analysis have been reported. For highly sensitive assays, numerous devices and systems and high-throughput analyses have been developed. Additionally, nanomaterials such as quantum dots (QDs) were developed for use as ECL tags [58], but we skip the detailed discussion of QDs in this chapter.

An ECL-based biosensor array was proposed for glucose, lactate, and choline detection [59]. The six working electrodes were modified with enzymes, carbon nanotubes, and chitosan. After the enzymatic reaction, ECL was generated using luminol and H_2O_2 produced by the enzyme-catalyzed oxidation of different substrates. In another study, dopamine released from living cells was detected using an ECL nanocage array in which luminophores were confined [60]. In this study, the cells were stimulated, and the supernatants were collected and measured using the platform. The approach relied on the quenching effect of dopamine on the ECL signal. An ECL imaging microarray was also used to monitor dopamine released from single cells (Fig. 7) [61]. A microfluidic device with microwells was used to trap cells and concentrate released dopamine. At the sensing points, an ITO electrode was modified with co-reactant-embedded polymer dots (Pdots), resulting in decreased ECL signals in the presence of dopamine. Under hypoxic conditions, the concentration of dopamine released from single cells was 50–130 pM or 3×10^4–7×10^4 per cell, and the low concentration was successfully monitored.

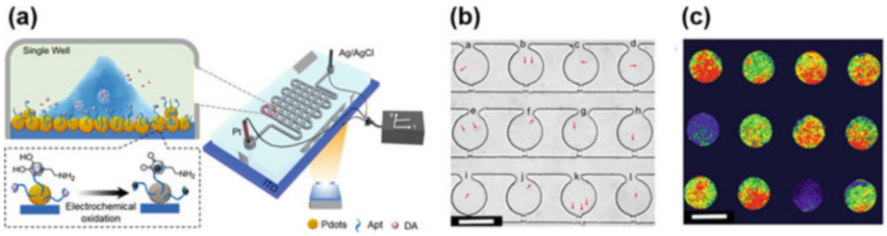

Fig. 7 ECL imaging of dopamine (DA) release from a PC12 cell culture array. (**a**) Schematic illustration of the system. Cells are cultured in a microfluidic device containing microwells modified with Pdots and aptamers (Apt). (**b**) Bright-field and (**c**) ECL images of cells. Reproduced with permission from [71]. Copyright 2022, Elsevier

ECL was also applied to bead-based immunoassays for multiplex detection (Fig. 8) [62]. In this study, the antigen was sandwiched between biotinylated antibodies and antibody-modified microbeads, and the beads were then treated with a streptavidin-$Ru(bpy)_3^{2+}$ complex. The beads were trapped in a microwell array of etched Au electrodes. Three types of microbeads were prepared for VEGF, IL-8, and TIMP-1 detection. The concentrations of Eu^{3+} in the beads differed, which allowed them to be distinguished in the assay using fluorescence signals. The ECL emission was observed to evaluate immunoreactions.

Array-based genotoxicity screening has been performed using an ECL approach [63]. In this study, DNA, the CYP450 enzyme, and $[Ru(bpy)_2(PVP)_{10}]^{2+}$ were spotted in an array on a pyrolytic graphite electrode. The ECL signals derived from damaged DNA were larger than those from normal DNA. Because DNA damage depends on CYP450 activity, the enzymatic activity was evaluated based on the ECL intensity.

ECL imaging is also applicable to single-cell analysis [64]. Cholesterol from single cells was monitored using an ECL device. Microwells were prepared on an ITO electrode, which was modified with graphitic carbon nitride ($g\text{-}C_3N_4$) nanosheets to enhance ECL emission. Single HeLa cells were trapped in the microwells, and cholesterol oxidase in solution reacted with membrane cholesterol to generate H_2O_2. A luminol analog, L012, was loaded into the cell chamber and used for ECL imaging. The same group reported the detection of intracellular glucose in single cells with ECL imaging using a similar device and glucose oxidase [65].

5 Bipolar Electrode Arrays

To address the issue of the complex wiring of electrode arrays, wireless electrochemical sensing systems have been developed using a strategy based on bipolar electrochemistry [66].

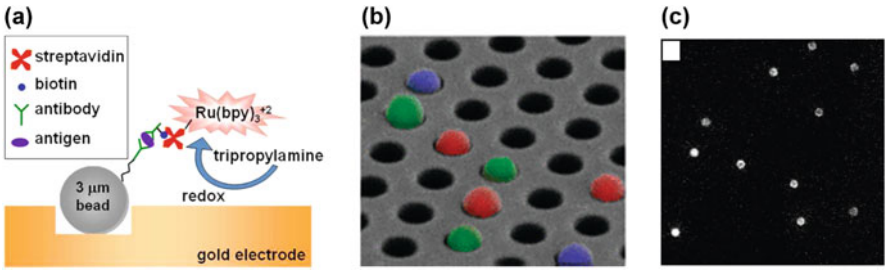

Fig. 8 ECL imaging of immunobeads on the Au electrode. (**a**) Schematic illustration. (**b**) Bead array on the electrode. The image was pseudo-colorized. Four types of immunobeads were trapped and observed under a fluorescence microscope. (**c**) ECL images of the beads. The intensities in the ECL image indicated the quantity of the analytes. Reproduced with permission from [62]. Copyright 2009, American Chemical Society

A BPE consists of a conducting material in an electrolytic solution containing a pair of driving electrodes with a potential bias. When the bias is sufficient, an anodic reaction is induced at one end of the BPE and a cathodic reaction is induced at the other end (Fig. 9a), even though the BPE is not connected to the driving electrodes. In general, an electrochemical reaction at either pole of the BPE is converted into an optical signal, such as fluorescence or ECL at another pole. By monitoring the optical signal, the electrochemical reaction at the other pole can be evaluated because the anodic and cathodic currents of the BPE are equal. Thus, the BPE-based strategy can provide electrochemical sensing without complex wiring, and large electrochemical sensors can be incorporated into small chip devices. For example, a small chip with 1,000 individual BPEs was reported [67]. In contrast, it is difficult to stimulate cells locally using BPEs as shown in previous figures, because a single pair of driving electrodes simultaneously control all BPEs in the array, and the BPEs do not operate individually. Additionally, potentiometric assays of cellular functions have not been described yet, because no strategy for converting active potentials to optical signals using BPEs has been reported, to the best of our knowledge. BPEs can be categorized as open (Fig. 9a) or closed (Fig. 9b). For open BPEs, the cathodic and anodic poles are in the same solution. In contrast, for closed BPEs, the solutions in contact with the anodic and cathodic poles are physically separated. In the closed system, there is a single current path via the BPE. Therefore, the applied potential between the driving electrodes can be set lower in the closed system than in the open system, which is advantageous. Moreover, the physical separation of the reporter and sample cells aids in eliminating crosstalk. In this section, we focus on closed systems for array-based assays. Although many sensors can be incorporated using this strategy, there are limited systems that combine analyte electrochemical reactions and ECL, which is a disadvantage compared with conventional electrode array devices.

A closed BPE array was applied to detect cancer biomarkers [68]. In this study, parallel ITO BPEs were placed on a glass substrate. Au films were electrodeposited

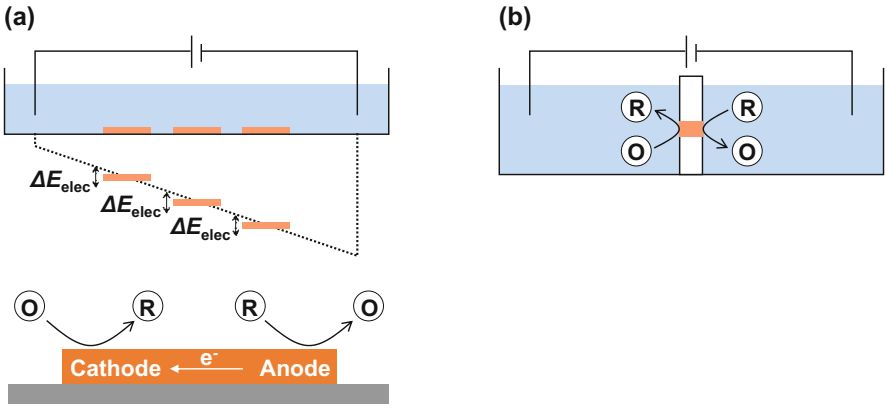

Fig. 9 BPE types. (**a**) Open and (**b**) closed BPEs. Reproduced with permission from [5]. Copyright 2021, Elsevier

on the BPE cathodes, which were also modified with aptamers or first antibodies. In the presence of the biomarkers, thionine with second antibodies was immobilized at the cathodic pole as an electrochemical tag. $[Ru(bpy)_3]^{2+}$ underwent a reaction at the anodic pole, and the resulting ECL signal was monitored. Thus, electrochemical arrays can be utilized for detection of high-throughput assays of multiple analytes and samples.

DNA detection has also been achieved using a closed BPE array [69]. In this system, single-stranded DNA probes were immobilized on Au electrodes as cathodic poles. During the hybridization of the target single-stranded DNA, methylene blue (MB) was intercalated into the resulting double-stranded DNA. MB was reduced at the cathodic pole, while $[Ru(bpy)_3]^{2+}$/TPA was oxidized to produce ECL emission. The concentration of the target DNA was successfully determined using the ECL signal.

Closed BPE arrays have been applied for cell analysis. For example, the respiratory activity of cancer spheroids was monitored [70], as outlined in Fig. 10. Briefly, a BPE array of Pt electrodes was prepared. Cancer spheroids of MCF-7 were manually arranged using a micropipette at the cathodic poles of the BPEs, whereas $[Ru(bpy)_3]^{2+}$ and TPA were placed at the anodic poles. During detection, dissolved oxygen was reduced to water at the cathodic pole, and ECL emission occurred at the anodic pole. Cell respiration caused the concentration of dissolved oxygen to decrease at the cathodic pole, resulting in low ECL emission. Using this strategy, the respiratory activity of cellular spheroids was successfully evaluated. Because cellular spheroids are widely utilized for cellular transplantation and drug screening, this method can also be applied for these purposes.

Typically, BPE arrays are 2D and prepared on flat substrates such as glass. To fabricate high-density BPE array membranes, several methods have been proposed,

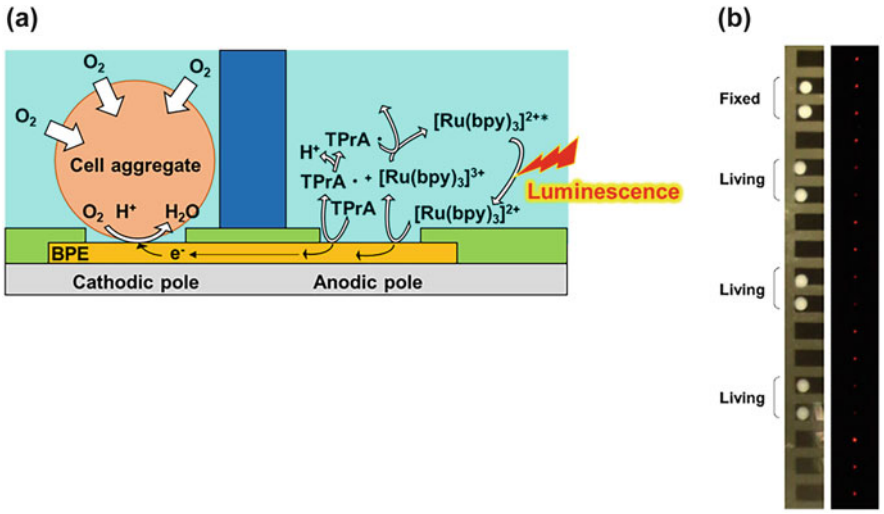

Fig. 10 BPEs for detection of respiratory activity of cellular spheroids in an array. (**a**) Schematic illustration. (**b**) Optical image of spheroids at the cathodic poles and ECL images of the sensing areas of anodic poles. Reproduced with permission from [70]. Copyright 2021, Elsevier

in which BPEs are vertically embedded in thin films (Fig. 11a) [71–75]. For example, a carbon electrode array obtained by SU-8 pyrolysis was prepared in a parylene C film [72, 74]. In another approach, a track-etched membrane was used and Au BPEs were prepared using electroless plating [73]. In addition to ECL imaging, fluorescence imaging of resazurin/resorufin was reported using a BPE array film [76]. In this study, resazurin was reduced to resorufin at the cathodic poles, and the resorufin was fluorescently monitored. BPE array membrane was successfully applied for the visualization of cellular adhesion [77]. In this study, Au electrodes were electrodeposited in the pores of an anodic aluminum oxide membrane to prepare a nanoelectrode array. This fabrication strategy resulted in an electrode diameter of 140 nm and a pitch of 450 nm. Single cells were cultured on the cathodic poles of the membrane, and $(Ru(bpy)_3)^{2+}$/2-(dibutylamino)ethanol were used as the luminophore/co-reactant for ECL imaging at the anodic poles of the membrane. When cells were attached to the membrane, oxygen reduction was inhibited because the cells covered the electrodes (Fig. 11b).

Commercially available BPE arrays are desirable for researchers with no instruments to fabricate them. Anisotropic conductive film (ACF) can also be used as a commercially available BPE array, although ACFs are generally applied for vertical and horizontal conduction and lead-free adhesion in the production of display panels and camera modules. Generally, an ACF comprises a thermosetting resin and conductive particles/rods, and the construction is similar to that in Fig. 11a. Therefore, commercially available ACFs have been used as BPEs in ECL imaging [78].

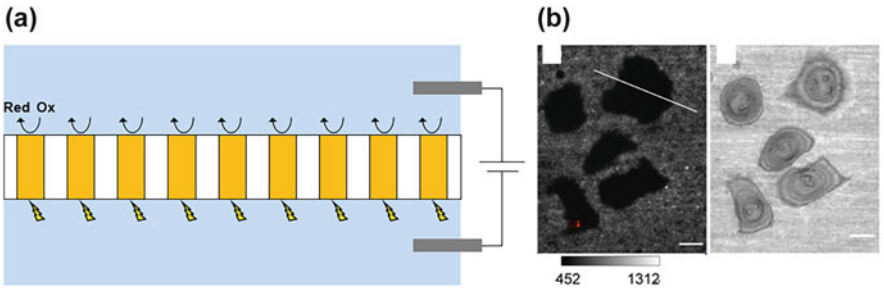

Fig. 11 Closed BPE array in a thin film. (**a**) Schematic of device. (**b**) ECL imaging of single cells. Left: ECL image. Right: bright-field image. Scale bar: 20 μm. Reproduced with permission from [77]. Copyright 2021, Wiley-VCH GmbH

Closed and open BPE arrays have also been combined with DEP techniques to trap cells. Such a device was applied for the high-throughput selective capture of circulating tumor cells [79].

In addition to the chip devices for bioanalysis discussed in this section, BPEs have also been incorporated into probe devices [80–81]. BPEs have also been utilized for other applications such as electrosynthesis [82, 83] and biofabrication [84]. Thus, bipolar electrochemical systems are of considerable interest in several fields, including bioanalysis.

In addition to cell analysis as mentioned above, a microfluidic system was combined with BPE arrays in multiplexed detection [85]. Using this system, rapid, automatic multiple sampling was realized, resulting in an improved efficiency and a reduced use of reagents. As microfluidic systems can be utilized in organs-on-a-chip and microphysiological systems, BPE-microfluidic system should be used in cellular analyses based on chips.

6 Perspective and Conclusions

This chapter provides an overview of microarray-based electrochemical biosensing approaches, including SECM, electrode arrays, ECL techniques, and BPEs, and discusses their advantages, disadvantages, and bioanalysis applications. Although electrochemical biofabrication [86] was omitted from this chapter, the aforementioned electrochemical devices and systems can be utilized for biofabrication in arrays. Such arrays can be used as cell culture platforms and bioanalysis chips.

Although we focused on SECM in this chapter, several other electrochemical microscopic techniques have been proposed, including scanning ion conductance microscopy (SICM) and scanning electrochemical cell microscopy (SECCM) [87]. The SICM and SECCM techniques are capable of visualizing samples on the nanometer scale. In addition, SECCM can be used to prepare arrays of chemicals on electrodes using a scanning droplet cell [88]. Furthermore, these techniques can be

combined with SECM for bioanalysis [89]. We anticipate that these techniques will be utilized for array-based bioanalysis in the future.

As discussed in this chapter, electrode arrays are applicable for single-cell analysis and the evaluation of cellular spheroids. In the near future, further advances will allow these devices to be widely used to evaluate organoids [90] and microphysiological systems [91] for drug discovery.

References

1. Grieshaber D, MacKenzie R, Voros J, Reimhult E (2008) Electrochemical biosensors – sensor principles and architectures. Sensors 8:1400–1458
2. Rissin DM, Kan CW, Campbell TG, Howes SC, Fournier DR, Song L, Piech T, Patel PP, Chang L, Rivnak AJ, Ferrell EP, Randall JD, Provuncher GK, Walt DR, Duffy DC (2010) Single-molecule enzyme-linked immunosorbent assay detects serum proteins at subfemtomolar concentrations. Nat Biotechnol 28:595–599
3. Heath JR, Ribas A, Mischel PS (2016) Single-cell analysis tools for drug discovery and development. Nat Rev Drug Discov 15:204–216
4. Trouillon R, Passarelli MK, Wang J, Kurczy ME, Ewing AG (2013) Chemical analysis of single cells. Anal Chem 85:522–542
5. Ino K, Shiku H, Matsue T (2017) Bioelectrochemical applications of microelectrode arrays in cell analysis and engineering. Curr Opin Electrochem 5:146–151
6. Ding H, Su B, Jiang DC (2022) Recent advances in single cell analysis by electrochemiluminescence. ChemistryOpen:e202200113
7. Wang J (2002) Electrochemical nucleic acid biosensors. Anal Chim Acta 469:63–71
8. Blair EO, Corrigan DK (2019) A review of microfabricated electrochemical biosensors for DNA detection. Biosens Bioelectron 134:57–67
9. Trotter M, Borst N, Thewes R, von Stetten F (2020) Review: electrochemical DNA sensing – principles, commercial systems, and applications. Biosens Bioelectron 154:112069
10. Maduraiveeran G, Sasidharan M, Ganesan V (2018) Electrochemical sensor and biosensor platforms based on advanced nanomaterials for biological and biomedical applications. Biosens Bioelectron 103:113–129
11. Amemiya S, Bard AJ, Fan FRF, Mirkin MV, Unwin PR (2008) Scanning electrochemical microscopy. Annu Rev Anal Chem 1:95–131
12. Mirkin MV, Horrocks BR (2000) Electroanalytical measurements using the scanning electrochemical microscope. Anal Chim Acta 406:119–146
13. Kwak J, Bard AJ (1989) Scanning electrochemical microscopy. Theory of the feedback mode. Anal Chem 61:1221–1227
14. Wang X, Askarova G, Mirkin MV (2021) Chapter 4 – electrochemical microscopy at the nanoscale. Elsevier
15. Lesch A, Momotenko D, Cortés-Salazar F, Wirth I, Tefashe UM, Meiners F, Vaske B, Girault HH, Wittstock G (2012) Fabrication of soft gold microelectrode arrays as probes for scanning electrochemical microscopy. J Electroanal Chem 666:52–61
16. Lesch A, Momotenko D, Cortés-Salazar F, Roelfs F, Girault HH, Wittstock G (2013) High-throughput scanning electrochemical microscopy brushing of strongly tilted and curved surfaces. Electrochim Acta 110:30–41
17. Kai TH, Chen S, Monterroso E, Zhou FM (2015) Continuous nanoflow-scanning electrochemical microscopy: voltammetric characterization and application for accurate and reproducible imaging of enzyme-labeled protein microarrays. Anal Chem 87:4523–4529

18. Gdor E, Shemesh S, Magdassi S, Mandler D (2015) Multienzyme inkjet printed 2D arrays. ACS Appl Mater Interfaces 7:17985–17992
19. Chen BP, Hu QQ, Xiong Q, Zhang F, He PG (2016) An ultrasensitive scanning electrochemical microscopy (SECM)-based DNA biosensing platform amplified with the long self-assembled DNA concatemers. Electrochim Acta 192:127–132
20. Fan HJ, Wang XL, Jiao F, Zhang F, Wang QJ, He PG, Fang YZ (2013) Scanning electrochemical microscopy of DNA hybridization on DNA microarrays enhanced by HRP-modified SiO_2 nanoparticles. Anal Chem 85:6511–6517
21. Sridhar A, de Boer HL, van den Berg A, Le Gac S (2014) Microstamped petri dishes for scanning electrochemical microscopy analysis of arrays of microtissues. PloS One 9:e93618
22. Torisawa Y, Takagi A, Nashimoto Y, Yasukawa T, Shiku H, Matsue T (2007) A multicellular spheroid array to realize spheroid formation, culture, and viability assay on a chip. Biomaterials 28:559–566
23. Zhao L, Shi M, Liu Y, Zheng X, Xiu J, Liu Y, Tian L, Wang H, Zhang M, Zhang X (2019) Systematic analysis of different cell spheroids with a microfluidic device using scanning electrochemical microscopy and gene expression profiling. Anal Chem 91:4307–4311
24. Murata T, Yasukawa T, Shiku H, Matsue T (2009) Electrochemical single-cell gene-expression assay combining dielectrophoretic manipulation with secreted alkaline phosphatase reporter system. Biosens Bioelectron 25:913–919
25. Şen M, Ino K, Shiku H, Matsue T (2012) A new electrochemical assay method for gene expression using HeLa cells with a secreted alkaline phosphatase (SEAP) reporter system. Biotechnol Bioeng 109:2163–2167
26. Wang M, Liu S, Li F (2019) Imaging oxygen microenvironment in hydrogel microwell array. Acta Mech Sinica 35:321–328
27. Mayer FD, Hosseini-Benhangi P, Sánchez-Sánchez CM, Asselin E, Gyenge EL (2020) Scanning electrochemical microscopy screening of CO_2 electroreduction activities and product selectivities of catalyst arrays. Commun Chem 3:155
28. Ye H, Lee J, Jang JS, Bard AJ (2010) Rapid screening of $BiVO_4$-based photocatalysts by scanning electrochemical microscopy (SECM) and studies of their photoelectrochemical properties. J Phys Chem C 114:13322–13328
29. Preet A, Lin T-E (2021) A review: scanning electrochemical microscopy (SECM) for visualizing the real-time local catalytic activity. Catalysts 11:594
30. Layqah LA, Eissa S (2019) An electrochemical immunosensor for the corona virus associated with the Middle East respiratory syndrome using an array of gold nanoparticle-modified carbon electrodes. Mikrochim Acta 186:224
31. Neves MMPS, González-García MB, Hernández-Santos D, Fanjul-Bolado P (2014) Screen-printed electrochemical 96-well plate: a high-throughput platform for multiple analytical applications. Electroanalysis 26:2764–2772
32. Piermarini S, Micheli L, Ammida NHS, Palleschi G, Moscone D (2007) Electrochemical immunosensor array using a 96-well screen-printed microplate for aflatoxin B_1 detection. Biosens Bioelectron 22:1434–1440
33. Frank R, Prönnecke C, Azendorf R, Jahnke H-G, Beck-Sickinger AG, Robitzki AA (2020) Advanced 96-microtiter plate based bioelectrochemical platform reveals molecular short cut of electron flow in cytochrome P450 enzyme. Lab Chip 20:1449–1460
34. Ino K, Kanno Y, Yamada Y, Shiku H, Matsue T (2017) Binary-number-based digital electrochemical detection using a single working electrode with multiple sensors. Electrochem Commun 77:76–80
35. Madden J, O'Mahony C, Thompson M, O'Riordan A, Galvin P (2020) Biosensing in dermal interstitial fluid using microneedle based electrochemical devices. Sens Bio-Sens Res 29:100348
36. Zhang BL, Zhang XP, Chen BZ, Fei WM, Cui Y, Guo XD (2021) Microneedle-assisted technology for minimally invasive medical sensing. Microchem J 162:105830

37. Delle LE, Pachauri V, Vlandas A, Riedel M, Lägel B, Lilischkis R, Vu XT, Wagner P, Thoelen R, Lisdat F, Ingebrandt S (2018) Scalable fabrication and application of nanoscale IDE-arrays as multi-electrode platform for label-free biosensing. Sens Actuator B-Chem 265:115–125
38. Elsholz B, Wörl R, Blohm L, Albers J, Feucht H, Grunwald T, Jürgen B, Schweder T, Hintsche R (2006) Automated detection and quantitation of bacterial RNA by using electrical microarrays. Anal Chem 78:4794–4802
39. Ino K, Kanno Y, Nishijo T, Komaki H, Yamada Y, Yoshida S, Takahashi Y, Shiku H, Matsue T (2014) Densified electrochemical sensors based on local redox cycling between vertically separated electrodes in substrate generation/chip collection and extended feedback modes. Anal Chem 86:4016–4023
40. Ino K, Nishijo T, Arai T, Kanno Y, Takahashi Y, Shiku H, Matsue T (2012) Local redox-cycling-based electrochemical chip device with deep microwells for evaluation of embryoid bodies. Angew Chem Int Edit 124:6752–6756
41. Ino K, Saito W, Koide M, Umemura T, Shiku H, Matsue T (2011) Addressable electrode array device with IDA electrodes for high-throughput detection. Lab Chip 11:385–388
42. Zhang H, Oellers T, Feng W, Abdulazim T, Saw EN, Ludwig A, Levkin PA, Plumeré N (2017) High-density droplet microarray of individually addressable electrochemical cells. Anal Chem 89:5832–5839
43. Ino K, Kanno Y, Nishijo T, Goto T, Arai T, Takahashi Y, Shiku H, Matsue T (2012) Electrochemical detection for dynamic analyses of a redox component in droplets using a local redox cycling-based electrochemical (LRC-EC) chip device. Chem Commun 48:8505–8507
44. Bhaskara S, Sakorikar T, Chatterjee S, Girishan KVS, Pandya HJ (2022) Recent advancements in micro-engineered devices for surface and deep brain animal studies: a review. Sens Bio-Sens Res 36:100483
45. Hong JW, Yoon C, Jo K, Won JH, Park S (2021) Recent advances in recording and modulation technologies for next-generation neural interfaces. iScience 24:103550
46. Jeong YC, Lee HE, Shin A, Kim DG, Lee KJ, Kim D (2020) Progress in brain-compatible interfaces with soft nanomaterials. Adv Mater 32:1907522
47. Huang D, Li JS, Li TY, Wang ZY, Wang QN, Li ZH (2021) Recent advances on fabrication of microneedles on the flexible substrate. J Micromech Microeng 31:073001
48. Park Y, Franz CK, Ryu H, Luan HW, Cotton KY, Kim JU, Chung TS, Zhao SW, Vazquez-Guardado A, Yang DS, Li K, Avila R, Phillips JK, Quezada MJ, Jang H, Kwak SS, Won SM, Kwon K, Jeong H, Bandodkar AJ, Han MD, Zhao HB, Osher GR, Wang HL, Lee K, Zhang YH, Huang YG, Finan JD, Rogers JA (2021) Three-dimensional, multifunctional neural interfaces for cortical spheroids and engineered assembloids. Sci Adv 7:eabf9153
49. Yuan X, Schröter M, Obien MEJ, Fiscella M, Gong W, Kikuchi T, Odawara A, Noji S, Suzuki I, Takahashi J, Hierlemann A, Frey U (2020) Versatile live-cell activity analysis platform for characterization of neuronal dynamics at single-cell and network level. Nat Commun 11:4854
50. Abbott J, Mukherjee A, Wu W, Ye T, Jung HS, Cheung KM, Gertner RS, Basan M, Ham D, Park H (2022) Multi-parametric functional imaging of cell cultures and tissues with a CMOS microelectrode array. Lab Chip 22:1286–1296
51. Pethig R (2010) Review article-dielectrophoresis: status of the theory, technology, and applications. Biomicrofluidics 4:022811
52. Yang S-M, Lin Q, Zhang H, Yin R, Zhang W, Zhang M, Cui Y (2021) Dielectrophoresis assisted high-throughput detection system for multiplexed immunoassays. Biosens Bioelectron 180:113148
53. Yasukawa T, Hatanaka H, Mizutani F (2012) Simple detection of surface antigens on living cells by applying distinct cell positioning with negative dielectrophoresis. Anal Chem 84:8830–8836
54. Taff BM, Voldman J (2005) A scalable addressable positive-dielectrophoretic cell-sorting array. Anal Chem 77:7976–7983

55. Hata M, Suzuki M, Yasukawa T (2022) Selective retrieval of antibody-secreting hybridomas in cell arrays based on the dielectrophoresis. Biosens Bioelectron 209:114250
56. Ino K, Ishida A, Inoue KY, Suzuki M, Koide M, Yasukawa T, Shiku H, Matsue T (2011) Electrorotation chip consisting of three-dimensional interdigitated array electrodes. Sens Actuator B-Chem 153:468–473
57. Kawai S, Suzuki M, Arimoto S, Korenaga T, Yasukawa T (2020) Determination of membrane capacitance and cytoplasm conductivity by simultaneous electrorotation. Analyst 145:4188–4195
58. Chen X, Liu Y, Ma Q (2018) Recent advances in quantum dot-based electrochemiluminescence sensors. J Mater Chem C 6:942–959
59. Zhou ZY, Xu LR, Wu SZ, Su B (2014) A novel biosensor array with a wheel-like pattern for glucose, lactate and choline based on electrochemiluminescence imaging. Analyst 139:4934–4939
60. Ding H, Guo W, Zhou P, Su B (2020) Nanocage-confined electrochemiluminescence for the detection of dopamine released from living cells. Chem Commun 56:8249–8252
61. Wang N, Ao H, Xiao W, Chen W, Li G, Wu J, Ju H (2022) Confined electrochemiluminescence imaging microarray for high-throughput biosensing of single cell-released dopamine. Biosens Bioelectron 201:113959
62. Deiss F, LaFratta CN, Symer M, Blicharz TM, Sojic N, Walt DR (2009) Multiplexed sandwich immunoassays using electrochemiluminescence imaging resolved at the single bead level. J Am Chem Soc 131:6088–6089
63. Hvastkovs EG, So M, Krishnan S, Bajrami B, Tarun M, Jansson I, Schenkman JB, Rusling JF (2007) Electrochemiluminescent arrays for cytochrome P450-activated genotoxicity screening. DNA damage from benzo[a]pyrene metabolites. Anal Chem 79:1897–1906
64. Xu J, Jiang D, Qin Y, Xia J, Jiang D, Chen H-Y (2017) C_3N_4 nanosheet modified microwell array with enhanced electrochemiluminescence for total analysis of cholesterol at single cells. Anal Chem 89:2216–2220
65. Xu J, Huang P, Qin Y, Jiang D, Chen H-Y (2016) Analysis of intracellular glucose at single cells using electrochemiluminescence imaging. Anal Chem 88:4609–4612
66. Fosdick SE, Knust KN, Scida K, Crooks RM (2013) Bipolar electrochemistry. Angew Chem Int Ed 52:10438–10456
67. Chow K-F, Mavré F, Crooks JA, Chang B-Y, Crooks RM (2009) A large-scale, wireless electrochemical bipolar electrode microarray. J Am Chem Soc 131:8364–8365
68. Wu M-S, Liu Z, Shi H-W, Chen H-Y, Xu J-J (2015) Visual electrochemiluminescence detection of cancer biomarkers on a closed bipolar electrode array chip. Anal Chem 87:530–537
69. Hsueh A-J, Mutalib NAA, Shirato Y, Suzuki H (2022) Bipolar electrode arrays for chemical imaging and multiplexed sensing. ACS Omega 7:20298–20305
70. Ino K, Yaegaki R, Hiramoto K, Nashimoto Y, Shiku H (2020) Closed bipolar electrode array for on-chip analysis of cellular respiration by cell aggregates. ACS Sens 5:740–745
71. Iwama T, Komatsu M, Inoue KY, Shiku H (2021) Detection and 2D imaging of dopamine distribution using a closed bipolar electrode system by applying a cathodic luminophore. ChemElectroChem 8:3492–3498
72. Anderson TJ, Defnet PA, Cheung RA, Zhang B (2021) Electrocatalyst screening on a massive array of closed bipolar microelectrodes. J Electrochem Soc 168:106502
73. Iwama T, Inoue KY, Abe H, Matsue T, Shiku H (2020) Bioimaging using bipolar electrochemical microscopy with improved spatial resolution. Analyst 145:6895–6900
74. Anderson TJ, Defnet PA, Zhang B (2020) Electrochemiluminescence (ECL)-based electrochemical imaging using a massive array of bipolar ultramicroelectrodes. Anal Chem 92:6748–6755
75. Iwama T, Inoue KY, Abe H, Matsue T (2018) Chemical imaging using a closed bipolar electrode array. Chem Lett 47:843–845
76. Guerrette JP, Percival SJ, Zhang B (2013) Fluorescence coupling for direct imaging of electrocatalytic heterogeneity. J Am Chem Soc 135:855–861

77. Qin X, Jin H-J, Li X, Li J, Pan J-B, Wang K, Liu S, Xu J-J, Xia X-H (2022) Label-free electrochemiluminescence imaging of single-cell adhesions by using bipolar nanoelectrode array. Chem A Eur J 28:e202103964
78. Akasaka R, Ino K, Iwama T, Inoue KY, Nashimoto Y, Shiku H (2022) Electrochemiluminescence imaging based on bipolar electrochemistry using commercially available anisotropic conductive films. Sens Mater 34:3113–3122
79. Li M, Anand RK (2017) High-throughput selective capture of single circulating tumor cells by dielectrophoresis at a wireless electrode array. J Am Chem Soc 139:8950–8959
80. Fakhruddin SMB, Inoue KY, Tsuga R, Matsue T (2018) Closed bipolar electrode system for a liquid-junction-free reference electrode integrated in an amperometric probe sensor. Electrochem Commun 93:62–65
81. Santos CS, Conzuelo F, Eßmann V, Bertotti M, Schuhmann W (2019) Enhanced sensitivity of scanning bipolar electrochemical microscopy for O_2 detection. Anal Chim Acta 1087:36–43
82. Chen ZH, Villani E, Inagi S (2021) Recent progress in bipolar electropolymerization methods toward one-dimensional conducting polymer structures. Curr Opin Electrochem 28:100702
83. Shida N, Zhou YQ, Inagi S (2019) Bipolar electrochemistry: a powerful tool for electrifying functional material synthesis. Acc Chem Res 52:2598–2608
84. Ino K, Matsumoto T, Taira N, Kumagai T, Nashimoto Y, Shiku H (2018) Hydrogel electrodeposition based on bipolar electrochemistry. Lab Chip 18:2425–2432
85. Liu Y, Zhang N, Pan J-B, Song J, Zhao W, Chen H-Y, Xu J-J (2022) Bipolar electrode array for multiplexed detection of prostate cancer biomarkers. Anal Chem 94:3005–3012
86. Ino K, Ozawa F, Dang N, Hiramoto K, Hino S, Akasaka R, Nashimoto Y, Shiku H (2020) Biofabrication using electrochemical devices and systems. Adv Biosyst 4:1900234
87. Bentley CL, Kang M, Unwin PR (2020) Scanning electrochemical cell microscopy (SECCM) in aprotic solvents: practical considerations and applications. Anal Chem 92:11673–11680
88. Clausmeyer J, Henig J, Schuhmann W, Plumeré N (2014) Scanning droplet cell for chemoselective patterning through local electroactivation of protected quinone monolayers. ChemPhysChem 15:151–156
89. Takahashi Y, Shevchuk AI, Novak P, Murakami Y, Shiku H, Korchev YE, Matsue T (2010) Simultaneous noncontact topography and electrochemical imaging by SECM/SICM featuring ion current feedback regulation. J Am Chem Soc 132:10118–10126
90. Lancaster MA, Knoblich JA (2014) Organogenesis in a dish: modeling development and disease using organoid technologies. Science 345
91. Low LA, Mummery C, Berridge BR, Austin CP, Tagle DA (2021) Organs-on-chips: into the next decade. Nat Rev Drug Discov 20:345–361

Adv Biochem Eng Biotechnol (2024) 187: 339–380
https://doi.org/10.1007/10_2024_251

Published online: 27 February 2024

Trends in Development of Aptamer-Based Biosensor Technology for Detection of Bacteria

Tibor Hianik, Sandro Spagnolo, and Michael Thompson

Contents

Abstract The contamination of food by bacterial pathogens represents a substantial hazard for human and animal health. Therefore, considerable effort is focused on the development of effective methods for monitoring food safety. A current trend in this field is the development of biosensors that can be used in remote food laboratories and even in farms to check food contamination prior to its delivery to consumers or its further processing in the food industry. Among receptors that can recognize proteins or lipopolysaccharides (LPS) on bacterial surfaces, aptamers play an important role. An aptamer consists of a single strand of DNA or RNA that folds into a 3D structure when placed in a solution, forming a binding site for the target. This chapter presents an overview of recent achievements in bacterial pathogen detection through the development of electrochemical, optical, and acoustic biosensors based on DNA

T. Hianik (✉) and S. Spagnolo
Faculty of Mathematics, Physics and Informatics, Comenius University, Bratislava, Slovakia
e-mail: tibor.hianik@fmph.uniba.sk

M. Thompson
Department of Chemistry, University of Toronto, Toronto, ON, Canada

aptamers. Thus far, these biosensors exhibit good sensitivity and selectivity, comparable with conventional methods currently used in food laboratories. However, these biosensors offer several advantages over conventional methods: they are of low cost, easier to handle, and respond more quickly. Biosensor technology is therefore an important tool for monitoring food safety.

Graphical Abstract

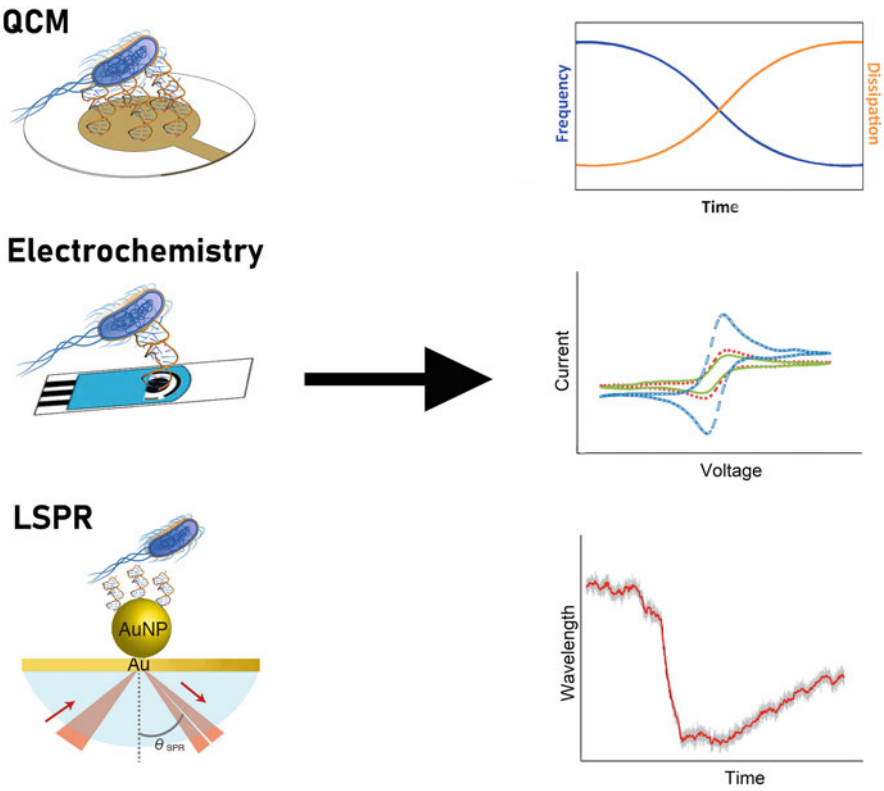

Keywords Bacteria, Biosensors, DNA aptamers, Food contamination

1 Introduction

Food and waterborne pathogens present a substantial threat to human and animal health. They are the source of over 200 diseases. The World Health Organization (WHO) reports that over 600 million people worldwide are infected with

contaminated food each year, leading to over 420,000 deaths. The most common symptom of foodborne illness is diarrhea, although severe symptoms may also occur, such as renal failure, liver failure, central nervous system disorders, reactive arthritis, cancer, and death. Among the most dangerous sources of foodborne pathogens are *Listeria monocytogenes*, *Escherichia coli O157:H7*, *Staphylococcus aureus*, *Salmonella enterica*, *Salmonella typhimurium, Bacillus cereus*, *Vibrio* spp., *Campylobacter jejuni*, *Clostridium perfringens*, and *Shiga toxin*-producing *Escherichia coli* (STEC) [1, 2].

The pathogens are especially prevalent in insufficiently cooked foods, such as vegetables and fruits, raw milk, dairy products, and processed and raw meat. These pathogens pose a serious problem in foods that do not undergo sufficient heat treatment prior to consumption, including seafood. Seafood can contain pathogens such as *Vibrio*, *Listeria*, *Yersinia*, *Salmonella*, *Shigella*, *Clostridium*, *Campylobacter*, and *Hepatitis A*, as the infection dose of these pathogens is very low (10–1,000 bacterial cells/mL) [3].

According to the European Food Safety Authority (EFSA) in 2021 the first and second most common cause of foodborne illnesses in the European Union has been related to *Campylobacter* and *Salmonella*, respectively. *Campylobacter* is the most common cause of foodborne illnesses annually within the European Union (EU). The data presented shows over 246,000 human cases each year; however, the actual number of annual cases is estimated to be up to nine million. The EFSA estimates that campylobacteriosis costs EU nations alone approximately 2.4 billion EUR annually through productivity losses and expenses related to public health systems [4].

Listeria contains 10 species within its family; *Listeria monocytogenes* is the cause of the disease known as listeriosis. Listeriosis infections can be severe, especially for pregnant women, newborns, people with weak immune system, and the elderly, with a mortality rate of 15.6% according to EFSA from data collected in 2018. Food contamination can occur even after production, since unlike other bacteria, *Listeria* specimens can survive and multiply in salty environments and low temperatures (2 and 4°C). The most common source of listeriosis is from contaminated smoked fish, meats, soft cheeses, and raw vegetables. Several methods are currently available to prevent and control bacterial contamination of food.

Waterborne pathogens pose another serious threat to human and animal health. These bacterial contaminants must be removed before water distribution; in cases of insufficient decontamination, water may contain various bacterial pathogens such as *Cryptosporidium*, *Giardia*, *Campylobacter*, and *E. coli* that cause gastroenteritis. Other waterborne pathogens that grow within water distribution systems or within engineered water systems include *Legionella pneumophila*, *Pseudomonas* spp., and non-tuberculosis mycobacteria. Among them, the *L. pneumophila* that is responsible for Legionnaires disease has attracted the most attention in recent years [5, 6].

Conventional methods in dairy and food laboratories can detect foodborne pathogens with high specificity. The most frequently used methods are microbiological in nature: that is, they are based on the incubation of the sample on an agar plate. However, these methods are affected by several factors, such as the presence

of other microbes or viable but not culturable cells (VBNC). In addition, these methods require specialized microbiological laboratories, and the assay takes up to 2–3 days. Qualified staff and expensive consumables are required [6, 7]. These drawbacks can be avoided through molecular biology methods such as polymerase chain reaction (PCR), high throughput sequencing, and immunoassays such as enzyme-linked immunosorbent assay (ELISA), immunochromatography, and immuno-lateral flow assays. The advantages of qPCR in comparison with microbiological culture methods are shorter detection time, higher sensitivity, and higher specificity. qPCR can also detect VBNC cells. However, detecting these cells as well as dead cells results in overestimations of pathogen concentration. Additionally, PCR requires multiple sample processing steps [8].

Biosensor technology can overcome existing difficulties in the detection of pathogens. Therefore, while efforts are being made to improve conventional technologies, these sensor technologies constitute a rapidly growing field. In the development of the bacterial sensors, it is crucial to select the proper receptors and to ensure that they are immobilized and supported such that bacteria have adequate access to the receptors' binding sites without a loss of affinity. Among the targets for whole bacteria detection may be bacterial proteins, lipopolysaccharides (LPS) embedded at their outer membrane. DNA/RNA aptamers and antibodies are the most common receptors, although other receptors such as lectins have been also reported [9]. It should be mentioned here that the detection of bacterial nucleic acids is not the focus of this chapter.

In bacterial biosensors, the most common methods for detection are electrochemical, optical, and acoustic. Electrochemical methods are based on detection potential, or current originated from redox processes at the sensing surface as well as impedance changes connected with the adsorption of bacteria at the sensing surface. Redox labels, enzyme labels, and redox mediators are often used to enhance the electrical signal. In addition, the surface for the immobilization of these receptors should also be conductive. Many nanomaterials such as graphene or metal nanoparticles are used for this purpose. Optical sensors are based mostly on surface plasmon resonance (SPR) or colorimetry, while acoustic sensors typically use quartz crystal microbalance (QCM) and surface acoustic wave (SAW) techniques. In acoustic methods, changes in resonance frequency and dissipation occur when bacteria bind with the sensing surface.

2 DNA Aptamers for Bacterial Biosensors

2.1 Selection of Aptamers: Cell-SELEX

Nucleic acid aptamers, mostly DNA, are extensively used in the development of various biosensors, including those for the determination of bacteria. DNA aptamers are known as chemical antibodies. However, in contrast to antibodies, they are selected in vitro by a combinatorial chemistry method known as SELEX (Systematic

Table 1 Comparison of the properties of the aptamers and antibodies

Aptamers	Antibodies
High affinity and specificity for the target	High affinity and specificity for the target
In vitro selection	In vivo biological methods – monoclonal antibodies. In vitro – recombinant monoclonal antibodies
Extended storage time	Limited storage time
Reversible denaturation	Irreversible denaturation
Labeling at precise location not involving the binding site	Labeling at Fc region is well established
Possibility of sensor regeneration	Sensor regeneration is possible in certain cases
Analyte recognition mostly under the conditions of selection	Analyte binding under different conditions in solution
3D structure is rather labile and may cause inactivation under immobilization	3D structure is rather robust, binding is mostly not affected by immobilization

Evolution of Ligands by Exponential Enrichment). This method allows the development of aptamers with high specificity in laboratory conditions without the need for antibodies generated from animals. At the same time, the affinity of aptamers to various targets is similar to that of monoclonal antibodies to these targets (dissociation constant, $K_d \sim 1$ pM to 1 nM). Aptamers can be selected for practically unlimited kinds of compounds, such as small molecules, toxins, proteins, bacteria, viruses, or cancer cells. Another advantage that aptamers have over antibodies is the ability to label them through various labeling methods (redox or optical) at precise location. (An excellent summary of the issue of choice of aptamers versus use of antibodies was published recently by [10].) Table 1 compiles some of the advantages of aptamers as compared to antibodies as determined by the authors.

Despite aptamers' advantages, antibodies are still used in many detection assays such as ELISA, dot-immunobinding assay (DIA), and Western blot [11]. Antibodies are also used in various biosensors [12, 13].

The principles of SELEX, invented by Tuerk and Gold [14], have been described in many excellent reviews [15]. This method is based on the creation of a random library of short single-stranded DNA (ssDNA) containing up to 80–100 bases with high nucleotide sequence variation (10^{13}–10^{15}). The addition of the target results in the formation of complexes with certain oligos. After the separation of the complexes from non-interacted DNA and elution, the amplification of the selected sequences by PCR results in a new pool of ssDNA. This pool is used for the next SELEX round. After approximately 10–15 rounds, the aptamer with the highest affinity to the target is selected. However, the detection of cells or bacteria requires the recognition of the proteins or lipopolysaccharides (LPS) incorporated into the lipid membrane. For this purpose, the Cell-SELEX assay has been developed. This method also involves a random ssDNA library, but instead of isolated proteins or LPS, whole cells or bacteria are used [16]. The scheme of Cell-SELEX is presented in Fig. 1.

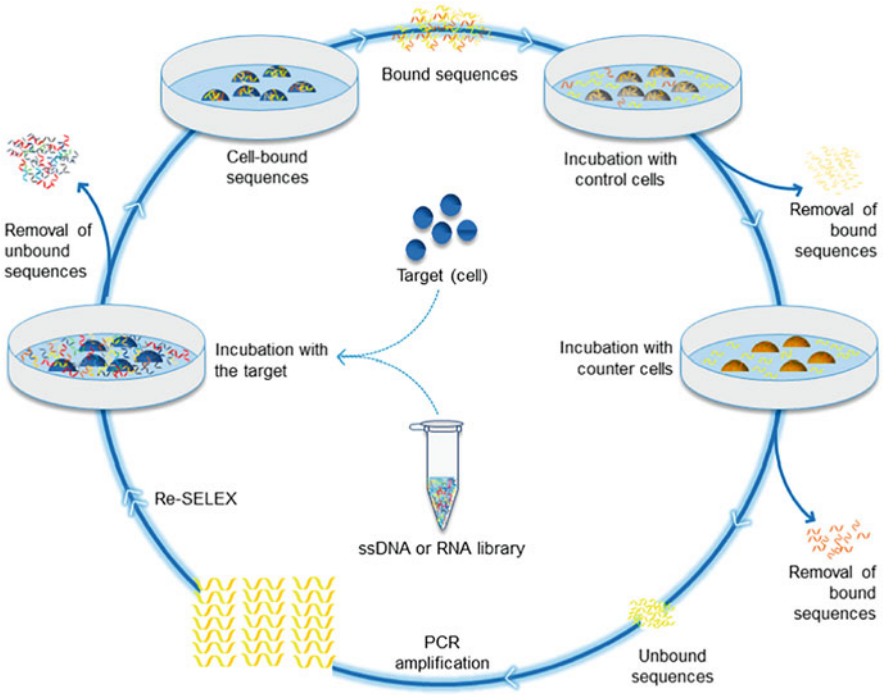

Fig. 1 The scheme of Cell-SELEX. Incubation of aptamers with control cells allowing removal of the oligonucleotides that interacts with other components of the cells, for example, lipid membranes (Reproduced from [17])

The aptamers are developed after multiple rounds. However, to increase specificity and to avoid non-specific interactions, negative Cell-SELEX is also used. This process involves the incubation of the selected aptamers with other bacteria. Thus, for the next round of selection, only the sequences that did not interact with control (non-specific) bacteria are used. Cell-SELEX is advantageous because the aptamers are specific to the bacterial proteins or LPS in their natural membrane environment. To date, several aptamers have been selected to target various bacterial proteins or LPS. Table 2 shows examples of aptamers used in aptasensors.

2.2 Methods of Aptamer Immobilization on Surfaces

Among various chemical modifications, biotin, thiol, and amino groups are often used. Control of the surface chemistry is important for orienting aptamers, providing access to the target, and avoiding non-specific binding or adsorption especially in complex samples [24]. Convenient methods of aptamer immobilization include biotin-avidin technology and chemisorption. In the first method, aptamers are

Table 2 Sequences of DNA aptamers most frequently used for the detection of selected bacteria and constant of dissociation K_d, that characterizes the stability of the aptamer-bacteria complex. Lower K_d means higher stability. (Reproduced from [13])

Bacteria	Aptamer sequence, 5′ → 3′	K_d, nM	Reference
Listeria monocytogenes	TACTATCGCGGAGACA GCGCGGGAGGCACCGGGGA	48.74 ± 3.11	Duan et al. [18]
E. coli O157H7	GGTCGTGGTGAGGTG CGTGTATGGGTGGTGGATGA GTGTGTGGC	10.30	Yu et al. [19]
Salmonella typhimurium	CTTGGGCGGTTGGTG TGATGGGCTTTTTTCGTT GGGCCGG	1,730 ± 540	Dwivedi et al. [20]
Shigella spp.	ATACCAGCTTATTCAA TTCCACACATACCAAAAACACAG CACACTTCATCAA TTTCACGAGATTGCA CTTACTATCT	15.89 ± 1.77	Song et al. [21]
Staphylococcus aureus	CACACCGCAGCAGT GGGAACGTTTCAGCCA TGCAAGCATC ACGCCCGT	3.49 ± 1.43	Moon et al. [22]
Yersinia enterocolitica	AGCAGCACAGAGG TCAGATGATATAACCTTAAT AAATAAAATATAAATTATTTAAT CTTACCTATGCGT GCTACCGTGAA	37.93 ± 7.88	Shoaib et al. [23]

modified by biotin and then bound to a monolayer of neutravidin, avidin, or streptavidin. The interaction of biotin with these proteins results in the strongest non-covalent bond in nature, with a dissociation constant of approximately 10^{-15} M [25]. This method of aptamer immobilization has been used, for example, by Duan et al. [26] for the detection of *Salmonella typhimurium*, and by Tatarko et al. [27] for detection of *Listeria innocua*. The modification of the aptamers by thiol groups is another frequently used method. In this case, the aptamers can be immobilized by chemisorption at the clean gold surface. However, often backfilling of the space between the aptamers with another short thiol is necessary.

Carbodiimide chemistry is also suitable for aptamer immobilization. This method uses 1-ethyl-3-(3-(dimethylaminopropyl)-carbodiimide (EDC) and N-hydroxysuccinimide (NHS) to activate carboxylic groups at the surfaces of carboxy-terminated thiol layers. The addition of amino-group-modified aptamers resulted in strong covalent binding and the formation of a stable sensor [13]. Gupta et al. [28] used this approach for the modification of graphene oxide-gold nanoparticles by aptamers for colorimetric *E. coli* detection. Thiol-maleimide chemistry can also be used for the preparation of the aptasensor at the gold surface. However, the aptamer layer can be unstable in real samples or in the presence of thiol-containing compounds. Figure 2 summarizes the most frequently used methods of aptamer immobilization at gold surfaces [13].

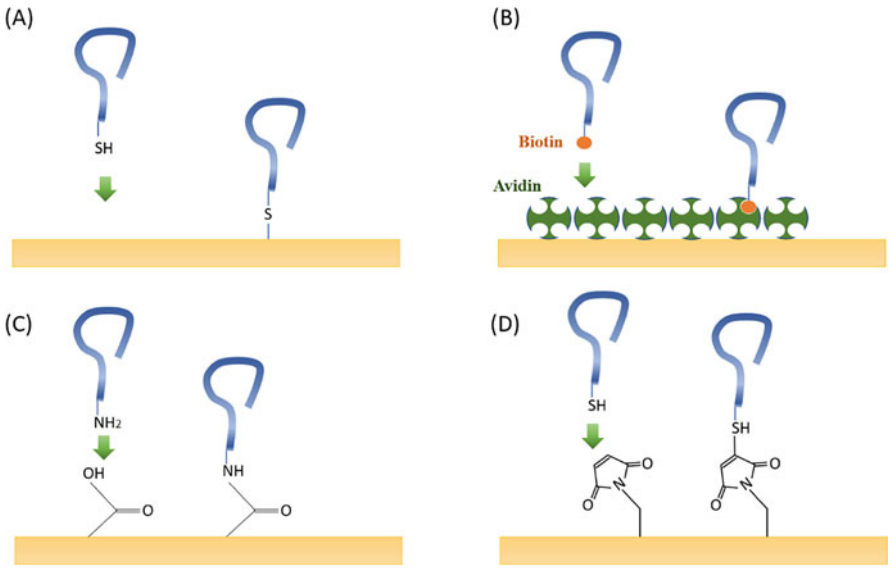

Fig. 2 Most frequently used methods of immobilization of aptamers at gold surfaces. (**a**) Chemisorption; the thiolated aptamers form a self-assembled monolayer. (**b**) Avidin-biotin coupling. (**c**) Carbodiimide (EDC/NHS) chemistry. (**d**) Thiol-maleimide immobilization. (Reproduced from [13])

Aptamers can also be immobilized at various carbon-based surfaces, such as carbon nanotubes, graphene, and graphene oxide using EDC/NHS chemistry. As there is an available carboxylic group at the surface of these materials, no additional modification is required. Some methods also use the physical adsorption of aptamers for sensor preparation. However, such systems do not provide stable detection because the binding of the aptamers with the target often results in the removal of the aptamer-target complexes from the surface.

When preparing sensing surfaces, it is important to avoid non-specific interactions with compounds that are present in the complex, such as food samples. For this purpose, special linkers and surface modification are needed [29, 30]. It is also crucial to control the surface density of aptamers to provide sufficient space for their conformational flexibility. This can be achieved by, for example, combining aptamers with other molecules during their adsorption at the surface. For instance, a biotinylated aptamer can be added to an avidin layer together with biotin at a specific optimal aptamer:biotin ratio. Increased biotin concentration results in the blockage of the avidin's binding sites, leading in turn to lower aptamer surface density.

3 Aptasensors for the Detection of Bacteria

3.1 Electrochemical Transduction Principles for the Detection of Bacteria

Of all aptasensors currently used in the detection of bacterial pathogens, electrochemical ones appear most often in recent literature. This can be explained by several factors: they provide straightforward detection of bacteria-aptamer interactions using various sensor designs. Furthermore, these methods are relatively inexpensive due to the availability of low-cost miniature potentiostats as well as electrodes of various types. Screen-printed electrodes (SPE) of various design and various material, such as gold or carbon are rather common. SPE has advantage of combination of a working (mostly gold or carbon) electrode (WE) together with reference (RE) and counter (CE) electrodes. The potentiostats offer various electrochemical techniques for detection; commonly used techniques include cyclic voltammetry (CV), differential pulse voltammetry (DPV), square wave voltammetry (SWV), and electrochemical impedance spectroscopy (EIS) [24]. However, other amperometric and potentiometric methods can be useful for the detection of bacteria-aptamer interactions.

The potentiometric method measures an electric potential generated between a reference and a working electrode at zero current. These sensors are typically based on an ion-selective electrode. For example, a light addressable potentiometric sensor (LAPS) for the detection of *E. coli* was proposed by Shaibani et al. [31] based on pH-responsive hydrogel nanofibers combined with a photoelectrochemical sensor. Here it should be mentioned that an indirect detection has been applied: It is based on the metabolic activity of the bacteria in the presence of glucose resulting in the appearance of acidic products such as lactates and acetates that affect the potential of the pH sensor. The LAPS sensor allowed the detection of *E. coli* in orange juice at 1 h with an LOD of 10^2 CFU/mL.

Among voltamperometric techniques, those based on DPV and SWV [32] are of particular interest. They are based on the application of the staircase potential in pulses. When the aptamer is modified by a redox label (e.g., methylene blue (MB) or ferrocene (Fc)) at the DNA end responsible for bacteria recognition, the maximum current is influenced by the bacteria binding to the aptamer since it modifies the distance of the redox label to the electrode surface.

The EIS method is powerful as a non-destructive technique for studying the aptamer–bacteria interaction in a label-free format by analyzing a) the interfacial resistance of the electron transfer or b) by measuring the changes in the capacitance [33]. The method can be used in faradaic mode in the presence of redox indicators such as $Fe(CN_6)^{3-/4-}$ (ferricyanide/ferrocyanide) or $Ru(NH_3)_6^{3+/2+}$ (hexaammineruthenium III/II ions) as well as in non-faradaic mode when no redox indicators are present. In this method, an alternating sinusoidal voltage with a small amplitude (5–20 mV – depending on the linearity of the system) and a different frequency (typically in the range of 0.01 Hz to 100 kHz) is applied to the working

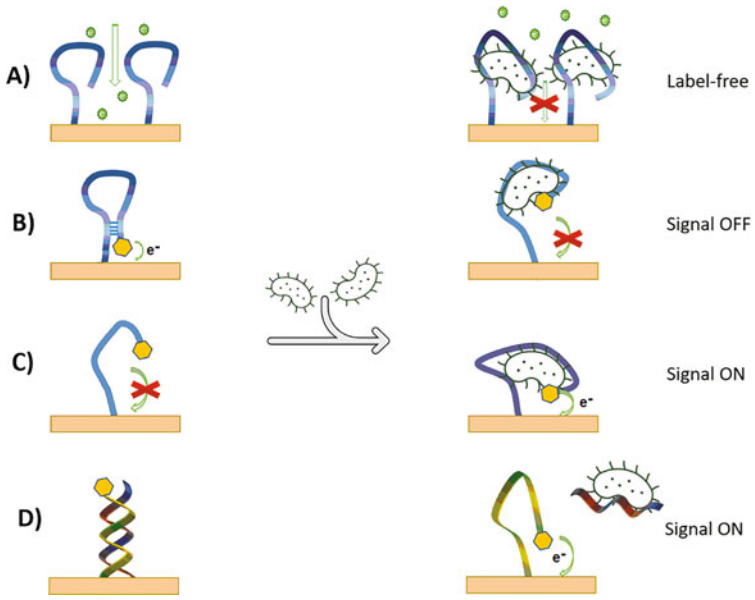

Fig. 3 Schematic illustration of aptasensor sensing in the absence of analyte (bacteria) (left side) and in presence of analyte (right side). (**a**) A label-free system, (**b**) a labeled aptamer resulting on signal OFF detection, (**c**) a labeled aptamer resulting in signal ON detection, (**d**) duplex aptamer followed by displacement of one strand. The figure is not in the scale. While the size of aptamer is several nm, the dimension of bacteria is in μm scale. (Reproduced from [35])

electrode. The impedance data can be represented in a Bode or Nyquist diagram. The latter plots the dependence of the negative imaginary component of the impedance vs. its real part. The plots can be modeled with a Randles equivalent circuit describing the electrochemical processes at the electrode. Different circuit components characterize a solution (R_s), charge transfer resistance (R_{ct}), double layer capacitance (C), and the Warburg element, Z_W, which is related to the diffusion of the species, such as ions to the sensor surface [33, 34].

Figure 3 shows various detection strategies using electrochemical methods. For label-free detection, the EIS method is useful. In this case, the binding of bacteria to the sensing surface blocks the diffusion of redox probes to the electrode surface, which results in increased charge transfer resistance (R_{ct}) (Fig. 3a). This change is reflected in the increased diameter of the semicircles in the Nyquist plot.

Label-based aptasensors use the conformational changes that their secondary structures undergo following the binding of bacteria. In most cases, the aptamers are labeled with MB or Fc (MB is preferable due to its better stability in comparison with Fc). The intensity of the electron transfer between a redox probe and the electrode depends on the distance. The signal OFF configuration detects a decreased signal upon binding (Fig. 3b). The aptamer is in a beacon configuration that is stabilized by hydrogen bonds at the terminal complementary part. The addition of the bacteria causes changes in aptamer conformation and moves the redox label

away from the electrode surface. In the signal ON configuration (Fig. 3c), the aptamer without bacteria is in a random conformation. The addition of bacteria results in conformational changes. The redox label moves closer to the electrode surface and the charge transfer increases. The duplex aptamer configuration is also effective (Fig. 3d). In the presence of bacteria, the single aptamer strand is displaced due to the conformational change. Then, a labeled aptamer is brought close to the electrode surface, which results in an increased electrochemical signal [36].

As mentioned above, aptamers are a new class of receptors that possess several advantages compared to the more expensive monoclonal antibodies. However, the number of studies that use antibodies as receptors for the detection of bacteria (immunosensors) remains greater in comparison with aptasensors. For example, according to the Scopus database, the first electrochemical immunosensor for bacteria detection (*Staphylococcus aureus*, LOD: 80 CFU/mL) was reported by Hadas et al. [37]. Up to now, according to Scopus approximately 210 papers on electrochemical bacterial immunosensors have been published; but only 100 papers were related to the electrochemical bacterial aptasensors (i.e., half as many). One possible reason for this disparity is that monoclonal antibodies are more often used in traditional bacterial assays (e.g., ELISA). Among the first bacterial electrochemical aptasensors were those reported by Zelada-Guillen et al. [38] in the detection of *Salmonella typhimurium* using potentiometry. In this work, amino-modified DNA aptamers were chemically linked to the carboxylated single-walled carbon nanotubes (SWCNTs) at the surface of a glassy carbon electrode (GCE). SWCNTs served as ion-to-electron transducers [39]. The selective binding of bacteria to the aptamers resulted in increase of the concentration of ions that naturally surround the bacteria. The SWCNTs thus transduced the ionic concentration into the potential changes that served as sensor response. The interaction of bacteria with aptamers significantly changed the electrical potential. High sensitivity of several units of CFU/mL was achieved with a rapid detection time of less than 1 min. The sensor was applied for the detection of *E. coli* in milk (6 CFU/mL) and apple juice (26 CFU/mL). These SWCNTs-based aptasensors exhibited exceptionally good selectivity related to other bacteria as well as a capacity for sensing surface regeneration (by immersion for 30 min in 2 M NaCl). A high ionic strength resulted in the dissociation of the bacteria from the surface without a loss of sensitivity.

Electrochemical immunosensors for bacteria detection were recently reviewed by Subjakova et al. [13] and Chadha et al. [40]. Aptasensors have been described in several recent reviews [13, 41–43]. The latest achievements in electrochemical bacterial aptasensor development are reviewed below and some examples are presented in Table 3.

Thus far, various electrochemical biosensors for the detection of bacteria have been reported. They can be categorized by receptor used (antibody, aptamer, lectin, etc.), method of sensing layer preparation (gold, carbon, carbon nanotubes, graphene, etc.), and receptor immobilization (physical adsorption, avidin-biotin technology, covalent attachment, etc.). To compare various approaches, we will review the aptasensors according to the type of bacteria they detect.

Table 3 An overview of some reported electrochemical aptasensors used for the detection of various bacteria (2015-the present)

Target bacteria	Material platform	Electrochemical method	Linear range/ LOD (buffer), CFU/mL	Real sample/ LOD CFU/mL	Recovery, %	Reusability, regeneration method	Reference
Escherichia coli O78: K80:H11	SCPE/MWCNTs/ TPA	EIS	$10–10^6$/10	Water, juice, milk/10	–	–	Kaur et al. [44]
Escherichia coli O157: H7	SCPE/BC-Ni	EIS	$1–10^6$/10	Water, juice, stool/10	–	–	Kaur et al. [45]
Escherichia coli O157: H7	3D-IDEA	EIS	$10–10^5$/2.9×10^2	Water	92.3 ± 1.1	80°C/30 min	Brosel-Oliu et al. [33]
Escherichia coli O157: H7	3D ZnO/AuNPs/CdS	Photocurrent	$10–10^7$/1.125	–	–	–	Dong et al. [46]
Escherichia coli O157: H7	AuNPs/rGO-PVA/ GCE	EIS	$9.2–9.2 \times 10^8$/ 9.34	Tap water, mil, meat	–	–	Qaanei et al. [47]
Escherichia coli	IDE	EIS	$2.5 \times 10–10^3$/9	–	–	–	Abdelrasoul et al. [48]
Salmonella typhimurium	GE/poly[pyrrole-co 3-carboxyl-pyrrole] copolymer	EIS	$10^2–10^8$/3	Apple juice	11	–	Sheikhzadeh et al. [49]
Salmonella typhimurium	SCPE/Diazonium	EIS	$10–10^8$/6	Apple juice	–	2 M NaCl/ 30 min	Bagheryan et al. [50]
Salmonella typhimurium	GCE/ rGO-CHI/MB	DPV	$10–10^6$/10	Chicken meat	–	–	Dinshaw et al. [51]
Salmonella typhimurium	GCE/rGO-AP	DPV	$10–10^8$/10	Chicken meat	99	–	Muniandy et al. [52]
Salmonella typhimurium	GE/AuNPs	DPV	$20–2 \times 10^8$/16	Mineral water/ 15	95–102	–	Ge et al. [53]
Salmonella typhimurium	ITO/MWCNTs	EIS	$67–6.7 \times 10^5$/67	Chicken meat	–	–	Hasan et al. [54]

Salmonella typhimurium	GCE/Au/NPG	EIS	6.5×10^2–6.5×10^8/1	Egg	84.6–109.1	2 M NaCl/1 h	Ranjbar et al. [55]
Salmonella typhimurium	GCE/rGO-CNTs	DPV	10–10^8/10	Chicken meat	–	–	Appaturi et al. [56]
Salmonella typhimurium	IDE/NiNWs	EIS	10^2–10^6/80	Chicken meat	98.6–109.0	–	Wang et al. [57, 58]
Salmonella enteritidis	ITO/MWCNTs	EIS	55–5.5×10^6/55	Chicken meat	–	–	Hasan et al. [54]
Staphylococcus aureus	SCPE/MBs/AgNPs (S)	DPASV	10–10^6/1	Tap and river water	101–102	–	Abbaspour et al. [59]
Staphylococcus aureus	Gold surface	EIS	10–10^4/10	–	–	–	Reich et al. [60]
Staphylococcus aureus	GCE/AuNPs/CNPs/CNFs	EIS	12–1.2×10^8/1	Human blood	87.5–113.3	–	Ranjbar et al. [55]
Staphylococcus aureus	Gold surface	DPV/triple helix molecular switch	3–3×10^8/8	Like water Tape water 10 × diluted honey	96.8–101 93.9–98.9 98–101.8	–	Cai et al. [61]
Staphylococcus aureus	Gold surface	DPV/DNA nanoflowers	60–6×10^7 /9	Tape water 10 × diluted honey	–	–	[62]
Staphylococcus aureus	SPGE	Chrinoampero-metry	–/39	–	–	–	Nguyen et al. [63]
Staphylococcus aureus	Chitosan/catechol/GCE	CV	10–10^8/2	Whole blood	90.5–100.1	–	Chen et al. [64]
Staphylococcus aureus	ML-Cu2O@Cu-MOF	EIS/DPV	10–10^8/1.6	Milk Honey Biscuit	91.6–105.5 93.8–100.2 97.9–103.2	0.1 M NaOH/2 min	Tian et al. [65]
Listeria monocytogenes	Au/AAO	Amperometry	10^2–1.25×10^3/100	Fish water	–	–	Zhou et al. [66]

(continued)

Table 3 (continued)

Target bacteria	Material platform	Electrochemical method	Linear range/ LOD (buffer), CFU/mL	Real sample/ LOD CFU/mL	Recovery, %	Reusability, regeneration method	Reference
Listeria innocua	Pt-IME	EIS	$10–10^6/6$	Vegetable broth	86–96	2 N NaOH or Piranha (20 times)	Sidhu et al. [67]
Shigella dysenteriae	GCE/AuNPs	EIS	$10–10^6/1$	Water and milk	93.26–132.95	–	Zarei et al. [68]
Vibrio parahaemolyticus	SCPE/ Fe_3O_4@NMOF/ AuNPs@Fc-PBA (S)	SWV	$10–10^9/3$	Shrimp	94–107	60 times	Wang et al. ([57], [58])
Virulence factor YadA of *Yersinia enterocolitica*	SPGE	SWV	$7 \times 10^4–7 \times 10^7/7 \times 10^4$	–	–	–	Sande et al. [69]

3D-IDEA three-dimensional interdigitated electrode array, *AAO* anodic aluminum oxide, *AP* azophloxine, *AgNPs* silver nanoparticles, *AuNPs* gold nanoparticles, *BC-Ni* boron-carbon nanorods decorated by nickel nanoparticles, *CHI* chitosan, *CNFs* cellulose nanofibers, *CNPs* carbon nanoparticles, *CNTs* carbon nanotubes, *CV* cyclic voltammetry, *DPASV* differential pulse anodic stripping voltammetry, *DPV* differential pulse voltammetry, *EIS* electrochemical impedance spectroscopy, *Fc* ferrocene, *GCE* glassy carbon electrode, *GE* gold electrode, *IDE* interdigitated electrode, *ITO* indium tin oxide, *MB* methylene blue, *MBs* magnetic beads, *MOF* metal-organic frameworks, *MWCNTs* multi-walled carbon nanotubes, *NiNWs* nickel nanowires, *NMOF* nanoscale metal-organic frameworks, *NPG* nanoporous gold, *PBA* phenylboronic acid, *PGE* pencil graphite electrode, *PVA* poly(vinyl alcohol), *Pt-IME* platinum interdigitated microelectrodes, *rGO* reduced graphene oxide, *SPGE* screen-printed gold electrode, *SPE* screen printed electrode, *SWV* square wave voltammetry, *TPA* terephthalaldehyde, *S* sandwich format

3.1.1 Escherichia coli

E. coli is a Gram-negative, anaerobic rod-shaped bacteria (2.0–6.0 μm in length and 1.1–1.5 μm in width). It has rounded ends and is motile with flagella. *E. coli* is typically found in the gastrointestinal tract. Most of its serogroups are non-pathogenic; however, some strains can cause acute urinary tract infection, urinary tract sepsis, neonatal meningitis, hemorrhagic colitis, and other diseases [70]. *E. coli* O157:H7 is the most pathogenic strain. Therefore, substantial effort has been focused on the development of biosensors for its detection [71]. Besides aptamers, a substantial number of electrochemical biosensors for *E. coli* O157:H7 are based on antibodies.

In a paper by Kaur et al. [44], a DNA aptamer specific for *E. coli* O78:K80:H11 has been developed using Cell-SELEX with constant of dissociation, $K_d \sim 14$ nM. The sensor was prepared by the adsorption of the aptamers onto multi-walled carbon nanotubes (MWCNTs) followed by bridging with terephthalaldehyde (TPA) on a screen-printed carbon electrode (SPCE). The aptasensor revealed an LOD as low as 10 CFU/mL and ranging from 10 to 10^6 CFU/mL, as determined by EIS within 8 min. The sensor has been verified in spiked juice and milk samples. This laboratory also selected a DNA aptamer for *E. coli* O157:H7 with $K_d = 69$ nM and applied it to the detection of bacteria using a label-free EIS method [45]. The DNA aptamers were immobilized via a poly-L-lysine linker on a surface of SPCE modified by boron-carbon nanorods and decorated by nickel nanoparticles (BC-Ni nanorods). The addition of the bacteria resulted in an increase of charge transfer resistance, R_{ct}. Using this value, an LOD of 10 CFU/mL and a linear range from 1 to 10^5 CFU/mL were determined (here and below, the linear range is expressed as a logarithmic scale of bacteria concentrations). Good selectivity has been confirmed using various bacteria. However, in the case of *Citrobacter freundi*, a higher response was observed, which has been attributed to the presence of polysaccharide O-antigen. The sensor has been analyzed in several samples, such as water, juice, and stool with satisfactory recovery (see Table 3).

The use of interdigitated electrodes (IDE) as transducer with a very small distance between the electrodes offers some advantages with respect to sensitivity for surface changes and enables the detection of bacteria in very small volumes after aptamer immobilization. This has been demonstrated by Brosel-Oliu et al. [72], who used a three-dimensional interdigitated electrode array (3D-IDEA) for the immobilization of DNA aptamers and detection of *E. coli* O157:H7 using an EIS method. The 3D-IDEA was constructed using highly conductive tantalum silicide ($TaSi_2$), onto which the dithiol-modified DNA aptamers were covalently attached using 3-mercaptopropyl-trimethoxysilane (MPTES). The addition of the bacteria resulted in an increase of R_{ct} value. The sensor enabled the detection of *E. coli* O157:H7 with an LOD of 10^2 CFU/mL and high selectivity compared to other bacteria tested (*E. coli* K12, *Salmonella typhimurium*, *Staphylococcus aureus*). Another IDE application was reported by Abdelrasoul et al. [48], who developed a portable lab-on-chip aptasensor for the detection of *E. coli*. The IDE's surface was functionalized with

carboxy aliphatic thiol compounds and modified through EDC/NHS linkers with an amino-labeled DNA aptamer specific for the outer membrane protein of *E. coli*. The IDE was made on a glass or SiO_2-coated silicon substrate. The sensor revealed an LOD of 9 CFU/mL in a linear range from 20 to 10^3 CFU/mL using non-faradaic EIS. The sensor includes a disposable IDE chip connected to the reader, enabling signal analysis via smartphone.

A high sensitivity of *E. coli* O157:H7 detection has been obtained by immobilization of DNA aptamers at nanocomposite surfaces. For example, Qaanei et al. [47] immobilized amino-modified aptamers at the surface of a GCE electrode covered by a reduced graphene oxide-poly (vinyl alcohol) and gold nanoparticles (AuNPs/rGO-PVA/GCE). This increased the surface area and hence the density of the aptamers. Using EIS, they obtained a LOD of 9.34 CFU/mL and a linear range of logarithmic concentrations from 9.2 to 9.2×10^8 CFU/mL. The sensor has been validated in tap water, milk, and meat. An interesting approach to the detection of *E. coli* O157:H7 using specific DNA aptamers has been proposed by Dong et al. [46]. In their study, thiol-modified DNA aptamers were immobilized at the surface of 3D ZnO nanowires decorated by AuNPs and CdS quantum dots. This design enabled the high-sensitivity detection of bacteria by means of a photoelectrochemical method with an LOD of 1.125 CFU/mL and in a wide linear range of 10–10^7 CFU/mL.

As is evident in Table 3, aptasensors based on 3D ZnO/AuNPs/CdS and photoelectrochemical detection demonstrated the highest sensitivity to *E. coli* O157:H7, with an LOD of 1.125 CFU/mL [46]. However, the detection of *E. coli* O157:H7 in real samples has not been reported in this work. The EIS method for detecting this bacterium with aptasensors of various design provide excellent sensitivity and has been verified in real samples.

3.1.2 Salmonella

Salmonella is a Gram-negative, rod-shaped anaerobe bacterium belonging to the Enterobacteriaceae family. Pathogenic *Salmonella enterica* causes four major syndromes: enteric fever (typhoid), enterocolitis/diarrhea, bacteremia, and chronic asymptomatic carriage [73]. The primary sources of *Salmonella* infections are raw and uncooked foods (e.g., vegetables, fruits, poultry, meat, eggs, etc.). In humans, the *Typhi* and *Paratyphi* serovars cause enteric fever, while the *Typhimurium* serovar is associated with self-limiting gastroenteritis [74, 75]. *Salmonella* is one of the major global causes of diarrheal diseases; due to its high prevalence, an extremely low limit of detection (1 CFU/mL) is desirable [76] to control food safety.

Several electrochemical aptasensors for *Salmonella* detection have been reported so far. Appaturi et al. [56] used a reduced graphene oxide-carbon nanotubes (rGO-CNTs) nanocomposite for the immobilization of DNA aptamers selective to *S. typhimurium*. For bacteria detection, the authors used DPV in the presence of 3 mM $K_3Fe(CN)_6$ that served as a redox probe. With an increased concentration of bacteria, the current density at the maximum DPV peak (0.23 V vs. Ag/AgCl reference electrode) increased. However, the mechanism of current increase is not

clear considering that the increased concentration of bacteria should cause in an increase of negative charge at the electrode surface and hence repulse the negatively charged redox probe. An LOD of 10 CFU/mL with a linear range of 10–10^8 CFU/mL of concentration on a logarithmic scale was determined. The aptasensor was verified in homogenized, centrifuged, and diluted chicken meat. The sensor is stable for 20 days.

Ge et al. [53] reported another method for detecting *S. typhimurium*: gold nanoparticles (AuNPs) were deposited on a gold electrode that allowed chemisorption of a thiol-modified DNA capture probe that hybridized with an aptamer specific to *S. typhimurium*. The addition of bacteria resulted in the release of the primer binding part and led to the anchoring of multiple circular templates on the surface of the aptasensor. RCA served for production of long DNA molecules that hybridized with biotinylated detection probe that interacted with streptavidin-modified alkaline phosphatase at the sensor surface through streptavidin-biotin binding. DPV was applied for the detection of the current generated by the enzymatic reaction in the presence of α-naphthyl phosphate (α-NP) as a substrate. The aptasensor detected bacteria with an LOD of 16 CFU/mL in a linear range 20–2 × 10^8 CFU/mL. The aptasensor revealed good reproducibility and selectivity and was validated in spiked mineral water with good recovery (95–102%). The disadvantages of the sensor are its long detection time (more than 3 h) and its stability (no more than 10 days).

A label-free biosensor was reported by Sheikhzadeh et al. [49] for the detection of *S. typhimurium.* They used amino-modified aptamers attached to a copolymer poly [pyrrole-co-3-carboxyl-pyrrole] film via EDC/NHS chemistry. The presence of bacteria resulted in an increased R_{ct} value, as recorded by EIS. High sensitivity (LOD = 3 CFU/mL) in a linear range 10^2–10^8 CFU/mL has been achieved. The aptasensor was verified in spiked filtered and diluted apple juice. A label-free aptasensor for the detection of *S. typhimurium* was reported also by Dinshaw et al. [51]. They used an SPCE modified with a diazonium salt layer grafted either electrochemically or Zn-mediated. Amino-modified aptamers were immobilized on the electrode's surface using EDC/NHS chemistry. The electrochemically grafted surface resulted in higher density of aptamers and an LOD of 6 CFU/mL with a linear range from 10 to 10^8 CFU/mL, as determined by EIS. The aptasensor was tested in spiked undiluted apple juice. However, a certain matrix effect has been observed (see Table 3). Ranjbar et al. [55] developed a highly sensitive label-free aptasensor for the detection of *S. typhimurium* based on nanoporous gold (NPG), onto which the thiolated aptamers were chemisorbed. The size of the pores affected the surface to volume ratio, which allowed for the regulation of target molecules' binding density. After 40 min of incubation with various bacteria concentrations a typical LOD of 1 CFU/mL in a dynamic range of 6.5 × 10^2–10^8 CFU/mL was obtained. The senor has been verified in spiked egg samples with 84.61–109.07% recovery. The samples were pretreated in methanol and the proteins were removed by centrifugation. The resulting diluted supernatant was used for bacteria detection.

An electrochemical sensor based on IDE modified with a biotinylated aptamer via streptavidin for the detection of *S. typhimurium* was reported by Wang et al. [57, 58]. They used nickel nanowires (NiNWs) to amplify the impedance signal

(a phenomenon caused by the formation of bridges across microelectrodes) and to separate the target bacterial complex with a magnetic field. This sensor's LOD was 80 CFU/mL in a linear range 10^2–10^6 CFU/mL. The selectivity of the aptasensor was verified in the presence of several bacteria, such *as E. coli*, *S. aureus*, *Bacillus*, and *vibrio*; its accuracy was 93% compared to the culture planting method in real chicken samples.

As mentioned above, due to the serious effects of *Salmonella* on human health, the sensitivity of detection should be extremely high: ideally 1 CFU/mL. A degree of sensitivity close to this value (LOD 3 CFU/mL) was achieved using an EIS aptasensor with aptamers immobilized on a surface of poly[pyrrole-co-3-carboxyl-pyrrole] copolymer [49]. The sensor has been validated in apple juice. Various approaches for *Salmonella* detection have also been reviewed recently by Awang et al. [77].

3.1.3 Staphylococcus Aureus

S. aureus is a round-shaped, Gram-positive bacteria. It is both a commensal bacterium that naturally colonizes the skin, nasal cavity and pharynx and a common human pathogen responsible for many infections (e.g., bacteremia, infective endocarditis, osteoarticular infections, skin and soft tissue infections) [78, 79]. The development of biosensors is important to the prevention of infections caused by multi-drug-resistant *S. aureus* [80].

Abbaspour et al. [59] proposed a sandwich configuration for sensing *S. aureus* using streptavidin-modified magnetic beads (MNBs) and silver nanoparticles (AgNPs) functionalized with biotinylated and thiolated DNA aptamers. In this approach, the aptamer was attached to MNBs via streptavidin-biotin interaction, after which the bacteria sample was added to the solution, and the aptamer-conjugated AgNPs were added to complete the sandwich complex. The separation of MNB conjugates using an external magnet followed by the dissolution of the AgNPs enabled the measurement of a current of Ag ions on an SPCE using differential pulse anodic stripping voltammetry. The concentration of Ag^+ was proportional to the concentration of *S. aureus.* The LOD achieved by this aptasensor was as low as 1 CFU/mL in a linear range from 10 to 10^6 CFU/mL. The aptasensor showed good selectivity with interfering bacteria and has been verified in tap and river water samples compared to a standard method.

Reich et al. [60] developed a highly sensitive EIS-based aptasensor for the detection of *S. aureus*. The DNA aptamers that specifically bind to protein A at the bacteria's surface were immobilized by chemisorption at the gold surface. The binding of bacteria resulted in an increase of charge transfer resistance, R_{ct}, which was used for quantitative determination. The sensor detected bacteria with an LOD of 10 CFU/mL.

An impedimetric aptasensor for *S. aureus*. has been reported by Ranjbar et al. [55]. This sensor is based on a nanocomposite of gold nanoparticles, carbon nanoparticles, and cellulose nanofibers (AuNPs/CNPs/CNFs) at the surface of a

glassy carbon electrode (GCE). In this study, the thiolated DNA aptamers specific for *S. aureus* were chemisorbed on AuNPs. The prepared nanocomposite layer exhibited a high surface area. Using EIS, an LOD of 1 CFU/mL in a wide linear range of 12–1.2 × 10^8 CFU/mL in 30 min response time has been reported. The sensor was selective in the presence of various other bacteria and has distinguished between live and dead bacteria. The sensor has been validated in a spiked blood serum with 87.5–113.3% recovery. Cai et al. [61] proposed an interesting triple-helix molecular switch for the detection of *S. aureus*. Using DPV as a detection technique, they achieved high sensitivity in a dynamic range (30–3 × 10^8 CFU/mL) and low LOD (8 CFU/mL). The same laboratory [62] reported an aptasensor based on a nanomachine composed of a DNA walker and DNA nanoflowers. In this approach, two groups of double-stranded DNA were immobilized on the surface of a gold electrode. The binding of *S. aureus* with the aptamer resulted in the disintegration of the long double strands, which released the DNA walker. In the presence of exonuclease III (Exo III), the DNA walker moved along the electrode surface and hydrolyzed the anchored short double strands. The involvement of circular DNA and phi29 DNA polymerase started a rolling circle amplification (RCA) reaction. DNA nanoflowers were formed at high DNA concentration in the solution, which provided binding sites for electroactive methylene blue (MB). At optimal conditions, the DPV from MB enabled the detection of bacteria with an LOD of 9 CFU/mL in a dynamic range of 60 to 6 × 10^7 CFU/mL. The sensor has been verified in water and diluted honey samples with good recovery.

Nguyen et al. [63] developed several aptamers sensitive to *S. aureus* using Cell-SELEX. Bacteria detection was performed using a signal-on sandwich assay. In this assay, the captured DNA aptamers were immobilized by chemisorption on the surface of screen-printed gold electrodes (SPGE). After the addition of the bacteria, DNA aptamers conjugated with horseradish peroxidase (HRP) were applied. The bacteria were detected by chronoamperometry in the presence of TMB and H_2O_2. The current was proportional to the bacterial concentration. The best detection limit achieved with the most specific aptamers was 39 CFU/mL. The sensor has been verified in spiked tap water.

Chen et al. [64] proposed a method for aptasensor-based *S. aureus* detection in blood samples using a redox capacitor system. The redox capacitor is composed of chitosan electrodeposited on glassy carbon electrode (GCE) and anodically grafted catechol. This chitosan-catechol film is not conductive but redox active. It can exchange the electrons with the redox mediators that are present in solution, for example, ferrocene (Fc)–ruthenium (Ru^{3+}) [81]. It has been shown that negatively charged bacteria that interacted with the aptamers immobilized at the chitosan-catechol surface via amino-aldehyde bridge, reduced the oxidation peak of Fc that served as the detection signal. Using this approach, it was possible to detect bacteria within relatively a short time (25 min), and high sensitivity (LOD = 2 CFU/mL). The sensor has been verified in spiked whole blood samples with good recovery (90.5–100.1%), which is appropriate for clinical applications.

Tian et al. [65] have most recently proposed an interesting strategy for the preparation of an aptasensor for *S. aureus* detection using a copper-based

metal–organic framework encapsulated with Cu_2O nanocrystals (ML-Cu2O@Cu-MOF). A high sensitivity of detection was demonstrated, with an LOD of 2.0 and 1.6 CFU/ mL using EIS and DPV methods, respectively, in a concentration range from 10 to 1×10^8 CFU/mL. The sensor has been regenerated up to 8 times (immersion into 0.1 M NaOH for 2 min). The sensor capacity for bacteria detection was verified in several food samples (milk, honey, biscuit) with good recovery (see Table 3).

As shown in Table 3, and for comparison of so far reported immunosensors (see [13]) the best LOD = 1 CFU/mL has been achieved only by aptamer-based biosensors.

3.1.4 Listeria Monocytogenes

L. monocytogenes is a rod-shaped, anaerobic, Gram-positive bacteria. This bacterium can grow at low temperatures, but its optimal temperature is 37°C. It is resistant to low pH and high salt concentrations. *Listeria* is a foodborne pathogen that causes a disease called listeriosis. The most common human pathogenic species are *L. monocytogenes* and *L. ivanovii* [82]. *L. monocytogenes* can contaminate milk and dairy products, vegetables, meat, poultry, and seafood [83]. Several biosensors have been developed for the detection of *L. monocytogenes*; some are based on the detection of the *hly*A gene using DNA hybridization [84, 85]. For whole bacteria detection, Zhou et al. [66] developed a label-free electrochemical aptasensor based on a porous anodic aluminum oxide (AAO) with sputtered Au film on one side membrane. Aldehyde-modified DNA aptamers specific to *Listeria monocytogenes* were adsorbed on an AAO surface treated with a silane linker. A cathodic current originating from a redox probe $Fe(CN)_6^{3-}$ was used as the detection signal. The interaction of the bacteria with the aptamers reduced the current due to steric blockage and charge repulsion. The effect of pore sizes in the AAO membrane was also examined. The pore size of 20 nm was determined to be optimal for bacteria detection. An LOD of 100 CFU/mL was reached in 10 min but in a narrow linear range (100–1,250 CFU/mL). The selectivity of the sensor was analyzed at 10^8 CFU/mL of control bacteria (*S. aureus* or *E. coli*). The aptasensor was verified in water samples from a fish market and confirmed by a standard plate count method.

An aptasensor based on platinum interdigitated microelectrodes (Pt-IME) on SiO_2 wafers was also used in the real-time detection of *Listeria* in hydroponic media [67]. In this work, thiolated DNA aptamers specific for *Listeria*'s surface proteins were immobilized via chemisorption at the electrode surface. Using the EIS method, an LOD of 6 CFU/mL in a linear range from 10 to 10^6 CFU/mL was reported. The sensor was connected to a smartphone through a potentiostat; it indicated an LOD of 23 CFU/mL (linear range from 10^2 to 10^6 CFU/mL) in a steady condition and 48 CFU/mL (linear range 10^2–10^4 CFU/mL) in a flow system. Sensor recovery in hydroponic media was 90%. The Pt-IME chip can be reused 20 times after treatment with Piranha solution and subsequent aptamer functionalization. The

aptasensor can be reused after washing with 2 N NaOH at 25°C with subsequent rinsing in PBS for 10 min.

The aptasensors described above exhibit higher sensitivity to *Listeria* in comparison with immunosensors (see [13]). In addition, the possibility of sensor regeneration and application in real samples has been convincingly demonstrated.

3.1.5 Other Bacteria

Several other bacteria have been also detected by aptasensors. For example, Zarei et al. [68] developed a highly sensitive aptasensor for the detection of *Shigella dysenteriae* (*S. dysenteriae*), which is responsible for gastrointestinal problems with an infective dose of less than 10 bacteria. Thiolated DNA aptamers were chemisorbed on AuNPs electrodeposited on a glassy carbon electrode (GCE) and mercaptohexanol (MCH) for blocking non-specific interaction. It has been shown that the charge transfer resistance (R_{ct}) determined by EIS increased with bacteria concentration in a linear logarithmic range between 10 and 10^6 CFU/mL. High sensitivity with an LOD of 1 CFU/mL has been demonstrated. The interaction of dead *S. dysenteriae* bacteria caused substantially lower changes of the R_{ct} values. However, the reason of this effect has not been explained. The sensor has been validated in spiked water, unpasteurized milk, and pasteurized milk with 93.26 to 132.95% recovery.

Wang et al. [57, 58] proposed a sandwich configuration for an electrochemical aptasensor for the detection of the foodborne pathogen *vibrio parahaemolyticus.* In this study, a metal-organic framework (Fe_3O_4@NMOF-Apt) labeled with an amino-modified aptamer served as a capture probe; nanoconjugates of gold nanoparticles, phenylboronic acid and ferrocene (Au@Fc-PBA) were used as an electroactive label. NMOFs are porous crystalline nanostructures with high surface area, which allows for greater aptamer surface density. The sandwich complex and labels were magnetically adsorbed to the SPCE. The current that originated from the ferrocene was measured using square wave voltammetry (SWV). The aptasensor exhibited high sensitivity and low LOD (3 CFU/mL). The current vs. logarithm of the bacteria's concentration was linear in a wide range from 10 to 10^9 CFU/mL. The sensor was rather stable. After 90 days storage the signal did not decrease less than by 9%. The proposed regeneration method allowed the sensor to be reused up to 60 times. The sensor has been verified in spiked supernatant from shrimp samples with 94–107% recovery.

Most recently, Sande et al. [69] reported a new Cell-SELEX-based aptamer that selectively bound to the virulence factor Yersinia adhesin A (YadA) of *Yersinia enterocolitica.* The most sensitive aptamer revealed binding to YadA which was characterized by K_d value of 11 nM. The selected aptamer has been used for the development of electrochemical aptasensors. Thiol-modified aptamers were chemisorbed on the surface of a gold screen-printed electrode. SWV was used to detect YadA at the surface of *E. coli* YadA in the presence of 5 mM $[Fe(CN)_6]^{3-}$ and 5 mM $[Fe(CN)_6]^{4-}$ redox probes in phosphate buffer, at a pH of 7.4. The

electrochemical aptasensor enabled the detection of bacteria with an LOD of 7.0×10^4 in a range of up to 7.0×10^7 CFU/mL.

3.2 *Optical Aptasensors for the Detection of Bacteria*

3.2.1 Overview of Applied Optical Transduction Principles

Optical transducers convert an optical signal into an electrical signal and are based on the detection of changes in the properties of emitted, reflected, or transmitted light induced by a biorecognition process [86]. The physical values that can be analyzed in optical sensors are mostly absorbance, reflectance, fluorescence, Raman vibrations, and surface plasmon resonance effects (SPR) [87, 88].

Optical biosensors can be differentiated by the presence or absence of a label. In label-based detection, biomolecules are tagged with specific molecules, which are chemically or physically attached to the analyte to detect the biomolecules' presence or activity (e.g., fluorescent molecules, nanoparticles). However, labels can potentially alter the properties intrinsic to the biological molecule [89]. In contrast, label-free detection methods rely on changes in physico-chemical properties on the transducer's surface to detect the presence or activity of the analyte without the need to bind a tag. These methods can be used to monitor molecular events in real time and under physiological conditions. They are also time- and cost-effective [90].

A special labeling method consists of the interaction between nucleic acids and nanoclusters or nanoparticles. This interaction can change the state of aggregation or dispersion of these nanosystems, causing color or fluorescence variations [91]. This phenomenon is widely used in the design of colorimetric biosensors. Alternatively, these devices may be designed without labeling, as in detection by SPR or optical resonance. The addition of optical fibers allows for the capture of high-performance and high-speed measurements for use under various conditions, such as the investigation of biomolecular events in situ or even in vivo [92].

Various types of optical aptasensors are used for bacteria detection. *Fluorescent aptasensors* can be label-free: the conformational changes that aptamers can undergo following interaction with the analyte can cause changes in their optical properties, such as the emission of fluorescence associated with nitrogenous bases. These emissions are affected by variations in the chemical environment, such as changes in the distance between specific atomic groups or the presence of solvent or analyte [93].

Alternatively, these aptasensors can be label-bound: the fluorescence is due to specific fluorophores coupled to a nucleic acid. The fluorescent properties that undergo variation are mostly intensity and decay time of the emitted fluorescence [94]. However, the emission of fluorescence has several limits, among which the most common is quenching, i.e., the damping of its intensity. This process underlies the phenomenon of the Förster resonance energy transfer (FRET), which occurs between a donor and an acceptor under some conditions, which can also

advantageously be used for detection purpose. In this case an aptamer labeled by fluorophore can undergo a conformational change following interaction with the analyte, which results in a variation in the distance between the fluorophore and quencher. Consequently, the absorption and emission of fluorescence varies with an intensity proportional to distance [45]. The decay properties of the emitted fluorescence are also used in the design of optical biosensors, as the time required for the fluorophore to pass from the excited state to the fundamental one varies due to the interaction of the labeled aptamer with the fluorophore and the analyte. An advantage of this type of analysis is its high sensitivity; however, as temporal measurements occur in the order of nanoseconds, the main drawback is that complex, expensive devices are required, such as lasers, modulators, mirrors, and optic fibers [95].

Colorimetric techniques are used for detecting an analyte in a biological sample by developing or changing the color of the solution following a recognition event. Particularly advantageous are color changes occurring during analyte detection that can be easily observed with the naked eye. However, in common colorimetric assays, the detection is often only qualitative (i.e., the presence or absence of analyte). In the case of biosensors that use these techniques, conversely, the detection is also quantitative: it is possible to determine concentrations, even in complex biological samples like serum and blood. This method is mainly used in colorimetric assays, or through the use of optical detectors that are part of the set-up of a colorimetric biosensor [96].

Colorimetric aptasensors commonly consist of aptamers conjugated with an enzymatic probe capable of metabolizing a chromogenic substrate and releasing a colored product. In this set-up, a sandwich configuration is very common. The aptamer specific for an analyte is immobilized on a surface or on nanoparticles to anchor the analyte and move it away from the rest of the sample, while another pool of this aptamer is labeled with an enzyme that produces color in the presence of a chromogenic substrate. The first aptamer is incubated with the analyte and then incubated again with the second aptamer, which produces a color whose intensity is proportional to the concentration of the analyte and can be captured and measured by a photodiode [97].

Aptasensors based on metal nanoparticles are more common. These nanoparticles are capable of changing color when the surroundings vary near their surface (e.g., when the nanoparticles pass from a monodisperse state to an aggregate state). A fundamental property of these materials is an effect called localized surface plasmon resonance (LSPR). The electromagnetic radiation interacts with a nanoparticle, the conducting electrons begin to absorb energy and oscillate, generating a plasma. This movement is confined to the volume of a nanoparticle; the plasma is localized and superficial, and it oscillates with a certain frequency. When this frequency is the same as the incident light, the plasma resonates, and consequently the associated electromagnetic field is amplified. These physical characteristics depend on the shape and size of the nanoparticle, the distance between them, and on the surrounding environment. Due to LSPR the metal nanoparticles strongly absorb visible light and have colors such as red, purple, or orange, depending on the size and the

environment. For example, the dispersed gold nanoparticles (AuNPs) adsorb the light in a blue-green region of the spectra. Therefore, the sample has a red color. If the AuNPs are modified for example by DNA aptamers specific to bacteria, addition of the bacteria resulted in their aggregation and shift of the color to the blue part of the spectra due to the dependence of absorbance on the size of nanoparticles [98, 99].

Many optical *aptasensors are based on the SPR*. This technology is increasingly associated with other spectroscopic techniques (Raman, absorbance, or fluorescence) and is used in combination with technologies based on optical fibers [100, 101]. SPR is similar to the previously described LSPR. It occurs when electromagnetic radiation hits the surface covered by thin metallic film. At a certain angle, the energy associated with the light beam moves the surface electrons with a wave that propagates parallel to the metal surface, creating a plasmon [102].

SPR aptasensors are designed by binding nucleic acids to the surface of the metal. The sensing surface is incubated with the biological sample and, when the analyte interacts with the aptamer, a variation in the refractive index near the metal surface occurs, which can be detected by measuring the variation of the incident angle of the light radiation. During an SPR experiment, the resonance unit parameter (RU) is recorded, in which 1 RU is equivalent to a critical angle shift of 10^{-6}° which corresponds to 1 pg/mm^2 of mass linked to the surface [103].

Waveguide interferometry is equipped with an optical fiber made of polymeric material or glass inside which light can propagate by total reflection. Like SPR, this technique measures changes in the refractive index on the sensor surface. However, the aptamer is bonded to the fiber surface and radiation propagates along this surface's entire length. During an interferometric reading, the phase change is converted into intensity and correlated with the concentration of the analyte – very

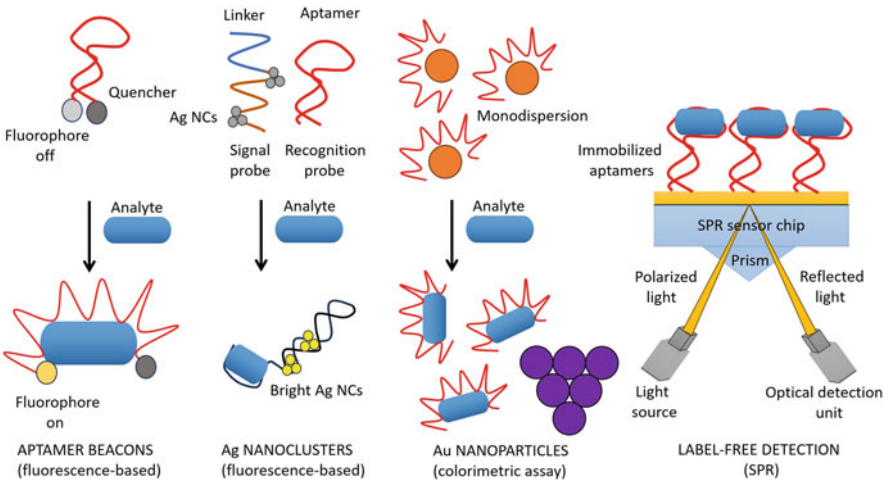

Fig. 4 Optical aptasensors based on fluorophores, nanoclusters, and nanoparticles that use on-off strategies or colorimetric properties. A label-free aptasensors use the changes of optical signal occuring on the surface of the sensing area

often by detecting an interference spectrum. With this type of sensor, the incident light generates an evanescent field that penetrates the sample to a lesser extent, and thus the disturbance due to spurious changes in the refractive index is reduced, increasing the signal-to-noise ratio [104]. The general scheme of various optical aptasensors is presented in Fig. 4.

3.2.2 Examples of Sensorial Bacteria Detection Applying Optical Transduction

In recent years, significant progress has been made in the development and construction of optical biosensors for bacteria detection. The employment of aptamers as bioreceptors has greatly increased in biosensor development. For example, nanoparticles can be conjugated with aptamers specific for bacteria. Once the aptamer-nanoparticle bioconjugate recognizes and binds to bacteria, detecting or sorting techniques such as flow cytometry can be used [105]. In a *fluorescence-based detection* the aptamers have a hairpin structure in which the 3′ end is bonded to a fluorophore, while the 5′ end is bound to a quencher capable of absorbing the electromagnetic energy after the excitation of the fluorophore at the 3′ end according to the FRET principle. In work by Bruno and Carrillo [106] this approach has been applied to the detection of *Bacillus anthracis* spores. When the aptamer binds to the target, a conformational rearrangement of the aptamer occurs, moving the quencher away from the fluorophore. In this case, FRET cannot occur, and consequently the excitation of the fluorophore causes an easily detectable emission signal. This method was found to have a detection limit of 3×10^4 spores per mL. Spore detection has useful applications in fields ranging from food safety to counter-bioterrorism; as such, further efforts to improve these systems are highly desirable.

An interesting study was performed by Liu et al. [107], who developed an optical method for the sensitive detection of *Escherichia coli* based on liquid crystals and their rearrangement in the presence of organic molecules such as hexadecyl trimethyl ammonium bromide. When this molecule is bound to an aptamer, it cannot self-assemble. The binding of the nucleic acid to the bacterium causes the release of the organic molecule, which assembles itself and causes in turn an optical transition from light to dark. This method was found to have a detection limit of 27 CFU/mL.

Another type of fluorescent aptasensor using DNA-silver nanoclusters (DNA-AgNCs) and polypyrrole nanoparticles (PPyNPs) was developed by Zhang et al. [108] for the detection of staphylococcal enterotoxin A, which is the cause of one of the major food poisonings produced by *Staphylococcus aureus* (*S. aureus*). The DNA-AgNCs nanoclusters were formed by DNA aptamers in the presence of $AgNO_3$ and served as an energy donor, while PPyNPs have been used as a quencher. Following the binding of the aptamer with the enterotoxin the DNA-AgNCs were dissociated from PPyNPs and the fluorescence was restored. This method is highly sensitive: the study quantified a detection limit of approximately 0.34 ng/mL in milk samples.

Fu et al. [109] designed a rapid and sensitive fluorescent aptasensor for *Salmonella typhimurium* (*S. typhimurium*). They incorporated magnetic spheres, aptamers, and gold nanoparticles to create a fluorescence quenching sandwich system. Fluorescent silver nanoclusters linked to DNA were also used. In both systems, the binding of the aptamer to the bacterium caused the release of the nanoparticles or nanoclusters; changes in fluorescence intensity were related to the bacterial concentration. A detection limit of 98 CFU/mL was achieved.

The fluorescence technique has also been adopted for the development of aptamer-based assay to detect *S. typhimurium* in food. The method is based on biotinylated DNA aptamers and streptavidin-conjugated silica fluorescence nanoparticles (SA-FSiNPs). The sample containing bacteria has been incubated with DNA aptamers. Addition of SA-FSiNPs strongly bonds to the surface of bacteria. The fluorescence microscope allowed the imaging of the fluorescently labeled bacteria and thus qualitatively detects the bacterial contamination [110].

In a study by Duan et al. [111], a fluorescent aptasensor was designed for the detection of *S. typhimurium*. The aptamer was labeled with 5-carboxyfluorescein (FAM) and suspended in a solution with graphene oxide (GO), as GO behaves as an energy acceptor during FRET. In the presence of bacteria, the FAM-aptamer separated from the GO to bind to the pathogen surface. Without bacteria, the FAM-aptamer remained adsorbed on the GO, which quenched the fluorescence due to FRET. Fluorescence intensity therefore correlated with the bacteria's concentration. The sensor achieved a detection limit of 100 CFU/mL.

Yang et al. [112] used Cell-SELEX for the development of DNA aptamer specific to *Salmonella Paratyphi A*. The most selective aptamer has been characterized by $K_d = 47 \pm 3$ nM. These aptamers were used for the detection of bacteria using single-walled carbon nanotubes (SWCNTs). A specific oligonucleotide sequence that served as DNAzyme has been used as an extended part of the aptamer. This aptamer probe has been wrapped around the SWCNTs. In the presence of bacteria the aptamers were dissociated from SWCNTs. The extended aptamer part responsible for DNAzyme has been folded into guanine quadruplex. Then they added hemin that self-assembled with the quadruplex. This hemin-quadruplex served as a peroxidase mimicking system. The DNAzyme acted as a catalyst for the generation of chemiluminescence through the oxidation of luminol in the presence of H_2O_2. The proposed assay was able to detect bacteria with an LOD of 10^3 CFU/mL.

In addition to applications involving fluorescent probes, *colorimetric assays* based on aptamers have been developed, with the advantage of quick and easy analyte detection. For example, Gupta et al. [28] developed a colorimetric assay that allowed the detection of *E. coli* by *the* naked eye. In this assay, the gold nanoparticles (AuNPs) were modified by graphene oxide (GO) to increase the aptamer loading capacity. Without bacteria, the AuNPs-GO were dispersed in a solution. Addition of *E. coli* resulted in nanoparticle aggregation due to the bridging of nanoparticles caused by bacteria-aptamer interactions. The originally red color of the sample has been changed to blue due to the localized plasmon resonance effect. The AuNPs-GO allowed the detection of bacteria with an LOD of 10^2 CFU/mL, while those without

GO revealed an LOD of 10^3 CFU/mL, confirming the enhanced density of aptamers at the AuNPs-GO surface.

In colorimetric assays, a common method for immobilizing aptamers on surfaces takes advantage of the strong affinity between avidin and biotin. For example, Yuan et al. [113] developed a colorimetric-based assay to detect *S. typhimurium*. This assay involved biotinylated DNA aptamers that were immobilized on the streptavidin adsorbed at the microliter plates. After the addition of the sample containing bacteria the thiol-modified DNA aptamers chemisorbed at AuNPs were added and allowed to interact with bacteria. After the addition of a silver enhancement solution based on $AgNO_3$ (in order to be deposited on the AuNPs), the absorbance detected by the microplate reader has been observed at 630 nm, which was proportional to the bacteria concentration.

Antibodies and aptamers have been used together in a sandwich configuration for microbial detection. For example, an enzyme-linked antibody-aptamer sandwich (ELAAS) biosensor has been used to quickly detect and quantify *S. typhimurium*. After the immobilized aptamers bind to a target bacteria molecule, the system is incubated with labeled antibodies, where the label is usually an enzyme. Subsequently, a detection method is used depending on the type of antibody label, and the pathogen is then titrated and quantitatively measured. A study by Duan et al. [114] altered this method by using aptamers, which were immobilized onto gold (AuNPs) and magnetic nanoparticles (MNPs). AuNPs served as a probe for colorimetric measurements, while MNPs were used for bacteria preconcentration. During incubation with *S. typhimurium*, the binding of aptamers to the target created a MNPs-aptamer-pathogen-aptamer-AuNPs sandwich. The use of MNPs allowed the sandwiches to be magnetically removed from the solution. When the bacteria were present in the solution, a color change was observed due to aggregation of AuNPs and the LSPR effect. This method achieved a detection limit of 10 CFU/mL.

One category of label-free optical aptasensors uses *SPR or LSPR technologies*. SPR is also useful in the aptamer selection process (SELEX) as it is able to determine the binding constant between nucleic acid and the target. Khateb et al. [115] used the LSPR method based on metal nanostructures with aptamers to detect *S. aureus* in milk samples with a detection limit of 10^3 CFU/mL.

SPR technology can be suitably modified to allow for ultra-sensitive and rapid quantification of analytes, facilitating point-of-care testing and diagnosis. In the field of bacterial contamination monitoring, Shin et al. [116] have developed an SPR sensor for the detection of *Vibrio fischeri* with a detection limit of around 40 CFU/mL. This technology was also used by Dursun et al. [117] to develop an SPR aptasensor for the detection of *Brucella melitensis* (*B. melitensis*) in milk. The aptamers were selected using the standard SELEX procedure and their affinity constants were characterized. Finally, two aptamers were chosen and then immobilized on magnetic nanoparticles and on the SPR sensors. The nanoparticles extracted the bacteria from the milk samples, while the SPR aptasensor was used for detection. A detection limit of 27 CFU/mL was demonstrated with this method.

Another optical technique that can detect low concentrations of bacterial contamination is *interferometry*. This method was used to design a sensor specific for

Lactobacillus, a bacterium that is not commonly pathogenic but can cause opportunistic infections such as endocarditis. This sensor involves a capture probe that is functionalized on porous silicon. The concentration of bacteria is determined by analyzing the change in the reflexivity spectrum [118]. A further evolution of this technology came with the introduction of optical fibers. The fibers act as guides for light waves, which propagate within them by total internal reflection with extremely low losses They are suitable for incorporation into smaller and less expensive platforms in point-of-care systems, and are capable of carrying out more sensitive and faster analyses [119].

Table 4 summarizes the optical aptasensors published for the detection of various bacteria since 2016 to the present day. Earlier studies have been reviewed in several papers (e.g., [131]). In some cases, optical aptasensors have demonstrated high bacteria sensitivity (less than 3 CFU/mL, see Table 4). Optical methods of bacteria detection are thus able to achieve a level of sensitivity close to that of electrochemical approaches (see Table 3). However, optical sensors were verified in real food samples only in a very limited number of cases.

3.3 Acoustic Aptasensors for the Detection of Bacteria

Acoustic wave sensors are a type of mechanical transducer that detects changes in force or mass. These sensors are obtained using biologically functionalized piezoelectric materials that convert an electrical signal into an acoustic signal. When the piezoelectric crystal is excited by an alternating electric field, it behaves as a harmonic oscillator at a particular frequency, called the resonant frequency. The value of the resonant frequency depends on the physical characteristics of the oscillator, such as dimensions, geometry, and the piezoelectric material used; it also depends on the contact medium and the material adsorbed on the surface. Therefore, when the crystal is electrically brought into resonance, it is possible to record some acoustic parameters such as the oscillation frequency and its damping due to the interaction with the analyte on the sensor surface [132]. Within this category, one can distinguish devices that employ bulk acoustic waves (BAW), such as quartz crystal microbalances (QCM), or devices based on surface acoustic waves (SAW). Alternative to QCM is electromagnetic piezoelectric acoustic sensor (EMPAS) that works at ultra-high frequencies (up to 1.06 GHz), while QCM uses the frequency range typically 5–20 MHz.

Acoustic aptasensors based on QCM, EMPAS, and SAW have been developed for detecting bacterial pathogens – mostly based on the mass sensitivity of the devices. QCM aptasensor studies for monitoring and/or detecting bacteria have been particularly successful. Functionalizing QCM discs requires modifying the gold electrodes using Au-S chemistry. For example, thiol molecules can provide both linking and antifouling properties, such as in our recent work, where the dithiol molecule 3-dithiothreitol propanoic acid was shown to bind to aptamers while also facilitating an antifouling layer against human serum [30].

Table 4 An overview of some reported optical aptasensors used for the detection of various bacteria (2016-the present)

Target bacteria	Material platform	Optical method	Linear range/LOD (buffer), CFU/mL	Real sample/ LOD CFU/mL	Recovery, %	Reusability, regeneration method	Reference
Escherichia coli O157:H7	Glass-silane-glutaraldehyde/ CdTe-QDs-streptavidin	Fluorescence	$100–10^7/10^2$	Meat, milk, green sprouts	76.75–91.25	–	Renuka et al. [120]
Escherichia coli	Gold-polyA-aptamer	SPR	$10^5–10^8/10^5$	–	–	–	Wang et al. [121]
Escherichia coli ATCC 8739	AuNPs/UCNPs	FRET	$5–10^6/3$	Water, milk/–	–	–	Jin et al. [122]
Salmonella typhimurium	AuNPs- and MNPs-aptamer	Colorimetry	$25–10^5/10$	Milk/–	–	–	Duan et al. [114]
Salmonella typhimurium	AuNPs	LSPR	$10^4–10^6/10^4$	Pork meat/10^4	–	–	Oh et al. [123]
Salmonella enterica	Au-AgNPs - 4-MBA	SERS	$4.17 \times 10^2–1.39 \times 10^7$	Wenxin granule/ 52	–	–	Jin et al. [124]
Staphylococcus aureus ATCC6538	AgNPs-4-mercaptobenzonitrile-MPNs	SERS	$10^2–10^8/2.6$	Milk/–	94.8–112	–	Huang et al. [125]
Staphylococcus aureus	ELISA plate-streptavidin-biotinylated probe-aptamer	Colorimetry	$10^2–10^7/81$	Milk/–	–	–	Yu et al. [126]
Staphylococcus aureus	Gold-polyA-aptamer	SPR	$10^5–10^8/10^6$	–	–	–	Wang et al. [121]
Campylobacter jejuni/coli	AuNPs	Colorimetry	$10^5–10^8$	Chicken/ 7.2×10^5	–	–	Kim et al. [127]

(continued)

Table 4 (continued)

Target bacteria	Material platform	Optical method	Linear range/LOD (buffer), CFU/mL	Real sample/ LOD CFU/mL	Recovery, %	Reusability, regeneration method	Reference
Campylobacter jejuni	Au-PdNPs	Colorimetry	$10–10^6/10$	Milk/100	98–113	–	Dehghani et al. [128]
Brucella melitensis	Gold-avidin-biotinylated aptamer	SPR	$10^2–10^6$	Milk/27	85.4	8 times, 10 mM NaOH	Dursun et al. [117]
Vibrio fischeri	AuNPs/nitrocellulose	Colorimetric	$40–4 \times 10^5/10^3–10^4$	–	–	–	Shin et al. [116]
Pseudomonas aeruginosa PAO1	Gold-biotinylated PEG-SH-neutravidin-biotinylated aptamer	LSPR	$10–10^3/10$	–	–	–	Hu et al. [129]
Pseudomonas aeruginosa	GOQDs	FRET	$1.28 \times 10^3–2 \times 10^7/100$	Water, orange juice and popsicle	93.9–108	–	Gao et al. [130]

AgNPs silver nanoparticles, *MPNs* metal-phenolic networks, *SERS* surface-enhanced Raman spectroscopy, *ELISA* enzyme-linked immunosorbent assay, *AuNPs* gold nanoparticles, *Poly A* polyadenine, *SPR* surface plasmon resonance, *LSPR* localized surface plasmon resonance, *PEG* polyethylene glycol, *PDA-PEI* polydopamine-polyethyleneimine, *QD* quantum dot, *4-MBA* 4-mercaptobenzoic acid, *FRET* Förster resonance energy transfer, *UCNP* upconversion nanoparticle, *GOQD* graphene oxide quantum dots

Bayramoglu et al. [133] designed a QCM aptasensor for detecting *B. melitensis* in milk. The system used aptamer-functionalized magnetic nanoparticles to isolate the bacteria from milk with the use of a magnet. Afterward, the new concentrated solution with captured bacteria was processed to separate the bacteria from the magnetic nanoparticles. The bacteria were then quantitatively measured via QCM involving discs functionalized with the same aptamer. This method achieved a low detection limit of 100 CFU/mL. Yu et al. [19] selected DNA aptamers specific for *E. coli* O157:H7 using Cell-SELEX method. Using these aptamers they developed a QCM sensor that allowed to monitor bacteria with a detection limit of about 10^3 CFU/mL.

In addition to analyte detection, QCM can also be used to more precisely select new aptamers. Wang et al. [7] reported an efficient method of selecting DNA aptamers for *S. typhimurium* using a combined QCM-Cell SELEX method. In this method after each round of the SELEX the pool of aptamers were added to the surface of QCM crystal with immobilized bacteria. The binding of aptamers has been characterized by the decay of the resonant frequency. The bounded aptamers were eluted from the QCM surface and used for the next round of selection. After 8 rounds of selection and 2 rounds of counter-selection, an aptamer with high binding affinity ($K_d = 59.5$ nM) was identified. This aptamer was used to design a QCM sensor for the detection of bacteria with an LOD of 10^3 CFU/mL.

Aptasensors capable of detecting pathogenic bacteria can thus be designed not only to achieve very low detection limits, but also to study the specificity of these nucleic bioreceptors. Oravczová et al. [134] developed an acoustic aptasensor for the detection of *Listeria innocua*. They also studied the specificity of the aptamer for this bacterium and determined that the frequency shift was specific to the bacteria, as negligible variation occurred for another pathogen, *E. coli*. The aptasensor had a detection limit of 1.6×10^3 CFU/mL.

An evolution of the aptasensors based on piezoelectric transduction was the advent of SAW, which further improved the sensitivity of mass detection (Fig. 5). For example, Xu and Yuan [135] compared QCM and SAW sensors for the quantitative detection of *S. aureus*. QCM had a detection limit of 2×10^5 to 2×10^6 CFU/mL, while the SAW sensor achieved a much lower limit of 2×10^3 CFU/mL.

Acoustic detection techniques can also be combined with other methods that allow the analyte to be enriched in a solution before its detection. Zhang et al. [136] used dielectrophoresis to enrich *E. coli* close to the microelectrodes that made up a SAW module. Using this method, they achieved a detection limit of 100 CFU/mL with a sensor response time of approximately 30 s. They also tested specificity using *S. aureus* and showed that this gram-positive bacterium did not cause a significant change in the SAW response.

To our knowledge, there is currently only one study that has used an EMPAS aptasensor for bacteria detection. Our research group studied *E. coli* detection in milk, where quartz crystals were functionalized with an antifouling aptamer layer. The EMPAS system achieved a highly sensitive detection limit of 8 CFU/mL in cow's milk, which is significantly lower than the safe limit of *E. coli* in milk. The

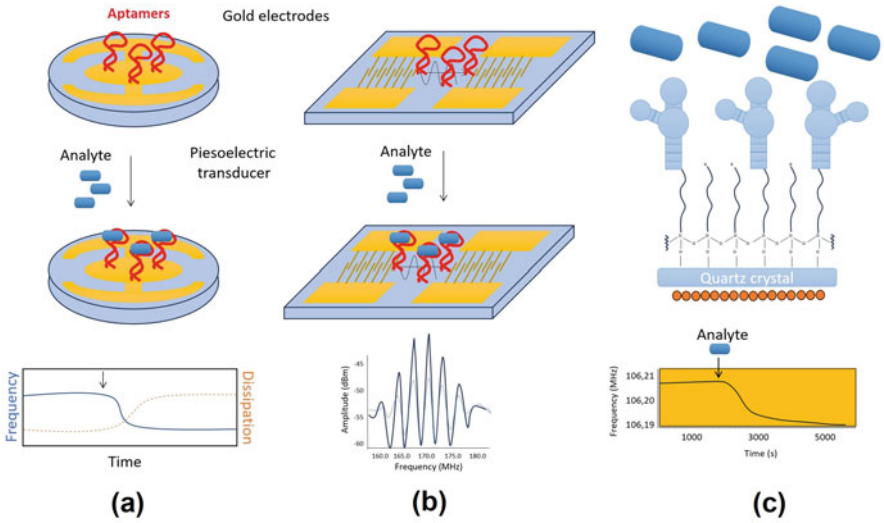

Fig. 5 Acoustic aptasensors based on gold electrodes and piezoelectric transducers: (**a**) quartz crystal microbalance (QCM) detection of bacteria by frequency and dissipation variation of the disc. Addition of bacteria (arrow) results in their binding to the aptamers, which is typically accompanied by a decrease in resonant frequency and increase in dissipation; (**b**) surface acoustic wave biosensor (SAW) detection of bacteria by means of aptamers bound in the area between two pairs of interdigitated electrodes, recording variations of the acoustic intensity (decibels) vs. frequency; (**c**) cross-section of the electromagnetic piezoelectric acoustic sensor (EMPAS) showing the copper coil that generates a secondary electric field in the piezoelectric quartz crystal. The crystal is functionalized via silanol groups, linking the aptamers that bind target bacteria, which the sensor detects by a frequency shift. Arrow shows the addition of *E. coli* in a concentration of 10^7 CFU/mL

sensor's selectivity was also tested by exposing it to *S. aureus* and *P. aeruginosa*, which had negligible frequency shifts compared to measurements with *E. coli* [137]. Table 5 summarizes the findings of studies in acoustic bacterial aptasensor development published since 2015. Works published prior to 2015 are discussed in a paper by Ozalp et al. [139]. As noted in Table 5, the highest degree of bacterial sensitivity was achieved by our EMPAS system for *E. coli* detection.

4 Conclusion

In this chapter, we demonstrated several approaches for bacteria detection using aptamer-based biosensors and various techniques such as electrochemical, optical, and acoustic methods. As is evident from this review, the advantages of aptamers are obvious. Immune- and aptasensors are comparable in terms of sensitivity, but nucleic acid aptamers have several advantages: they are more stable, their preparation is more reproducible, and it is possible to reuse these sensors following relatively simple regeneration processes [10]. At the same time, the disadvantage of the aptasensor is the sensitivity of aptamer folding to the environment that differs

Table 5 An overview of some reported acoustic aptasensors used for the detection of various bacteria (2015-the present)

Target bacteria	Material platform	Acoustic method	Linear range/LOD (buffer), CFU/mL	Real sample/ LOD CFU/mL	Recovery, %	Reusability, regeneration method	Reference
Escherichia coli DH5α	SiO_2-MEG-NH_2-aptamer	EMPAS	$10–10^7/35$	Not diluted milk/8	127.4	–	Spagnolo et al. [137]
Escherichia coli KCTC 2571	Gold-biotinylated thiol-streptavidin-biotinylated aptamer	QCM	$10^5–10^8/10^4$	–	–	–	Khobragade et al. [138]
Escherichia coli O157:H7	Gold-MHDA-streptavidin-biotinylated aptamer	QCM	$5 \times 10^2–5 \times 10^5/1.46 \times 10^3$	–	–	–	Yu et al. [19]
Escherichia coli 87,399 (crooks strain)	Gold-thiolated aptamer	QCM	$–/10^7$	–	–	–	Urmann et al. [118]
Salmonella typhimurium	Gold-MHDA-aptamer	QCM	$7.9 \times 10^2–7.9 \times 10^6/7.9 \times 10^3$	–	–	–	Wang et al. [7]
Salmonella enterica	Gold-MHDA-aptamer	QCM	$100–4 \times 10^4$	Milk/10^2	–	6 times, 20 mM NaOH solution	Ozalp et al. [139]
Listeria innocua	Gold-streptavidin-biotinylated aptamer	QCM	$5 \times 10^3–10^6/1.6 \times 10^3$	–	–	–	Oravczová et al. [134]
Listeria innocua	Gold-neutravidin- biotinylated aptamers	QCM	$5 \times 10^3–10^6/–$	–	–	–	Tatarko et al. [27]
Brucella melitensis	Gold-MHDA-aptamer	QCM	$10^2–10^7$	Milk/100	79	8 times, NaOH solution	Bayramoglu et al. [133]

(continued)

Table 5 (continued)

Target bacteria	Material platform	Acoustic method	Linear range/LOD (buffer), CFU/mL	Real sample/ LOD CFU/mL	Recovery, %	Reusability, regeneration method	Reference
Staphylococcus aureus ATCC 25923	Aptamer/graphene modified gold electrode	IDE-SPQC	41–4.1 × 10^5	Milk/41	–	10 times, acetonitrile and acetone	Lian et al. [140]
Pseudomonas aeruginosa	SiO_2 surface with Ti intermediate layer and Au outermost layer	Au IDE-MSPQC	81–8.1 × 10^5 /9	Sheep blood/ 52	–	–	Shi et al. [141]

EMPAS electromagnetic piezoelectric acoustic sensor, *QCM* quartz crystal microbalance, *MHDA* 16-mercaptohexadecanoic acid, *IDE* interdigitated electrode, *MSPQC* multichannel series piezoelectric quartz crystal, *SPQC* series electrode piezoelectric quartz crystal

from those used in selection procedure. Moreover, the components present in real samples, for example, sugars or proteins in milk, can affect the binding properties of the aptamers. In this respect, the antibodies are most robust and usually not so sensitive to the surrounding water solution. Therefore, further effort is required for the stabilization of the 3D structure of aptamers to make them less sensitive to solvent composition.

The comparison of various detection techniques demonstrated that electrochemical methods are the most widely used. This can be explained by several factors: sensor preparation is a simple process, screen-printed electrodes are inexpensive and readily available in the market, as are advanced potentiostats. The sensitivity of electrochemical and optical methods is comparable. Acoustic bacterial sensors are generally less sensitive, but they have several advantages over other methods. They do not require the labels, and binding events are easily evaluated through the measurement of frequency changes. There is, however, still a gap in terms of application between acoustic bacterial sensors and other methods, as few studies have examined their effectiveness in real food samples. This gap is significant, as species present in food samples (such as proteins in milk) influence signals via the matrix effect. Current studies in acoustic aptasensor development are thus focused on methods of aptamer immobilization using specially synthesized antifouling linkers [30]. Moreover, rather wide range of the concentration of bacteria demonstrated in various papers is linear only in a logarithmic scale. The typical S-shaped binding curve is usually not presented. In addition, the detection of 1–10 CFU/mL is complicated by the fact that few bacteria are not reaching the sensing surface and thus, strategies have been developed to enhance the interaction probability (e.g., by magnetic beads, turbulent flow conditions, etc.). Thus, additional pre-concentration steps are required to improve the limit of detection of very low bacteria concentrations in real samples.

Acknowledgments This work was funded under the European Union's Horizon 2020 research and innovation program through the Marie Skłodowska-Curie grant agreement No. 101007299 (T.H. and M.T.), The Science Agency VEGA, project No. 1/0445/23 (T.H.), and by the Natural Sciences Engineering Research Council of Canada (M.T., NSERC 9522). We are grateful to Katharina Davoudian and Marek Tatarko for help with preparation of Figs. 4 and 5.

References

1. Scallan E, Hoekstra RM, Angulo FJ, Tauxe RV, Widdowson M-A, Roy SL, Jones JL, Griffin PM (2011) Foodborne illness acquired in the United States-major pathogens. Emerg Infect Dis 17:7–15
2. Zhao X, Lin CW, Wang J, Oh DH (2014) Advances in rapid detection methods for foodborne pathogens. J Microbiol Biotechnol 24:297–312
3. Mandal P, Biswas AK, Choi K, Pal UK (2011) Methods for rapid detection of foodborne pathogens: an overview. Am J Food Technol 6:87–102
4. European Food Safety Authority (2022) The European Union one health 2021 zoonoses report. EFSA J 20:7666

5. McClung RP, Roth DM, Vigar M et al (2017) Waterborne disease outbreaks associated with environmental and undetermined exposures to water – United States, 2013–2014. Morbid Mortal Weekly Rep 66:1222
6. Saad M, Faucher SP (2021) Aptamers and aptamer-coupled biosensors to detect water-borne pathogens. Front Microbiol 12:643797
7. Wang J, Wang R, Chen F, Jiang T, Wang H, Slavik M, Wei H, Li Y (2017) QCM-based aptamer selection and detection of *Salmonella typhimurium*. Food Chem 221:776–782
8. Gentry-Shields J, Wang A, Cory RM, Stewart JR (2013) Determination of specific types and relative levels of QPCR inhibitors in environmental water samples using excitation-emission matrix spectroscopy and PARAFAC. Water Res 47:3467–3476
9. Mi F, Guan M, Hu C et al (2021) Application of lectin-based biosensor technology in the detection of foodborne pathogenic bacteria: a review. Analyst 146:429–443
10. Arshavsky-Graham S, Heuer C, Jiang X, Segel E (2022) Aptasensors versus immunosemsors – which will prevail? Eng Life Sci 22:319–333
11. Charlermroj R, Oplatowska M, Kumpoosiri M, Himananto O, Gajanandana O, Elliott CT, Karoonuthaisiri N (2012) Comparison of techniques to screen and characterize bacteria-specific hybridomas for high-quality monoclonal antibodies selection. Anal Biochem 421: 26–36
12. Byrne B, Stack E, Gilmartin N, O'Kennedy R (2009) Antibody-based sensors: principles, problems and potential for detection of pathogens and associated toxins. Sensors (Basel) 9: 4407–4445
13. Subjakova V, Oravczova V, Tatarko M, Hianik T (2021) Advances in electrochemical aptasensors and immunosensors for detection of bacterial pathogens in food. Electrochim Acta 389:138724
14. Tuerk C, Gold L (1990) Systematic evolution of ligands by exponential enrichment: RNA ligands to bacteriophage T4 DNA polymerase. Science 249:505–510
15. Zhuo Z, Yu Y, Wang M, Li J, Zhang Z, Liu J, Wu X, Lu A, Zhang G, Zhang B (2017) Recent advances in SELEX technology and aptamer applications in biomedicine. Int J Mol Sci 18: 2142
16. Yahyaabadi MY, Dorraj GS, Heiat M, Latifi AM (2017) Utilizing cell-SELEX, as a promising strategy to isolate ssDNA aptamer probes for detection of *Staphylococcus aureus*. Appl Biotechnol Rep 4:633–638
17. Ali MH, Elsherbiny ME, Emara M (2019) Updates on aptamer research. Int J Mol Sci 20:2511
18. Duan N, Ding X, He L, Wu S, Wei Y, Wang Z (2013) Selection, identification and application of a DNA aptamer against *Listeria monocytogenes*. Food Contr 33:239–243
19. Yu X, Chen F, Wang R, Li Y (2018) Whole-bacterium SELEX of DNA aptamers for rapid detection of *E. coli* O157:H7 using a QCM sensor. J Biotechnol 266:39–49
20. Dwivedi HP, Smiley RD, Jaykus LA (2013) Selection of DNA aptamers for capture and detection of *Salmonella typhimurium* using a whole-cell SELEX approach in conjunction with cell sorting. Appl Microbiol Biotechnol 97:3677–3686
21. Song MS, Sekhon S, Shin WR, Kim H, Min J, Ahn JY, Kim YH (2017) Detecting and discriminating *Shigella sonnei* using an aptamer-based fluorescent biosensor platform. Molecules 825:22
22. Moon J, Kim G, Park S, Lim J, Mo C (2015) Comparison of whole-cell SELEX methods for the identification of *Staphylococcus aureus*-specific DNA aptamers. Sensors 15:8884–8897
23. Shoaib M, Shehzad A, Mukama O, Raza H, Niazi S, Khan IM, Ali B, Akhtar W, Wang Z (2020) Selection of potential aptamers for specific growth stage detection of *Yersinia enterocolitica*. RSC Adv 10:24743–24752
24. Hianik T, Wang J (2009) Electrochemical aptasensors – recent achievements and perspectives. Electroanalysis 21:1223–1235
25. Green NM (1963) Avidin. 1. The use of (14-C) biotin for kinetic studies and for assay. Biochem J 89:585–591

26. Duan N, Sun W, Wu S, Liu L, Hun X, Wang Z (2018) Aptamer-based F0F1-ATPase biosensor for *Salmonella typhimurium* detection. Sens Actuat B Chem 255:2582–2588
27. Tatarko M, Spagnolo S, Oravczová V, Süle J, Hun M, Hucker A, Hianik T (2021) Changes of viscoelastic properties of aptamer-based sensing layers following interaction with *Listeria innocua*. Sensors 21:5585
28. Gupta R, Kumar A, Kumar S, Pinnaka AK, Singhal NK (2021) Naked eye colorimetric detection of *Escherichia coli* using aptamer conjugated graphene oxide enclosed gold nanoparticles. Sens Actuat B Chem 329:129100
29. Spagnolo S, De La Franier B, Hianik T, Thompson M (2020) Surface probe linker with tandem anti-fouling properties for application in biosensor technology. Biosensors 10:20
30. Spagnolo S, Davoudian K, Ahmadi S, Chan E, Hianik T, Thompson M (2022) Thiol-based probe linker with antifouling properties for aptasensor development. Chemosensors 10:435
31. Shaibani PM, Etayash H, Jiang K, Sohrabi A, Hassanpourfard M, Naicker S, Sadrzadeh M, Thundat T (2018) Portable nanofiber-light addressable potentiometric sensor for rapid *Escherichia coli* detection in orange juice. ACS Sens 3:815–822
32. Wang J (2006) Analytical electrochemistry.3rd edn. Wiley, Hoboken
33. Brosel-Oliu S, Ferreira R, Uria N, Abramova N, Gargallo R, Muñoz-Pascual FX, Bratov A (2018) Novel impedimetric aptasensor for label-free detection of *Escherichia coli* O157:H7. Sens Actuat B Chem 255:2988–2995
34. Lisdat F, Schäfer D (2008) The use of electrochemical impedance spectroscopy for biosensing. Anal Bioanal Chem 391:1555–1567
35. Hianik T (2021) Advances in electrochemical and acoustic aptamer-based biosensors and immunosensors in diagnostics of leukemia. Biosensors 11:177
36. Rozenblum GT, Pollitzer IG, Radrizzani M (2019) Challenges in electrochemical aptasensors and current sensing architectures using flat gold surfaces. Chemosensors 7:57
37. Hadas E, Soussan L, Rosen-Margalit I, Farkash A, Rishpon J (1992) A rapid and sensitive heterogeneous immunoelectrochemicall assay using disposable electrodes. J Immunoassay 13: 231–252
38. Zelada-Guillen GA, Riu J, Düzgün A, Rius FX (2009) Immediate detection of living bacteria at ultralow concentrations using a carbon nanotube based potentiometric aptasensor. Angew Chem Int Ed 48:7334–7337
39. Crespo GA, Macho S, Rius FX (2008) Ion-selective electrodes using carbon nanotubes as ion-to-electron transducers. Anal Chem 80:1316–1322
40. Chadha U, Bhardwaj P, Agarwal R, Rawat P, Agarwal R, Gupta I, Panjwani M, Singh S, Ahuja C, Selvaraj SK, Banavoth M, Sonar P, Badoni B, Chakravorty A (2022) Recent progress and growth in biosensors technology: a critical review. J Industrial Eng Chem 109: 21–51
41. Pham TD, Phan LMT, Park J, Cho S (2022) Review – electrochemical aptasensor for pathogenic bacteria detection. J Electrochem Soc 169:087501
42. Yi J, Xiao W, Li G, Wu P, He Y, Chen C, He Y, Ding P, Kai T (2020) The research of aptamer biosensor technologies for detection of microorganism. Appl Microbiol Biotechnol 104:9877–9890
43. Zhang W, Cui C, Chen H, Liu H, Bin S, Wang D, Wang Y (2022) Advances in electrochemical aptamer biosensors for the detection of food-borne pathogenic bacteria. ChemistrySelect 7:e202202190
44. Kaur H, Shorie M, Sharma M, Ganguli AK, Sabherwal P (2017) Bridged rebar graphene functionalized aptasensor for pathogenic *E. coli O78:K80:H11* detection. Biosens Bioelectron 98:486–493
45. Kaur A, Kaur P, Ahuja S (2020) Förster resonance energy transfer (FRET) and applications thereof. Anal Methods 12:5532–5550
46. Dong X, Shi Z, Xu C, Yang C, Chen F, Lei M, Wang J, Cui Q (2020) CdS quantum dots/Au nanoparticles/ZnO nanowire array for self-powered photoelectrochemical detection of *Escherichia coli* O157:H7. Biosens Bioelectron 149:111843

47. Qaanei M, Taheri RA, Eskandari K (2021) Electrochemical aptasensor for: *Escherichia coli* O157:H7 bacteria detection using a nanocomposite of reduced graphene oxide, gold nanoparticles and polyvinyl alcohol. Anal Methods 13:3101–3109
48. Abdelrasoul GN, Anwar A, MacKay S, Tamura M, Shah MA, Khasa DP, Montgomery RR, Ko AI, Chen J (2020) DNA aptamer-based non-faradaic impedance biosensor for detecting *E. coli*. Anal Chim Acta 1107:135–144
49. Sheikhzadeh E, Chamsaz M, Turner APF, Jager EWH, Beni V (2016) Label-free impedimetric biosensor for *Salmonella typhimurium* detection based on poly [pyrrole-co-3-carboxyl-pyrrole] copolymer supported aptamer. Biosens Bioelectron 80:194–200
50. Bagheryan Z, Raoof JB, Golabi M, Turner APF, Beni V (2016) Diazonium-based impedimetric aptasensor for the rapid label-free detection of Salmonella typhimurium in food sample. Biosens Bioelectron 80:566–573
51. Dinshaw IJ, Muniandy S, Teh SJ, Ibrahim F, Leo BF, Thong KL (2017) Development of an aptasensor using reduced graphene oxide chitosan complex to detect *Salmonella*. J Electroanal Chem 806:88–96
52. Muniandy S, Dinshaw IJ, Teh SJ, Lai CW, Ibrahim F, Thong KL, Leo BF (2017) Graphene-based label-free electrochemical aptasensor for rapid and sensitive detection of foodborne pathogen. Anal Bioanal Chem 409:6893–6905
53. Ge C, Yuan R, Yi L, Yang J, Zhang H, Li L, Nian W, Yi G (2018) Target-induced aptamer displacement on gold nanoparticles and rolling circle amplification for ultrasensitive live *Salmonella typhimurium* electrochemical biosensing. J Electroanal Chem 826:174–180
54. Hasan MR, Pulingam T, Appaturi JN, Zifruddin AN, Teh SJ, Lim TW, Ibrahim F, Leo BF, Thong KL (2018) Carbon nanotube-based aptasensor for sensitive electrochemical detection of whole-cell *Salmonella*. Anal Biochem 554:34–43
55. Ranjbar S, Shahrokhian S, Nurmohammadi F (2018) Nanoporous gold as a suitable substrate for preparation of a new sensitive electrochemical aptasensor for detection of *Salmonella typhimurium*. Sens Actuat B Chem 255:1536–1544
56. Appaturi JN, Pulingam T, Thong KL, Muniandy S, Ahmad N, Leo BF (2020) Rapid and sensitive detection of *Salmonella* with reduced graphene oxide-carbon nanotube based electrochemical aptasensor. Anal Biochem 589:113489
57. Wang L, Huo X, Qi W, Xia Z, Li Y, Lin J (2020) Rapid and sensitive detection of *Salmonella Typhimurium* using nickel nanowire bridge for electrochemical impedance amplification. Talanta 211:120715
58. Wang W, Tan L, Wu J, Li T, Xie H, Wu D, Gan N (2020) A universal signal-on electrochemical assay for rapid on-site quantitation of vibrio parahaemolyticus using aptamer modified magnetic metal–organic framework and phenylboronic acid-ferrocene co-immobilized nanolabel. Anal Chim Acta 1133:128–136
59. Abbaspour A, Norouz-Sarvestani F, Noori A, Soltani N (2015) Aptamer-conjugated silver nanoparticles for electrochemical dual-aptamer-based sandwich detection of *Staphylococcus aureus*. Biosens Bioelectron 68:149–155
60. Reich P, Stoltenburg R, Strehlitz B, Frense D, Beckmann D (2017) Development of an impedimetric aptasensor for the detection of *Staphylococcus Aureus*. Int J Mol Sci 18:2484
61. Cai R, Zhang Z, Chen H, Tian Y, Zhou N (2021) A versatile signal-on electrochemical biosensor for *Staphylococcus aureus* based on triple-helix molecular switch. Sens Actuat B Chem 326:128842
62. Cai R, Zhang S, Chen L, Li M, Zhang Y, Zhou N (2021) Self-assembled DNA nanoflowers triggered by a DNA walker for highly sensitive electrochemical detection of *Staphylococcus aureus*. ACS Appl Mater Interfaces 13:4905–4914
63. Nguyen TT-Q, Kim ER, Gu MB (2022) A new cognate aptamer pair-based sandwich-type electrochemical biosensor for sensitive detection of *Staphylococcus aureus*. Biosens Bioelectron 198:113835

64. Chen W, Chen Z, Lai Q, Zhang Y, Long M, Liang B, Liu Z (2022) Specific and ultrasensitive detection of *Staphylococcus aureus* with a catechol-chitosan redox capacitor based electrochemical aptasensor. J Electroanal Chem 916:116357
65. Tian J-Y, Liu X, Zhang S, Chen K, Zhu L, Song Y, Wang M, Zhang Z, Du M (2023) Novel aptasensing strategy for efficiently quantitative analyzing *Staphylococcus aureus* based on defective copper-based metal–organic framework. Food Chem 402:134357
66. Zhou CX, Mo RJ, Chen ZM, Wang J, Shen GZ, Li YP, Quan QG, Liu Y, Li CY (2016) Quantitative label-free *Listeria* analysis based on aptamer modified nanoporous sensor. ACS Sens 1:965–969
67. Sidhu RK, Cavallaro ND, Pola CC, Danyluk MD, McLamore ES, Gomes CL (2020) Planar interdigitated aptasensor for flow-through detection of *Listeria spp*. in hydroponic lettuce growth media. Sensors 20:5773
68. Zarei SS, Soleimanian-Zad S, Ensafi AA (2018) An impedimetric aptasensor for *Shigella dysenteriae* using a gold nanoparticle-modified glassy carbon electrode. Microchim Acta 185: 538
69. Sande MG, Ferreira D, Rodrigues JL, Melo LDR, Linke D, Silva CJ, Moreira FTC, Sales MGF, Rodrigues LR (2022) Electrochemical aptasensor for the detection of the key virulence factor YadA of *Yersinia enterocolitica*. Biosensors 12:614
70. Percival SL, Williams DW (2014) Escherichia coli. In: Percival SL, Yates MV, Williams DW, Chalmers RM, Gray NF (eds) Microbiology of waterborne diseases. Academic Press, London, pp 89–117
71. Razmi N, Hasanzadeh M, Willander M, Nur O (2020) Recent progress on the electrochemical biosensing of *Escherichia coli* O157:H7: material and methods overview. Biosensors 10:1–18
72. Brosel-Oliu S, Abramova N, Uria N, Bratov A (2019) Impedimetric transducers based on interdigitated electrode arrays for bacterial detection – a review. Anal Chim Acta 1088:1–19
73. Coburn B, Grassl GA, Finlay BB (2007) *Salmonella*, the host and disease: a brief review. Immunol Cell Biol 85:112–118
74. Eng SK, Pusparajah P, Ab Mutalib NS, Ser HL, Chan KG, Lee LH (2015) *Salmonella*: a review on pathogenesis, epidemiology and antibiotic resistance. Front Life Sci 8:284–293
75. Johnson R, Ravenhall M, Pickard D, Dougan G, Byrne A, Frankel G (2018) Comparison of *Salmonella enterica* serovars *Typhi* and *Typhimurium* reveals typhoidal serovar-specific responses to bile. Infect Immun 86:1–16
76. Shen Y, Xu L, Li Y (2021) Biosensors for rapid detection of *Salmonella* in food: a review. Compr Rev Food Sci Food Saf 20:149–197
77. Awang MS, Bustami Y, Hamzah HH, Zambry NS, Najib MA, Khalid MF, Aziah I, Manaf AA (2021) Advancement in *Salmonella* detection methods: from conventional to electrochemical-based sensing detection. Biosensors 11:346
78. Ansari N, Yazdian-Robati R, Shahdordizadeh M, Wang Z, Ghazvini K (2017) Aptasensors for quantitative detection of *Salmonella typhimurium*. Anal Biochem 533:18–25
79. Tong SYC, Davis JS, Eichenberger E, Holland TL, Fowler VG (2015) *Staphylococcus aureus* infections: epidemiology, pathophysiology, clinical manifestations, and management. Clin Microbiol Rev 28:603–661
80. Rubab M, Shahbaz HM, Olaimat AN, Oh FH (2018) Biosensors for rapid and sensitive detection of *Staphylococcus aureus* in food. Biosens Bioelectron 105:49–57
81. Liu Z, Liu YI, Kim E, Bentley WE, Payne GF (2016) Electrochemical probing through a redox capacitor to acquire chemical information on biothiols. Anal Chem 88:7213–7221
82. Radoshevich L, Cossart P (2018) *Listeria monocytogenes*: towards a complete picture of its physiology and pathogenesis. Nat Rev Microbiol 16:32–46
83. Shamloo E, Hosseini H, Moghadam AZ, Larsen HM, Haslberger A, Alebouyeh M (2019) Importance of *Listeria monocytogenes* in food safety: a review of its prevalence, detection, and antibiotic resistance. Iran J Vet Res 20:241–254
84. Soni DK, Ahmad R, Dubey SK (2018) Biosensor for the detection of *Listeria monocytogenes*: emerging trends. Crit Rev Microbiol 44:590–608

85. Vizzini P, Braidot M, Vidic J, Manzano M (2019) Electrochemical and optical biosensors for the detection of *Campylobacter* and *Listeria*: an update look. Micromachines 10:500
86. Baldini F, Giannetti A (2005) Optical chemical and biochemical sensors: new trends. OPTO-Ireland 5826:485–499
87. Bosch ME, Sánchez AJR, Rojas FS, Ojeda CB (2007) Recent development in optical fiber biosensors. Sensors 7:797–859
88. McDonagh C, Burke CS, MacCraith BD (2008) Optical chemical sensors. Chem Rev 108: 400–422
89. Xu C, He P, Fang Y (2000) Electrochemical labeled DNA probe for the detection of sequence-specific DNA. Anal Chim Acta 411:31–36
90. Syahir A, Usui K, Tomizaki K-y, Kajikawa K, Mihara H (2015) Label and label-free detection techniques for protein microarrays. Microarrays 4:228–244
91. Xu J, Wei C (2017) The aptamer DNA-templated fluorescence silver nanoclusters: ATP detection and preliminary mechanism investigation. Biosens Bioelectron 87:422–427
92. Shevchenko Y, Francis TJ, Blair DAD, Walsh R, DeRosa MC, Albert J (2011) In situ biosensing with a surface plasmon resonance fiber grating aptasensor. Anal Chem 83:7027–7034
93. Xu Y, Cheng N, Luo Y, Huang K, Chang Q, Pang G, Xu W (2022) An Exo III-assisted catalytic hairpin assembly-based self-fluorescence aptasensor for pesticide detection. Sens Actuat B Chem 358:131441
94. Liu H, Bai Y, Qin J, Wang H, Wang Y, Chen Z, Geng F (2018) Exonuclease I assisted fluorometric aptasensor for adenosine detection using 2-AP modified DNA. Sens Actuat B Chem 256:413–419
95. Zhou Y, Zuo L, Wei Y, Dong C (2020) Development of fluorescent aptasensing system for ultrasensitive analysis of kanamycin. J Luminescence 222:117124
96. Zahra QA, Luo Z, Ali R, Khan MI, Li F, Qiu B (2021) Advances in gold nanoparticles-based colorimetric aptasensors for the detection of antibiotics: an overview of the past decade. Nanomaterials 11:840
97. Wu S, Wang Y, Duan N, Ma H, Wang Z (2015) Colorimetric aptasensor based on enzyme for the detection of *vibrio parahemolyticus*. J Agric Food Chem 63:7849–7854
98. Melikishvili S, Piovarci I, Hianik T (2021) Advances in colorimetric assay based on AuNPs modified by proteins and nucleic acid aptamers. Chemosensors 9:281
99. Soongsong J, Lerdsri J, Jakmunee J (2021) A facile colorimetric aptasensor for low-cost chlorpyrifos detection utilizing gold nanoparticle aggregation induced by polyethyleneimine. Analyst 146:4848–4857
100. Loyez M, DeRosa MC, Caucheteur C, Wattiez R (2022) Overview and emerging trends in optical fiber aptasensing. Biosens Bioelectron 196:113694
101. Song M, Khan IM, Wang Z (2021) Research progress of optical aptasensors based on AuNPs in food safety. Food Anal Methods 14:2136–2151
102. Lan L, Yao Y, Ping J, Ying Y (2017) Recent progress in nanomaterial-based optical aptamer assay for the detection of food chemical contaminants. ACS Appl Mater Interfaces 9:23287–23301
103. Nguyen HH, Park J, Kang S, Kim M (2015) Surface plasmon resonance: A versatile technique for biosensor applications. Sensors 15:10481–10510
104. Kozma P, Kehl F, Ehrentreich-Förster E, Stamm C, Bier FF (2014) Integrated planar optical waveguide interferometer biosensors: a comparative review. Biosens Bioelectron 58:287–307
105. He X, Li Y, He D, Wang K, Shangguan J, Shi H (2014) Aptamer-fluorescent silica nanoparticles bioconjugates based dual-color flow cytometry for specific detection of *Staphylococcus aureus*. J Biomed Nanotechnol 10:1359–1368
106. Bruno JG, Carrillo MP (2012) Development of aptamer beacons for rapid presumptive detection of *Bacillus spores*. J Fluoresc 22:915–924

107. Liu M, Zhang M, Chen J, Yang R, Huang Z, Liu Z, Li N, Shui L (2022) Liquid crystal-based optical aptasensor for the sensitive and selective detection of gram-negative bacteria. Sci China Chem 65:2023–2030
108. Zhang X, Khan IM, Ji H, Wang Z, Tian H, Cao W, Mi W (2020) A label-free fluorescent aptasensor for detection of *Staphylococcal* enterotoxin A based on aptamer-functionalized silver nanoclusters. Polymers 12:152
109. Fu S, Yang X, Pang L, Cheng S, Song D, Qin X, Man C, Jiang Y (2022) A novel fluorescence aptasensor based on magnetic beads/gold nanoparticles/DNA-stabilized silver nanoclusters for detection of *Salmonella typhimurium*. Food Secur 11:595
110. Wang Q-Y, Kang Y-J (2016) Bioprobes based on aptamer and silica fluorescent nanoparticles for bacteria *Salmonella typhimurium* detection. Nanoscale Res Lett 11:150
111. Duan YF, Ning Y, Song Y, Deng L (2014) Fluorescent aptasensor for the determination of *Salmonella typhimurium* based on a graphene oxide platform. Microchim Acta 181:647–653
112. Yang M, Peng Z, Ning Y, Chen Y, Zhou Q, Deng L (2013) Highly specific and cost-efficient detection of *Salmonella paratyphi* a combining aptamers with single-walled carbon nanotubes. Sensors 13:6865–6881
113. Yuan J, Tao Z, Yu Y, Ma X, Xia Y, Wang L, Wang Z (2014) A visual detection method for *Salmonella typhimurium* based on aptamer recognition and nanogold labeling. Food Control 37:188–192
114. Duan N, Xu B, Wu S, Wang Z (2016) Magnetic nanoparticles-based aptasensor using gold nanoparticles as colorimetric probes for the detection of *Salmonella typhimurium*. Anal Sci 32: 431–436
115. Khateb H, Klös G, Meyer RL, Sutherland DS (2020) Development of a label-free LSPR-apta sensor for *Staphylococcus aureus* detection. ACS Appl Bio Mat 3:3066–3077
116. Shin W-R, Sekhon SS, Rhee S-K, Ko JH, Ahn J-Y, Min J, Kim Y-H (2018) Aptamer-based paper strip sensor for detecting *Vibrio fischeri*. ACS Comb Sci 20:261–268
117. Dursun AD, Borsa BA, Bayramoglu G, Arica MY, Ozalp VC (2022) Surface plasmon resonance aptasensor for *Brucella* detection in milk. Talanta 239:123074
118. Urmann K, Arshavsky-Graham S, Walter JG, Scheper T, Segal E (2016) Whole-cell detection of live L*actobacillus acidophilus* on aptamer-decorated porous silicon biosensors. Analyst 141:5432–5440
119. Janik M, Brzozowska E, Czyszczoń P, Celebańska A, Koba M, Gamian A, Bock WJ, Smietana M (2021) Optical fiber aptasensor for label-free bacteria detection in small volumes. Sens Actuat B Chem 330:129316
120. Renuka RM, Achuth J, Chandan HR, Venkataramana M, Kadirvelu K (2018) A fluorescent dual aptasensor for the rapid and sensitive onsite detection of *E. coli* O157: H7 and its validation in various food matrices. New J Chem 42:10807–10817
121. Wang WW, Han X, Chu LQ (2019) Polyadenine-mediated immobilization of aptamers on a gold substrate for the direct detection of bacterial pathogens. Anal Sci 35:967–972
122. Jin B, Wang S, Lin M, Jin Y, Zhang S, Cui X, Gong Y, Li A, Xu F, Lu TJ (2017) Upconversion nanoparticles based FRET aptasensor for rapid and ultrasenstive bacteria detection. Biosens Bioelectron 90:525–533
123. Oh SY, Heo NS, Shukla S, Cho HJ, Vilian AT, Kim J, Lee SY, Han YK, Yoo SM, Huh YS (2017) Development of gold nanoparticle-aptamer-based LSPR sensing chips for the rapid detection of *Salmonella typhimurium* in pork meat. Sci Rep 7:1–10
124. Jin L, Wang S, Shao Q, Cheng Y (2022) A rapid and facile analytical approach to detecting *Salmonella enteritidis* with aptamer-based surface-enhanced Raman spectroscopy. Spectrochim Acta A Mol Biomol Spectrosc 267:120625
125. Huang Z, Yu X, Yang Q, Zhao Y, Wu W (2021) Aptasensors for *Staphylococcus aureus* risk assessment in food. Front Microbiol 12:714265
126. Yu T, Xu H, Zhao Y, Han Y, Zhang Y, Zhang J, Xu C, Wang W, Guo Q, Ge J (2020) Aptamer based high throughput colorimetric biosensor for detection of *Staphylococcus aureus*. Sci Rep 10:9190

127. Kim YJ, Kim HS, Chon JW, Kim DH, Hyeon JY, Seo KH (2018) New colorimetric aptasensor for rapid on-site detection of *Campylobacter jejuni* and *Campylobacter coli* in chicken carcass samples. Anal Chim Acta 1029:78–85
128. Dehghani Z, Hosseini M, Mohammadnejad J, Bakhshi B, Rezayan AH (2018) Colorimetric aptasensor for *Campylobacter jejuni* cells by exploiting the peroxidase like activity of Au@ Pd nanoparticles. Microchim Acta 185:1–9
129. Hu J, Fu K, Bohn PW (2018) Whole-cell *Pseudomonas aeruginosa* localized surface plasmon resonance aptasensor. Anal Chem 90:2326–2332
130. Gao R, Zhong Z, Gao X, Jia L (2018) Graphene oxide quantum dots assisted construction of fluorescent aptasensor for rapid detection of *Pseudomonas aeruginosa* in food samples. J Agric Food Chem 66:10898–10905
131. Wu W, Yu C, Qi W, Zhao F, He H, Liu C, Yang Q (2020) Research advances of DNA aptasensors for foodborne pathogen detection. Crit Rev Food Sci Nutr 60:2353–2368
132. Nirschl M, Reuter F, Vörös J (2011) Review of transducer principles for label-free biomolecular interaction analysis. Biosensors 1:70–92
133. Bayramoglu G, Ozalp VC, Oztekin M, Arica MY (2019) Rapid and label-free detection of *Brucella melitensis* in milk and milk products using an aptasensor. Talanta 200:263–271
134. Oravczová V, Tatarko M, Süle J, Hun M, Kerényi Z, Hucker A, Hianik T (2020) Detection of *Listeria innocua* by acoustic aptasensor. Proceedings (MDPI) 60:18. https://doi.org/10.3390/IECB2020-07079
135. Xu Z, Yuan YJ (2019) Quantification of *Staphylococcus aureus* using surface acoustic wave sensors. RSC Adv 9:8411–8414
136. Zhang J, Oueslati R, Cheng C, Zhao L, Chen J, Almeida R, Wu J (2018) Rapid, highly sensitive detection of gram-negative bacteria with lipopolysaccharide based disposable aptasensor. Biosens Bioelectron 112:48–53
137. Spagnolo S, De La Franier B, Davoudian K, Hianik T, Thompson M (2022) Detection of *E. coli* bacteria in milk by an acoustic wave aptasensor with an anti-fouling coating. Sensors 22:1853
138. Khobragade S, Granja CDS, Sandström N, Efimov I, Ostanin VP, van der Wijngaart W, Klenerman D, Ghosh SK (2020) Direct detection of whole bacteria using a nonlinear acoustic resonator. Sens Actuat B Chem 316:128086
139. Ozalp VC, Bayramoglu G, Erdem Z, Arica MY (2015) Pathogen detection in complex samples by quartz crystal microbalance sensor coupled to aptamer functionalized core–shell type magnetic separation. Anal Chim Acta 853:533–540
140. Lian Y, He F, Wang H, Tong F (2015) A new aptamer/graphene interdigitated gold electrode piezoelectric sensor for rapid and specific detection of *Staphylococcus aureus*. Biosens Bioelectron 65:314–319
141. Shi X, Zhang J, He F (2019) A new aptamer/polyadenylated DNA interdigitated gold electrode piezoelectric sensor for rapid detection of *Pseudomonas aeruginosa*. Biosens Bioelectron 132:224–229

Adv Biochem Eng Biotechnol (2024) 187: 381–412
https://doi.org/10.1007/10_2023_244

Published online: 10 February 2024

Signal-Amplified Nanobiosensors for Virus Detection Using Advanced Nanomaterials

Akhilesh Babu Ganganboina and Enoch Y. Park

Contents

Abstract Rapid diagnosis and treatment of infectious illnesses are crucial for clinical outcomes and public health. Biosensing developments enhance diagnostics at the point of care. This is superior to traditional procedures, which need centralized lab facilities, specialized personnel, and large equipment. The emerging coronavirus epidemic threatens global health and economic security. Increasing viral surveillance and regulatory actions against disease transmission necessitate rapid, sensitive testing tools for viruses. Due to their sensitivity and specificity, biosensors offer a possible reliable and quantifiable viral detection method. Current advances in genetic engineering, such as genetic alteration and material engineering, have provided several opportunities to enhance biosensors' sensitivity, selectivity, and recognition efficiency. This chapter explains biosensing techniques, biosensor

A. B. Ganganboina (✉)
International Center for Young Scientists ICYS-NAMIKI, National Institute for Materials Science, Ibaraki, Japan
e-mail: ganganboina.AkhileshBabu@nims.go.jp

E. Y. Park (✉)
Research Institute of Green Science and Technology, Shizuoka University, Shizuoka, Japan
e-mail: park.enoch@shizuoka.ac.jp

varieties, and signal amplification technologies. Challenges and potential developments for viral microorganisms based on biosensors and signal amplification were also investigated.

Graphical Abstract

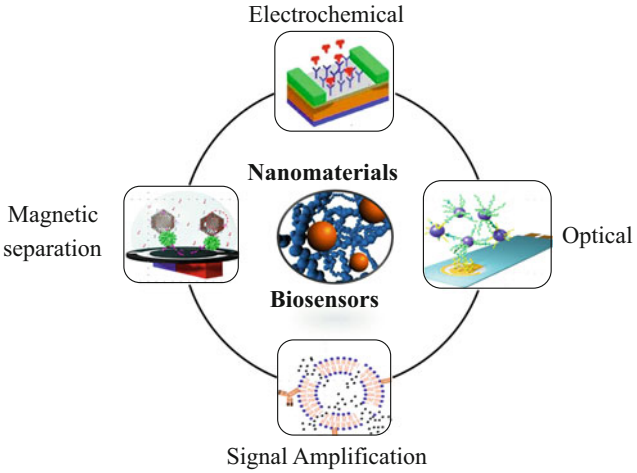

Keywords Biosensor, Diagnostics, Nanocage, Nanomaterial, Nanozyme, Signal amplification, Virus detection

1 Introduction

In light of the ongoing COVID-19 epidemic, infectious illness has risen to the forefront of world attention. It is vital to comprehend the global burden of these diseases to enhance population-wide outcomes and treat patients individually. Inequality in access to healthcare resources, particularly diagnostics, impedes getting this information [1]. Thus, much effort has been directed toward developing technologies to increase diagnostics accessibility equality, particularly in settings with limited resources. Nanotechnology-enabled biosensors, which provide quantitative target readings with affordable, basic equipment, are an essential field of study for developing such platforms.

There are rapidly developing technologies to perform early screening of pathogenic viruses since this would significantly lower the incidence of viral infections. Electrochemical biosensors offer sensitive and specific sensing by combining biorecognition components, or biomolecules that precisely identify and bind an analyte with electrochemical readout [2]. The glucose meter has revolutionized healthcare and made a dramatic difference in the lives of patients with diabetes. A measurable electrical signal

is produced when the enzyme reduces an electroactive mediator which is subsequently oxidized at an electrode surface [3]. Signal amplification methods, including but not limited to biological components like enzymes, are crucial for laboratory and point-of-care (POC) diagnostics since they increase the device's precision and accuracy while simultaneously decreasing the limit of detection (LOD) [4].

Viruses are quite small just 20–500 nm in size and come in various shapes and sizes, but they are responsible for significant harm to human health [5]. Viruses including the influenza virus, SARS coronavirus, Ebola virus, Zika virus (ZIKV), Middle East respiratory syndrome coronavirus (MERS-CoV), and SARS coronavirus-2 have been responsible for certain recent epidemics [6]. Compared to other microorganisms, viruses present unique challenges in identification and bioimaging due to their nanoscale size. Influenza and other viruses pose severe threats to human health due to their ability to spread quickly and easily [7]. The inadequate detection tools are one of the reasons why health consequences are arising from viral infections. Numerous primary approaches exist for viral identification, each optimized for a specific type of virus. Time-consuming lab-based approaches involving complex analytical instrumentation are the norm regarding viral detection. While traditional lab-based approaches can identify viruses with a high degree of precision, they have several downsides [8]. These include the requirement for skilled individuals, the high cost of consumables, the length of the process, and the difficulty of preparing samples. As a result, it is crucial to create fast, accurate, and cost-effective tests for detecting viruses. Thus, nanomaterial- and bio-recognition-unit-based biosensors for detecting viruses have great promise. Colorimetric, fluorometric, surface-enhanced Raman scattering (SERS), and lateral flow immunoassay (LFIA) biosensors made from nanoscale materials are only a few of the many that have been proposed for viral detection [9].

In recent years, nanoscience and nanotechnology have been effective diagnostic and detection tools for infectious viruses [10]. As a result, nanomaterial-based biosensors have emerged as one of the most relevant topics in viral detection and diagnosis. Nanomaterials have distinctive optical, electrical, magnetic, and mechanical characteristics, which is a significant benefit of using them [11, 12]. In addition to their excellent sensitivity and selectivity, nanomaterials-based sensors are also widely used in bioimaging applications. Sensors based on nanomaterials can also respond quickly while maintaining a low detection limit [13]. New designs of biosensors based on various nanomaterials, such as quantum dots (QDs) [14], carbon nanomaterials [15], gold nanoparticles (AuNPs) [16], upconversion nanomaterials (UCNPs) [17], magnetic nanoparticles (MNPs) [18], and organic molecule-based nanostructures [19], have emerged as a result of recent research.

Here, we highlight new signal amplification methods for enhancing electrochemical sensors for infectious illness diagnostics. These techniques may be classified into **a)** signal-based amplification and **b)** target-based amplification. We define target-based amplification as an approach that increases the number of detectable targets, whereas signal-based amplification modifies the transducer to boost the detectable signal. Based on current technology for diagnosing infectious diseases, we believe that signal-based amplification methodologies will allow electrochemical POC devices to be used in various contexts for such diseases.

2 Biosensing Principles

Several biosensors have been developed due to the development and use of sensors in numerous fields. Currently, biosensors may be categorized based on their biorecognition element and transducer. Regarding the biosensitive element, enzyme, DNA, tissue, and immunosensor biosensors may be distinguished [20]. Based on the transducers employed, biosensors may be categorized as electrochemical, optical, piezoelectric, thermal, and acoustic [21]. Parallel to the development of microfluidic technology, a novel type of microfluidic biosensor with benefits in automation and miniaturization has been created. In recent years, electrochemical biosensors, optical biosensors, and microfluidic biosensors have garnered great interest and have become a hot research topic using aptamers or antibodies as recognition elements. Different approaches can be employed to detect viruses, which include targeting the whole virus, specific proteins, or using nucleic acids.

2.1 Electrochemical Biosensors for Virus Detection

An electrochemical biosensor is a common type of sensing device that converts biological activities into electrical signals [22]. The field of electrochemical biosensors is pivotal because it has the most established history, the broadest variety of applications, and the highest vitality of all biosensor subfields. The electrochemical biosensor generally works by biologically modifying the surface of particular electrodes to fix biological recognition components. The target molecules in the solution will be recognized by the biologically sensitive components that are permanently affixed and will trigger a binding response. Attaining quantitative or semi-quantitative detection is accomplished by converting the binding response into an electrical signal at an electrode [23]. There are various categories of electrochemical biosensors, but the two most utilized approaches for detecting viruses are amperometric and impedimetric because of their high sensitivity.

2.1.1 Impedimetric Biosensors

Impedance immunosensors are used to measure the change in impedance at the interface. This can be performed by evaluating the whole impedance or analyzing the resistive part (mostly the charge transfer resistance), or the capacity before and after the target molecule binds [24]. EIS has been shown to be a useful and effective method because small changes caused by how the solution interacts with the electrode can be easily tracked in real-time without needing labels [25–28]. Impedance spectroscopy allows for a comprehensive description of the system by resistive and capacitive (and diffusional) impedance elements; however, care has to be taken in analytical applications to discriminate non-specific binding – as for all label-free

approaches. Another aspect of impedance measurements is the composition of the solution. In most cases, a redox species (such as ferri-/ferrocyanide) is added to have a defined charge transfer process. However, this is not necessary for general, and impedance analysis in a buffer solution is feasible; capacitive measurements completely avoid such additions. Typically, impedance measurement is carried out at the sensing electrode's equilibrium potential to minimize the degree of conversion during the measurement. This approach ensures that only a small amount of conversion occurs during the measurement. Alternatively, one can detect impedance during a forced oxidation or reduction process. Here a constant dc potential is additionally applied to the ac signal.

Baek et al. aimed to identify noroviruses, the viruses responsible for acute foodborne gastroenteritis [29]. Figure 1a shows the schematic diagram of the electrochemical biosensor coated with peptides for detecting norovirus. The study examined eight different peptides coated on gold electrodes to identify norovirus, and it was found that the norovirus-binding peptide had a high degree of specificity for the virus. The detection process involved the addition of ferri-/ferrocyanide to the solution. The biosensor demonstrated an LOD of 1.7 copies/mL, which was three times lower than previous methods, and the signal intensity increased with increasing amounts of norovirus.

To detect influenza virus A (IVA), Hassen et al. presented an electrochemical impedance spectroscopy (EIS)-based electrochemical sensor [27]. Their sensor, consisting of a gold electrode with a conjugated particular antibody, can detect IVA in the presence of bovine serum albumin (BSA), fetal bovine serum (FBS), and hepatitis B virus (HBV). Electrochemical measurements were performed in a 5 mM solution of redox couple $[Fe(CN)_6]^{4-/3-}$ prepared in phosphate-buffered saline (PBS) solution. The sensor's high performance in detecting IVA was demonstrated by its low LOD of 8 ng/mL, which was not influenced by the presence of nontarget proteins at substantial levels. Trung group identified the Japanese encephalitis virus (JEV) using EIS and without any label [32]. The authors first electrochemically synthesized nanowires (NWs) on the surface of a Pt microelectrode, then bound a particular antibody there. This innovative manufacturing approach achieved a very low LOD with reasonable specificity against various irrelevant compounds without using any redox species.

Intriguingly, Lai et al. created a single-use, carbon NP-modified screen printed carbon electrode (SPCE) strip to quickly detect Japanese encephalitis virus (JEV) [33]. The antibodies were anchored to the surface using amide bonds between the amino groups of carbon NPs and the carboxylic group of JEV. It takes 10 min for the sensor to perform EIS readings. This biosensor has the potential for clinical use since it is disposable and eliminates the risk of cross-contamination. A polyaniline-coated glassy carbon electrode (GCE) synthesized with a particular anti-HEV antibody coupled to nitrogen- and sulfur-codoped graphene quantum dots (AbN,S-GQDs) and gold-embedded polyaniline nanowires were produced by the Park group as shown in Fig. 1b for detecting hepatitis E virus (HEV) (AuNP-PAni) [30]. Using a pulse-induced mechanism, the scientists improved impedimetric responses to a level

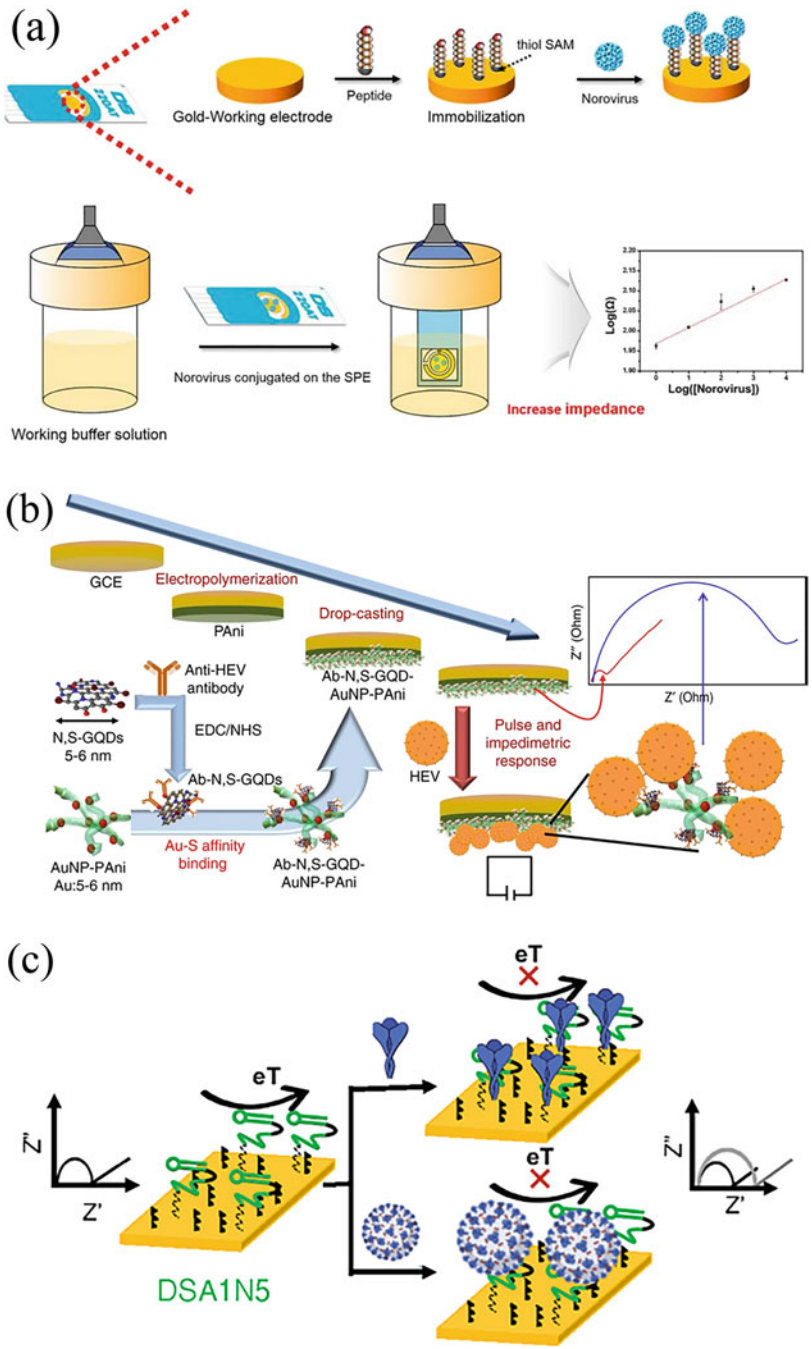

Fig. 1 Schematic illustration for the (**a**) detection of norovirus using novel peptide-coated electrochemical biosensor [29], (**b**) Ab-N,S-GQDs@AuNP-PAni nanocomposite-loaded sensor electrode and its pulse-induced impedimetric sensing of HEV [30], (**c**) electrochemical assay for the detection of SARS-CoV-2 using spike protein aptamer [31]

that allowed for an LOD of 0.8 fg/mL while maintaining a high degree of selectivity and specificity.

Zhang et al. recently published a detection method for SARS-CoV-2 that utilized a simple and fast saliva-based sensor [31]. The sensor was created by binding the novel dimeric DNA aptamer DSA1N5, which detects spike proteins, onto gold electrodes for EIS measurements (Fig. 1c). This study was one of the few with a large enough sample size to report on false-positive and false-negative results, and the authors found an extremely low LOD of 1,000 virus particles per milliliter in diluted saliva with 100% specificity for false positives and 80.5% sensitivity for actual positive cases. This sensor was capable of detecting the wild-type virus, as well as the Alpha and Delta variants, indicating the feasibility of a quick and reliable SARS-CoV-2 test.

Using boron-doped polycrystalline diamond electrodes functionalized with a biotin-streptavidin linker complex and biotinylated anti-SARS-CoV-2S1 antibodies, the Becker group also created an EIS sensor for SARS-CoV-2 detection using the changes to the electrode's charge transfer resistance (Rct) [34]. The electrolyte solution used in this study consisted of 1 mM potassium ferricyanide (III) [$K_3Fe(CN)_6$] in PBS. This sensor exhibited exceptional sensitivity and had a low limit of detection (LOD) of 1 fg/mL, making it a promising candidate among the various SARS-CoV-2 detection technologies available.

Various researchers have suggested different methods for enhancing the sensitivity of EIS-based detection, such as modifying the electrode surface, using interdigitated electrodes, or combining both cyclic voltammetry (CV) and EIS measurements for detection signals. Interdigitated gold microelectrodes (IDEs) are a type of electrode that feature closely spaced electrodes that allow for the more sensitive detection of surface events. One study, for instance, utilized a functionalized interdigitated gold microelectrode array to create an EIS-based EI for detecting the Zika virus (ZIKV) [30, 35]. In this case, the anti-ZIKV envelope antibody and the ZIKV protein combine to create an immunocomplex. For quick measurements of ZIKV, this sensor's high sensitivity, excellent selectivity, and stability make it a valuable resource. For the detection of Hantavirus Araucaria virus, Martins and coworkers have described a novel sensor that can do both CV and EIS measurements [36]. The authors mounted antibodies onto a commercial 3D conductive filament made of carbon black and poly (lactic acid) to identify Hantavirus Araucaria nucleoproteins with high selectivity and sensitivity.

2.1.2 Amperometric Biosensors

With amperometry, the analyte's oxidation or reduction processes provide a current response proportional to the analyte's concentration when diffusion conditions are controlled [37]. When detecting a signal, an electrode is positioned at a specific voltage to facilitate the flow of electrons to or from the electrode. Researchers have successfully combined immune technology with amperometric biosensors, leading to reduced detection times and limits. As a result, these biosensors are particularly

valuable for rapidly and accurately detecting pathogens in food and other compounds with multiple targets.

Using AuNPs, carbon nanotubes (CNTs), and other nanomaterials, the Sedghi group created a new nanocomposite film for the detection of the HIV-1 p24 antigen (Fig. 2a) [38]. An immunoassay format was employed to detect HIV-1 p24 Ag using a horseradish peroxidase streptavidin-labeled biotinylated polyclonal antibody to HIV-1 p24 (HRP-streptavidin-biotin-antip24 Ab) as a tracer and hydrogen peroxide as enzyme substrate. The analytical procedure for the immunosensor was based on the formation of the immunocomplex between the polyclonal HIV-1 p24 Ab and the HIV-1 p24 Ag which causes a decrease of the reduction current. Together, the large surface area of the electrodes and the bound p24 antibody allows for a sensitive amperometric immunosensor with a low LOD (6.4 pg/mL) and a short response time (18 s).

Recent work by the Dutra lab has resulted in a low-cost EI sensor capable of detecting Dengue virus nonstructural proteins (DENV) (Fig. 2b) [39]. Researchers used poly(allylamine) on carboxylated CNTs to fix anti-NS1 antibodies on an electrode surface, then used amperometry to quantify the antibodies' reactions. Electrochemical responses of the immunoassay are claimed to be based on a direct electron transfer of HRP conjugated to anti-NS1 antibodies. The novel sensor is highly reproducible, sensitive, and selective, allowing for an LOD of 0.035 μg/mL.

Mandli et al. [40] developed an indirect competitive immunosensor for detecting the hepatitis A virus (HAV) antigen using a carbon nanopowder paste electrode. The sensor works by immobilizing the target HAV antigen on the sensor surface and then using a capture antibody and a secondary antibody labeled with peroxidase to detect it. The amperometric current generated from adding hydrogen peroxide and hydroquinone as redox mediators is then used to determine the concentration of the antigen (Fig. 2c). One advantage of this sensor is its ability to tolerate complicated matrices, making it suitable for detecting HAV in water samples. This is an important feature since water samples can often contain various interfering substances that can affect measurement accuracy. The use of a secondary antibody labeled with peroxidase also enhances the sensitivity of the sensor, allowing it to detect low concentrations of HAV. Overall, this study demonstrates the potential of carbon nanopowder paste electrodes as a platform for developing sensitive and selective immunosensors for various applications, including the detection of viral pathogens in environmental samples.

2.2 Optical Biosensors for Virus Detection

Colorimetry, fluorescence, surface-enhanced Raman spectroscopy, and surface plasmon resonance spectroscopy are the four most appealing optical biosensors for viral detection based on the underlying principle utilized. Out of these, colorimetric and fluorescent biosensors are the most popular choices because their results can be interpreted simply and have a high sensitivity level.

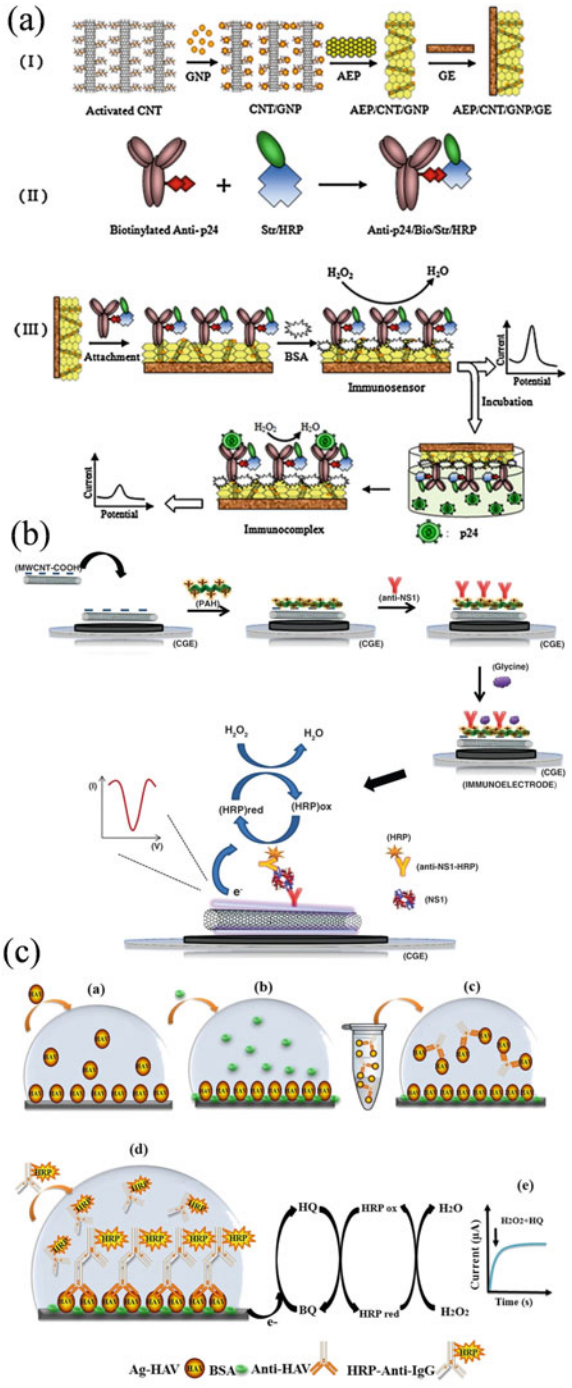

Fig. 2 A schematic diagram of the (**a**) fabrication steps and performance of a novel immunosensor for the detection of HIV-1 p24 Ag [38], (**b**) stepwise construction of immunoelectrode and principle of an immunoassay for dengue virus NS1 protein [39], (**c**) preparation of the electrochemical HAV competitive antibody immunosensor [40]

2.2.1 Colorimetric Biosensor

The color changes generated by the interaction between analytes of varying concentrations and experimental reagents are employed in colorimetric analysis, an analytical method for quantitatively detecting analytes [41]. There have been two distinct areas in colorimetric analytical technology: visual colorimetry and photometric colorimetry. In visual colorimetry, the concentration of the target is determined mostly by visually inspecting the color produced by the detecting reaction. The measurements are often easily performed and do not need instrumentation. However, the accuracy of this analytical approach is poor since experiments relying on visual observations depend on the individual person. As a result, throughout time, visual colorimetry has been adapted into a photometric colorimetry technique. Absorbance measurements are taken at various concentrations of a standard solution to create a standard curve. The measured material's absorbance can then be used for quantitative analysis. By removing the room for human mistakes, photometric colorimetry provides far more reliable findings in experiments than visual colorimetry. Its primary detecting devices of photoelectric colorimetry now rely on a spectrophotometer, ultraviolet-visible spectrophotometer, and microplate reader.

As the most practical optical sensors used to detect infectious viruses, those based on antibodies are becoming popular. Polyclonal, monoclonal, and recombinant antibodies have often been used in immunodiagnostics and biomarker detection [42].

A classical method for detecting analytes is lateral flow assays that rely on the accumulation of AuNPs in the detection zone to generate a color signal, as described by [43]. This approach has been modified to use enzymes as labels, but it requires a substrate to generate a color, necessitating modifying the test strip. Kogaki et al. [44] applied this method to detect virus particles; for instance, they utilized the virus's recombinant N protein antigen to detect SARS-CoV quickly. The detection zone of an immunochromatographic (ICT) device was built on a nitrocellulose strip. The SARS-CoV N protein and an anti-mouse IgG were immobilized on a control and test line. Alkaline phosphatase (AP) was used as an enzyme, and the blue color formation was used as the signal. The base of the ICT device contained two wells, one for the sample and one for the buffer. When the sample was added to the sample well, the AP-antibody-antigen complex flowed across the membrane through capillary action. The complex accumulated at the test line, causing it to turn blue if there was an antibody to SARS-CoV in the blood sample. A positive result displayed two colored lines, with one indicating device functionality and the other representing the existence of an antibody to SARS-CoV. The result was deemed unacceptable if the color was limited to the test line or no lines were visible.

Recently, Li et al. developed a point-of-care immunoassay kit based on a lateral flow test with gold nanoparticles to detect IgM and IgG antibodies in human blood concurrently in less than 15 min (Fig. 3a) [48]. The data show promise, demonstrating improved sensitivity and specificity in the fast detection of antibodies. After

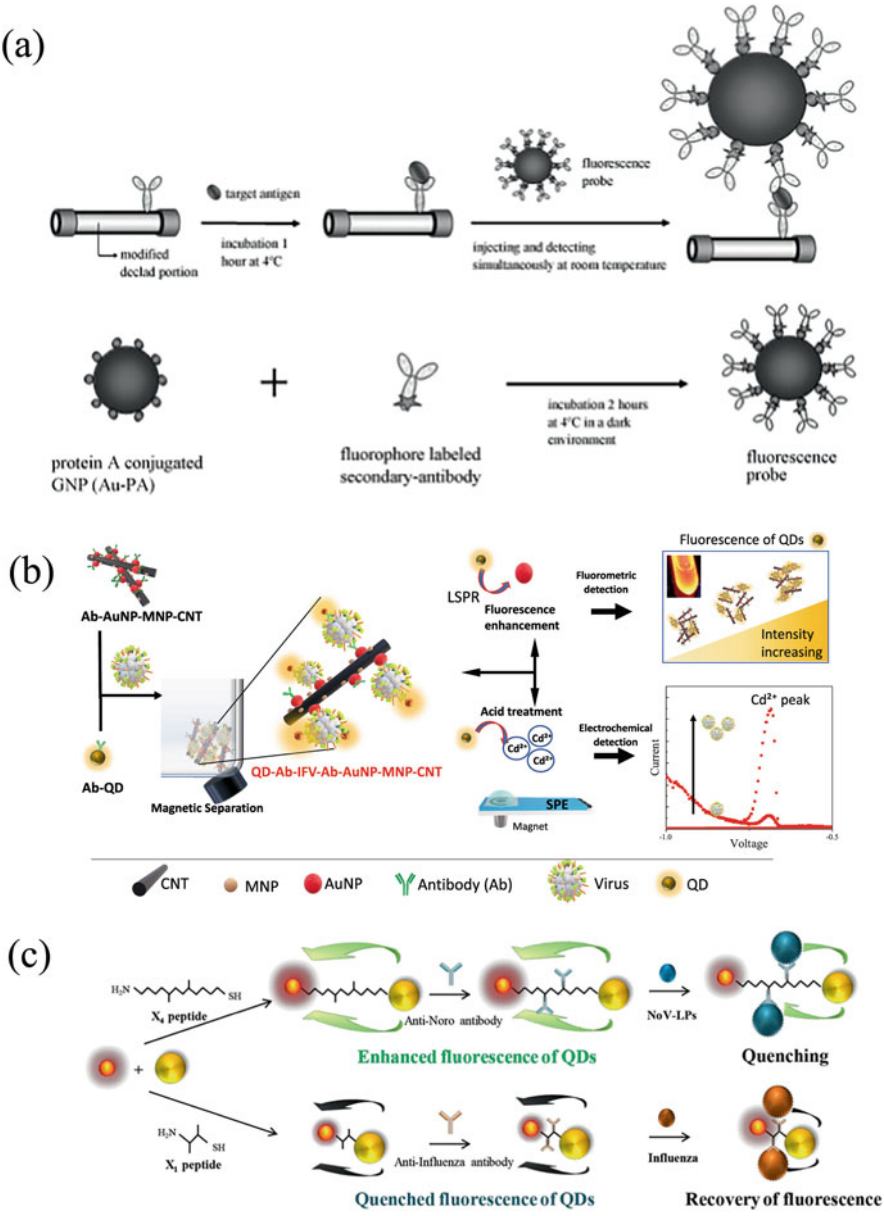

Fig. 3 Scheme of (**a**) rapid SARS-CoV-2 IgM-IgG combined antibody test [45], (**b**) optical and electrochemical IFV detection method [46], and (**c**) virus sensing using CdSe QD-peptide-AuNP system for two modes of detection [47]

successful trials, it has been approved for use in healthcare settings and research labs, making it a potent weapon in the battle against SARS-CoV-2.

Metal nanoparticles also allow the generation of a color by exploiting their enzyme-like behavior. This is a valuable alternative to surface plasmon effects and will be explained in Sect. 3.3.2.

2.2.2 Fluorescence Biosensor

A biosensor based on the fluorescent characteristics of substances is referred to as a fluorescence biosensor. At this time, the procedures of (a) fluorescence spectroscopy and (b) fluorescence energy resonance transfer are the ones that are utilized the most frequently [49]. After absorbing light energy when subjected to UV irradiation, various substances will emit at different wavelengths, and the emission intensity will be proportional to the substance's concentration [50]. Within the fluorescence resonance energy transfer methodology, the energy of an excited fluorescent material is radiationless transferred to another molecule at a close distance, which starts to emit light. This can be evaluated qualitatively and quantitatively. However, several preconditions must be fulfilled for this energy transfer [47, 51, 52]. In fluorescence spectroscopy, fluorescent dyes and nanomaterials with fluorescent properties, such as quantum dots (QDs), are frequently utilized [53–55].

A fiber optical biosensor based on localized surface plasmon coupled fluorescence (LSPCF) was later developed to improve detection (Fig. 3a). Here a concentration of 0.1 pg/mL of GST-N in PBS was sufficient for detection. When human serum was diluted by a factor of 10, the LOD was found to be 0.1 pg/mL, which is on par with the LOD in raw serum (1 pg/mL). LSPCF, by employing the same monoclonal antibodies, improved detection sensitivity by a factor of 104 [45, 56]. LSPCF has consistently proven to be the most advantageous approach regarding detection limit and cost-effectiveness for detecting SARS-CoV N protein in blood samples.

The plasmon effects present on metal nanoparticles and the light absorption by semiconductor nanoparticles can be exploited for an enhanced detection capability often combining optical and electrochemical detection. For example, CdSeTeS quantum dots (QDs) have been utilized to generate optical and electrochemical signals. Additionally, AuNP−magnetic nanoparticle−carbon nanotube (AuNP−MNP−CNT) nanocomposites are used to enhance signals and magnetically separate the virus from interference (Fig. 3b) [46]. The QDs exhibit virus concentration-dependent fluorescence enhancement due to localized surface plasmon resonance (LSPR) of AuNPs when the target virus is present. In terms of electrochemical signals, Cd ions released from acid degradation of QDs in solution exhibit a virus concentration-dependent increase in current peak on an electrode with improved electrochemical properties from deposition of these nanocomposites. Both nanomaterials are bound to specific antibodies for influenza virus A (IFV/A) in a sandwich structure for virus detection. This approach successfully detects the virus from these two signals even in the presence of a human serum matrix, with a

detection limit of 2.16 fg/mL for optical detection and 13.66 fg/mL for electrochemical detection.

Chowdhury et al. [47] utilized the physical significance of LSPR to establish an ultrasensitive biosensing system using CdSe QD-peptideAuNP nanoconjugates. Several CdSe QD-peptide-AuNP nanoconjugates have been designed by varying the length of the peptide chain, size, and concentration of AuNPs to investigate the resulting changes in fluorescence intensities (Fig. 3c). The experimental separation distance between the terminal nanoduos was validated through theoretical simulation. The strong quenching effect of QDs fluorescence was observed due to the close interaction of CdSe QDs and AuNP, which gradually showed fluorescence enhancement with the increment of distance. Two systems were chosen for the application and successfully applied for sensing NoV and influenza virus, respectively, using two different-sized peptides, following opposite sensing mechanisms. Excellent linearity was observed with virus concentration in both cases, with LODs of 124 fg/mL for NoV-LP and 14.6 fg/mL for the influenza virus. We believe that the thorough investigation of this study can provide useful directions in the emerging field of LSPR-based biosensing.

3 Signal Amplification Technology in Virus Biosensors

3.1 Magnetic Separation

Magnetic separation is a technique used to separate magnetic materials from non-magnetic ones. This technique has been extensively used in various fields, including biology and medicine, to isolate and purify specific cells, proteins, and nucleic acids. In recent years, magnetic separation has also been employed in detecting viral particles in biological samples, for medical diagnostics, environmental monitoring, and food safety. Magnetic separation-based virus sensing typically involves the use of magnetic nanoparticles (MNPs) that are functionalized with specific ligands that bind to viral particles. These particles can then be separated from the sample using an external magnetic field and be detected by various methods. For example, biosensors based on magnetic nanoparticles (MNPs) can detect respiratory viruses [57]. Alternatively, it was shown by Zhao et al. [18] found that carboxyl polymer-coated magnetic NPs (pcMNPs) were effective for COVID-19 detection by extracting the RNA.

Magnetic separation can also be coupled with other amplification technologies. Tian et al. show that MNPs-based biosensors may be employed for the detection of nucleic acids by utilizing iron oxide NPs (IONPs) and homogenous circle-to-circle amplification (HC2CA) [58]. Under the influence of an external magnetic field, both isolated and coupled IONPs exhibit the expected optical characteristics (absorption or scattering). However, when IONP detection probes are paired with HC2CA, combined IONPs are generated (ssDNA). Accordingly, the states of IONPs may be used to assess opto-magnetic characteristics. Since SARS-CoV-2 and SARS-CoV

gene sequences are so similar, this technique was proven to be highly specific. It was also used to identify SARS-CoV-2 RdRp sequences using synthetic complementary DNA [58].

The nanosystem based on carboxyl polymer-coated magnetic NPs (pcMNPs) demonstrated several beneficial properties, such as breaking down viruses and binding to RNA in a single step. This resulted in a pcMNPs-RNA complex that could be directly used in subsequent RT-PCR reactions. Additionally, the pcMNPs facilitated RT-PCR biosensing with a sensitivity of detecting 10 copies and a linearity range of 10–10^5 copies of SARS-CoV-2 pseudovirus particles by identifying the ORFlab and N gene of the viral RNA. Overall, this study highlights the potential of the pcMNPs-based RNA extraction approach as a viable alternative for addressing challenges in the timely diagnosis of SARS-CoV-2 through RT-PCR techniques [59].

3.2 Amplification of Analyte

Electrochemical biosensors' speed and quantitative accuracy make them a natural addition to well-established methods of amplifying nucleic acids. Here isothermal protocols are particularly beneficial since they can work without complicated temperature control systems and are also comparatively fast [60]. Isothermal amplification with modified primers and electrochemical detection was used in an assay to detect Leishmania DNA in blood samples, as described by the Merkoçi group [60]. Multiplex amplification with primers for Leishmania and endogenous control was performed using 14×10^{-3} M of magnesium, 300×10^{-9} M of Leishmania primers, 150×10^{-9} M of 18 s primers, 5 μL of DNA, and 37°C of reaction temperature during 10 min without agitation. The forward primer was linked to a AuNP to increase the signal by catalyzing the hydrogen evolution process. In contrast, the reverse primer was labeled with a magnetic bead to facilitate the purification and immobilization of the amplicon on the electrode. A potential technique for point-of-care testing on a clinical sample with little sample preparation, the complete operation took less than 20 min at a constant temperature of 37°C. The detection limit was around one parasite per milliliter of blood. The detection of SARS-CoV-2 may also be done effectively using an enzyme-linked immunoassay (ELISA) kit that employs a colloidal gold-immuno-chromatographic (GICA) technique based on RT-PCR.

3.3 Nanomaterial-Based Signal Amplification

Materials with at least one dimension in the nano-range, often below 100 nm, are collectively referred to as nanomaterials [61]. This includes nanowires, nanorods, nanosheets, and even bulk nanostructured materials like graphene. A new generation

of biosensors with improved sensitivity, specificity, stability, and cheap cost may be developed using nanoparticles due to their unique features, which constitute an opportunity and availability above traditional bulk state materials [62]. But there are still problems with using nanomaterials as biosensors, such as (a) with high quality and good repeatability; (b) with high stability and biocompatibility in complicated systems.

Signal amplification through the use of nanomaterials in biosensors is predicated on the following features: (a) Many nanomaterials have good conductivity, show fast charge transfer and a high surface area which results in higher signals and shorter response times when used in electrochemical biosensors; (b) nanomaterials may possess distinct optical properties which allow the detection of relatively small amounts; (c) nanomaterials can possess similar properties such as enzymes and thus, the catalytic activity can be used for significant signal enhancement; and (d) nanomaterials can load a large number of signal molecules to achieve signal amplification [63]. Because of these benefits, nanomaterials are increasingly being employed in domains such as ensuring the quality and safety of food, aiding in medical diagnostics, and analyzing and testing pharmaceuticals, among others. Nanoparticles like colloidal gold, quantum dots, and so on are the most common types of zero-dimensional nanomaterial [64]. Nanorods, nanowires, and nanotubes are the three most common types of one-dimensional nanomaterials. The graphene film is a prototypical example of a two-dimensional nanomaterial with a thin film structure. Flower-like, circularly porous, and dendritic shapes are three-dimensional nanomaterials' most common architectural features [65].

Organic-inorganic hybrid nanoflowers (NFs) are flower-shaped nanomaterials generated by self-assembling inorganic salt ions and organic ligands. In 2012, Ge et al. [66] created nanoflowers for the first time. Proteins such as bovine serum albumin, BSA, etc., served as organic ligands, whereas copper phosphate served as an inorganic salt ion. Since then, there has been an explosion of research and reports on nanoflowers, revealing new insights into their peculiar characteristics. Currently, available nanoflowers range in size from 0.5 to 2 μm, with a significant specific surface area capable of loading many signal molecules. Meanwhile, it has been established that nanoflowers can enhance biomolecular performance. The enhancement of the catalytic activity of biological enzymes is a frequent function. Therefore, nanoflowers have enormous potential as a signal-amplification medium in biosensors.

3.3.1 Optical Properties of Nanoparticles

The exceptional physicochemical features of gold nanostructures have led to their widespread use in medicine. Numerous biosensors utilize AuNPs to enable colorimetric detection of SARS-CoV-2. Research has demonstrated that biosensors utilizing AuNPs can effectively detect viruses through various mechanisms, offering the advantage of clear signal strength [16, 67]. One successful approach involves thiol-modified antisense oligonucleotides with AuNP capping for detecting the

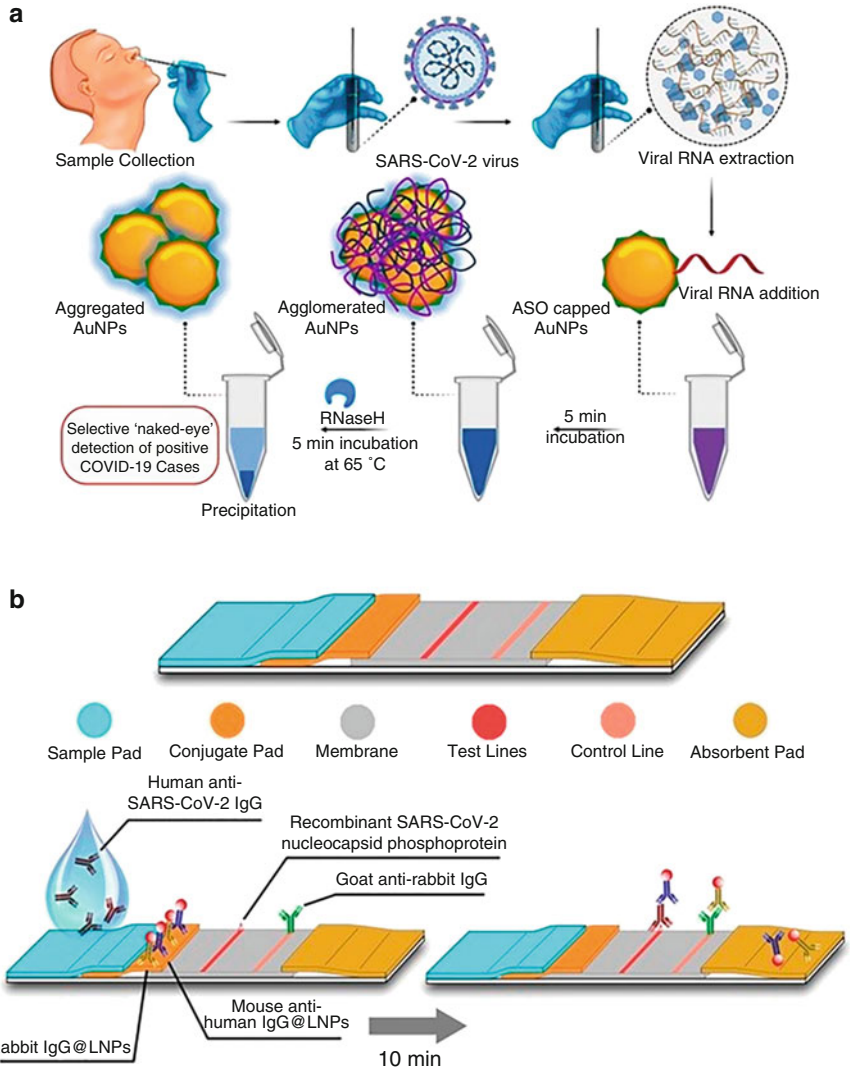

Fig. 4 Schematic design of (**a**) selective naked-eye detection of SARS-CoV-2 RNA mediated by the suitably designed ASO-capped AuNPs [67] and (**b**) design and fabrication of the developed assay and lateral flow test strip for SARS-CoV-2 detection [68]

nucleocapsid phosphor protein gene (N-gene) in RNA obtained from oropharyngeal swabs.

The ability to visually detect positive cases of COVID-19 without the need for advanced instrumental techniques is highly desirable. A colorimetric assay based on AuNPs capped with specially designed thiol-modified antisense oligonucleotides (ASOs) specific to the N-gene (nucleocapsid phosphoprotein) of SARS-CoV-2 was developed (Fig. 4a) [67]. This assay can diagnose positive COVID-19 cases in as

little as 10 min from isolated RNA samples. The thiol-modified ASO-capped AuNPs selectively agglomerate in the presence of the target RNA sequence of SARS-CoV-2, resulting in a change in surface plasmon resonance. The addition of RNaseH leads to the cleavage of the RNA strand from the RNA-DNA hybrid, causing visually detectable precipitation from the solution by further agglomeration among the AuNPs. The assay's selectivity was confirmed in the presence of MERS-CoV viral RNA, with a limit of detection of 0.18 ng/μL of RNA with SARS-CoV-2 viral load.

The RdRp gene of SARS-CoV-2 may be detected using a lateral flow biosensor in human nasopharyngeal samples. Furthermore, it was discovered that human blood samples could be used in a lateral flow immunoassay (LFIA) using AuNPs to simultaneously detect immunoglobulin M (IgM) and IgG antibodies of SARS-CoV-2 [48]. The test had a sensitivity of 88.66% and a specificity of 90.63%. Anti-human-IgG, anti-human-IgM, and anti-rabbit-IgG (control) were immobilized at specific locations along three test lines on a nitrocellulose (NC) membrane used to construct a test strip for this investigation. The conjugation pad was then sprayed with a mixture of AuNP-COVID-19 recombinant antigen conjugate and AuNP-rabbit IgG. It allows the detection of SARS-CoV-2 at many time points [69]. Moreover, sensitivity was 87.3% when using an ELISA kit and 82.4% when using a combined GICA-IgM and GICA-IgG (IgM and IgG antibodies) detection. In addition, GICA and ELISA were completely selective for normal patients [59]. Because of this, it serves as an effective method for identifying COVID-19.

The mini-emulsion polymerization process was used to create a biosensor based on lanthanide-doped polystyrene nanoparticles (LNPs) that can detect anti-SARS-CoV-2 IgG in human serum within 10 min (Fig. 4b) [68]. Unique properties, such as wide and crisp emission bands and extended luminescence lifetimes, are responsible for the exceptional optical features of lanthanide-doped NPs, which aid in very sensitive detection [70]. In addition, lanthanide-doped NPs were used to construct an LFIA-based biosensor for POC identification of viruses using luminescence [71]. In addition, the lanthanide-doped NPs were coupled via an EDC/NHS chemical reaction of rabbit IgG (R-IgG) and mouse anti-human IgG antibody (MH-IgG) to create fluorescent probes. The SARS-CoV-2 specific IgG, which can trap the recombinant nucleocapsid protein, was then immobilized utilizing a nitrocellulose membrane as a mold. Since there is currently no anti-SARS-CoV-2 IgG standard, it has been demonstrated that the LFIA does not provide accurate findings. Therefore, more research into LFIA for the diagnosis of COVID-19 is required [59, 68].

3.3.2 Exploitation of Catalytic Properties of Nanomaterials

Catalytic signal amplification has become an indispensable technique in bioanalysis, where colorimetric, fluorescent, and electrochemical detection methods, such as ELISA, are well-established [72, 73]. Proteins and RNAs having catalytic activity are called enzymes and ribozymes, and they are generated by living organisms to catalyze various chemical processes [74, 75]. Unfortunately, enzyme-based assays have several drawbacks that cannot be overcome by improving their activity or

specificity, including poor stability, high manufacturing costs, and storage complications [76]. None of these features is suitable for use in extreme or out-of-the-way places.

Multiple nanozymes have been demonstrated to possess properties similar to natural enzymes [77–81]. Although substrate specificity cannot be provided, they show good and excellent turnover rates, which allows their application in detection assays and sensors. Biomedical applications are broadened by the discovery and comprehension of nanozyme systems, allowing for the creation of biosensors and contrast agents to treat a wide range of diseases [82].

Initially, nanozymes were employed as substitutes for natural enzymes in biosensing and colorimetric research. In a groundbreaking study, Gao et al. [83] reported the use of magnetic Fe_3O_4 nanoparticles as peroxidase-mimicking nanomaterials. In this setup, nanoparticles are used to capture and extract target analytes from the sample matrix, and their signal is amplified for a colorimetric immunoassay. Conventional biomarker detection methods, such as ELISA, typically rely on HRP for TMB oxidation to initiate color development and aid in result quantification. HRP is only applicable within a narrow pH, temperature, and concentration range as a protein-based enzyme due to its instability in harsh conditions and expensive price [72]. So, metal and metal oxide nanoparticle-based nanozymes are a terrific alternative since they can work in a broader range of temperatures and pH levels, concentrate more when necessary, and even have better catalytic efficiency in some situations [84].

As already mentioned under Sect. 3.1. the magnetic separation capabilities of magnetic particles can be advantageously combined with other principles. For example, Fe_3O_4 nanoparticles due to their ferromagnetic features, which substantially assist the sample preconcentration and washing procedures due to their ferromagnetic features, were among the first nanocatalysts utilized for signal amplification in a biological experiment. Because of their versatility, new approaches to electrochemical biosensing have been made possible.

To screen for the Ebola virus efficiently, Duan et al. [85] developed an immunochromatographic strip with an anti-EBOV antibody-tagged Fe_3O_4 MNP probe, with detection limits as low as 1 ng/mL of EBOV glycoprotein. This study amplified the signal on the strip for better EBOV glycoprotein detection by 100-fold compared to the standard colloidal gold strip, thanks to the prominent peroxidase (POD)-like catalytic activity of Fe_3O_4. This activity is similar to natural enzymes and catalyzes POD substrates to produce a color reaction. Fe_3O_4 nanoparticles showed promise as a simple, quick, and accurate diagnostic tool with a broad detection range when used with specific antibodies to detect various illnesses.

Furthermore, several creative scientists have used a gold-and-metal combination to improve viral detection. The rubella virus was detected using an antibody-conjugated platinum-coated gold (Au@Pt NRs) nanozyme probe developed (Fig. 5a) [86, 88]. Specifically, rod-shaped gold has been shown to enhance the POD-like activity of Pt for color signal generation. Antigen-conjugated Au@Pt NRs maintained POD-like activity between 25°C and 85°C between pH 3 and 9. Their detection limit was 10 ng/mL, which is 1,000 times lower than commercial ELISA.

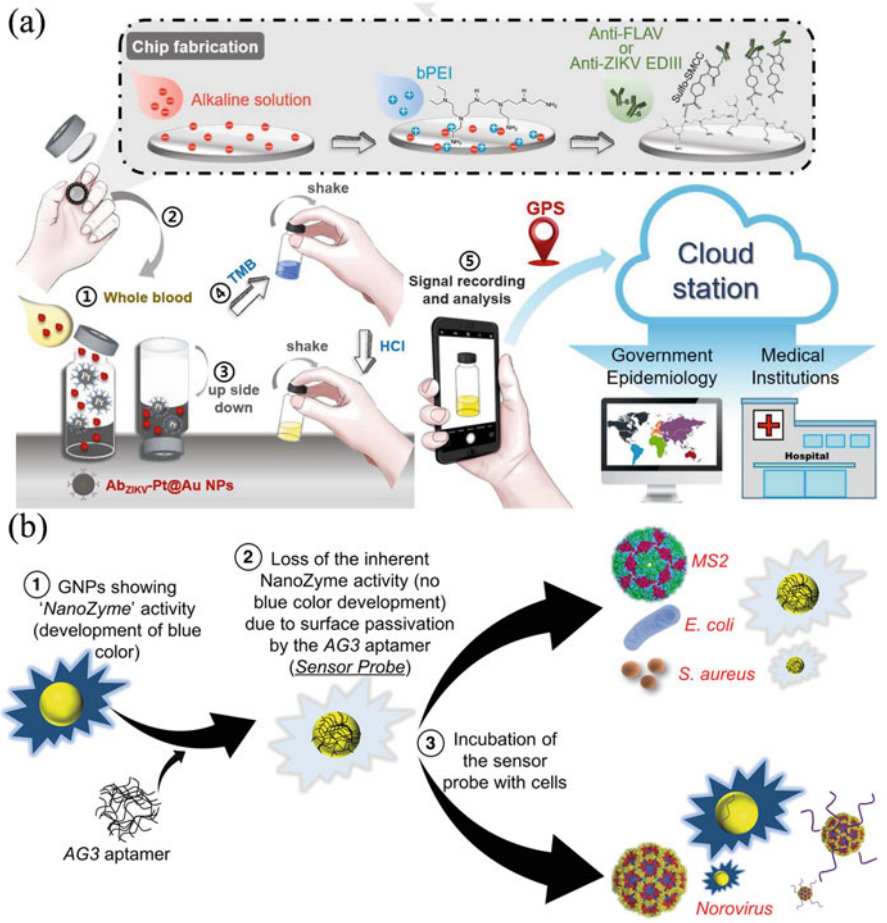

Fig. 5 Illustration of (**a**) fabrication processes and detection procedures: (1) addition of spiked whole blood sample into VISZIKV; (2) securing of the chip-containing lid; (3) shaking for 30 s, incubating upside-down for 15 min, and then transferring the lid to a new vial containing wash buffer (TBST); (4) transferring the lid to a new vial containing H_2O_2/TMB, securing the lid, shaking for 1 min, and allowing to stand for 3 min; and (5) signal recording by a smartphone for result determination, data storage, digital data transmission, and real-time geographical tagging of the results [86] and (**b**) principle of the norovirus nanozyme aptasensor; outlining the steps involved during norovirus sensing [87]

Because of this, antigen-conjugated Au@Pt NRs are preferable to antibody-conjugated HRP because they are more stable, robust, and economical. As such, it may serve as a suitable replacement. Increased sensitivity in an enzyme-linked immunosorbent assay using an antigen-conjugated Au@Pt NR was achieved thanks to the enhanced catalytic capabilities of this nanozyme probe.

Interestingly, metal-based nanomaterials, primarily AuNP, demonstrated POD-mimetic capabilities that work as an enzyme mimic, enabling superior, more

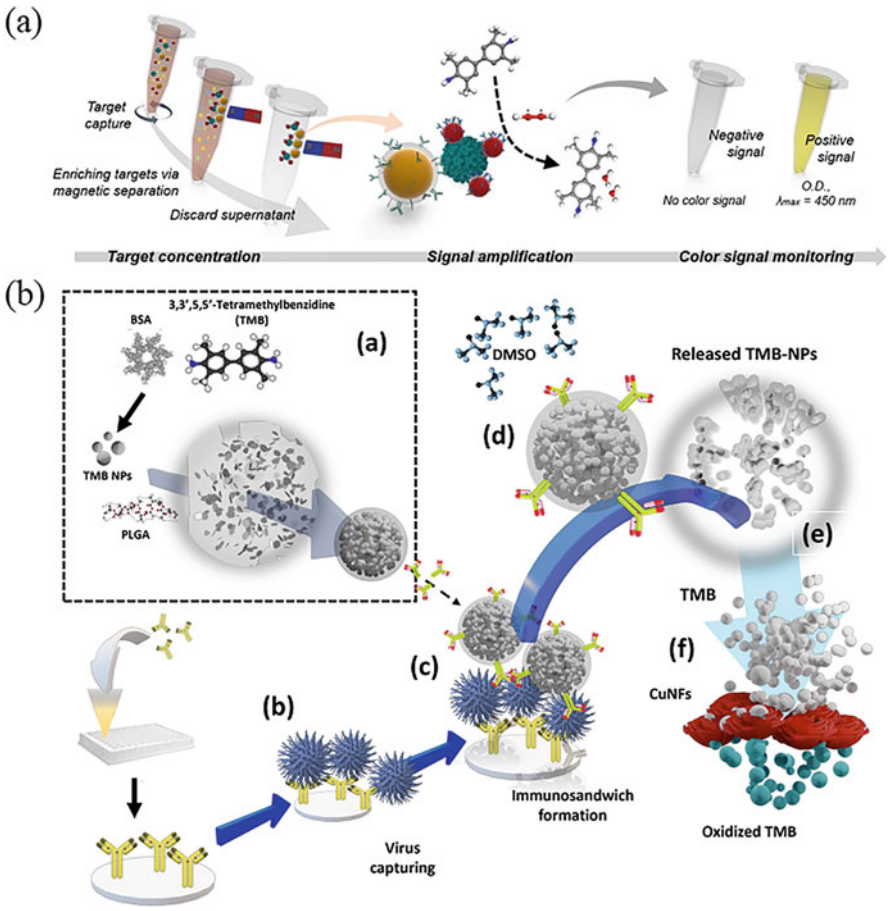

Fig. 6 (**a**) Working principle for the quantification of influenza viruses using MagLISA-based colorimetric diagnostics kit [90] and (**b**) TMB-NPs@PLGA-based signal amplification platform [91]

precise analytical methods [89]. For example, the quick and sensitive detection of murine norovirus by a colorimetric AuNP nanozyme aptasensor is shown in Fig. 5b [87]. Tyrosine-functionalized AuNPs' POD enzyme-mimicking ability and the antivirus aptamer's selectivity, sensor probes may be made that change blue in the presence of the virus, with a detection limit of 200 viruses/mL.

Various other nanozymes than AuNP have also been created for viral immunoassay detection. Oh et al. [90] developed a colorimetric test based on AuNPs and silica-coated magnetic nanobeads (MagNB), calling magnetic nanozyme-conjugated immunosorbent assay (MagLISA) to detect influenza A virus quantities as low as 44.2 fg/mL (Fig. 6a). In this research, AuNPs played a crucial role as the nanozyme to execute POD-like activity-driven color signal production. MagNBs are a cluster of 30 nm Fe_3O_4 nanoparticles linked to gold nanozymes; their enhanced magnetism

and sustained superparamagnetic characteristics facilitated magnetic separation and enrichment of biomarkers. To specifically attach to the influenza A virus, this probe was embellished with an anti-hemagglutinin monoclonal antibody. Therefore, MagLISA established a new benchmark for influenza virus screening using enzyme-linked immunosorbent assay-based technology, with a detection limit of 5.0 g/mL, measured by the naked human eye, and 44.2 fg/mL as measured by a microplate reader.

Khoris et al. [91] developed a poly(lactic-co-glycolic acid) (PLGA)-based nanocarrier loaded with chromogen substrate (Fig. 6b), TMB (TMB-NPs@PLGA), coupled with virus-specific antibodies to concentrate signal molecules inside a single nanocarrier, achieved magnified signal upon viral detection. After being incubated with the influenza virus, the TMB-NPs@PLGA nanocarrier generated an antibody-conjugated immunocomplex sandwich structure. TMB-NPs loaded with POD-like activity are released upon the addition of dimethyl sulfoxide, at which point the substrate solution comprising H_2O_2 and copper nanoflower nanozyme (CuNF) begins active oxidation of the TMB-NPs. Because of this, the presence of viruses may be detected by the solution's distinctive blue color. Viral quantities as low as 32.37 and 54.97 fg/mL could be detected in the buffer and serum, respectively.

Nanozymes have also been used for COVID-19 detection. It was used in a novel way by Liu et al. [92] to develop SARS-CoV-2 spike antigen detection chemiluminescence paper tests that could be applied anywhere. This research developed a paper test using the principle of an antibody sandwich lateral flow immunoassay and the Co-Fe@hemin-POD-like nanozyme. First, Co-Fe@hemin nanozyme chemiluminescence probes labeled with a receptor binding domain of SARS-CoV-2 spike protein (S-RBD) antibody (S-dAb) were dispersed onto the conjugate pad. Along with the lateral flow of the sample, nanozyme probes combined with S-RBD and antibody of S-RBD (S-cAb) form the sandwich immunocomplexes. The nanozyme probes exhibit excellent peroxidase activity and can catalyze the conversion of luminol substrate in the presence of H_2O_2 under alkaline conditions, generating chemiluminescence signals. It was particularly impressive that Co-Fe@hemin, with its catalytic activity of 69.915 U/mg, outperformed both Co-Fe NPs (9.836 U/mg) and Fe_3O_4 NPs (5.40 U/mg) in the TMB chromogenic reaction.

In 2006, Gao and coworkers (2006) reported employing OsO_2 nanoparticles to catalyze the breakdown of hydrazine to detect microRNA in an electrocatalytic amplification. Since indium tin oxide (ITO) electrodes are resistant to hydrazine at low potentials, they have been employed to obtain low and reproducible background levels, allowing for an 80 fM detection limit during RNA extraction from a buffer solution following a 60-min hybridization stage.

Support materials for catalytically active nanoparticles should optimize the ratio of catalytic sites to total mass, allowing for maximum activity with little waste [93, 94]. Pt nanoparticles supported by TiO_2 nanospheres (Fig. 7a, b) [94], Pt or Pd nanoparticles supported by metal-organic frameworks (MOFs) [95, 96], Pt nanoparticles supported by graphene [97], or fullerene-CeO_2 composites [98]. Fe_3O_4/CeO_2 composites decorated with AuNPs [99] are just some of the

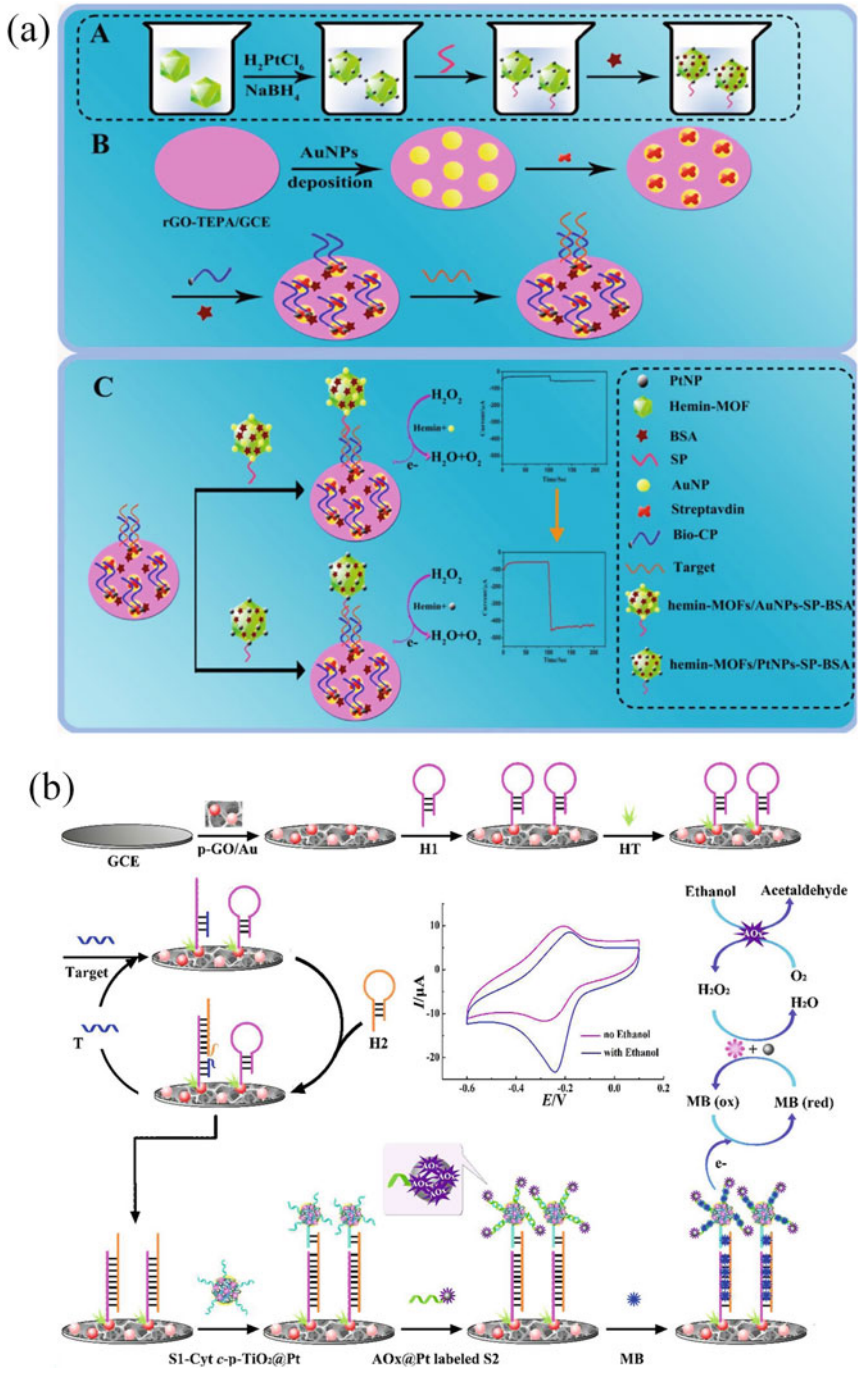

Fig. 7 Scheme illustration of (**a**) the preparation of hemin-MOFs/PtNPs-SP-BSA bioconjugates, stepwise assembly, and electrochemical DNA sensor [95] and (**b**) preparation process of the bio barcode conjugate labels. S1 and Cyt *c* are attached to the p-TiO_2@PtNPs and proposed strategy for miRNA-155 detection [94]

systems recently reported in the literature for miRNA and DNA detection using supported catalysts for signal amplification. Due to increased active surface area and synergistic interactions with the support materials, these methods exhibit higher performance compared to associated bare catalyst nanoparticle systems. However, the scalability of composite nanomaterial platforms is constrained by the necessity of numerous synthetic stages. In light of this, metal-organic frameworks (MOFs) have been proposed as valuable electrocatalysts for biosensing because of their easy one-step synthesis [100]. Their metal centers provide the catalytic activity of the MOF nanomaterials, and their surface is amenable to functionalization with biomolecules via organic ligands. Electrochemical signal amplification is a promising use for MOFs, which have recently progressed in catalysis and magnetic separation [101]. Several studies have shown that streptavidin-functionalized MOFs mimic the activity of the peroxidase enzyme, making them useful for DNA detection either as an indirect label (binding to an aptamer when the target DNA is absent) or a direct label (binding to a biotinylated strand of the complementary DNA) [102].

3.3.3 Nanocarrier-Based Signal Amplification

Using nanomaterials as the payload for redox reporters is one of the simplest methods for amplifying electrochemical signals. It has widespread application in nucleic acid detection [103, 104]. While nanocarrier approaches were among the initial tactics for enhancing biosensing signals, they have only witnessed modest improvement over the previous 5 years [105]. A cobalt-porphyrin redox marker-based DNA biosensor was described by Kaur et al. [105]. When the organometallic compounds were loaded onto AuNPs, the detection limit (3.8 aM) of short DNA sequences in the buffer was found to be increased by a factor of 1,000 [105, 106]. Recent years have seen numerous reports of different nanoparticle-marker systems, such as AuNPs labeled with methylene blue [107, 108] or ferrocene [107], Fe_3O_4 nanoparticles labeled with thionine [109] or ferrocene, thionine-labeled multi-walled carbon nanotubes [110], polymer nanoparticles labeled with Cu^{2+} ions [111], and Cd^{2+}-labeled titanium phosphate. Redox reporters come in the form of ions (e.g., Cd^{2+}, Pb^{2+}) [112], organometals (e.g., ferrocene) [113], and small molecules (e.g., methylene blue, 3,3′,5,5′-tetramethylbenzidine) [114]. More recently, adaptable nanoporous MOFs have shown good loading capacities for a range of redox reporters.

Several different types of interactions, such as covalent bonds, electrostatic interactions, nanopore intercalation, physisorption, and gold-thiol interactions, regulate the loading process of redox indicators onto nanoparticles. Loading nanoparticle labels with multiple signal probes permits a ratiometric signal analysis by employing a dual-probe method to determine the ratio of the probe signal in relation to a reference. With a ferrocene-labeled hairpin probe on the electrode surface and methylene blue on the nanoparticle tag, non-specific adsorption events of the nanoparticle labels on the electrode may be compensated for from the signal ratio, making detection of the target analyte more reliable.

More generally, current research has centered on the surface engineering of nanoparticle labels to boost redox indicator loading capacity. For example, one can functionalize AuNPs with dsDNA or ssDNA to enhance the number of potential binding sites for RuHex or methylene blue labels, respectively [115]. Following target identification, AuNPs can form aggregates through hybridization, providing additional binding sites for RuHex. Compared to using a single AuNP label, this method has increased detection limits by 32 [116].

Recently, Gooding and colleagues recently disclosed a novel method for miRNA identification [117]. Here, a sample solution containing target miRNAs was combined with gold-coated magnetic nanoparticles coupled with ssDNA labeled with methylene blue. To detect hybridized targets, a magnetic field was used to bring nanoparticles into contact with the electrode, creating a superlattice whose structure is sensitive to the presence of dsDNA. Due to the presence of stiff hybridized probes (dsDNA), the recorded signal was attenuated by using AuNPs as the electrode material. In this case, the nanoparticles are not only a nanocarrier for redox reporters but also enhance charge transport characteristics and signal transduction [117]. Targets as low as 10 aM were detected in whole blood using this approach, which has a remarkably wide linear range of approximately 7 orders of magnitude. Extracting target miRNAs from blood samples using magnetic core-shell nanoparticles requires a 30-min hybridization process, followed by a 5-min electrochemical measurement phase.

Liposomes are a type of carrier that can hold a significant quantity of signaling molecules, such as enzymes, fluorophores, and redox molecules. Chowdhury et al. [118] presented a fluorometric method to detect norovirus (NoV) by a newly developed fluorophore-labeled liposome and magnetically modified Fe_3O_4 combined system. Homogeneously distributed amine functionalized liposomes have been constructed and filled with a strong fluorophore of Calcein (Fig. 8a). Simultaneously, 3-aminopropyltriethoxysilane (APTES) functionalized Fe_3O_4 nanoparticles were also synthesized by standard silanization process, and these two separately synthesized nanoparticles were functionalized with antibodies to provide specificity. The Fe_3O_4 and Calcein-liposome systems have been applied for the NoV detection, which was magnetically separated from the analyte medium and then externally burst out to release the fluorophores from the core of the liposome. Ganganboina et al. [119] demonstrated a dual-modality sensing platform for ultrasensitive virus detection based on V_2O_5 nanoparticles-encapsulated liposomes (VONP-LPs). The sensing performance relies on intrinsic peroxidase and electrochemical redox properties of V_2O_5 nanoparticles (V_2O_5 NPs). The target-specific antibody-conjugated VONP-LPs and MNPs enrich the virus by magnetic separation. The separated VONP-LPs bound viruses are hydrolyzed to release the encapsulated V_2O_5 NPs (Fig. 8b). These released nanoparticles from captured liposomes act as peroxidase mimics and electrochemical redox indicators resulting in noticeable colorimetric and robust electrochemical dual signals. Utilizing the superiority of dual-modality sensors with two quantitative analysis forms, norovirus-like particles (NoV-LPs) can be detected by electrochemical signals with a wide linear range and low detection limit.

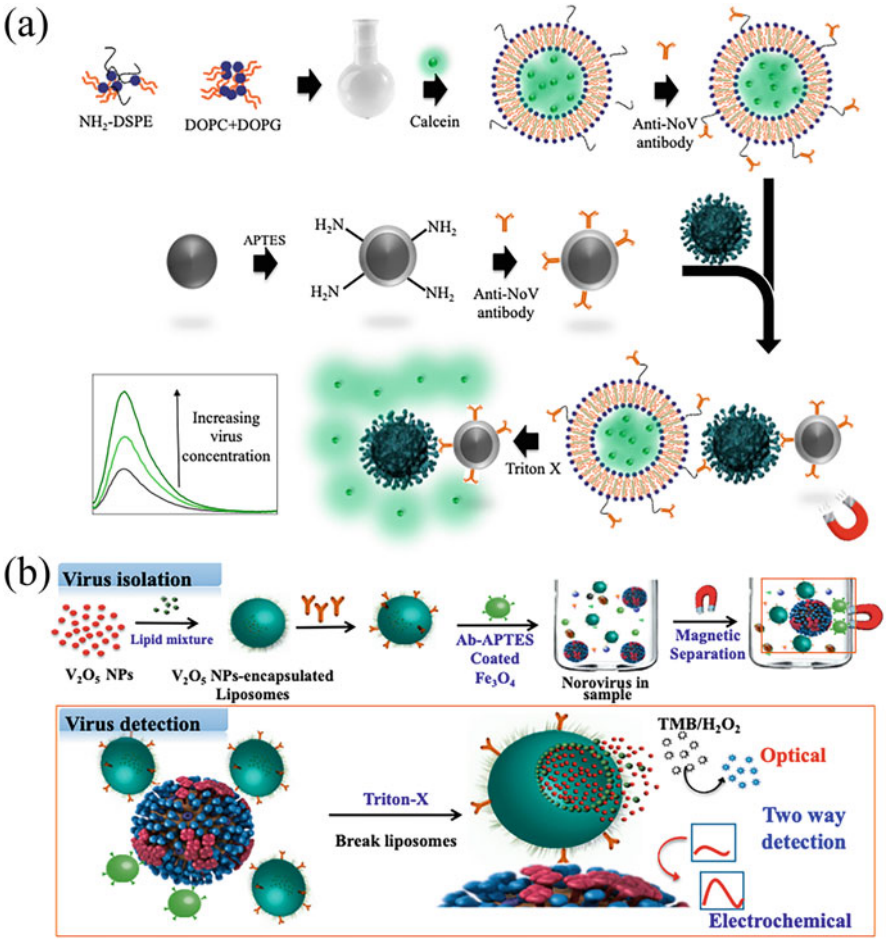

Fig. 8 Schematic representation of the (**a**) Calcein-liposome and Fe_3O_4 nanoparticles and the mechanism for the detection of NoV [118] (**b**) fabrication process of V_2O_5 NPs-encapsulated liposomes (VONP-LPs) and NoV detection principle [119]

4 Conclusions and Future Trends

Viral diseases pose a severe risk to the economy, the environment, and human health. The early detection of pathogenic virus is crucial to ensuring their absence. This study surveys recent detection developments, mainly focusing on biosensors and signal amplification techniques. Biosensors and signal amplification methods were compared and contrasted to provide a comprehensive resource for quickly and accurately detecting viral diseases. Furthermore, the detection time and sensitivity of the biosensors and signal amplification methods discussed in this article have been

impacted by various variables (such as human operation, detecting equipment, and environmental interference). Several approaches have fulfilled the analytical requirements for sensitivity and detection limits. However, a multistep approach is frequently required, and the biosensor is often only a portion of the experiment. More research is needed to combine the great practicability of lateral flow tests with accurate quantification.

Many scientists have worked hard to date to create new and improved methods of sensitive detection of the harmful virus. However, there are significant obstacles to screening for harmful viruses due to the often-low concentration of viruses in the screening samples. It is, therefore, crucial for the quick and sensitive identification of viruses that large-volume and complicated food samples be preprocessed. Using biosensors and signal amplification technologies, the next big thing in viral detection is the development of effective viral separation and enrichment technology for use with massive samples.

The fast progress of the biological sciences, information sciences, and materials sciences all point to exciting new possibilities for the future of biosensors as a multidisciplinary high-tech subject. To begin, biosensors may eventually get smaller and more complete. Medical diagnostics, food safety, and environmental surveillance sectors are just a few potential future applications of biosensors. In the future, biosensors will get even smaller because of developments in nanotechnology. The second is that in the near future, biosensors will be fully and intimately connected with computers, allowing for the collection and processing of data to be performed automatically, leading to more reliable scientific findings. Additionally, microfluidic technology will progressively enter the field of biosensors to accomplish the integration and integration of detecting systems. We anticipate increased biosensor efficacy due to the future refinement of essential technologies, including signal enrichment and processing, as well as the ongoing growth of a wide range of academic fields.

References

1. Kruk M, Gage A, Arsenault C, Jordan K, Leslie H, Roder-DeWan S, Adeyi O, Barker P, Daelmans B, Doubova S (2017) High-quality health systems in the sustainable development goals era: time for a revolution. Lancet Glob Health 6(11):e1196–ee252
2. Cesewski E, Johnson BN (2020) Electrochemical biosensors for pathogen detection. Biosens Bioelectron 159:112214
3. Zuccarello L, Barbosa C, Todorovic S, Silveira CM (2021) Electrocatalysis by heme enzymes—applications in biosensing. Catalysts 11(2):218
4. Kang T, Lu J, Yu T, Long Y, Liu G (2022) Advances in nucleic acid amplification techniques (NAATs): COVID-19 point-of-care diagnostics as an example. Biosens Bioelectron 206: 114109
5. Deshmukh SP, Patil S, Mullani S, Delekar S (2019) Silver nanoparticles as an effective disinfectant: a review. Mater Sci Eng C 97:954–965
6. Kikkert M (2020) Innate immune evasion by human respiratory RNA viruses. J Innate Immun 12(1):4–20

7. Ozer T, Geiss BJ, Henry CS (2019) Chemical and biological sensors for viral detection. J Electrochem Soc 167(3):037523
8. Younes N, Al-Sadeq DW, Al-Jighefee H, Younes S, Al-Jamal O, Daas HI, Yassine HM, Nasrallah GK (2020) Challenges in laboratory diagnosis of the novel coronavirus SARS-CoV-2. Viruses 12(6):582
9. Su L, Hu H, Tian Y, Jia C, Wang L, Zhang H, Wang J, Zhang D (2021) Highly sensitive colorimetric/surface-enhanced Raman spectroscopy immunoassay relying on a metallic core–shell Au/Au nanostar with clenbuterol as a target analyte. Anal Chem 93(23):8362–8369
10. Ramakrishnan SG, Robert B, Salim A, Ananthan P, Sivaramakrishnan M, Subramaniam S, Natesan S, Suresh R, Rajeshkumar G, Maran JP (2021) Nanotechnology based solutions to combat zoonotic viruses with special attention to SARS, MERS, and COVID 19: detection, protection and medication. Microb Pathog 159:105133
11. Ates HC, Yetisen AK, Güder F, Dincer C (2021) Wearable devices for the detection of COVID-19. Nat Electron 4(1):13–14
12. Khan I, Saeed K, Khan I (2019) Review nanoparticles: properties, applications and toxicities. Arab J Chem 12(2):908–931
13. Adam T, Gopinath SC (2022) Nanosensors: recent perspectives on attainments and future promise of downstream applications. Process Biochem 117:153–173
14. Mousavi SM, Hashemi SA, Yari Kalashgrani M, Omidifar N, Lai CW, Vijayakameswara Rao N, Gholami A, Chiang W-H (2022) The pivotal role of quantum dots-based biomarkers integrated with ultra-sensitive probes for multiplex detection of human viral infections. Pharmaceuticals 15(7):880
15. Ehtesabi H (2020) Application of carbon nanomaterials in human virus detection. J Sci Adv Mater Devices 5(4):436–450
16. Draz MS, Shafiee H (2018) Applications of gold nanoparticles in virus detection. Theranostics 8(7):1985
17. Song M, Yang M, Hao J (2021) Pathogenic virus detection by optical nanobiosensors. Cell Rep Phys Sci 2(1):100288
18. Zhao Z, Cui H, Song W, Ru X, Zhou W, Yu X (2020) A simple magnetic nanoparticles-based viral RNA extraction method for efficient detection of SARS-CoV-2. BioRxiv. https://doi.org/10.1101/2020.02.22.961268
19. Jose AD, Ghosh A (2022) Advances in nanomaterials-based biosensors for the development of virus detection. Advanced biosensors for virus detection. Elsevier, pp 203–217
20. Chambers JP, Arulanandam BP, Matta LL, Weis A, Valdes JJ (2008) Biosensor recognition elements. Curr Issues Mol Biol 10(1–2):1–12
21. Zhai J, Cui H, Yang R (1997) DNA based biosensors. Biotechnol Adv 15(1):43–58
22. Grieshaber D, MacKenzie R, Vörös J, Reimhult E (2008) Electrochemical biosensors-sensor principles and architectures. Sensors 8(3):1400–1458
23. Purohit B, Vernekar PR, Shetti NP, Chandra P (2020) Biosensor nanoengineering: design, operation, and implementation for biomolecular analysis. Sens Int 1:100040
24. Ganganboina AB, Dega NK, Tran HL, Darmonto W, Doong RA (2021) Application of sulfur-doped graphene quantum dots@ gold-carbon nanosphere for electrical pulse-induced impedimetric detection of glioma cells. Biosens Bioelectron 181:113151
25. Chowdhury AD, Ganganboina AB, Park EY, Doong R-A (2018) Impedimetric biosensor for detection of cancer cells employing carbohydrate targeting ability of Concanavalin A. Biosens Bioelectron 122:95–103
26. Ganganboina AB, Doong R-A (2019) Graphene quantum dots decorated gold-polyaniline nanowire for impedimetric detection of carcinoembryonic antigen. Sci Rep 9:7214
27. Hassen WM, Duplan V, Frost E, Dubowski JJ (2011) Quantitation of influenza A virus in the presence of extraneous protein using electrochemical impedance spectroscopy. Electrochim Acta 56(24):8325–8328
28. Lisdat F, Schafer D (2008) The use of electrochemical impedance spectroscopy for biosensing. Anal Bioanal Chem 391(5):1555–1567

29. Baek SH, Kim MW, Park CY, Choi C-S, Kailasa SK, Park JP, Park TJ (2019) Development of a rapid and sensitive electrochemical biosensor for detection of human norovirus via novel specific binding peptides. Biosens Bioelectron 123:223–229
30. Chowdhury AD, Takemura K, Li T-C, Suzuki T, Park EY (2019) Electrical pulse-induced electrochemical biosensor for hepatitis E virus detection. Nat Commun 10(1):3737
31. Zhang Z, Pandey R, Li J, Gu J, White D, Stacey HD, Ang JC, Steinberg CJ, Capretta A, Filipe CD (2021) High-affinity dimeric aptamers enable the rapid electrochemical detection of wild-type and B 1.1. 7 SARS-CoV-2 in unprocessed saliva. Angew Chem Int Ed Engl 60(45): 24266–24274
32. Tuan CV, Huy TQ, Hieu NV, Tuan MA, Trung T (2013) Polyaniline nanowires-based electrochemical immunosensor for label free detection of Japanese encephalitis virus. Anal Lett 46(8):1229–1240
33. Lai HC, Chin SF, Pang SC, Henry Sum MS, Perera D (2017) Carbon nanoparticles based electrochemical biosensor strip for detection of Japanese encephalitis virus. J Nanomater 2017: 3615707
34. Witt S, Rogien A, Werner D, Siegenthaler J, Lesiyon R, Kurien N, Rechenberg R, Baule N, Hardy A, Becker M (2021) Boron doped diamond thin films for the electrochemical detection of SARS-CoV-2 S1 protein. Diamond Relat Mater 118:108542
35. Kaushik A, Yndart A, Kumar S, Jayant RD, Vashist A, Brown AN, Li C-Z, Nair M (2018) A sensitive electrochemical immunosensor for label-free detection of Zika-virus protein. Sci Rep 8(1):9700
36. Martins G, Gogola JL, Budni LH, Janegitz BC, Marcolino-Junior LH, Bergamini MF (2021) 3D-printed electrode as a new platform for electrochemical immunosensors for virus detection. Anal Chim Acta 1147:30–37
37. Weltin A, Kieninger J, Urban GA (2016) Microfabricated, amperometric, enzyme-based biosensors for in vivo applications. Anal Bioanal Chem 408(17):4503–4521
38. Kheiri F, Sabzi R, Jannatdoust E, Shojaeefar E, Sedghi H (2011) A novel amperometric immunosensor based on acetone-extracted propolis for the detection of the HIV-1 p24 antigen. Biosens Bioelectron 26(11):4457–4463
39. Silva MM, Dias AC, Silva BV, Gomes-Filho SL, Kubota LT, Goulart MO, Dutra RF (2015) Electrochemical detection of dengue virus NS1 protein with a poly (allylamine)/carbon nanotube layered immunoelectrode. J Chem Technol Biotechnol 90(1):194–200
40. Mandli J, Attar A, Ennaji MM, Amine A (2017) Indirect competitive electrochemical immunosensor for hepatitis A virus antigen detection. J Electroanal Chem 799:213–221
41. Schanda J (2007) Colorimetry: understanding the CIE system. Wiley
42. Leow CH, Fischer K, Leow CY, Cheng Q, Chuah C, McCarthy J (2017) Single domain antibodies as new biomarker detectors. Diagnostics 7(4):52
43. Wu H-S, Chiu S-C, Tseng T-C, Lin S-F, Lin J-H, Hsu Y-F, Wang M-C, Lin T-L, Yang W-Z, Ferng T-L (2004) Serologic and molecular biologic methods for SARS-associated coronavirus infection, Taiwan. Emerg Infect Dis 10(2):305
44. Kogaki H, Uchida Y, Fujii N, Kurano Y, Miyake K, Kido Y, Kariwa H, Takashima I, Tamashiro H, Ling AE (2005) Novel rapid immunochromatographic test based on an enzyme immunoassay for detecting nucleocapsid antigen in SARS-associated coronavirus. J Clin Lab Anal 19(4):150–159
45. Chang Y-F, Chen R-C, Lee Y-J, Chao S-C, Su L-C, Li Y-C, Chou C (2009) Localized surface plasmon coupled fluorescence fiber-optic biosensor for alpha-fetoprotein detection in human serum. Biosens Bioelectron 24(6):1610–1614
46. Takemura K, Ganganboina AB, Khoris IM, Chowdhury AD, Park EY (2021) Plasmon nanocomposite-enhanced optical and electrochemical signals for sensitive virus detection. ACS Sens 6(7):2605–2612
47. Chowdhury AD, Nasrin F, Gangopadhyay R, Ganganboina AB, Takemura K, Kozaki I, Honda H, Hara T, Abe F, Park S (2020) Controlling distance, size and concentration of nanoconjugates for optimized LSPR based biosensors. Biosens Bioelectron 170:112657

48. Li Z, Yi Y, Luo X, Xiong N, Liu Y, Li S, Sun R, Wang Y, Hu B, Chen W (2020) Development and clinical application of a rapid IgM-IgG combined antibody test for SARS-CoV-2 infection diagnosis. J Med Virol 92(9):1518–1524
49. Nasrin F, Chowdhury AD, Ganganboina AB, Achadu OJ, Hossain F, Yamazaki M, Park EY (2020) Fluorescent and electrochemical dual-mode detection of chikungunya virus E1 protein using fluorophore-embedded and redox probe-encapsulated liposomes. Microchim Acta 187(12):674
50. Sohn M, Himmelsbach DS, Barton FE, Fedorka-Cray PJ (2009) Fluorescence spectroscopy for rapid detection and classification of bacterial pathogens. Appl Spectrosc 63(11): 1251–1255
51. Duan N, Wu S, Dai S, Miao T, Chen J, Wang Z (2015) Simultaneous detection of pathogenic bacteria using an aptamer based biosensor and dual fluorescence resonance energy transfer from quantum dots to carbon nanoparticles. Microchim Acta 182(5):917–923
52. Ganganboina AB, Chowdhury AD, Khoris IM, Doong RA, Li T-C, Hara T, Abe F, Suzuki T, Park EY (2020) Hollow magnetic-fluorescent nanoparticles for dual-modality virus detection. Biosens Bioelectron 170:112680
53. Allam Z, Jones DS (2020) On the coronavirus (COVID-19) outbreak and the smart city network: universal data sharing standards coupled with artificial intelligence (AI) to benefit urban health monitoring and management. Healthcare 8(1):46
54. Kargozar S, Mozafari M (2018) Nanotechnology and nanomedicine: start small, think big. Mater Today Proc 5(7):15492–15500
55. Saylan Y, Akgönüllü S, Yavuz H, Ünal S, Denizli A (2019) Molecularly imprinted polymer based sensors for medical applications. Sensors 19(6):1279
56. Hsieh B-Y, Chang Y-F, Ng M-Y, Liu W-C, Lin C-H, Wu H-T, Chou C (2007) Localized surface plasmon coupled fluorescence fiber-optic biosensor with gold nanoparticles. Anal Chem 79(9):3487–3493
57. Islam MA, Ahsan MZ (2020) Plausible approach for rapid detection of SARS-CoV-2 virus by magnetic nanoparticle based biosensors. Am J Nanosci 6(6):6–13
58. Tian B, Gao F, Fock J, Dufva M, Hansen MF (2020) Homogeneous circle-to-circle amplification for real-time optomagnetic detection of SARS-CoV-2 RdRp coding sequence. Biosens Bioelectron 165:112356
59. Srivastava M, Srivastava N, Mishra P, Malhotra BD (2021) Prospects of nanomaterials-enabled biosensors for COVID-19 detection. Sci Total Environ 754:142363
60. de la Escosura-Muñiz A, Baptista-Pires L, Serrano L, Altet L, Francino O, Sánchez A, Merkoçi A (2016) Magnetic bead/gold nanoparticle double-labeled primers for electrochemical detection of isothermal amplified Leishmania DNA. Small 12(2):205–213
61. Ganganboina AB, Doong RA (2018) Functionalized N-doped graphene quantum dots for electrochemical determination of cholesterol through host-guest inclusion. Microchim Acta 185(11):526
62. Zhang X, Guo Q, Cui D (2009) Recent advances in nanotechnology applied to biosensors. Sensors 9(02):1033–1053
63. Patel M, Agrawal M, Srivastava A (2022) Signal amplification strategies in electrochemical biosensors via antibody immobilization and nanomaterial-based transducers. Mater Adv 3: 8864–8885
64. Paramasivam G, Palem VV, Sundaram T, Sundaram V, Kishore SC, Bellucci S (2021) Nanomaterials: synthesis and applications in theranostics. Nanomaterials 11(12):3228
65. Léonard F, Talin AA (2011) Electrical contacts to one-and two-dimensional nanomaterials. Nat Nanotechnol 6(12):773–783
66. Ge J, Lei J, Zare RN (2012) Protein–inorganic hybrid nanoflowers. Nat Nanotechnol 7(7): 428–432
67. Moitra P, Alafeef M, Dighe K, Frieman MB, Pan D (2020) Selective naked-eye detection of SARS-CoV-2 mediated by N gene targeted antisense oligonucleotide capped plasmonic nanoparticles. ACS Nano 14(6):7617–7627

68. Chen Z, Zhang Z, Zhai X, Li Y, Lin L, Zhao H, Bian L, Li P, Yu L, Wu Y (2020) Rapid and sensitive detection of anti-SARS-CoV-2 IgG, using lanthanide-doped nanoparticles-based lateral flow immunoassay. Anal Chem 92(10):7226–7231
69. Xiang J, Yan M, Li H, Liu T, Lin C, Huang S, Shen C (2020) Evaluation of enzyme-linked immunoassay and colloidal gold-immunochromatographic assay kit for detection of novel coronavirus (SARS-Cov-2) causing an outbreak of pneumonia (COVID-19). MedRxiv. https://doi.org/10.1101/2020.02.27.20028787
70. Ma Q, Wang J, Li Z, Lv X, Liang L, Yuan Q (2019) Recent progress in time-resolved biosensing and bioimaging based on lanthanide-doped nanoparticles. Small 15(32):1804969
71. Banerjee R, Jaiswal A (2018) Recent advances in nanoparticle-based lateral flow immunoassay as a point-of-care diagnostic tool for infectious agents and diseases. Analyst 143(9): 1970–1996
72. Conyers SM, Kidwell DA (1991) Chromogenic substrates for horseradish peroxidase. Anal Biochem 192(1):207–211
73. Ganganboina AB, Khoris IM, Chowdhury AD, Li T-C, Park EY (2020) Ultrasensitive detection of the hepatitis E virus by electrocatalytic water oxidation using Pt-Co_3O_4 hollow cages. ACS Appl Mater Interfaces 12(1):50212–50221
74. Cooper GM (2000) The central role of enzymes as biological catalysts. Sinauer Associates
75. Dega NK, Ganganboina AB, Tran HL, Kuncoro EP, Doong R-A (2022) BSA-stabilized manganese phosphate nanoflower with enhanced nanozyme activity for highly sensitive and rapid detection of glutathione. Talanta 237:122957
76. Cass AE, Sharma S (2017) Microneedle enzyme sensor arrays for continuous in vivo monitoring. Methods in enzymology. Elsevier, pp 413–427
77. Ganganboina AB, Doong RA (2018) The biomimic oxidase activity of layered V_2O_5 nanozyme for rapid and sensitive nanomolar detection of glutathione. Sens Actuators B 273: 1179–1186
78. Lévy R (2006) Peptide-capped gold nanoparticles: towards artificial proteins. Chembiochem 7(8):1141–1145
79. Manea F, Houillon FB, Pasquato L, Scrimin P (2004) Nanozymes: gold-nanoparticle-based transphosphorylation catalysts. Angew Chem 43:6165–6169
80. Pasquato L, Pengo P, Scrimin. (2005) Nanozymes: functional nanoparticle-based catalysts. Supramol Chem 17(1–2):163–171
81. Singh S (2019) Nanomaterials exhibiting enzyme-like properties (nanozymes): current advances and future perspectives. Front Chem 7:46
82. Khoris IM, Kenta T, Ganganboina AB, Park EY (2022) Pt-embodiment ZIF-67-derived nanocage as enhanced immunoassay for infectious virus detection. Biosens Bioelectron 215: 114602
83. Gao L, Zhuang J, Nie L, Zhang J, Zhang Y, Gu N, Wang T, Feng J, Yang D, Perrett S (2007) Intrinsic peroxidase-like activity of ferromagnetic nanoparticles. Nat Nanotechnol 2(9): 577–583
84. Gao Y, Zhou Y, Chandrawati R (2019) Metal and metal oxide nanoparticles to enhance the performance of enzyme-linked immunosorbent assay (ELISA). ACS Appl Nano Mater 3(1): 1–21
85. Duan D, Fan K, Zhang D, Tan S, Liang M, Liu Y, Zhang J, Zhang P, Liu W, Qiu X (2015) Nanozyme-strip for rapid local diagnosis of Ebola. Biosens Bioelectron 74:134–141
86. Hsu Y-P, Li N-S, Chen Y-T, Pang H-H, Wei K-C, Yang H-W (2020) A serological point-of-care test for Zika virus detection and infection surveillance using an enzyme-free vial immunosensor with a smartphone. Biosens Bioelectron 151:111960
87. Weerathunge P, Ramanathan R, Torok VA, Hodgson K, Xu Y, Goodacre R, Behera BK, Bansal V (2019) Ultrasensitive colorimetric detection of murine norovirus using NanoZyme aptasensor. Anal Chem 91(5):3270–3276
88. Zhang T, Tian F, Long L, Liu J, Wu X (2018) Diagnosis of rubella virus using antigen-conjugated Au@ Pt nanorods as nanozyme probe. Int J Nanomedicine 13:4795

89. Mohamad A, Teo H, Keasberry NA, Ahmed MU (2019) Recent developments in colorimetric immunoassays using nanozymes and plasmonic nanoparticles. Crit Rev Biotechnol 39(1): 50–66
90. Oh S, Kim J, Tran VT, Lee DK, Ahmed SR, Hong JC, Lee J, Park EY, Lee J (2018) Magnetic nanozyme-linked immunosorbent assay for ultrasensitive influenza A virus detection. ACS Appl Mater Interfaces 10(15):12534–12543
91. Khoris IM, Ganganboina AB, Suzuki T, Park EY (2021) Self-assembled chromogen-loaded polymeric cocoon for respiratory virus detection. Nanoscale 13(1):388–396
92. Liu D, Ju C, Han C, Shi R, Chen X, Duan D, Yan J, Yan X (2021) Nanozyme chemiluminescence paper test for rapid and sensitive detection of SARS-CoV-2 antigen. Biosens Bioelectron 173:112817
93. Munnik P, de Jongh PE, de Jong KP (2015) Recent developments in the synthesis of supported catalysts. Chem Rev 115(14):6687–6718
94. Wu X, Chai Y, Zhang P, Yuan R (2015) An electrochemical biosensor for sensitive detection of microRNA-155: combining target recycling with cascade catalysis for signal amplification. ACS Appl Mater Interfaces 7(1):713–720
95. Chen J, Yu C, Zhao Y, Niu Y, Zhang L, Yu Y, Wu J, He J (2017) A novel non-invasive detection method for the FGFR3 gene mutation in maternal plasma for a fetal achondroplasia diagnosis based on signal amplification by hemin-MOFs/PtNPs. Biosens Bioelectron 91:892–899
96. Yan T, Zhu L, Ju H, Lei J (2018) DNA-walker-induced allosteric switch for tandem signal amplification with palladium nanoparticles/metal–organic framework tags in electrochemical biosensing. Anal Chem 90(24):14493–14499
97. Wang W, Bao T, Zeng X, Xiong H, Wen W, Zhang X, Wang S (2017) Ultrasensitive electrochemical DNA biosensor based on functionalized gold clusters/graphene nanohybrids coupling with exonuclease III-aided cascade target recycling. Biosens Bioelectron 91:183–189
98. Zhang C, He J, Zhang Y, Chen J, Zhao Y, Niu Y, Yu C (2018) Cerium dioxide-doped carboxyl fullerene as novel nanoprobe and catalyst in electrochemical biosensor for amperometric detection of the CYP2C19* 2 allele in human serum. Biosens Bioelectron 102:94–100
99. Liu S, Yang Z, Chang Y, Chai Y, Yuan R (2018) An enzyme-free electrochemical biosensor combining target recycling with Fe_3O_4/CeO_2@ Au nanocatalysts for microRNA-21 detection. Biosens Bioelectron 119:170–175
100. Kumar P, Deep A, Kim K-H (2015) Metal organic frameworks for sensing applications. Trends Anal Chem 73:39–53
101. Espallargas GM, Coronado E (2018) Magnetic functionalities in MOFs: from the framework to the pore. Chem Soc Rev 47(2):533–557
102. Ling P, Lei J, Ju H (2015) Porphyrinic metal-organic framework as electrochemical probe for DNA sensing via triple-helix molecular switch. Biosens Bioelectron 71:373–379
103. Ganganboina AB, Takemura K, Zhang W, Li T-C, Park EY (2021) Cargo encapsulated hepatitis E virus-like particles for anti-HEV antibody detection. Biosens Bioelectron 185: 113261
104. Khoris IM, Ganganboina AB, Park EY (2021) Self-assembled chromogenic polymeric nanoparticle-laden nanocarrier as a signal carrier for derivative binary responsive virus detection. ACS Appl Mater Interfaces 13(31):36868–36879
105. Kaur B, Malecka K, Cristaldi DA, Chay CS, Mames I, Radecka H, Radecki J, Stulz E (2018) Approaching single DNA molecule detection with an ultrasensitive electrochemical genosensor based on gold nanoparticles and cobalt-porphyrin DNA conjugates. Chem Commun 54(79):11108–11111
106. Grabowska I, Singleton DG, Stachyra A, Góra-Sochacka A, Sirko A, Zagórski-Ostoja W, Radecka H, Stulz E, Radecki J (2014) A highly sensitive electrochemical genosensor based on Co-porphyrin-labelled DNA. Chem Commun 50(32):4196–4199

107. Jolly P, Batistuti MR, Miodek A, Zhurauski P, Mulato M, Lindsay MA, Estrela P (2016) Highly sensitive dual mode electrochemical platform for microRNA detection. Sci Rep 6(1): 36719
108. Wang L, Ma R, Jiang L, Jia L, Jia W, Wang H (2017) A novel "signal-on/off" sensing platform for selective detection of thrombin based on target-induced ratiometric electrochemical biosensing and bio-bar-coded nanoprobe amplification strategy. Biosens Bioelectron 92: 390–395
109. Yuan Y-H, Wu Y-D, Chi B-Z, Wen S-H, Liang R-P, Qiu J-D (2017) Simultaneously electrochemical detection of microRNAs based on multifunctional magnetic nanoparticles probe coupling with hybridization chain reaction. Biosens Bioelectron 97:325–331
110. Deng K, Liu X, Li C, Huang H (2018) Sensitive electrochemical sensing platform for microRNAs detection based on shortened multi-walled carbon nanotubes with high-loaded thionin. Biosens Bioelectron 117:168–174
111. Gong D, Hui X, Guo Z, Zheng X (2019) The synthesis of PEI core@ silica shell nanoparticles and its application for sensitive electrochemical detecting mi-RNA. Talanta 198:534–541
112. Chen M, Gan N, Li T, Wang Y, Xu Q, Chen Y (2017) An electrochemical aptasensor for multiplex antibiotics detection using Y-shaped DNA-based metal ions encoded probes with NMOF substrate and CSRP target-triggered amplification strategy. Anal Chim Acta 968:30–39
113. Huang S, Gan N, Li T, Zhou Y, Cao Y, Dong Y (2018) Electrochemical aptasensor for multi-antibiotics detection based on endonuclease and exonuclease assisted dual recycling amplification strategy. Talanta 179:28–36
114. Chang J, Wang X, Wang J, Li H, Li F (2019) Nucleic acid-functionalized metal–organic framework-based homogeneous electrochemical biosensor for simultaneous detection of multiple tumor biomarkers. Anal Chem 91(5):3604–3610
115. Tunc I, Susapto HH (2020) Label-free detection of ovarian cancer antigen CA125 by surface enhanced Raman scattering. J Nanosci Nanotechnol 20(3):1358–1365
116. Miao X, Li Z, Zhu A, Feng Z, Tian J, Peng X (2016) Ultrasensitive electrochemical detection of protein tyrosine kinase-7 by gold nanoparticles and methylene blue assisted signal amplification. Biosens Bioelectron 83:39–44
117. Tavallaie R, McCarroll J, Le Grand M, Ariotti N, Schuhmann W, Bakker E, Tilley RD, Hibbert DB, Kavallaris M, Gooding JJ (2018) Nucleic acid hybridization on an electrically reconfigurable network of gold-coated magnetic nanoparticles enables microRNA detection in blood. Nat Nanotechnol 13(11):1066–1071
118. Chowdhury AD, Sharmin S, Nasrin F, Yamazaki M, Abe F, Suzuki T, Park EY (2020) Use of target-specific liposome and magnetic nanoparticle conjugation for the amplified detection of norovirus. ACS Appl Bio Mater 3(6):3560–3568
119. Ganganboina AB, Chowdhury AD, Khoris IM, Nasrin F, Takemura K, Hara T, Abe F, Suzuki T, Park EY (2020) Dual modality sensor using liposome-based signal amplification technique for ultrasensitive norovirus detection. Biosens Bioelectron 157:112169

Adv Biochem Eng Biotechnol (2024) 187: 413–442
https://doi.org/10.1007/10_2023_239

Published online: 26 January 2024

Progress on the Electrochemical Sensing of Illicit Drugs

Robin Van Echelpoel, Florine Joosten, Marc Parrilla, and Karolien De Wael

Contents

Abstract Illicit drugs are harmful substances, threatening both health and safety of societies in all corners of the world. Several policies have been developed over time to deal with this illicit drug problem, including supply reduction and harm reduction policies. Both policies require on-site detection tools to succeed, i.e. sensors that can identify illicit drugs in samples at the point-of-care. Electrochemical sensors are highly suited for this task, due to their short analysis times, low cost, high accuracy, portability and orthogonality with current technologies. In this chapter, we evaluate the latest trend in electrochemical sensing of illicit drugs, with a focus on detection of illicit drugs in seizures and body fluids. Furthermore, we will also provide an outlook on the potential of electrochemistry in wearable sensors for this purpose.

R. Van Echelpoel, F. Joosten, M. Parrilla, and K. De Wael (✉)
A-Sense Lab, UAntwerp, Antwerp, Belgium
e-mail: Karolien.DeWael@uantwerpen.be

Graphical Abstract

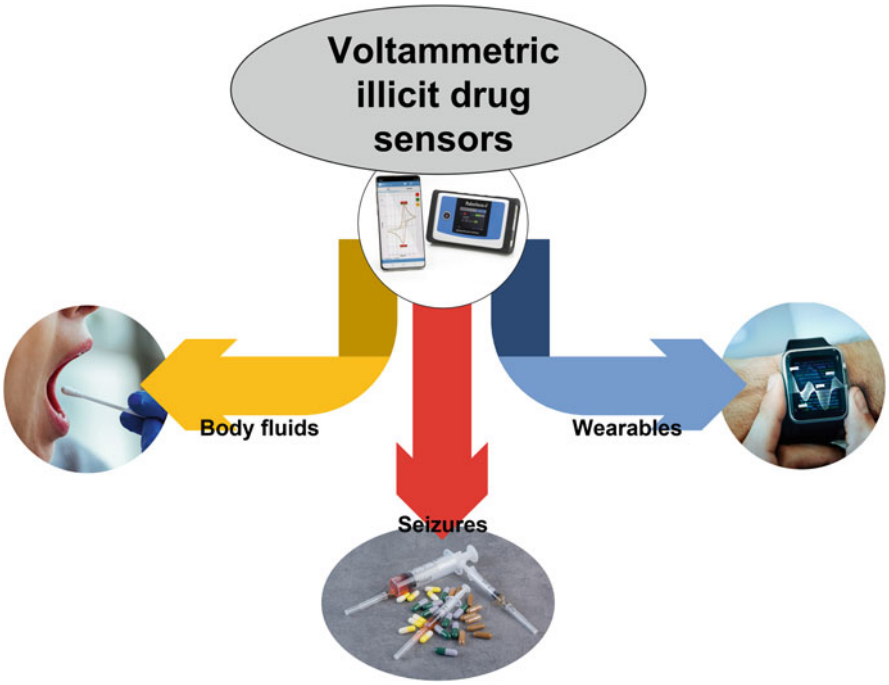

Keywords Drug seizures, Illicit drugs, Oral fluid detection, Voltammetric sensors, Wearable sensors

1 Importance of Illicit Drug Detection and Monitoring in Society

1.1 Detection in Drug Seizures

Illicit drugs are harmful substances, threatening both health and safety of societies in all corners of the world. Numerous statistics highlight the health-related risks, carefully listed each year in reports published by instances such as the United Nations Office on Drugs and Crime (UNODC) and European Monitoring Centre for Drugs and Drug Addiction (EMCDDA) [1, 2]. As an illustration, over half a million people died due to drugs in 2019, with drug use disorders resulting in 18 million years of healthy life lost [1]. Worryingly, statistics point out that these numbers are on the rise year after year, seemingly unaffected by the COVID-19

pandemic [3]. The aforementioned numbers are also reflected in the number of drug seizures, i.e. drug confiscations made by law enforcement personnel. In 2022, customs in Antwerp, one of the major entry ports for illicit drugs in Western Europe, seized a staggering 110 tons of cocaine [4]. Aside from the health risks, and sometimes overlooked, illicit drugs also bring safety hazards to our society. Think about violence between gangs that want control over the drug trade in an area, or the fact that drug use pushes people into poverty, making them more vulnerable to illicit practices [1].

In general, cannabis is the most used drug with 183 million consumers each year. This is followed by opioids and amphetamines with around 36 million users each year. Methylenedioxymethamphetamine (MDMA), opiates, and cocaine are next in line with approximately 20 million users each worldwide [5]. Specifically for Europe, cocaine is the second most used drug. Furthermore, new drugs and drug classes appear rapidly in a constant fight to beat the current legislation. Some important classes in this "designer drug" category are synthetic drugs such as cathinones, cannabinoids, and opioids [6].

Drugs appear in many forms and colors, often different forms of appearance exist for the same illicit drug. The most common appearance forms are resin, crystal, powder, liquid, pill, or blotter. Furthermore, due to their inherent illicit nature, many illicit drug's appearances are masked or altered by criminal organizations to circumvent detection by law enforcement. Additionally, licit cutting agents and adulterants, such as paracetamol or caffein, are sometimes added to illicit drugs to increase profits, mimic desired effects, or counter negative side effects.

The variety of effects induced by illicit drugs is enormous, and it is these effects that are sought after by the user. They can be categorized as stimulants, depressants, opioids, psychedelics, cannabinoids, dissociatives, and empathogens. Some drugs have no risk of dependence, others create mental dependence, and some even create physical dependence within the user [7].

It may be clear that illicit drugs are harmful, and it is no surprise that countless efforts have been done to deal with this problem. The classic approach to deal with illicit drugs is by attempting to limit the supply. Law enforcement is typically in charge of this task, and a common phrase is "the war on drugs." [8] Another approach, although less well known, is harm reduction. Here, it is acknowledged that people will use drugs, independent of legal status or price, and the objective is to limit the health-related risks of illicit drug use [9]. Determining the optimal approach is a task for policy makers. Nevertheless, it is clear that we as scientists can make a contribution by providing tools that allow both approaches to succeed in their goals.

One important example of such a tool is portable detection devices. They allow a user, typically a non-expert in science, to analyze a sample on the presence of an illicit drug, in a short time frame and on-site. If necessary, the suspicious sample is then sent to a laboratory for confirmation analysis by a gold-standard technique such as gas chromatography-mass spectrometry (GC-MS) or gas chromatography-flame ionization detection (GC-FID). Currently, the most frequently used on-site detection technologies are colorimetric tests and portable spectroscopic techniques.

Colorimetric tests target one specific drug or drug class. A change in color when coming into contact with the target confirms the presence of the drug (class) in the analyzed sample. A wide variety of tests exist, such as the Scott test for cocaine, Marquis test for MDMA, and the Mandelin reagent for ketamine. Overall, colorimetric tests are popular, especially in law enforcement, due to their high portability, ease of use, and low cost. However, their accuracy, sensitivity, and specificity are rather low, as shown by Shanmugam et al., commonly hindered by cutting agents, adulterants, and a difficult visual interpretation [10]. Another validation study was performed by de Jong et al., describing a sensitivity of 68% for the cocaine Scott color test [11]. It may be clear that colorimetric tests are prone to false positives and negatives when cutting agents or adulterants are present, which is very often the case.

Portable spectroscopic techniques, such as portable Fourier-transformed infrared (FTIR) and Raman devices, allow the recording of a spectrum which is then compared with a large internal library of spectra to find a match. FTIR devices can be considered portable; however, they remain quite bulky and their portability is hardly comparable to color tests or portable Raman devices. Attenuated total reflection FTIR (ATR-FTIR) is commonly used since it allows direct FTIR analysis without difficult sampling procedures, i.e. the sample (powder, liquid, crystal, etc.) simply needs to be placed below an ATR crystal. Nevertheless, a stable benchtop is required, and preferably lab conditions. This positions the technology between a pure on-site sensor and a lab-based sensor. Intrinsically, the ATR-FTIR technology has the potential to reach high accuracies, owing to a combination of good reproducibility and spectral features that are unique for individual compounds. However, the spectra interpretation strongly depends on the detection algorithm that is used. Since the detection algorithm is commonly a matching algorithm that compares the recorded spectrum with a database of spectra, the accuracy greatly depends on the quality of the database (TICTAC library for illicit drug detection). Furthermore, this task is greatly complicated in illicit drug detection by the often complex mixtures encountered in the field. Portable Raman devices have the same operating principle as ATR-FTIR, a Raman spectrum is recorded, and a library search algorithm is employed to find a match between the recorded spectrum and a spectrum in the TICTAC library. Contrary to ATR-FTIR, the portable Raman is highly portable, with a weight of approximately 1.5 kg. Additionally, the Raman device uses a laser for its spectrum recording, which allows for non-invasive sampling. Nevertheless, the same burdens as for ATR-FTIR affect the accuracy, and additionally, fluorescence has a negative impact on the accuracy as well, particularly if colored samples are involved. The latter brings down the overall accuracy considerably since many illicit drug samples are colored, be it for commercial purposes (e.g., ecstasy pills) or smuggling purposes (e.g., cocaine or heroin samples).

1.2 Detection in Body Fluids

It is widely known that drug abuse can have severe health consequences and can lead to death. In 2019, over half a million people died from overdoses and drug use disorders [12]. In both the United States of America (USA) and Europe, opioids were the main contributor to overdose deaths [13, 14]. In the USA, the Health and Human Services declared a national opioid epidemic, urging the country to tackle this crisis in 2017 [15]. As described above, one possible approach to overcome the opioid crisis, and the issue of illicit drug abuse in general is harm reduction. A pivotal aspect of this approach is the rehabilitation of drug users. While traditionally the analysis of illicit drugs in body fluids was performed to establish the cause of death in suspected overdoses and poisonings [16], it is nowadays also performed in rehabilitation centers. Additionally, testing body fluids for illicit drugs can play an important role in several aspects of forensic casework. The use of cocaine, opiates, and hallucinogens can induce violence, requiring police officers to test suspects on drug use [17]. Additionally, victims of sexual assault may be screened for the presence of date-rape drugs, such as benzodiazepines, ketamine, and gamma-hydroxybutyrate (GHB) [18]. Finally, roadside drug testing may be performed in suspected cases of driving under the influence of a drug.

Depending on the purpose of the drug test, several different body fluids can be analyzed. Post-mortem investigations, to establish the cause of death, usually involve the use of blood, urine, or vitreous humor [19]. Blood analysis may also be used in hospitals in case of suspected overdose where the patient is unable to speak. In rehabilitation centers, urine drug testing is employed to monitor patients in order to ensure they abstain from using [20]. Here, the advantage of urine testing is that it offers a wider detection window than blood and can be collected more easily. Even though in toxicological analysis, blood is the gold standard, it only allows for the detection of drugs and their metabolites for 24–48 h [18]. As sexual assault victims often take a longer time to report the attack, urine testing or hair analysis, which offers longer time frames for the detection, can be used [18]. Additionally, the collection of blood samples is more difficult outside the hospital. In recent years, oral fluid has become the preferred matrix of choice for roadside drug testing over urine [21]. Oral fluid provides a better indication of impairment as this matrix might reflect recent drug use. Moreover, oral fluid collection can easily be performed on-site under the supervision of a police officer without privacy concerns, contrary to the collection of urine. The use of oral fluid as a matrix makes the testing procedure easier for law enforcement, which drastically increases the number of performed roadside controls.

Similar to the detection of drugs in seizures, the gold-standard techniques for analytical toxicology continue to be liquid chromatography or gas chromatography (LC- or GC-MS) [22]. Unfortunately, these techniques are time-consuming (hours), expensive (starting at €100,000 for the entire system), and do not allow for on-site drug detection. However, in many cases, on-site drug detection in body fluids could aid in rapid decision making or prove more practical. Currently, the most widely

used on-site detection technique in biofluids is the lateral flow immunoassay (LFA) [23]. While LFAs are indeed practical for the detection on-site, they also exhibit some drawbacks: (i) lack of specificity from cross-reactivity with similar chemicals; (ii) time-consuming (>5 min); (iii) expensive (ca €25); and (iv) short shelf-lives due to the use of bioreceptors [24].

2 Current Trends in Electrochemical Sensing of Illicit Drugs

2.1 Electrochemical Sensors for Illicit Drug Detection in Seizures

Today, the majority of electrochemical sensors employ voltammetric techniques to gather the analytical output. Normally, a voltammetric profile is obtained by scanning a potential on the working electrode in a conventional three-electrode system. When there is the presence of the illicit drug in the sample, and thus at the surface of the working electrode, and the oxidation potential corresponding to the illicit drug is reached at the electrode, a current flows and an oxidation or reduction peak is depicted on the user interface [25]. This profile is characteristic for each electroactive illicit drug and adulterant (i.e., it depends on the structure and functionalities of the molecule) which allows for the discrimination between compounds and its quantification, as the peak intensity is dependent on the concentration of the analyte. Interestingly, the pH of the buffer solution has an impact on the electrochemical profile, e.g. the illicit drug MDMA has one anodic signal (around +1.10 V) in a pH 5 buffer, and three anodic signals (around +0.80 V, +0.95 V & +1.20 V) in a pH 12 buffer (Fig. 1) [10]. The origin of these oxidation peaks can be related to the presence of specific functional groups in the structure of the compounds. Van Echelpoel et al. investigated the electrochemical profile of MDMA and related the signal visible in

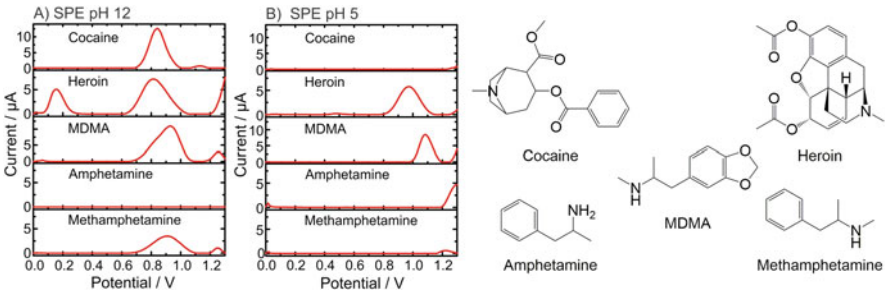

Fig. 1 Electrochemical profiles of the illicit drugs cocaine, heroin, MDMA, amphetamine, and methamphetamine in pH 12 and pH 5 buffer, recorded at unmodified screen-printed electrodes. The chemical structures of the illicit drugs are depicted on the right side of the figure

the pH 5 buffer to the oxidation of the methylenedioxy group [26]. The additional signals, visible in the pH 12 buffer, are related to oxidation of the secondary amine of MDMA. Absence of an electroactive functional group can lead to a chemical profile without oxidation signals, as is exemplified by amphetamine. Besides this concentration and pH influence, compounds present together sometimes influence each other's electrochemical signals. As an example, the local anesthetic benzocaine is known to shift the signal of cocaine to lower potentials in a pH 12 buffer [27]. Overall, the aforementioned behavior leads to a complex picture of electrochemical profiles that hold a wealth of information on the measured analyte(s). Building a library of peak potentials or electrochemical profiles and linking this library with advanced chemometric tools allows for the qualitative and/or quantitative determination of illicit drugs in unknown samples.

Typically, the operation of an electrochemical illicit drug sensor has several characteristic steps. First, a few milligrams of the suspicious samples is dissolved in a few milliliters of buffer solution. As discussed before, drugs appear in different forms (e.g., powder, liquid, etc.), and thus slightly different sampling procedures have to be developed to bring the illicit drug sample into the solution. Some unusual samples, such as in blotter or even impregnated in clothing, require additional sampling steps [28]. Additionally, if the illicit drug has low solubility in aqueous solutions (e.g., heroin), a small amount of organic solvent such as ethanol should be added to dissolve the sample. In general, low detection limits (μM) can be reached with electrochemical sensors, requiring thus little sample amount for identification. Further information on the strategies are described in the following sections. The buffer solution contains supporting electrolytes and ensures a constant pH. The type of buffer solution (e.g., phosphate buffer saline, acetate buffer, etc.) and pH of the buffer influence the electrochemical output, making it an important asset to allow diversification between target analytes. Choosing a favorable buffer is an important step in developing a successful electrochemical illicit drug sensor. Typically, a buffer solution has a stability of 3–6 months, which is something to consider when researching illicit drugs, as well as when bringing the technology to the market.

Second, a few droplets of the resulting solution are placed on the surface of a screen-printed electrode (SPE). The low cost and ease-of-use character of SPEs are some of the major contributors to the success of electrochemical sensors. A three-electrode configuration with a working, counter, and reference electrode is generally employed. Figure 2 shows different components of an SPE, on the left, the typical three-electrode system is shown, and on the right the different layers. The type of substrate (e.g., plastic, ceramic, or paper) and conductive ink influence the electrochemical output of the measurement. The reference electrode is usually made with silver ink, whereas the auxiliary/counter and working electrode are made from carbon-based inks [29]. The electrodes are printed on a substrate and covered with dielectric ink. Various types of conductive materials can be employed at the working electrode such as platinum [30]. Importantly, the nature of the screen-printed ink (which might vary depending on the supplier) can affect the electrochemical performance of the sensor. This favorably creates several additional variables that allow for optimization toward a specific target drug. At the same time, good control over the

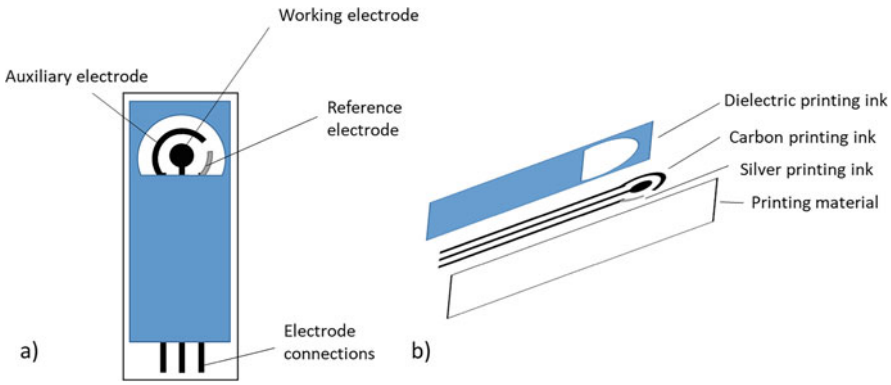

Fig. 2 Overview of the three-electrode system (**a**) and different layers (**b**) of a screen-printed electrode

quality of the SPE production process, short and long term, is required to ensure good reproducibility and reliability of the electrochemical illicit drug sensor. This is an important aspect to consider when designing strategies for real applications in the field.

Interestingly, the surface of the working electrode of the SPE can be modified with a large variety of compounds, altering the electrochemical output, improving detection limits, and in general facilitating an improved detection performance [31]. The improved detection performance is a major asset; however, the long incubation times and complex manufacturing process should not be overlooked, especially when considering bringing the technology to the market (higher cost and cumbersome quality control). Depending on the type of modification, a distinction can be made between chemical sensors (e.g., modified with polymers, ionic liquids, or nanoparticles) and biosensors (Fig. 3) (modified with enzymes, antibodies, or nucleic acids). Polymers, and molecularly imprinted polymers (MIPs) in particular, are artificial highly cross-linked polymeric receptors that are engineered toward the binding of specific analytes, in this case, illicit drugs [32]. Due to their high selectivity and excellent LOD in the μg L^{-1}-range, these sensors tend to be able to detect the illicit drugs in biofluids as well [33]. Akhoundian et al. employed a combination of nano-sized MIPS with multi-walled carbon nanotubes (MWCNTs) to perform ultra-trace detection of methamphetamine in biological samples [34]. Nanoparticles are another type of modification that is commonly employed, Zhang et al., for example, used Pt nanoparticles for the simultaneous detection of morphine and MDMA in biological samples [35]. Gold nanoparticles (modified exfoliated graphite electrode) are also employed, Masemola et al. successfully detected cocaine, heroin, amphetamine, 6-acetylmorphine, and methylphenidate using this strategy [36]. Furthermore, several other types of modifications can be used, such as graphene and multi-walled carbon nanotubes [37] aptamers [38] and ionic liquids [39].

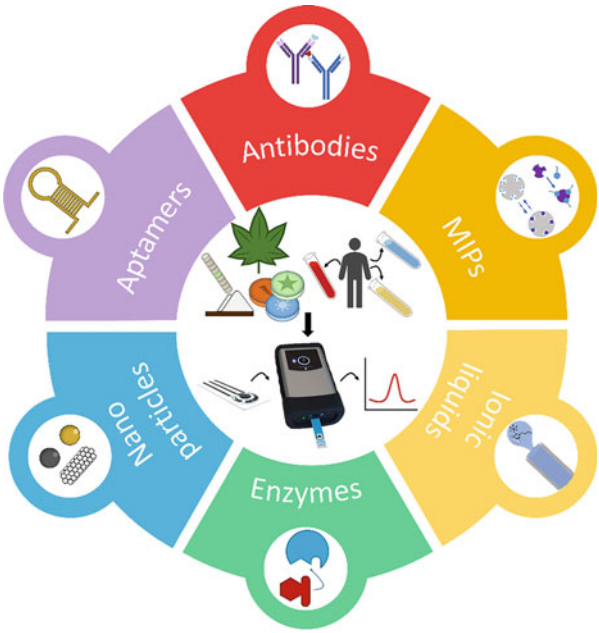

Fig. 3 Workflow of electrochemical sensors for the detection of illicit drugs in seizures and biological fluids, and overview of strategies to enhance sensor performance

2.1.1 Voltammetric Techniques

The SPE itself is inserted in a potentiostat that controls the electrochemical measurement. Typically, one of the following electrochemical techniques is used in electrochemical illicit drug sensors: cyclic voltammetry (CV) [40], square-wave voltammetry (SWV) [41], cyclic SWV [42], or differential pulse voltammetry (DPV) [43]. CV is usually employed to understand the electrochemical behavior of the analyte on the sensor (e.g., study the reversibility of the redox process). SWV and DPV are voltammetric techniques normally used for analytical purposes. Clearly, the electrochemical output will differ based on the employed technique and set of electrochemical parameters, again providing an opportunity to optimize the sensor toward a specific target drug. The choice of technique and parameters will depend on, e.g., the need for reductive and oxidative scan, time of response, or complexity of the voltammetric scan leading to higher or lower sensitivities and enhanced limit of detections (LODs). SWV and DPV are usually employed for the electrochemical detection of illicit drugs due to their low background currents (low contribution of the non-faradaic currents in the output signal) thus exhibiting higher sensitivities and better LODs. These features are mainly caused by the wave form of the applied voltammetric scan. The potentiostat is typically connected to a measuring device (computer, tablet, or smartphone) via cable or Bluetooth, which contains software that allows control over the measurement (parameters).

2.1.2 Software

The identification software can be integrated with the measurement software to perform an analysis of the electrochemical output data [41]. Such identification software makes the sensor accessible to non-expert end-users. Typically, some preprocessing steps (e.g., baseline correction) are employed, followed by pattern recognition approaches, although electrochemical fingerprint-based peak recognition approaches are also used [44]. Integrating the measurement and identification software into a user-friendly (mobile) application makes the technology fully usable by the non-expert target audience and as such bridges the gap between lab and real use.

SPEs as a point of test for illicit drugs have been used for the direct detection of cocaine [28], heroin [45], ketamine [46], MDMA [47], synthetic cathinones [48, 49], and many other illicit drugs [50, 51]. Here, a single drug is targeted, and it typically suffices to measure at a single SPE to get enough electrochemical information to identify the targeted drug. However, when expanding an electrochemical sensor to target multiple illicit drugs, a single SPE might not allow diversification between the targeted drugs and electroactive adulterants (e.g., overlapping signals). Relief is provided here by means of array approaches, that is, the combination of multiple, (different) SPEs, coupled with specific algorithms [52, 53]. It is important that the same sample is recorded under different conditions, providing diverse electrochemical profiles, resulting in an increased opportunity to diversify between the target compounds. These different conditions can be provided by employing different buffers [54, 55], electrode modifications [53, 56] or by employing electrode pretreatments [32, 41]. Van Echelpoel et al. reported a very nice demonstration of the array possibilities with a dual SPE array that allows simultaneous electrochemical detection of cocaine, heroin, ketamine, and MDMA in seizures. They developed dedicated software that interprets the combined EFs (coined a superfingerprint), recorded at two different electrodes with different measuring conditions (PBS7 buffer with formalin derivatization and PBS12 buffer) [54].

Overall, since there is no ideal technique available, there is an opportunity for electrochemistry to enter the on-site illicit drug detection field and make a difference. Electrochemical sensors have proven to reach good accuracies, with short analysis times while remaining inexpensive [25].

2.2 Electrochemical Sensors for Drug Detection in Body Fluids

Due to their high selectivity and sensitivity, versatility, portability, and simplicity of use, electrochemical sensors could show a promising alternative to LFAs for on-site testing in body fluids. The detection of illicit drugs in body fluids comes with new challenges compared to the detection in seizures, of which the first is the lower limits of detection required. For roadside drug testing purposes, analytical cut-off values

are in the low ng/mL range (low nM range) [57]. This requires increased efforts from the electrochemist to further enhance the electrochemical signals from the illicit drug detection. Different strategies to reach low LOD for illicit drugs in body fluids have been reported in the literature [23, 58]. Several studies involved the use of antibodies [59], aptamers [38], and MIPs [60].

Concerning the recognition elements mostly used for the analysis of biofluids, antibodies have been widely explored due to their high specificity toward the analyte of interest. Hence, the detection of cocaine abuse by employing antibodies selective to benzoylecgonine (i.e., a metabolite after cocaine intake) has been reported [61]. Depending on the region of an antigen that binds with an antibody, which is called the epitope, antibodies can be divided into two categories [62]. Monoclonal antibodies bind only one epitope and are thus more specific, resulting in decreased chances of cross-selectivity. Polyclonal antibodies, on the other hand, can interact with more than one epitopes. As a result, polyclonal antibodies may be more suitable when detecting a class of drugs instead of one specific drug. In electrochemical immunosensors, the antibodies are immobilized onto the surface of the working electrode. When these antibodies bind the target analyte, a stable complex is formed and the electrical signal generated during this binding event is measured. This signal usually originates from a catalytic reaction of an enzyme labeled as a signal tracer with the detection antibody [63].

Drug	Antibody	Matrix	LOD (μM)	Reference
Cocaine	scFv anti-cocaine GNC92H2	OF, S, Sw, U	12×10^{-3}	[64]
	Monoclonal anti-BZE (clone 2, ABCOC-0402)	OF[a], U[a]	0.41	[61]
	Monoclonal anti-BZE (clone IP3G2)	OF, U	3.3×10^{-6}	[59]
	Polyclonal sheep anti-cocaine (PAS10174)	OF, S, U	OF: 3.0×10^{-4} S: 2.1×10^{-4} U: 12×10^{-4}	[65]
Heroin	Morphine antibody	S	7.3×10^{-10}	[66]
	Monoclonal morphine antibody	OF, U	OF: 2.4×10^{-4} U: 3.2×10^{-6}	[67, 68]
Amphetamine	Amphetamine antibody from Syva EMIT II kit	U	2.5	[69]
Methamphetamine	Monoclonal anti-methamphetamine	U	1.3	[70]
	Anti-methamphetamine	B S[a]	7.5×10^{-3} 1.6×10^{-8} μmol	[71, 72]
	Methamphetamine antibody (Arista biologicals)	OF[a], U[a], S[a]	88	[73]

(continued)

Drug	Antibody	Matrix	LOD (μM)	Reference
	Methamphetamine antibody ABMET-0400 (Arista biologicals)	OF	PBS: 3.8×10^{-3} OF: 4.8×10^{-3}	[74]
MDMA	Antibody raised against methylenedioxy moiety of MDA-BSA conjugate	OF, U	OF: 5.3×10^{-3} U: 9.8×10^{-4}	[75]
THC	Monoclonal anti-THC	U	2.3×10^{-5}	[68]
Ketamine	Ketamine antibody	H	5.73 pg/g	[76]
	Anti-ketamine (Hangzhou Clongene Biotech Co., Ltd.)	P	PBS: 2.8×10^{-4}	[77]
	Ketamine antibody (Fankel Co. Ltd.)	S	0.41×10^{-6}	[78]

Abbreviations: B = blood; BZE = benzoylecgonine; H = hair; LOD = limit of detection; MDMA = 3,4-methylenedioxymethampetamine; OF = oral fluid; P = plasma; PBS = phosphate-buffered saline; S = serum; scFv = [X]; Sw = sweat; THC = tetrahydrocannabinol; U = urine

[a] Synthetic biofluids

Aptamers have recently been a promising recognition element due to their higher stability than antibodies [79]. Additionally, it is possible to regenerate aptamers without loss of selectivity and integrity [80]. To achieve immobilization of the aptamer at the working electrode, thiol groups are often added to an aptamer so that it can bind a gold surface. Importantly, aptamers allow their easy modification with redox probes which can provide direct output during the interaction with the analyte of interest [81]. Upon binding of the target analyte, a conformational change of the aptamer takes place which brings the redox probe closer or further away from the electrode surface [80]. This change in distance between the redox probe and the electrode surface results in a change of the redox current. However, it is essential to characterize the chemical interaction between the aptamer and the target before using the aptamer as the recognition element [82]. In this direction, aptamers have been used for the detection of cocaine [83], including their embodiment in gold nanoclusters to enhance the analytical properties [84].

Drug	Aptamer	Matrix	LOD (μM)	Reference
Cocaine	5′-C_6-NH_2-AGACAAGGAAA-ATCCTTCAATGAAGTGGG-TCG-SH_2-3′	S OF[a], U[a]	0.5×10^{-6} to 150×10^{-6} 1.5×10^{-3}	[85–90]
	5′-CCATAGGGAGACAAGG-ATAAATCCTTCAATGAAG-TGGGTCTCCC-3′	S	273×10^{-6} 136×10^{-6}	[83, 91]
	CoS: 5′-HO-$(CH2)_6$-S-S-$(CH_2)_6$-TTCGTTCTTCAAT-GAAGTGG-	S	0.02	[92]

(continued)

Drug	Aptamer	Matrix	LOD (μM)	Reference
	GACGACA-3′ CoB: 5′-GGGAGTCAAGAA-CGAA-biotin-3′			
	SH-C2: 5′-HS-$(CH2)_6$-TTTTT-GGGAGTCAAGAACGAA-3′ C1: 5′-TTCGTTCTTCAATG-AGTGGGACGACA-3′	OF, P, S, U	0.1	[93]
	5′-ferrocene-GACAAGGAAA-ATCCTTCAATGAAGTGGG-TC-3′	S	32×10^{-6}	[94]
	5′-GGCGACAAGGAAAATC-CTTCAACGAAGTGGGTCG-CC-3′	S	15×10^{-6}	[95]
	5′-GGGAGACAAGGATAAA-TCCTTCAATGAAGTGGGT-CTCCC- $(CH_2)_3$-SH-3′	S	0.3	[96]
	5′-GGGAGACAAGGATAAA-TCCTTCAATGAAGTGGGT-CTCCC- $(CH_2)_6$-SH-3′	S	0.3×10^{-3}	[97]
Heroin	–			
Amphetamine	5′-(HS)-$(CH_2)_6$-ACGGTTGC-AAGTGGGACTCTGGTAGG-CTGG-GTTAATTTGG-3′	U	0.51×10^{-3}	[98]
Methamphetamine	5′-SH-C_6-AGGAATTCAGAT-CTCCCTGCAGGTGGTGTTT-TTTTTGTGTGCTGTGTTTTT-GTGATGCATGCTCGAGGA-GCTCAGGATCCCG-3′	U[a]	3.13×10^{-3}	[99]
	5′-CGGTTGCAAGTGGGACT-CTGGTAGGCTGGGTTAATT-TG-3′	50% OF, S, U	OF: 20×10^{-3} S: 30×10^{-3} U: 50×10^{-3}	[100]
MDMA	–			
THC	HOC_6-S-S-5′-TGTCACATCTA-CACTGCTCGAAGGTCTTTC-GTATTTGCATTCCTCTCTTC-TTCATTTCGAGCAATTCAG-ACAGCGTTCCC-3′	OF	PBS: 1×10^{-3} OF: 5×10^{-3}	[101]
Ketamine	–			

Abbreviations: B = blood; LOD = limit of detection; MDMA = 3,4-methylenedioxymethampetamine; OF = oral fluid; P = plasma; PBS = phosphate-buffered saline; S = serum; THC = tetrahydrocannabinol; U = urine

[a] Synthetic biofluids

Finally, MIPs are an interesting approach as they are based on synthetic recognition elements, usually highly stable, with the potential to be included in the conductive ink to manufacture sensors at large scale. MIPs have been designed for the detection of ketamine and incorporated in a modified SPE for the analysis of

serum and saliva samples. Importantly, the research article described a very low LOD of only 400 fM [102].

The second challenge is the detection of metabolites. In several cases, the detection of the parent drug will not suffice for the determination of drug use. For example, the illicit drug heroin is quickly metabolized in the human body to 6-monoacetylmorphine (6-MAM) and morphine [103]. Therefore, the measurement of these metabolites is pivotal in the analysis of heroin in body fluids. Several studies have been performed on the voltammetric detection of the metabolites of cocaine [104], morphine [105], heroin [106], codeine [107], and amphetamine-type stimulants (ATS) [108]. However, these studies focus on the detection in buffer solution and not in the biofluid matrices.

This brings us to the third, and perhaps the largest, challenge which is the matrix effects that the body fluids may have on the electrochemical signals for the illicit drugs. Blood consists of approximately 55% blood plasma and 45% blood cells, such as red blood cells, white blood cells, and platelets [109]. In blood analysis, three different types of blood matrices can be used: whole blood, plasma, and serum. Both plasma and serum are obtained from whole blood. Both plasma and serum are acquired after the removal of cells, but while serum is obtained from blood after it has coagulated (or clotted), plasma is what remains after the addition of an anticoagulant [110]. More than 90% of the plasma matrix consists of water, with the other 10% made up of dissolved compounds [109]. These compounds include proteins, sugars, hormones, vitamins, and nitrogen-containing substances such as creatinine, uric acid, and urea [111]. According to Sviridov and Hortin, urine is a more complex matrix than serum and plasma in regard to matrix effects as it has a more variable composition [112]. Urine can contain proteins, uric acid, phenylacetylglutamine, and hippuric acids. Importantly, the amount of fluid that a person drinks and their diet can have a significant effect on the concentrations present. Oral fluid is a complex heterogeneous mixture containing over 1,000 different proteins, electrolytes, and small organic compounds and is rich in antioxidants [113–115]. Additionally, it can contain exogenous compounds present in food, drinks, or the use of therapeutic drugs.

The composition of the biofluids must be well understood as compounds present in these matrices can be electroactive and overlap with the electrochemical signals for the illicit drugs and their metabolites targeted in drug tests. Unfortunately, little research is performed on which components in body fluids are electroactive under the experimental conditions used for illicit drug detection. The importance of this type of research was highlighted by two studies that have shown that the presence of uric acid and albumin in the oral fluid matrix may result in peaks around +0.1 V and +0.5 V v. Ag/AgCl, respectively [116, 117]. The electrochemical signal for albumin overlapped with the potential window of the drug 4-chloro-alpha-pyrrolidinovalerophenone (Cl-PVP), thus hindering its detection at SDS/SPE. For a more detailed review of the use of cyclic voltammetry in biological samples for clinical settings, the reader is referred to the work of Wang et al. [118]. A possible solution to overcome the overlapping of signals from the matrix would be to remove the interfering compounds before analysis through filtration or centrifugation.

However, this could be challenging during on-site testing. Therefore, another option would be the use of data treatment methods such as digital filters or principal component analysis (PCA) [44, 119]. Besides the overlapping with drug signals, compounds present in the biomatrices might also cause the suppression of the drug signal. For example, the presence of the cutting agent levamisole has been demonstrated to suppress the cocaine signal [120]. To tackle this issue, De Jong et al. proposed a dual pH strategy. By measuring the cocaine signal at both pH 7 and pH 12 it was possible to detect cocaine in presence of this interferent. The use of such strategies may also prove useful in case components of the biofluid matrices are found to suppress the electrochemical drug signals. Suppression of the signals for illicit drugs can also be caused by biofouling. It is well known that the presence of proteins in biomatrices leads to biofouling of electrochemical sensors, due to the non-specific adsorption on the electrode's surface [121]. This can lead to a lowered performance of electrochemical sensors and loss in sensitivity and specificity for the target analyte. The effect of albumin biofouling has been studied for the electrochemical detection of cocaine [117]. Here, it was shown that increased amounts of the protein resulted in lower signals for the illicit drug. Multiple strategies to mitigate the biofouling effects have been discussed in the review by Russo et al. including (i) antifouling coatings, (ii) hydrogels, (iii) nanoengineered surfaces, and (iv) nanoporous membranes [121].

To overcome the biofouling issue, a lubricin coating has been deposited on SPE to avoid protein adsorption and allow the detection of clonazepam in saliva [122]. This approach is interesting as it allows small molecules to diffuse to the electrode's surface while blocking proteins to adsorb, thus keeping a similar analytical performance as in regular buffer solutions. Besides, the use of reduced graphene oxide enabled the nanomolar detection of the drug of abuse.

In summary, antibodies offer high selectivity and specificity but are expensive which hinders the multiplexing capability. Aptamers are a good alternative to antibodies offering lower costs but potentially lower specificity. However, validation of the binding capacity of the aptamer to the target analyte is required [123]. Alternatively, the design of MIPs is interesting for electrode modification with promising low LOD, but special attention needs to be considered in the selectivity. Finally, the functionalization of the electrode with nanomaterials and surfactants along with electrochemical pretreatments might offer a simpler and more straightforward way to detect illicit drugs in biofluids [116, 117]. Nevertheless, a suitable study of interferents, avoidance of biofouling, and proper LOD are challenges that still need to be overcome.

2.3 Wearable Electrochemical (Bio)sensors for Drug Detection

Electrochemical (bio)sensors can be easily miniaturized while maintaining excellent analytical performance for the desired application as has been shown in the use of

SPEs for illicit drug detection. Apart from the easy portability at the point of test provided by the planar configuration of the SPE (i.e., strip), the materials used for the fabrication of electrochemical (bio)sensors can be deposited on wearable substrates or embedded onto wearable platforms [124]. The seamless integration of electrochemical (bio)sensors in regular textiles or cloth is recently being explored for the detection of illicit drugs in powders for the detection of drug seizures or also in biofluids (e.g., saliva, interstitial fluid) [125].

The most used wearable platform for illicit drug detection in seizures is the glove [126]. This sensing concept called "lab-on-a-glove" is an interesting approach for law enforcement, as this garment is regularly used during daily activities, thus making it widely available in real scenarios and easy to introduce during their routine. For the purpose of the fabrication of glove-based sensors, tailor-made materials such as stress-enduring inks made of conductive nanomaterials and inherently stretchable polymers have been developed [127], which offer stretchability and resilience to the printed electrodes without affecting the tactile ability and user protection. Moreover, customized designs can be printed on each fingertip allowing multiplexed analysis of different analytes. Glove-based wearables allow for an electrochemical direct detection of illicit drugs dissolved in solution by dipping the fingertip and in powders by performing a "swiping method" where the sampling and the electrochemical steps are carried out in the thumb and index fingertip, respectively [128]. The swiping method consists of first swiping on the suspicious powder with a mixing step with a gel-based electrolyte on the index finger to close the electrochemical cell. Glove-based electrochemical sensors were primarily reported for the detection of cocaine among their cutting agents [128]. Later, a glove-based sensor has been also reported for the detection of fentanyl [129]. These reports used the same principle of voltammetric profile to identify the target analyte among other potential interferences following the same strategy of regular SPE. Indeed, the manufacturing process used on the glove-based electrochemical sensors is by employing the screen-printing technique with a high potential for scalability.

Apart from drug seizures, wearable electrochemical (bio)sensors have been reported for the monitoring of illicit drug consumption. For this purpose, microneedle-based electrochemical sensors have been reported for the monitoring of fentanyl in interstitial fluid [130]. Interstitial fluid exhibits a correlation with blood levels of several analytes which makes it relevant for physicians and toxicologists while preserving the non-invasiveness character [131]. This application can be interesting to detect overdose cases with corresponding reversal interventions and to follow up on recovery patients with addictions. Another interesting application is the monitoring of drug consumption through saliva, a well-known biofluid for drug testing at the roadside. In this direction, a wearable ring platform was designed to accommodate saliva analysis for THC and alcohol. Still, the limitation is on the sampling pretreatment, thus an incorporated strategy to remove debris and interferents from the saliva matrix needs to be integrated with the whole analytical system [132]. Last but not least, sweat has the potential to be a biofluid for the detection of illicit drug consumption. Currently, sweat has been tested for this

purpose, although using laboratory-based analysis to confirm the drug's presence [133]. Hence, wearable electrochemical sensors in epidermal patches for the in situ detection of the drug in sweat would be highly valuable for on-site testing. To induce active perspiration, an iontophoretic system needs to be coupled prior to the analysis by the sensor. In this direction, a set of electrodes (anode and cathode for the iontophoretic system and a regular SPE setup) were printed for the non-invasive monitoring of alcohol consumption [134]. This design can be easily extrapolated to the detection of illicit drugs following the voltammetric profiling approach.

Many opportunities are still ahead for the detection and monitoring of illicit drugs by wearable electrochemical systems. However, the challenges for the use of wearable electrochemical (bio)sensors rely on: (i) the full wearability of the device with seamless integration on the body; (ii) minimal user interaction which limits the sampling preparation for enhanced selectivity; and (iii) the incorporation of a miniaturized potentiostat easy to wear. Importantly, these challenges can be, respectively, addressed by: (i) using conformal substrates of polymeric nature which provide excellent adhesion of the conductive inks; (ii) modification of the working electrode with electrocatalytic materials or bioreceptors toward the analyte of interest; and (iii) the employment of flexible printed circuit boards as the electrochemical readers which can be reused. Overall, wearable electrochemical devices are an advent in sensing technology with countless opportunities. In contrast, the end-user case needs to be carefully studied in advance to know when a wearable system is needed (e.g., continuous monitoring) or when a low-cost point-of-test device is sufficient for a rapid decision-making process on-site.

3 Challenges

It should come as no surprise that electrochemical illicit drug sensors, just as every other sensing technology, have several challenges to overcome: (i) accuracy, (ii) validation with a large set of samples, (iii) affordability, easy to use, and short time of analysis, (iv) ability for multidrug detection, and (v) secure data processing and tailored data display for forensic applications. Some of these challenges are associated with the technology itself, whereas others are linked to the field and (complexity of the) market that is targeted.

Overall, the grand objective is to develop sensors that address the needs of society. Scientists, in general, will mainly use their time and energy to develop a sensor that ticks off scientific objectives such as high accuracy, excellent reproducibility, low LOD, short analysis time, etc. By trying to tick all these boxes, a disconnect might occur between the "scientific" solution and a realistic application of the technology in the real world. Indeed, keeping the target market in mind, other aspects such as secure data handling and transmission, low cost, and portability are important as well. There is often a trade-off between all these aspects, improving one might compromise another. Nevertheless, the objective should be to develop sensors that perform well in all areas. In the coming section, we will discuss the challenges of

electrochemical illicit drug sensors, with a special focus on bringing the advancements in the research field to fruition in a real-world application.

The accuracy of an illicit drug sensor is typically expressed as the amount of true positive and negative analysis, divided by the total amount of analysis (including true positive and negative and false positive and negative). As such, good accuracy is obtained by developing a sensor that allows differentiation between target compounds and non-target compounds via a different electrochemical output, and by developing a data analysis approach that is capable of diversifying between these different electrochemical outputs. Electrochemical output after an electrochemical measurement is typically quite scarce in information, that is, a pure compound usually has a maximum of three signals to work with. On the upside, this typically provides the researcher with a good insight into the data since it is much more straightforward to interpret a voltammogram and understand the origin of each signal in comparison with, e.g., an NMR or Raman spectrum. However, the flip side is that there is often not as much information in the data to work with, which can make the unique identification of a target compound cumbersome. In addition, cutting agents and adulterants that are added to the drugs for profit can suppress or shift the signals of an illicit drug in a voltammogram and add their own signals to the voltammogram. These different factors make it challenging, not impossible, to reach good accuracies with electrochemical illicit drug sensors. On the flip side, the possibility to identify cutting agents and adulterants grants the technology an edge over the competitive technologies, i.e. by facilitating drug profiling. Besides the previously discussed electrode modifications, which allow a more target-specific electrochemical profile, the electrochemist has another powerful tool: chemometrics. This chemical discipline uses mathematical and statistical methods to maximally extract (electro)chemical information from (electro)chemical data. Linking chemometric tools to electrochemical illicit drug research has time and again proven successful to push accuracies to higher levels [52, 53]. Especially for applied illicit drug research, it seems unthinkable not to use chemometrics. Nevertheless, this is far from the standard, and it is a challenge for electrochemical illicit drug research to make more use of the tools provided by chemometrics.

Due to the constant emergence of NPS, there is an unrelenting supply of new drugs to develop electrochemical detection strategies. Research papers describing such novel strategies for NPS appear relatively fast after an NPS rises to the forefront [48, 49, 60]. This highlights one of the qualities of electrochemical illicit drug research: its versatility and ability to quickly adapt to novel compounds. Typically, these research papers describe that the targeted drug has an electrochemical signal that can be used for detection. However, only a small amount of confiscated samples is included to prove that indeed, the drug can be detected with the new approach, followed by a statement in the conclusion that law enforcement agencies (LEAs) will greatly benefit from the new methodology. Importantly, LEAs are not too interested in these studies as long as no follow-up validation studies are performed with a larger number of confiscated samples, a substantial part of which should consist of negative samples. Only then will the new method be effectively validated, and LEAs will become familiar with electrochemical technology at the same time. From time to

time, validation studies of this kind are carried out, but this still happens far too infrequently.

Similarly, it is a common sight in electrochemical illicit drug research, manuscripts that describe a certain type of modified electrode with great selectivity toward a target drug, obtaining great accuracies. Although very interesting and innovative from a research point of view, these modifications don't make the road to a real application shorter. Challenging reproducibility, long incubation times, and an increased price are factors to be reckoned with. Little information can be found on modified electrode applications that made it out of academic research into a commercial application that is used in real life. This is not a statement to say it is impossible, but a critical look at the potential of a modification to make it to such a stage would be beneficial for the research field. After all, the research field itself will blossom if at some point a commercial electrochemical illicit drug sensor is used by end-users.

Furthermore, as already mentioned previously, most electrochemical illicit drug research focuses on the detection of a single drug or single drug class. This is a drawback compared to other techniques, e.g., portable Raman or NIR [135–137], that can detect all illicit drug classes at once. Multiplexing, that is combining the electrochemical output of an array of SPEs, will open up electrochemical illicit drug detection to the simultaneous detection of multiple drug classes. It is expected that the field will evolve in this direction in the coming years as new fabrication technologies and nanomaterials use is converging. Similar to the single drug sensors, sufficient attention should be paid to the feasibility of these multidrug sensors for use in real scenarios. Aspects such as portability, easy sampling, short analysis time, and low cost should be kept in mind during development besides the typical parameters such as reaching high accuracies.

A final challenge for electrochemical illicit drug sensors is the specific end-user requirements. Ultimately, the sensors will be used by law enforcement, bringing with them some very specific needs concerning data security and transmission. Preferably, the employed methodology and data analysis algorithms should be protected to give the drug cartels and dealers as little opportunity as possible to circumvent or sabotage the detection strategy. Furthermore, a report is preferably generated after a measurement to facilitate the follow-up steps. It is important then to decide if this report is stored locally or cloud-based, same for the generated data during the measurement. These are important questions to ask when bringing an electrochemical illicit drug sensor to the market, and the answers and solutions should be as close as possible to the specific end-user requirements.

To summarize, electrochemistry and biosensors have the potential to deliver tools that meet the end-user requirements: high accuracy, portable, low cost, short analysis time, excellent reproducibility, safe data handling and transmission, and easy to use by non-experts. For some end-users, it is sufficient to develop single drug sensors that target one specific drug. The current state of the art is close to delivering sensors for this purpose to the field if the previously mentioned challenges (modifications, chemometrics, etc.) are properly addressed. However, some end-users require simultaneous detection of multiple drugs at once. Substantial research is necessary for this

purpose, but electrochemistry clearly has the capability to eventually deliver sensors for this purpose as well, as indicated by several proof-of-concept studies reported in the chapter.

4 Prospects

4.1 Vision of Illicit Drug Detection in Seizures

Currently, the law enforcement process of drug analysis consists of two parts. First a presumptive test is performed, often in the form of a color test, to determine the presence or absence of an illicit drug. These tests can be executed on-site or in the laboratory. If the results of this test are positive, they need to be confirmed in the laboratory using gold-standard techniques such as GC- or LC-MS. While the presumptive tests are generally fast and can be performed by non-trained personnel, the confirmatory tests are more time-consuming and require the analyst to be educated in the use of the technique. Improving the accuracy of the on-site tests would lead to a lower amount of confirmatory tests in the laboratory thereby reducing the workload of law enforcement. Especially if this improved accuracy is, in part, achieved through correct identifications in difficult matrices that pose problems for the currently established detection technologies. The absence of matrix effects as such becomes a major asset that will make the novel technology attractive to end-user for point-of-care usage. Next to a lower workload, more accurate on-site tests will facilitate better and faster decision-making at the point of care. Important is that electrochemical sensors couple this improved accuracy to the assets – easy to use, fast, wide sampling concentration range, and low cost – that make color tests so attractive to law enforcement. After all, improved accuracy is needed, but the new technology will only be adopted if the end-user sees the benefit of the technology and prefers to use it over (or next to) the existing technologies. Developing an elegant sampling method for the electrochemical sensors is thus of utmost importance since this will be a crucial factor for end-users that determines if they will use the technology. Overall, if all these desired specifications can be stringed together in a single product, and this is possible for electrochemical sensors, the result will truly be an asset for law enforcement.

Specifically for forensic institutes, due to increasing numbers of cases and the emergence of novel psychotic substances such as NPS which result in more complex analysis, forensic chemistry laboratories have problems overcoming backlogs. In order to replace confirmatory laboratory testing, it is important to consider that at least two techniques should be used for on-site detection, as in the forensic field it is not acceptable to solely rely upon one technique. Two techniques that are promising for on-site detection, besides electrochemistry, are portable NIR [136] and portable Raman spectroscopy [135]. Due to the orthogonality of electrochemistry with these two techniques, the combination with electrochemistry is an attractive possibility for

the decentralization of the forensic laboratory. Additionally, electrochemistry may be used to overcome the challenges of NIR and Raman spectroscopy regarding colored samples and mixtures for on-site detection.

Contrary to law enforcement, harm reduction is not aware of the latest developments in electrochemical drug detection, few in harm reduction are even aware of the existence of electrochemical drug sensors. Harm reduction studies are performed on point-of-care drug detection, however typically with color tests and portable spectroscopic techniques. Therefore, the first step would be to make the electrochemical technology aware of the field of harm reduction, e.g., through collaborations or demonstrations. These should then lead to the next stage to a better understanding of the needs and requirements of this group of end-users. It is envisioned that electrochemical sensors can contribute to several harm reduction initiatives. Pill testing services at, e.g., festivals are an obvious candidate, but also studies on the currently used cutting agents might be relevant. A possibility would be to, e.g., screen heroin samples in drug consumption rooms on the presence of fentanyl (analogs) to monitor the latter's prevalence.

4.2 Vision of Illicit Drug Detection in Body Fluids

Due to the high costs of lateral flow immunoassays and their associated problems regarding cross-reactivity, there is an opportunity for electrochemical sensors to take over part of the global drugs screening market. This market was $5.3 billion last year and is rapidly expanding to reach an expected $11.6 billion by 2026, at a compound annual growth rate of 16.8%. However, to reach the market electrochemical sensors for illicit drug detection in body fluids should first be able to overcome the challenges of low LODs required (low nM levels), the detection of metabolites, and matrix effects as described above. Importantly, for the application of electrochemical sensors for detection in body fluids, user-friendly consumables need to be developed to allow point-of-care detection. Here, the desired application and, as a consequence of that, the appropriate biological matrix need to be considered. The detection of different body fluids will require different consumables for collection and possibly for sample preparation. The integration of collection devices for body fluids with electrochemical sensors is necessary to assure hygienic handling of the samples. It is pivotal that this sample preparation is kept as simple as possible, which requires that steps such as centrifugation are avoided. To this end, platforms allowing the straightforward removal of interferences from the biological matrix will need to be designed and established. While the current state of the art is mostly concerned with the detection aspect of developing sensors for illicit drugs in body fluids, collaboration with product designers will be necessary for electrochemical sensors to reach this market.

4.3 Vision of Wearable Illicit Drug Detection

The recent gadgets based on glove- or ring-based platforms have demonstrated the great potential of wearable electrochemical sensors for on-site and rapid screening of illicit drugs and cutting agents in street samples and biofluids. However, further developments and new features such as in situ sampling pretreatments and miniaturized electrochemical readers are still necessary for a full user experience. Innovative wearable electrochemical systems can address the limitations of currently used portable analytical systems while maintaining the reliability of benchtop standard techniques. In this way, LEAs will be only willing to adopt wearable and portable devices for an accurate and rapid decision-making process in the field if the new tools comply with current analytical standards or even improve the performance of the analysis. Although the wearability of the device is not an essential feature for LEAs, it might be useful for the operation in some cases such as road testing of drugs of abuse users. In these cases, a wearable device on the subject at the test would avoid direct contact with the agent, thus preventing interaction with contaminated samples from the subject (particularly interesting in outbreaks such as the COVID-19 pandemic) [138]. Another important aspect is to incorporate wearable electrochemical sensors in regularly used garments by the agents (e.g., gloves). The use of common tools or gadgets will increase the end-user adherence to the new system while providing an easy-to-use device.

Interstitial fluid and sweat are promising biofluids for drug monitoring. Hence, wearable electrochemical sensors can offer groundbreaking illicit drug detection activities, including remote monitoring of individuals on probation or for rapid detection of an overdose in first-responder settings. Moreover, these wearable systems have the potential to be integrated as a feedback-controlled wearable closed-loop device for autonomous mitigation of drug overdose, thus avoiding death in emergency settings. The same technology offers easy translation to clinical decision-making processes during therapeutic drug monitoring, thus showing the potential for a broader market. In this direction, wearable electrochemical sensors for drug monitoring are capable of providing time-resolved data on drug concentrations, which can unravel any fluctuation of the therapeutic concentration and identify drug−drug interactions through the analysis of unusual behavior in the drug pharmacokinetics [125]. This feature will enable personalized drug dosing toward enhanced healthcare. Besides, wearable electrochemical sensors can improve patient compliance with medication by sending alert messages to wearers and caregivers regarding the frequency of medication intake.

These wearable devices manage sensitive data, thus high-security standards are required for the processing and transmission of the data. Importantly, drug seizure information needs to be encrypted to prevent sensitive data (e.g., location and drug composition) to reach criminal organizations (e.g., through a data breach).

The embodiment of regular electrochemical sensors in wearable platforms can pave the way to rapid and user-friendly analysis in the field thus increasing the safety

and security of our society. However, high analytical standards and affordable prices on these devices need to be complied with for early adoption by end-users.

5 Conclusions

The progression of electrochemical sensors for illicit drug detection has been discussed. First, the need for the detection and monitoring of illicit drugs in our society has been pointed out. Sensors and devices able to rapidly detect illicit drugs in powder or another type of form in the field facilitate the identification of illegal trading and confiscation of cargo before reaching drug consumers. This is an important step for LEAs to block the spreading of drug abuse in society. Moreover, electrochemical sensors can also be applied in the detection of the consumption of illicit drugs by users which brings dangerous situations in daily activities (e.g., at the workplace, driving under the influence of drugs, etc.). These sensors can detect the illicit drug in several matrices, ranging from non-invasive biofluids such as saliva or sweat to invasive matrices such as blood or serum. The ability to quickly identify drug consumption can be an ideal situation for first responders when dealing with intoxication. Thus, electrochemical sensors can be beneficial in daily situations: (i) fast confiscation of illicit drugs; (ii) detection of drug consumption; (iii) identification of intoxications; and (iv) analysis of the purity of the illicit drug for harm reduction purposes.

Despite the advances in nanomaterials and sensing strategies, there are some challenges that still researchers need to address such as: (i) accuracy to avoid false positives and false negatives; (ii) detection of multiple drugs in a single analysis; (iii) low limit of detection in biofluids; and (iv) user-friendliness, meaning low to none sample preparation being able to be performed by non-trained personnel; among others. The most used designs for on-site detection and monitoring of illicit drugs are based on point-of-care detection, and more recently, wearable sensors seamlessly integrated with the body. Each design can be advantageous in different situations. For example, a point-of-care test to quickly identify a suspicious sample for confiscation is used by LEAs, or a wearable device to monitor illicit drug intake in an individual on probation. Interestingly, the integration of data treatment and cloud-based software with the electrochemical sensors is a necessary step to bring the technology to a fruitful outcome truly valuable for end-users.

Unfortunately, the use of illicit drugs is still increasing which translates into the necessity to bring highly accurate and user-friendly devices that assist in rapid on-site detection. Fortunately, electrochemical (bio-)sensors can be part of such devices and contribute to the fight against drugs by providing cost-effective tools to LEAs and first responders.

References

1. United Nations Office on Drugs and Crime. World Drug Report 2021 (2021)
2. European Monitoring Centre for Drugs and Drug Addiction (2019) Eur Drug Rep. https://doi.org/10.1097/JSM.0b013e31802b4fda
3. Addiction, E. M. C. for D. and D. Impact of COVID-19 on drug markets, use, harms and drug services in the community and prisons : results from an EMCDDA trendspotter study. (Publications Office, 2021). https://doi.org/10.2810/498734
4. VRT. Recordhoeveelheid van 110 ton cocaïne onderschept in haven van Antwerpen: grote vangst of druppel op hete plaat? Preprint at https://www.vrt.be/vrtnws/nl/2023/01/10/cocaine-belgie-nederland-douane/
5. Florea A, de Jong M, De Wael K (2018) Electrochemical strategies for the detection of forensic drugs. Curr Opin Electrochem 11:34–40
6. European Monitoring Centre for Drugs and Drug Addiction (2019) EU Drug Markets Rep. https://doi.org/10.2810/53181
7. Mégarbane B et al (2020) Management of pharmaceutical and recreational drug poisoning. Ann Intensive Care 10:157
8. Babor TF et al (2019) Drug policy and the public good: a summary of the second edition. Addiction 114:1941–1950
9. Ciccarone D (2012) Henceforth harm reduction? Int J Drug Policy 23:16–17
10. Thiruvottriyur Shanmugam S et al (2021) Towards developing a screening strategy for ecstasy: revealing the electrochemical profile. ChemElectroChem 8:4826–4834
11. de Jong M et al (2018) Tackling poor specificity of cocaine color tests by electrochemical strategies. Anal Chem 90:6811–6819
12. United Nations Office on Drugs and Crime (UNODC) (2022) World drug report 2022 executive summary. www.unodc.org/unodc/en/data-and-analysis/world-drug-report-2022.html
13. National Institute on Drug Abuse (NIDA) (2022) Overdose death rates. https://nida.nih.gov/research-topics/trends-statistics/overdose-death-rates
14. European Monitoring Centre for Drugs and Drug Addiction (EMCDDA) (2022) Eur Drug Rep 2022 Trends Dev. wwwemcddaeuropaeu. https://doi.org/10.2810/715044
15. About the Epidemic | HHS.gov. https://www.hhs.gov/opioids/about-the-epidemic/index.html
16. Curry AS, Alan S (1976) Poison detection in human organs. Thomas
17. Anderson PD, Bokor G (2012) Forensic aspects of drug-induced violence. J Pharm Pract 25:41–49
18. de Costa YRS, Lavorato SN, de Baldin JJCMC (2020) Violence against women and drug-facilitated sexual assault (DFSA): a review of the main drugs. J Forensic Leg Med 74:102020. https://doi.org/10.1016/j.jflm.2020.102020
19. Iskierka M, Zawadzki M, Szpot P, Jurek T (2021) Detection of drugs in postmortem specimens of blood, vitreous humor and bone marrow aspirate. J Anal Toxicol 45:348–355
20. Center for Substance Abuse Treatment (2006) Appendix B. Urine collection and testing procedures and alternative methods for monitoring drug use
21. Navazesh M, Ahmadieh A (2020) Salivary bioscience. In: Granger DA, Taylor MK (eds) Salivary bioscience, pp 371–393. https://doi.org/10.1007/978-3-030-35784-9
22. Scientific Working Group for the Analysis of Seized Drugs (SWGDRUG). Scientific Working Group for the Analysis of Seized Drugs (SWGDRUG) Recommendations (2019). www.swgdrug.org
23. Ahmed SR et al (2020) Recent biosensing advances in the rapid detection of illicit drugs. Trends Anal Chem 131:116006
24. Posthuma-Trumpie GA, Korf J, van Amerongen A (2009) Lateral flow (immuno)assay: its strengths, weaknesses, opportunities and threats. A literature survey. Anal Bioanal Chem 393:569–582

25. Moro G et al (2020) Unlocking the full power of electrochemical fingerprinting for on-site sensing applications. Anal Bioanal Chem 412:5955–5968
26. Van Echelpoel R et al (2023) Validated portable device for the qualitative and quantitative electrochemical detection of MDMA ready for on-site use. Microchem J 190:108693
27. de Jong M et al (2021) A benzocaine-induced local near-surface pH effect: influence on the accuracy of voltammetric cocaine detection. Anal Sens 1:54–62
28. de Jong M et al (2022) Real-time electrochemical screening of cocaine in lab and field settings with automatic result generation. Drug Test Anal
29. Singh S, Wang J, Cinti S (2022) Review – an overview on recent progress in screen-printed electroanalytical (bio)sensors. ECS Sens Plus 1:23401
30. González-Hernández J, Alvarado-Gámez AL, Arroyo-Mora LE, Barquero-Quirós M (2021) Electrochemical determination of novel psychoactive substances by differential pulse voltammetry using a microcell for boron-doped diamond electrode and screen-printed electrodes based on carbon and platinum. J Electroanal Chem 882
31. Ren S, Zeng J, Zheng Z, Shi H (2021) Perspective and application of modified electrode material technology in electrochemical voltammetric sensors for analysis and detection of illicit drugs. Sens Actuators A Phys 329:112821
32. Singla P et al (2020) MIPs for commercial application in low-cost sensors and assays – an overview of the current status quo. Sens Actuators B Chem 325:128973
33. Sorribes-Soriano A, Herrero-Martínez JM, Esteve-Turrillas FA, Armenta S (2020) Molecularly imprinted polymer-based device for field collection of oral fluid samples for cocaine identification. J Chromatogr A 1633:461629
34. Akhoundian M, Alizadeh T, Ganjali MR, Norouzi P (2019) Ultra-trace detection of methamphetamine in biological samples using FFT-square wave voltammetry and nano-sized imprinted polymer/MWCNTs-modified electrode. Talanta 200:115–123
35. Zhang R et al (2021) Highly sensitive electrochemical sensor based on Pt nanoparticles/carbon nanohorns for simultaneous determination of morphine and MDMA in biological samples. Electrochim Acta 370:137803
36. Masemola DP, Mafa PJ, Nyoni H, Mamba BB, Msagati TAM (2020) Gold nanoparticles modified exfoliated graphite electrode as electrochemical sensor in the determination of psychoactive drug. J Environ Sci Health B 0:1–7
37. Dragan AM et al (2021) Electrochemical fingerprints of illicit drugs on graphene and multi-walled carbon nanotubes. Front Chem 9
38. Mao K et al (2020) Nanomaterial-based aptamer sensors for analysis of illicit drugs and evaluation of drugs consumption for wastewater-based epidemiology. Trends Anal Chem 130:115975
39. Goodchild SA et al (2019) Ionic liquid-modified disposable electrochemical sensor strip for analysis of fentanyl. Anal Chem 91:3747–3753
40. Balbino MA et al (2016) Use of screen-printed electrodes for quantification of cocaine and Δ9-THC: adaptions to portable systems for forensic purposes. J Solid State Electrochem 20:2435–2443
41. Parrilla M et al (2022) Rapid on-site detection of illicit drugs in smuggled samples with a portable electrochemical device. Chemosensors 10:108
42. de Faria LV et al (2022) Cyclic square-wave voltammetric discrimination of the amphetamine-type stimulants MDA and MDMA in real-world forensic samples by 3D-printed carbon electrodes. Electrochim Acta 429:141002
43. Teófilo KR et al (2020) Electrochemical detection of 3,4-methylenedioxymethamphetamine (ecstasy) using a boron-doped diamond electrode with differential pulse voltammetry: simple and fast screening method for application in forensic analysis. Microchem J 157:105088
44. Van Echelpoel R, de Jong M, Daems D, Van Espen P, De Wael K (2021) Unlocking the full potential of voltammetric data analysis: a novel peak recognition approach for (bio)analytical applications. Talanta 233:122605

45. Felipe Montiel N et al (2021) The opportunity of 6-monoacetylmorphine to selectively detect heroin at preanodized screen printed electrodes. Talanta 226:122005
46. Schram J et al (2020) Identifying electrochemical fingerprints of ketamine with voltammetry and liquid chromatography–mass spectrometry for its detection in seized samples. Anal Chem 92:13485–13492
47. Shanmugam ST, van Echelpoel R, Boeye G (2021) Towards developing a screening strategy for ecstasy: revealing the electrochemical profile. ChemElectroChem 8:4826–4834
48. Schram J et al (2021) Electrochemical profiling and LC-MS characterization of synthetic cathinones : from methodology to detection in forensic samples. Drug Test Anal 13:1282–1294
49. Arrieiro MOB et al (2022) Electrochemical detection of eutylone using screen-printed electrodes: rapid and simple screening method for application in forensic samples. Electrochim Acta 412:140106
50. Ameen A, Brown K, Dennany L (2022) Can synthetic cannabinoids be reliably screened with electrochemistry? An assessment of the ability to screen for synthetic cannabinoids STS-135 and BB-22 within a single sample matrix. J Electroanal Chem 909:116141
51. Mynttinen E et al (2020) Electrochemical detection of oxycodone and its main metabolites with Nafion-coated single-walled carbon nanotube electrodes. Anal Chem 92:8218–8227
52. Ortiz-Aguayo D, de Wael K, del Valle M (2021) Voltammetric sensing using an array of modified SPCE coupled with machine learning strategies for the improved identification of opioids in presence of cutting agents. J Electroanal Chem 902:115770
53. Ortiz-Aguayo D, Cetó X, de Wael K, del Valle M (2022) Resolution of opiate illicit drugs signals in the presence of some cutting agents with use of a voltammetric sensor array and machine learning strategies. Sens Actuators B Chem 357
54. van Echelpoel R et al (2022) Electrochemical methods for on-site multidrug detection at festivals. Sens Diagn 1:793–802
55. Schram J et al (2022) Paraformaldehyde-coated electrochemical sensor for improved on-site detection of amphetamine in street samples. Microchem J 179:107518
56. Ghorbanizamani F, Moulahoum H, Guler E, Timur S (2022) Ionic liquid-hydrogel hybrid material for enhanced electron transfer and sensitivity towards electrochemical detection of methamphetamine. J Mol Liq 361:119627
57. Verstraete A et al (2011) Per se limits – methods of defining cut-off values for zero tolerance. https://biblio.ugent.be/publication/1988464/file/1988490.pdf
58. de Rycke E, Stove C, Dubruel P, de Saeger S, Beloglazova N (2020) Recent developments in electrochemical detection of illicit drugs in diverse matrices. Biosens Bioelectron 169:112579
59. Abdelshafi NA, Bell J, Rurack K, Schneider RJ (2019) Microfluidic electrochemical immunosensor for the trace analysis of cocaine in water and body fluids. Drug Test Anal 11:492–500
60. Couto RAS et al (2020) Methylone screening with electropolymerized molecularly imprinted polymer on screen-printed electrodes. Sens Actuators B Chem 316:128133
61. Yilmaz Sengel T et al (2017) An immunoelectrochemical platform for the biosensing of 'Cocaine use'. Sens Actuators B Chem 246:310–318
62. Felix FS, Angnes L (2018) Electrochemical immunosensors – a powerful tool for analytical applications. Biosens Bioelectron 102:470–478. https://doi.org/10.1016/j.bios.2017.11.029
63. Cho IH et al (2018) Current technologies of electrochemical immunosensors: perspective on signal amplification. Sensors (Basel) 18
64. Sanli S et al (2020) Screen printed electrode-based biosensor functionalized with magnetic cobalt/single-chain antibody fragments for cocaine biosensing in different matrices. Talanta 217
65. Vidal JC et al (2016) A multi-electrochemical competitive immunosensor for sensitive cocaine determination in biological samples. Electroanalysis 28:685–694

66. Ya Y, Jinyin P, Weijie H, Yifeng T (2014) An approach for the preparation of highly sensitive electrochemical impedimetric immunosensors for the detection of illicit drugs. J Electroanal Chem 726:1–6
67. Eissa S, Zourob M (2017) Competitive voltammetric morphine immunosensor using a gold nanoparticle decorated graphene electrode. Microchim Acta 184:2281–2289
68. Eissa S, Almthen RA, Zourob M (2019) Disposable electrochemical immunosensor array for the multiplexed detection of the drug metabolites morphine, tetrahydrocannabinol and benzoylecgonine. Microchim Acta 186
69. Ivison FM, Kane JW, Pearson JE, Kenny J, Vadgama P (2000) Development of a redox mediated amperometric detection system for immunoassay. Application to urinary amphetamine screening. Electroanalysis 12:778–785
70. Luangaram K, Boonsua D, Soontornchai S, Promptmas C (2002) Development of an amperometric immunosensor for the determination of methamphetamine in urine. Biocatal Biotransformation 20:397–403
71. Zhang LY, Liu YJ (2014) Label-free amperometric immunosensor based on prussian blue as artificial peroxidase for the detection of methamphetamine. Anal Chim Acta 806:204–209
72. Wang X et al (2019) A convenient electrochemiluminescent immunosensor for detecting methamphetamine antibody. Anal Sci 35:875–882
73. Demir B et al (2016) Polypeptide with electroactive endgroups as sensing platform for the abused drug 'methamphetamine' by bioelectrochemical method. Talanta 161:789–796
74. Ghorbanizamani F, Moulahoum H, Guler Celik E, Timur S (2022) Ionic liquid-hydrogel hybrid material for enhanced electron transfer and sensitivity towards electrochemical detection of methamphetamine. J Mol Liq 361
75. Butler D, Pravda M, Guilbault GG (2006) Development of a disposable amperometric immunosensor for the detection of ecstasy and its analogues using screen-printed electrodes. Anal Chim Acta 556:333–339
76. Yang Y, Zhai S, Liu C, Wang X, Tu Y (2019) Disposable immunosensor based on electrochemiluminescence for ultrasensitive detection of ketamine in human hair. ACS Omega 4:801–809
77. Li Q et al (2015) Electrochemiluminescence immunosensor for ketamine detection based on polyamidoamine-coated carbon dot film. J Solid State Electrochem 19:2973–2980
78. Chen Y, Yang Y, Tu Y (2013) An electrochemical impedimetric immunosensor for ultrasensitive determination of ketamine hydrochloride. Sens Actuators B Chem 183:150–156
79. Radi AE, Abd-Ellatief MR (2021) Electrochemical aptasensors: current status and future perspectives. Diagnostics 11. https://doi.org/10.3390/diagnostics11010104
80. Hianik T, Wang J (2009) Electrochemical aptasensors – recent achievements and perspectives. Electroanalysis 21:1223–1235. https://doi.org/10.1002/elan.200904566
81. Cánovas R et al (2022) Novel electrochemiluminescent assay for the aptamer-based detection of testosterone. Talanta 239
82. Daems E, Moro G, Campos R, de Wael K (2021) Mapping the gaps in chemical analysis for the characterisation of aptamer-target interactions. Trends Anal Chem 142:116311
83. Abnous K, Danesh NM, Ramezani M, Taghdisi SM, Emrani AS (2016) A novel electrochemical aptasensor based on H-shape structure of aptamer-complimentary strands conjugate for ultrasensitive detection of cocaine. Sens Actuators B Chem 224:351–355
84. Su F et al (2017) Two-dimensional zirconium-based metal-organic framework nanosheet composites embedded with Au nanoclusters: a highly sensitive electrochemical aptasensor toward detecting cocaine. ACS Sens 2:998–1005
85. Roushani M, Shahdost-Fard F (2016) Fabrication of an electrochemical nanoaptasensor based on AuNPs for ultrasensitive determination of cocaine in serum sample. Mater Sci Eng C 61:599–607
86. Shahdost-Fard F, Roushani M (2016) Conformation switching of an aptamer based on cocaine enhancement on a surface of modified GCE. Talanta 154:7–14

87. Roushani M, Shahdost-Fard F (2015) A novel ultrasensitive aptasensor based on silver nanoparticles measured via enhanced voltammetric response of electrochemical reduction of riboflavin as redox probe for cocaine detection. Sens Actuators B Chem 207:764–771
88. Roushani M, Shahdost-fard F (2016) An aptasensor for voltammetric and impedimetric determination of cocaine based on a glassy carbon electrode modified with platinum nanoparticles and using rutin as a redox probe. Microchim Acta 183:185–193
89. Roushani M, Shahdost-Fard F (2015) A highly selective and sensitive cocaine aptasensor based on covalent attachment of the aptamer-functionalized AuNPs onto nanocomposite as the support platform. Anal Chim Acta 853:214–221
90. Bozokalfa G et al (2016) Polypeptide functional surface for the aptamer immobilization: electrochemical cocaine biosensing. Anal Chem 88:4161–4167
91. Taghdisi SM, Danesh NM, Emrani AS, Ramezani M, Abnous K (2015) A novel electrochemical aptasensor based on single-walled carbon nanotubes, gold electrode and complimentary strand of aptamer for ultrasensitive detection of cocaine. Biosens Bioelectron 73:245–250
92. Zhang DW et al (2012) An electrochemical aptasensor based on enzyme linked aptamer assay. Biosens Bioelectron 31:363–368
93. Du Y et al (2010) Solid-state probe based electrochemical aptasensor for cocaine: a potentially convenient, sensitive, repeatable, and integrated sensing platform for drugs. Anal Chem 82: 1556–1563
94. Chen Z, Lu M (2016) Target-responsive aptamer release from manganese dioxide nanosheets for electrochemical sensing of cocaine with target recycling amplification. Talanta 160:444–448
95. Abnous K et al (2022) A highly sensitive electrochemical aptasensor for cocaine detection based on CRISPR-Cas12a and terminal deoxynucleotidyl transferase as signal amplifiers. Talanta 241
96. Hua M et al (2010) Label-free electrochemical cocaine aptasensor based on a target-inducing aptamer switching conformation. Anal Sci 26:1265–1270
97. Hua M et al (2011) Quantum dots as immobilized substrate for electrochemical detection of cocaine based on conformational switching of aptamer. J Electroanal Chem 662:306–311
98. Soni S, Jain U, Burke DH, Chauhan N (2022) A label free, signal off electrochemical aptasensor for amphetamine detection. Surf Interfaces 31
99. Bor G et al (2022) Synthetic antibodies for methamphetamine analysis: design of high affinity aptamers and their use in electrochemical biosensors. J Electroanal Chem 921
100. Xie Y, Wu S, Chen Z, Jiang J, Sun J (2022) Rapid nanomolar detection of methamphetamine in biofluids via a reagentless electrochemical aptamer-based biosensor. Anal Chim Acta 1207
101. Kékedy-Nagy L, Perry JM, Little SR, Llorens OY, Shih SCC (2023) An electrochemical aptasensor for Δ9-tetrahydrocannabinol detection in saliva on a microfluidic platform. Biosens Bioelectron 222
102. Fu K, Zhang R, He J, Bai H, Zhang G (2019) Sensitive detection of ketamine with an electrochemical sensor based on UV-induced polymerized molecularly imprinted membranes at graphene and MOFs modified electrode. Biosens Bioelectron 143:111636
103. Rook E, Huitema A, Brink W, Ree J, Beijnen J (2008) Pharmacokinetics and pharmacokinetic variability of heroin and its metabolites: review of the literature. Curr Clin Pharmacol 1:109–118
104. Pavlova V, Mirčeski V, Komorsky-Lovrić Š, Petrovska-Jovanović S, Mitrevski B (2004) Studying electrode mechanism and analytical determination of cocaine and its metabolites at the mercury electrode using square-wave voltammetry. Anal Chim Acta 512:49–56
105. Garrido JMPJ, Delerue-Matos C, Borges F, Macedo TRA, Oliveira-Brett AM (2004) Voltammetric oxidation of drugs of abuse: I. Morphine and metabolites. Electroanalysis 16: 1419–1426
106. Garrido JMPJ, Delerue-Matos C, Borges F, Macedo TRA, Oliveira-Brett AM (2004) Voltammetric oxidation of drugs of abuse III. Heroin and metabolites. Electroanalysis 16: 1497–1502

107. Garrido JMPJ, Delerue-Matos C, Borges F, Macedo TRA, Oliveira-Brett AM (2004) Voltammetric oxidation of drugs of abuse: II. Codeine and metabolites. Electroanalysis 16: 1427–1433
108. Garrido EMPJ, Garrido JMPJ, Milhazes N, Borges F, Oliveira-Brett AM (2010) Electrochemical oxidation of amphetamine-like drugs and application to electroanalysis of ecstasy in human serum. Bioelectrochemistry 79:77–83
109. Institute for Quality and Efficiency in Health Care (IQWiG) (2006) What does blood do? – InformedHealth.org – NCBI Bookshelf. https://www.ncbi.nlm.nih.gov/books/NBK279392/
110. Yu Z et al (2011) Differences between human plasma and serum metabolite profiles. PloS One 6
111. Krebs HA (1950) Chemical composition of blood plasma and serum. Annu Rev Biochem 19: 409–430
112. Sviridov D, Hortin GL (2009) Urine albumin measurement: effects of urine matrix constituents. Clin Chim Acta 404:140–143
113. Battino M, Ferreiro MS, Gallardo I, Newman HN, Bullon P (2002) P: the antioxidant capacity of saliva. J Clin Periodontol 29:189–194
114. del Vigna de Almeida P, Trindade Grégio AM, Naval Machado MÂ, Adilson Soares de Lima A, Reis Azevedo L (2008) Saliva composition and functions: a comprehensive review. J Contemp Dental Practic 9:72–80
115. Inzitari R et al (2006) Detection in human saliva of different statherin and P-B fragments and derivatives. Proteomics 6:6370–6379
116. Parrilla M, Joosten F, de Wael K (2021) Enhanced electrochemical detection of illicit drugs in oral fluid by the use of surfactant-mediated solution. Sens Actuators B Chem 348:130659
117. Joosten F, Parrilla M, de Wael K (2022) Electrochemical detection of cocaine in authentic oral fluid. Eng Proc 16(1):13. https://doi.org/10.3390/IECB2022-12284
118. Wang H-W et al (2021) Cyclic voltammetry in biological samples: a systematic review of methods and techniques applicable to clinical settings. Signals 2:138–158
119. Cetó X, O'Mahony AM, Wang J, del Valle M (2013) Simultaneous identification and quantification of nitro-containing explosives by advanced chemometric data treatment of cyclic voltammetry at screen-printed electrodes. Talanta 107:270–276
120. de Jong M et al (2018) Levamisole: a common adulterant in cocaine street samples hindering electrochemical detection of cocaine. Anal Chem 90:5290–5297
121. Russo MJ et al (2021) Antifouling strategies for electrochemical biosensing: mechanisms and performance toward point of care based diagnostic applications. ACS Sens 6:1482–1507
122. Russo MJ et al (2020) A simple electrochemical swab assay for the rapid quantification of clonazepam in unprocessed saliva enabled by Lubricin antifouling coatings. ChemElectroChem 7:2851–2858
123. Bottari F et al (2020) Do aptamers always bind? The need for a multifaceted analytical approach when demonstrating binding affinity between aptamer and low molecular weight compounds. J Am Chem Soc 142:19622–19630
124. Parrilla M, De Wael K (2021) Wearable self-powered electrochemical devices for continuous health management. Adv Funct Mater 31:2107042
125. Teymourian H et al (2020) Wearable electrochemical sensors for the monitoring and screening of drugs. ACS Sens 5:2679–2700
126. Hubble LJ, Wang J (2019) Sensing at your fingertips: glove-based wearable chemical sensors. Electroanalysis 31:428–436
127. Cánovas R, Parrilla M, Mercier P, Andrade FJ, Wang J (2016) Balloon-embedded sensors withstanding extreme multiaxial stretching and global bending mechanical stress: towards environmental and security monitoring. Adv Mater Technol 1:1600061
128. de Jong M et al (2016) Electrochemical fingerprint of street samples for fast on-site screening of cocaine in seized drug powders. Chem Sci 7:2364–2370
129. Barfidokht A et al (2019) Wearable electrochemical glove-based sensor for rapid and on-site detection of fentanyl. Sens Actuators B Chem 296:126422

130. Mishra RK et al (2020) Continuous opioid monitoring along with nerve agents on a wearable microneedle sensor array. J Am Chem Soc 142:5991–5995
131. Heikenfeld J et al (2019) Accessing analytes in biofluids for peripheral biochemical monitoring. Nat Biotechnol 37:407–419
132. Mishra RK et al (2020) Simultaneous detection of salivary Δ9-tetrahydrocannabinol and alcohol using a wearable electrochemical ring sensor. Talanta 211:120757
133. Hudson M et al (2019) Drug screening using the sweat of a fingerprint: lateral flow detection of Δ^9-tetrahydrocannabinol, cocaine, opiates and amphetamine. J Anal Toxicol 43:88–95
134. Sempionatto JR et al (2021) An epidermal patch for the simultaneous monitoring of haemodynamic and metabolic biomarkers. Nat Biomed Eng 5:737–748
135. Kranenburg RF et al (2020) Performance evaluation of handheld Raman spectroscopy for cocaine detection in forensic case samples. Drug Test Anal 13:1054–1067
136. Kranenburg RF et al (2020) Rapid and robust on-scene detection of cocaine in street samples using a handheld near-infrared spectrometer and machine learning algorithms. Drug Test Anal 12:1404–1418
137. Kranenburg RF, Ramaker H, van Asten AC (2022) On-site forensic analysis of colored seized materials: detection of brown heroin and MDMA-tablets by a portable NIR spectrometer. Drug Test Anal 14:1762–1772
138. Dragan AM et al (2021) Analytical techniques for the determination of amphetamine-type substances in different matrices: a comprehensive review. Trends Anal Chem 145:116447